FACILITY FORM 602
N68-35984
(ACCESSION NUMBER)
514
(PAGES)
(NASA CR OR TMX OR AD NUMBER)
(THRU)
1
(CODE)
31
(CATEGORY)

NASA CONTRACTOR REPORT

NASA CR-66678-5

NASA CR-66678-5

GPO PRICE $ _____

CFSTI PRICE(S) $ _____

Hard copy (HC) ____

Microfiche (MF) ____

ff 653 July 65

MARS HARD LANDER CAPSULE STUDY

OCT 1968
RECEIVED
NASA STI FACILITY
INPUT BRANCH

Volume IV
Capsule Point Designs and Supporting Analysis

Prepared by
GENERAL ELECTRIC
RE-ENTRY SYSTEMS
for Langley Research Center

31 JULY 1968

NATIONAL AERONAUTICS AND SPACE ADMINISTRATION–WASHINGTON, D. C.

NASA CR-66678-5

MARS HARD LANDER CAPSULE STUDY

Volume IV
(Book #1)

CAPSULE POINT DESIGNS AND SUPPORTING ANALYSIS

Distribution of this report is provided in the interest of information exchange. Responsibility for the contents resides in the author or organization that prepared it.

Issued by Originator as General Electric Document No. 68SD952-5 (Vol. IV, Book 1)

PREPARED UNDER CONTRACT NO. NAS 1-8098 BY

GENERAL ELECTRIC
RE-ENTRY SYSTEMS
3198 Chestnut Street, Philadelphia, Pa. 19101

FOR
LANGLEY RESEARCH CENTER

NATIONAL AERONAUTICS & SPACE ADMINISTRATION

PRECEDING PAGE BLANK NOT FILMED.

FOREWORD

The Mars "Hard Lander" Study Final Report is divided into four volumes and bound in eight books. The titles of the volumes and a brief description of the contents of each book are presented below.

VOLUME I - SUMMARY (CR-66678-1)

Volume I contains a summary of the study activity, the conclusions reached, and a description of a possible design implementation suggested by the study results.

This study indicates that meaningful scientific payloads of approximately 1500 pounds can be placed on the Mars surface, survive for several months, and transmit more than a hundred million bits of data to Earth.

In addition, the study provided data which shows that a smaller Capsule of 700 to 900 pounds has the ability to transmit approximately 10 million bits of imagery and additional scientific surface data.

VOLUME II - MISSION AND SCIENCE DEFINITION (CR-66678-2)

Volume II contains a description of the 'reference' mission plans, both direct entry and out-of-entry, the mission analyses conducted to define the reference plans, the assumed Mars models considered, and the science definition tasks accomplished to select entry and surface science packages/measurement sequences specifically designed to satisfy LRC's scientific goals.

VOLUME III - CAPSULE PARAMETRIC STUDY (CR-66678-3, -4)

A discussion of the analysis and results derived in determining the Capsule subsystems' design characteristics parametrically is provided for the range of assumed Mars Models and the reference mission plans. The synthesis of these subsystems into complete Capsule systems is presented in terms of Capsule performance, total imagery data obtainable, and surface lifetime.

CR-66678-3 presents the Capsule System Parametric Synthesis and Entry and Retardation Subsystem Studies. CR-66678-4 presents both studies of the Lander and Re-entry Subsystems and Appendices associated with the Parametric Study.

VOLUME IV- CAPSULE POINT DESIGNS AND SUPPORTING ANALYSES
(CR-66678-5, -6, -7, -8)

Volume IV contains a presentation of the detailed Capsule 'Point Designs', and their supporting analyses, derived to identify specific hardware approaches, weights, and system configurations; and confirm the correctness of the parametric results. In addition to the Capsule's engineering and design details, the results include development status, probability of success, and constraints imposed on the Orbiter by the Capsule mission.

CR-66678-5 contains a definition of the Capsule Point Design Requirements and descriptions of Point Designs 1 and 2. CR-66678-6 contains descriptions of Point Designs 3 and 4 and CR-66678-7 of Point Designs 5 and 6. CR-66678-8 provides additional information on Impact Attenuation, Surface Environment Definition, Effects on Point Designs due to Variations in Assumed Design Parameters as well as the Effects of a Lander on the Mariner Orbiter.

TABLE OF CONTENTS

BOOK 1

Section			Page
1	INTRODUCTION		1-1
	1.1	Introduction	1-1
	1.2	Summary	1-4
	1.3	Component Development Status of Equipment	1-8
2	POINT DESIGN REQUIREMENTS		2-1
	2.1	Definition of Six Point Designs	2-1
	2.2	Baseline Mission Constraints for Point Designs	2-3
		2.2.1 Langley Research Center Guidelines and Constraints	2-3
		2.2.2 Out-of-Orbit Entry - Baseline Mission Data	2-4
		2.2.3 Direct Entry - Baseline Mission Data	2-6
	2.3	Capsule System Design Criteria and Constraints	2-8
		2.3.1 Capsule Launch Envelope	2-8
		2.3.2 Environments	2-8
		2.3.3 Entry Science Instrumentation	2-16
		2.3.4 Surface Science Instrumentation	2-25
		2.3.5 Landing Parameters	2-35
		2.3.6 Structural Loading Criteria	2-35
	2.4	References	2-37
3	POINT DESIGN 1		3-1
	3.1	Mission Sequence	3-1
	3.2	Capsule System Design Description	3-9
		3.2.1 Science Data Reference	3-11
		3.2.2 Capsule Systems Configuration	3-13
		3.2.3 Capsule Systems Weight	3-13
		3.2.4 Functional Block Diagram	3-13
		3.2.5 Power Profiles, Point Design 1	3-23
	3.3	Pre-entry Systems	3-25
		3.3.1 Canister	3-25
		3.3.2 Pressure and Venting System	3-32
		3.3.3 Separation Subsystem Description	3-36
		3.3.4 Environmental Control	3-46
		3.3.5 De-orbit Propulsion System	3-49
		3.3.6 Electrical Equipment, Pre-entry	3-53
		3.3.7 De-orbit System	3-56
		3.3.8 Pre-entry Systems Weight	3-59
	3.4	Entry Systems	3-61
		3.4.1 Configuration	3-61
		3.4.2 Heat Shield	3-64

Section			Page
	3.4.3	Aeroshell and Structure	3-72
	3.4.4	Lander/Aeroshell Separation	3-79
	3.4.5	Entry Systems Equipment	3-81
	3.4.6	Retardation Subsystem	3-81
	3.4.7	Roll Control Subsystem	3-97
	3.4.8	Entry Systems Weight	3-98
3.5	Lander Systems		3-100
	3.5.1	Configuration Constraints and Description	3-100
	3.5.2	Science Payload Equipments	3-107
	3.5.3	Telecommunications	3-121
	3.5.4	Electrical Power Equipment	3-158
	3.5.5	Environmental Control	3-162
	3.5.6	Deployment Mechanisms	3-165
	3.5.7	Lander Container Structure	3-170
	3.5.8	Impact Attenuation and Structure	3-176
	3.5.9	Mass Property and Inertia Data	3-193
3.6	Constraints Imposed on Orbiter		3-197
3.7	Probability of Success		3-203
	3.7.1	Introduction	3-203
	3.7.2	Results	3-203
	3.7.3	Capsule Analysis	3-204
	3.7.4	Orbiter Support Analysis	3-211
3.8	References		3-212
4	POINT DESIGN 2		4-1
4.1	Mission Sequence		4-1
4.2	Capsule System Design Description		4-9
	4.2.1	Science Data Reference	4-12
	4.2.2	Capsule Systems Configuration	4-13
	4.2.3	Capsule Systems Weight	4-13
	4.2.4	Functional Block Diagrams	4-14
	4.2.5	Power Profiles, Point Design 2	4-23
4.3	Pre-entry Systems		4-25
	4.3.1	Canister	4-25
	4.3.2	Pressure and Venting System	4-34
	4.3.3	Separation Subsystem	4-38
	4.3.4	Environmental Control	4-48
	4.3.5	De-orbit Propulsion System	4-51
	4.3.6	Electrical Equipment, Pre-entry	4-57
	4.3.7	De-orbit System	4-58
	4.3.8	Pre-entry Systems Weight	4-62

Section			Page
4.4	Entry Systems		4-63
	4.4.1	Configuration	4-63
	4.4.2	Heat Shield	4-67
	4.4.3	Aeroshell and Structure	4-75
	4.4.4	Lander/Aeroshell Separation	4-82
	4.4.5	Entry System Equipment	4-82
	4.4.6	Retardation Subsystem	4-82
	4.4.7	Roll Control Subsystem	4-101
	4.4.8	Entry Systems Weight	4-104
4.5	Lander Systems		4-105
	4.5.1	Configuration Constraints and Description	4-105
	4.5.2	Science Payload Equipments	4-111
	4.5.3	Telecommunications	4-125
	4.5.4	Electrical Power Equipment	4-158
	4.5.5	Environmental Control	4-169
	4.5.6	Deployment Mechanisms	4-170
	4.5.7	Lander Container Structure	4-174
	4.5.8	Impact Attenuation and Structure	4-183
	4.5.9	Mass Property and Inertia Data	4-202
4.6	Constraints Imposed on Orbiter		4-207
4.7	Probability of Success - Point Design 2		4-214
	4.7.1	Introduction	4-214
	4.7.2	Results	4-214
	4.7.3	Capsule Analysis	4-215
	4.7.4	Orbiter Support Analysis	4-222
4.8	References		4-224

LIST OF ILLUSTRATIONS

Figure		Page
2.3.1-1	Titan III-C Standard Fairing	2-9
2.3.1-2	Titan III-C Fairing - Bulbous Payload	2-10
2.3.1-3	Capsule and Orbiter Adapter Interface with Launch Vehicle, Standard Fairing	2-11
2.3.1-4	Capsule and Orbiter Adapter Interface with Launch Vehicle, Bulbous Fairing	2-11
2.3.4-1	Silicon Solar Cell Wavelength Response and ASOS Vidicon Wavelength Response	2-31
3.1-1	Operational Flight Sequence from Separation to Impact	3-5
3.1-2	Landed Operations	3-7
3.2.2-1	Mars Hard Lander, Point Design 1	3-15
3.2.4-1	Electrical System Signal and Power, Functional Block Diagram, Point Design 1	3-19
3.2.5-1	Power Profile, Point Design 1	3-24
3.3.1-1	Aeroshell/Canister Clearances	3-26
3.3.1-2	Inboard Profile, Point Design 1	3-27
3.3.1-3	Canister Field Joint	3-30
3.3.1-4	Required Ring Inertia for Stability as a Function of Critical Load	3-31
3.3.2-1	Pressure and Venting Subsystem, Block Diagram	3-33
3.3.2-2	Flow Rate and Differential Pressure vs Time After Lift-off	3-35
3.3.3-1	Separation Subsystem, Block Diagram	3-38
3.3.3-2	Hot-Wire Tension Bolt	3-41
3.3.3-3	Capsule Separation Adjustable Spring Assembly	3-41
3.3.3-4	Aft Canister Ring	3-43
3.3.3-5	Forward Canister Ring	3-44
3.3.4-1	Super Insulation Requirements to Maintain 310°R on Compartment Wall and Heat Shield	3-47
3.3.4-2	Transit Mode Power and Insulation Requirements for Various Canister Areas	3-48

Figure		Page
3.3.5-1	Solid Propellant System	3-51
3.3.5-2	De-Orbit Rocket and Thrust Cone Structure	3-54
3.3.5-3	Thrust Cone Separation	3-55
3.3.7-1	Spin and Roll Control Subsystem, Block Diagram	3-58
3.4.1-1	Aeroshell Geometry, Point Design 1	3-64
3.4.2-1	Cold Wall Convective and Radiative Heat Flux Histories, Point Design 1	3-67
3.4.2-2	Heat Shield Thickness Requirements, Point Design 1	3-69
3.4.2-3	Surface and Backface Temperature Histories, Point Design 1	3-70
3.4.2-4	Temperature Gradients Through the Shield, Point Design 1	3-71
3.4.3-1	Axial Deflection - Aeroshell 2A vs Radial Distance	3-73
3.4.3-2	Axial Bending Moment (M_x) - Aeroshell 2A vs Radial Distance	3-73
3.4.3-3	Shell Transverse Shear - Aeroshell 2A vs Radial Distance	3-74
3.4.3-4	Axial In-plane Load - Aeroshell 2A vs Radial Distance	3-74
3.4.3-5	Axial Honeycomb Facing Stress - Aeroshell 2A vs Radial Distance	3-75
3.4.3-6	Performance Characteristics of 2024-T4	3-77
3.4.3-7	Mechanical Design Yield Strength for 2024-T4	3-77
3.4.4-1	Lander Installation into Aeroshell	3-80
3.4.5-1	Entry Systems Instrumentation	3-82
3.4.6-1	Pilot Deployment Trajectory Study, Point Design 1	3-85
3.4.6-2	Main Parachute Trajectory in VM-8 Atmosphere, Point Design 1	3-88
3.4.6-3	Retardation Deployment Sequence	3-95
3.5.1-1	General Assembly, Point Design 1	3-103
3.5.2-1	Water Vapor Detector, Block Diagram	3-111
3.5.2-2	Wind Velocity Sensor	3-115
3.5.2-3	Alpha Back Scatter Instrument	3-116
3.5.2-4	High and Low Speed TV Cameras	3-118
3.5.2-5	Silicon Photo-voltaic Cell Spectral Response	3-119
3.5.2-6	Rotary Potentiometer Clinometer	3-119

Figure		Page
3.5.3-1	Telecommunications Subsystem, Functional Block Diagram	3-122
3.5.3-2	Available Data Rate vs Time with Adverse Tolerances	3-126
3.5.3-3	Relay and Beacon Link, Block Diagram	3-126
3.5.3-4	Reference Orbit Communications Parameters	3-129
3.5.3-5	400 MHz Antenna Pattern	3-133
3.5.3-6	400 MHz Transmitter, Block Diagram	3-134
3.5.3-7	Duplexer and Antenna Selector	3-135
3.5.3-8	Beacon Receiver	3-136
3.5.3-9	Orbiter 400 MHz Radio Subsystem	3-138
3.5.3-10	Data Handling System	3-140
3.5.3-11	Command Word Format	3-143
3.5.3-12	Operation of Command Storage Control Unit	3-144
3.5.3-13	Entry Data Storage Routine	3-148
3.5.4-1	Electrical Power Subsystem Block Diagram, Point Design 1	3-151
3.5.4-2	Battery Redundancy Circuit	3-153
3.5.5-1	Battery Temperature Profile and Heater Power Requirements, Minimum Environment	3-163
3.5.5-2	Battery Temperature Profile and Heater Power Requirements, Maximum Environment	3-163
3.5.5-3	Payload Temperature Profile, Minimum Environment	3-164
3.5.5-4	Payload Temperature Profile, Maximum Environment	3-164
3.5.6-1	Camera Deployment (Includes Wind Velocity and Temperature Transducers	3-167
3.5.6-2	Operation of Alpha Back Scatter Deployment Mechanism	3-169
3.5.7-1	Structure Assembly	3-171
3.5.7-2	Four Conditions Used for Preliminary Loading Analysis	3-174
3.5.7-3	Typical Interaction Radial Loads Between Torus and Cylinder, Edge-on Condition	3-174
3.5.7-4	Typical Interaction Moment Between Torus and Cylinder, Edge-on Condition	3-175
3.5.7-5	Typical Interaction Shear Flow Between Torus and Cylinder, Edge-on Condition	3-175
3.5.8-1	Lander Attenuation, Point Design 1	3-179
3.5.8-2	Gross Cross-sectional Area vs Stroke	3-180
3.5.8-3	Effective Cross-sectional Area vs Stroke	3-182

Figure		Page
3.5.8-4	Design Guide for Reduction in Honeycomb Properties for Non-axial Impacts	3-183
3.5.8-5	Comparison of Crushing Stress vs Angle-of-Impact for Static and Dynamic Loading	3-183
3.5.8-6	Stroke Efficiency vs Bulk Density	3-185
3.5.8-7	Stroke Efficiency	3-185
3.5.8-8	Crushable Honeycomb Properties	3-187
3.5.8-9	General Internal Geometry, Point Design 1	3-187
3.5.8-10	Layup of Honeycomb Attenuator	3-190
3.6-1	Capsule/Bus Interface	3-199
4.1-1	Operational Flight Sequence from Separation to Impact	4-5
4.1-2	Landed Operation	4-7
4.2.2-1	Mars Hard Lander, Point Design 2A	4-15
4.2.2-2	Mars Hard Lander, Point Design 2B	4-17
4.2.4-1	Electrical System Signal and Power, Functional Block Diagram, Point Design 2	4-19
4.2.5-1	Power Profile, Point Design 2 (Nominal Mission)	4-24
4.3.1-1	Aeroshell/Canister Clearances	4-26
4.3.1-2	Inboard Profile, Point Design 2A	4-27
4.3.1-3	Inboard Profile, Point Design 2B	4-29
4.3.1-4	Canister Field Joint	4-32
4.3.1-5	Required Ring Inertia for Stability as a Function of Critical Load	4-33
4.3.2-1	Pressure and Venting System, Block Diagram	4-35
4.3.2-2	Flow Rate and Differential Pressure vs Time After Lift-off	4-37
4.3.3-1	Separation Subsystem, Block Diagram	4-40
4.3.3-2	Hot-wire Tension Bolt	4-43
4.3.3-3	Capsule Separation Adjustable Spring Assembly	4-44
4.3.3-4	Aft Canister Ring	4-45
4.3.3-5	Forward Canister Ring	4-46
4.3.4-1	Super Insulation Requirements to Maintain 310° R on Compartment Wall and Heat Shield	4-49
4.3.4-2	Transit Mode Power and Insulation Requirements for Various Canister Areas	4-50

LIST OF ILLUSTRATIONS (Continued)

Figure		Page
4.3.5-1	Solid Propellant System	4-53
4.3.5-2	De-orbit Propulsion Installation, Point Designs 2A and 2B	4-55
4.3.5-3	Thrust Cone Separation	4-57
4.3.7-1	Spin and Roll Control Subsystem, Block Diagram	4-60
4.4.1-1	Aeroshell Geometry, Point Design 2A	4-66
4.4.1-2	Aeroshell Geometry, Point Design 2B	4-66
4.4.2-1	Cold Wall Convective and Radiative Heat Flux Histories, Point Design 2B	4-71
4.4.2-2	Heat Shield Thickness Requirements, Point Design 2B	4-72
4.4.2-3	Surface and Backface Temperature Histories, Point Design 2B	4-73
4.4.2-4	Temperature Gradients Through the Shield, Point Design 2B	4-74
4.4.3-1	Axial Deflection - Aeroshell 2A vs Radial Distance	4-76
4.4.3-2	Axial Bending Moment (M_x) - Aeroshell 2A vs Radial Distance	4-76
4.4.3-3	Shell Transverse Shear - Aeroshell 2A vs Radial Distance	4-77
4.4.3-4	Axial In-plane Load - Aeroshell 2A vs Radial Distance	4-77
4.4.3-5	Axial Honeycomb Facing Stress - Aeroshell 2A vs Radial Distance	4-78
4.4.3-6	Shield-Structure Interface Temperature, Point Design 2A	4-80
4.4.4-1	Lander Installation into Aeroshell, Point Designs 2A and 2B	4-83
4.4.5-1	Entry Systems Instrumentation	4-84
4.4.6-1	Pilot Deployment Trajectory Study, Point Design 2A	4-88
4.4.6-2	Pilot Deployment Trajectory Study, Point Design 2B	4-89
4.4.6-3	Main Parachute Trajectory in VM-8 Atmosphere, Point Design 2A	4-93
4.4.6-4	Main Parachute Trajectory in VM-8 Atmosphere, Point Design 2B	4-94
4.4.6-5	Retardation System Sequence of Events	4-99
4.5.1-1	General Assembly, Point Design 2	4-109

Figure		Page
4.5.2-1	Water Vapor Detector, Block Diagram	4-115
4.5.2-2	Wind Velocity Sensor	4-119
4.5.2-3	Alpha Back Scatter Instrument	4-120
4.5.2-4	High and Low Speed TV Cameras	4-121
4.5.2-5	Silicon Photo-Voltaic Cell Spectral Response	4-122
4.5.2-6	Rotary Potentiometer Clinometer	4-124
4.5.3-1	Telecommunications Subsystem, Functional Block Diagram	4-125
4.5.3-2	First Orbit Pass Communication Parameters	4-130
4.5.3-3	Available Data Rate vs Time with Adverse Tolerances, Entry Pass and Nominal Orbital Passes	4-131
4.5.3-4	Available Data Rate vs Time with Adverse Tolerances, First Orbiter Pass, -3.4 hr Period Error	4-132
4.5.3-5	Available Data Rate vs Time with Adverse Tolerances, First Orbiter Pass, +3.4 hr Period Error	4-133
4.5.3-6	Relay and Beacon Link, Block Diagram	4-134
4.5.3-7	400 MHz Antenna Pattern	4-140
4.5.3-8	400 MHz Transmitter, Block Diagram	4-141
4.5.3-9	Duplexer and Antenna Selector	4-142
4.5.3-10	Beacon Receiver	4-143
4.5.3-11	Orbiter 400 MHz Radio Subsystem	4-146
4.5.3-12	Data Handling System	4-147
4.5.3-13	Command Word Format	4-151
4.5.3-14	Operation of Command Storage Control Unit	4-152
4.5.3-15	Entry Data Storage Routine	4-155
4.5.4-1	Electrical Power Subsystem, Point Design 2, Block Diagram	4-159
4.5.4-2	Battery Redundancy Circuit	4-161
4.5.5-1	Battery Temperature Profile and Heater Power Requirements, Minimum Environment	4-171
4.5.5-2	Battery Temperature Profile and Heater Power Requirements, Maximum Environment	4-171
4.5.5-3	Payload Temperature Profile, Minimum Environment	4-172
4.5.5-4	Payload Temperature Profile, Maximum Environment	4-172
4.5.6-1	Camera Deployment, Includes Wind Velocity and Temperature Transducers	4-175
4.5.6-2	Operation of Alpha Back Scatter Deployment Mechanism	4-177
4.5.7-1	Structure Assembly	4-179
4.5.7-2	Four Conditions Used for Preliminary Loading Analysis	4-181
4.5.7-3	Typical Interaction Radial Loads Between Torus and Cylinder, Edge-on Condition	4-182

Figure		Page
4.5.7-4	Typical Interaction Moment Between Torus and Cylinder, Edge-on Condition	4-182
4.5.7-5	Typical Interaction Shear Flow Between Torus and Cylinder, Edge-on Condition	4-183
4.5.8-1	Lander Attenuation, Point Design 2A	4-186
4.5.8-2	Lander Attenuation, Point Design 2B	4-186
4.5.8-3	Gross Cross-sectional Area vs Stroke	4-188
4.5.8-4	Effective Cross-sectional Area vs Stroke	4-190
4.5.8-5	Design Guide for Reduction in Honeycomb Properties for Non-axial Impacts	4-191
4.5.8-6	Comparison of Crushing Stress vs Angle-of-Impact for Static and Dynamic Loading	4-191
4.5.8-7	Stroke Efficiency vs Bulk Density	4-193
4.5.8-8	Residual Honeycomb and Debris	4-193
4.5.8-9	Crushable Honeycomb Properties	4-194
4.5.8-10	General Internal Geometry, Point Design 2A	4-195
4.5.8-11	Layup of Honeycomb Arrangement (Omni Direction)	4-198
4.5.8-12	Layup of Honeycomb Attenuator (Multi-direction)	4-199
4.6-1	Capsule/Bus Interface	4-209

LIST OF TABLES

Table		Page
1.1-1	Summary of Capsule Design Characteristics	1-2
1.2-1	Capsule System Weights	1-4
1.2-2	Telecommunications Subsystem Characteristics	1-6
1.3-1	Component Development Status Matrix	1-9
2.1-1	Six Point Designs, System Requirements	2-2
2.2.2-1	Point Design Values of Out-of-Orbit Entry Trajectory Parameters	2-6
2.2.2-2	Point Design Values of Direct Entry Trajectory Parameters	2-7
2.3.2-1	Mars Atmospheric Models	2-13
2.3.2-2	Mean Wind Model for Mars Atmospheric Models	2-14
2.3.2-3	Wind Shear Model for Mars Atmospheric Models	2-15
2.3.6-1	Point Design Loads	2-36
3.1-1	Mission Sequence of Events, Point Design No. 1	3-1
3.2-1	Comparative Weight Summary of Minimum Mission Systems	3-11
3.2-2	Science Weight Summary	3-12
3.2-3	Weight and Inertia Composition, Point Design 1	3-17
3.3.1-1	Structural Analysis, Canister Loads	3-29
3.3.3-1	Separation Spring Data	3-46
3.3.5-1	Performance, Weight, and Envelope Data	3-50
3.3.7-1	Spin and Roll Control Requirements, Point Design 1	3-56
3.3.8-1	Pre-entry Systems Weight Summary	3-60
3.4.1-1	CONSEP Program Results, Point Design 1	3-61
3.4.1-2	Point Design Loads	3-63
3.4.2-1	Entry Conditions and Geometry of Point Designs 1 through 6	3-65
3.4.2-2	Thermophysical Properties of ESM Materials	3-68
3.4.3-1	Final Aluminum Honeycomb Requirements for Aeroshells	3-75
3.4.3-2	Point Design Configuration Data	3-78
3.4.6-1	Pilot Parachute Deployment Trajectory Study Parameters	3-86
3.4.6-2	Main Parachute Design Parameters	3-89
3.4.6-3	Parachute Trajectory Parameters, Point Design 1	3-89
3.4.6-4	Retardation System Weight Breakdown	3-97
3.4.7-1	Spin and Roll Control Subsystem Fixed Hardware Weight, Point Design 1	3-98
3.4.7-2	Spin and Roll Control Subsystem, Point Design 1 Parameters	3-99
3.4.8-1	Entry System Weight Summary, Point Design 1	3-99
3.5.2-1	Entry Science Payload	3-108
3.5.2-2	Surface Science Payload	3-112
3.5.2-3	Typical Camera Specifications	3-120
3.5.3-1	Design Summary, Point Design 1	3-122
3.5.3-2	Telecommunications Sequence	3-123
3.5.3-3	Measurements List	3-124
3.5.3-4	Data Transmitted	3-125

Table		Page
3.5.3-5	Design Control Tables - Relay (Landed) and Beacon	3-127
3.5.3-6	Early Turn-on Intervals	3-130
3.5.3-7	Entry Link Design Control Table	3-131
3.5.3-8	Data Transferable After Impact Plus 2.5 Min (bits/10^7)	3-132
3.5.3-9	Entry Data	3-145
3.5.3-10	Landed Science (Non-imaging)	3-146
3.5.3-11	Physical Characteristics	3-149
3.5.4-1	Electrical Equipment Hardware Matrix, Point Design 1	3-155
3.5.9-1	Weight Summary	3-193
3.5.9-2	Detailed Weight Breakdown, Subsystems Components	3-194
3.6-1	Major Subsystem Changes	3-201
3.6-2	Orbiter Propulsion Summary	3-202
3.7.2-1	Mission Success Probability, Point Design 1	3-203
3.7.3-1	Reliability Estimates, Point Design 1 Components	3-208
3.7.3-2	Reliability Summary, Point Design 1 Capsule System and Subsystem	3-210
4.1-1	Mission Sequence of Events, Point Design 2	4-1
4.2-1	Comparative Weight Summary of Minimum Mission Systems	4-10
4.2-2	Science Weight Summary	4-12
4.2-3	Weight and Inertia Composition, Point Design 2A	4-13
4.2-4	Weight and Inertia Composition, Point Design 2B	4-14
4.3.1-1	Interface Ring Loads	4-31
4.3.3-1	Separation Spring Data	4-48
4.3.5-1	Performance, Weight, and Envelope Data, Point Designs 2A and 2B	4-52
4.3.7-1	Spin and Roll Control Requirements, Point Design 2	4-59
4.3.8-1	Pre-entry Systems Weight Summary, Point Designs 2A and 2B	4-62
4.4.1-1	CONSEP Program Results - Point Design 2A	4-64
4.4.1-2	Point Design Loads	4-65
4.4.2-1	Entry Conditions and Geometry of Point Designs 1 through 6	4-68
4.4.2-2	Thermophysical Properties of ESM Materials	4-70
4.4.2-3	Shield Thickness Requirements for Point Designs 1 through 6	4-75
4.4.3-1	Final Aluminum Honeycomb Requirements for Aeroshells	4-78
4.4.3-2	Point Design Entry Data	4-79
4.4.6-1	Pilot Parachute Design Parameters	4-87
4.4.6-2	Main Parachute Design Parameters	4-92
4.4.6-3	Parachute Trajectory Parameters, Point Design 2	4-92
4.4.6-4	Retardation System Weight Breakdown	4-98
4.4.7-1	Spin and Roll Control Subsystem Fixed Hardware Weight, Point Designs 2A and 2B	4-102
4.4.7-2	Spin and Roll Control Subsystem, Point Design 2 Parameters	4-103
4.4.8-1	Entry Systems Weight Summary, Point Designs 2A and 2B	4-104
4.5.2-1	Entry Science Payload	4-112

Table		Page
4.5.2-2	Surface Science Payload	4-116
4.5.2-3	Typical Camera Specifications	4-123
4.5.3-1	Design Summary	4-126
4.5.3-2	Telecommunications Sequence	4-127
4.5.3-3	Measurements List	4-128
4.5.3-4	Data Transmission	4-128
4.5.3-5	Design Control Tables, Relay (Landed) and Beacon	4-135
4.5.3-6	Data Transferable After Impact +2.5 Min (bits/10^7)	4-136
4.5.3-7	Entry Link Design Control Table	4-138
4.5.3-8	Entry Data	4-153
4.5.3-9	Landed Science (Non-imaging)	4-154
4.5.3-10	Physical Characteristics	4-157
4.5.4-1	Electrical Equipment Hardware Matrix, Point Design 2	4-163
4.5.9-1	Weight Summary, Point Design 2A	4-202
4.5.9-2	Weight Summary, Point Design 2B	4-203
4.5.9-3	Detailed Weight Breakdown, Subsystems Components	4-204
4.6-1	Major Subsystem Changes	4-211
4.6-2	Orbiter Propulsion Summary, Point Design 2A	4-212
4.6-3	Orbiter Propulsion Summary, Point Design 2B	4-213
4.7.2-1	Mission Success Probability, Point Design 2	4-214
4.7.3-1	Reliability Estimates, Point Design 2 Components	4-219
4.7.3-2	Reliability Summary, Point Design 2 Capsule System and Subsystems	4-221

1. INTRODUCTION

1. INTRODUCTION

1.1 DESCRIPTION

Volume IV of this Final Report documents the six Point Designs prepared as part of the Mars Hard Lander Capsule Study. The requirements of Langley Research Center call for three similar Capsule pairs. One of the Capsules in each pair is designed for out-of-orbit entry and the other is for direct entry. The first Capsule pair (designated Point Designs 1 and 2) has a surface lifetime of one diurnal cycle, a data requirement of 10^7 bits surface imagery and meteorological data (relayed via a synchronous Orbiter) and a "minimum" science package. The second design pair (Point Designs 3 and 4) has a surface lifetime of more than 90 days, direct and relay radio links, an Earth-controlled command link, and is powered by battery and regenerative solar electric systems. This pair also has the minimum science package. The third design pair (Point Designs 5 and 6) has lifetime and support equipment requirements identical with Point Designs 3 and 4; the difference is in an "increased" science package. The same entry science subsystem has been used in all the Capsule designs.

All of the Landers have been designed to attenuate the impact landing loads by dissipating the landing energy in mechanical crush-up of a toroidal ring made of phenolic glass honeycomb material. The stroke of the material has been selected to limit maximum landing body deceleration to 1000 g's, and the volume has been determined for the particular requirements. One configuration, termed "omni", means that the Lander may strike the surface in any orientation. The "multi" configuration means that Lander is constrained to initial by impact in a predicted direction. The landed equipment has been arranged so that the surface operations can be performed by the Lander in either a heads-up or tails-up final attitude.

Table 1.1-1 summarizes the principal design characteristics of the various Mars Hard Lander point designs studied. Two versions of the direct entry, one diurnal cycle, "minimum" science Capsule (Point Designs 2A and 2B) were examined to demonstrate the influence of omni-versus multi-impact capability. The effect of the new Mars Model Environment was explored by Point Design 7. Investigations of the capability of lifting body and inflatable afterbody vehicles (not shown in Table 1-1) were also conducted.

This report has been prepared with Point Designs 1 through 6 in a single volume but the order is arranged so that each point design may be considered independently of the other five. The section designations are:

Section 1. Introduction

Section 2. Requirements - All Designs

Section 3. Point Design 1

Section 4. Point Design 2

TABLE 1.1-1. SUMMARY OF CAPSULE DESIGN CHARACTERISTICS

	Point Design							
	1	2A	2B	3	4	5	6	7
Landing attenuation	omni-	omni-	multi-	multi-	multi-	multi-	multi-	multi- (New Mars Model Environment)
Launch weight	1626 lb	1882 lb	1463 lb	1846 lb	1977 lb	2114 lb	2227 lb	1581 lb
Landed weight	858 lb	858 lb	623 lb	934 lb	934 lb	1053 lb	1053 lb	753 lb
Entry science weight	15.5 lb	15.5 lb	15.5 lb	15.5 lb	15.5 lb	15.5 lb	15.5 lb	15.5 lb
Surface science weight	35.3 lb	35.3 lb	35.3 lb	35.3 lb	35.3 lb	75.7 lb	75.7 lb	35.3 lb
Surface lifetime	25 hr	25 hr	25 hr	more than 90 days	more than 90 days	more than 90 days	more than 90 days	more than 90 days
Telecommunications	UHF relay	UHF relay	UHF relay	UHF relay + S-band Direct	UHF relay + S-band Direct	UHF relay + S-band Direct	UHF relay + S-band Direct	UHF relay + S-band Direct
Electric power (average watts)	batteries (64)	batteries (64)	batteries (64)	battery + solar (25 + 15)	battery + solar (25 + 15)	battery + solar (27 + 20)	battery + solar (27 + 20)	battery + solar (25 + 10)
Entry mode	out-of-orbit	direct	direct	out-of-orbit	direct	out-of-orbit	direct	out-of-orbit
Attitude control	spin de-spin+ roll control	spin de-spin+ roll control	spin de-spin+ roll control	spin de-spin+ roll control	spin de-spin+ roll control	spin de-spin+ roll control	spin de-spin+ roll control	spin de-spin+ roll control
De-orbit propulsion	solid	solid	solid	liquid-mono-propellant	liquid-mono-propellant	liquid-mono-propellant	liquid-mono-propellant	liquid-mono-propellant
Aeroshell base diameter	8.3 ft	12.7 ft	11.4 ft	8.3 ft	12.7 ft	10 ft	14 ft	8.3 ft
Parachute deployment	Mach 2	Mach 2	Mach 2	altitude	altitude	altitude	altitude	altitude

Section 5. Point Design 3

Section 6. Point Design 4

Section 7. Point Design 5

Section 8. Point Design 6

Section 9. Other Designs

Appendix

If, for example, Point Design 5 is to be considered independently, Sections 1, 2, and 7 give the complete descriptions of that design.

The engineering details, analyses, drawings, weight, balance and inertial properties, pre-entry systems, entry systems, Lander systems, mission sequence, development status, and estimates of probable success are given separately for each point design in the applicable section. Each point design section also identifies the constraints imposed by the Capsule on a modified Mariner '71 Orbiter.

The study results show that the out-of-orbit entry Capsule has more design and performance capability than the direct entry Capsule in each point design pair. The principal reason is that the out-of-orbit entry systems can have a ballistic coefficient at entry (W/C_DA) that is almost twice that allowed for the direct entry Capsules. Consider identical 934 lb Landers (e.g., Point Designs 3 and 4): the direct entry Capsule (20,800 ft/sec and 25^o) requires a 12.7 ft base diameter aeroshell compared to an 8.3 ft diameter for the out-of-orbit entry aeroshell. For the same aeroshell size, the direct entry landed weight would be limited to approximately half that of the out-of-orbit Capsule. A steeper direct entry path angle (40^o) would show that the out-of-orbit entry Capsule is still more advantageous.

The study results show that the direct entry Capsule has some significant advantages. A very important advantage of the direct entry Capsule is that it places minor design and mission constraints on the Orbiter compared to the out-of-orbit entry Capsule that requires orbit insertion and heavier Orbiter structure.

Volume I of this report contains a comparison of each entry mode. As stated there, the final choice between entry modes requires that other constraints, such as resources available to the mission, be considered in the trade-off before ultimate selection is made.

1.2 SUMMARY

1. The limiting ballistic entry coefficient for the out-of-orbit Capsule designs is about two times the limit coefficient for direct entry designs with nominal entry path angles of 25°.

2. The out-of-orbit entry Capsules equipped to conduct the basic entry and surface science measurements specified for this study and having surface lifetimes greater than 90 days are compatible with a 10 ft diameter flight shroud. The required Capsule base diameter of the direct entry designs with similar capabilities is 12.7 ft. The out-of-orbit entry designs require an 8.3 ft aeroshell.

3. The ballistic entry designs for direct and out-of-orbit entry are based on current ballistic entry design approaches for aeroshell structure and heat shield.

4. The weight of crush-up material to attenuate the impact loads of hard landing is about 44 percent of the total touchdown system weight for multi- Landers and about 56 percent for omni-Landers. The depth of material required is based on providing a 5 in. rock clearance, and the deceleration stroke required for the touchdown velocity and the limiting deceleration level selected; (1000-g deceleration and touchdown velocity components of 220 ft/sec horizontal and 100 ft/sec vertical). In all the designs, the vertical component is limited by aerodynamic drag (aeroshell and parachute design), but the Landers are passive to the Mars surface low atmosphere winds.

   For 1000-g deceleration and 5 in. rock clearance, but with the touchdown velocity reduced to 110 ft/sec horizontal and 100 ft/sec vertical, the weight fraction of attenuation material to touchdown weight is about 32 percent.

5. Approximately 50 percent of the Capsule system weight at launch, for both out-of-orbit and direct entry missions, is landed on the Martian surface. The weight tabulation for the Capsules designed in this study can be seen in Table 1.2-1.

TABLE 1.2-1. CAPSULE SYSTEM WEIGHTS

	1	2A	2B	3	4	5	6	7
At Launch	1626	1882	1463	1846	1977	2114	2217	1581
At Separation	1415	1551	1184	1624	1647	1856	1875	1359
At Entry	1246	1480	1127	1324	1558	1530	1766	1087
Landing	858	858	623	934	934	1053	1053	753

6. After each of the above Capsule designs were completed, the list of equipment in each was reviewed to predict what the increase in weight would be. Well defined equipment was forecast to grow 12 percent in weight while new designs could grow as much as 30 percent to the final flight system design. The average weight growth was predicted to be 20 percent.

7. The out-of-orbit entry Capsule places a larger constraint on the Orbiter than the direct entry and the booster Capsule (as illustrated by the following comparison):

	Out-of-Orbit Entry (lb)	Direct Entry (lb)
Orbiter (MM '73)	963	930
Propulsion propellant	2319	796
Burn-out	421	182
Capsule adapter	70	200
Capsule (Point Designs 3 and 4)	1846	1977
Spacecraft launch weight	5619	4085

8. Based on a 50 watt transmitter and a 160 kbps data rate, the maximum data obtainable on a periapsis relay link by the out-of-orbit entry Lander is 8.1×10^7 bits per transmission period. For four possible transmissions in the two days for a relay link to the Orbiter, the total data transmitter can be 32.4×10^7 bits.

   For the direct entry Lander, with the greater transmission distance to the Orbiter at periapsis, the data return capability of the relay communication link is influenced by the uncertainty of the orbit. The data rate for the first Orbiter pass is reduced to 31 kbps or a total of 2.5×10^7 bits transmission. The relay link for the second Orbiter pass is further reduced to 1090 bps for a 1.5×10^6 total bits transmission. In extreme cases, no communications to the Orbiter, may be possible. The total data that could be transmitted to the Orbiter in 3 days, therefore, is dependent upon the orbit inclination and period error. For the reference mission selected and optimum communication conditions, the total bits in two days is 5.2×10^7 or about 16 percent of the out-of-orbit entry data.

9. The characteristics of the telecommunications subsystem in the point designs are given in table 1.2-2.

10. Most components planned for the '73 Mars Hard Lander will meet the sterilization and shock requirements as currently available, or only minor modification. Documentation of this capability from suppliers is lacking. It will be necessary to demonstrate these capabilities for many current and all modified items.

TABLE 1.2-2. TELECOMMUNICATIONS SUBSYSTEM CHARACTERISTICS

Mission Phase	Point Designs	Radio Link	Data Rate (bps)	Transmission Time	Total Data (bits) Mission
Post Separation	All	400 MHz FSK, relay	1090	30 min	2.0×10^6
Entry	1	400 MHz FSK, relay	1090	460 to 1250(1) sec	0.50 to 1.4×10^6
	2	400 MHz FSK, relay	1090	350 to 1216(1) sec	0.38 to 1.3×10^6
	3	400 MHz FSK, relay	1090	450 to 630(1) sec	0.49 to 0.69×10^6
	4	400 MHz FSK, relay	1090	302 to 566(1) sec	0.33 to 0.62×10^6
	5	400 MHz FSK, relay	1090	450 to 630(1) sec	0.49 to 0.69×10^6
	6	400 MHz FSK, relay	1090	302 to 566(1) sec	0.33 to 0.62×10^6
	7	400 MHz FSK, relay	1090	450 to 630(1) sec	0.49 to 0.69×10^6
Post Impact					
Deployment	All	400 MHz FSK, relay	1090	2.5 min	1.6×10^5 (2)
Orbiter pass	1	400 MHz FSK, relay	160×10^3	10.4 min	0 to 10.3×10^7 (4)
	3	400 MHz FSK, relay	160×10^3	10.4 min	0 to 10.3×10^7 (4)
	5	400 MHz FSK, relay	160×10^3	10.4 min	0 to 10.3×10^7 (4)
	7	400 MHz FSK, relay	160×10^3	10.4 min	0 to 10.3×10^7 (4)
Entry pass	2	400 MHz FSK, relay	31×10^3	-	See table 4.5.3-6
	4	400 MHz FSK, relay	31×10^3	-	See table 6.5.3-6
	6	400 MHz FSK, relay	31×10^3	-	See table 8.5.3-5

TABLE 1.2-2. TELECOMMUNICATIONS SUBSYSTEM CHARACTERISTICS (Concluded)

Mission Phase	Point Designs	Radio Link	Data Rate (bps)	Transmission Time	Total Data (bits) Mission
Post Impact (Continued)					
Each periapsis pass	1	400 MHz FSK, relay	160×10^3 (3)	20.5 min	8.1×10^7
	3	400 MHz FSK, relay	160×10^3 (3)	20.5 min	8.1×10^7
	5	400 MHz FSK, relay	160×10^3 (3)	20.5 min	8.1×10^7
	7	400 MHz FSK, relay	160×10^3 (3)	20.5 min	8.1×10^7
1st periapsis pass	2	400 MHz FSK, relay	31×10^3	800 sec	2.5×10^7
2nd periapsis pass			1090	1400 sec	1.5×10^6
3rd periapsis pass			-	No communication in extreme case	
1st periapsis pass	4	400 MHz FSK, relay	31×10^3	800 sec	2.5×10^7
2nd periapsis pass			1090	1400 sec	1.5×10^6
3rd periapsis pass			-	No communication in extreme case	
1st periapsis pass	6	400 MHz FSK, relay	31×10^3	800 sec	2.5×10^7
2nd periapsis pass			1090	1400 sec	1.5×10^6
3rd periapsis pass			-	No communication in extreme case	
Direct Link (daily)	3	S-band PSK, direct	24	1.6 hr (5)	138,000
				1750 sec (6)	42,000
				133 sec (7)	3,184
	4	S-band PSK, direct	11	4.2 hr (5)	166,320
				1580 sec (6)	17,000
				290 sec (7)	3,184
	5	S-band PSK, direct	24	1.6 hr (5)	138,000
				2200 sec (6)	52,800
				187 sec (7)	4,484
	6	S-band PSK, direct	11	4.2 hr (5)	166,320
				2050 sec (6)	22,250
				408 sec (7)	4,484
	7	S-band PSK, direct	24	1.6 hr (5)	138,000
				1750 sec (6)	42,000
				133 sec (7)	3,184

NOTES

(1) Atmospheric dependent.
(2) Data during this period may be lost because entry antenna may be underneath Lander.
(3) Includes maximum beacon turn-on error of 12 min and 8.5 min minimum effective transmission interval.
(4) Atmosphere and tilt dependent.
(5) Antenna beam width limited.
(6) Average daily. Limited by Solar Array Size.
(7) Nominal data transmission time.

1.3 COMPONENT DEVELOPMENT STATUS OF EQUIPMENT

A '73 Mars Hard Lander Mission incorporates several unique requirements that have not been necessary on prior space missions. The most outstanding of these requirements is the fact that any item which enters the Martian atmosphere must be sterilized so as not to breech COSPAR planetary quarantine regulations. A second major constraint is the fact that components in the Lander must be capable of withstanding a landing shock impulse on the order of 1000 g's and still continue to function satisfactorily.

Due to the uniqueness of these requirements, it was felt advisable to conduct a survey to determine the current and/or potential development status of components which are applicable for a '73 Mars Hard Lander Mission. The following information sources were included as a part of this survey:

1. General Electric Missile and Space Division flight, test, and development laboratory data

2. Component manufacturers

3. External development and research laboratories.

The survey was conducted in the following manner:

1. Potential mission components were identified by generic type.

   Information sources were searched to determine:

   a. Development status of the equipment (in production, redesign required, new development, etc.)

   b. Will, (or is it reasonable to expect that) components withstand currently defined sterilization procedures. (Qualification tests consisting of six cycles of 96 hr each at 135° C.)

   c. What is maximum shock impact force that component can (or can reasonably be expected to) withstand.

A tabulation of information obtained from this survey is presented in table 1.3-1. Based on the information obtained from this survey, the following conclusions can be drawn concerning the development status of potential '73 Mars Hard Lander components.

1. With the primary exceptions of scientific instruments and operational batteries, most items either are in a current production status or require minor modification to existing equipment.

2. In all but one exception (tape recorder), the equipment is, or is reasonably expected to be, capable of experiencing sterilization procedures without detrimental effect.

TABLE 1.3-1. COMPONENT DEVELOPMENT STATUS MATRIX

Generic Component Type	Development Status*	Steril-izable	Maximum Shock (g's)	Applicable Capsule Usage	Information Source
Accelerometer, Triaxial	2	NFP	3,000	1,2,3,4,5,6	Systron - Donner Corp.
Accelerometer, Impact	1	Yes	10,000	1,2,3,4,5,6	GE/MSD Data
Antenna, S-band	4	Yes	500/1000(2)	3,4,5,6	GE/MSD Data
Antenna, UHF	4	Yes	500/1000(2)	1,2,3,4,5,6	GE/MSD Data
Breaker and Limiter Unit	2	Yes	10,000(1)	1,2,3,4,5,6	GE/MSD Data
Battery, Dual	5	NFP	2,000	1,2,3,4,5,6	GE/MSD Data
Battery, Operational	5	NFP	2,000	1,2,3,4,5,6	GE/MSD Data
Battery, Thermal	1	Yes	15,000	1,2,3,4,5,6	GE/MSD Data and The Wurlitzer Co.
Charge Amplifier	1	Yes	2,000	1,2,3,4,5,6	GE/MSD Data
Cable and Wire	1	Yes	2,000	1,2,3,4,5,6	Ray Chem Corp. and GE/MSD Data
Cable, Connectors, and Cable Assemblies	3	Yes	2,000	1,2,3,4,5,6	Times Wire & Cable Co. and GE/MSD Data
Camera, Facsimile	4	NFP	3,000(1)	1,2,3,4,5,6	Philco-Ford
Commutator, Cruise	1	Yes	2000/5000(2)	1,2,3,4,5,6	Fifth Dimension, Inc.
Conditioner, Data Signal	2	Yes	500/3000(2)	1,2,3,4,5,6	Fifth Dimension, Inc.
Controller, Power	5	NFP	500/1000(2)	1,2,3,4,5,6	GE/MSD Data
Circulator, UHF	3	Yes	3,000	1,2,3,4,5,6	GE/MSD Data
Circulator, S-band	3	Yes	3,000	3,4,5,6	GE/MSD Data
Decoder, Command	2	Yes	2,000(1)	1,2,3,4,5,6	GE/MSD Data
Detector, Airborn Dust	5	NFP	1,000(1)	5,6	GE/MSD Data
Detector, Large Molecule	2	Yes	300(1)	5,6	Consolidated Systems
Ejector, Nozzle	1	NFP	NR	1,2	Gould Laboratories
Explosive Nut	2	Yes	1,000(1)	1,2,3,4,5,6	Link Ordinance Div., General Precision Systems Co.
Fan, Circulating	1	Yes	NR	1,2,3,4,5,6	Rotron Mfg., Co.
Filter, EMC	2	Yes	5,000	1,2,3,4,5,6	GE/MSD Data
Filter, Vent Valve	4	Yes	NR	1,2,3,4,5,6	Pall Trinity Micro Corp.
Fitting, Parachute Release	1	NFP	2,000(1)	1,2,3,4,5,6	Gould Laboratories
Fuses	1	Yes	200(1)	1,2,3,4,5,6	Little Fuse, Inc.

*Development Status Code: 1 - as is, 2 - Modify, 3 - Redesign, 4 - New Design, 5 - New Development.

LEGEND:
(1) EXPECTED OR ESTIMATED - NOT DOCUMENTED
(2) CURRENT CAPABILITY/EXPECTED CAPABILITY
NR - NOT REQUIRED
NFP - NO FORSEEABLE PROBLEM
UNK - UNKNOWN

TABLE 1.3-1. COMPONENT DEVELOPMENT STATUS MATRIX (Continued)

Generic Component Type	Development Status*	Steril-izable	Maximum Shock (g's)	Applicable Capsule Usage	Information Source
"G" Switch Assembly	2	NFP	NR	1,2,3,4,5,6	Systron-Donner Corp. and J.E. Cuesta Co.
Guillotine Assembly, Parachute Disconnect	1	Yes	1,000	1,2,3,4,5,6	Link Ordinance Div.
Guillotine Assembly, Reefing Cutter	1	Yes	NR	1,2,3,4,5,6	Link Ordinance Div.
Gyro, Rate	2	NFP	NR	1,2,3,4,5,6	U.S. Time
Heater, Electronic	1	Yes	NR	1,2,3,4,5,6	GE/MSD Data
Inclinometer	5	NFP	2,000(1)	1,2,3,4,5,6	Diamond Laboratories
In-flight Disconnect	3	Yes	NR	1,2,3,4,5,6	GE/MSD Data and Link Ordinance
Initiator, Squib	1	Yes	1,000	1,2,3,4,5,6	Link Ordinance Div.
Motor, Controller	5	NFP	700/2000(1)	3,4,5,6	GE/MSD Data
Motor, Stepping	3	Yes	100/1000(1)	3,4,5,6	GE/MSD Data
Mass Spectrometer	2	Yes	NR	1,2,3,4,5,6	Consolidate Systems
Module, Diode Blocking	2	Yes	20,000	1,2,3,4,5,6	GE/MSD Data
Module, Power Distribution	3	Yes	500/3000(2)	1,2,3,4,5,6	Fifth Dimension Inc.
Module, Thermal Relay	4	Yes	700/2000(2)	1,2,3,4,5,6	GE/MSD Data
Moisture Sensor	5	NFP	1,500(1)	1,2,3,4,5,6	GE Experimental Data
Mortar, Drogue Ejector	5	NFP	2,000(1)	1,2,3,4,5,6	Link Ordinance & Gould Laboratories
Multicoder	3	Yes	500/2000(2)	1,2,3,4,5,6	GE/MSD Data
Panel, Solar	4	Yes	1,000(1)	3,4,5,6	GE/MSD Data
Processor, Data Handling	2	Yes	500/3000(2)	1,2,3,4,5,6	Fifth Dimension
Programmer	4	Yes	2,000(1)	1,2,3,4,5,6	GE/MSD Data
Radar Altimeter	3	NFP	7,000	3,4,5,6	GE/MSD Data
Receiver, Beacon	4	Yes	UNK	1,2,3,4,5,6	GE/MSD Data
Regulator, Charge	3	Yes	1,000	1,2,3,4,5,6	GE/MSD Data
Regulator, Voltage	3	Yes	1,000	1,2,3,4,5,6	GE/MSD Data
Release, Hot-wire	1	Yes	NR	1,2,3,4,5,6	Link Ordinance
Recorder, Tape	1	No	No	-	Ampex

*Development Status Code: 1 - as is, 2 - Modify, 3 - Redesign, 4 - New Design, 5 - New Development.

LEGEND:
(1) EXPECTED OR ESTIMATED - NOT DOCUMENTED
(2) CURRENT CAPABILITY/EXPECTED CAPABILITY
NR - NOT REQUIRED
NFP - NO FORSEEABLE PROBLEM
UNK - UNKNOWN

TABLE 1.3-1. COMPONENT DEVELOPMENT STATUS MATRIX (Concluded)

Generic Component Type	Development Status*	Sterilizable	Maximum Shock (g's)	Applicable Capsule Usage	Information Source
Switch, Antenna	1	Yes	3,000	1,2,3,4,5,6	GE/MSD Data
Storage Unit, Data	4	NFP	1,000(1)	1,2,3,4,5,6	GE/MSD Data
Switch, Hg.	4	Yes	50/1000(2)	1,2,3,4,5,6	GE/MSD Data
Switch, Microwave	1	Yes	1,500	1,2,3,4,5,6	Hewlett-Packard
Switch, Power Transfer	3	Yes	400	1,2,3,4,5,6	GE/MSD Data
Surface Composition (Alpha Scatter)	5	NFP	500(1)	1,2,3,4,5,6	A. L. Turkevitch (Univ. of Chicago)
Sensor, Linear Velocity	2	NFP	3,000(1)	1,2,3,4,5,6	Systron-Donner Corp.
Sensor, Differential Pressure	1	Yes	NR	1,2,3,4,5,6	J. E. Cuesta & Co.
Thermostat, Heater	1	Yes	NR	1,2,3,4,5,6	GE/MSD Data
Transducer, Pressure	1	Yes	1,750(1)	1,2,3,4,5,6	Servonic Inc. & Bourns Inc.
Transducer, Temperature	1	Yes	2,000(1)	1,2,3,4,5,6	Hy-Cal Engineering Co.
Transmitter, S-band	1	Yes	9,600	3,4,5,6	GE/MSD Data
Transmitter, UHF	1	Yes	7,000	1,2,3,4,5,6	GE/MSD Data
Transponder, Exciter	2	Yes	7,000	3,4,5,6	GE/MSD Data
Ultraviolet, Radiometer	5	NFP	1,000(1)	5,6	GE/MSD Data
Valve, Purge	1	Yes	NR	1,2,3,4,5,6	GE/MSD Data
Valve, Relief/Vent	2	Yes	NR	1,2,3,4,5,6	GE/MSD Data
Valve, Solenoid	1	NFP	2,000(1)	1,2,3,4,5,6	Wright Components
Valve, Squib	3	NFP	2,000(1)	1,2,3,4,5,6	Conax Corp. & Link Ordinance Corp.
Water Detector, Subsurface	5	NFP	1,500(1)	5,6	GE/MSD Data

*Development Status Code: 1 - as is, 2 - Modify, 3 - Redesign, 4 - New Design, 5 - New Development.

LEGEND:
(1) EXPECTED OR ESTIMATED - NOT DOCUMENTED
(2) CURRENT CAPABILITY/EXPECTED CAPABILITY
NR - NOT REQUIRED
NFP - NO FORSEEABLE PROBLEM
UNK - UNKNOWN

3. In general, components are capable of or are reasonably expected to be capable of withstanding shock impulses in the 500 to 2000 g range.

4. As was expected, negative information was received concerning tape recorder sterilizability on this type mission. This equipment has not been used for either parametric or point designs in this study.

2. POINT DESIGN REQUIREMENTS

2. POINT DESIGN REQUIREMENTS

2.1 DEFINITION OF SIX POINT DESIGNS

The six point designs developed during this study and discussed in this volume are designed in pairs that conduct the same entry and science experiments and have the same surface lifetime. One Capsule of each pair is designed for out-of-orbit entry and the other for direct entry from the interplanetary trajectory. The Capsules are delivered to the de-orbit maneuver point in the mission sequence by the spacecraft. The Orbiter remains in view of the Capsule throughout the Capsule entry and descent, and the Lander touchdown. At periapse passage, it is available to relay the post-impact data of the Lander.

The Orbiter is placed in a synchronous orbit with a periapsis altitude of 1000 km and apoapsis altitude of 33,100 km.

The entry science measurements are used in reconstructing the atmospheric profile of Mars and consist of pressure, temperature, density (entry body deceleration), and atmospheric composition. The basic surface science measurements include pressure, temperature, moisture and wind readings, surface imagery data of at least 10^7 bits with a design goal of 10^8 bits and soil composition measurements with a Surveyor-type alpha back scatter device.

Table 2.1-1 summarizes the design and performance characteristics of the six point designs developed in this Hard Lander study. The Capsules of the first design pair (Point Designs 1 and 2) are designed to transmit a minimum of 10^7 bits of surface imagery and to acquire the meteorological data over one diurnal cycle. The entry and surface science data is relayed to the Orbiter.

The next design pair (Point Designs 3 and 4) have the increased capacity to perform the surface operations on Mars for more than 90 days. The data acquired during entry is relayed to the Orbiter and the surface imagery data is transmitted, real time, to the Orbiter after impact and again at periapsis passage. A third and a fourth transmission are made during periapsis passage of the Orbiter in the second and the third day.

The Lander of each Capsule in the second design pair also is equipped for direct transmission of data to the Earth Goldstone Station. After the third day of this Mars mission concept, the Orbiter ephemeris is changed to conduct a mapping mission and the Lander radio relay link is discontinued. The meteorological data acquired thereafter is transmitted directly to Earth. The Lander is designed with battery and solar panel electric power for data transmission on both direct and relay links and with equipment to receive Earth commands.

The third design pair (Point Design 5 and 6) are models with the increased capability of conducting additional surface science experiments and transmitting more data, including surface imagery acquired later in the Lander lifetime.

TABLE 2.1.1. SIX POINT DESIGNS, SYSTEM REQUIREMENTS

Point Design	Entry Mode	Surface Lifetime	Entry Science	Surface Science	Telecom-munications	Power Source	Command Link	Notes
1	Out-of-Orbit	25 hr +	Basic package	Minimum package	Relay only	Batteries	No	• Surface Imagery + 1 diurnal cycle of meteorology
2	Direct							
3	Out-of-Orbit	90 days or more	Basic package	Minimum package	Relay and/ or direct	Batteries plus solar cells	Yes	• Surface Imagery 1st day • Meteorology for full mission
4	Direct							
5	Out-of-Orbit	90 days or more	Basic package	Increased package	Relay and/ or direct	Batteries plus solar cells	Yes	• Imagery 1st day plus later • Meteorology full mission
6	Direct							

2.2 BASELINE MISSION CONSTRAINTS FOR POINT DESIGNS

2.2.1 LANGLEY RESEARCH CENTER GUIDELINES AND CONSTRAINTS

The guidelines and constraints that formed the basis for this contract were placed on the Contractor by Langley Research Center. The following summary represents the major boundaries on the point designs.

2.2.1.1 Overall

1. Dry heat sterilization required. ETO compatibility not required. Sterile insertion of propellants permitted.

2. '73 opportunity of prime interest.

2.2.1.2 Interplanetary, Entry, and Retardation

1. Type I and Type II transfers

2. C3 $\approx$ 25 to 40 km^2/sec^2

3. Direct entry and out-of-orbit entry

4. For direct entry, deflection maneuver must be made by Capsule

5. VM-1 through VM-10 atmospheric models

6. Utilize aeroshell/parachute deceleration

7. Parachute deployment not over Mach 2.0

8. Maximum shroud diameter 16 ft, 10 ft desired

9. Entry science consisting of temperature, pressure, density, and composition.

2.2.1.3 Planetary Impact

1. Voyager Environmental Standard of September 1967

2. Landing site - near Equator (e.g., Syrtis Major) 30° from either terminator.

2.2.1.4 Data Return

1. Orbiter in synchronous orbit for few days after landing, then Orbiter asynchronous to enhance mapping mission, inclination 60°.

2. 10^7 bits imagery minimum, 10^8 bits or more desired.

3. Surface science consisting of imagery, pressure, temperature, wind velocity, and moisture, soil composition desired.

4. Communication mode may be relay to Orbiter, direct to Earth, or combination of these.

5. DSN capability is either one 210 ft antenna and two 85 ft antennas or, three 210 ft antennas.

6. Imagery mission performed immediately after landing before Orbiter flys over horizon.

2.2.1.5 Surface Lifetime

1. One day minimum. Several months desired.

2.2.1.6 Point Design Requirements

	Direct Entry	Out-of-Orbit Entry
1.	Minumum science per objectives of document of May 3, 1968. One diurnal cycle minimum. Battery only - relay communication only.	same
2.	Minimum science as above. 90 day lifetime goal with battery plus solar cell. Imagery first day, meteorology data only afterward. S-band command link required. Initial imagery first day, metero-logical data - low bit rate after.	same
3.	Increased science over above, S-band command battery + solar cell for 90 day life. Relay and direct communication. Low total bit imagery periodically beyond the initial first day imagery.	same

2.2.2 OUT-OF-ORBIT ENTRY - BASELINE MISSION DATA

2.2.2.1 Pre-entry Data

Launch date	29 August '73
Arrival data	30 April '74
Launch energy	25.48 km^2/sec^2
Flight time to Mars encounter	244 days

Communication distance, Earth to Mars at encounter	294.7×10^6 km
Approach velocity	2.594 km/sec
Spacecraft orbit about Mars	1000 km x 33.084 km
Orbit inclination	60°
Landing site location	30° before evening terminator and 10°N to 20°N latitude
De-orbit true anomaly	235°
De-orbit velocity increment	234.8 m/sec
Entry altitude	244 km
Time from de-orbit to entry	5330 sec
Entry velocity and path angle	15,300 ft/sec and 16°
Anomaly entry to impact (average)	14.5°

2.2.2.2 Entry to Landing Data

The transfer trajectory is selected to meet the requirements of landings at 10° and 20°N latitudes, surface imagery conducted 30° from a terminator and an Orbiter inclination of 60°. The de-orbit conditions chosen for the baseline trajectory in the Mars atmospheric models VM-1 through -10 are:

De-orbit true anomaly	235°
De-orbit velocity increment	235 meters/sec
Entry velocity and angle	15,300 ft/sec and 16°
Nominal ballistic entry parameter	16 lb/ft^2

Aero retardation is utilized from entry to parachute deployment. The parachute is deployed at speeds not greater than Mach 2 (in the VM-8 model atmosphere) and sized to reach terminal velocity above a 6000 ft altitude in the VM-7 model atmosphere. Subsequent to parachute deployment, the Lander is separated from the aeroshell.

The baseline parameters for the combined ballistic entry and chute descent trajectory to impact in the VM-3, -7, -8 and -9 atmospheric models of Mars are summarized in table 2.2.2-1.

TABLE 2.2.2-1. POINT DESIGN VALUES OF OUT-OF-ORBIT ENTRY TRAJECTORY PARAMETERS

	VM-3	VM-7	VM-8	VM-9
Time-entry to Mach 5 (sec)	229	243	255	217
Altitude at Mach 5 (km)	33.7	23.8	11.5	42.9
Time-entry to Mach 2 (sec)	273	287	285	259
Altitude at Mach 2 (km)	22.7	12.9	6.66	32.4
Maximum deceleration (g)	5.43	5.28	12.70	5.59
Time-entry to impact (Mach 2 parachute deployment) (sec)	830	531	460	1251
Time-entry to impact (altitude deployment of parachute) (sec)			452.5	630

2.2.3 DIRECT ENTRY - BASELINE MISSION DATA

2.2.3.1 Pre-entry Data

A summary of the flight data for the combination of launch and arrival dates for which the Sun angle is 60° and the entry path angle is 25° for landings at 10° and 20°N latitude is given below. The orbit inclination for this case is about 11°.

Launch data	30 July '73
Arrival date	10 January '74
Launch energy	16 km^2/sec^2
Flight time to Mars encounter	164 days
Communication distance to Earth at encounter	137.5 x 10^6 km
Approach velocity	4.028 km/sec

Spacecraft orbit	**1000 km x 33.054 km at 11° inclination**
Separation velocity	45 meters/sec
Entry velocity and path angle	20800 ft/sec and 25°

Conditions for Lander deceleration are the same as given for the out-of-orbit entry Capsule.

The trajectory parameters in the VM-3,-7,-8, and -9 atmospheres is given in the table 2.2.2-2.

TABLE 2.2.2-2. POINT DESIGN VALUES OF DIRECT ENTRY TRAJECTORY PARAMETERS

	VM-3	VM-7	VM-8	VM-9
Time-entry to Mach 2 (secs)	124	128	120	118
Altitude at Mach 2 (km)	29	19	9.3	38.9
Maximum deceleration (g)	18.3	18.2	48.2	18.5
Time-entry to impact (Mach 2 parachute deployment) (sec)	784	466	351	1217
Time-entry to impact (altitude deployment of parachute) (sec)			302	566

2.3 CAPSULE SYSTEM DESIGN CRITERIA AND CONSTRAINTS

2.3.1 CAPSULE LAUNCH ENVELOPE

The launch vehicle shroud envelope constraints placed on the point designs were that Capsule systems maximum diameters fit within a 10 ft or 16 ft diameter shroud. Based on these two extremes in size, the maximum diameter aeroshells were determined.

Figure 2.3.1-1 shows a Titan III-C standard fairing with the required internal clearances and resulting payload envelope shown. Fig. 2.3.1-2 shows a Titan III-C fairing for bulbous payloads with the required internal clearances and resulting payload envelope shown. These two envelopes limit the maximum Capsule system diameters to 109.27 in. and 181.0 in., respectively.

In addition to the shroud constraint, there is the constraint imposed by the Capsule arrangement with respect to the Orbiter. The Capsule system, in configurations considered, is located beneath the Orbiter in the launch vehicle configuration and an adapter is used to mount the Capsule system beneath the Orbiter and also ties into the launch vehicle, thereby providing a direct load path for the inertial loads of launch and powered flight of the Orbiter and Capsule system to the launch vehicle. This adapter requires a ring be added to the launch vehicle for attachment and separation purposes. Figs. 2.3.1-3 and -4 show the Capsule-to-adapter and adapter-to-shroud mounting arrangements and clearances.

Analysis of the layouts in figs. 2.3.1-3 and -4 show that the major clearance problem for the Capsule system is that of being within the inside diameter of the launch vehicle mounting ring. Comparing the allowable diameters, figs. 2.3.1-1 and -3, indicates that a smaller maximum diameter is required on the Capsule system for the latter arrangement than for the shroud alone.

The resulting clearances, to allow for a clean separation with no interferences, limit the Capsule maximum diameters to 105.1 in. for the 10 ft shroud configuration and 176.8 in. for the 16 ft shroud configuration. Making an additional allowance of 0.6 in. on all sides, to eliminate the possibility of interference due to large tip-off angles and booster motions during the separation event, further reduces these diameters to 103.9 in. and 175.6 in., respectively. These dimensions, with the resulting clearances and angles between the shroud ring flange and separation device, are all reflected in figs. 2.3.1-3 and -4.

2.3.2 ENVIRONMENTS

2.3.2.1 Reference Documents

Natural Environments Definition - Voyager Environmental Standards, 25 September ber, 1967, NASA-Office of Space Science and Applications.

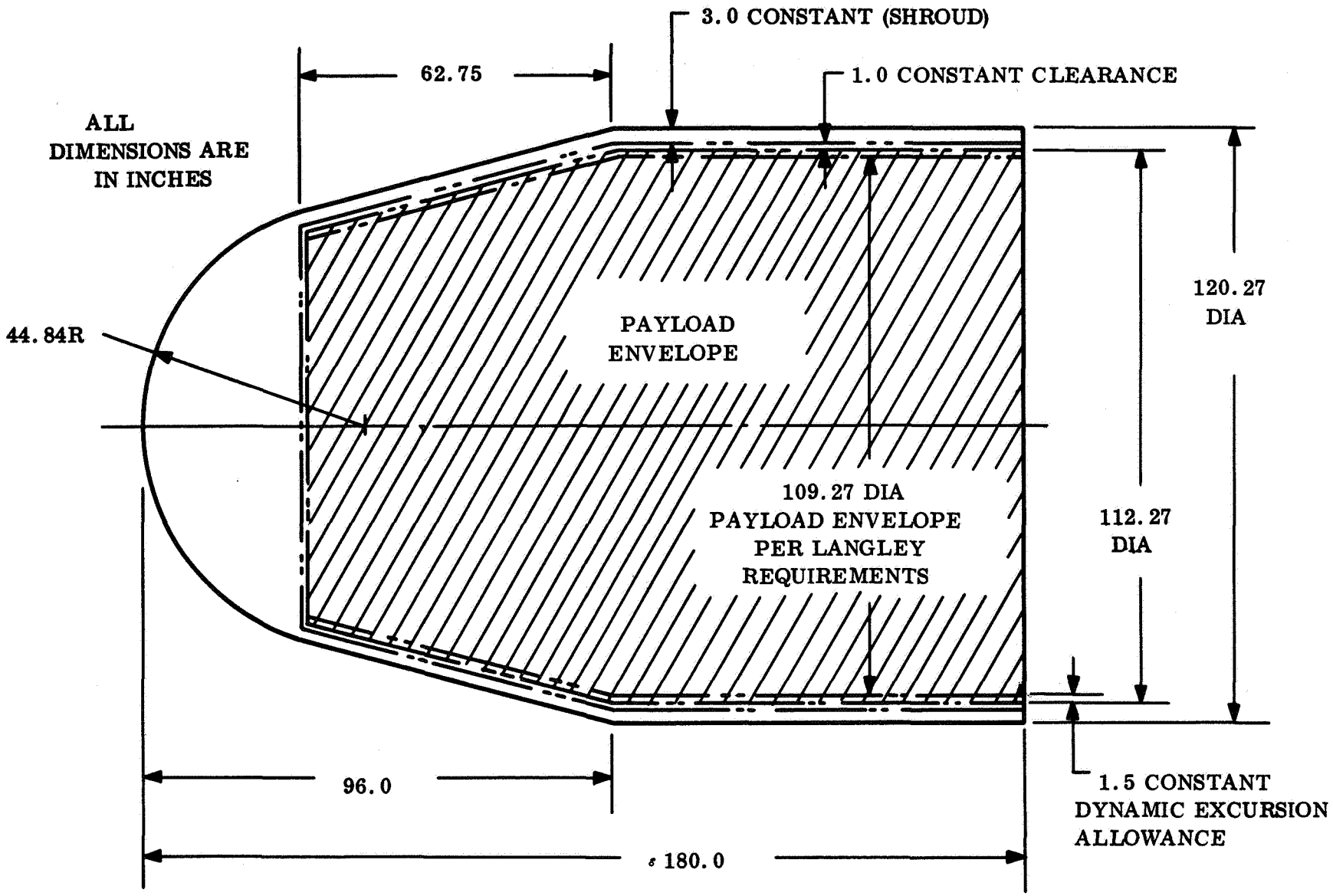


Figure 2.3.1-1. Titan III-C Standard Fairing

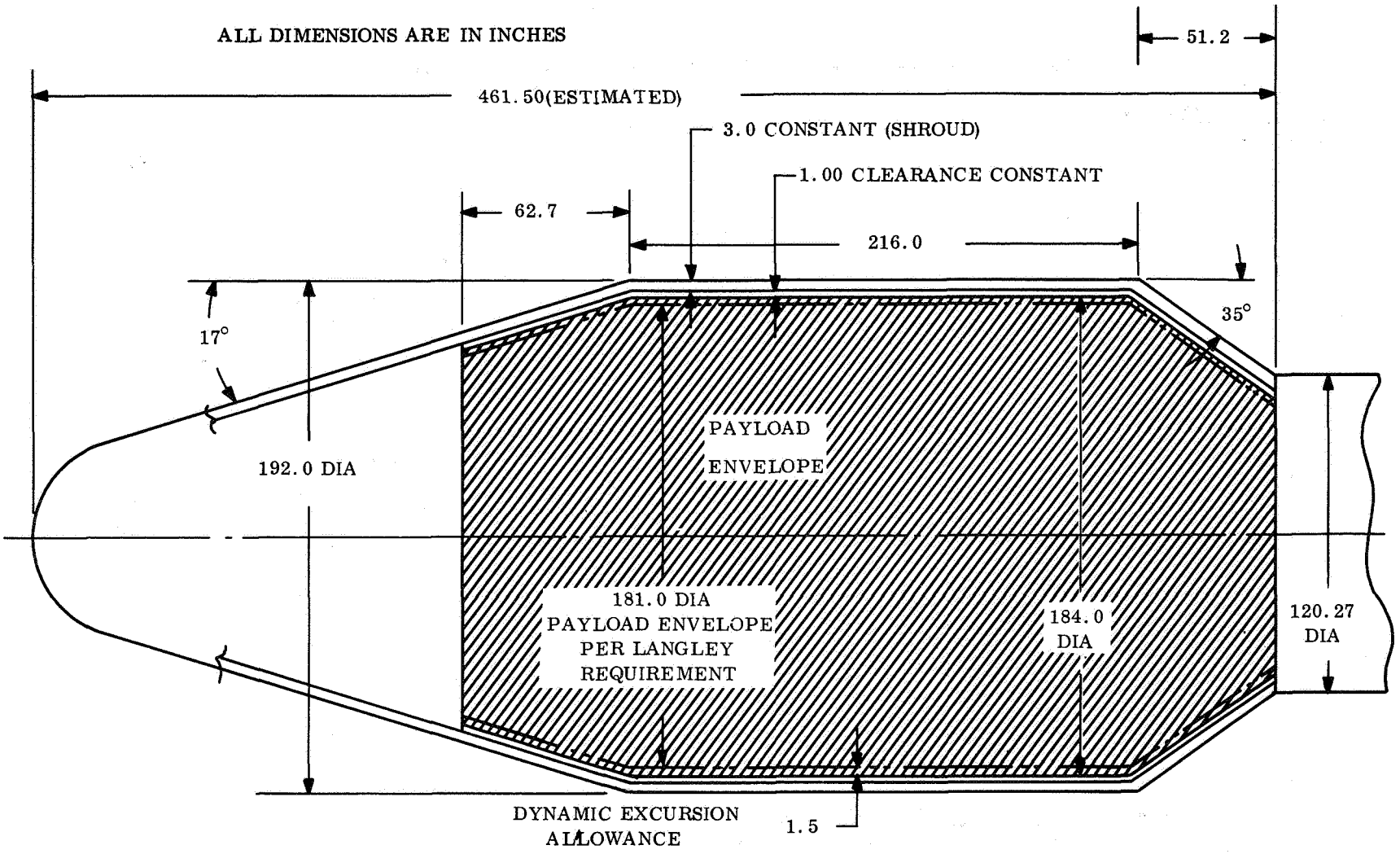


Figure 2.3.1-2. Titan III-C Fairing - Bulbous Payload

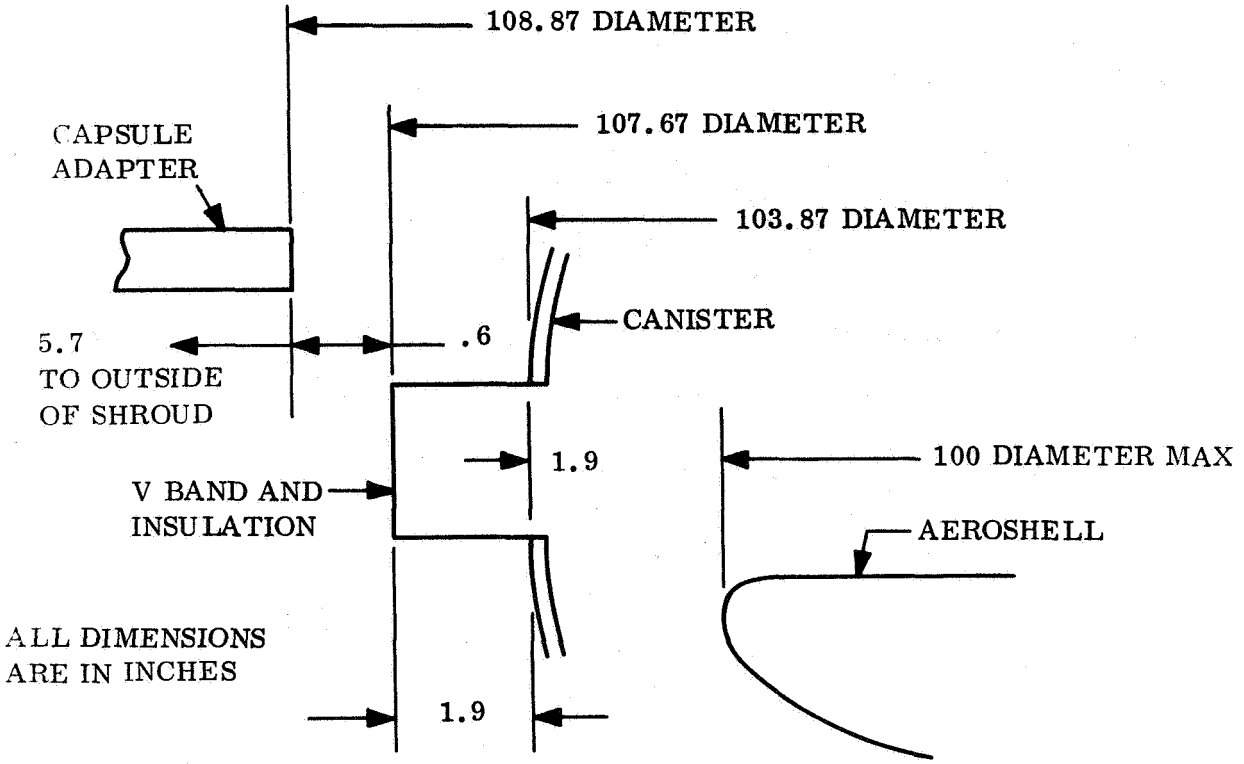


Figure 2.3.1-3. Capsule and Orbiter Adapter Interface with Launch Vehicle, Standard Fairing

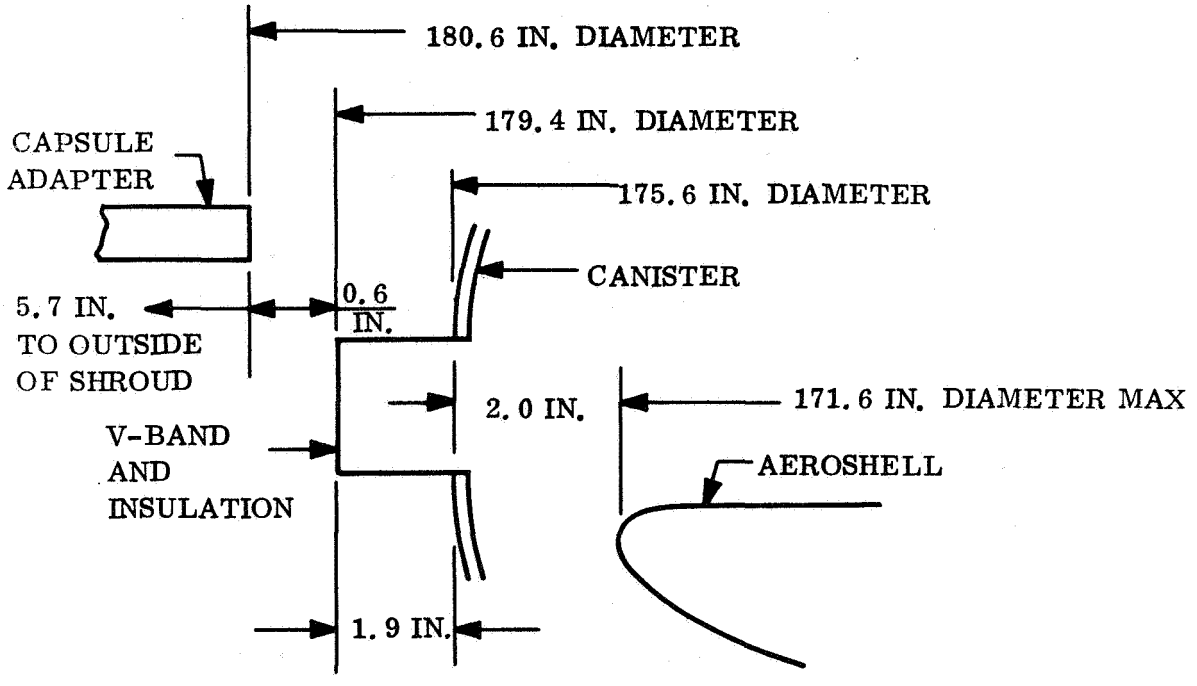


Figure 2.3.1-4. Capsule and Orbiter Adapter Interface with Launch Vehicle, Bulbous Fairing

Mars Engineering Model Parameters for Mission and Design Studies, May 1968, NASA Langley Research Center.

1973 Voyager Capsule Systems Constraints and Requirements Document, 18 May 1967, Jet Propulsion Laboratory - California Institute of Technology.

2.3.3.2 Mars Atmospheric Properties

The atmospheric models VM-1 through VM-10, shown in table 2.3.2-1, have been used in the design of the Capsules.

The mean wind model for the Mars atmospheric models is given in table 2.3.2-2 and the corresponding wind shear model in table 2.3.2-3. Wind directions may be normal to the local vertical or parallel to the local terrain blowing up, down or cross slope. The wind direction should be assumed normal to the local vertical at elevations above 1000 ft.

2.3.3.3 Mars Surface Conditions

Surface slope	inclinations up to 34°
Surface roughness	particles up to rocks of 5 in. diameter
Surface mechanical properties	minimum bearing capacity = 6 psi
	dissipates none of the energy of Lander impact
	coefficient of friction = up to 1
Thermal characteristics	322° K maximum temperature
	150° K minimum temperature

2.3.2.4 Sterilization Environment

Terminal sterilization shall be effected prior to launch and shall be by means of dry heat. The heat cycle shall be performed to assure that all points have been at 125 °C for not less than 24.5 hr.

2.3.2.5 Launch Environment

Titan III-C

TABLE 2.3.2-1. MARS ATMOSPHERIC MODELS

Property	Symbol	Dimension	VM-1	VM-2	VM-3	VM-4	VM-5	VM-6	VM-7	VM-8	VM-9	VM-10
Surface Pressure	P_o	mb	7.0	7.0	10.0	10.0	14.0	14.0	5.0	5.0	20.0	20.0
		lb/ft^2	14.6	14.6	20.9	20.9	29.2	29.2	10.4	10.4	41.7	41.7
Surface Density	ρ_o	$(gm/cm^3)\ 10^5$	0.955	1.85	1.365	2.57	1.91	3.08	0.68	1.32	2.73	3.83
		$(slugs/ft^3)\ 10^5$	1.85	3.59	2.65	4.98	3.7	5.97	1.32	2.56	5.30	7.44
Surface Temperature	T_o	^oK	275	200	275	200	275	200	275	200	275	200
		^oR	495	360	495	360	495	360	495	360	495	360
Stratospheric Temperature	T_s	^oK	200	100	200	100	200	100	200	100	200	100
		^oR	360	180	360	180	360	180	360	180	360	180
Acceleration of Gravity at Surface	g	cm/sec^2	375	375	375	375	375	375	375	375	375	375
		ft/sec^2	12.3	12.3	12.3	12.3	12.3	12.3	12.3	12.3	12.3	12.3
Composition (percent)												
CO_2 (by mass)			28.2	100.0	28.2	70.0	28.2	35.7	28.2	100.0	28.2	13.0
CO_2 (by volume)			20.0	100.0	20.0	68.0	20.0	29.4	20.0	100.0	20.0	9.5
N_2 (by mass)			71.8	0.0	71.8	0.0	71.8	28.6	71.8	0.0	71.8	62.0
N_2 (by volume)			80.0	0.0	80.0	0.0	80.0	32.2	80.0	0.0	80.0	70.5
A (by mass)			0.0	0.0	0.0	30.0	0.0	35.7	0.0	0.0	0.0	25.0
A (by volume)			0.0	0.0	0.0	32.0	0.0	38.4	0.0	0.0	0.0	20.0
Molecular Weight	M	mol^{-1}	31.2	44.0	31.2	42.7	31.2	36.6	31.2	44.0	31.2	31.9
Specific Heat of Mixture	C_p	cal/gm^oC	0.230	0.166	0.230	0.1530	0.23	0.174	0.230	0.166	0.230	0.207
Specific Heat Ratio	α		1.38	1.37	1.38	1.43	1.38	1.45	1.38	1.37	1.38	1.41
Adiabatic Lapse Rate	Γ	$^oK/km$	-3.88	-5.39	-3.88	-5.85	-3.88	-5.14	-3.88	-5.39	-3.88	-4.33
		$^oR/1000$ ft	-2.13	-2.96	-2.13	-3.21	-2.13	-2.82	-2.13	-2.96	-2.13	-2.38
Tropopause Altitude	h_T	km	19.3	18.6	19.3	17.1	19.3	19.4	19.3	18.6	19.3	23.1
		kilo ft	63.3	61.0	63.3	56.1	63.3	63.6	63.3	61.0	63.3	75.8
Inverse Scale Height (stratosphere)	β	km^{-1}	0.0705	0.199	0.070	0.193	0.0705	0.1655	0.0705	0.199	0.0705	0.145
		$ft^{-1} \times 10^5$	2.15	6.07	2.15	5.89	2.15	5.05	2.15	6.07	2.15	4.41
Continuous Surface Wind Speed	$\bar{v}$	ft/sec	186.0	186.0	155.5	155.5	131.5	131.5	220.0	220.0	110.0	110.0
Maximum Surface Wind Speed	v_{max}	ft/sec	470.0	470.0	390.0	390.0	330.0	330.0	556.0	556.0	278.0	278.0
Design Vertical Wind Gradient	$\frac{d\bar{v}}{dh}$	ft/sec/1000 ft	2	2	2	2	2	2	2	2	2	2
Design Gust Speed	v_g	ft/sec	200.0	200.0	150.0	150.0	150.0	150.0	200.0	200.0	100.0	100.0

TABLE 2. 3. 2-2. MEAN WIND MODEL FOR MARS ATMOSPHERIC MODELS

Altitude feet	Wind Gradient	Shear Gradient	Horizontal Wind Speeds				
			VM-1, 2	VM-3, 4	VM-5, 6	VM-7, 8	VM-9, 10
	fps/1000'	fps/1000'	fps	fps	fps	fps	fps
0	+2	±20	186.0	156.0	132.0	220.0	110.0
2,500	↓	↓	191.0	161.0	137.0	225.0	115.0
7,500	↓	↓	201.0	171.0	147.0	235.0	125.0
12,500	↓	↓	211.0	181.0	157.0	245.0	135.0
17,500	↓	↓	221.0	191.0	167.0	255.0	145.0
22,500	↓	↓	231.0	201.0	177.0	265.0	155.0
27,500	↓	↓	241.0	211.0	187.0	275.0	165.0
32,500	↓	↓	251.0	221.0	197.0	285.0	175.0
37,500	↓	↓	261.0	231.0	207.0	295.0	185.0
42,500	↓	↓	271.0	241.0	217.0	305.0	195.0
47,500	↓	↓	281.0	251.0	227.0	315.0	205.0
50,000	0	±40	286.0	256.0	232.0	320.0	210.0
52,500	↓	↓	↓	↓	↓	↓	↓
55,000	↓	↓	↓	↓	↓	↓	↓
57,500	↓	↓	↓	↓	↓	↓	↓
60,000	↓	↓	↓	↓	↓	↓	↓
62,500	↓	↓	↓	↓	↓	↓	↓
65,000	↓	↓	↓	↓	↓	↓	↓
67,500	↓	↓	↓	↓	↓	↓	↓
70,000	↓	↓	↓	↓	↓	↓	↓
72,500	↓	↓	↓	↓	↓	↓	↓
75,000	↓	↓	↓	↓	↓	↓	↓
77,500	↓	↓	↓	↓	↓	↓	↓
80,000	↓	↓	↓	↓	↓	↓	↓
82,500	↓	↓	↓	↓	↓	↓	↓
85,000	↓	↓	↓	↓	↓	↓	↓
87,500	↓	↓	↓	↓	↓	↓	↓
90,000	↓	↓	↓	↓	↓	↓	↓
790,000	0	0	0	0	0	0	0

TABLE 2.3.2-3. WIND SHEAR MODEL FOR MARS ATMOSPHERIC MODELS

Altitude Feet	Wind Shear Speeds				
	VM-1,2	VM-3,4	VM-5,6	VM-7,8	VM-9,10
0	186.0	156.0	132.0	220.0	110.0
2,500	241.0	211.0	187.0	275.0	165.0
7,500	151.0	121.0	97.0	185.0	75.0
12,500	261.0	231.0	207.0	295.0	185.0
17,500	171.0	141.0	117.0	205.0	95.0
22,500	281.0	251.0	227.0	315.0	205.0
27,500	191.0	161.0	137.0	225.0	115.0
32,500	301.0	271.0	247.0	335.0	225.0
37,500	211.0	181.0	157.0	245.0	135.0
32,500	321.0	291.0	267.0	355.0	245.0
42,500	231.0	201.0	177.0	265.0	155.0
50,000	336.0	306.0	282.0	380.0	260.0
52,500	236.0	206.0	182.0	280.0	160.0
55,000	336.0	306.0	282.0	380.0	260.0
57,500	236.0	206.0	182.0	280.0	160.0
60,000	336.0	306.0	282.0	380.0	260.0
62,500	236.0	206.0	182.0	280.0	160.0
65,000	336.0	306.0	282.0	380.0	260.0
67,500	236.0	206.0	182.0	280.0	160.0
70,000	336.0	306.0	282.0	380.0	260.0
72,500	236.0	206.0	182.0	280.0	160.0
75,000	336.0	306.0	282.0	380.0	260.0
77,500	236.0	206.0	182.0	280.0	160.0
80,000	336.0	306.0	282.0	380.0	260.0
82,500	236.0	206.0	182.0	280.0	160.0
85,000	336.0	306.0	282.0	380.0	260.0
87,500	236.0	206.0	182.0	280.0	160.0
90,000	336.0	306.0	282.0	380.0	260.0
790,000	0	0	0	0	0

2.3.3 ENTRY SCIENCE INSTRUMENTATION

2.3.3.1 General

Direct and parametric measurement of density, pressure, and temperature profiles and atmospheric composition is accomplished by the instrumentation characterized in table 3.5.2.1. Descriptions of each of the entry science devices employed are given in Section 3.5.2.

2.3.3.2 Density Profile Measurement

Atmospheric density profile may be measured either directly by radiation back scatter techniques or indirectly by measurement of entry Capsule accelerations.

2.3.3.2.1 Back Scatter Densitometer

Radiation back scatter devices exist that can accurately determine the density of the gas by measuring the gamma back scatter from a given volume of the gas when illuminated by a known source. This technique employs a radiation detector and counts the number of photons back scattered from the gas in a finite time. This leads to serious measurement limitations in very low density environments since the statistical accuracy of the measurement is proportional to the inverse square root of the number of counts. Either an unreasonably large source is required (this also means more shielding) or the measurement period must be relatively long. The former solution is undesirable from a physical standpoint while the latter is not recommended because of the altitude variation that can occur during long sampling periods at high velocity. In addition, this technique requires auxiliary information such as acceleration, velocity, or altitude if an accurate density profile is desired. This is especially true if the entry body experiences large angles-of-attack during the entry. For these reasons, direct density measurements have not been considered for point design purposes.

2.3.3.2.2 Entry Capsule Acceleration Interpretation

A more reasonable approach to atmospheric density profile measurement has been discussed by several investigators (ref. 2-1 through 2-4). This approach relies on the post-flight interpretation of triaxial accelerometer data to determine both the altitude vs time and density vs time profiles. Recorded accelerometer measurements are smoothed and integrated downward to obtain density beginning at entry using the vehicle drag history as previously described by Seiff et al (refs. 2-1, 2-6). The integrating logic is based on using measured acceleration and gravitational attraction. The sensitivity of this approach to body dynamics and its dependence on other measurements to minimize bias errors has been discussed by deVries et al (ref. 2-4). Acceleration sensing transducers generally take the

form of a supported mass that is allowed to undergo a limited displacement depending upon the acceleration force (F = Ma) and the supporting structure deformation forces (e.g., F = -KX). Triaxial accelerometers may simply be combinations of orthogonally mounted linear accelerometers in a single package or special devices in which the moving mass is allowed to move in any direction and readout of the motion is resolved into three orthogonal components. Cross coupling between axes can be a serious problem in the less sophisticated designs.

Cross coupling is also a function of location of the sensor on the vehicles. Exact location of the accelerometer on the vehicle's c.g. is sometimes impractical or even impossible. Every attempt must be made, however, to place the accelerometer as near the c.g. as possible since interpretation of the data becomes difficult when large cross coupled components are present.

Accuracies in the higher ranges of better than 0.5 percent are easily attainable and low range accelerometers with better than 1.0 percent accuracies are common.

The development of a "Magnetic Force Balance" accelerometer has increased the accuracy of acceleration measurement while reducing the degree of cross coupling between axes. This device uses a single mass whose motion is restrained by a magnetic field. The magnetic field has three orthogonal components separately controlled by high gain servo amplifiers. The position of the mass is sensed by a three axis sensing circuit and any displacement from the rest position results in an error signal in one or more of the three axes. These error signals are applied to the servo amplifiers and the magnetic field is altered a sufficient amount to return the mass to its rest position. Either the servo amplifier currents or the error signal potentials may be used to indicate the acceleration in each of the axes.

2.3.3.2.3 Point Design Selection - Density Measurement

The measurement approach chosen for point design evaluation is the body acceleration interpretation approach. The choice is based upon consideration of weight, volume, and system compatibility. Back scatter devices for this purpose would weigh upwards of 15 lb and seriously limit the design flexibility due to their shielding and orientation requirements. By sampling the accelerometer at high rates, the body dynamics sensitivity of the evaluation is minimized and bias errors are significantly reduced by virtue of the fact that pressure and temperature profiles are measured during the low velocity portion of the entry. It is anticipated that the atmospheric density profile may be reconstructed to within 5 percent by this technique based upon results of computerized experiment simulation.

2.3.3.3 Temperature Profile Measurement

The two basic types of temperature sensors considered for use in the entry science package are the resistance thermometer and the thermistor.

2.3.3.3.1 Resistance Thermometer

The resistance thermometer employs a temperature sensitive element, usually platinum or nickel, to parametrically measure temperature by measurement of the elements electrical resistance. The temperature dependence of the resistance takes the form of

$$R_T/R_o = 1 + \alpha f(t)$$

where

R_T = resistance at temperature T

R_o = resistance at 0° centigrade

α = temperature coefficient of resistivity

f(t) = temperature dependent function peculiar to the particular metal

In general, the best resistance thermometers use platinum as the variable element. f(t) for pure platinum is given in the Callendar-Van Dusen equation:

$$\frac{R_T}{R_o} = 1 + \alpha \left[T - \delta \left(\frac{T}{100} - 1 \right) (T/100) - \beta \left(\frac{T}{100} - 1 \right) (T/100)^3 \right]$$

where δ and β are constants for the individual platinum element which are determined during calibration of the element. Typically, $\beta = 0.1$ for negative T(°C) and 0 for positive T. δ is typically 1.49.

The electrical stability of platinum over long periods of time is excellent and its high melting point, coupled with its extreme resistance to chemical deterioration lend to its use over extended temperature ranges (14 °K to 1075 °K). Platinum temperature elements display fairly high sensitivity (dR/dT) and the output voltage from the sensor can be quite large. Accuracies on the order of 0.02 percent at 500 °C are possible.

If economy is a factor in selection of the thermometer element, nickel may be substituted for platinum. Nickel has a high temperature coefficient but is limited in range from 175 °K to 575 °K. Nickel also is prone to contamination by various materials and this also reduces its attractiveness as a potential resistive element.

2.3.3.3.2 Thermistor

Thermistors are non-metallic, temperature sensitive resistive elements that have a negative thermal coefficient of resistivity. They exhibit somewhat poorer calibration stability than platinum resistance thermometers and have a highly non-linear R-T response. The dR/dT for thermistors is considerably higher than that of metallic resistance elements and thus provides great sensitivity over their operating range. Because of their large dR/dT, thermistors cannot be used for measurements much below 200 °K. Rapid increases in resistance occur between 275 °K and 200 °K resulting in unreasonably high resistance values. Until recently, the upper limit for thermistor measurements was approximately 400 °K. General Electric Company is now fabricating thermistors in which the active element is a man-made diamond. These thermistors are reported to operate over the temperature range of 75 °K to 725 °K in an oxidizing atmosphere and 75 °K to 925 °K in a non-oxidizing atmosphere.

2.3.3.3.3 Point Design Selection - Temperature Measurement

The platinum resistance thermometer was selected for use in the entry science payload since it has superior performance characteristics in the temperature regime (100-300 °K) of interest. Additionally, its excellent calibration stability provides a high confidence level in the ultimate measurement accuracy.

2.3.3.4 Pressure-Profile Measurement

Pressure transducers that effectively operate over the pressure range anticipated in the Martian atmosphere are basically divided into two categories: referenced and unreferenced. The former category of transducers include most of the diaphragm types. They sense a difference in pressure between the sample being measured and a reference carried in a hermetically sealed chamber. Calibration stability of these devices is therefore dependent upon the stability of the pressure in the reference chamber. At atmospheric pressure, even with the best hermetic seals, the self life of these units is limited by calibration drift. The units are typically rather heavy and bulky because of the requirement of hermetic sealing.

The deflection of the diaphragm may be sensed in any of several ways. The following are examples of referenced pressure transducers. In each case, the diaphragm deflection is sensed in a different manner.

2.3.3.4.1 Referenced Pressure Transducers

A. Variable Reluctance Transducer

If the diaphragm can be used to vary the reluctance of a magnetic circuit, the position of the diaphragm may be determined by measurement of the reluctance of the circuit. The magnetic circuit can be made quite small. This type of transducer could probably withstand the high temperature sterilization soak without difficulty. The major disadvantage of this scheme is the requirement of a somewhat more complicated electronics package and the large size and weight of the reference chamber. The total sensor weight would typically be 10 oz.

B. Potentiometer Pressure Transducer

The deformation of a thin diaphragm can be used to mechanically vary the resistance of a potentiometer. Voltage variations across the potentiometer (carrying constant current) can thus be used as a measure of the diaphragm deformation. Because of the small deforming forces involved at such low pressures, the frictional forces in the mechanical system seriously limit the accuracy that can be attained by this device. If an attempt is made to minimize the frictional forces in the potentiometer and reduce the thickness of the diaphragm in order to improve the systems accuracy, serious penalties must be imposed on the devices ability to withstand extreme environments. Sensor weights and volumes about the same as those for the variable reluctance sensor should be attainable.

C. Variable Capacitance Transducer

This device measures pressure by measuring the change in capacitance between the diaphragm and one or more reference surfaces located near the diaphragm. Motion of the diaphragm causes changes in the capacitive reactance of one leg of an unbalanced capacitance bridge network. The resulting bridge output potential indicates the pressure difference between the reference chamber and the sample. This type of transducer is similar to the potentiometer type; however, the accuracy of the device is not dependent upon friction induced errors since the only motion that takes place is in the diaphragm. Again, as in the other referenced pressure transducers, the weight and volume of the sensitive element is only a small fraction of the total sensor weight. The reference chamber is the size and weight limiting factor.

Sensor developments (ref. 2-5) in the Aeromechanics and Materials Laboratory in the General Electric Company's Re-entry Systems Organization have resulted in the generation of a unique variable capacitance-type transducer in which the large reference pressure chamber is greatly reduced in weight and volume. Basically, the reference pressure is derived from the pressure of interplanetary space and maintained in a small reference chamber. This chamber is not hermetically sealed. A vent tube

allows the pressure in the chamber to equalize to the transducer's local environment pressure. The leak rate of this vent tube is controlled by a slug of porous material located within the tube. Response time (1/e) as short as a few seconds or as long as many minutes can be achieved conveniently. The sensors are currently in use in the shock tunnel at the Space Technology Center, weigh less than 4 oz and occupy less than 1 $in.^3$.

2.3.3.4.2 Unreferenced Pressure Transducers

A sensor developed by the Ames Research Center is a prime candidate in the unreferenced category of pressure transducers. This device, called the Dimeff Viscosity Pressure Transducer, is a form of the variable capacitance transducer in which the diaphragm acts as one plate of the capacitor. The diaphragm is caused to vibrate at the resonant frequency of the mechanical system. The capacitance between the vibrating diaphragm and a small metal plate located near the diaphragm reaches its peak value when the diaphragm is at its maximum deflection during each cycle of its oscillation. This amplitude is held constant by a servo loop in the electronics. The work done on the gas by the diaphragm (P dv and kinetic energy) varies with the pressure. The pressure is thus relatable to the input energy - a measured parameter. This type of transducer has the following advantages:

1. Relatively high accuracy may be maintained at low pressure.

2. Very rapid response to pressure changes is possible due to the small volume of the sample used.

3. Shelf life of the sensor should exceed that of competitive referenced pressure sensors.

4. The sensor can be manufactured in a small light weight version (8 oz. - 6 in^3).

One serious disadvantage of this type of pressure measurement lies in its dependence upon atmospheric composition. Composition variations result in rather large errors in pressure determination by the viscosity technique. It is thus imperative that some form of composition measurement device be operated in conjunction with this pressure transducer during the entry.

2.3.3.4.3 Point Design Selection - Pressure Measurement

Based upon its demonstrated reliability, independence from other measurements, and the accuracy requirements of the measurement, the variable capacitance transducer was selected for point design evaluation. The controlled leak rate differential transducer being developed by General Electric has not been flight tested as yet but is a prime contender for this application when fully developed.

2.3.3.5 Atmospheric Composition

Although other approaches, including gas chromatography and chemical reaction analyses, have been proposed for atmospheric composition determination during entry, mass spectrographic analysis leads the field of contenders to the point of being universally accepted as the best overall approach. The ability of the mass spectrometer to operate at velocities as high as Mach 5, withstand sterilization environments, and accommodate all of the potential atmospheric constituents with equal facility in measurement coupled with its relatively advanced state of development for this application are all strong influencing factors in its favor.

Mass spectrometers have the following basic elements in common:

1. A leak valve to introduce low pressure gas to the evacuated spectrometer chamber

2. An ion source and pump which ionizes inflowing gas for mass separation

3. A mass separator utilizing electric and magnetic fields singly or in combination

4. Ion detectors to measure the quantity of separated constituents

5. A vacuum pump

6. Electronic control and readout circuitry.

The various classes of spectrometers are distinguished by their mass separation technique. The three classes of spectrometers that have been designed as prototype flight hardware and are applicable to measurements during Marian entry are:

1. R-F quadrapole

2. Double-focusing

3. Monopole analyzer.

2.3.3.5.1 R-F Quadrapole Mass Spectrometer

The quadrapole spectrometer operates on the principle of applied dc and ac fields to perform molecular mass isolation. The component that characterizes the system consists of four rods to which the two fields are applied. A particular setting of the ac voltage, the ratio of ac to dc voltages, the ac voltage frequency, and the rod spacing will permit only ions of a given mass to undergo a stable but complicated

oscillatory motion along the rods' axis and be collected. Detection of different ionic masses typically requires a change in the first three variables. The rod spacing is fixed in the instrument's design and is dictated in part by the mass range over which the system is to operate.

A system typical of this class of spectrometer has been built for flight application and can be heat sterilized, tolerate up to 300g loads, and provide good magnetic cleanliness. The ion source and sputter ion pump in addition to the mass analyzer are non-magnetic in their design. Application to Martian atmospheric measurements during entry has been considered in its design. In particular, the unit uses a molecular leak valve which can adequately operate up to external pressures of 500 mb without the use of auxiliary vacuum pumps. Molecular flow valves were selected instead of viscous flow valves to permit the molecular specie flow rate to be directly proportional to the species' partial pressure. This feature allows sensitivity calibration for direct introduction of unknown gas samples into the spectrometer.

The quadrapole spectrometer utilizes a single detector in either of its two possible modes of operation. The system can perform either a preselected scan of specific masses or a continuous scan of the entire mass range. The former scan mode requires less bits per scan and shorter scan times, but relies on the assumption that the interesting mass values can be reliably predicted. However, the assumption does not appear limiting since present quadrapoles can scan five to eight mass units and this quantity should provide adequate coverage of the major Martian atmospheric constituents.

2.3.3.5.2 Double-Focusing Mass Spectrometer

This class of spectrometer utilizes an electrostatic sector and magnetic sector to accomplish mass separation with first order angle focus and second order energy focus. The magnetic sector permits mass separation which is generated by ions of different masses and kinetic energies traveling paths of distinctive radii of curvature for a specific field strength. This sector, through straightforward kinetics, provides first order angle focus. The electric sector acts as an energy-compensating device to minimize the undesirable spread in the focal plane caused by the energy variations for given ion types. The use of the two sectors makes this type of spectrometer a highly accurate instrument with good mass resolution and small size.

The development of a miniaturized version of this type of spectrometer has been underway at JPL with help provided by the University of Minnesota. The instrument has a 60° sector magnet of 4.4 cm radius. A single-focusing device has been flown on sounding rockets. The addition of the electrostatic sector permits the spectrometer to act as a 15 cm radius, 60° sector device that has increased resolution. The unit can have a non-magnetic ion source and ion pump. It uses a molecular flow leak valve that possibly can operate up to external pressures of 0.5 atmospheres.

The spectrometer can be operated in two modes. In one case, the ion source and electrostatic sector voltages are held constant and a series of detectors are spread along the collector plane at positions corresponding to specific masses. This mode while limited to specific mass values does provide very sensitive response to trace components. The detectors are usually read in parallel although serial readout can be performed.

The second operating mode uses one to two detectors and the masses are scanned by varying the ion source and electrostatic sector voltages. The advantages of continuous mass scan and the use of a single detector come at the price of sensitivity loss in detecting minor constituents that fall at interferring mass positions.

2.3.3.5.3 Monopole Mass Spectrometer

A third class of mass spectrometer is the monopole analyzer. Its primary advantage is its sensitivity for the detection of gases in extremely low pressures and at fast scan rates (< 1 sec). Serious consideration cannot be given to the unit at this time since it has not been completely designed as a flight prototype instrument.

2.3.3.5.4 Point Design Selection - Atmospheric Composition Measurement

For reasons of magnetic cleanliness and state of development, the r-f quadrapole mass spectrometer was selected for point design evaluation. In addition to the above, the r-f quadrapole has the desirable feature of requiring only one detector telemetry channel.

2.3.3.6 Atmospheric Water Vapor Detection

Currently, there are two promising techniques for the detection of trace amounts of water vapor in a gaseous medium. They are the aluminum oxide hygrometer and chemical/radiological hygrometer.

2.3.3.6.1 Aluminum Oxide Hygrometer

This sensor consists of an aluminum plate on which is deposited a porous layer of aluminum oxide. A semi-porous coating of metal is formed over the oxide layer thus forming a simple capacitor in which the aluminum plate and metal coating are the electrodes and the oxide layer is the dielectric. Gases coming in contact with the semi-porous metal coating generally have no affect on the impedance of the aluminum oxide capacitor unless the gas contains water vapor. In this case, the water vapor diffuses through the metal coating and deposits on the pore walls of the aluminum oxide until equilibrium is reached. This causes both resistive and reactive changes to

take place in the capacitor. These changes are proportional to the number of molecules of water deposited in the oxide layer and are thus a measure of water vapor partial pressure. This type of device has been tested to water vapor levels as low as one part per million.

One unfavorable characteristic of this device is its sensitivity to certain agents other than water. In particular, NH_3 appears to be a serious problem. In addition, since the concentration of water vapor likely to be present in the Martian atmosphere will be quite small, there may be some difficulty in operating this system cyclically during the entry period due to a degraded time constant.

2.3.3.6.2 Chemical/Radiological Hygrometer

This system is based on a technique that involves the quantitative reaction of water with a radioisotopically labeled reagent so that one of the resulting products is a labeled gas. Thus the measurement of water is translated to a measurement of radioactivity. Such a system is currently under development at GE/RS. It employs tritium labeled calcium hydride. The reaction for this system is:

$$Ca\ T_2 + 2HOH \rightarrow Ca\ (OH)_2 + 2HT$$

This is a highly specific reaction and can be made completely insensitive to any other gaseous material. Laboratory demonstration of one part per million sensitivity has been accomplished. This concentration sensitivity is well below the theoretical limit and has not yet been approached because of difficulties in preparing calibrated samples of gas at these extremely low water vapor concentrations.

2.3.3.6.3 Point Design Selection - Atmospheric Water Measurement

The chemical/radiological technique has been chosen for point design evaluation because of its potentially great flexibility, sensitivity and specificity. It also appears that this device has an inherently greater ability to deal with cyclic measurements.

2.3.4 SURFACE SCIENCE INSTRUMENTATION

2.3.4.1 General

The surface science instrumentation package is made up of a number of basic instruments used in measurement of the meteorological, and surface characteristics of Mars. In the case of Point Designs 5 and 6, when power, volume, and weight considerations permit, certain advanced experiments are carried on the 1973 Mars Lander. These experiments will provide information about the surface, subsurface, and atmosphere that cannot be collected by the simple experiments included in the minimum science payload. Since there is no universal set of criteria for experiment evaluation, it is difficult to rank these experiments in terms of their merit.

As a result, the experiments described in para 2.3.4.3 are those for which no preferred ranking is possible with the exception of the subsurface water detector. The detection of subsurface water is generally accepted by the scientific community as the one most significant surface experiment relating to Martian biology that can be performed.

2.3.4.2 Minimum Science Payload

2.3.4.2.1 Surface Pressure

The ambient pressure on the Martian surface may be measured by any of the devices considered in para 2.3.3.4 Once again, for reasons of reliability, independence from uncontrollable variables (atmospheric composition) and ease of implementation, a capacitor-type pressure transducer has been selected for point design evaluation. A sufficiently high sampling rate is provided for the transducer so that diurnal variations may be identified.

2.3.4.2.2 Surface Temperature

Either resistance thermometers or thermistors may be used to measure the atmospheric temperature on the surface of Mars since the anticipated temperature range is within the operating range of both devices. The selection of a platinum resistance thermometer is based on its extreme stability and the evidence of its ability to withstand high level shocks. Resistance thermometers used on military programs have been successfully tested to shock levels in excess of 600 g's and manufacturers of these devices feel confident that extension of existing designs to the 1000 g range is feasible.

2.3.4.2.3 Wind Velocity

Wind velocity measurements have been conducted on the Earth by employing any number of different techniques. Most of these techniques do not lend themselves to planetary exploration applications. Only three approaches are considered to be reasonable candidates for planetary exploration. These are mechanical wind velocity mechanisms such as the conventional cup anemometer, the hot anemometer, and acoustic propagation devices. For specific application to a Hard Lander, use of a mechanical mechanism is usually avoided due to their inherent sensitivity to severe shock and their requirement for orientation. Thus, only the hot element anemometer and the acoustic devices have been evaluated for use in the 1973 Mars Hard Lander.

A. Hot Element Anemometry

Hot element anemometers, and most specifically hot wire anemometers, have been used extensively for mass flow measurements for both subsonic and supersonic velocities. The principal for these measurements was first described by King with the relationship

$$Nu = A + B\,Re^{1/2} \qquad (1)$$

where Nu is the Nusselt number $I^2R/lk\ (t-T_o)$ and Re is the Reynolds number and A and B are constants.

However, for low velocities and densities, the mechanism for heat transfer changes and free convection and conduction play important roles. When natural convection is negligible, it has been found that for long wires (1/d = 200) and zero velocity that Nu = A 0.30, and Kings' Law may be used down to zero velocity. However, a long thin wire may be prone to breakage under the impact conditions of a Mars Lander. In addition, a wire only measures the wind velocity component normal to the length of the wire, and two crossed wires would be required.

To reduce the effect of natural convection and conduction which will limit the minimal measurable wind velocity, the anemometer may be operated at a temperature only slightly greater than the ambient temperature. This, however, will also reduce the signal. A material may be chosen with a much greater thermal coefficient of resistivity, such as a thermistor, than the metals generally used. This would increase the signal by several orders of magnitude and perhaps make low temperature operation feasible.

Thermistors are available as small beads of the order of 10^{-2} in. in diameter. This is much larger than the diameter of the wires which are normally used. This increases the response time of the sensor, even if constant temperature operation is employed rather than constant current operation. However, a fast response is not considered essential to the Mars measurements.

A spherical hot element anemometer would be omni-directional and only one would be required for wind velocity measurements. However, as low temperature operation is necessary to reduce conduction and natural convection, the solar heat input to the sensor would become important and of unknown quantity.

Two identical sensors would allow the solar heating effect to be subtracted, provided this heat input is less than the heat loss due to forced convection. The heat loss h, would be

$$h = f(\Delta T) = F(I^2R + Q)$$
$$h' = f(\Delta T)' = F(I'^2R + Q) \qquad (2)$$

where the prime indicates the second sensor. If h is known as a function of ΔT and the mass velocity, we have two equations and the two unknowns, the solar input Q and the mass velocity, and it is possible to solve for both.

Another shortcoming of the hot element anemometer is that erroneous results would be obtained if foreign particles adhere to the sensor. This, plus the probability that such an element might act more like a Pirani gauge, being more sensitive to density than to wind velocity as outlined above, present major difficulties in the development of a suitable hot element anemometer for the low density atmosphere of Mars.

B. Acoustical Methods

Wind velocities can be determined by measuring the perturbation of sound transit time between fixed transducers due to the transport of the medium. It is not necessary to know the absolute velocity of sound in the medium if the sound transit time is measured in opposing directions.

Consider two transducers separated a distance, d, the sound transit time from transducer 1 to transducer 2 is related by

$$\frac{d}{t_{12}} = U_x + \left| W_x \right| \tag{3}$$

where U_x is the apparent velocity of sound in the medium and W_x is the wind velocity component in the 1-2 direction. The sound transit time from transducer 2 to 1 is related by

$$\frac{d}{t_{21}} = U_x - \left| W_x \right| \tag{4}$$

Subtracting (4) from (3) we have

$$d \left[\frac{1}{t_{12}} - \frac{1}{t_{21}} \right] = 2 W_x \tag{5}$$

and the direction of W_x is known by the sign of (5). If these transducers are in a horizontal plane, and another set of transducers are placed in the same plane with a direction perpendicular to the first pair, then the two vector components of the horizontal wind velocity, W_x and W_y, can be determined. Similarly, the W_z component may be determined by using a third set of transducers located orthagonally to the first two sets. These components may then be vectorially added to obtain the wind velocity and relative direction regardless of the Lander's attitude after impact. It must be assumed that the wind velocity and direction do not change between successive transit time measurements used for computation. These measurements could be completed in tens of milliseconds.

The apparent sound velocities, U_x and U_y, are not necessarily the real velocity of sound in the medium. For simplicity, consider a wind velocity, W_y, normal to the 1-2 direction, then $t_{12} = t_{21}$ and $W_x = 0$. If V is the absolute velocity of sound in the medium, then

$$V = \sqrt{U_x^2 - W_y^2} \tag{6}$$

Thus, the absolute sound velocity in the medium can be determined in addition to the wind velocity and this will provide an independent appraisal of the atmosphere constituents, density, and temperature.

Several methods can be used to make the above measurements. In any case, the transducers should be capable of either transmitting or receiving. A single source of transmitting power and a single receiver should be sufficient if a gating network is employed to select the proper transducers for sending and receiving. The method could consist of actual time delay measurements of a short pulse of energy, or possibly phase measurements of a modulated sinusoidal carrier. It seems that a pulse technique would be more economical in power requirements and bulk of electronic circuitry.

It should be noted that the acoustical method of measuring the wind velocity as outlined is independent of the atmospheric density, constituency, and temperature, although the absolute velocity of sound is dependent on these factors. In addition, foreign particles on the transducers should not affect the accuracy of the measurement.

If high sound frequencies are used, the transducers may be quite small. Magnetostriction transducers should be quite rugged and shock resistant and piezoelectric transducers may also be feasible, although inherently less rugged.

The velocity of sound should be of the order of 250 $msec^{-1}$. For a 1 meter separation distance, the transit time would be of the order of 4.0 msec. Wind component velocity resolution of 1 meter sec^{-1}, would require a timing accuracy of 0.4 percent or 16 μsec with 1 meter spacing. Such timing seems readily achievable.

C. Point Design Selection

The acoustic propagation wind sensor was selected for point design evaluation since it appears to provide more flexibility in its application than does the hot element anemometer. It also is significantly less sensitive to its environment (solar flux, airborne particles, etc.). A design capable of being incorporated into the Lander does not currently exist. Engineering estimates of the physical and electrical characteristics of a conceptual design appear in the Science Payload Requirements paragraphs of Sections 3 through 8.

2.3.4.2.4 Water Vapor Detector

The water vapor detector selected for the entry science payload (Section 2.3.3) will also be used for the detection of atmospheric water vapor during the landed phase of operation.

2.3.4.2.5 Surface Composition

Definition of the chemical composition of the Martian surface is a difficult task when weight and volume are at a premium. The high impact loads encountered at

touchdown preclude making this measurement to any reasonable accuracy. At present, the most likely candidate for this experiment is a modified version of the Lunar, Surveyor Vehicle-alpha back scatter spectrometer. This device has not yet been designed for Mars, but will probably take a form similar to that of the Surveyor device. The operation of the device will be upgraded to include proton and x-ray spectrometic measurements to provide better accuracy for high Z elements. The source is expected to change from curium (Cm^{242}) to einsteinium (Es^{254}) if sufficient einsteinium can be accumulated. Tests using several potential sources are expected sometime in the future (no date). Current tests on various components of the device indicate a shock capability of about 500 g's. The Surveyor spectrometer made use of alpha back scatter and alpha-proton reactions to determine composition. The sample is irradiated with mono-energetic alpha particles. Rutherford scattering takes place and the energy of the scattered alpha particle is a function of the mass number of the sample. Similarly, the energy of the protons produced in the alpha-proton reactions is dependent on target mass number. The Surveyor instrument experiences some difficulties with mass number resolution when the number exceeds about 40. The addition of an x-ray detector and utilization of sources such as einsteinium allow x-ray fluorescence measurements to be made, thus materially improving the instruments' ability to resolve large mass numbers.

2.3.4.2.6 Imagery

The photoimaging task is to take pictures of the planetary surface and the design goal is taken to be that the returned pictures contain the maximum amount of surface coverage permitted by engineering and naturally occurring restraints. The type of camera chosen for this task is a Philco-Ford facsimile camera made specially for the Hard Lander mission. In effect, it will be two cameras in one unit. The advantage of this approach is that extraneous weight is cut down and the weight required for camera supports is also decreased. The facsimile is also very versatile in that a range of detectors can be used with it and the flexibility of format construction is extremely desirable in view of likely changes in the bits allotted to the imaging program. A further desirable feature is the choice of a silicon solar cell as the basic detector. This can be subjected to direct sunlight behind a small lens, and has a very extensive dynamic range of signal response that is clearly needed in this mission. It has a broader spectral response than the vidicon photocathode (see fig. 2.3.4-1) that permits the utilization of some of the peak of the Martian surface radiance. It further allows a wide range of filters to be employed for multispectral analysis should this technique become a requirement.

The ability of the cameras to withstand g-loads of impact and a complete sterilization procedure before launch has been fully tested in the laboratory (see Sections 3.5.2 through 8.5.2 for data.)

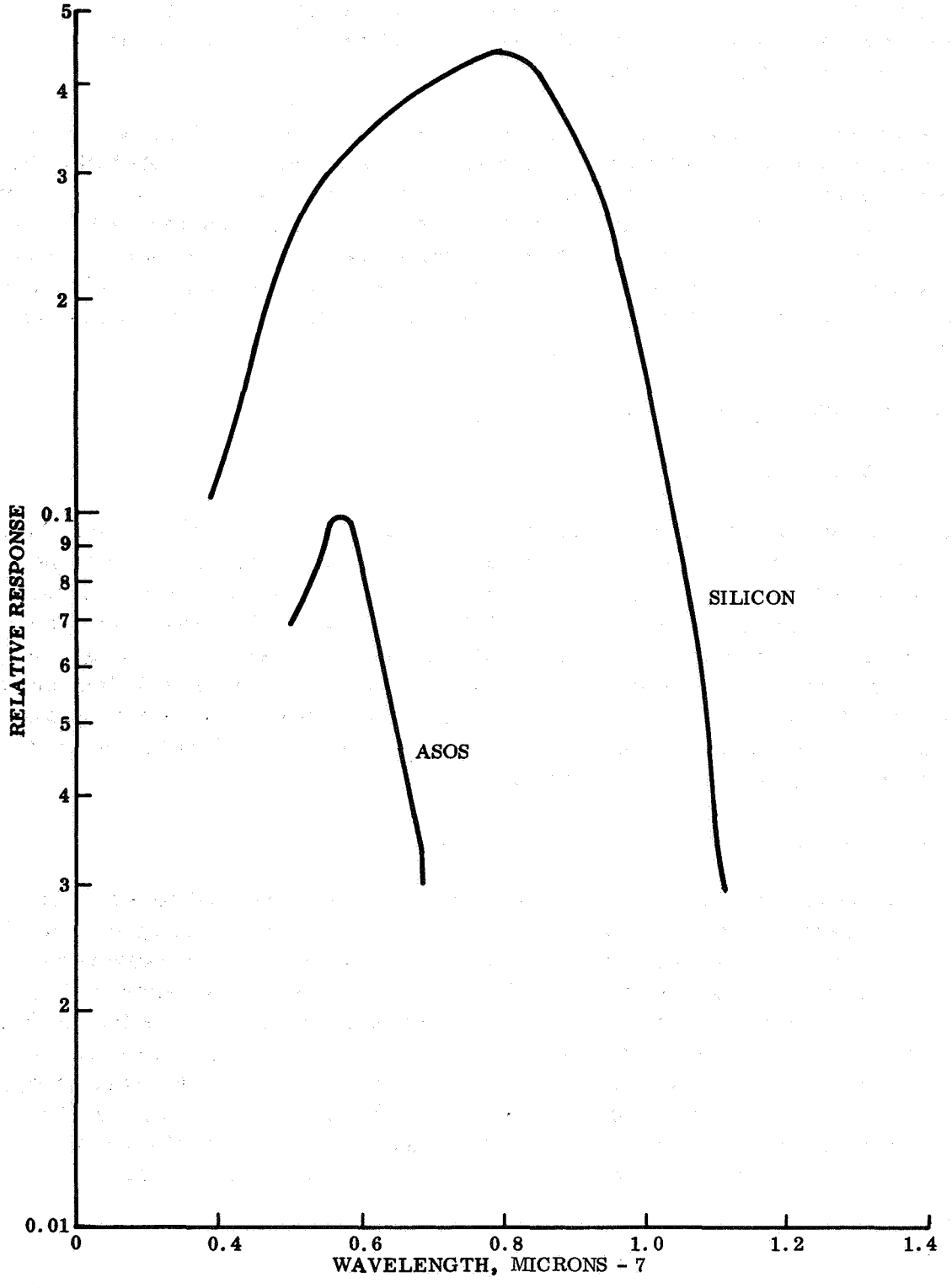


Figure 2.3.4-1. Silicon Solar Cell Wavelength Response and ASOS Vidicon Wavelength Response

2.3.4.2.7 Vehicle Inclination

Knowing the inclination of the vehicle is useful in the interpretation of the results of various experiments carried on the Lander. Further, this information is invaluable in providing the required signals to the various deployment mechanisms for heads or tails Lander operational attitude.

The simple approach to this measurement is to provide two rotary potentiometers with unbalanced pendulums affixed to their shafts. Each would be mounted with the shafts in the plane parallel to the top of the Lander and at right angles to each other. Thus the angle formed by the normal to the plane of the Lander and the local vertical will be a function of the resistance values (output voltages in the case where a constant current generator is used with each potentiometer) of each potentiometer. Small, ruggedized potentiometers have been tested at Diamond Laboratories to shocks as high as 2000 g's with successful results.

2.3.4.3 Expanded Science Payload Candidates

2.3.4.3.1 Subsurface Water Detection

This experiment requires the collection of a sample of material from the planet. This collection process can be accomplished by using a miniaturized borer being developed by JPL in conjunction with Philco-Ford. This device can remove a sample from the surface down to a depth of about 1 ft in 10 min. The sample is pulverized in the process until it assumes the consistency of a fine pumice. This grinding process can supply the necessary heat to drive off any water contained in the sample without transporting the sample to a pyrolizer. A low pressure dry carrier gas may be used to transport the water vapor to a detector located in the Lander (part of a minimum payload) via a flexible ducting system.

2.3.4.3.2 Airborne Dust Detection

This experiment uses technology developed for micrometeoroid detection in space. Basically, a microphone is used to detect sonic vibrations set up in a sounding board when dust particles with momentum above a minimum detectable level impact on the sounding board. The sounding board takes the form of either a 5 in. cube or a sphere with equivalent volume. An electronic counter records the number of impacts in a given time and readout is accompanied by a reset pulse to return the counter to zero. Several micrometeoroid detector devices may be considered for development to meet the exact requirements of this experiment. High level impacts may materially increase the weight of this system since it employs a very delicate microphone element. No sterilization problems can be foreseen.

2.3.4.3.3 Ultraviolet Radiometery

A four channel ultraviolet radiometer will measure the ultraviolet flux reaching the planet's surface. Four wavelength bands will be employed so that radiation in specific bands of interest, such as those containing the absorption lines for DNA, O, and O_3

can be measured. For proper analysis of the data, a Sun angle sensor is also included in this package. It measures the angle of the line of sight to the Sun with respect to a plane passing through the Lander perpendicular to its axis of symmetry. No scanning will be attempted with this device, and hence a rather rugged construction seems feasible. Sterilization should not be a problem.

2.3.4.3.4 Large Molecule Detector

The large molecule detector will take the form of a mass spectrometer/gas chromatograph combination. It is anticipated that the same sample that is collected by the borer in the subsurface water experiment will be transported from the borer proper to an oven located inside the detector subsystem by a high pressure pneumatic system (pulsed gas system). Following pyrolysis of the sample, the gases evolved will be transported via duct system to the mass spectrometer/gas chromatograph by a helium carrier gas system. Analysis of the gas sample will take place for the next 30 min period. The gas chromatograph will look for 30 specific species while the mass spectrograph will perform a mass number scan from mass numbers of 25 to 200. A similar device of this type is currently under development for planetary exploration applications and thus no problems concerning sterilizability are anticipated. High 'g' requirements will probably be one of the key limiting factors in this system.

2.3.4.3.5 Life Detection

No life detection techniques have yet been identified that will determine with certainty whether life exists outside the terrestrial biosphere. Greater confidence may be placed in our judgment concerning the existence of extraterrestrial life as the amount of correlative information increases. Two relatively well known biological detection instruments have been developed for planetary exploration application. These are called Gulliver and Wolf Trap.

A. Gulliver

Gulliver detects bacterial reproduction and/or metabolism by identifying the formation of radioactive CO_2 from C^{14} labeled substrates such as formate, glucose, lactate, or glycine. Growth or reproduction is indicated by an exponential increase in the counting rate of the radioactive gas. If metabolism occurs without growth or reproduction, the count rate also increases. The count rate curve of the test is calibrated against one obtained from a bacterial growth chamber in which an inhibitor of growth has been introduced.

If $C^{14}O_2$ production is not exponential, it may not be clear whether the gaseous release is due to degradative metabolism process in the absence of growth or chemical degradation of the radioactive material. However, the proper choice of controls will help eliminate this ambiguity. An inhibitor to growth or metabolism (heat is the best antimetabolite) will stop the emission of $C^{14}O_2$ from biological sources.

The small Capsule is ejected from the Lander by a compressed spring or pyrotechnic device. An umbilical cord is connected with the Lander for data transmission. The module erects itself on landing. Pliable bellows on the bottom portion rest on the planetary surface to confine the radioactive broth which is released at the proper time. If microbiota are present and will grow in the broth provided to release $C^{14}O_2$, a geiger counter located in the top portion of the module will detect it. The geiger counter is not located in direct line of sight to the broth on the planetary surface. It will detect the radioactive gas which rises in the module.

However, since the Martian atmosphere is known to contain CO_2, it is desirable that entrapped native CO_2 be removed from the interior of the module prior to the deposition of radioactive broth on the surface. A getter ($B_a(OH)_2$ or L_i OH) removes native CO_2 soon after the bellows are implanted on the surface. In order to increase the efficiency of the geiger tube in detecting $C^{14}O_2$, a getter is also coated on the tube surface. This begins functioning after release of the broth.

No attempt is made to seal a portion of the soil and broth inside the "in site" model. The vapor pressure of the broth inside produces a greater pressure than atmospheric pressure outside. However, some gas from outside will be available if needed for Martian growth. This experiment attempts to change ambient conditions as little as possible.

Gulliver's 3 oz weight does not include the weight of the umbilical cord which can easily weigh more than the life detector. The required ejection distance has not been studied carefully. This will depend partially on the mission. Gulliver is currently described as being in a state of engineering readiness. Heat sterilization should offer no serious problems. High 'g' impact may once again be the limiting item in application of this device to a Hard Lander mission.

B. Wolf Trap

In this device, micro-organism growth is detected by light scattering measurements. Relative concentrations of microbiota in a turbid culture may be determined by measuring either the attenuation of a beam of collimated light traversing the suspension or the intensity of light scattered by the organisms. Due to greater inherent sensitivity, the measurement of scattered light (nephelometry) has been selected.

It was planned that Wolf Trap would also detect organism growth by change of pH. Unfortunately, no electrodes are available which will withstand sterilization by heat. The pH determination has been dropped until satisfactory electrodes are made available.

The sampling system is quite often one of the unsolved problems for Lander science instruments. This is also true for Wolf Trap. The earlier designs, which assumed a Martian atmospheric pressure up to about 50 mb, utilized Bernoulli-principle vacuum cleaners which are marginal at a pressure as low as 10 mb. Very little recent study has been directed toward the solution of the sampling problem. Probably some kind of mechanical sampler will be desirable. Once again, the high 'g' levels encountered by a Hard Lander will force special mounting of this device since there is little doubt that it will not withstand shocks of the 1000 'g' variety.

C. Point Design Selection - Life Detection Instrument

Based solely on its more advanced state-of-development engineering and testing, the Wolf Trap has been selected for point design evaluation.

2.3.5 LANDING PARAMETERS

Landing parameters for the Point Design are as follows:

1. Lander velocity components at touchdown are 220 ft/sec horizontal and 100 ft/sec vertical.

2. Lander vertical axis can be 40° off local vertical at touchdown.

3. Surface slopes at impact up to 34° with particles up to rocks of 5 in. diameter.

4. All energy at impact is dissipated in Lander attenuation equipment — none by the surface or particles.

5. Lander footprint must be compatible with minimum surface bearing pressure of 6 psi.

6. Maximum Lander deceleration from touchdown velocity to rest is 1000 g's for attenuation design.

2.3.6 STRUCTURAL LOADING CRITERIA

2.3.6.1 Point Design Loads

The point design analysis consists of the aeroshell, the Hard Lander and the protective canister. The critical structural loadings are shown in table 2.3.6-1. In addition to the above loads, there are vibration requirements. The sterilization temperature (condition O) consists of 300 °F constant for six cycles of 24.5 hr each at 0.5 psi differential pressure. Also, interplanetary temperatures (condition P) consists of temperature extremes of -300 °F to 150 °F. The launch vibration frequencies of 10-15 cps with 140 dB acoustic environment are the high frequency requirements.

2.3.6.2 Critical Loadings

The critical loadings are as follows:

1. The aeroshell critical design condition is the entry condition (J). The direct entry designs (Point Designs 2A, 2B, 4, and 6) are designed to withstand 48 g's. The out-of-orbit designs (Point Designs 1, 3, and 5) are designed to withstand 5.5 g's with the structural temperature at 320 °F as well as 12.7 g's with the structural temperature of 200 °F. These loadings override the axial vibration loadings.

2. The canister critical design loads consist of the internal pressure loadings of 0.5 psi at 275°F and 1.0 psi at ambient temperature. A relief valve limits the pressure differential to these levels. For limit loadings, a factor of 1.33 is used on the pressure and for burst (ultimate), a factor of 1.66 is used on these pressures. The second critical loadings is the separation band clamp strap load of 48 lb/in.

3. The Hard Lander critical loading is the dynamic response loading of 1000 g's.

TABLE 2.3.6-1. POINT DESIGN LOADS
(all loads are limit)

Loading Condition	Accelerations		Notes
	G_X	G_N	
A. Ground handling	2.0	2.0	
B. Band clamp	N/A	N/A	83 lb/in. Radial
C. First stage burnout	5.2	2.0	
D. Second stage burnout	4.0	2.0	
E. Axial vibration	+6.0 -3.0	—	
F. Lateral vibration	—	±2.0	
G. Canister separations	Negligible	Negligible	
H. Entry systems separation	Negligible	Negligible	
I. T/C separation	Negligible	Negligible	
J. Entry (Maximum G_X)	5.5	Negligible	Out-of-orbit 320°F Interface
	12.7	Negligible	Out-of-orbit 200°F Interface
	48.0	Negligible	Direct Entry 200°F Interface
K. Parachute opening	10.0	—	
L. Impact	1000.0		
M. Canister pressure	N/A	N/A	ΔP = 0.5 psi at 275°F
N. Canister pressure	N/A	N/A	ΔP = 1.0 psi maximum at ambient
O. Sterilization	N/A	N/A	300°F soak and 0.5 psi internal pressure in canister (6 cycle-24 hr +3 cycle 96 hr)
P. Interplanetary temperature	N/A	N/A	-300°F to 100°F

2.4 REFERENCES

2-1 Seiff, "Some Possibilities for Determining the Characteristics of the Atmospheres of Mars and Venus from Gas Dynamic Behavior of a Probe Vehicle", NASA TN D-1770, 1963.

2-2 Peterson, "A Technique for Determining Planetary Atmosphere Structure from Measured Accelerations of an Entry Vehicle", NASA TN D-2669, 1965.

2-3 Peterson, "Analysis of the Errors Associated with the Determination of Planetary Atmospheric Structure from Measured Accelerations of an Entry Vehicle", NASA TR R-225, July, 1965.

2-4 Smith, DeVries, and Homsey, "Synthesis Techniques for Experiments in Planetary Atmospheres", AIAA Paper number 68-155.

2-5 General Electric Re-entry Systems Technical Brief, "Development of a Lightweight, Low-Range Pressure Transducer for Planetary Entry Applications", November 1967.

2-6 Seiff and Reese, "Use of Entry Vehicle Responses to Define the Properties of the Mars Atmosphere", reprint 65-24, American Astronautical Society Symp. an Unmanned Exploration of the Solar System, 1965.

3. POINT DESIGN 1

3. POINT DESIGN 1

3.1 MISSION SEQUENCE

The operational flight sequence for the interval from start of separation operations to impact is illustrated by fig. 3.1-1. This profile depicts the sequence of events for the out-of-orbit mission of Point Design 1. Fig. 3.1-2 illustrates the landed operations of the same mission.

Point Design 1 is an out-of-orbit mission with a nominal interplanetary flight time of 244 days and a Mars orbital flight of up to 30 days before Capsule separation. The Lander Capsule is stabilized by spin-up prior to de-orbit propulsion ignition and roll control during entry. Deceleration is accomplished by parachute whose deployment is actuated by a g-switch at Mach 2. The Capsule is programmed to relay the data real time to the Orbiter, which is to remain in synchronous orbit for one full diurnal cycle. Entry and surface science and surface imaging is performed at the beginning of the cycle with data transmitted real time to the Orbiter for relay to earth. Surface meteorology and composition measurements will continue for the entire cycle period, and the data is stored while the Orbiter is beyond communication (periapsis) range. When the Orbiter enters communication range it will signal the Lander, and stored data plus an additional complete set of real time data will be sent to the Orbiter for relay to the Earth. A more detailed sequence of events, from launch to mission completion, is shown for this mission in Table 3.1-1.

TABLE 3.1-1. MISSION SEQUENCE OF EVENTS, POINT DESIGN 1

Item	Event	Time
A.	Launch to Impact	
1.	Launch	TL
2.	First mid course maneuver (if required)	TL + 30 days
3.	Second mid course maneuver (if required)	TL + 234 days
4.	Mars orbit insertion	TL + 244 days
5.	Start final Capsule diagnostic checkout	To (entry - 24 hr)
6.	Complete diagnostic checkout	To + 120 min
7.	Update programmers complete	To + 20 hr
8.	Turn on Lander power, T/M, sequencer diagnostic data	T1 (To + 21.7 hr)
9.	Canister separation	T2 (T1 + 5 min)
10.	Spacecraft maneuvers to Capsule separation attitude	T2 + 10 min

TABLE 3.1-1. MISSION SEQUENCE OF EVENTS - POINT DESIGN 1 (Continued)

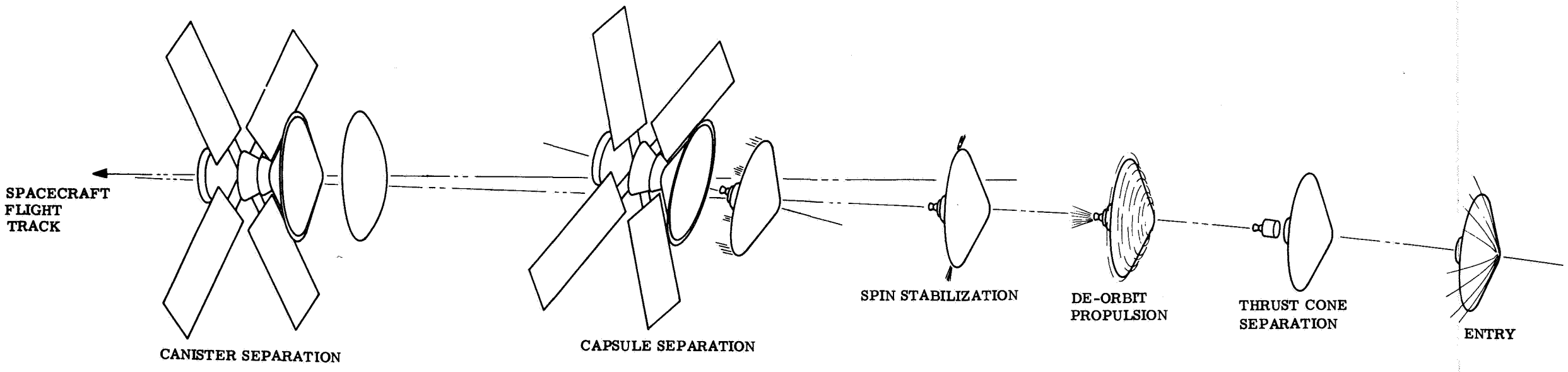
Item	Event	Time	
11.	Capsule separates from spacecraft	T3 (T2 + 10.1 min)	
12.	Initiate spin stabilization	T3 + 0.5 sec	
13.	Ignite de-orbit propulsion	T3 + 30 min	
14.	Terminate de-orbit propulsion	T3 + 30.3 min	
15.	Initiate de-spin	T3 + 30.5 min	
16.	Separate thrust cone	T3 + 30.6 min	
17.	Turn power and T/M off	T3 + 30.7 min	
18.	Turn on mass spectrometer for warm-up	T4 - 15 min	
19.	Turn on T/M (low data rate), initiate accelerometer and pressure sensor reading	T4 - 60 sec	
20.	Entry	T4 (T3 + 119 min)	
		VM-8	VM-9
21.	Mach 5 - Initiate mass spectrometer water vapor, and temperature sensor readings	T4 + 255 sec	T4 + 217 sec
22.	Mach 2 - deploy parachute	T4 + 285 sec	T4 + 259 sec
23.	Aeroshell separation	T4 + 295 sec	T4 + 269 sec
24.	Jettison parachute	T4 + 459 sec	T4 + 1250 sec
25.	Impact - Force sensed and transmitted to spacecraft (with redundant storage)	T5 (T4 + 460 sec)	T5 (T4 + 1251 sec)
B.	Landed Operations		
1.	Diagnostic and stored entry data transmitted to Orbiter (low data rate)	T5 + 0.1 min	
2.	Lander comes to rest - up direction sensed	T5 + 2 min	
3.	Initiate hatch cover and boom deployments	T5 + 2.1 min	

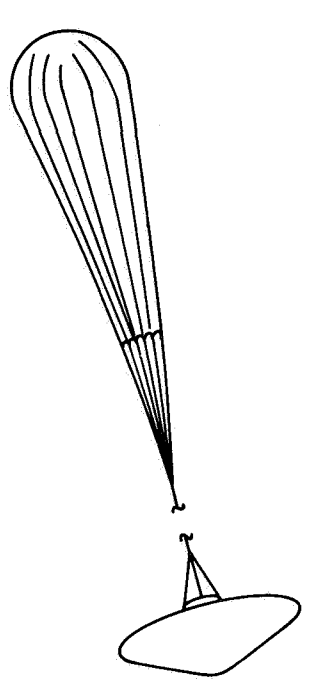
TABLE 3.1-1. MISSION SEQUENCE OF EVENTS - POINT DESIGN 1 (Concluded)

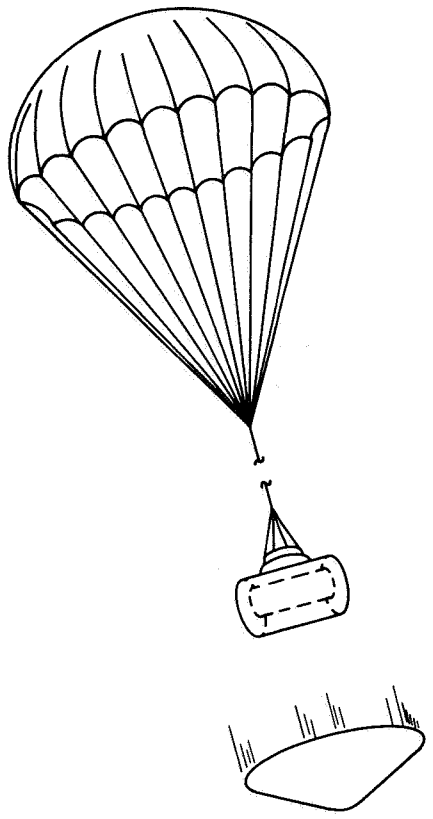
Item	Event	Time
4.	Switch to high data rate transmission mode	T6 (T5 + 2.5 min)
*5.	Initiate stored diagnostic, entry, and impact data transmission to Orbiter	T6 + 0.1 min
*6.	Initiate imagery, meteorology, and inclinometer measurements and transmit to Orbiter for relay to Earth	T6 + 0.2 min
*7.	Repeat items 5 and 6	T6 + 8.5 min
8.	Turn off imagery and T/M systems	T6 + 20 min
9.	Repeat surface science measurements (excluding imagery) at 20 min intervals and store data	--
10.	Initiate surface composition (alpha back scatter) measurement cycle and store data	T7 (T5 + 1 hr)
11.	Complete initial surface composition cycle	T7 + 5 hr
12.	Repeat surface composition measurements every 3 hr	--
13.	Receive signal that Orbiter is returning to range	T8 (T6 + 24.5 hr)
14.	Turn on T/M system (high data rate) and transmit stored science data to spacecraft	T9 (T6 + 24.6 hr)
15.	Perform imagery and surface science measurements and transmit data to Orbiter for relay to Earth	T9 + 0.1 min
16.	Repeat items 14 and 15	T9 + 8.5 min

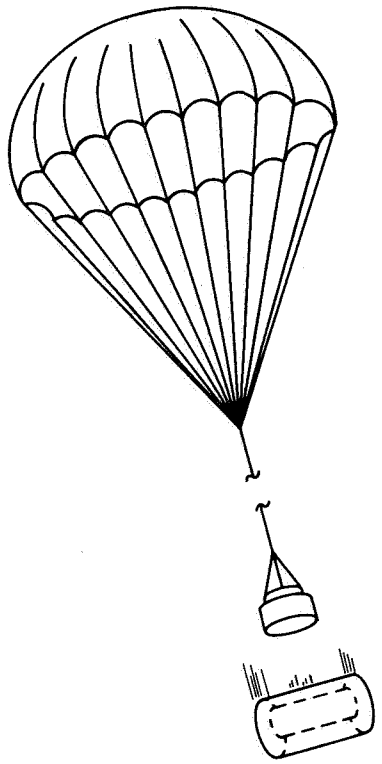
* If impact occurs too late for relay to Orbiter (VM-9), gate switch delays function until item 14

FOLDOUT FRAME




DEPLOY PARACHUTE

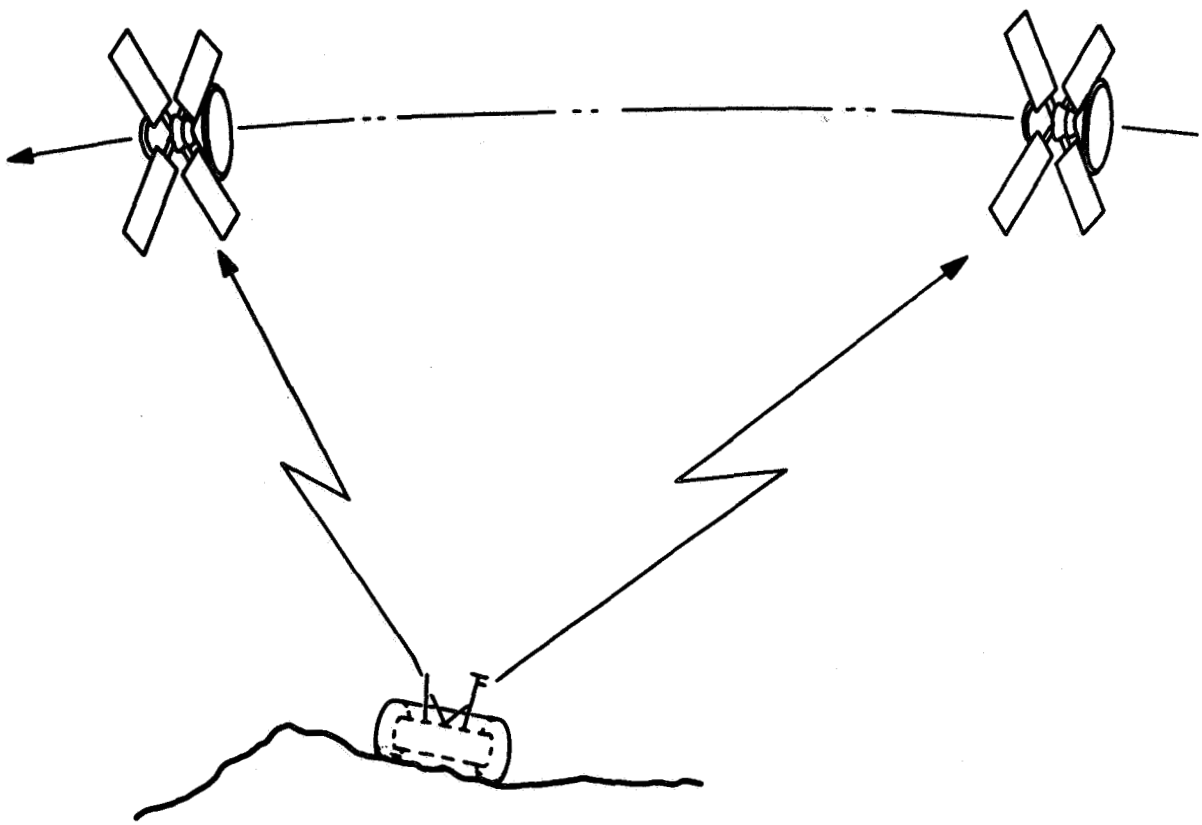

AEROSHELL SEPARATION


JETTISON PARACHUTE

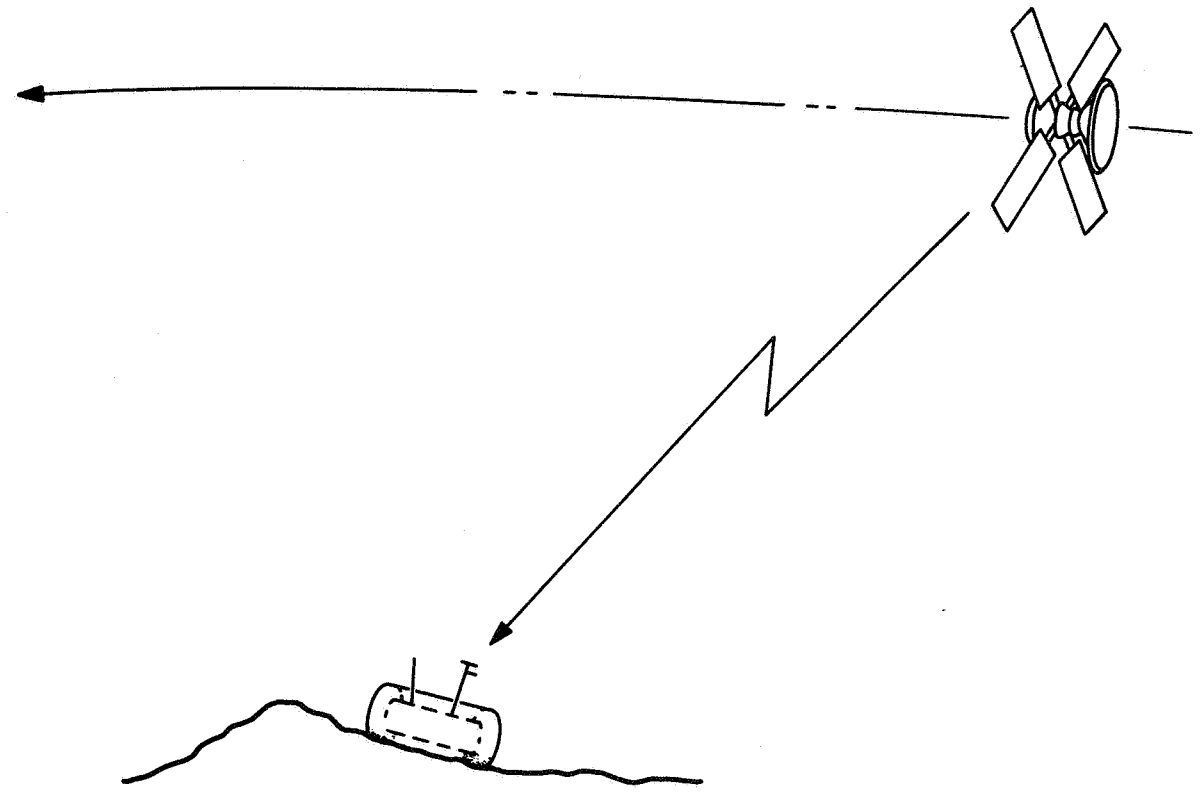
FOLDOUT FRAME


CAPSULE IMPACTS ON SURFACE

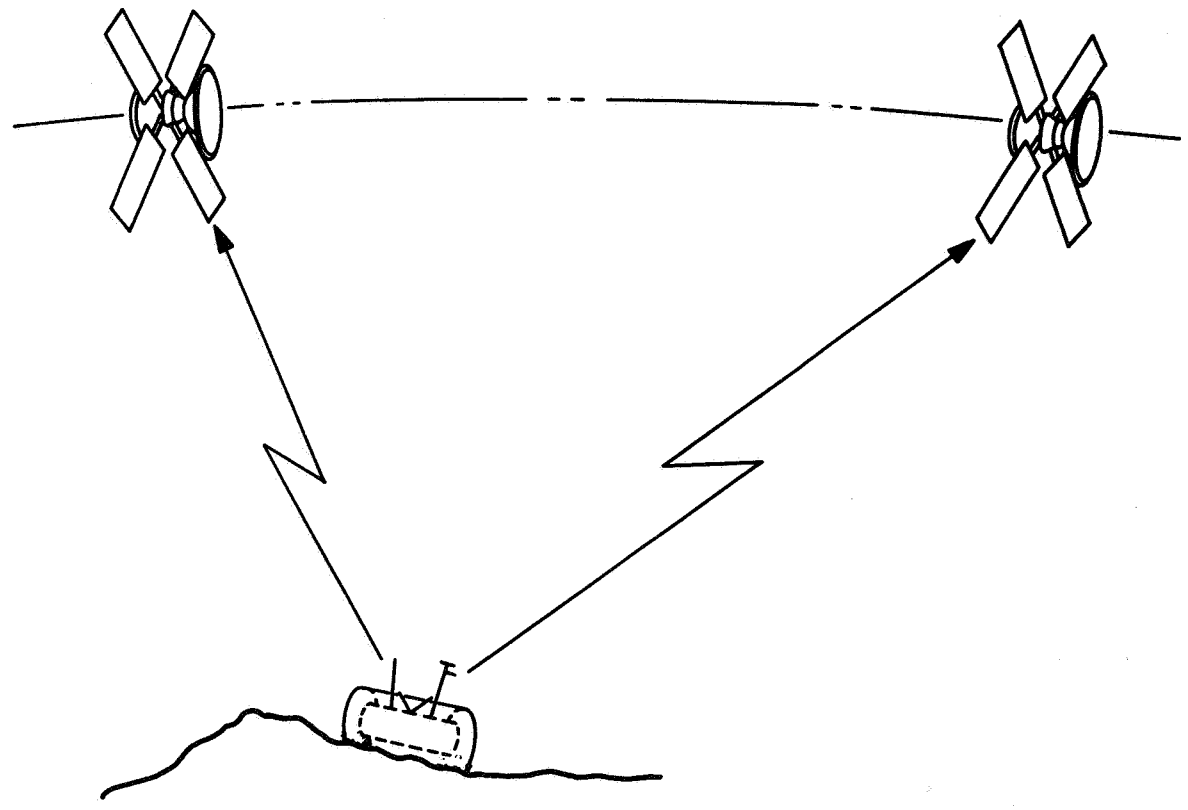
Figure 3.1-1. Operational Flight Sequence from Separation to Impact



DATA TRANSMITTED TO SPACECRAFT



LANDER RECEIVES SIGNAL THAT
SPACECRAFT IS RETURNING
(24.5 HRS LATER)



STORED DATA, TRANSMITTED TO SPACECRAFT

Figure 3.1-2. Landed Operations

3.2 CAPSULE SYSTEM DESIGN DESCRIPTION

A basic difference in the direct entry system and the out-of-orbit entry system in a given point design pair is that the ballistic entry parameter (W/C_DA) for the direct entry vehicle (20.8 kft/sec entry velocity and 25° path angle) is approximately 0.6 the value appropriate for the out-of-orbit entry system (15.3 kft /sec and 16° at entry). Direct entry systems entering at a path angle increased to 40° require a ballistic parameter about 0.4 times smaller than the out-of-orbit entry vehicle.

The allowable or limiting ballistic coefficient is determined for the different entry modes by selecting the best combination of aeroshell drag area, parachute deployment, size and landing load attenuation in the deceleration profile to Lander touchdown. The entry system velocity must be reduced to Mach 2 before parachutes are deployed and this deceleration increment must occur at a sufficiently high altitude that the Capsule Lander system can be decelerated by parachute to the acceptable touchdown velocity increment. In this study, the ballistic entry parameter limit is determined for each entry mode based on parachute deployment in the VM-8 Mars model atmosphere (lowest altitude at Mach 2) and parachute sizing for descent in the VM-7 atmosphere, the model having the lowest atmospheric density at the surface.

The effect of the limiting ballistic coefficient is that the direct entry Capsules are designed with considerably larger base diameter and heavier aeroshells than the slower entry, out-of-orbit vehicle of the point design pair. The design approach taken for each vehicle in the particular design pair is the same and the system weight difference in the launch configuration, separation and entry is primarily due to the entry shell size because it directly affects the weight of aeroshell structure and heat shield and the canister (larger size and inertial loading).

The aeroshell designs selected for each of the six Capsule point designs incorporate blunt body, sphere cone shell structures with ablative heat shields using elastomeric formulations such as GE's ESM 1004 X at 16 lb/ft^3 density for the out-of-orbit vehicles and ESM 1004 AP at 35 lb/ft^3 density for the direct entry vehicles. The selected entry system structure and shield design is an extension of ICBM technology and the integrity of the approach in either of the bonded shields or film adhesive shields has been proved. The shield materials referenced are typical of the application but the exact formulation required would be specified in a more detailed engineering phase of a Mars mission program.

The Lander system of the Capsule is retained within the aeroshell by a tension strap arrangement and released by burning the wire wrap of the hot-wire bolts with 30 msec of 10 to 15 amp current. It is separated from the aeroshell by the parachute drag differential. The preferred release, separation and deceleration sequence is initiated with an altimeter. G-level switch and timing units as well as an axial g-level and base pressure measurement approach have been considered for the parachute deployment device. The altimeter approach is preferred because it can be used to delay parachute opening (below Mach 2) to match the descent time of the Lander to the view time available for communication with the Orbiter before and after landing. The requirement for shortening the descent time is most necessary if the flight was made in a VM-9 type atmosphere.

The Lander contains the instruments, power, sequencing, telemetry, and communication equipment to perform the surface science operations. The equipment is contained within a torroidal rim-stiffened cylinder that is equipped with a deep ring of phenolic glass, honeycomb structure that is sized and positioned to attenuate the landing loads by mechanical crush-up of the honeycomb material. The first point design pair developed for the minimum surface lifetime mission were prepared with both omni-directional and multi-directional Landers to develop the weight and size difference in the out-of-orbit and direct entry vehicles due to the design approach taken for impact attenuation. The difference in the weight of attenuation material between omni- and multi- landing (522 and 287 lb respectively) is the difference in the omni- and multi- Lander total weights (weight suspended on parachute) of 858 and 623 lb. The following weight statement (table 3.2-1) summarizes the comparison of the out-of-orbit and direct vehicles and the influence of Lander type for the minimum lifetime mission. The comparison is based on the first design pair data but the results are typical of like comparison studies of the other design pairs.

The pre-entry systems of the Capsule consist of the sterilization canister, adapter attitude control and the de-orbit maneuver hardware. The prime function of the canister is to encapsulate the entry vehicle and maintain a physical, biological barrier to prevent contamination of the entry vehicle during:

1. The terminal sterilization cycle
2. Post sterilization operations in the ground environment
3. During launch and powered flight
4. The cruise and up to the sequence for Capsule-Orbiter separation.

The canister design approach for the six capsule designs is a semi-monocoque construction in minimum manufacturing gauge (0.012), 7075 aluminum. The rear shell of the canister assembly contains the Capsule-to-Orbiter adapter within the sterilized envelope and connections to the Orbiter are made outside this envelope. The forward shell is released by applying 24 amps for 30 msec to the four hot-wire bolts of the V-ring type clamp segments. The shell is separated by two mechanical springs with a velocity of 2 ft/sec.

The adapter provides the structural transition between the Capsule and the Orbiter and contains the equipment for separating the flight systems. The Capsule is released by applying 48 amps to four explosive nuts and is separated at approximately 1 ft/sec by four springs.

Both spin, de-spin and three axis control systems were studied for Capsule attitude control for the de-orbit maneuver, for entry path angle control, and for vehicle control up to Lander separation from the aeroshell. The six point designs have been detailed with spin/de-spin for pre-entry and roll control during entry. The final system would be selected after more detailed error analyses are made and the principle trade-offs in landing site location, data communication and trajectory design are completed.

TABLE 3.2-1. COMPARATIVE WEIGHT SUMMARY OF MINIMUM MISSION SYSTEMS

Aeroshell base diameter	Out-of-Orbit Entry		Direct Entry	
	8.3 ft	8.3 ft	12.7 ft	11.4 ft
Lander type - weight (lb)	Omni-858	Multi-623	Omni-858	Multi-623
Retardation weight (lb)	228	172	228	172
Aeroshell and Propulsion (lb)	329	329	465	389
	---	---	---	---
Capsule weight at spearation from spacecraft (lb)	1415	1124	1551	1184
Capsule weight at entry (lb)	1246	955	1480	1127
Ballistic entry coefficient $\frac{(lb)}{ft^2}$	15.2	11.7	7.9	7.3
Capsule weight at launch (lb)	1626	1335	1882	1463

Based on the baseline missions data, the out-of-orbit entry vehicles require a velocity increment of 235 meters/sec and the direct vehicles 45 meters/sec. Both solid propellant systems and liquid propulsion systems have been detailed in the point designs. The liquid systems are more easily adapted to de-orbit maneuver changes as weight and velocity requirements are modified. In the low impulse requirements range, the liquid systems have disproportionate weights for the propulsion hard parts compared to the total and, generally, the liquid systems applicable to these study vehicles are about three times heavier and require considerably larger packaging volumes than the solids. Both systems have been designed into the Capsules and the pertinent trades and the engineering details in each design application are given in the following Paragraph 3.3 of this volume. In all six design applications the de-orbit maneuver system is arranged to be jettisoned before entry by release of preloaded, hot-wire bolts of the thrust cone and separated by mechanical springs.

The following sections give engineering details and analyses of the out-of-orbit, one diurnal cycle surface lifetime Capsule shown as Point Design 1 in the list of six prepared in this study.

3.2.1 SCIENCE DATA REFERENCE

The weight of the sensors selected and a baseline reference of the atmospheric data acquired from entry to impact in the maximum flight time range of atmospheres is shown on table 3.2-2. Pressure and temperature readings are taken at both the stagnation and the base region of the aeroshell. The atmospheric density profile is determined from the vehicle aerodynamic data and the measured deceleration profile of the Capsule.

TABLE 3.2-2. SCIENCE WEIGHT SUMMARY

	Weight (lb)	Data Load (bits)	
		VM-8*	VM-9*
Entry Science			
Pressure	3.0	1.3×10^4	2.7×10^4
Temperature	1.5	5.7×10^3	2.0×10^4
Composition	8.0	8.6×10^3	10.2×10^3
Density	2.0	1.1×10^5	2.9×10^5
Water Vapor (ducting)	1.0	7.5×10^1	3.75×10^2
	15.5	1.37×10^5	3.47×10^5
Landed Science			
Pressure	1.4	1.35×10^3	
Temperature	2.0	2.7×10^3	
Wind	5.0	4.9×10^3	
Moisture	10.0	1.77×10^3	
Photo imaging	4.8	1.02×10^7	
Clinometer	2.6	7.0×10^1	
Soil sampler	9.5	3.0×10^4	
	35.3	1.02×10^7	

*Time from entry to impact in VM-8 = 460 sec
in VM-9 = 1251 sec

The landed science consists of meteorological data and surface imagery taken with (Philco) facsimile cameras that take four scenes of low resolution data and four nested scenes of high resolution data. The low resolution scenes are each $35^{o} \times 50^{o}$ segments imaged with $1/10^{o}$ Instantaneous Field of View (IFOV) and the high resolution scenes are $5^{o} \times 5^{o}$ segments imaged with $1/100^{o}$ IFOV. The total data acquired in four high and four low scenes (63 gay shades) is $6 \times 10^{6} + 4.2 \times 10^{6}$ or 1.02×10^{7} bits. A typical data summary for the surface operations included in table 3.2-1.

The surface imagery is transmitted real time to the Orbiter after impact and again at periapsis passage. The meteorological data is read out from the magnetic core storage unit and the first readout includes stored entry science data. To preclude possible loss of entry data due to plasma sheath blocking, the entry data is interleaved for two transmissions, with the readout portion delayed about 70 sec.

3.2.2 CAPSULE SYSTEMS CONFIGURATION

The Capsule for Point Design 1 is an omni-directional Lander containing the minimum surface science with a surface lifetime of one diurnal cycle. It will be delivered to the Martian surface in an out-of-orbit mode. Telecommunications will be accomplished by a UHF relay to the Orbiter. A solid propellant propulsion system is used to de-orbit the entry vehicle. Parachute deployment will be initiated by a Mach 2 sensor. Fig 3.2.2-1 shows the Point Design 1 Capsule configuration.

3.2.3 CAPSULE SYSTEMS WEIGHT

The weight and inertias of the out-of-orbit entry Capsule with a surface design goal of one diurnal cycle are given in table 3.2-3. The table gives the basic composition of the Capsule and the weights and inertia at key mission events - launch, separation, entry, and landing. The more detailed statements of the weight, balance, and inertial properties are given for the major systems of the Capsule in Sections 3.3 (Pre-entry), 3.4 (Entry) and 3.5 (Landing).

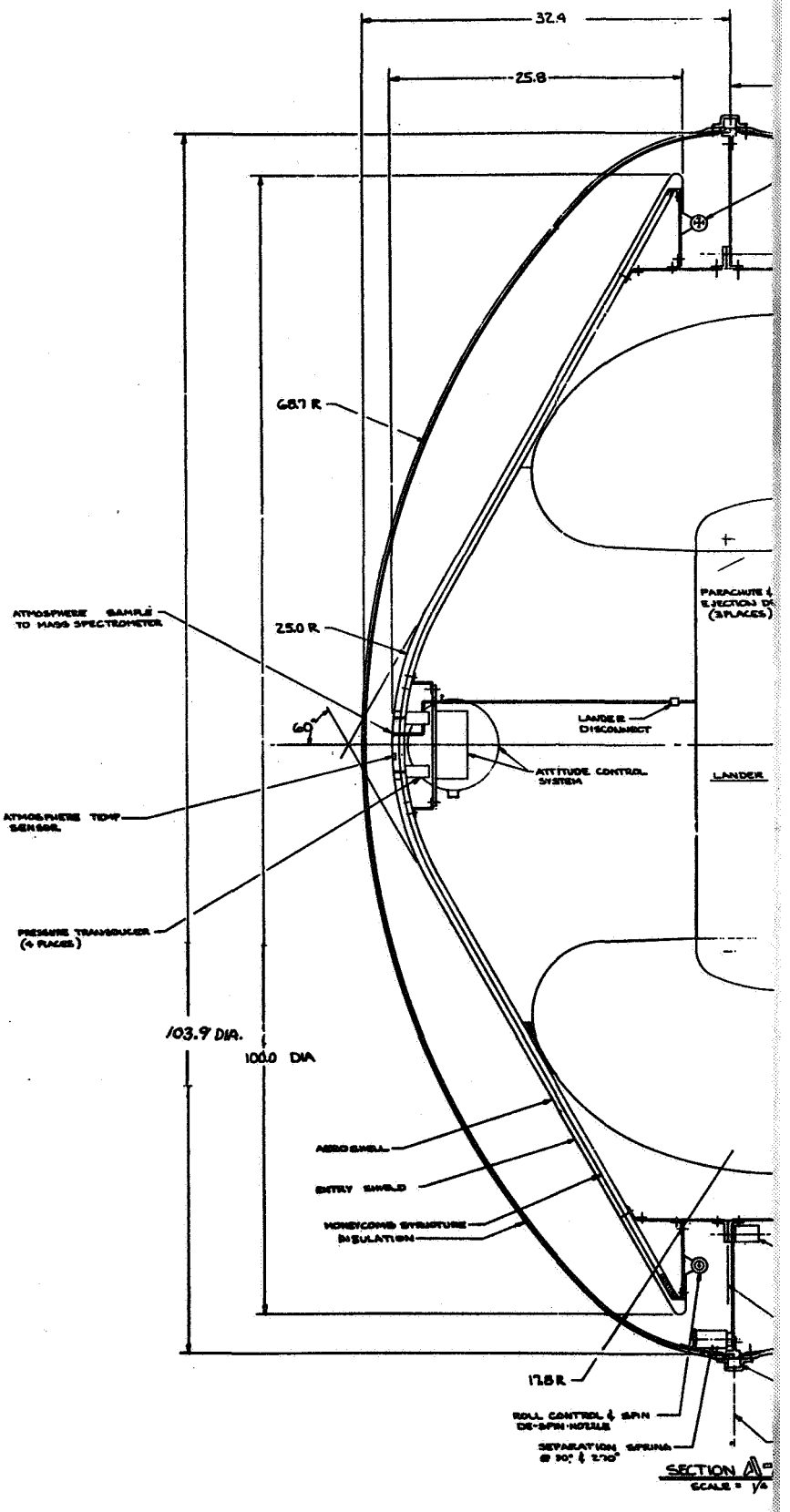
3.2.4 FUNCTIONAL BLOCK DIAGRAM

The functional block diagram, fig. 3.2.4-1 is the complete system delineation of events from launch until the end of the mission. Each functional component is located with respect to functional criteria.

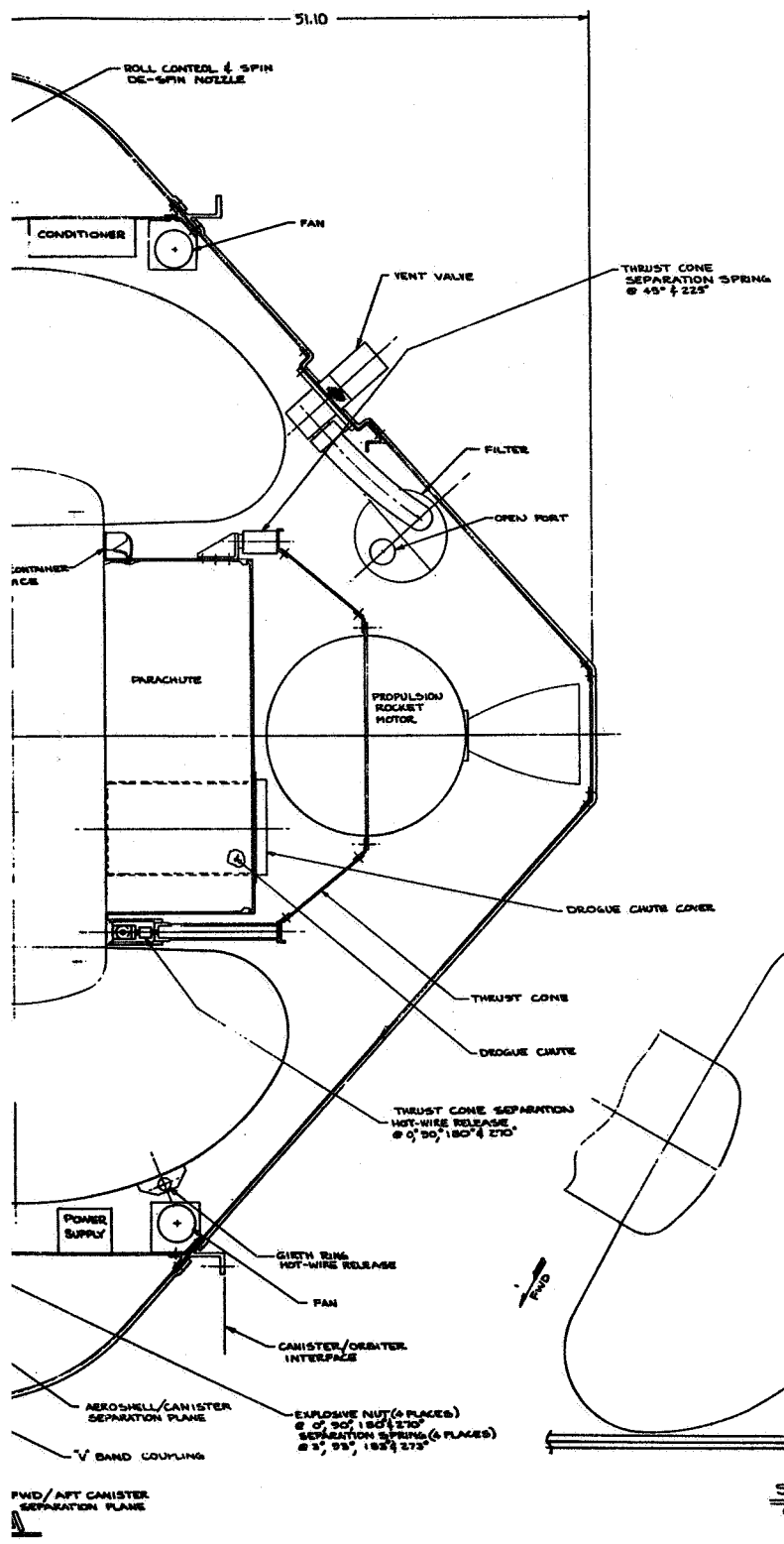
The horizontal axis can be considered a relative time axis with each mission phase occupying a discrete time segment. Each segment, however, does not represent a linear time scale since the total cumulative length would become unreasonable. The time axis then, indicates the sequence of events rather than the time at which they occur. Whenever components operate in multiple events, either the primary event or the typical mode of operation is indicated. Although the component location indicates the relative beginning of the event, the duration, repetitive rate, or the stop time of the event is not indicated.

The vertical axis is used to group the components by subsystem. The subsystem grouping, indicated on both the right and left hand borders, is maintained throughout the drawing. Therefore, for any given event, all components within the system used to perform that event will be shown within the same vertical time boundaries designated at the borders, and the components within a given subsystem are aligned from top to bottom in order of the first function of operation.

FOLDOUT FRAME 1



FOLDOUT FRAME 2



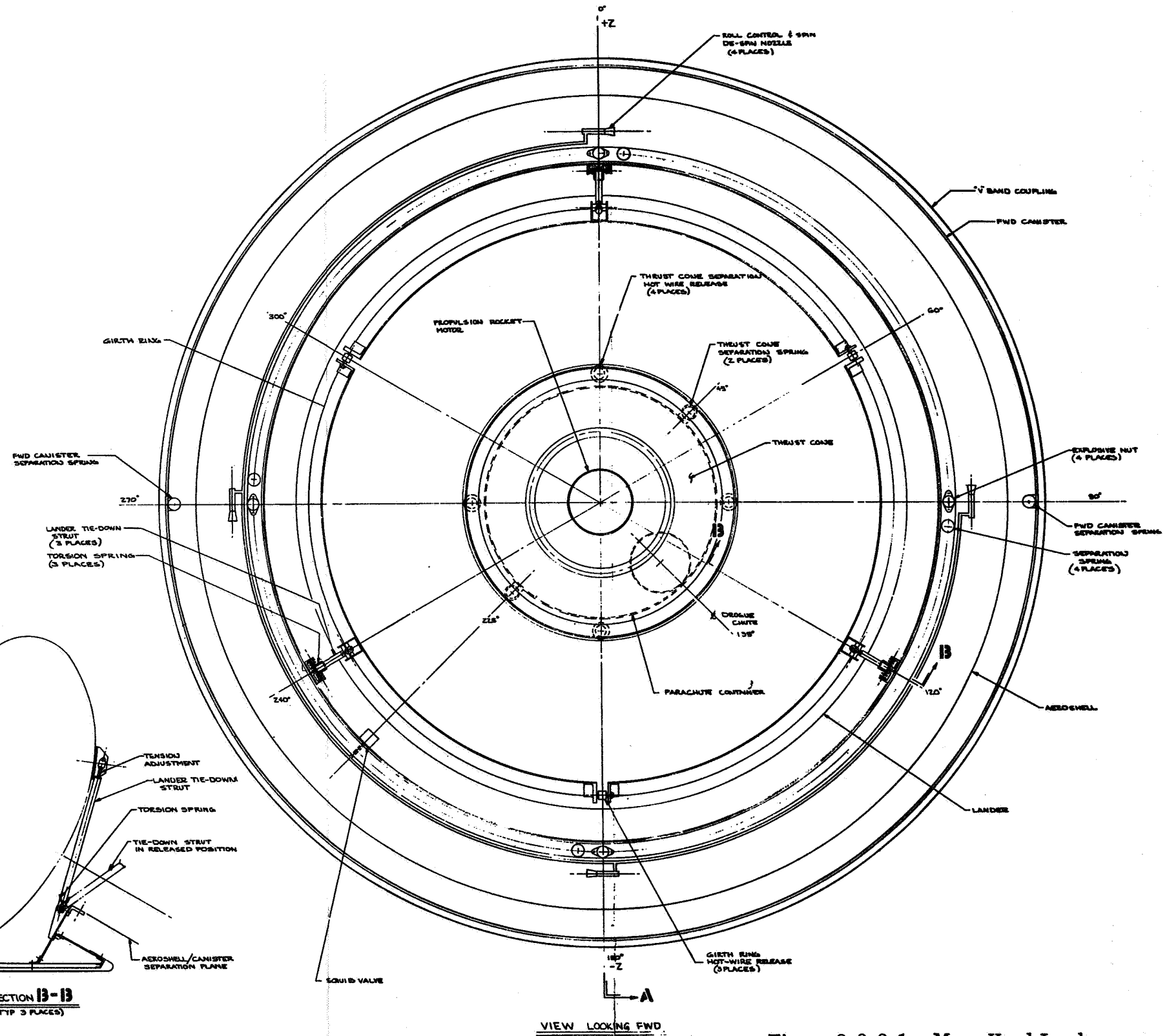


Figure 3.2.2-1. Mars Hard Lander, Point Design 1

TABLE 3.2-3. WEIGHT AND INERTIA COMPOSITION, POINT DESIGN 1

Capsule Systems	Weight (lb)	Roll ($slug/ft^2$)	Pitch ($slug/ft^2$)	Yaw ($slug/ft^2$)
Lander	858			
Aeroshell	160			
Retardation	228			
Propulsion	169			
Canister and thermal blanket	211			
Capsule at launch	1626	172	185	185
Capsule at separation	1415	140	138	138
Entry system	1246	138	136	136
Lander system	858	92	61	60

The interrelationship of the components has been separated into four classifications as indicated on the drawing: (1) unregulated power, (2) regulated power, (3) signals, and (4) data. For clarity, components are shown with the most meaningful functions indicated. For example ON/OFF signals are often considered to originate by correct power switching and are thus designated by a power flow line rather than a signal line. Furthermore, each individual line may carry one or more similar functions, such as different power levels.

The components are represented by uniform blocks with a common notation. The electrical reference designator is assigned in accordance with MIL-STD-16. The component's name is listed below and the location of the component is noted by the appropriate letter abbreviation at the extreme right of the block.

The electrical connections between individual components and between subsystems is designed such that it allows the appropriate operations to be performed. By referring to fig. 3.2.4-1, it can be seen that for a particular event, such as UHF transmission, there exists a specific group of components that must operate. These components are linked by several of the function lines. The sequence of events and flow of data can be traced as shown below. The appropriate type of power is switched through the power controller. This signal is supplied by the Lander programmer which initiates the power controller switching of all components required for the transmission of the data, whether in the electrical, telecommunication or scientific payload subsystem. The correct interconnections then allow data flow from the science subsystem to the telemetry subsystem.

Although other events require a different series of components, the relationship of component functional line designations to events is similar. A separation event is

FOLDOUT FRAME (1)

FOLDOUT FRAME

FOLDOUT FRAME

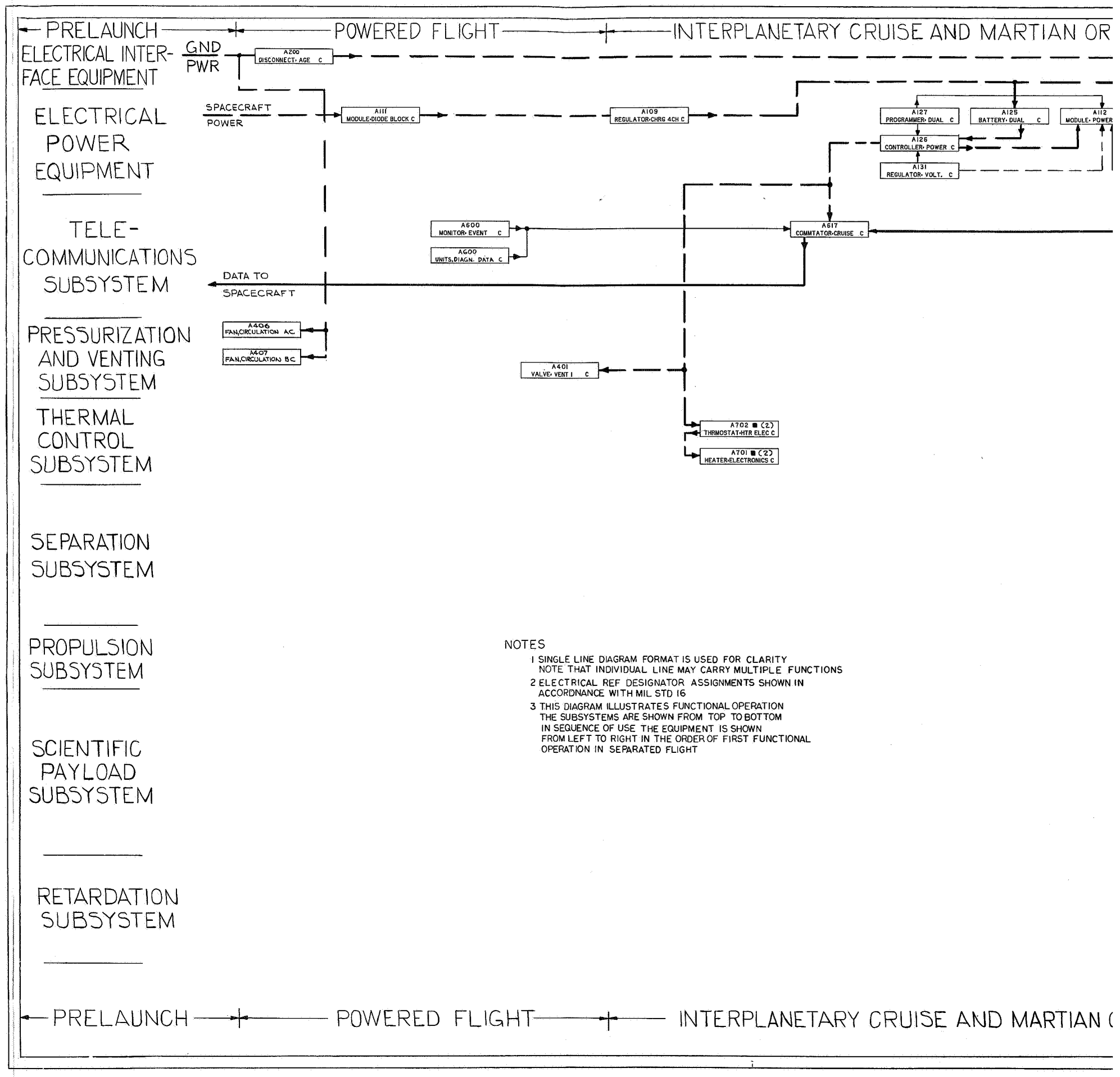
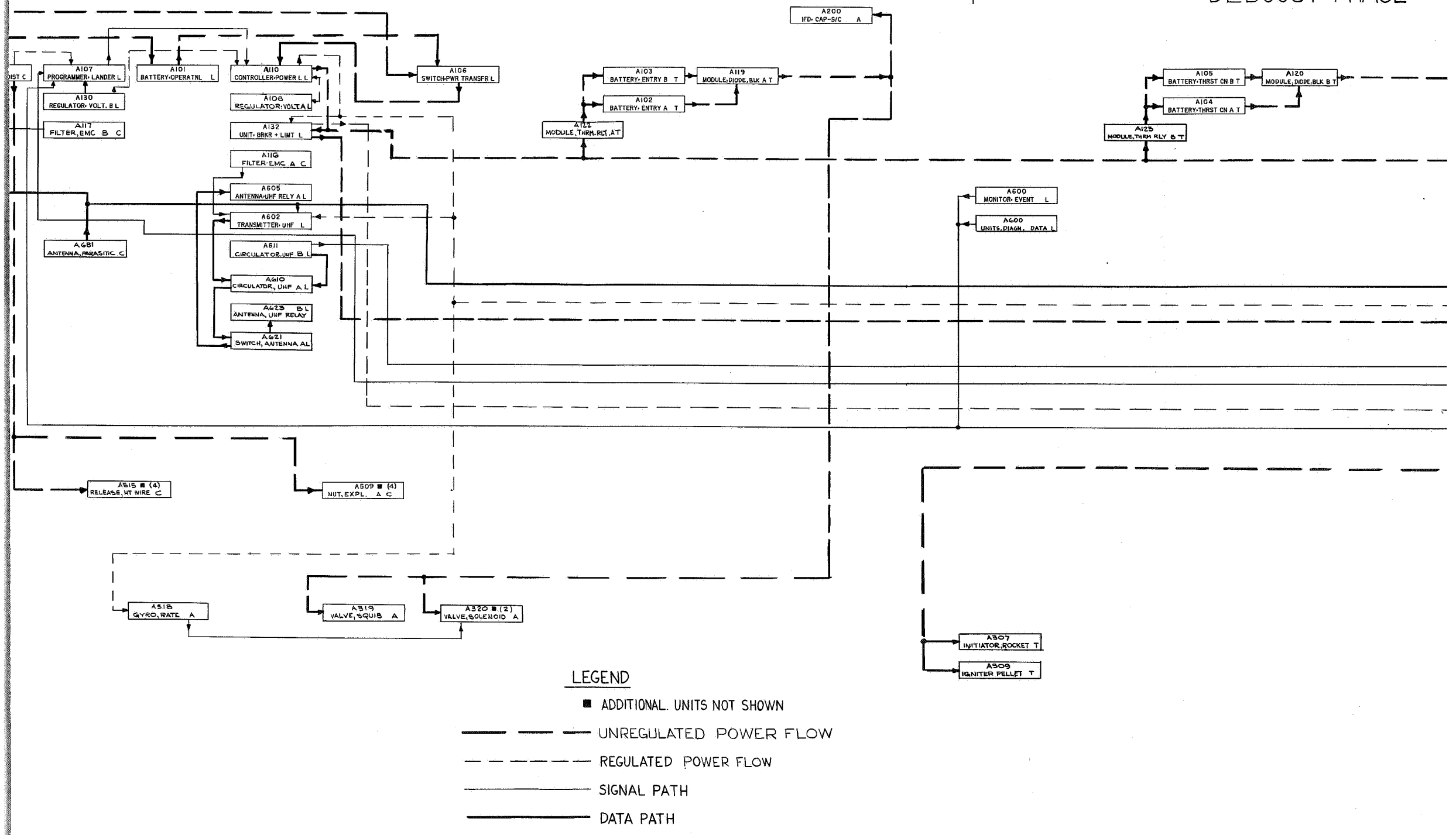


Figure 3.2.4-1. Electrical System Signal and Power, Functional Block Diagram, Point Design 1 (Sheet 1 of 2)

FOLDOUT FRAME (2)

BITAL FLIGHT — SEPARATION PHASE — DEBOOST PHASE



LEGEND

■ ADDITIONAL. UNITS NOT SHOWN

UNREGULATED POWER FLOW

REGULATED POWER FLOW

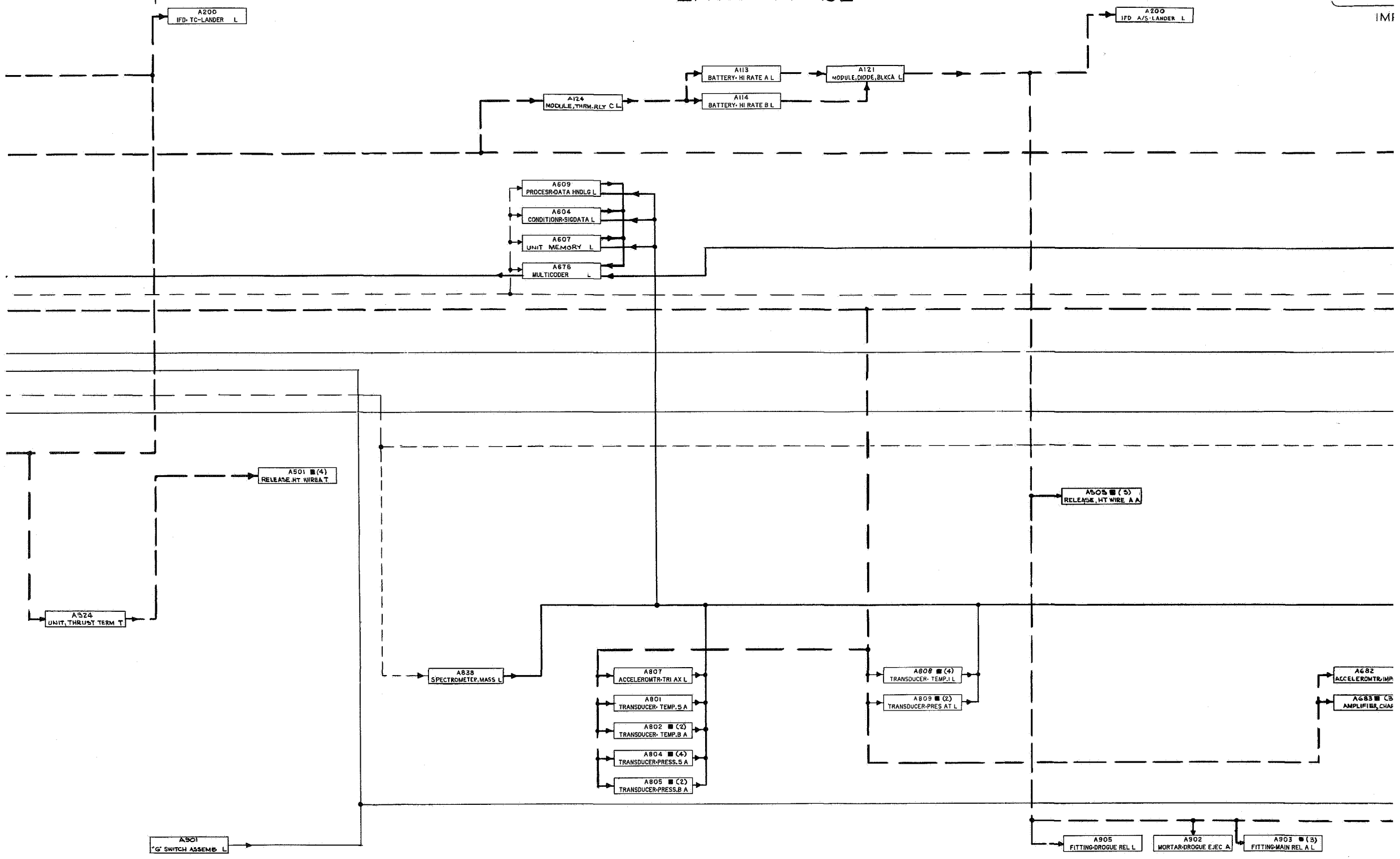
SIGNAL PATH

DATA PATH

RBITAL FLIGHT — SEPARATION PHASE — DE BOOST PHASE

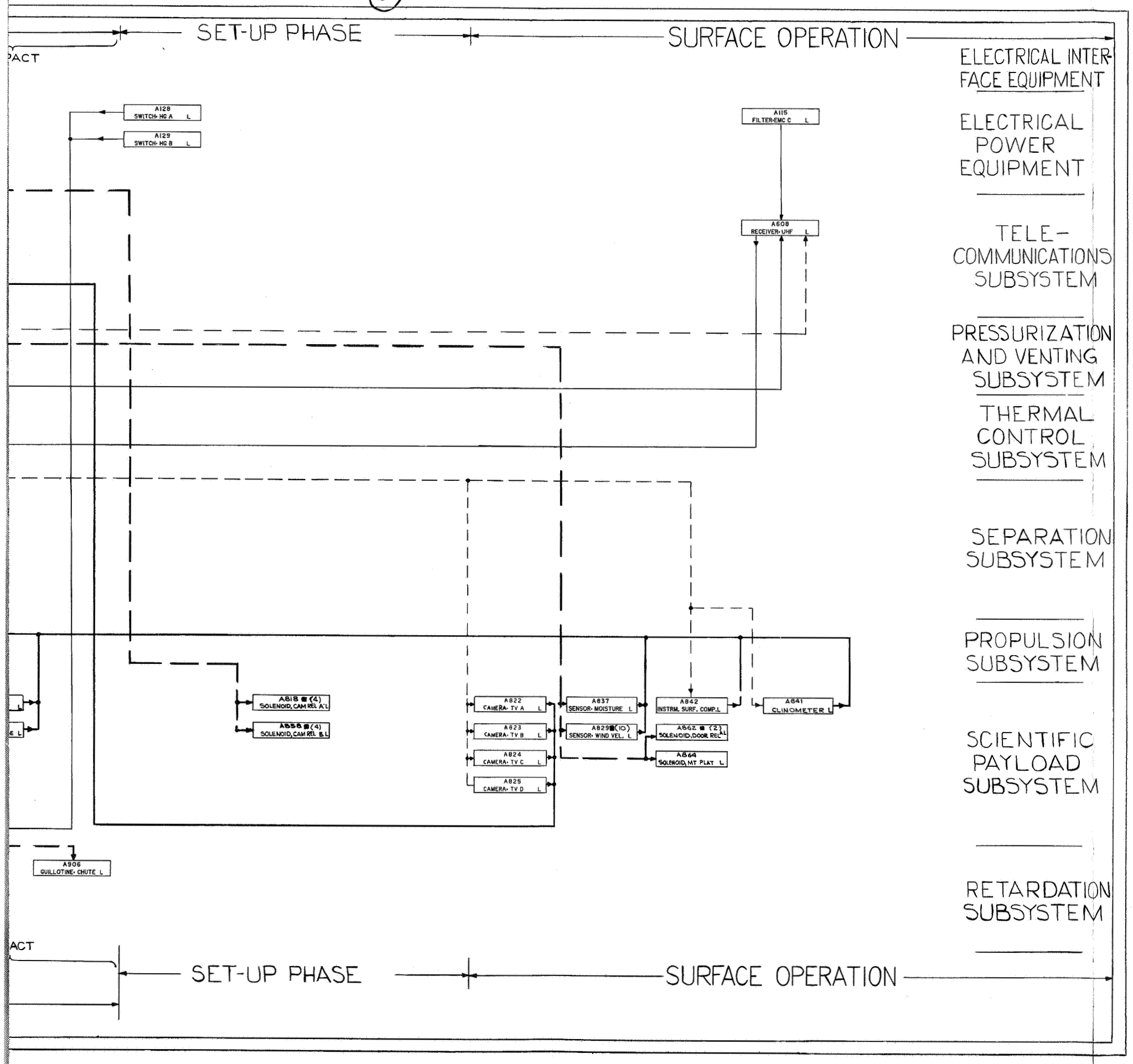
FOLDOUT FRAME (1)

ENTRY PHASE



ENTRY PHASE

FOLDOUT FRAME (2)



FOLDOUT FRAME

Figure 3.2.4-1. Electrical System Signal and Power, Functional Block Diagram, Point Design 1 (Sheet 2 of 2)

preceded by the Lander programmer signalling the power controller which turns on the stepping switch and connects the capacitor discharge circuit. These then supply the pulse loads as required.

Similar interconnections exist for all other events and the same scheme of functional operations is carried throughout the drawing. These component-subsystem relationships then become the foundation for the harnesses that physically supply the required electrical interconnections.

3.2.5 POWER PROFILES, POINT DESIGN 1

The power profile, as illustrated in fig. 3.2.5-1, represents the power demand sequence on the operational battery. By relating these demands to the event times, the curves reflect the mission sequence of events, since each pulse is the power required by all the components operating at the event.

Superimposed on a continuous level of power are the various events. The operational battery is activated prior to Capsule/spacecraft separation. It then supplies the required power for telemetry transmission during de-orbit and entry. In addition, entry science data is transmitted until impact.

After impact, the UHF relay link transmits the stored data with a real time imagery period. The meteorological sampling period begins at 20 min intervals with clinometer readings every 6 hr. The surface composition instrument represents the relatively high continuous power level during the first day. The diurnal day concludes with another UHF relay transmission of stored data and real time imagery.

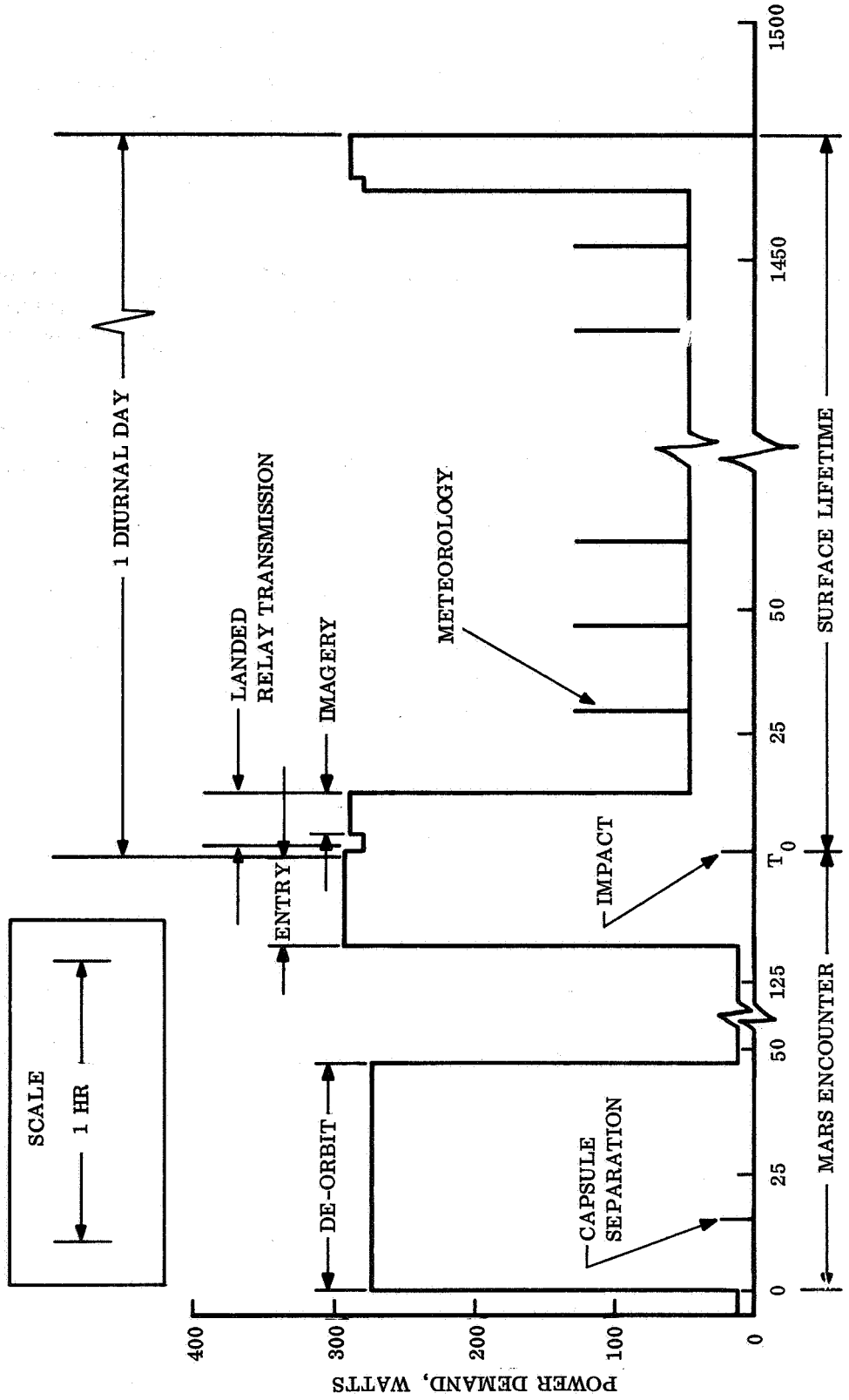


Figure 3.2.5-1. Power Profile, Point Design 1

3.3 PRE-ENTRY SYSTEMS

3.3.1 CANISTER

3.3.1.1 Design Constraints

Canister design constraints for Point Design 1 were as follows:

1. Maximum diameter less than specified in Section 2.3.1 (103.9 in.)
2. Withstand an internal pressure
3. Withstand the inertial loads of launch and powered flight
4. Provide adequate clearance between the aeroshell heat shield and canister
5. Provide a separation and field joint as one and the same joint
6. Provide support for the entry system.

Diameter constraints on the maximum allowable canister diameter are fully described in Section 2.3.1 and were imposed by the internal envelope available for the Capsule system installation.

Due to the requirement to maintain biological integrity within the internal portion of the canister, it was necessary to evaluate the effects of an internal pressure on the shape, material and construction of both the forward and aft canisters. Inertial loading of the canister during flight and handling conditions, including equipment loadings on the aft canister, was a constraint which was traded off against the differential pressure to determine the more severe loading environment for the canister structure.

A driving influence on the canister size was the allowance necessary for clearances between the entry system and canister. This clearance has been estimated to be 1.9 in., as shown in fig. 3.3.1-1, to allow for Capsule system dynamic excursions.

The field joint for the canister could be combined with the device used for in-flight separation as it could be entirely separated. Maximum leak tightness was an over-riding criteria in either case.

The entry system must be supported within the Capsule system and a means of support had to be designed. This design considered that in addition to support, it must have the capability of withstanding and transferring the entry system inertia loads through the structure and to the Capsule bus interface to the bus adapter ring.

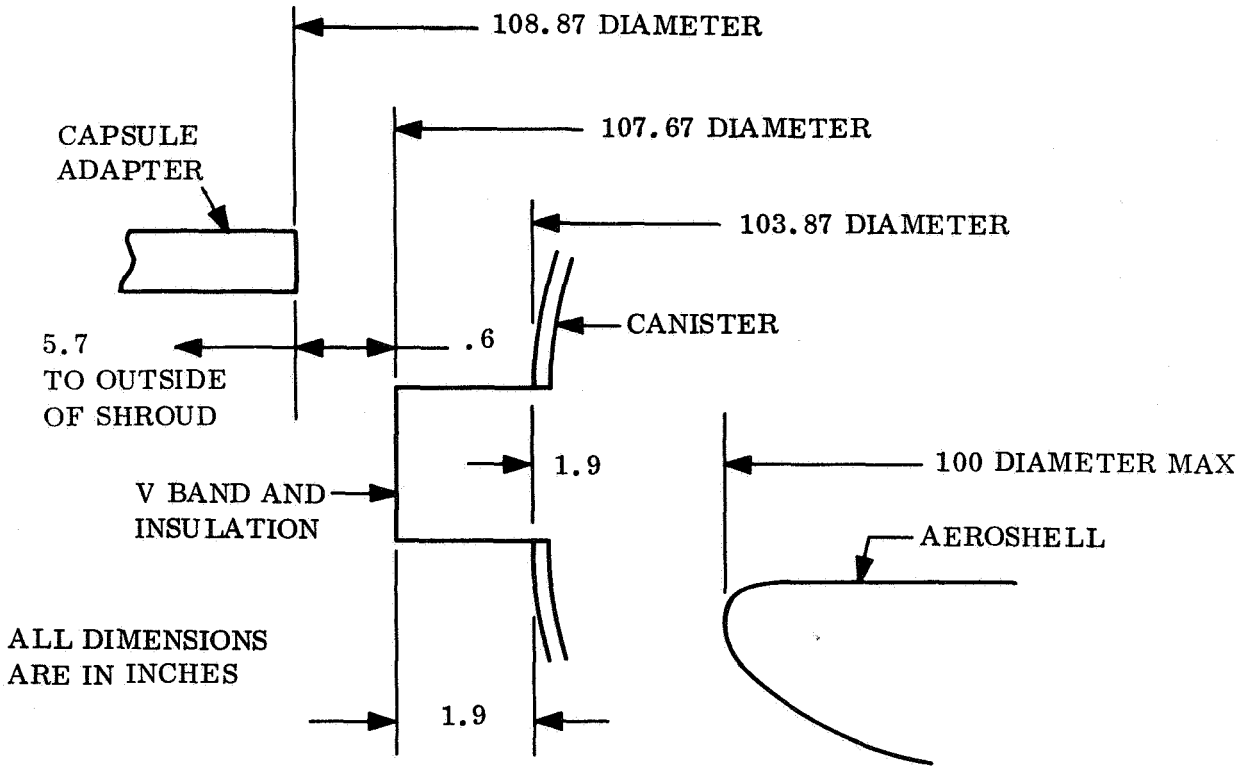


Figure 3.3.1-1. Aeroshell/Canister Clearances

3.3.1.2 Canister Structural Description

The forward canister is a hemispherically-shaped minimum gauge aluminum shell making a tangent at its maximum diameter through a quarter torus section, fig. 3.3.1-2. This structure has been designed to act as a pressure vessel, and the torus section provided to eliminate the inboard kick loads and minimize shell bending at the field joint ring due to the internal pressure. The minimum gauge aluminum material is more than adequate to withstand the pressurization and inertial loads imposed on it. The hemispherical shape has been shown in previous analyses (Voyager Phase B Study) to be considerably stiffer from a dynamics standpoint than a conical shape.

The forward canister has been designed such that there will be no yielding under design load conditions and no failure under ultimate design load conditions. This includes the transient and steady state loads encountered under the conditions of handling, transportation, sterilization, pre-flight, powered flight, transit, and separation.

Inertial loading conditions were determined to be less severe than the internal pressurization condition in the design of the canister and the field joint ring. This can be seen in table 3.3.1-1, where the running loads on the interface ring are

FOLDOUT FRAME

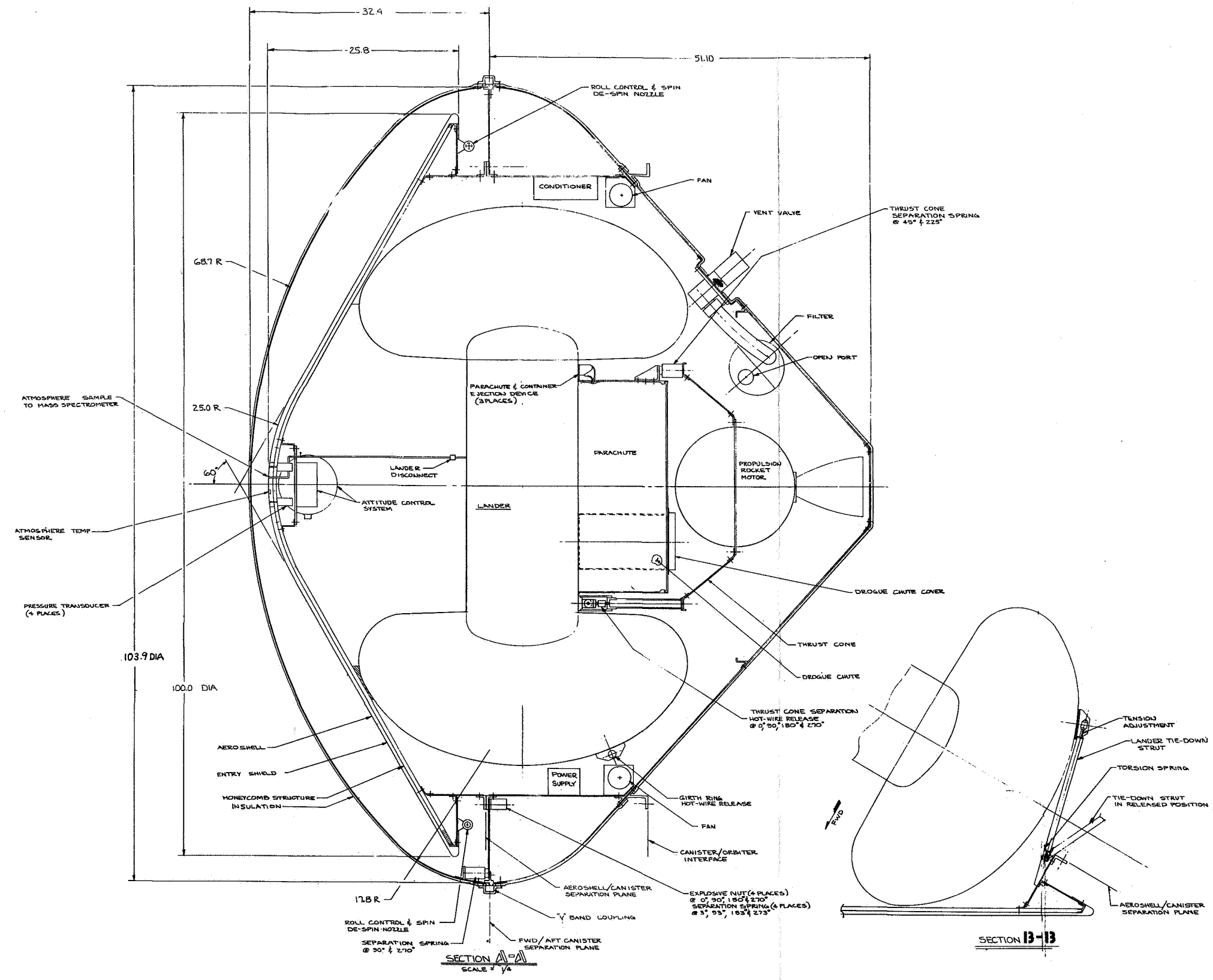


Figure 3.3.1-2. Inboard Profile, Point Design 1

TABLE 3.3.1-1. STRUCTURAL ANALYSIS, CANISTER LOADS

Load Condition	Vertical Load W_V (lb/in.)	Inboard (horizontal) Load W_H (lb/in.)	
C	1.06	0.38	
E	1.92	0	
F	0.30	1.92	
C&E	2.98	0.38	
C&F	1.38	2.27	
M	27.85	0	0.5 psi skin pressure
N	55.7	0	1.0 psi skin pressure

tabulated for both inertial and pressure loading conditions. As a result, the pressure loading condition determined the desired construction, material and thicknesses to be used in the structural design of both the forward and aft canister.

Minimum sheet gages were the over-riding constraint on the thicknesses selected for the canister design. Stiffeners to rigidize the shell for dynamic and ground handling loads have been provided. The limit pressure condition for the canister is 1.0 psid internal pressure, and the structure is adequate to withstand a 1.7 psid burst pressure, which results in a safety factor of 1.7 on the limit pressure.

The field joint rings for the forward and aft canisters provide a seat for the band clamp, which holds the canister halves together, resists the loads imposed by the internal pressure and the band clamp, and provide for the pressure tight sealing of the canister assembly. The aft canister ring slides under the forward mating ring and has an internal leg, as shown in fig. 3.3.1-3, which is connected to a bulkhead joining the ring with the internal adapter. This arrangement provides a torque box in the aft canister, increasing both its stiffness and structural load carrying capability.

The combined inertia of the forward ring, aft rings, and bulkhead is more than adequate to insure structural stability of the field joint under the critical load condition. Fig. 3.3.1-4 shows a plot of the required inertias for ring stability as a function of critical load in lb/in.

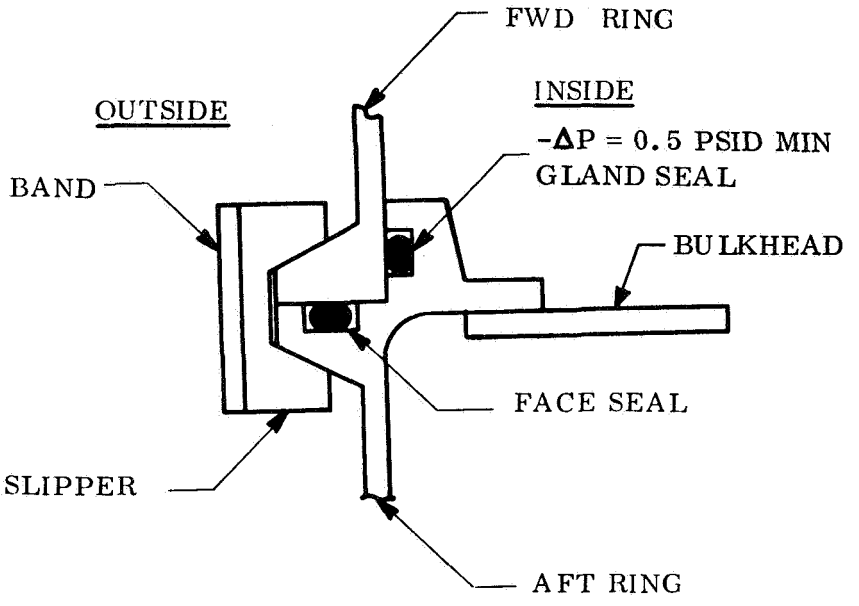


Figure 3.3.1-3. Canister Field Joint

Structurally, the aft canister is sized for the internal pressure which dictates the same minimum sheet gauge as the forward canister. The aft canister is essentially conical in shape with the forward end, a quarter torus making a tangent with the maximum diameter and the conical afterbody as shown in fig. 3.3.1-2. Stiffening members are located between the adapter to canister ring and the end bulkhead ring. These members also act as supports for the electrical equipment and vent system equipment in the aft canister.

3.3.1.3 Internal Adapter

The adapter for Point Design 1 is designed to support the entry system and transfer loads introduced by the entry system to the Capsule bus interface ring. This adapter is internal to the sterilization canister and interfaces with it at the aft canister ring. The adapter picks up the entry system at four points and attaches to the Capsule bus interface ring through the canister skin.

Structurally, the internal adapter is a cylindrical aluminum shell with longitudinal stiffeners, as shown in fig. 3.3.1-2. The shell and stiffeners have been sized such that the section modulus and working area are more than adequate to withstand the bending moment and axial loads which the structure will experience. The inertial loads used in determining the necessary section properties of the cylindrical skin and stiffeners were 6 g's limit in the axial direction and 2 g's limit in the lateral direction.

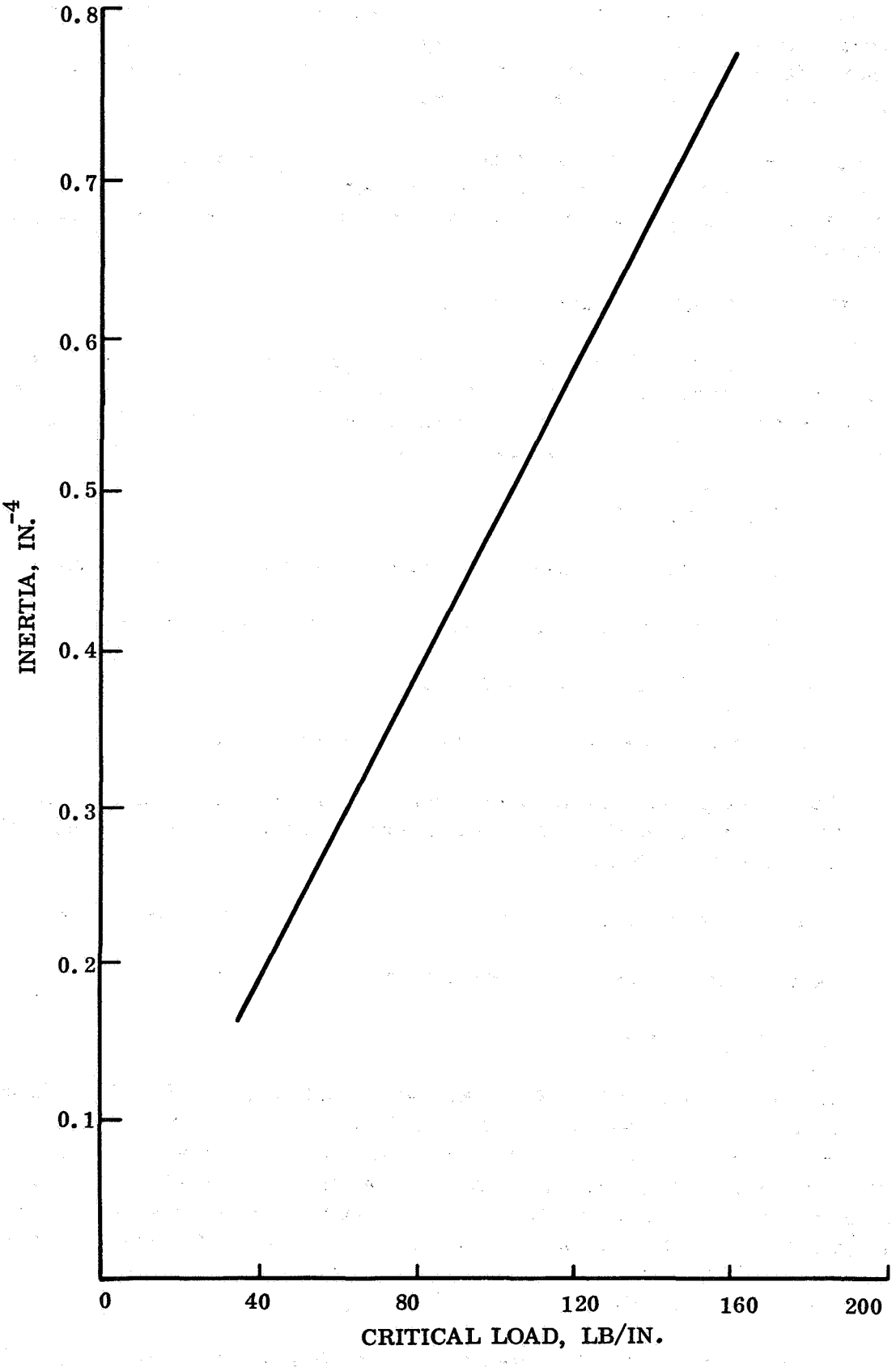


Figure 3.3.1-4. Required Ring Inertia for Stability as a Function of Critical Load

The forward ring, at the entry vehicle interface, attaches to a lateral interconnection to the aft canister interface ring. Lightening holes have been placed in the cylindrical structure to allow for free passage of heated gases between the canister and adapter during heat sterilization cycles. The lateral interconnection or bulkhead provides support for the aft canister ring as well as the adapter.

The spring-pusher housing is located on the inside of the adapter at the interface with the entry system. This device provides the separation force necessary to eject the entry system from the bus. Separation forces are reacted through the adapter skin and stiffeners.

3.3.2 PRESSURE AND VENTING SYSTEM

The basic function of the pressure and venting (P&V) system for Point Design 1 is to prevent recontamination of the Capsule by maintaining a minimum specified differential pressure (ΔP) between the canister and the ambient environment. This positive ΔP is maintained from sterilization until prior to canister separation.

3.3.2.1 Design Constraints

The P&V system has been designed to fulfill the following design constraints:

1. Provide inlet and outlet ports into the canister for sterilization
2. Provide for circulation of air during sterilization
3. Provide pressure relief - due to temperature variations
4. Maintain a positive ΔP between 0.5 and 1.0 lb/in.^{2} differential (psid) between the canister and ambient atmosphere from sterilization until exit from the earth's atmosphere.
5. Vent 70 ft^3 of internal air during ascent to maintain ΔP below 1 psid.
6. Evacuate all entrapped gases to ambient space vacuum.

3.3.2.2 System Description

The primary function of the P&V system is to vent the internal canister during sterilization, after sterilization and during flight to prevent the internal pressure from exceeding 1 psid. This is accomplished using a combination relief valve with a solenoid over-ride which opens at a nominal pressure of 15.6 psia with increasing pressure and closes at a nominal pressure of 15.3 psia with decreasing pressure. A biological filter is installed upstream of the valve to filter out any bacteria flowing upstream. Relief of a pressure build-up due to a temperature increase is accomplished using the same valve described above.

The block diagram of the P&V system for Point Design 1 is shown in fig. 3.3.2-1.

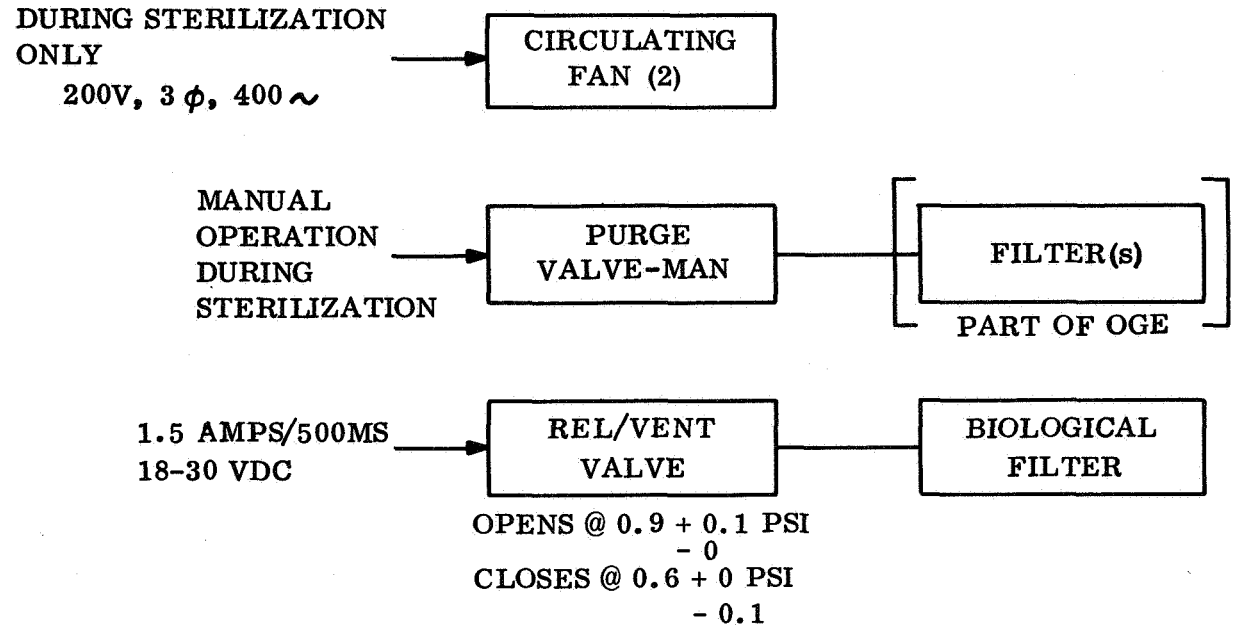


Figure 3.3.2-1. Pressure and Venting Subsystem, Block Diagram

During sterilization, the P&V system provides for inlet and exit of sterilized gas (and decontaminating gases if used) by using a manually operated inlet valve connected to the sterile, filtered air supply, and electrically opening the vent valve for use as the outlet port. Since the gas will pass through the biological filter, it must be prefiltered to prevent clogging of the prime flight filter. Two circulating fans are used to speed up the heating and cooling cycles and to eliminate hot spots. These fans are used only during sterilization and their power will be provided by GSE. After sterilization, the make-up gas supply is connected to the manually operated valve. The canister is vented after launch and throughout powered flight until the internal pressure reaches 0.5 psia. The canister remains pressurized at ~ 0.5 psia less leakage, after exiting the Earth's atmosphere until prior to canister separation; at which time the vent valve will be electrically opened to evacuate the canister to near space vacuum.

To minimize the possibility of backflow during venting, the exit port from the canister is shaped as a convergent nozzle. It has been shown that in a convergent nozzle flow separation does not occur. Thus the possibility of gas flow upstream during venting is almost nil. This fact would preclude the entry of bacteria during the venting process when the valve is open.

3.3.2.2.1 Canister Venting

The vent valve is used to vent the canister during powered flight. Its size is determined by the amount of gas and maximum permissible Δ P. For Point Design 1 there is an initial volume of 70 ft^3 of air, and the maximum allowable Δ P is 1 psid. The nominal fill pressure will be 15.45 psia at 70°F. From the P&V parametric study, the vent area required for 70 ft^3 of air is 0.75 $in.^2$; and assuming a C_D for the value of 0.7 gives a required valve aperture equivalent to a 1.07 $in.^2$ circular orifice.

The valve is a spring-loaded, pilot-operated relief valve with a latching, override solenoid, and a position indicating switch. This valve design permits its use for relief, venting, purging and evacuation. The proposed design will be similar to Sterer P/N 19260, Pneumatic and Pressure Control Valve Assembly. The basic changes required to the valve relate to operating pressure and orifice area. The reference valve weighed 3.0 lb, and it is estimated that the proposed valve will weigh 4.0 lb. Electrical power required for the solenoid is 1.5 amps at 30 vdc at 70°F for 1/2 sec maximum.

The outline of the proposed valve is:

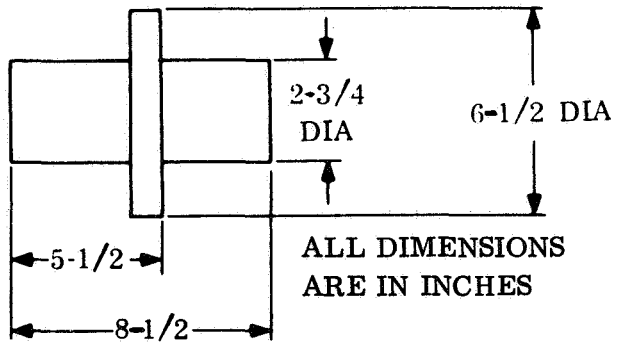


Fig. 3.3.2-2 shows the approximate Δ P time history for a valve that opened and remained opened. Obviously, this method will not meet the requirement for maintaining the Δ P > 0.5 psid. The relief valve will act as a controller and it is expected that the valve will close in the cross-hatched portion of the curve. The valve will be set to open at $0.9^{+0.1}_{-0}$ psid on increasing pressure and to close at $0.6^{+0}_{-0.1}$ psid on decreasing pressure. The valve will most likely cycle several times during the first 20 sec and remain open until L.O. +90, after which time it will remain closed until opened prior to canister separation.

The biological filter is used to prevent bacteria migration into the Capsule through the vent valve. The filter is installed in series with the valve and upstream of it. The filter is required then, to filter bacteria (0.3 microns) in the backward direction while presenting a low pressure drop to the air being vented. The filter size is governed by the maximum flow, the pressure drop and the differential pressure (Δ P).

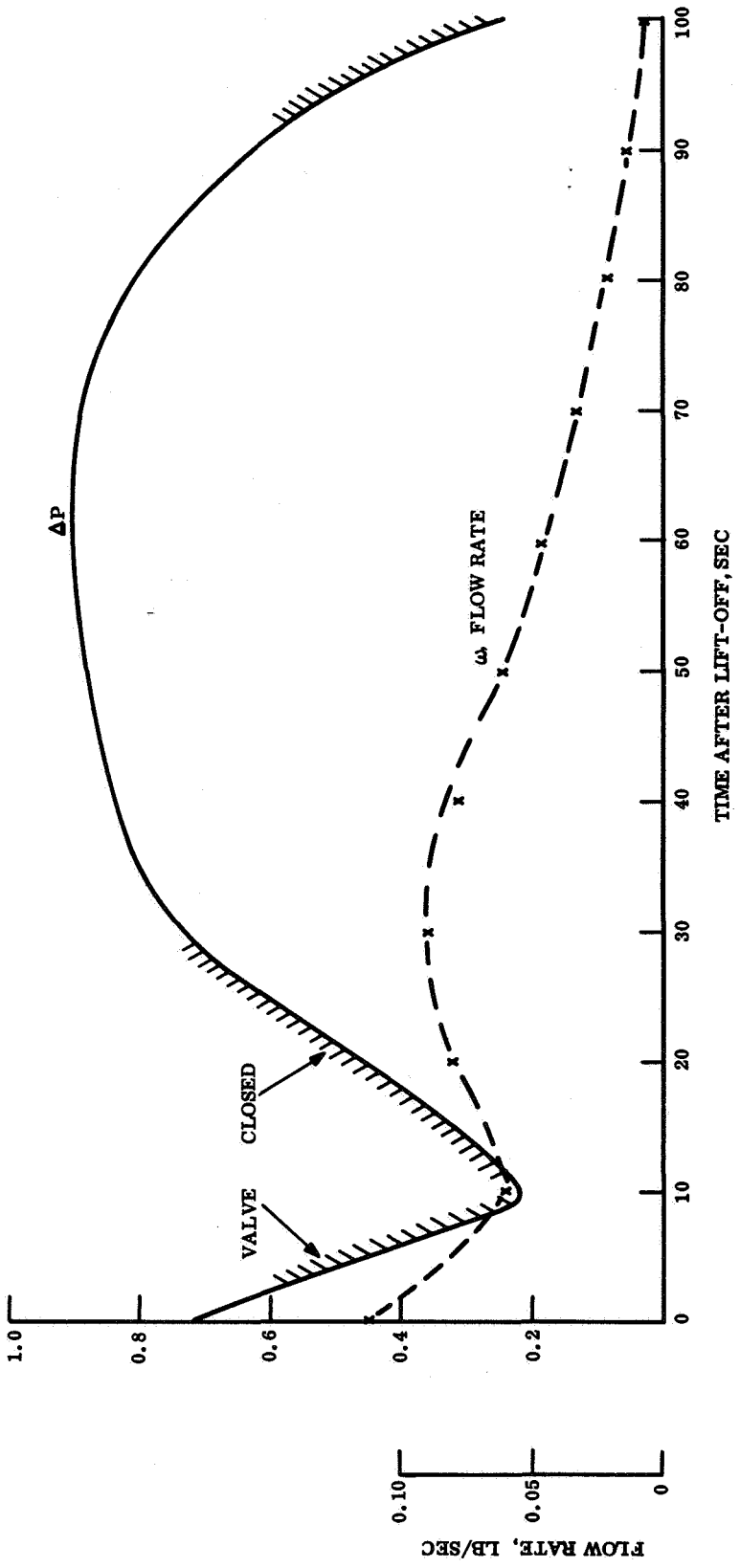


Figure 3.3.2-2. Flow Rate and Differential Pressure vs Time After Lift-off

The maximum calculated flow for Point Design 1 (70 ft^3 of air) was 0.116 lb/sec or 91 scfm. For the 1 psid Δ P system and a specified pressure drop of 0.3 psi, a filter area of approximately 2.6 ft^2 is required. Using Pall Corporation's Ultipor 0.9 medium, an element size of 6.6 in. long x 2.5 in. diameter is obtained. The filter assembly will be 7.6 in. long x 3.0 in. diameter and would weigh approximately 1 lb.

The choice of Ultipor 0.9 was made because it presents a lower pressure drop than Ultipor 0.15, while satisfying the filtering requirements. It has a catalog rating of 100 percent removal of 0.08 micron particles in dry air. The filter can be decontaminated with ETO and has a temperature rating of 350°F in air.

To maintain the necessary flow, the filter housing requires 1-1/8 in. ports and will be connected to the vent valve with 1-1/8 in. aluminum tubing.

3.3.2.2.2 Canister Sterilization

During canister sterilization, air will be introduced into the canister to speed up heating or cooling through the manually operated valve. Using 1/4 in. tubing and a valve with an area of 0.25 $in.^2$, 5.4 cfm of air can be introduced at 1 psid (15.7 psia); thus the canister air will be changed 4+ times in one hour.

Two fans, Rotron Manufacturing Company, type AXIMAS 1, Model 367 QS, with a delivery of 19 cfm at 1 in. H_2O sp. will be used to circulate air during sterilization, thus reducing warm up times, eliminating hot spots, and insuring that the entire Capsule reaches sterilization temperature.

Power required for the fans will be provided by OGE and shall be as follows: 200v, 3 φ, 400 $\sim$, 0.1 amp line current per motor. Fan size is 1.75 in. diameter x 1-1/2 in. long and weight is 4 oz.

3.3.3 SEPARATION SUBSYSTEM DESCRIPTION

3.3.3.1 Design Constraints, Functions and Requirements, Point Design 1

The separation subsystem performs the following pre-entry functions:

1. Separation of the forward canister
2. Separation of the Capsule assembly
3. Separation of the thrust cone assembly
4. Separation of the aeroshell.

The subsystem has been designed to meet the following requirements in addition to the usual environmental criteria:

1. Provide field and separation joints for the canister

2. Eject the canister for Point Design 1 at 2.5 ± 0.3 fps

3. Maintain a pressure-tight joint from sterilization through exit from the Earth's atmosphere for a maximum internal pressure of 1.67 psid. Pressure-tight is defined as leakage which results in less than 0.002 psi drop/hr at 70^{o}F.

4. Maintain maximum attainable pressure tightness during space cruise where outside temperature may be as low as -300^{o}F

5. Maintain sterility of Capsule

6. Separation shall not produce debris or loose objects

7. Attach the Capsule at four points

8. Eject the Capsule at 1.5 ± 0.25 fps separation velocity from the Orbiter with tip-off rates of $< 0.5^{o}$/sec to the Capsule. Orbiter's pitch inertia equals Capsule's.

9. Separation shall not cause collision with any of the remaining payload

10. Attach and separate the thrust cone at 1.0 fps minimum

11. Attach and release the aeroshell

12. Provide electrical separation as required

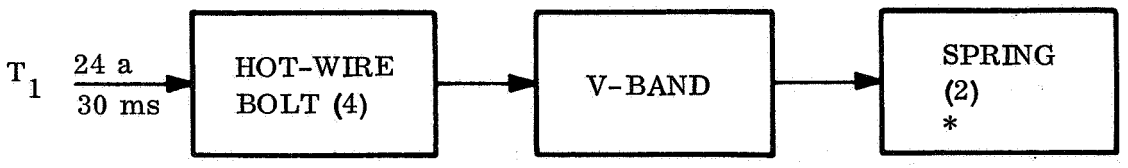
13. Optimum reliability and subsystem performance is paramount to mission success. Use proven concepts.

Other system constraints - electrical power, distribution, timing, and signal lockout shall be provided by the EP&D subsystem.

3.3.3.2 General Subsystem Description - (see fig. 3.3.3-1)

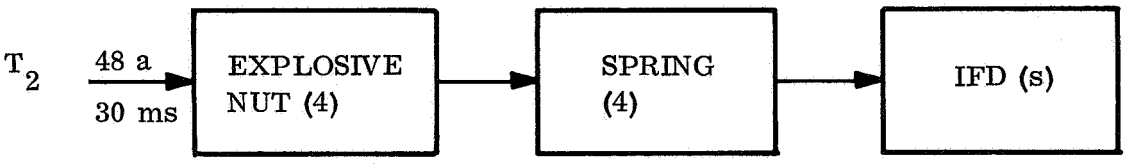
The canister halves are joined by a V-band assembly consisting of independent slippers attached to a strap. The band is made in four equal segments joined by hot-wire tension bolts. The hot-wire bolt is a nonpyrotechnic, mechanical device consisting of a turnbuckle coupling which separates when an electrical signal is applied to a hot-wire element which kept the turnbuckle together. The forward canister is ejected using two helical coil compression springs. The rings, to which the V-band clamps, perform double duty by providing the groove and sealing surfaces for the O-ring type pressure seal. After separation, the V-band segments remain attached to the aft canister via springs and lanyards. The canister is completely evacuated by the P&V S/S prior to separation.

FWD CANISTER SEPARATION

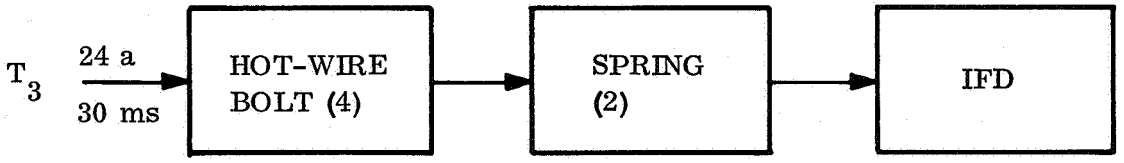


* 4 SPRINGS FOR POINT DESIGNS 2A, 2B, 4, 6

CAPSULE SEPARATION



THRUST CONE SEPARATION



AEROSHELL SEPARATION

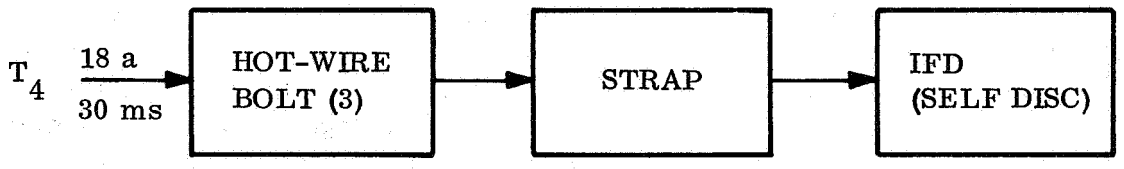


Figure 3.3.3-1. Separation Subsystem, Block Diagram

The Capsule assembly is separated from the Orbiter approximately 10 min after canister separation. The Capsule is attached to the adapter at four points by explosive nuts, but a hot-wire type of coupling is also being investigated. The Capsule is ejected at 1.5 fps nominally, by four helical coil compression springs.

The thrust cone assembly is attached to the Lander/aeroshell assembly by four hot-wire tension bolts. Two helical coil compression springs identical to the ones used for canister ejection are used to eject the thrust cone at 3.1 fps, nominally. The thrust cone is separated after the de-orbit function is completed.

The aeroshell is attached to the Lander by a strap assembly retained by three hot-wire tension bolts and released after parachute deployment. This system is described in Section 3.4.4 of Volume IV.

The weight of the subsystem as described above based on an 8.7 ft diameter canister is:

Canister	
V-band assembly	7.0
4 hot-wire bolts	0.8
2 springs	0.2
2 spring housings, adjustable	0.7
Capsule	
4 explosive nuts	1.0
4 springs	0.8
4 spring housings, adjustable	1.4
Thrust Cone	
4 hot-wire bolts	1.0
2 springs	0.2
Aeroshell	
1 strap	1.2
3 hot-wire bolts	0.6
TOTAL	14.9 lb

The following sections discuss the detail designs.

3.3.3.2.1 Canister Separation

The selection of the separation method for the canister is governed by the requirement for a sterile, pressure-tight joint for a large, flexible structure. This basic requirement limits the separation joint design to one that can apply a continuous distributed force, such as, flexible shape charge, various types of MDC or primer cord, V-bands, closely spaced bolted joint, pyro fuze joint system, or a thermal heat pad joint system. The V-band system was selected because of its simplicity, reliability, low separation shock, lack of debris, tolerance to temperature environment, elimination of the need for a field joint, and because it presents a tortuous path for microbial access to the separation interface.

The band must meet the following specific requirements:

1. Contain proof pressure without yielding
2. Provide the necessary clamping force without yielding
3. Contain the burst pressure without breaking
4. Make allowance for creep at low temperature over a 9 month period.

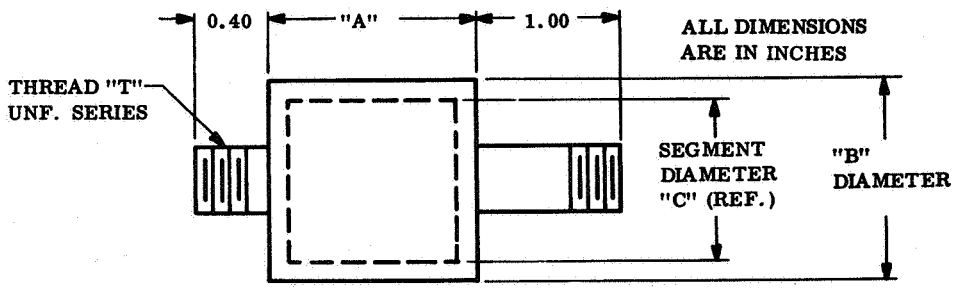
The V-band assembly is made in four segments, with the strap material being 2024T86 aluminum, 1 in. wide x 0.032 in. thick. The slippers, which are attached to the band by clips, are made of 7075T73 aluminum. The band is preloaded to 1100 pounds ±10% in order to sustain all loads, allow for creep during cruise and tension variations during assembly. (See Volume III, Appendix B for load and stresses in band.)

The V-band segments are held in tension by the four hot-wire* bolt assemblies. The choice of four points for attaching and torquing was made to maintain nearly uniform tension on the entire band and to facilitate band disengagement. The hot-wire bolt is a mechanical separation device which utilizes the reduction of tensile strength property of a material upon heating to actuate. Upon application of 6 amps for 30 msec the hot-wire element breaks and separation occurs. The hot-wire bolt consists of two separate studs connected by a segmented coupling. The coupling is held together by the hot-wire element, so that tension can be carried by the mechanism.

The required preload can be applied through 3/8 in. diameter thread and a 0.69 in. outside diameter coupling (see fig. 3.3.3-2) made of 17-4 PH, Cond 1050, with an ultimate load capacity of 8000 lb tension. Nine turns of 0.014 in. diameter 302 stainless wire form the hot-wire element. The segments of the coupling are retained so that there is no debris. This unit is ideal for long service in space because of its all metal design. The band will separate if any of the four bolts operate.

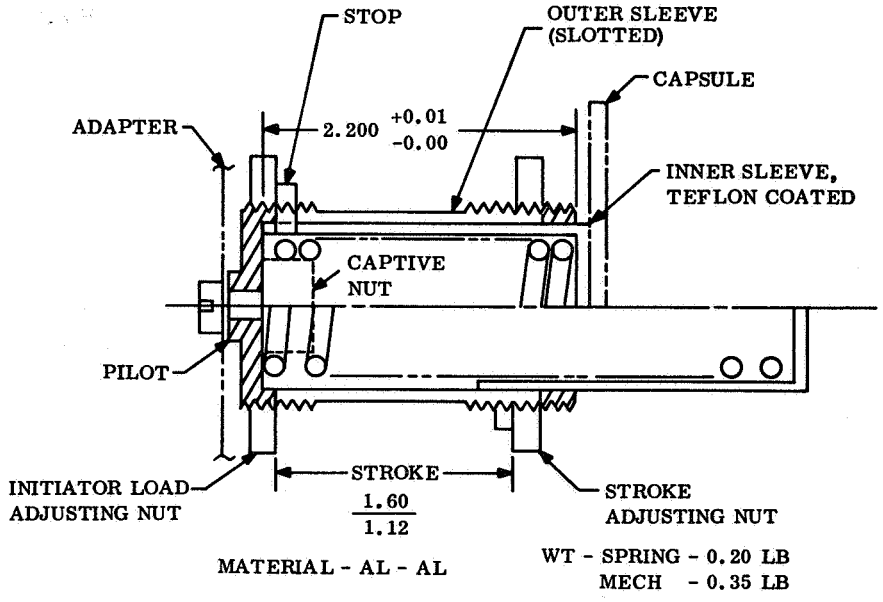
The forward canister is ejected by two helical coil compression springs. The springs provide 35 lb of initial force each and have a working stroke of 2 in. They will impart a velocity of 2.7 ± 0.25 fps to the canister. The springs are of 302 stainless steel, stressed at 90,000 psi and are retained with the aft canister, in an adjustable subassembly (see fig. 3.3.3-3). Tip-off rates will be less than 2.0 deg/sec about any axis. Center of gravity offsets are expected to be minimal since the forward canister is of symmetric construction.

* (The hot-wire bolt is GE-RS proprietary design)



MAX LOAD (LB)	PHYSICAL DATA				HOT WIRE DATA				
	A	B	T	C	WIRE DIA	NOTCH DIA	NO. OF TURNS	A. F. CURRENT	WT LB
8000	0.90	1.00	3/8	0.69	0.014	0.0040	9	6.0	0.20
12,000	1.15	1.32	7/16	1.00	0.020	0.0660	11	9.0	0.44
19,000	1.40	1.62	1/2	1.30	0.025	0.0075	13	12.0	0.81

Figure 3.3.3-2. Hot-wire Tension Bolt



SPRING DATA

WIRE DIA	-	0.148 IN.
O. D.	-	1.034 IN.
SPS. CONST	-	75 LB/IN.
TOTAL TURNS	-	14.7
MAX LOAD	-	120 LB
NOM LOAD	-	108 LB
LS	-	2.19 LB
LF	-	3.79 IN.
NOMINAL STROKE	-	.128 IN.

Figure 3.3.3-3. Capsule Separation Adjustable Spring Assembly

The canister separation joint seal utilizes two silicone rubber O-rings to attain a pressure-tight seal. The O-rings are used in two different modes to enhance sealing capabilities, one O-ring being a face seal and the other a gland seal (see fig. 3.3.1-3). This arrangement utilizes the axial and radial clamping forces of the V-band and closes off the clearances resulting from manufacturing tolerances, while retaining a machineable and structurally sound ring design. The basic cross section of the ring is depicted in figs. 3.3.3-4 and -5 for the Point Design 1 ring. The face seal O-ring is nominally 0.139 in. diameter and is compressed from 0.014 in. to 0.041 in., or 10 to 30 percent. The force necessary to compress this O-ring using 50 durometer silicone is from 1.2 to 12.0 lb/linear in. The gland seal is nominally 0.210 in. diameter and is compressed from 0.015 to 0.045 in., or 7 to 22 percent. The radial force to compress this ring is from 1 to 16 lb/linear in. The radial clamping force available, if the nominal axial clamping force of 45.1 lb/in. is attained, is

$$FR = FN\ (TAN) = 45.1\ (TAN\ 20^{o}) = 16.4\ lb/in.$$

which is adequate.

Silicone rubber material was selected because it has the best low temperature properties -- rated to -80°F for seals, but doesn't harden until -150 to -180°F. Therefore, it is expected that the seal will degrade during the space cruise. If it is mandatory that a seal be maintained, then thermal insulation could be applied to the band to keep the temperature above -150°F.

The ability of the separation joint to inhibit the penetration of bacteria is further enhanced by the tortuous path which they must follow to gain entry into the Capsule. The slipper is in full contact with the ring except for a 1/4 in. gap between the 5.75 in. long slippers, or a total of 96 percent of the circumference is covered by the slippers. The band, of course, covers the entire circumference except at openings for the hot-wire bolts, which probably will be about 1-1/2 in. long each, or 94.5 percent band coverage.

3.3.3.2.2 Capsule Separation

The main consideration for Capsule separation and ejection was the stringent tip-off rate requirement. To meet this requirement, it is necessary that the impulse generated by the separation device be either very low or nearly the same at all points. Likewise the ejection system must have controlled force and energy, with low variances; and c.g. offsets, and ejection system force axes must be controlled.

Separation devices that meet the above needs are ball locks, collet releases and explosive nuts. The latter were chosen because of their compactness and ease of use and installation. All of the above utilize pressure cartridges for operation, and for high reliability dual cartridges will be used. This introduces the problem of wide impulse variance as a function of gas pressure (a function of cartridge design, simultaneity, and number of cartridges firing).

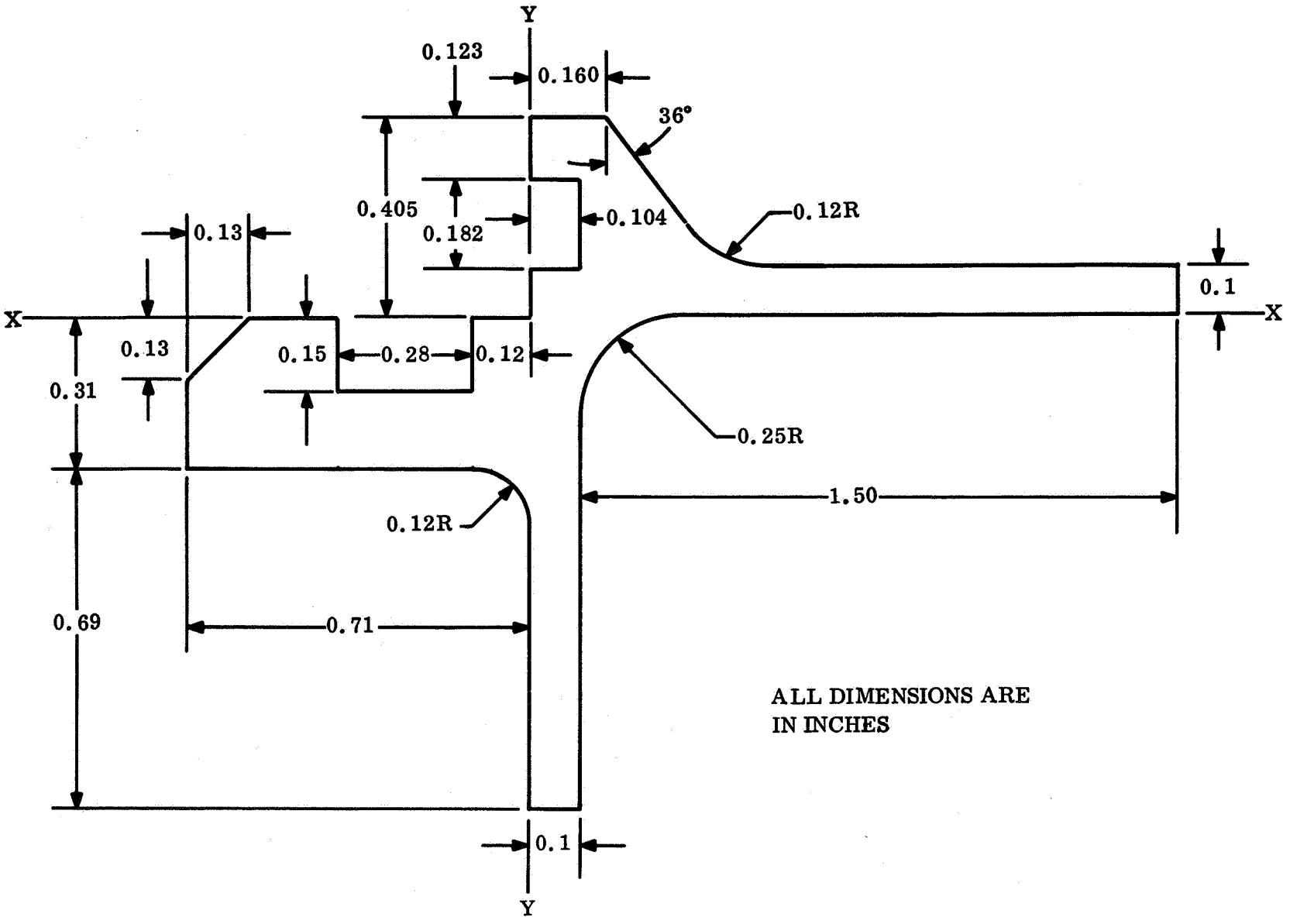


Figure 3.3.3-4. Aft Canister Ring

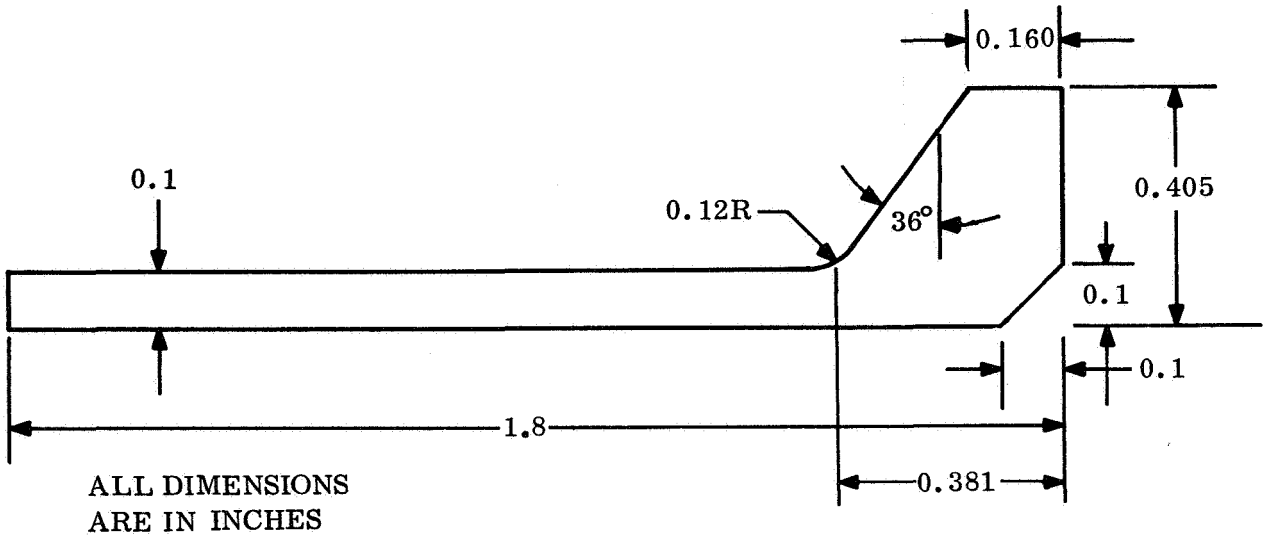


Figure 3.3.3-5. Forward Canister Ring

A non-pyrotechnic device, similar to the hot-wire tension bolt previously discussed, will be seriously considered, because of its obvious advantages. Its main drawback is that it is new and needs to be developed.

The ejection systems available are pneumatic pistons, pyrotechnic thrusters, reaction systems and springs. Springs were selected for their obvious simplicity. To minimize tip-off rates, the energy and force of the ejection system must be controlled. A guide/roller system may also be required if rates are too high. The proposed solution uses preset springs in an energy package, with selective assembly and gives a maximum tip-off rate of 0.34°/sec when the maximum and minimum spring forces are combined with the worst case c.g. offset.

The Capsule is attached to the adapter by four 1/4 in. explosive nuts, each having dual cartridges. The explosive nut is of the captive type, with all loose pieces contained within the unit. The gas generated by the squibs is also contained. The choice of an explosive nut was made because of its reliability, capability for dual squib initiation, low weight, and high load carrying ability. The 1/4 in. size nut can carry the full load of a 1/4 in. 160,000 psi UTS bolt, which is 3600 lb. The applied limit load is 2600 lb and therefore there is ample margin. Four nuts were selected based on the four pickup points on the structure.

Capsule ejection is accomplished by four helical coil compression springs. The springs exert 108 lb of force each, and have a working stroke of 1.28 in. The springs are stable ($L/D < 5$) and will impart a separation velocity of 1.5 ± 0.15 fps to the Capsule. Thus, the Capsule will acquire a positive ΔV of 3/4 fps, whereas the forward canister was ejected at 2-1/2 fps. Tip-off imparted to the Capsule will be 0.34^{o}/sec obtained by trimming and selecting the springs. The Orbiter will acquire a negative or retrograde ΔV of 3/4 fps and a tip-off rate of 0.34^{o}/sec as a result of Capsule separation. It was assumed that this small motion was not detrimental to the mission. (See Volume III, Appendix B for tip-off analysis.)

The spring assembly is shown in fig. 3.3.3-3. It provides for adjustment of initial load - one turn of the adjustment nut gives approximately a 2 lb load change - it provides for adjustment of total stroke, it retains the spring at the end of the stroke and provides a locating pilot. The inner sleeve is coated with teflon on both inner and outer surfaces to reduce friction. Operation of the spring over the inner 80 percent of its total possible stroke assures nearly constant spring rate.

The following summarizes the recommended spring design (see table 3.3.3-1 for spring detail data).

Spring material - National Standard NS355 stainless steel

Ultimate tensile strength = 330,000 psi for up to 0.159 in. wire

Torsional shear - 45 percent x UTS = 148,000 psi

Initial load - 108 lb @ 0.16 in. from solid

Final load - 12 lb @ 1.44 in. from solid

Maximum load - 120 lb @ solid height

Maximum stroke, Xm - 1.60 in.

Operating stroke - 1.60 - 20 percent (1.60) = 1.28:

Energy required - 25.5 ft/lb

Energy available - $\frac{(108 + 12)}{2} \quad \frac{(1.28)}{12}$ (4 springs) = 25.6 ft-lb

Control spring rate to 75 ± 3 percent lb/in

Adjust spring to 108 ± 2 lb initial load

Install springs so that diametrically opposite springs have an initial load within 0.5 lb

IFD's for electrical separation will be self disconnect type or electrically actuated, hot-wire type depending on size and location on the vehicle.

TABLE 3.3.3-1. SEPARATION SPRING DATA

	Canister	Thrust Cone	Capsule
Wire diameter (in.)	0.107	0.107	0.148
Mean coil diameter (in.)	1.07	1.07	1.034
Number of springs	2	2	4
Component length (in.)	1.29	1.29	2.35
Solid height (in.)	1.09	1.09	2.19
Free length (in.)	3.29	3.29	3.79
Total weight (lb)	0.17	0.17	0.80
Number of active coils	8.4	8.4	12.7
Stress (psi)	90,000	90,000	110,000
Nominal Δ V (fps)	2.5	2.5	1.5

3.3.3.2.3 Thrust Cone Separation

The thrust cone is attached to the aeroshell/Lander through a hot-wire bolt to a male fitting which is internal and pinned to a female fitting on the Lander cover. The hot-wire separation occurs as described for the canister.

The thrust cone is ejected at 3.1 fps using two helical coil compression springs identical to the ones used for canister separation. The springs remain with the thrust cone.

IFD's for electrical separation will be of the spring self-disconnect type.

3.3.4 ENVIRONMENTAL CONTROL

Thermal control of the Lander components during interplanetary travel will be accomplished by insultaing the Lander from the space environment and using heater power from the spacecraft to control the Lander temperatures. The insulated blanket will be a multi-radiation barrier type composed of a number of layers of either aluminized mylar or aluminum foils separated by an insulating material. An effective thermal conductivity of 1×10^{-4} btu/hr-ft-^{o}R was selected for this type of insulation. Definition of the insulation details and heater power requirements will be dependent on the surface radiative properties, payload allowable temperatures and canister surface area. A low emissivity coating (EoS = 0.1) on the outside insulation surface will be utilized to maintain minimum heat loss through the canister. From fig. 3.3.4-1 insulation and heater power requirements can be determined on a unit surface area basis for a compartment temperature requirement of 310 ^{o}R. Total heater power can be evaluated from fig. 3.3.4-2 at the design values.

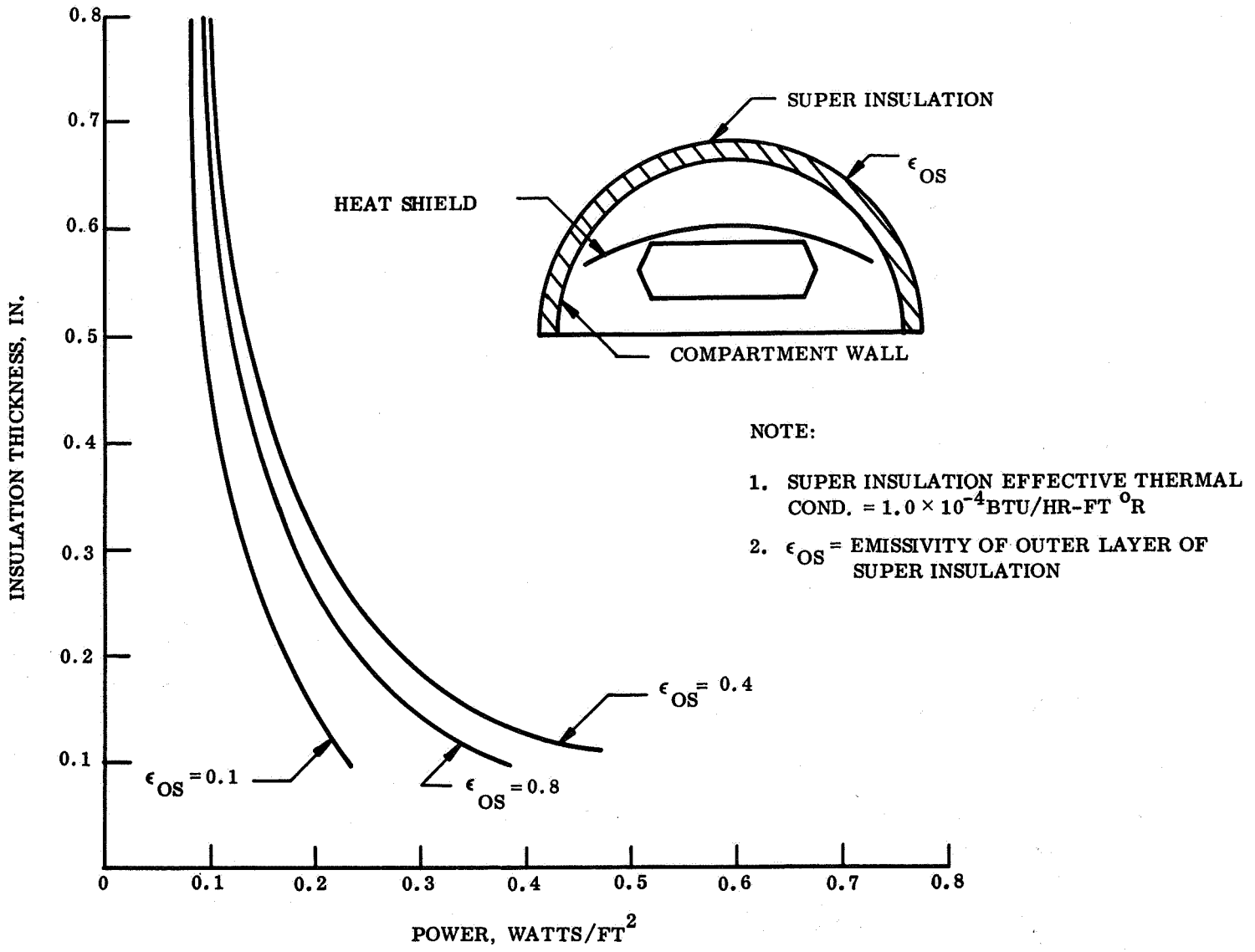


Figure 3.3.4-1. Super Insulation Requirements to Maintain 310 ^{o}R on Compartment Wall and Heat Shield

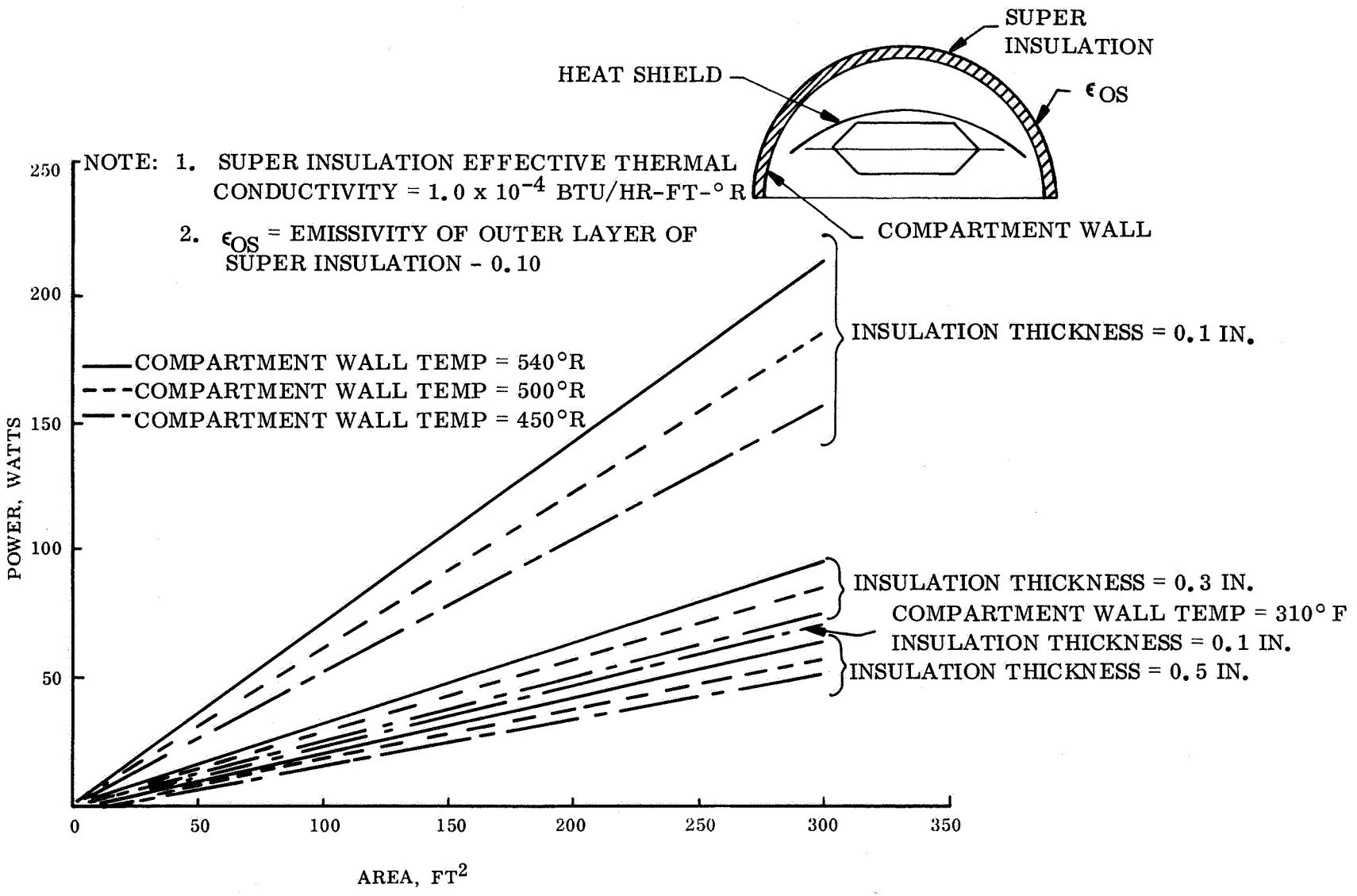


Figure 3.3.4-2. Transit Mode Power and Insulation Requirements for Various Canister Areas

3.3.5 DE-ORBIT PROPULSION SYSTEM

3.3.5.1 Design Constraints

The design constraints for the de-orbit propulsion system for Point Design 1 were as follows:

1. De-orbit weight of 1350 lb (less propulsion)
2. Velocity increment 235 meters/sec
3. Motor burn time 20 to 30 sec
4. Solid propellant system.

3.3.5.2 System Description

3.3.5.2.1 De-orbit Propulsion Equipment

The selected propulsion equipment for the Mars Hard Lander Point Design 1 is a solid propellant system conforming to the requirements presented below. This portion of the report presents the performance data, and system description of the selected de-orbit propulsion equipment.

The de-orbit propulsion system must impart a velocity increment of 235 meters/sec to a 1350 lb vehicle for out-of-orbit planet entry at 15,300 ft/sec and a path angle of 16^{o}. The vehicle weight does not include the propulsion system weight. Thrust termination is required and the system must be aligned to within $\pm 2^{o}$ with respect to the principal axis. Motor burn time is to be approximately 20 to 30 sec.

The performance, weight, and basic envelope data is presented in table 3.3.5-1. The propellant weight shown in the table is useful propellant weight. Inert weights consist of the case, liner, insulation, nozzle, igniter, and thrust termination mechansim for the solid system.

The velocity increment variation for the solid system has been estimated not to exceed plus or minus 1 meter/sec. Using statistical data obtained primarily from Minuteman motor firings, the variation in specific impulse was estimated at ± 0.338 percent (3-sigma). Propellant and inert weight variations can be held to limits approaching weighing system accuracies of +0.05 percent (3-sigma). Therefore, assuming no variation in payload weight, the resulting velocity increment variation is 0.34 percent (3-sigma), or less than plus or minus 1 meter/sec.

Table 3.3.5-1 also presents data on two solid propellant compositions. These propellants are Aero-Jet General's ANB-3289-2 and United Technology's UTREZ. ANB-3289-2 is higher performing than UTREZ, and, from preliminary data, more capable of surviving the heat sterilization cycles. The increased performance is due to 15 percent aluminum in the propellant. A disadvantage is that ANB-3289-2 has yet to be cast and fired in a motor. However, based on the satisfactory results of propellant physical property testing and the increased performance potential, ANB-3289-2 is the preferred solid propellant.

TABLE 3.3.5-1. PERFORMANCE, WEIGHT, AND ENVELOPE DATA

Propellant	ANB 3289-2	UTREZ
ΔV in meters/sec	235	235
Payload weight less propellant (lbm)	1350	1350
Total propulsion system weight (lbm)	140	147
Propellant weight (lbm)	119	126
Propulsion inert weight (lbm)	21	21
Mass fraction (propellant weight to total weight) (lbm)	0.85	0.86
I_{sp} (VAC sec)	276.3	244.4
Nozzle expansion ratio	40	40
Total impulse (lb-ft-sec)	34492	30816
Burn time (t_b) (sec)	20.0	20.1
Thrust, total (lbf)	1725	1530
Approximate dimensions (spherical diameter in inches)		
Case	16.3	17.2
Throat area (in^2)	1.33	1.18

A representative solid propellant propulsion system as designed by Aerojet-General is shown in fig. 3.3.5-1. Major components include a case bonded, saturated, hydroxy terminated polybutadiene sterilizable propellant grain with a stress relief boot; a titanium alloy case; a single, fixed, semi-submerged nozzle; an epoxy-cured, saturated, polybutadiene insulation system; a BPN pellet igniter; and a shaped charge thrust termination unit which allows jettisoning the nozzle.

All materials and component configurations, except the propellant, have been used successfully for other solid rocket motors, and the manufacturing and assembly techniques are well established. State-of-the-art inert materials and procedures will be used to fabricate and process the motor. The propellant is an 85 percent solid

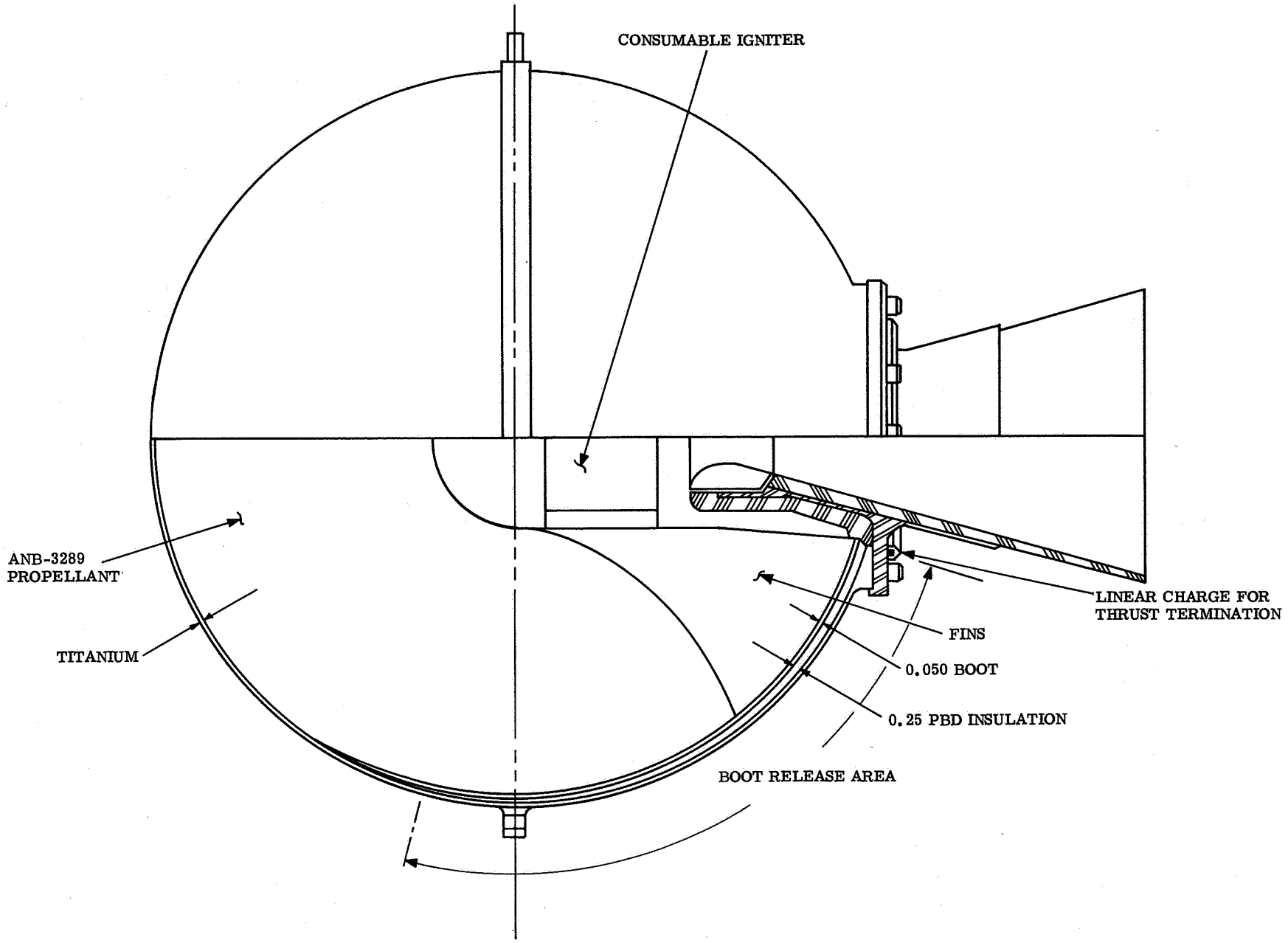


Figure 3.3.5-1. Solid Propellant System

loaded propellant with a saturated hydrocarbon binder and stabilized ammonium perchlorate oxidizer that has been recently developed by Aerojet-General for use in sterilizable motors.

ANB-3289-2 is a heat sterilizable propellant manufactured by Aerojet-General Corporation. It is formulated from stabilized ammonium perchlorate and a binder based on saturated hydroxy terminated polybutadiene binder cured with an isocyanate. Only slight changes in mechanical properties (with respect to a conventional propellant) were detected when 3 x 5 in. blocks of this propellant were exposed to six successive 53 hr exposures at 275°F in air.

Achievement of satisfactory heat sterilization performance requires the use of (1) a stable propellant formulation with good high temperature strength and stress relaxation properties and good flow and pot-life characteristics, and (2) controlled processing procedures which minimize defects in the cured grain or specimen.

The combination of the ANB-3289-2 binder system formulated at a high cross link density and a process based on vacuum stripped prepolymer, very dry oxidizer, high vacuum mixing and bayonet casting appears to satisfy all requirements.

The propellant grain configuration is designed to minimize stresses during sterilization heat cycling. The forward portion of the grain is case bonded and the aft end is released from the chamber by the release boot. Fins in the aft portion of the grain neutralize the progressive burning surface nature of the grain and provide a grain with low inner bore strains.

The selection of SD-850-2 liner was made on the basis of tests of the effect of heat sterilization on the bond strength of a saturated HTPB/Aromatic isocyanate propellant. The bond strength appeared good and was not degraded by heat sterilization.

The motor case will be insulated with IBT insulation, a filled epoxy-cured, saturated, polybutadiene insulation system, developed by Aerojet-General specially for sterilization requirements. The propellant release boots are made of the same material.

The case is made of 6A1-4V titanium alloy, spun in halves and welded together at the centerline. An increased thickness is provided in the weld area to compensate for reduced strength. A single aft opening is provided for attaching the nozzle, and tabs are located at the equator for mounting the motor.

Since no opening is available at the forward end of the case, a phenolic boss is bonded to the center of the forward dome to act as a guide for locating the insulation installation tooling.

The nozzle consists of a forged titanium housing, graphite throat insert, silica-phenolic exit cone and IBT insulation on the outside of the submerged portion of the expansion cone. A circular shaped charge is mounted on the nozzle flange to release the nozzle when the thrust termination device is actuated. The angular displacement

of the nozzle centerline with respect to the motor centerline is plus or minus 10 min and the radial displacement shall not exceed 0.030 in.

A consumable BPN pellet igniter will be used. The igniter, inserted into the bore of the propellant grain and bonded in place before the nozzle is installed, consists of a BPN pellet charge and an initiator in a foamed plastic housing.

Thrust termination is accomplished by releasing the nozzle from the chamber when the shaped charge is actuated to cut the nozzle flange. (This well-proven technique is currently used on the third stage Minuteman III to release the head end thrust termination ports.) The resultant vent area increase will be approximately 17 times the throat area. A case blowdown analysis shows that the motor will extinguish itself by a $\dot{P}$ extinguishment phenomena (rapid depressurization) in 18 msec when 50 percent of the propellant is consumed and in 28 msec when 99 percent of the propellant is consumed.

3.3.5.2.2 De-orbit Structure

The de-orbit engine is supported by a conical sheet metal thrust cone which is attached to the Lander cover by means of four tubular trusses. Fig. 3.3.5-2 depicts the complete assembly and the associated attachments.

An aluminum ring provides the interconnection between the engine and a conical aluminum adapter or thrust cone. The thrust cone is an aluminum sheet metal construction with longitudinal stiffeners to aid in taking the axial and bending loads introduced during flight conditions and during de-orbit motor burn. Gussets are provided at two locations to provide a means of installation and a load path for the separation springs. Another aluminum ring, at the larger diameter end of the thrust cone, provides the attachment for the main support members. This ring takes the shear loads, due to lateral loading conditions, and redistributes them to the support members and stiffens the thrust cone to resist torsional forces during spin and de-spin.

The main support members are aluminum tubes approximately 10 in. long. These tubes act as short columns taking the axial loads and re-distributing them as four point loads into the Lander structure. The column is attached to the Lander, as shown in fig. 3.3.5-3, through a hot-wire bolt to a male fitting which fits into and is pinned to a female fitting on the Lander cover. The lower end of the column is threaded to match a threaded pre-load sleeve which, when tightened, puts tension in the hot-wire bolt. The de-orbit engine and all of the structure is released when the hot-wire separates.

3.3.6 ELECTRICAL EQUIPMENT, PRE-ENTRY

The canister is equipped with electrical/electronic equipment which provides status monitoring during cruise, preseparation, check-out, arming, electrical disconnection, separation initiations and separation event monitoring.

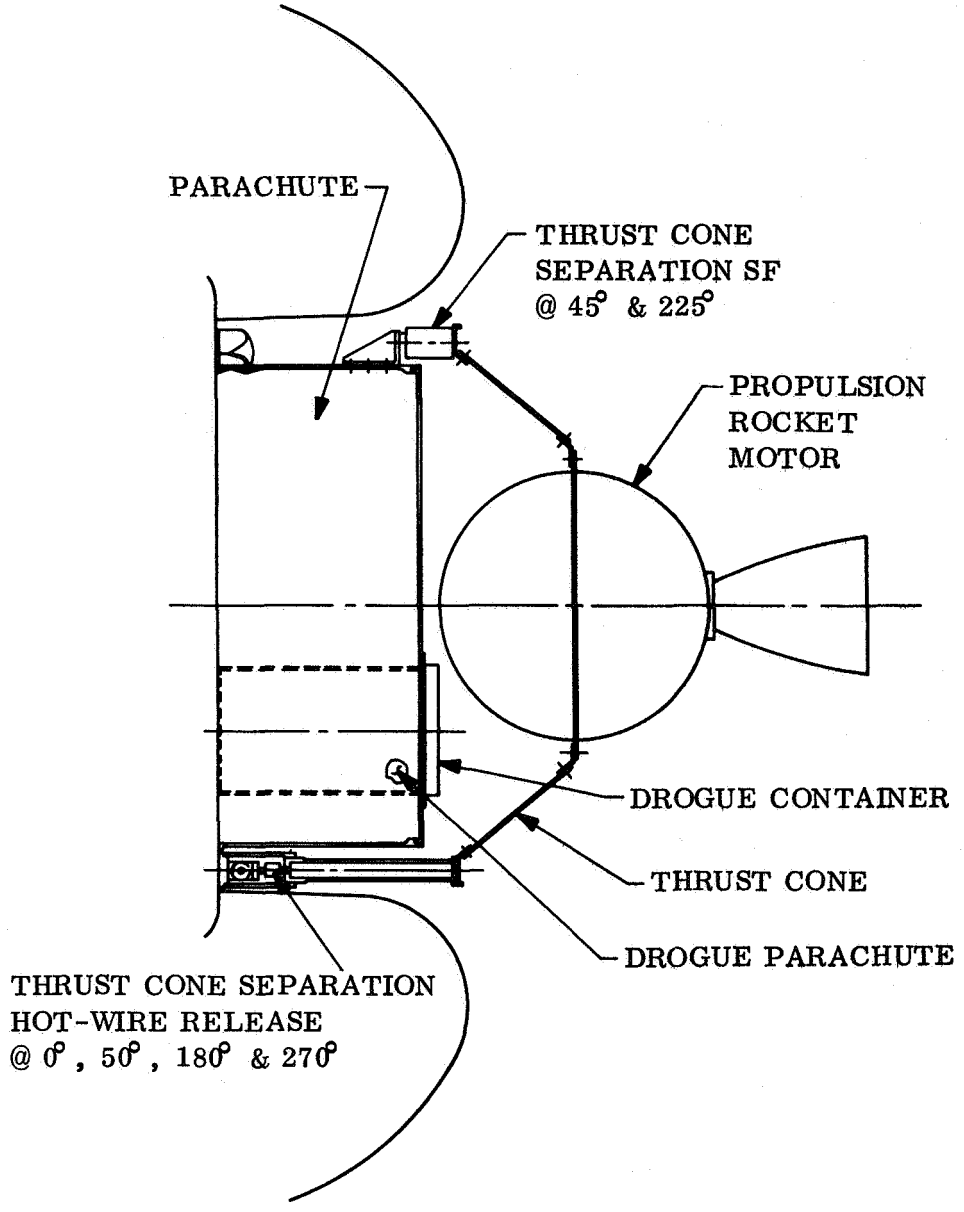


Figure 3.3.5-2. De-orbit Rocket and Thrust Cone Structure

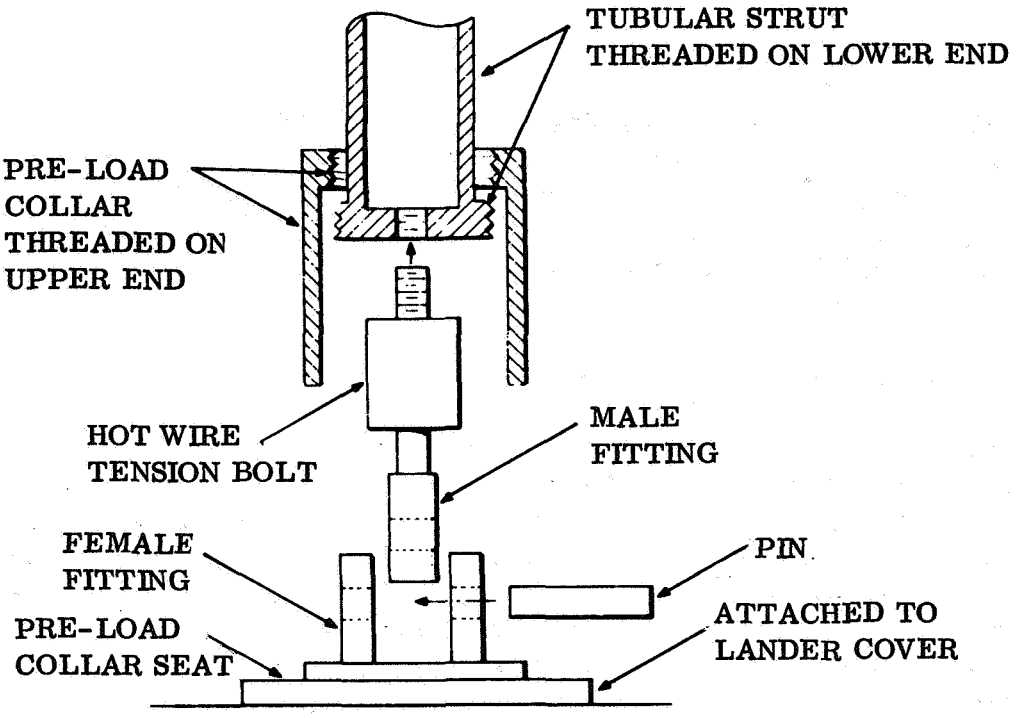


Figure 3.3.5-3. Thrust Cone Separation

Commands from the Orbiter CC&S are sent to the canister via hardwire where decoding takes place in the dual canister programmer. Signals from the programmer operate the power controller which contains redundant capacitor discharge energy storage units. Energy from these capacitors provide electrical initiation.

All canister equipment is powered from a sterilized dual silver-zinc secondary battery. This battery is similar in design to the Lander battery and its development is described in para. 4.3.1.3 of Volume III. This provides an independent energy source for operation when the Orbiter solar arrays are pointed away from the Sun, e.g., maneuver and separation attitude, for separation event monitoring after Lander disconnection, and to avoid sending initiation energy across an interface.

Thermal batteries located on the thrust cone provide high level currents for the electrical initiation events associated with spin, de-boost and de-spin. These are ignited from the Lander battery through thermal relay modules which protect the operational battery against initiation circuit faults. The thermal batteries are used in redundant pairs with diode blocking for isolation.

3.3.7 DE-ORBIT SYSTEM

3.3.7.1 Spin Control Subsystem

The subsystem configuration described here for Point Design 1 performs attitude control for the de-orbit system and roll control for the entry system. By combining these functions, the overall equipment design is simpler, weighs less, and since fewer components are needed, is more reliable. In the following discussion, reference will be made to the entry system description, Volume IV, Section 3.4.7, where appropriate.

3.3.7.1.1 Spin Requirements

The most important requirement for the spin control subsystem is to control the Capsule attitude during firing of the propulsion system so that the error in direction of the velocity increment (ΔV) will not cause excessive entry path angle or down range dispersions. Errors will be caused by thrust misalignment of the propulsion engine, center-of-mass offset of the Capsule, separation tip-off rates, and by other sources to be discussed later. The spin control subsystem provides a combination of gyroscopic stability and cyclical averaging to reduce the effect of these error sources to less than 2.1^{o}, 3-sigma, error on the ΔV orientation.

Another requirement for the subsystem is to control the Capsule attitude at the beginning of entry into the atmosphere so that a large initial angle-of-attack, or even backward entry, is avoided. Since the initial angle-of-attack can be as large as 40^{o}, the requirement is met by maintaining until entry the same inertial orientation established for de-orbit propulsion firing. Again, the gyroscopic stability of the spin control performs this function.

The requirements for roll control during entry are discussed in Volume IV, Section 3.4.7 under entry systems. Additional requirements and constraints for the spin control are summarized in table 3.3.7-1. These requirements determine the required torque level and impulse.

TABLE 3.3.7-1. SPIN AND ROLL CONTROL REQUIREMENTS, POINT DESIGN 1

Capsule weight	1500 lb
Roll inertia	140 slug-ft^2
P/Y inertia	138 slug-ft^2
Moment arm	46 in.
Separation rate	0.5 deg/sec
CM offset	0.3 in.
Nozzle alignment error	0.5 deg
Velocity increment	771 ft/sec
Separation to entry time	4700 sec
Entry spin rate	5 rpm
Entry roll torque	12 ft-lb
Entry roll impulse	510 ft-lb-sec

3.3.7.1.2 Description of the Spin Control Subsystem

The spin control subsystem consists of a small monopropellant hydrazine reaction control, a single rate gyro, and an electronic assembly. A block diagram is shown in fig. 3.3.7-1. The rate gyro measures Capsule roll rate, which is compared with the output of the roll rate generator. When the spin command is given, the high rate (50 rpm) mode is used for spin-up for engine firing. When the de-spin command is given, the low rate (5 rpm) mode is used for both de-spin and entry roll control. When the error voltage is larger than the preset threshold, the valve drivers operate the appropriate valve to generate corrective roll torques.

Reaction control is provided by a blow-down hydrazine system using nitrogen as a pressurant. An aluminum tank less than 8 in. in diameter is used. Its size is chosen so that the initial gas pressure of 400 psi is reduced to 300 psi when all of the hydrazine has been expelled. This limits the thrust decrease to approximately 25 percent. All control torques are provided as couples. The system is sealed off until Capsule separation by the explosive squib shown in fig. 3.3.7-1.

Power requirement for the gyros and electronic assembly is 5 watts. When one of the valves is energized, an additional 2 watts is required. The size of the combined gyro and electronics is 5 x 6 x 3 in.

The operational sequence of the subsystem is as follows:

1. The spacecraft orients the Capsule in the proper direction for firing the de-orbit propulsion engine. The gyros and electronics are energized just prior to separation. The high rate mode of operation is commanded.

2. At 1.5 sec after separation, the explosive squib is fired, initiating spin-up.

3. A spin rate of 50 rpm is reached at 25 sec after spin-up is started. This rate is maintained during propulsion firing.

4. After propulsion firing, and prior to entry, the low rate mode of operation is commanded. The subsystem remains in this mode throughout entry.

3.3.7.1.3 Spin Control Subsystem Performance

The pointing accuracy of the spin control subsystem is, of course, directly dependent on the accuracy with which the spacecraft orients the Capsule prior to separation. Two major additional errors are introduced by the Capsule separation subsystem and the spin control subsystem. These errors are the tip-off error and the coning error during propulsion firing.

The tip-off error is caused by the Capsule angular rate uncertainty at separation from the Capsule. This rate produces an attitude deviation from the separation spacecraft attitude proportional to the time interval from separation to spin-up command. It is estimated that the separation tip-off rate can be held to less than 0.5^{o}/sec. For spin-up occurring 1.5 sec from separation, this creates an angular error of 0.75^{o}, 3-sigma.

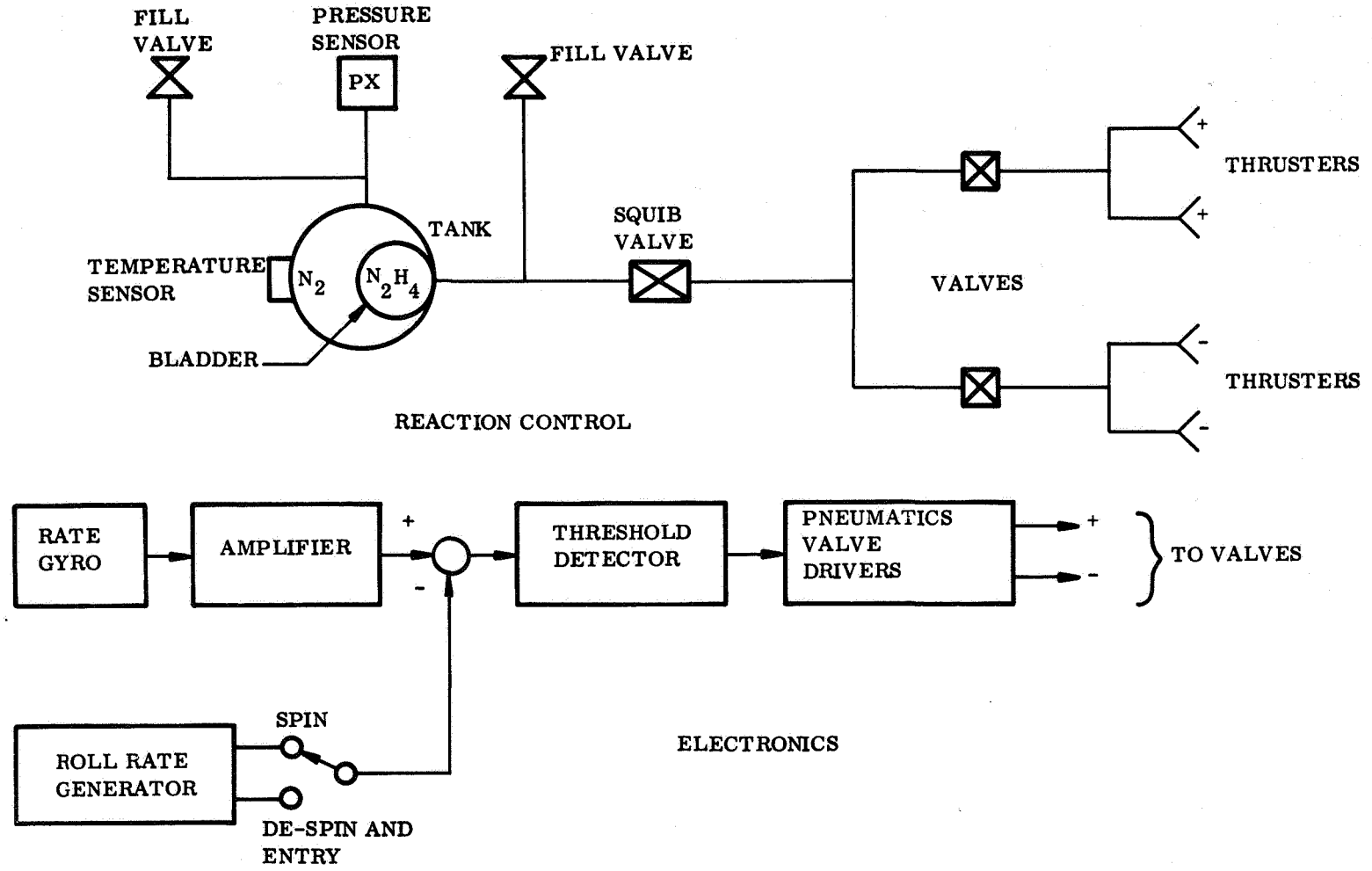


Figure 3.3.7-1. Spin and Roll Control Subsystem, Block Diagram

The coning error is caused by the upsetting torque created by the propulsion thrust not acting through the Capsule center-of-mass. Gyroscopic action reacts to the torque by producing a spiralling increase in the attitude error. To maintain a required ΔV orientation error, the spin rate must be increased as the propulsion thrust level is made larger. For the selected spin rate of 50 rpm, the ΔV orientation error will be held to less than 0.75^{o}, 3-sigma.

An error analysis, including these and other error sources, was described in Volume III, para. 5.2.5.3. The overall error in ΔV orientation is estimated to be 2.1^{o}, 3-sigma.

The attitude error of the Capsule at entry into the atmosphere is dependent on the stability of the spinning Capsule from the time of propulsion burnout to entry. To use spin stabilization during this period, the problem of energy dissipation which could lead to attitude divergence must be considered. Since a vehicle is stable about the axis of maximum moment of inertia, even with energy dissipation, the majority of the point designs will present no problem since their roll (spin) axis inertia is much larger than that of the pitch/yaw axes. However, Point Design 1 has nearly equal inertias about all axes. Since this is an out-of-orbit mission with a relatively short flight time prior to entry, the possible attitude divergence is probably small enough not to create a significantly large inertial angle-of-attack. This potential problem should be examined further if significant body flexibility or other energy dissipation means are present.

3.3.8 PRE-ENTRY SYSTEMS WEIGHT

The weights of those items contained within the pre-entry systems for Point Design 1 are listed in table 3.3.8-1. The weight of the attitude control system equipment is carried in the entry system weight summary, table 3.4.8-1. Total pre-entry system weight for this point design is 379.8 lb.

TABLE 3.3.8-1. PRE-ENTRY SYSTEMS WEIGHT SUMMARY

Item	Weight (lb)
Thrust Cone Assembly	168.7
Structure	20.0
Propulsion system (less propellant)	21.0
Propellant	119.0
Separation system	1.2
Electronics	7.5
Canister and Adapter	211.1
Shell	38.0
Internal structure	40.7
Separation rings	25.9
Separation system	11.9
Pressure and venting system	6.0
EP&D	53.4
Thermal blanket	16.0
Hardware and miscellaneous	19.2
Pre-entry system Total	379.8

3.4 ENTRY SYSTEMS

3.4.1 CONFIGURATION

3.4.1.1 Constraints

Constraints for Point Design 1 were placed on the following parameters:

1. Ballistic coefficient
2. Entry system weight
3. Maximum aeroshell diameter
4. Entry angle and velocity
5. Payload weight and volume
6. Powered flight and entry loads
7. Materials and construction techniques.

The design goal was to achieve a vehicle design with a ballistic coefficient of 14 psf. This had to be achieved within the envelope constraints discussed in Section 2.3.1, which limited the Capsule system maximum diameter to 103.9 in. and the entry system diameter to 100 in. as was shown in fig. 3.3.1-1.

Entry system weight was an important parameter, since along with the half cone angle and base diameter it determined the final ballistic coefficient achieved for a given design. It must be pointed out that the ballistic coefficient was the overriding criteria since it was this factor that had the most effect on heating rates, trajectories, loading and determined the retardation system of deployment regime. Table 3.4.1-1 shows a tabulation from the Configuration Selection Program (CONSEP) for Point Design 1. It can be seen from looking at this table that for a fixed base radius of 50 in., a varying half cone angle of 50 to 70°;the ballistic coefficient varies from 20.9 down to 14.2 for a change of greater than 25 percent while the weight change is only 20 lb (less than 1.5 percent). This points up the fact that the ballistic coefficient is the important factor and must be held constant.

TABLE 3.4.1-1. CONSEP PROGRAM RESULTS, POINT DESIGN 1

Cone Angle (°)	Ballistic Coefficient (lb/ft^2)	Entry Weight (lb)	Aeroshell Base Radius (in.)
50	20.9	1331.8	50
60	16.6	1320.5	50
65	15.2	1315.8	50
70	14.2	1311.2	50

Internal clearances between the canister and the aeroshell limit the aeroshell diameter to 100 in. Additionally the aeroshell could not be so small as to adversely affect the packaging of the Lander system. Working with both the 100 in. diameter and the packaging volume necessary for the Lander, Point Design 1 configuration was evolved.

The entry angle and entry velocity, along with the ballistic coefficient, base diameter and bluntness ratio were important factors in determining the thickness of heat shield material necessary for this out-of-orbit mission.

The payload weight was an important factor for determining internal shell loads and for sizing the retardation system since it was this weight which contributed greatly to the total decelerator load.

The critical loading conditions for the entry system in the out-of-orbit mode were conditions J, K, O, and P as shown in table 3.4.1-2. It was based on these conditions and the entry heating environment that the aeroshell structure was selected. Also important in selection of the material and construction of the aeroshell was its ease of fabrication, cost, and light weight.

3.4.1.2 Configuration Description

Geometrically, Point Design 1 is a blunt sphere cone vehicle with a nose radius to base radius ratio (R_N/R_B) of 0.5. The spherically shaped nose has a radius of 25 in. making a tangent with a frustum of a cone with a half angle of 60°, and a base diameter of 100 in. as shown fig. 3.4.1-1.

The heat shield is an ablative design with elastomeric shield material (ESM) 1004X with a tapering thickness from the stagnation region to the end of the skirt. Density of this selected heat shield material is 16 lb/ft^3. Corner heating effects were accounted for in the design and protection has been provided in the form of a peripheral edge protection. To protect against the possibility of backface heating around edge of the entry vehicle; the backface, for a short distance, is coated with a heat shield material.

The aeroshell structure is an aluminum honeycomb shell with a core thickness of 0.75 in. and facing sheets 0.020 in. thick to form a total shell thickness of 0.79 in. In the aft end of the aeroshell is a torque box structure made up of webs and rings with periodic ribs to provide internal stiffness. This structure tends to stiffen the shell and minimize local shell bending and rotation as well as providing a load path for the Lander loads introduced by securing the Lander into the aeroshell. The combined spin, de-spin and roll control nozzles are mounted on the aft web of the torque box. Separation forces, which occur at separation from the adapter and at Lander release, are taken in the longitudinal web of the box.

The Lander is held in by a strap arrangment which consists of strap or bellyband which runs completely around the Lander (see fig. 3.3.1-2), hot-wire device, T-bolt, tie-down strap and torsion spring. The load in the tie-down strap is sufficient to overcome the rotational forces due to spin and de-spin and thus restrain the Lander from moving during these events.

TABLE 3.4.1-2. POINT DESIGN LOADS

Letter	Condition	Limit Load (Gx)	Acceleration (Gn)	Remarks
A	Ground handling	2.0	2.0	
B	Band Clamp	N/A	N/A	83 lb/in.radial
C	First stage burnout	5.2	2.0	
D	Second stage burnout	4.0	2.0	
E	Axial vibration	+6.0 -3.0	---	
F	Lateral vibration	---	±2.0	
G	Canister separation	Negligible	Negligible	
H	Entry systems separation	Negligible	Negligible	
I	Thrust cone separation	Negligible	Negligible	
J	Entry (max Gx)	5.5	Negligible	Out-of-Orbit 320°F interface
		12.7	Negligible	Out-ofOrbit 250°F interface
		48.0	Negligible	Direct Entry 200°F interface
K	Parachute opening	10.0	---	
L	Impact	1000.0	---	
M	Canister pressure	N/A	N/A	ΔP = 0.5 psi at 275°F
N	Canister pressure	N/A	N/A	ΔP = 1.0 psi at Ambient
O	Spin	N/A	N/A	50
P	Sterilization	N/A	N/A	

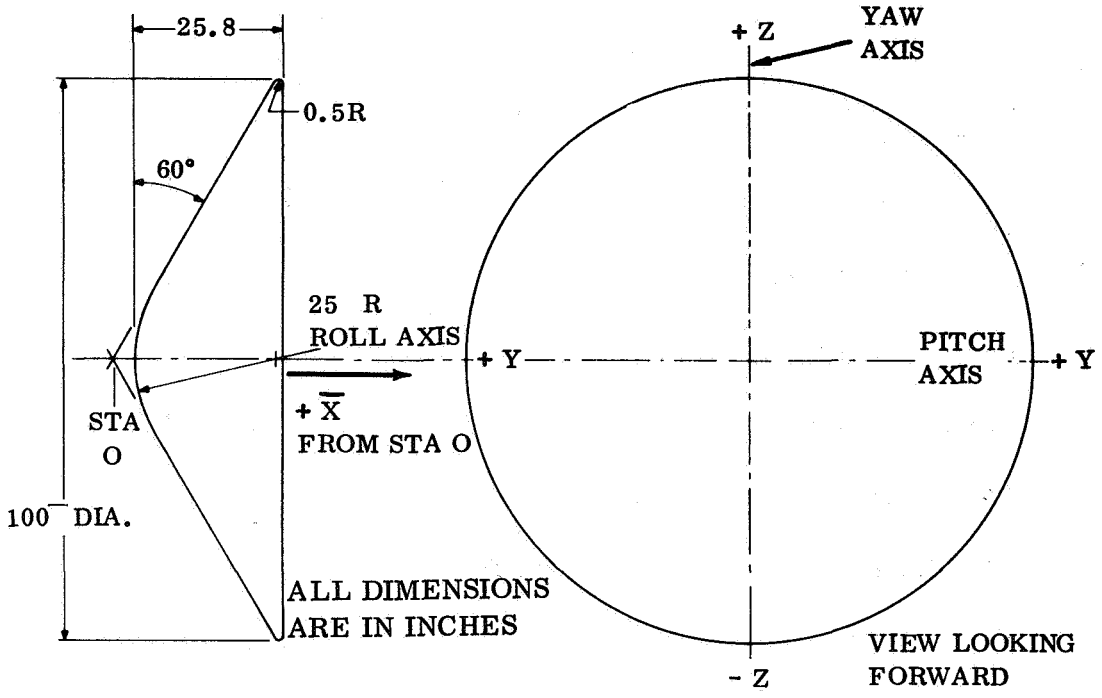


Figure 3.4.1-1. Aeroshell Geometry, Point Design 1

The forward portion of the Lander sits in a phenolic glass honeycomb saddle which has a teflon lining between it and the Lander to eliminate the possibility of adhesion of the saddle and Lander to each other during the long space flight while under the tie-down load.

Pressure sensors, a temperature sensor, and an air intake which leads into the mass spectrometer located in the Lander, are located in the nose of the aeroshell.

3.4.2 HEAT SHIELD

At the heating rates expected for the out-of-orbit Point Design 1 mission, described in table 3.4.2-1, the most efficient materials on a weight basis are, in general, members of the low density charring ablator class. Thus, because of the relatively mild Martian entry environment, where total surface recession is small in most cases and thermal insulation is of prime importance, the low density charring ablator, ESM 1004X was selected to be a design solution for the Mars Hard Lander heat protection system for out-of-orbit entry modes.

The basis for selection of this material was:

1. Minimum system weight
2. Maximum flexibility to accommodate non-design conditions

TABLE 3.4.2-1 ENTRY CONDITIONS AND GEOMETRY OF POINT DESIGNS 1 THROUGH 6

Point Design	Mission Entry Mode	Entry Velocity (kft/sec)	Entry Angle (deg)	Ballistic Coefficient (lb/ft^2)	Aeroshell Base Diameter (ft)	Half Cone (deg)	R_N/R_B
1	Out-of-Orbit	15.3	14	14	8.33	60	0.5
2A	Direct	20.8	16	7	12.7	60	0.5
2B	Direct	20.8	16	7	11.4	60	0.5
3	Out-of-Orbit	15.3	14	14	8.33	60	0.5
4	Direct	20.8	16	7	12.7	60	0.5
5	Out-of-Orbit	15.3	14	14	10.0	60	0.5
6	Direct	20.8	16	7	14.0	60	0.5

3. Fewer anticipated fabrication and development problems than with other approaches

4. Sensitivity to the sterilization/decontamination and low temperature/hard vacuum environments can be circumvented by proper material formulation.

ESM 1004X (16 lbs/ft^3 density) was selected as the preferred shield material for the out-of-orbit Point Design 1 mission since no surface melting is anticipated, even for the steep angle entries of 16° Nom (+2°) into the VM-8 atmosphere. However, ESM 1004X is not the most efficient shield material in the flight regime where surface melting occurs.

It has been shown in Volume III, para 3.1.2.1, that the maximum heat shield thickness requirement is dictated by the shallowest path entry angle attainable. The heating histories which include both convective heating and equilibrium and nonequilibrium radiative heating for Point Design 1 are shown in fig. 3.4.2-1 for the stagnation point and end of skirt locations.

Employing the thermo-physical properties described in table 3.4.2-2 and the convective and radiative heat flux histories shown in fig. 3.4.2-1, the heat shield thickness requirements were generated using the techniques described in Volume III, para 3.1.2.1, and are shown for Point Design 1 in fig. 3.4.2-2. The shield thickness requirements are those required to hold the design bondline temperature to 600° F with a safety factor of 1.0. In lieu of a detailed evaluation to justify a statistical safety margin it is suggested that a safety factor of 1.2 be applied to the shield thickness requirements presented for Point Design 1. This would result in a margin of about 200° F on the backface temperature. Analysis has shown that one of the most significant factors which affects the estimation of the shield thickness is the tolerance on the entry path angle. Designing the heat shield thickness to the lower limit on entry angle results in a safety margin of about 10 percent for Point Design 1 when compared to the nominal entry condition.

The backface and frontface temperature histories of the shield material for Point Design 1 are shown in fig. 3.4.2-3. Fig. 3.4.2-4 shows the thermal gradients through the ESM material at selected times in the Martian entry corresponding to peak surface temperature and peak bondline temperature. These results are presented for entry into the VM-3 atmosphere.

Since the total heat load on the afterbody of the sphere cone is expected to be small compared with the forebody, an ablating material for thermal protection is unnecessary, and a high emissivity coating would be an adequate protection. An analysis* indicated that for Voyager the peak cold wall heat flux on the afterbody was small, the resultant temperature rise being only 256° F.

*McDonnell Astronautics Voyager Capsule, Phase B Final Report, F694, Volume II, Part b, 31 August 1967

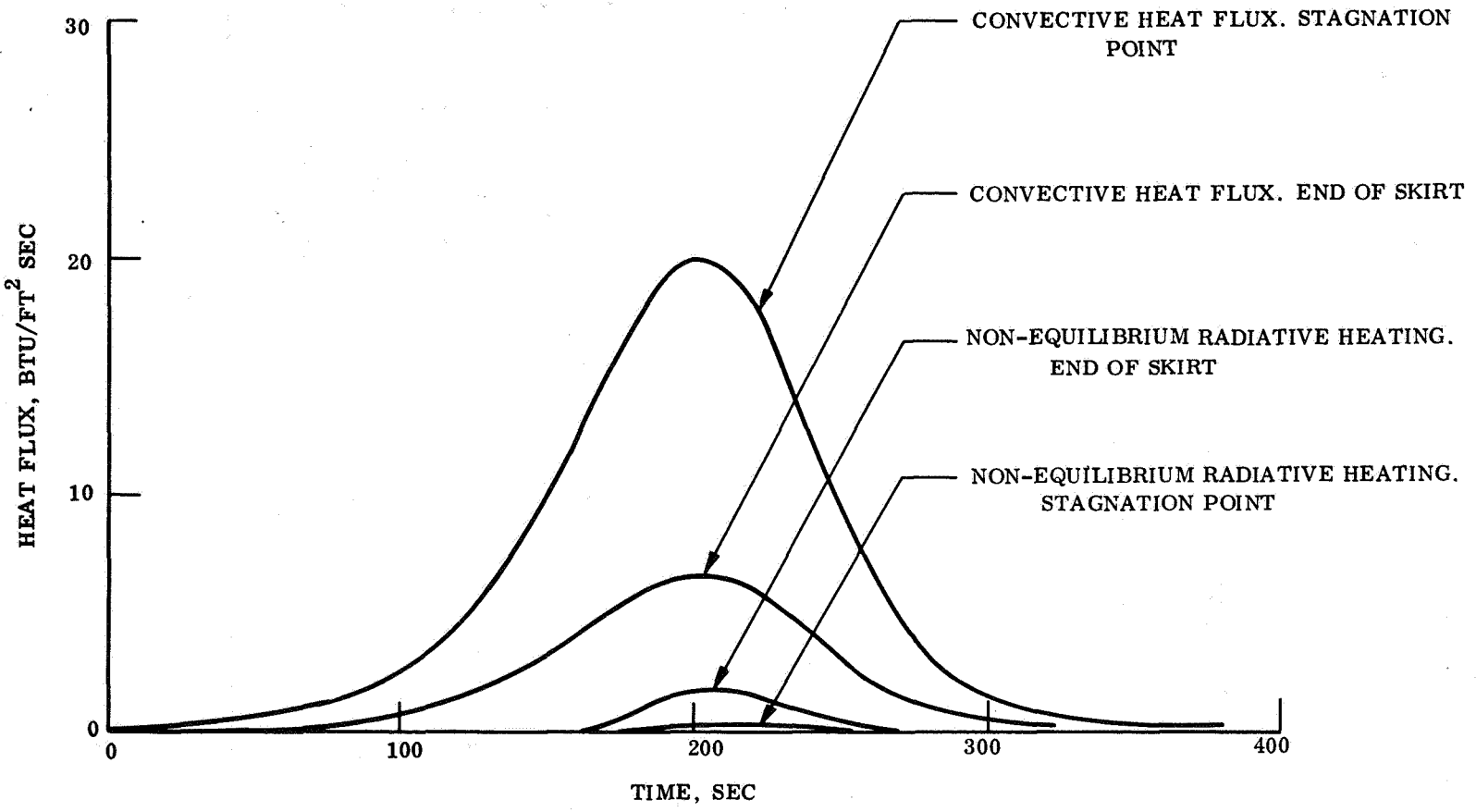


Figure 3.4.2-1. Cold Wall Convective and Radiative Heat Flux Histories, Point Design 1

TABLE 3.4.2-2. THERMOPHYSICAL PROPERTIES OF ESM MATERIALS

		ESM 1004X	ESM 1004AP
Virgin density (P_v lb/ft^3)		16.6	35.0
Char density (P_c lb/ft^3)		6.7	14.0
Pyrolysis gas specific heat (Cpg Btu/lb$^\circ$P)		.4	0.384
Molecular weight of injected species (Mg)		24.5	24.5
Order of reaction (N)		2	2
Pre-exponential factor (A sec^{-1})		15000	30000
Activation Energy (E Btu/lb mole)		44700	47500
Heat Decomposition (HGF) (Btu/lb gas generated)	1335°R	0	50
	1460°R		45
	1710°R		1000
	1960°R		2610
Specific Heat (Cp) (Btu/lb °R)	600°R	0.31	0.305
	710°R	0.33	0.360
	1210°R	0.44	0.44
	2075°R	0.44	0.44
Conductivity (k) Virgin (Btu/ft - sec °R)	610°R	0.0000115	0.0000237
	800°R	0.0000170	0.0000220
	1335°R	0.0000220	0.0000210
	1710°R	0.0000260	0.0000231
Char	1335°R	0.0000740	0.0000777
	1710°R	0.0000850	0.0000855
	2210°R	0.0001000	0.000104

For the decomposition reaction described by the following Arrhenius type equation

$$\frac{1}{W_o}\frac{dw}{dt} = \frac{(W-Wf)^N}{(Wo)} Ae^{-\delta E/RT}$$

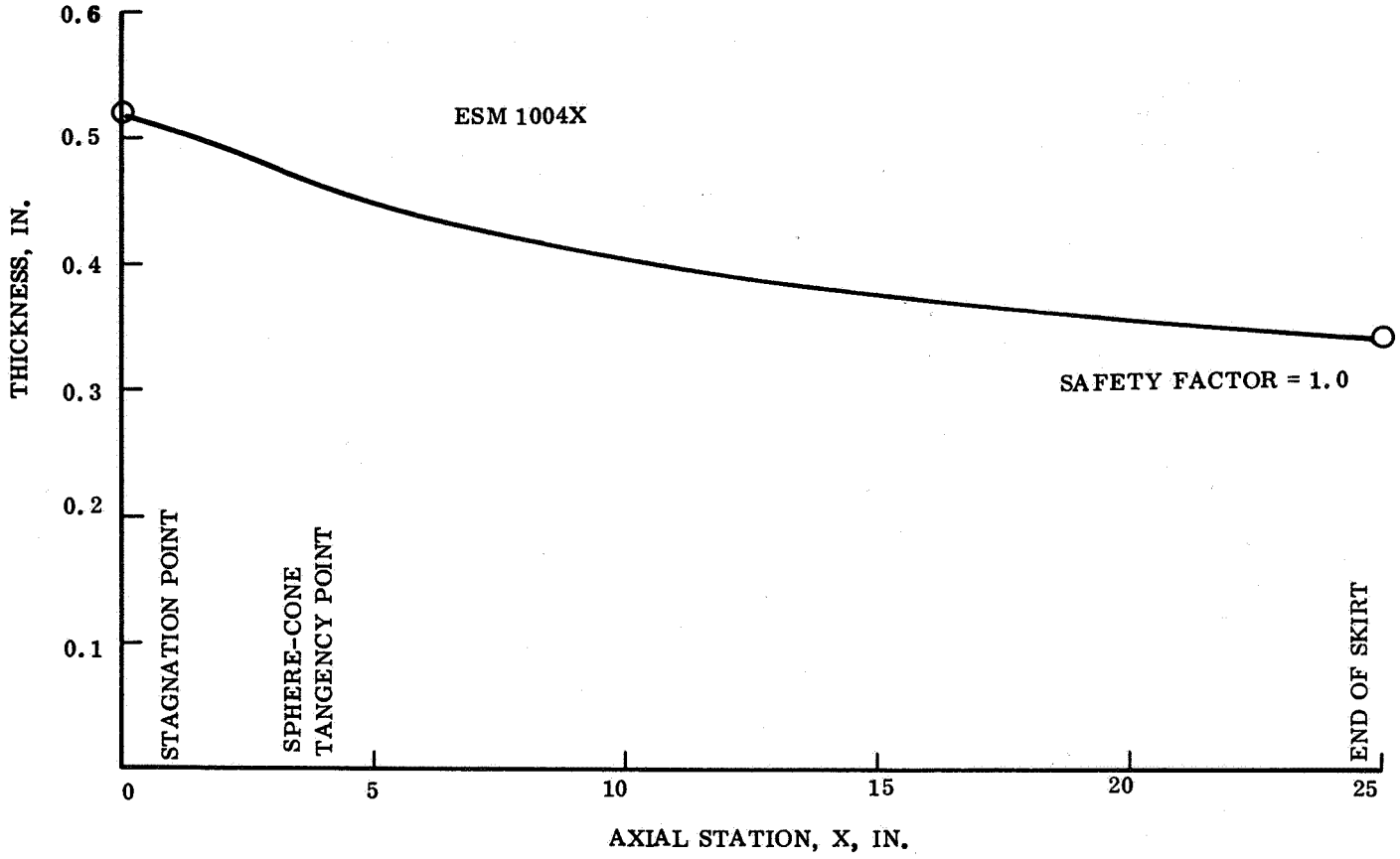


Figure 3.4.2-2. Heat Shield Thickness Requirements, Point Design 1

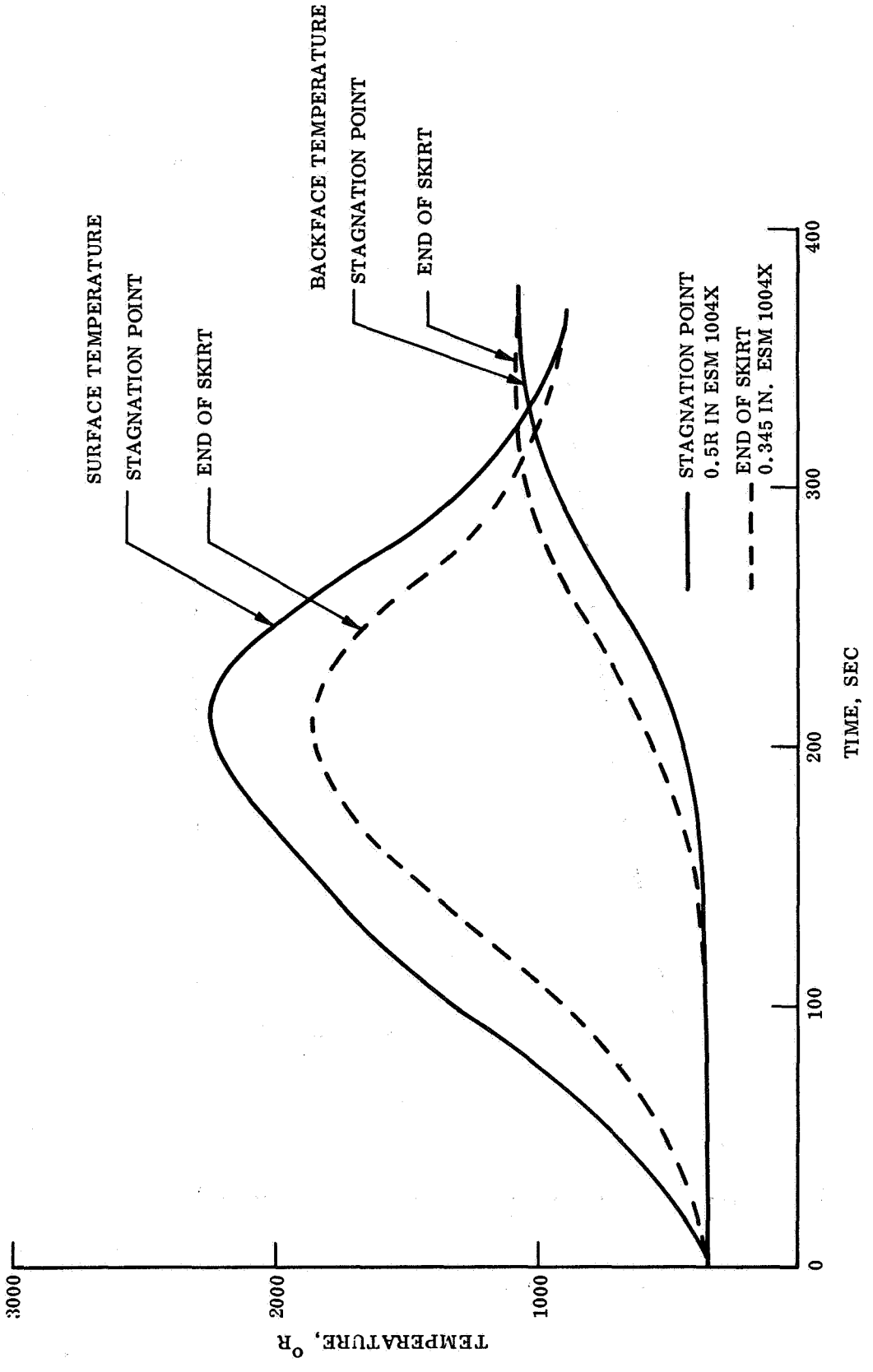


Figure 3.4.2-3. Surface and Backface Temperature Histories, Point Design 1

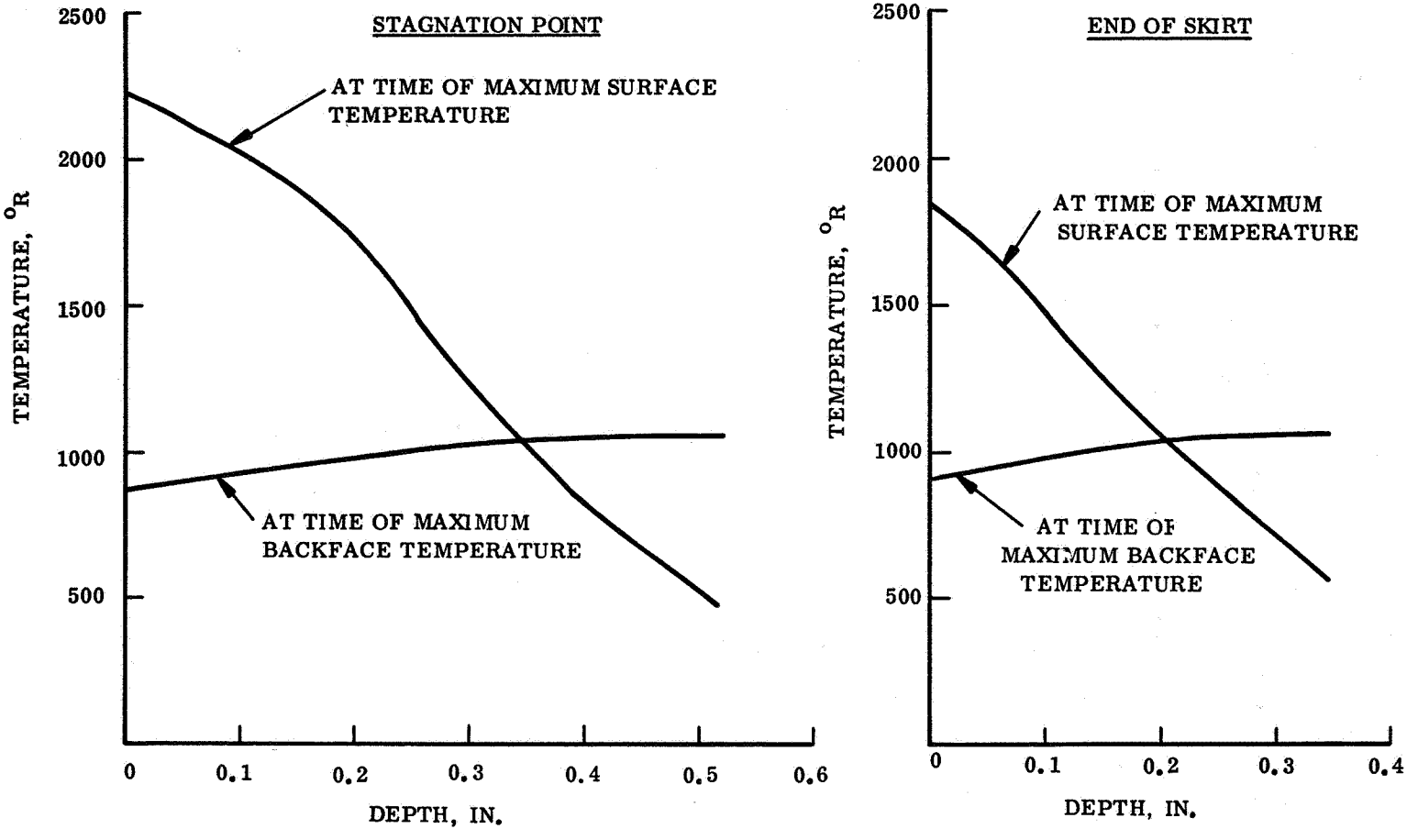


Figure 3.4.2-4. Temperature Gradients Through the Shield, Point Design 1

The current design for the ESM 1004X heat shield allows for ease of fabrication, handling, and final assembly. The heat shield material is designed to be fabricated in panel sections using maximum panel sizes, from a fabrication standpoint, of approximately 10 ft^2. Additional advantages of the segmented shield are that it allows for 100 percent inspection, does not require the aeroshell during manufacturing operations, and allows for finish machining prior to its being bonded to the aeroshell.

Design considerations have also taken into account the necessity for steps between the segmented panels both longitudinally and circumferentially. These steps were determined by both the bond and heat shield thickness tolerances.

Corner heating effects have been taken into consideration at the base of the entry vehicle and a peripheral edge protection of ESM 1004AP is provided around the corner of the heat shield at the base of the aeroshell. To protect against the possibility of backface heating around the edge of the entry vehicle, the exposed aeroshell structure at the base and inboard on the vehicle is coated with ESM 1004X.

3.4.3 AEROSHELL AND STRUCTURE

The aeroshell for Point Design 1 is an aluminum honeycomb shell 0.75 in. thick. It is comprised of a 3 lb/ft^3 core 0.75 in. thick with 0.020 in. thick 2024 aluminum facing sheets bonded on with HT 424 bond. This shell material has been selected for its light weight, ease of fabrication and much lower cost than other types of honeycomb materials. It has been designed to take the axial, bending and shear loads encountered during powered flight and planetary entry.

The detailed analysis of the aeroshell to withstand the entry inertial loads and aerodynamic pressure loadings has been performed by MULTISHELL, a GE computer program. The inputs to this program to perform the analysis consist of the entire aeroshell configuration upon which are imposed the inertia and pressure loadings. Output from the program consists of the shell internal stresses, moments, shear, in-plane shell loads, and in addition the complete shell deformations. These deformations include all local discontinuity deformations of the shell. Figures 3.4.3-1 through -5 present the deflection, moment, shear and in-plane load distributions for Point Design 2A which would be comparable to Point Design 1.

Approximate structural analysis was performed to determine the initial core and facing thicknesses to be used in the computer program. Upon completion of the first MULTISHELL analysis, any necessary changes to the structural material gages were made to result in small positive margins of safety for all of the elements of the shell as shown in table 3.4.3-1.

Analysis of Point Design 1 indicates that the shell bending is critical and that aluminum honeycomb is just as efficient as titanium honeycomb, lighter than stainless steel honeycomb and easier to fabricate than both materials. The aluminum honeycomb is just as efficient as the titanium or steel honeycomb because local shell bending is the critical loading condition and the minimum gage is no longer the controlling factor. This local shell bending is induced by the loading of the aeroshell internally by the Lander and the aerodynamic pressure externally.

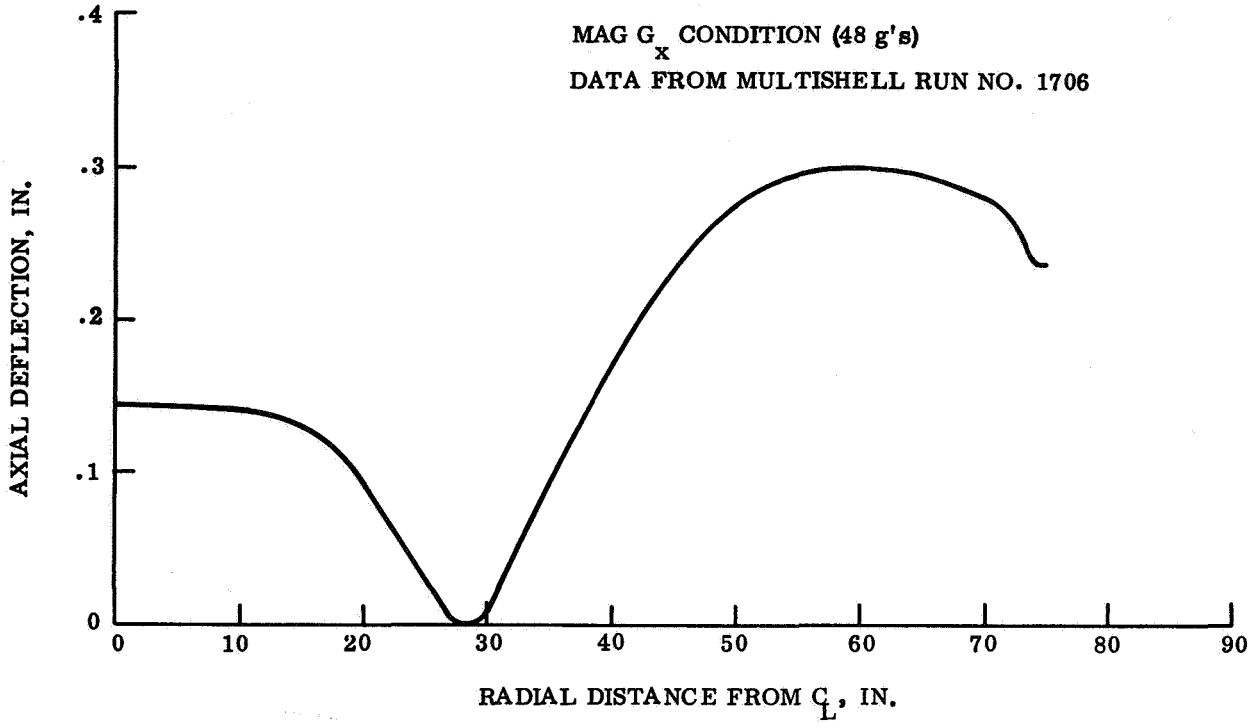


Figure 3.4.3-1. Axial Deflection-Aeroshell 2A vs Radial Distance

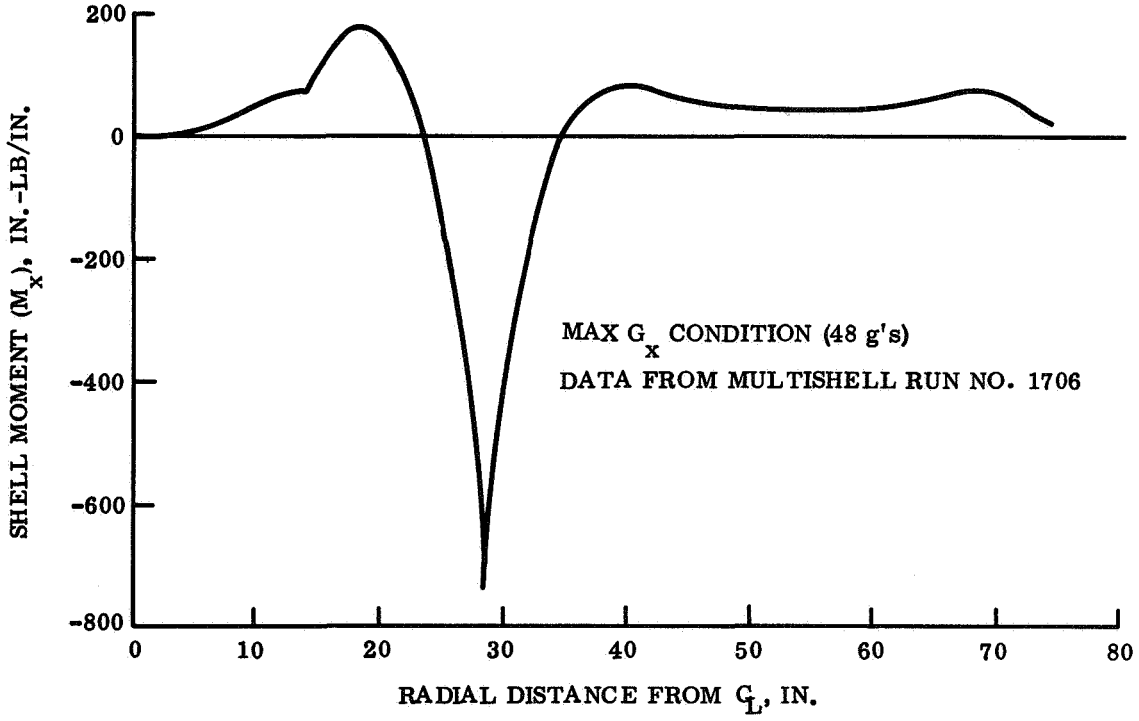


Figure 3.4.3-2. Axial Bending Moment (M_x)-Aeroshell 2A Versus Radial Distance

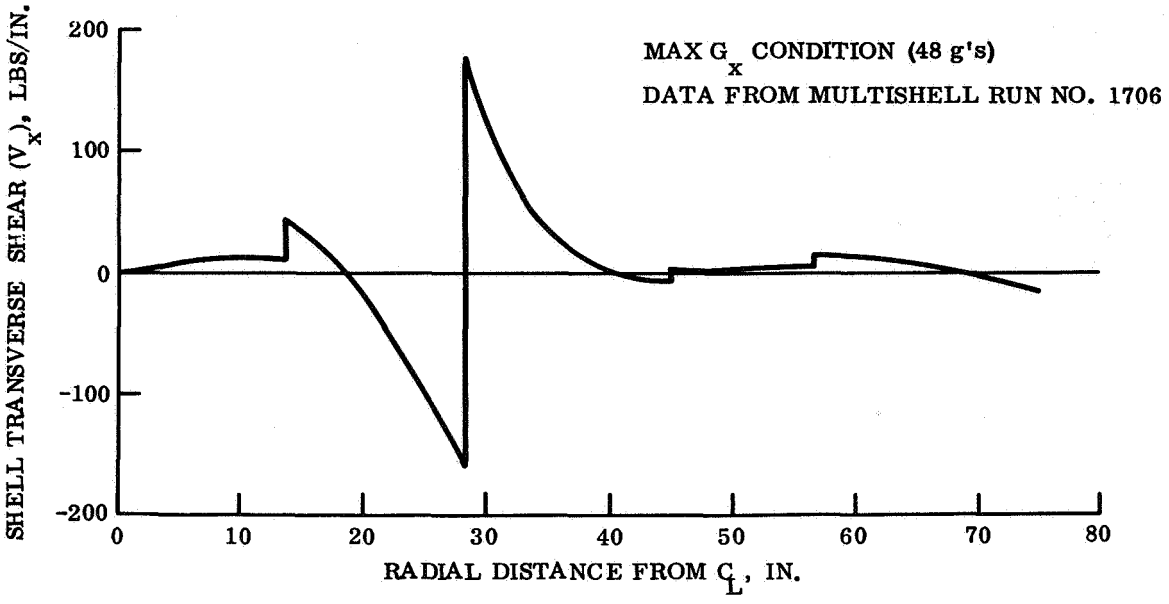


Figure 3.4.3-3. Shell Transverse Shear-Aeroshell 2A Versus Radial Distance

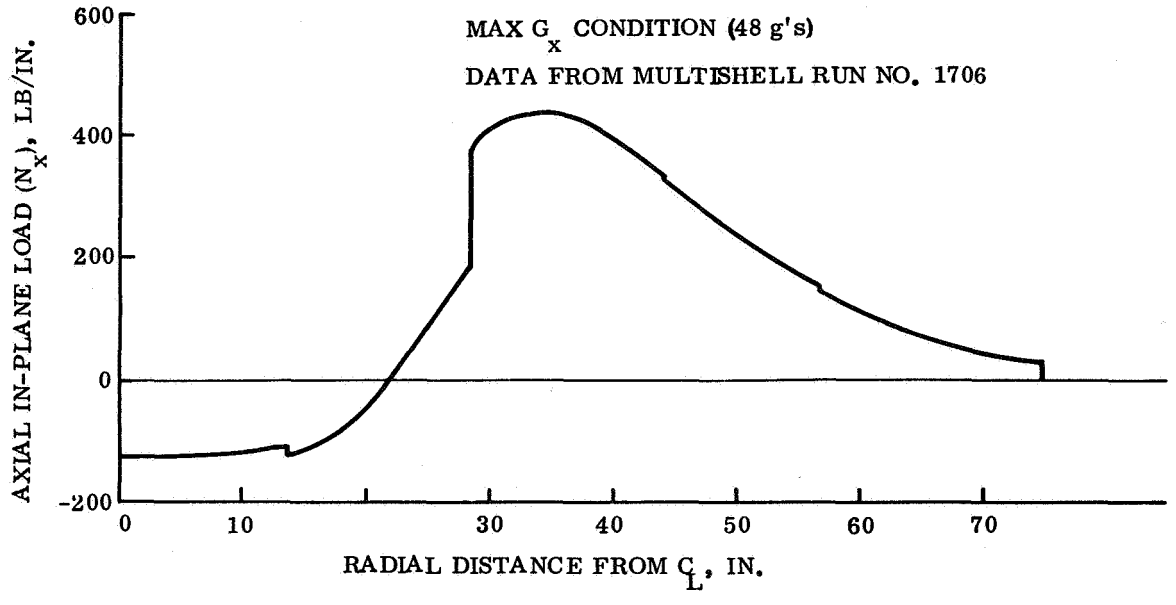


Figure 3.4.3-4. Axial In-Plane Load-Aeroshell 2A Versus Radial Distance

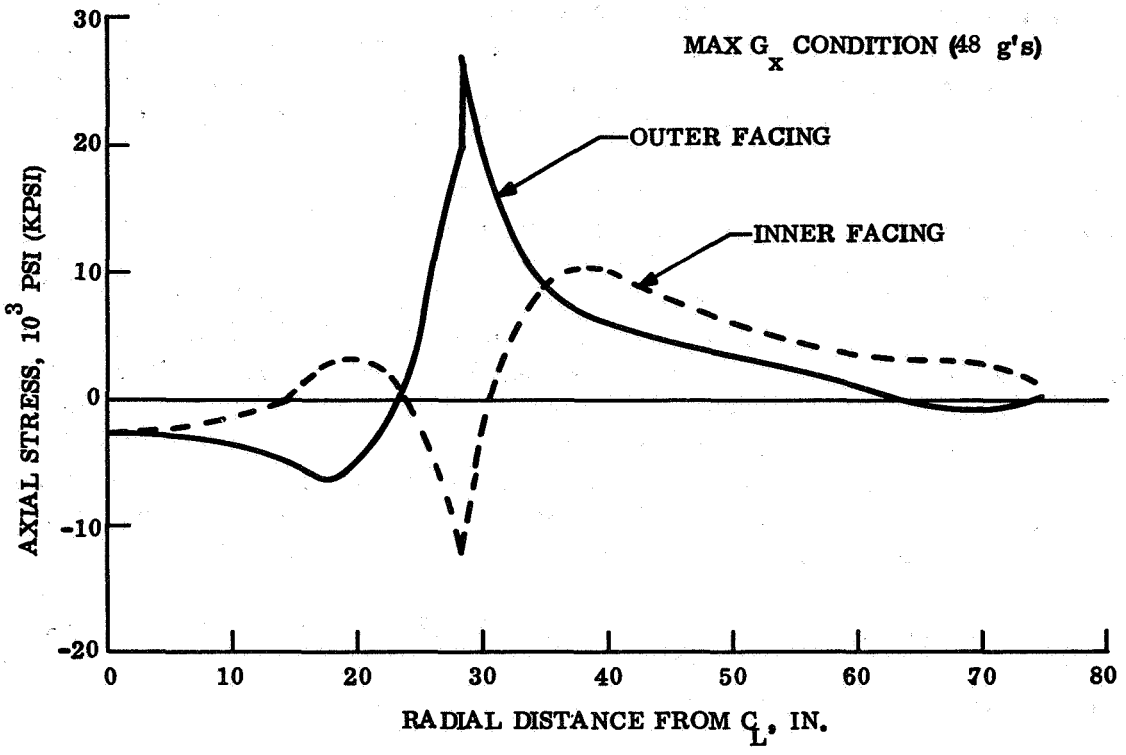


Figure 3.4.3-5. Axial Honeycomb Facing Stress-Aeroshell 2A Versus Radial Distance

TABLE 3.4.3-1. FINAL ALUMINUM HONEYCOMB REQUIREMENTS FOR AEROSHELLS

Point Design	Honeycomb		Minimum Safety Margin	Facing Material
	Facing Thickness	Core Thickness		
1	0.020	0.75	0.50	2024-T4
2A	0.025	1.50	0.09	7075-T6
2B	0.025	1.50	0.15	7075-T6
3	0.020	0.75	0.65	2024-T4
4	0.025	1.50	0.09	7075-T6
5	0.020	0.75	0.21	2024-T4
6	0.030	1.50	0	7075-T6

The heat shield structure interface temperature is only 200° F at the time of maximum loading (12.7 g's limit) and the loadings are lower at times of higher temperatures. At a temperature of 32° F the acceleration is reduced to 5.5 g's limit. The temperature at parachute deployment, at the heat shield structure interface, can by 600° F since at this time the loading on the aeroshell is negligible.

Figure 3.4.3-6 shows the relative load imposed on the aeroshell, the interface temperature and the yield strength of 2024-T4 aluminum as a function of time from entry. The maximum load occurs 40 sec after peak heating for this out-of-orbit condition. At this time the heat shield structure interface temperature is 325° F. When parachute deployment occurs (348 sec from entry), the load has reduced to 25 percent of the maximum value while the interface temperature has increased to 600° F. The total time at elevated temperature, prior to parachute deployment, is 150 sec or 2.5 min. The allowable tensile and compressive yield strengths for the 2024-T4 aluminum that have been plotted are a percentage of the allowable room temperature strength. These allowables are for the 1/2 hr (30 min) temperature exposure data from Mil Handbook 5 and are reflected in fig. 3.4.3-7.

At an elevated temperature of 600° F the allowable stresses for a 30 min exposure indicate a compressive yield strength 37 percent of room temperature strength compared with loads that are 25 percent of the maximum values.

For Point Design 1, the temperature of the aluminum honeycomb at time of maximum loading and the thermal stress levels due to the differential temperature between the outer and inner facing becomes significant. In order to consider these effects, the modified design allowable yield curve of fig. 3.4.3-7 was used for 2024-T4. The aluminum, 2024-T4 was used for the out-of-orbit design because of the retention of strength to 600° F. The 0.04 hr data was derived using the Larson parameter T (C + log t) to represent the maximum time from the start of heating to chute deployment (144 sec). The thermal stress due to the temperature differential between the outer and inner facing was calculated using the following equation:

$$Sf = \frac{\alpha \Delta T}{\left[\frac{1}{E_1} + \frac{1}{E_2}\right](1 - \gamma)}$$

where

α coefficient of thermal expansion

Δ_T differential temperature between inner and outer facing

E_1 & E_2 Modulus of Elasticity in outer and inner facing respectively

γ Poisson's Ratio

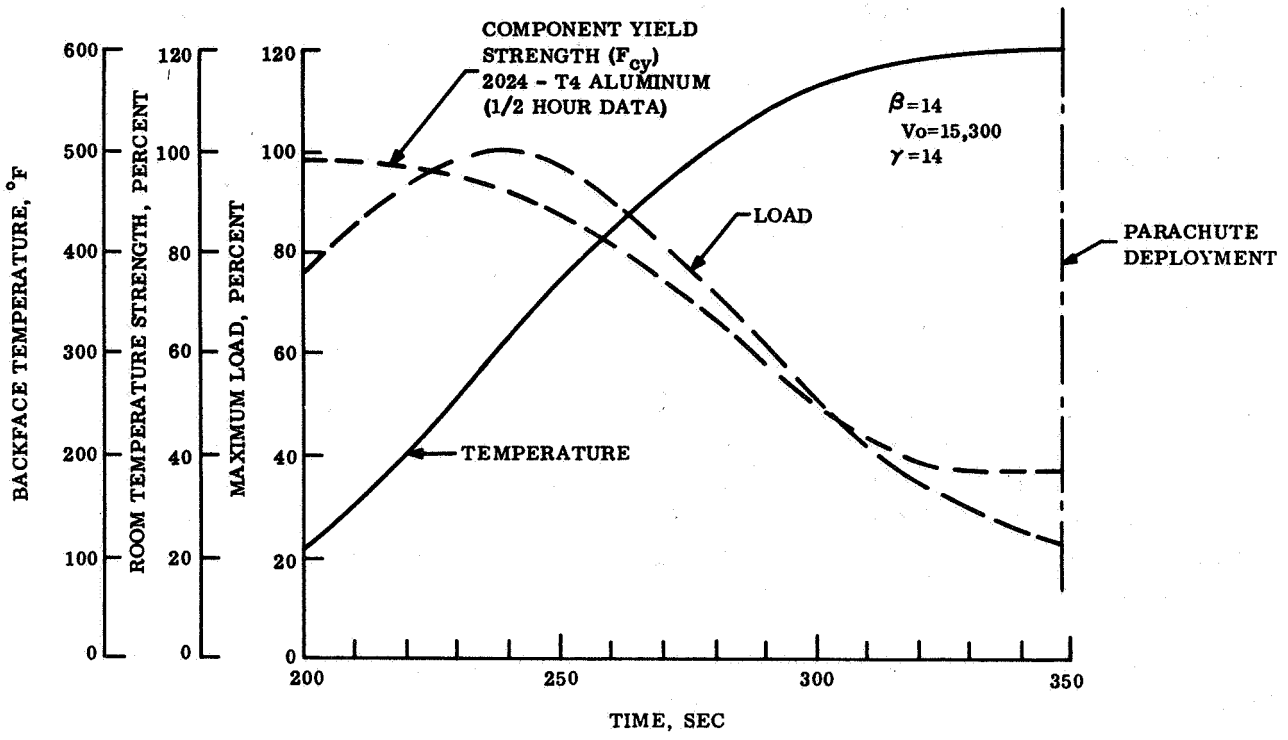


Figure 3.4.3-6. Performance Characteristics of 2024-T4

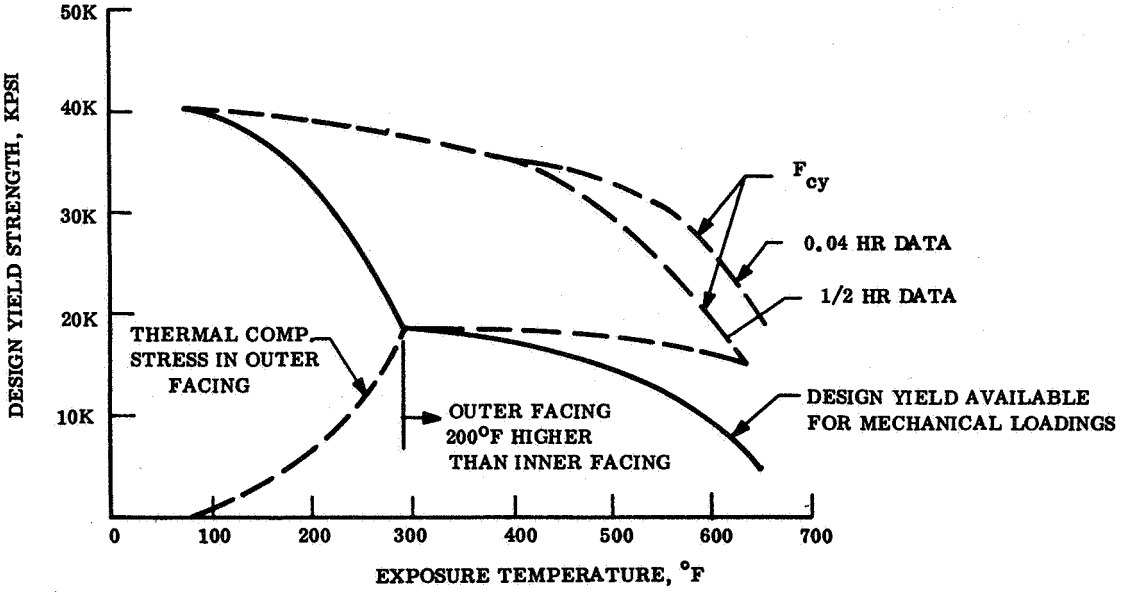


Figure 3.4.3-7. Mechanical Design Yield Strength For 2024-T4

The final design curve shown in fig. 3.4.3-7 is the compression yield minus the thermal stress level. For additional conservatism, the allowable strength was reduced to 1/2 of the design value shown in fig. 3.4.3-7. Three conditions were evaluated for the out-of-orbit point design:

Condition	G_x	Outer Facing (deg F)	Inner Facing (deg F)
1	12.7	200	70
2	5.5	320	130
3	1.375	600	400

Point Design 1 configuration parameters are presented in table 3.4.3-2. The honeycomb core and facing thickness requirements and minimum margin's of safety are presented in table 3.4.3-1. The critical condition was number 1 above, when the outer facing was 200° F.

The aluminum honeycomb weight is 0.82 psf of surface area (including bond) compared with 0.69 psf for titanium honeycomb.

TABLE 3.4.3-2. POINT DESIGN CONFIGURATION DATA

Point Design	Entry Weight (lb)	Diameter (in.)	Radius To Bearing Load (in.)	Radius To Box Structure A (in.)
1 (out-of-orbit)	1246	100.0	27.0	41.5
2A (direct)	1480	152.4	32.0	44.0
2B (direct)	1127	135.6	27.0	37.0
3 (out-of-orbit)	1324	100.0	31.0	41.5
4 (direct)	1558	152.4	31.0	44.0
5 (out-of-orbit)	1530	120.0	32.5	42.5
6 (direct)	1766	168.0	31.0	46.5

At the maximum base diameter is a box structure which extends forward into the aeroshell. This box structure is made up of a circular radial web and cylindrical longitudinal web with periodic ribs joined together by a ring at the base and tied into the aft ring of the aeroshell and a frustum ring internal and forward in the aeroshell.

The cylindrical longitudinal web extends beyond the maximum base diameter of the aeroshell to provide a support for the entry system separation device. At this point is the mating interface with the internal adapter.

This box like outer structure of the aeroshell acts as a torque box and restrains the rotation of the outer edge of the aeroshell. The construction of this torque box structure and the radial distance from the point of application of the load due to the payload bearing against the honeycomb shell determines the magnitude of the shell bending loads. With the torque box structure made very stiff, to allow very little torsional rotation, the maximum honeycomb shell bending moment and highest facing stresses would occur in the outer portions of the aeroshell. A reduction in the torsional box stiffness results in the maximum shell bending moments shifting to the center portion of the aeroshell. The ideal situation is then where some rotation is allowed such that the shell bending is reduced over the entire shell and the moments are of the same order of magnitude in the center and outer portions.

3.4.4 LANDER/AEROSHELL SEPARATION

The Lander is attached to the aeroshell by a strap assembly retained by three hot-wire tension bolts. The strap assembly, shown in fig. 3.4.4-1, consists of a strap or bellyband which runs completely around the Lander. As a part of the strap are cushioning pads and a teflon spacer to eliminate the possibility of damage to the crush-up material. The strap is in three segments connected by three hot-wire tension bolts. In the middle of each segment is a fitting which is attained by a T-bolt to the tie-down strap. The tie-down strap is attached to a fitting on the box structure in the aft end of the aeroshell. A torsion (or mousetrap) spring is also attached to this fitting and fits around the tie-down strap. To obtain the required restraining loads for the Lander, tension is placed in the entire assembly by torquing the T-bolt to a predetermined torque.

In order to separate the system, which occurs after parachute deployment, a current of 6 amps for 30 msec is fed to the hot-wire bolts causing them to separate. At this instant the torsion springs snap the tie-down strap and attached segments of the bellyband outboard and clear of the Lander, which is extracted from the aeroshell by the parachute.

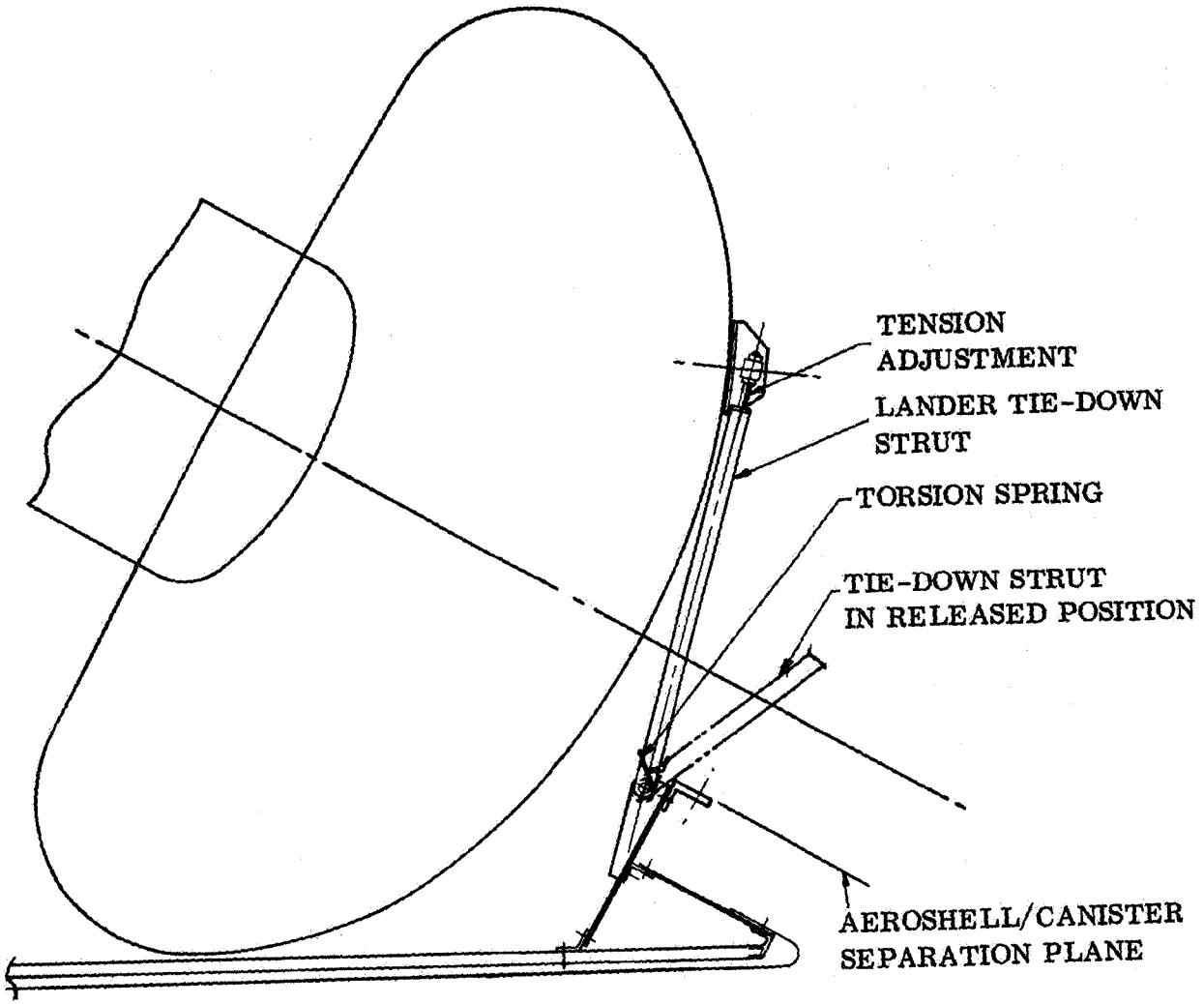


Figure 3.4.4-1. Lander Installation into Aeroshell

3.4.5 ENTRY SYSTEMS EQUIPMENT

With the exception of the four pressure and one temperature transducer for stagnation region measurements, all of the entry science instruments and support equipment (13.0 lb of the basic 15.5 lb package of instruments) is incorporated in the Lander module (fig. 3.4.5-1).

3.4.6 RETARDATION SUBSYSTEM

The retardation subsystem requirements are so similar for all of the point designs that a single subsystem design approach appears to be adequate. The design evolved for Point Design 1 will permit deployment and proper landing impact velocity to meet the required conditions of the mission. These are: deployment at speeds not greater than Mach 2, terminal velocity on main parachute at altitude not less than 6000 ft, and the velocity vertical descent occurring in the least dense atmosphere (VM-7) at 100 fps.

3.4.6.1 Retardation Performance

3.4.6.1.1 Mortared Pilot Parachute Selection

The use of a mortared pilot extraction parachute was selected over direct mortar ejection of the main parachute. The size of mortar required to directly eject such a large mass from the decelerating vehicle would take more weight than the selected arrangement. Furthermore, a more orderly deployment of the large diameter main parachute is ensured by using the pilot parachute extraction technique.

3.4.6.1.2 Trajectory Considerations

It is desired to minimize descent time on the main parachute while insuring that the main parachute will be at equilibrium terminal velocity at the time of its separation for Lander impact. Deployment based on sensing altitude alone would not be optimum. For the case where Mach 2 occurs at 11,000 ft in the VM-8 atmosphere, deploying at 11,000 ft in the VM-7 or VM-1 atmospheres would result in reaching terminal velocity on the main parachute at a lower altitude than in the VM-8 case even though the initial deployment would be below Mach 2.

Deploying on Mach number alone would produce high altitude deployment and a long descent time on the main parachute if the atmosphere is dense (i.e., VM-9). If the deployment sensing coupled a Mach 2 gate with a time gate and an altitude gate, deployment below Mach 2 and minimum descent time would be assured. The logic for this arrangement would probably be as discussed below. Further trajectory investigations would be necessary for any particular point design for optimization.

Parachute deployment will occur between 11 and 20 kft. A 20 kft signal from the radar altimeter would enable parachute dployment. On receipt of the Mach 2 signal, the timer would be started. If the 20 kft signal were received before the preset time-out, parachute deployment would occur. This would indicate a rare atmosphere. If Mach 2 did not occur until the receipt of the 11 kft signal from the radar altimeter, this would

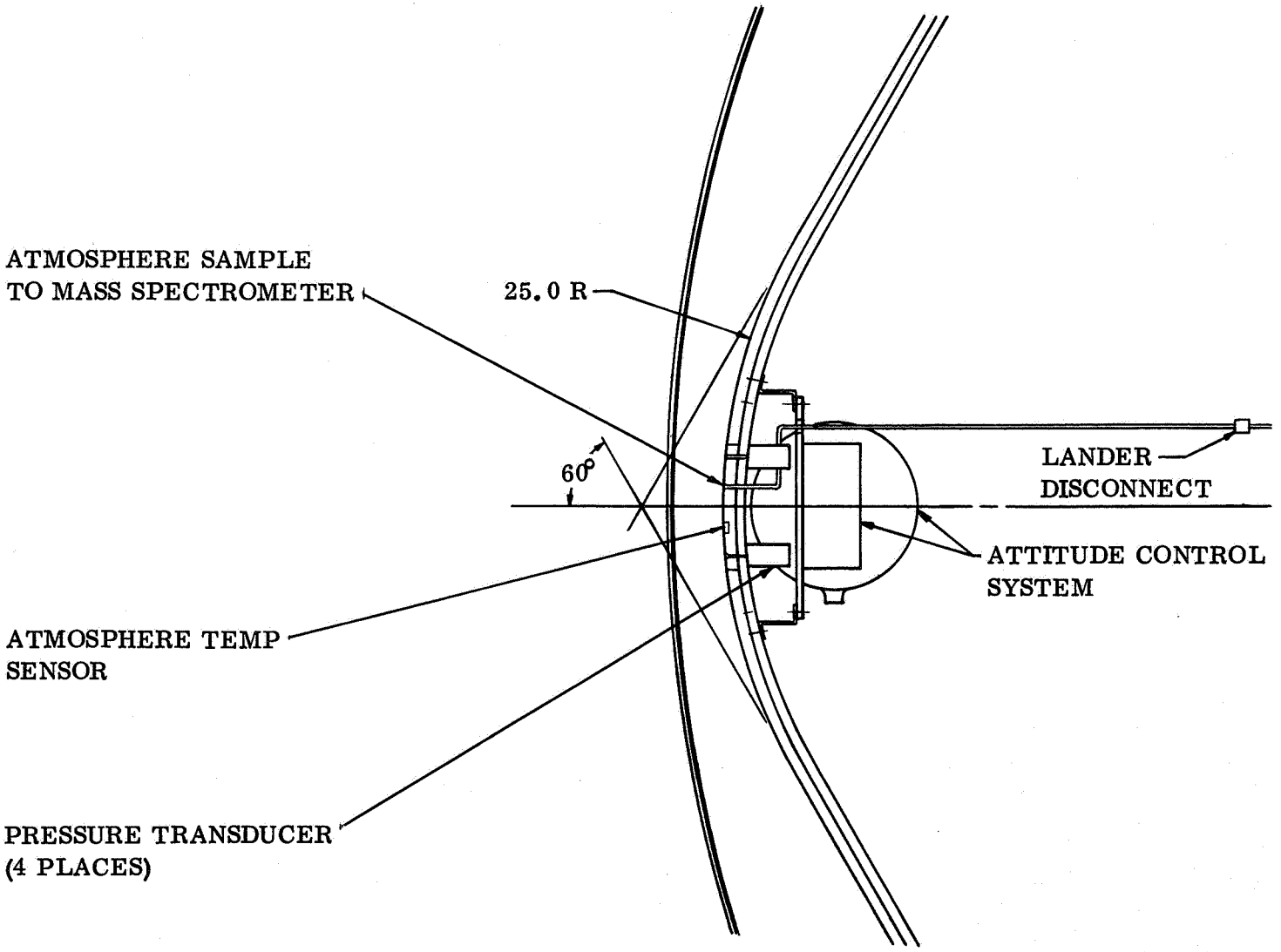
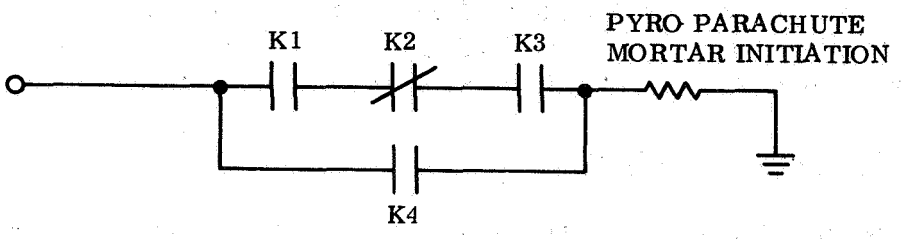


Figure 3.4.5-1. Entry System Instrumentation

indicate very rare atmosphere, such as VM-8. If the Mach 2 signal were received and time-out of the timer occurred prior to the 20 kft signal from the altimeter, this would indicate a dense atmosphere such as VM-9 or -10. In this case, parachute deployment initiation is delayed until the 11 kft signal from the altimeter. In any case, deployment would be initiated at 11 kft.

The following schematic clarifies this deployment logic.



K1 - closes at Mach 2 signal
K2 - opens at end of timer time-out
K3 - closes at 20 kft signal
K4 - closes at 11 kft signal

3.4.6.2 Parachute Design

The modified Ringsail parachute configuration, as tested in the PEPP program, was selected for the parachute design. To assure reliable deployment, a single large diameter main canopy deployed by an extraction pilot parachute was selected. The main parachute will be deployed with one stage of reefing to minimize opening loads and parachute weight. The technique of reefing is a proven and commonly used method of controlling parachute inflation and loads. It has been used in numerous applications in the past with complete success in all sizes of parachutes including Ringsail parachutes of the size that would be required for the Hard Lander of this study.

The single large diameter main canopy was selected over a cluster of smaller parachutes. More complexity is involved in deploying clustered canopies. The use of a cluster would increase the development risk for this application. Providing reefing with clustered canopies is much more complex than in the case of a single canopy because of the interactions of the clustered canopies. This interaction problem created a great deal of difficulty in applying reefing to the clustered parachutes used in the Apollo development. None of the inflation problems encountered in the Apollo development should be experienced in applying reefing to a single main parachute design investigated here.

With a reefed stage, the deployment loads experienced by the main canopy will be low enough to allow the use of light weight parachute construction. Analyses substantiating the materials and construction selected are presented in Volume III under Parachute Deceleration. The parachute system weights used were calculated using the RESEP program, which is described in Volume III, Appendix A.4.

Parachute design drag performance was based on results obtained in the PEPP program. A constant value for C_D of 0.52 was used. Other test data on Ringsail parachutes indicates a higher value for C_D should be obtainable. This would cause a reduction in parachute size, weight and opening loads. The use of $C_D = 0.52$ should therefore be conservative.

Available test data indicates that the Ringsail parachute inflation will follow the performance curve of figs. 4-49 and 4-50 of "Performance of and Design Criteria for Deployable Aerodynamic Decelerators", ASD-TR-61-579 (referred to as the parachute handbook). This data was used for this preliminary design analysis. The parachute inflation characteristic was assumed to be linear with time for each stage of deployment, i.e., $C_D S$ increases linearly with filling time. This is a good assumption for a first cut design analysis and is fairly representative of test data.

3.4.6.3 Design Trajectory Example

The purpose of the trajectory study was to verify that the selected point design could perform under the worst case deployment conditions and meet the established design requirements of parachute deployment at Mach No. ≤ 2.0 and reach main parachute full open terminal velocity at approximately 6 kft.

In some of the worst case design trajectories investigated, the main parachute does not reach terminal velocity until altitude is down to almost 4 kft. When further work is done to finalize a planned vehicle design and re-entry trajectory, the deployment altitude of the parachute system can be adjusted to reach terminal velocity at 6 kft.

The worst design conditions for the parachute occur in the rarest atmosphere represented by VM-8. The trade-off studies indicate that the vehicle will not decelerate to Mach 2 until approximately 11 kft altitude. For all other atmospheres, Mach 2 occurs at a higher altitude. Parachute performance was designed to meet the worst case deployment conditions of the VM-8 deployment. The study included the extraction and deployment of the main parachute by the pilot parachute.

The pilot parachute deployment occurred at 11 kft, Mach 2, and q = 20 psf. The trajectory of the pilot parachute extracting the main parachute was examined and compared to the trajectory of the vehicle now minus the weight of parachutes. This study was used to determine the point of start of main parachute reefed inflation where the main parachute skirt has been deployed. The results of this study are shown in fig. 3.4.6-1 and the parameters selected for use in the Point Design 1 study are listed in table 3.4.6-1.

3.4.6.3.1 Parachute Staging Design and Trajectory

Parachute reefing and duration of the reefed stage were determined using existing computer programs to produce opening loads for both main parachute stages to be within the strength capability of the suspension lines and minimize altitude loss during deployment.

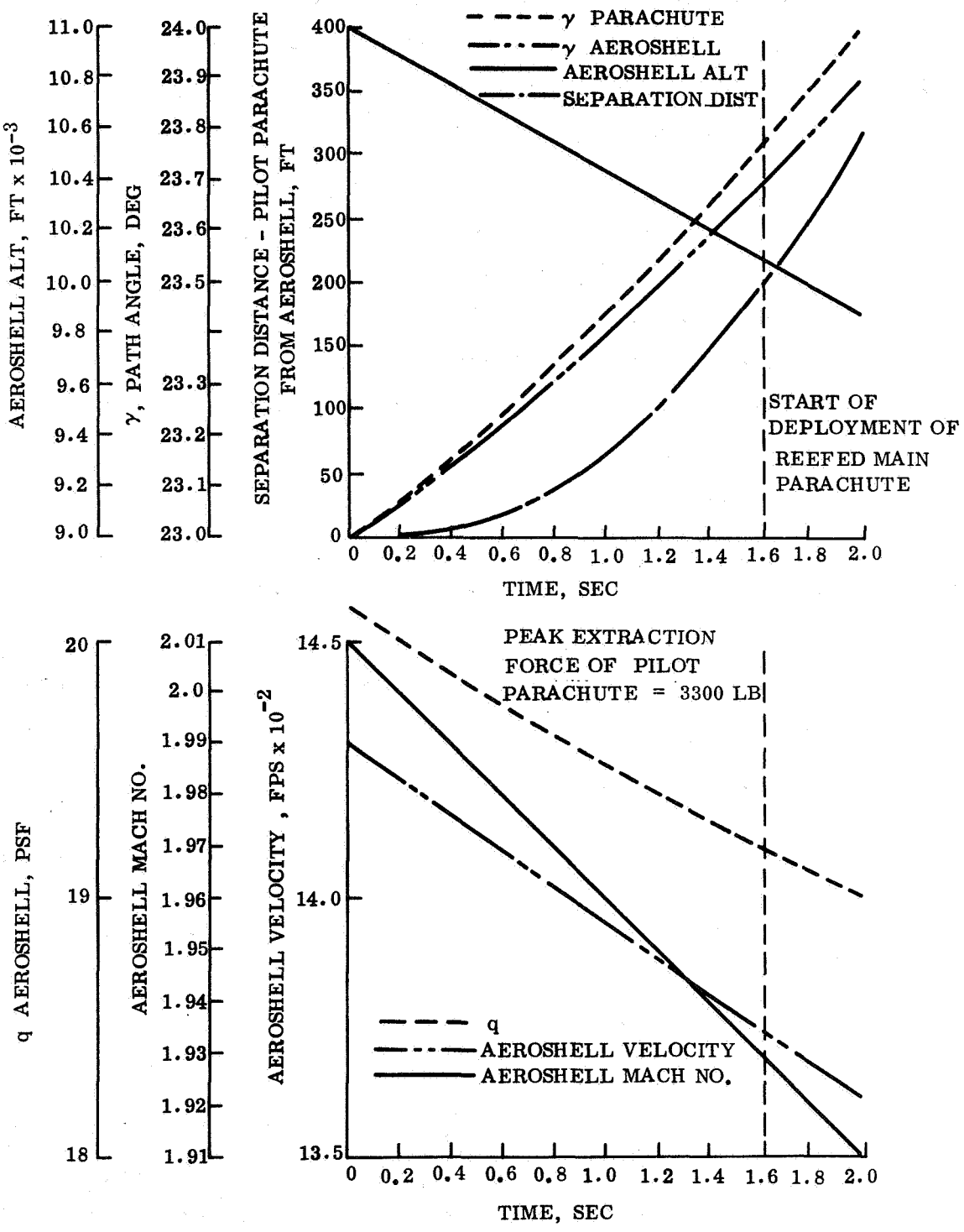


Figure 3.4.6-1. Pilot Deployment Trajectory Study, Point Design 1

TABLE 3.4.6-1. PILOT PARACHUTE DEPLOYMENT TRAJECTORY STUDY PARAMETERS

Atmosphere = VM-8
Initial deployment altitude = 11 kft
Weight being decelerated by pilot parachute = 193 lb
Vehicle weight minus the parachutes = 893 lb
Path angle below horizontal = 23°
Pilot parachute fill time = 0.24 sec
Linear pilot parachute inflation with time assumed
Pilot parachute D_o = 15.7 ft
Pilot parachute C_D = 0.52
Pilot parachute C_DS = 101 ft^2
Pilot parachute opening shock factor = 2.0
Average wake reduction effect during pilot parachute extraction = 0.85
Aeroshell D_o = 8.34 ft
Aeroshell C_D = 1.46

The analysis to establish reefing ratio is based on a simultaneous solution of the following equations for the two stage main parachute deployment:

$$F_1 = C_D S_1 \cdot X_1 \cdot q_1$$

$$F_2 = C_D S_2 \cdot X_2 \cdot q_2$$

$$q_2 = \frac{W_1 \cdot LF_1}{C_D A_1}$$

where:

C_DS	=	effective drag - ft^2
F	=	opening force - lb
X	=	opening shock factor
q	=	dynamic pressure - psf
W	=	Weight in local gravity - lb
LF	=	force along Z axis in local gravity - 'g's

subscripts:

1	=	stage one
2	=	stage two

The quantities C_DS_2, q_1, X_1, X_2, LF_1 and W_1 must be known. Without accurate performance data on a given design, assumptions must be made for X_1, X_2, and LF_1. If the correct characteristics are used, the performance can be verified in a computer trajectory analysis with a program designed to vary the C_DS during parachute inflation.

Optimum reefing should produce equal opening load peaks for both stages. However, a reefed design can be satisfactory if other objectives are met and the peak loads are not balanced. In this case, if the opening forces are within the structural capability of the parachute and the total altitude loss during deployment is not excessive, the performance will meet the requirements.

In the staging study below values were selected based on past experience and data. Reefing ratio was selected, using the approach described above, to produce equal stage loads. In the trajectory study, fill time was based on data from the parachute handbook (ASD-TR-579) and C_DS growth was assumed to be linear with time. The disreef opening force from the trajectory analysis (shown on fig. 3.4.6-2) came out lower than the reefed opening force. By iteration, the opening forces in the reefing ratio selection analysis and the trajectory analysis could be made to come out equal. However, at this point, the exercise would be academic. Slight changes in the disreef fill time, or some non-linearity in C_DS growth, or a combination of the two could significantly affect the resulting disreef open force. At this point, there is higher confidence that the reefed opening force is correct than there is in the disreef opening force.

In the hardware development program, the reefing line length to produce the desired reefing ratio will be selected based on the best existing data available. After first test data is obtained necessary adjustments would be made to obtain the desired reefed performance based on data from the actual system. There is high confidence that required reefed performance can be achieved with little difficulty.

The PEPP program demonstrated satisfactory inflation characteristics in Mach 2 deployment in a rare atmosphere. With reefing, inflation will proceed in the same manner as without reefing until the point where the reefing line restricts and delays full inflation. In all cases, a reefing design must be verified in the parachute development test program.

The parameters selected for the staging optimization study are shown for Point Design 1 in table 3.4.6-2.

The parachute trajectory was calculated by computer using the established or calculated parameters shown in table 3.4.6-3.

The results of this trajectory study are shown on fig. 3.4.6-2. These calculations are conservative inasmuch as the aeroshell or Lander drag area is not considered as part of retardation drag area after main parachute deployment.

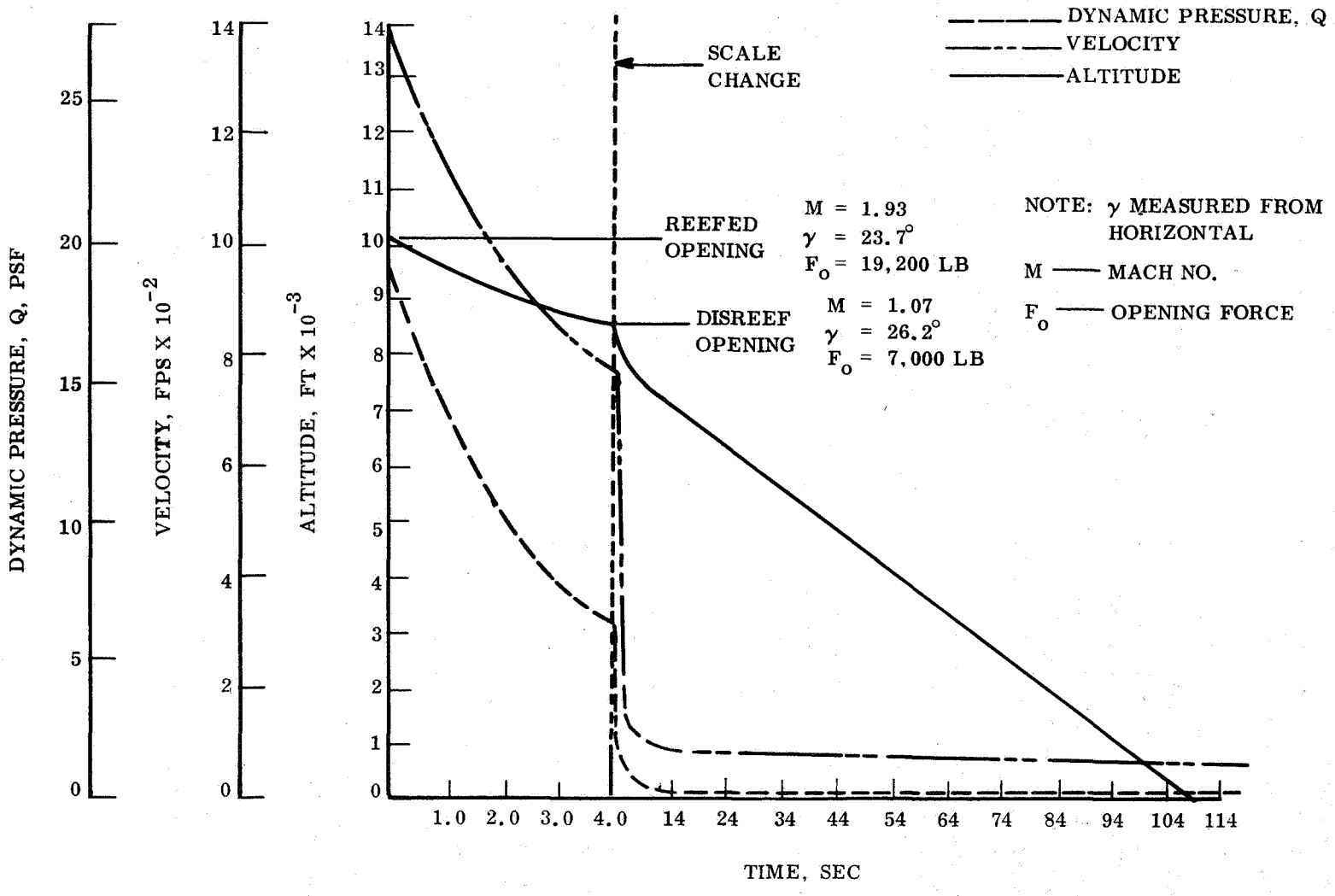


Figure 3.4.6-2. Main Parachute Trajectory in VM-8 Atmosphere, Point Design 1

TABLE 3.4.6-2. MAIN PARACHUTE DESIGN PARAMETERS

Main parachute fill open $C_DS = 6587$ ft^2
Initial reefed deployment q = 19.22 psf
Reefed stage opening shock factor = 2.0
Disreef opening shock factor = 0.5
Axial deceleration at disreef ~ 7 g's, Martian
Total weight being decelerated = 1086 lb
Main parachute C_D = 0.52

TABLE 3.4.6-3. PARACHUTE TRAJECTORY PARAMETERS, POINT DESIGN 1

Atmosphere = VM-8
Total weight being decelerated = 1086 lb
Initial deployment altitude = 10,108 ft
Initial velocity, reefed deployment = 1377 fps
Initial path angle = 23.7°
Linear reefed opening inflation with time assumed
Reefing ratio = 7.74 percent
Reefed filling time = 0.16 sec
Total time of reefed stage = 4.0 sec
Main parachute D_o = 127 ft
Main parachute C_D = 0.52
Main parachute full open C_DS = 6587
Main parachute full open fill time = 3.04 sec
Linear full opening inflation with time assumed

3.4.6.4 Hardware Description and Function

The basic hardware concepts selected for Point Design 1 have been previously used, tested, and proven in other programs. The mortared parachute deployment is a commonly used technique and the thermal cover concept and deployment arrangement has been used by GE on the 698 BJ program and the Maneuvering Ballistic Re-entry Vehicle (MBRV) program. The method of main parachute release has also been verified on these programs using explosive nuts. The parachute designs selected in the point designs of this study are based on the designs and results to date of the NASA PEPP program. The aeroshell release and fall-away is similar to the re-entry heat shield separation used by GE in the A-45 program.

3.4.6.4.1 Pilot Parachute Mortar Thermal Cover

The thermal cover provides the means for securing the pilot extraction parachute in the mortar prior to mortar deployment. It also anchors one end of the main parachute thermal cover and provides thermal protection from wake heating to the pilot parachute, mortar gas source and the pull-away electrical disconnect. The cover will be secured to the mortar tube by a break cord or shear pins until mortar firing. A bag handle on the pilot parachute deployment bag will be secured to the thermal cover in a recess within the cover. Thus, the thermal cover will also provide a mass to assist in stripping the deployment bag from the pilot parachute during deployment.

3.4.6.4.2 Pilot Extraction Parachute

The pilot extraction parachute will be similar in design to modified Ringsails tested in the NASA PEPP program. All parachute lines and material will be sterilizable dacron, and lightweight construction is envisioned using 1.1 oz cloth and 300 lb suspension lines. In a development program, an investigation would be made to determine the suitability of utilizing 0.8 oz material in the lower panels near the skirt to save weight. The pilot parachute will be pressure packed to a 40 lb/ft^3 density or slightly higher.

3.4.6.4.3 Pilot Parachute Riser Line

The pilot extraction parachute will be provided with a riser line to provide a minimum length of six aeroshell base diameters to the skirt at parachute inflation. This line will also be used to provide a mouth lock for the pilot parachute bag and to extract the main parachute bag for main deployment. It will attach to two fittings, one at each end of the main parachute thermal cover, for extraction and deployment of this cover. The end of this line, at the main parachute bag, will be used for form a tuck bight through a locking loop of the three tie-down straps securing the main parachute in its compartment.

3.4.6.4.4 Main Parachute Compartment Thermal Cover

The main compartment thermal cover provides thermal protection for the main parachute pack from re-entry wake heating. It is deployed by the pilot extraction parachute and permanently attached to the pilot parachute riser. This cover can also serve

as a mounting point for spring pushers to jettison the de-orbit propulsion and thrust structure. The cover will be aluminum with necessary reinforcement to sustain the loads of deployment. All edges will be well rounded to prevent damage to the pilot parachute riser line. The outside surface will be covered with thermal protective coating to preserve the cover's structure and control main parachute temperature from re-entry wake heating.

3.4.6.4.5 Main Parachute, Two Stage Deployment, Modified Ringsail, 15 Percent Geometric Porosity

The main parachute will be a single large diameter parachute with one stage of reefing. Existing design hermetically sealed reefing line cutters, manufactured by Technical Ordnance Products Co., will be used. The parachute will be made of sterilizable dacron material, in lightweight construction similar to the constructions tested in the PEPP program. At present the parachute, would be made of 1.1 oz cloth with 300 lb suspension lines since deployment q will be 20 psf or less. In a development program to optimize weight and volume, the use of 0.8 oz cloth in the lower panels near the skirt would be investigated. A higher weight, lower mechanical porosity material is needed in the crown area to facilitate initial reefed deployment. If added strength is required, 1.6 oz material will be used in the crown area. The main parachute will be pressure packed to 38 to 40 lb/ft^3 density. Parachute reefing will be established to produce approximately equal opening loads at each stage of deployment to a level that utilizes the full structural strength capability of the suspension lines, considering appropriate design derating factors. The reefed stage time will be set as short as possible to minimize altitude loss during this stage and provide a high opening velocity for rapid full open inflation. The trajectory in the VM-8 atmosphere, where Mach 2.0 occurs at the lowest altitude, will be used to determine staging time and reefing ratio. The opening loads in any other atmosphere will be lower than those for the VM-8 atmosphere as the deployment is presently envisioned.

3.4.6.4.6 Main Parachute Riser

The attachment risers will connect the main parachute at the suspension line confluence to the three tie-down fittings at the bottom of the parachute compartment. At main parachute release, the parachute compartment including the mortar will remain with the main parachute.

3.4.6.4.7 Parachute Compartment Including Mortar

The parachute compartment will be an aluminum sheet metal fabrication to confine the parachute and provide thermal protection from re-entry wake heating. The outside surface of the compartment will be provided with the required thermal protective coating. The attachment and tie-down fittings will be attached to the rim at the bottom of the compartment. The pilot parachute mortar will be built into one side of the compartment. It will consist of a mortar tube and a sabot for the pilot parachute to seat against. The gas for mortar ejection will enter through tubing at the bottom of the mortar under the sabot. The area on each side of the mortar will be used for mounting the gas source for mortaring and the pull-apart electrical disconnect to

separate the power supply from the mortar pyrotechnic. The side of the parachute compartment opposite the mortar will provide a slotted projection to receive a tang on the main thermal cover that secures that end of the thermal cover.

3.4.6.4.8 Parachute Attachment and Tie-down Fittings

Three fittings, one for each of the three risers, are attached to the parachute compartment at the bottom flange and will be provided with two pins for webbing attachment. One pin will attach the main parachute risers (3), and the second pin will attach tie-down straps that secure the main parachute in a position such that it does not put a load on the main parachute thermal cover by pressing against it. The three tie-down straps will secure the main parachute using a locking loop and a tuck bight formed by the pilot parachute riser.

3.4.6.4.9 Mortar Pyro Gas Generator or Compressed Gas Supply

The gas for mortar ejection can be provided by either a pyro gas generator or a compressed gas supply. The compressed gas supply can be provided at a slight weight increase over the gas generator. Standard components are available from Conax Corporation (Conax Eager Paks) for the compressed gas supply. It would consist of a small hermetic cylinder (10 to 15 $in.^3$ capacity) containing compressed nitrogen at 3000 psi and a pyro valve that fires, piercing the cylinder allowing flow out through a connecting tube. This arrangement offers several advantages. There is no hot gas that could damage fabrics or components used for mortaring. There will be less problem of pyro development for the Mars mission in that the valve uses a standard squib and does not need the special gas generating materials. Reaction forces and performance will be more predictable. The compressed gas can be sterilized readily where this may be a problem with the gas generator materials.

3.4.6.4.10 Pull-apart Electrical Disconnect

This component consists of an electrical connector, half of which is mounted captive to the main parachute compartment. At main parachute release, when the parachute compartment is pulled away, the two halves of the connector are separated. This component has been used successfully in a number of GE vehicle designs in the past.

3.4.6.4.11 Parachute Compartment Separation

The parachute compartment will be secured to the payload by three explosive nuts, each having dual cartridges, attached to bolts passing through the attachment and tie-down fittings. These will be similar to the explosive nuts used for Capsule separation and described in Section 3.3.3. The main parachute tie-down and deployment loads will be carried by these separation devices and fittings.

3.4.6.4.12 Mach 2 Sensor

This device will sense Mach No. as a function of vehicle base pressure divided by axial acceleration. (Point Designs 3, 4, 5, and 6 incorporate an altitude marking radar for parachute deployment and release before Lander impact.)

3.4.6.5 Sequence of Retardation Subsystem Events

The series of deployment events described are depicted in fig. 3.4.6-3.

On receipt of the signal for parachute system deployment, power from the vehicle power supply will be applied to the mortar pyro initiation. Mortar firing will release and deploy the pilot parachute thermal cover and the pilot parachute. After stripping off the pilot parachute, the pilot parachute deployment bag and attached thermal cover free-fall away.

As the pilot parachute is being deployed, the main compartment thermal cover will be deployed by the snatch force of the pilot parachute. One end of the main thermal cover is released by the pilot parachute cover separation. The main cover is attached to the pilot parachute riser at two points for deployment and retention to the riser. As the cover is rotated out by the pull from the pilot parachute, the hold-down tang on the edge of the cover opposite the mortar will rotate out of a slot in the main parachute compartment completely releasing the cover.

The snatch force of the main compartment thermal cover on the pilot parachute riser will pull out the tuck bight securing the main parachute tie-down straps. This releases the main parachute pack for deployment. Further pull force on the pilot parachute riser will be applied to the main parachute bag handles for main parachute extraction and deployment.

The main parachute is extracted and deployed in a reefed condition by the pilot parachute. During this deployment, the mechanically initiated pyro time delay reefing line cutters are actuated. As the drag of the reefed main parachute develops, the aeroshell is released and allowed to free-fall away. After time-out of the redundant reefing line cutters, the cutters actuate, severing the reefing line. This event permits main parachute full open deployment.

A 150 ft drop line is used to sense the distance of the Lander above the touch-down surface. When the line makes ground contact a signal is given to release the explosive nuts, which in turn cause separation of the parachute compartment/mortar assembly from the Lander. The Lander will free-fall to surface impact. The jettisoned main parachute will collapse and spill to one side due to the sudden release of loading from the suspension lines while the parachute was fully inflated. (Point Designs 3, 4, 5 and 6 incorporate a radar altimeter for this purpose.)

3.4.6.6 Retardation Subsystem Weight

The subsystem equipment weight for Point Design 1 is tabulated in table 3.4.6-4.

FOLDOUT FRAME

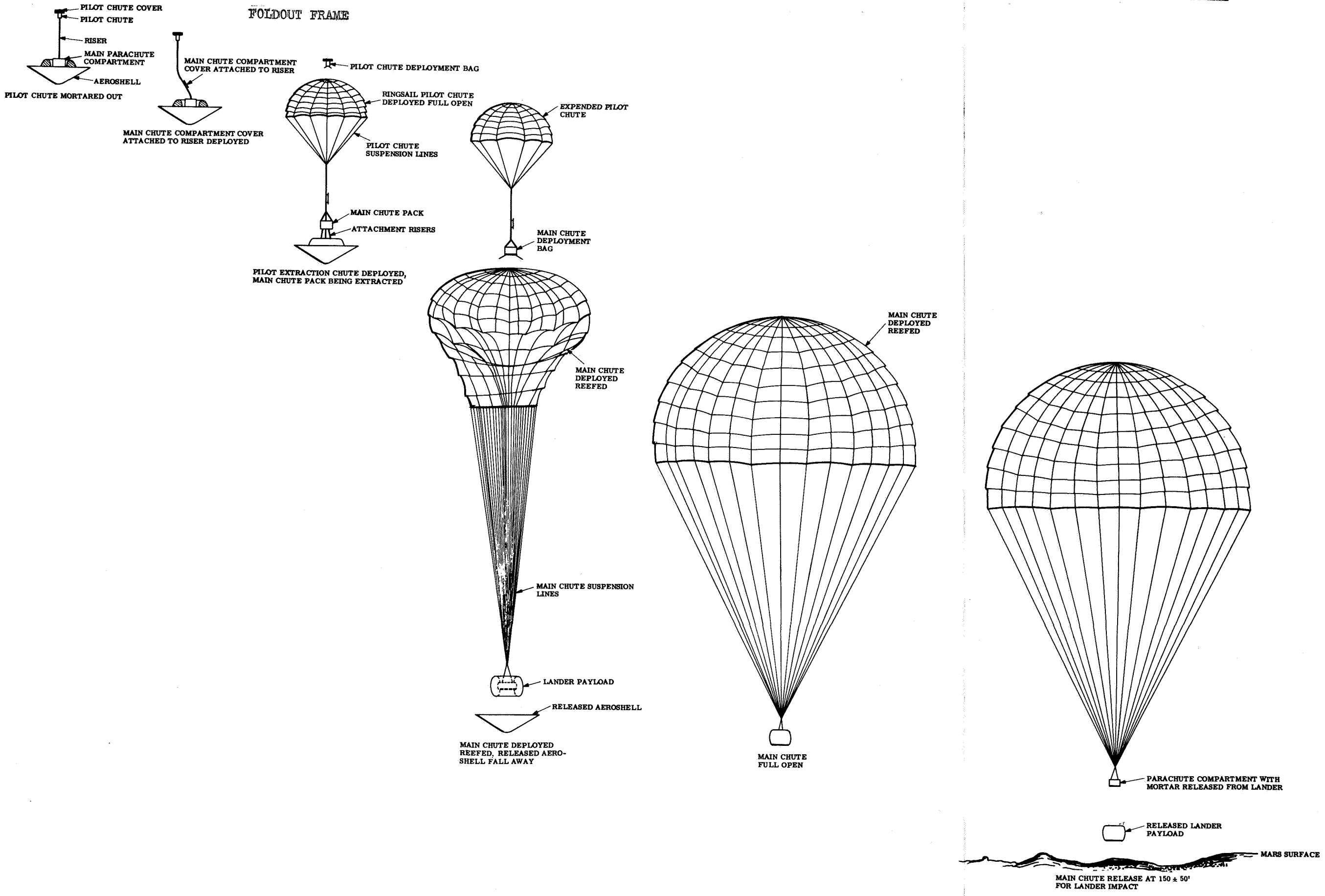


Figure 3.4.6-3. Retardation Deployment Sequence

TABLE 3.4.6-4. RETARDATION SYSTEM WEIGHT BREAKDOWN

	Weight (lb)
Pilot parachute mortar thermal cover	1.5
Pilot extraction parachute (modified Ringsail)	7.0
Main parachute compartment thermal cover	7.0
Main parachute, two stage deployment (modified Ringsail)	188.0
Main parachute attachment riser (3 legs)	2.0
Parachute compartment including mortar	15.0
Parachute attachment and tie-down fittings (3)	2.0
Mortar pyro gas generator or compressed gas supply	3.0
Pull-apart electrical disconnect	.2
Explosive nuts (3)	2.5
Total Subsystem Weight	228.2

3.4.7 ROLL CONTROL SUBSYSTEM

The roll control function is performed by the de-orbit equipment described in Volume IV, para 3.3.7.1. A single monopropellant hydrazine control is used, in conjunction with a rate gyro, to perform both the functions of spin and entry roll control.

3.4.7.1 Roll Control Requirements

At very low dynamic pressures, blunt bodies can be made unstable at zero angle-of-attack by spin. This phenomenon occurs after peak pressure where the pressure is decreasing with time. The effect here is that in the terminal steady state condition the vehicle will diverge to a trim angle-of-attack (dependent on configuration, spin rate, ballistic coefficient, and inertia properties) and follow a helical flight path.

The effects of this divergence may or may not be significant depending on requirements. Specific items that would be affected are base pressure measurements, radar altimeter measurements, vehicle ballistic coefficient (increases at angle-of-attack), and communication aspect angle.

In order to insure stability in this region a maximum roll rate must not be exceeded. However, roll torques will develop during entry due to built-in and ablation induced asymmetries. An estimate of this roll torque and the total roll impulse during entry was listed in table 3.4.3-1.

TABLE 3.4.7-1. SPIN AND ROLL CONTROL SUBSYSTEM FIXED HARDWARE WEIGHT, POINT DESIGN 1

Component	Quantity	Weight (lb)
Rate gyro	1	1.0
Spin electronics	1	2.4
Fill valve	2	0.5
Squib valve	1	0.5
Pressure sensor	1	0.5
Temperature Sensor	1	0.25
Valves	2	0.6
Thrusters	4	1.0
Tubing, fittings	-	1.05
Supports	-	2.5
Total weight		10.3

The Capsule will tend to spin up under the action of this roll torque and it is necessary to provide sufficient roll control torque and impulse to prevent Capsule roll rate from exceeding a maximum limit. The list of fixed hardware is given in table 3.4.7-1 for a total fixed weight of 10.3 lb. The weight of the remainder of the subsystem (hydrazine, pressurant, and tankage) is included in the design data shown in table 3.4.7-2. Total subsystem weight is 14.9 lb. The control torque and impulse provided for roll control also is listed in table 3.4.7-2.

3.4.8 ENTRY SYSTEMS WEIGHT

A summary weight statement for the items comprising the entry system weight (less Lander and pre-entry systems weight) for Point Design 1 is shown in table 3.4.8-1. Total entry system weight for this point design is 387.6 lb.

TABLE 3.4.7-2. SPIN AND ROLL CONTROL SUBSYSTEM, POINT DESIGN 1 PARAMETERS

Separation to spin-up, time	1.5 sec
Spin rate	50 rpm
Spin-up time	25 sec
Roll thrust	3.8 lb
Roll torque	29.1 ft-lb
Impulse requirements	
spin/de-spin	368 lb-sec
roll control	133 lb-sec
Weight of Hydrazine	
spin/de-spin	1.6 lb
roll control	0.6 lb
Tank weight	2.0 lb
Pressurant weight	0.4 lb
Fixed hardware weight	10.3 lb
Total Subsystem Weight	14.9 lb

TABLE 3.4.8-1. ENTRY SYSTEM WEIGHT SUMMARY, POINT DESIGN 1

Item	Weight (lb)
Aeroshell skin	51.0
Miscellaneous structure	41.0
Heat shield	39.0
Separation system	1.8
Attitude control	14.9
Retardation	228.2
Harness and cabling	6.2
Entry science	2.5
Mach 2 sensor	3.0
Total Entry System Weight	387.6

3.5 LANDER SYSTEMS

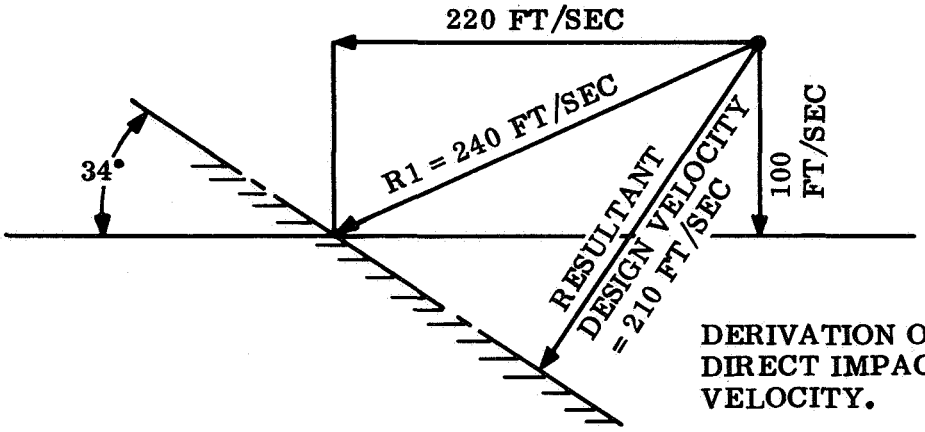
3.5.1 CONFIGURATION CONSTRAINTS AND DESCRIPTION

3.5.1.1 Constraints and Design Parameters for Vehicle Point Design 1

1. Maximum horizontal velocity of Lander at impact due to winds: 220 ft/sec.

2. Maximum vertical velocity of Lander at impact: 100 ft/sec. Selected based on the optimization of the deceleration and impact attenuation subsystems.

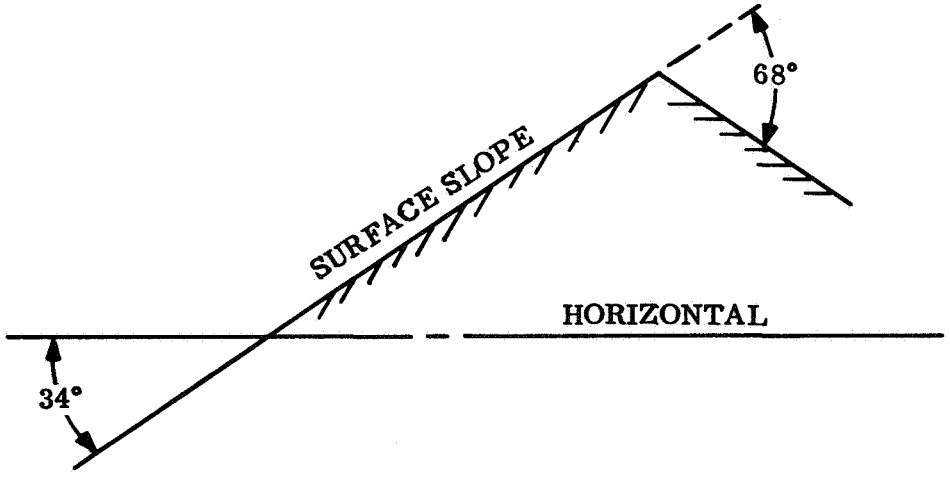
3. Maximum resultant direct impact design velocity: 210 ft/sec.



DERIVATION OF DIRECT IMPACT DESIGN VELOCITY.

4. Surface characteristics (to Langley requirements)

   a. Surface slopes: zero to $\pm 34^{\circ}$ relative to horizontal, with abrupt slope changes of $\pm 68^{\circ}$ forming hills (or valleys). As shown in the following sketch:



   b. Continuous slopes are defined as being as long or longer than the base diameter of the Lander.

   c. Maximum surface rock diameter: 5.0 in.

5. Maximum total Lander design g-level: 1000. Selected for point design, as a compromise between conflicting influences of structure and impact attenuation system design; volume for aeroshell packaging and weight.

6. Vehicle attitude and impact system design: Omni-directional full attenuation capability for maximum design velocity and g-level.

7. Landed temperature conditions assumed for environmental control design

   a. Ambient: -152°F to +114°F (to specification*)

   b. Component tolerance (non operating): -40°F to +160°F. Except for battery where the allowable temperature range is +50°F to +80°F.

8. Surface mechanical properties

   a. Bearing capacity: 6 psi to infinity

   b. Coefficient of friction: up to 1.0

   (Infinite strength surface assumed as the limiting design case for impact attenuation).

9. Geometrical, weight and c.g. constraints

   a. Packaging objective: approximately 40 lb/ft^3 in central cylinder of payload container.

   b. Center-of-gravity: on or forward of horizontal center line of Lander container.

3.5.1.2 Lander Description

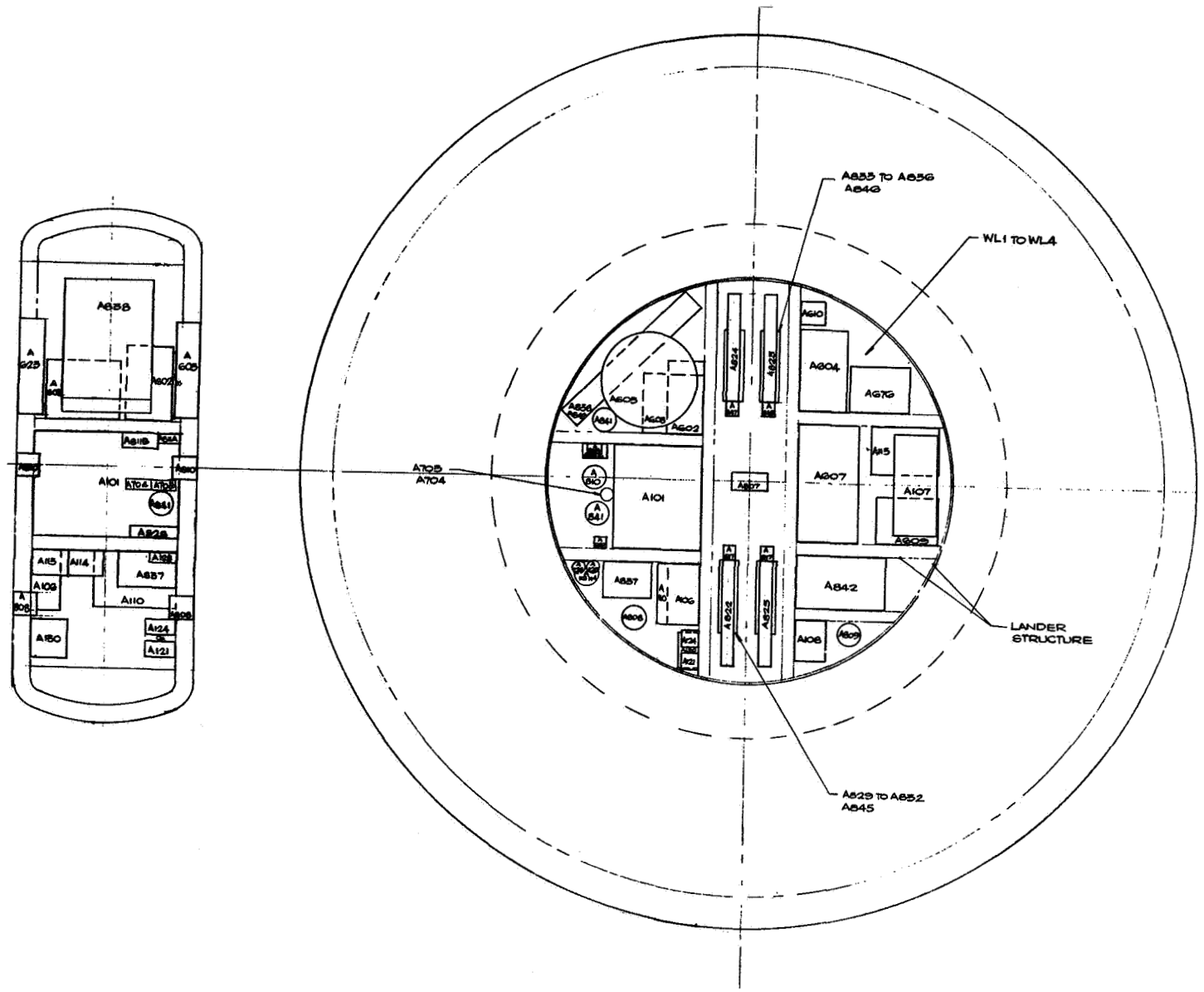
3.5.1.2.1 Configuration

The Lander concept is a doughnut shaped vehicle, with a central circular flat pack payload container. Either side of the vehicle may be face up after landing. It utilizes a completely passive landing system. The configuration of Point Design 1, illustrated in fig. 3.5.1-1, general assembly of Lander, shows the layout of and the volume required for a solid core memory and dual multicoder telecommunication system. A thin film memory and single multicoder system was evolved during the Point Design 3 effort and has been included in Point Design 1 performance and weight descriptions without revising the Lander general assembly.

*Mars Engineering Model Parameters for Mission and Design Studies. Langley Research Center, May 1968.

FOLDOUT FRAME

FOLDOUT FRAME



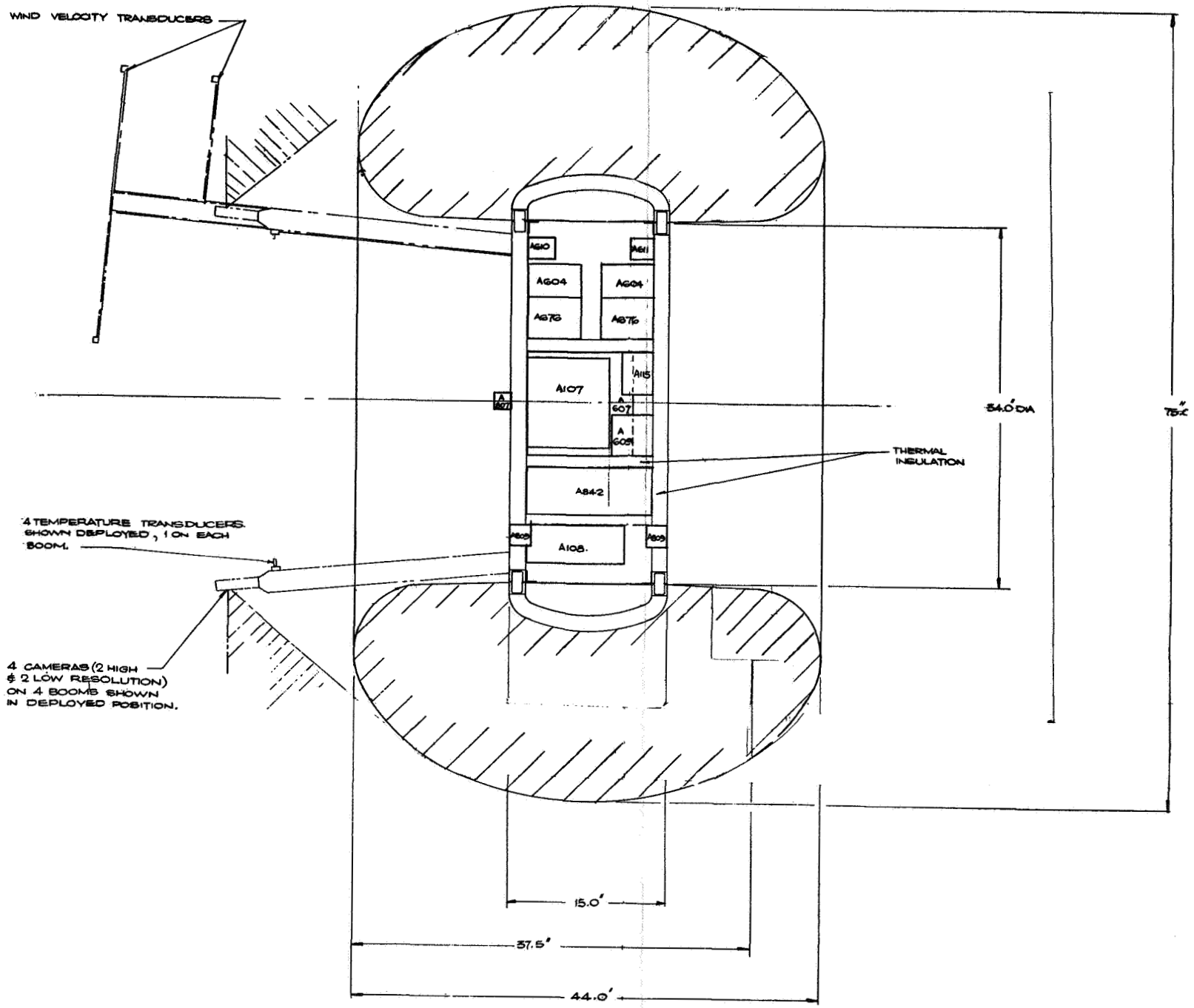


Figure 3.5.1-1. General Assembly Point Design 1

The central container, a short large diameter cylinder with a D-shaped edge structure, houses all the science and supporting subsystem equipment. A deep ring phenolic glass impact attenuation system is bonded to the edge structure of the payload container. Provision is made for science instruments and other equipment to be deployed from the Lander. The degree and type of deployment necessary varies between point designs and is discussed in detail in Section 3.5.6 for Point Design 1.

Depending upon the vehicle mission, electrical power and telecommunication subsystems vary between point designs and these subsystems and other vehicle equipment for Point Design 1 are discussed in detail in the following Lander sections.

Point Design 1 is the smallest and simplest Lander system with a minimum payload and the shortest operational surface lifetime. It is designed with an omnidirectional landing capability, and serves to illustrate the penalties paid for this capability over a multi-directional Lander; in weight and volume in the impact attenuation system, in vehicle packaging in the aeroshell, and to some extent, added complexity in the required instrument deployment.

3.5.1.2.2 Science Payload

Science instrument payload installed is the specified minimum listed and is discussed in Section 3.5.2. The Lander carries the majority of the entry science as well as the surface science, to avoid duplication of supporting subsystems and instruments and for flexibility of data acquisition and storage.

Provision is made for deployment of cameras, wind measuring instruments, temperature transducers and the alpha back scatter instrument head. The cameras and wind velocity and temperature instruments are housed in a central bay, which is the full width and depth of the Lander payload container. They are mounted on short spring-loaded swinging booms primarily provided for camera deployment. The wind velocity instrumentation requires secondary spring-loaded arms, which unfold at right angles to a spring-loaded extension of the camera booms when the booms are deployed, to provide correct relative location. Deployment of equipment from this bay is substantially automatic following selection and jettison of the bay door on the uppermost and exposed side of the Lander. With the current provision of four separate cameras and deployment booms and the capability to deploy all four from either side of the Lander for high and low resolution imaging, some boom deployment sequencing will be necessary, but can be kept relatively simple.

A gravity sensing device determines the uppermost side of the Lander and releases the upper door. Doors are spring-loaded and secured with bolts incorporating hot-wire devices.

The alpha back scatter instrument is located in a separate full depth bay and the instrument heat can be deployed downward onto the planet's surface, through whichever side of the Lander constitutes the underside. To facilitate this operation with a minimum of rotational movement of the instrument head, the alpha back scatter instrument is

installed on its side in the bay. Sensing for operation of inward hinging doors enclosing the alpha back scatter bay is by the gravity device provided for the camera bay doors. A full detailed description of the deployable instrument installation and mechanical operations, with illustrations, is given in Section 3.5.6.

The remainder of the payload (science and supporting subsystems) is housed in other compartments formed by the inner framework of the payload container. Access to this equipment is available through either the top or bottom bolted covers of the container, or by removal of the inner framework from the Lander, complete with all equipment. The installation is compact to achieve low weight and volume, but consistent with requirements for assembly, service and operational functions.

3.5.1.2.3 Lander Support Subsystems

To perform the one diurnal cycle mission of Point Design 1, the telecommunications link is designed to provide a relay link for transmission of imagery data for the periapsis passage of the Orbiter immediately after impact on the surface of the planet and at the end of each succeeding diurnal period. The telecommunications system consists of a 400 MHz transmitter with a dual power amplifier output stage, memory with 180 kbit storage capacity and the appropriate signal conditioning and data handling equipment.

The electrical power and distribution equipment located in the Lander provides all the primary power required of the Lander and the appropriate programming and sequencing functions. The main power source for this mission is a silver-zinc battery of approximately 30 lb. This battery was sized based on a 30 watt-hr/lb rating.

As stated, surface science equipment consists of the minimum science package including equipment to measure wind velocity, surface temperature, and pressure, alpha back scatter, imagery, a clinometer and moisture detector. Imagery data will be taken and transmitted to the Orbiter during the periapsis passage for each of the four available transmission periods, and will be transmitted real time. Additionally, stored entry and surface science data, diagnostic, and real time surface science data is alternately transmitted between the picture taking sequence.

Environmental control, primarily an insulation problem, is achieved by the use of honeycomb panels with fiberglass core for the outer shell of the Lander container, coupled with the application of thick layers of foam on exposed surfaces, such as the sidewalls of the camera bay. Batteries, which are the component most sensitive to the cold environment, are maintained at a working temperature by a combination of heat dissipated from other components and an individual electric heater.

A complete description of science and Lander sub-systems including structural and mechanical components is given in the sections following, together with detailed weight information.

3.5.2 SCIENCE PAYLOAD EQUIPMENTS

3.5.2.1 General

The various instruments carried by the Hard Lander to Mars can be classified into two general categories. They are the entry phase instruments, which require no special compatibility with unusually high deceleration loading, and the landed phase instruments which must survive the extreme loads and shocks encountered during impact and maintain their calibration and state of operability. In most cases, the entry phase instrumentation can be rather well defined in terms of the state-of-the-art; however, certain devices, such as the water vapor detector, will require some development before a device is available that will fulfill the scientific requirements of the measurement. The landed phase instrumentation includes a minimum science payload and certain other devices that may feasibly be carried by the Lander. In this group of instruments there are several devices that do not physically exist at the present. Others in this group are at some point in their development that provides sufficient confidence in their design to consider them in this mission even though serious doubts exist concerning their ability to withstand the high 'g' impact of the hard Lander. For these designs, additional shock attenuation can be considered for isolating the instrument from the extreme environment. However, this additional weight and volume appears prohibitive at the present time.

This section provides a brief summary of the scientific instrumentation selected for inclusion in the point designs. Detailed descriptions of the equipment and the studies performed in their selection have been given in previous sections (2.3.3 and 2.3.4) of this volume. Considerations used for identifying the implementation approaches best suited for the missions have been discussed in Volume II, Section 4.0.

3.5.2.2 Entry Science Payload

3.5.2.2.1 Tri-axial Accelerometer

The tri-axial accelerometer is mounted at the entry system c.g. Several varieties are currently available, however the magnetic force balance type seems to have the most desirable characteristics. Table 3.5.2-1 shows the mechanical and electrical characteristics of an accelerometer that is currently being used on various military programs. Also shown are the sequencing, sampling, and data format requirements for the accelerometer. No significant problems are foreseen in sterilizing the device.

3.5.2.2.2 Temperature Transducers

Atmospheric temperature measurements during the entry phase are performed by three temperature transducers. These are platinum resistance thermometers. One is located in the stagnation region of the aeroshell and measures the stagnation temperature from the beginning of entry down to aeroshell ejection.

TABLE 3.5.2-1. ENTRY SCIENCE PAYLOAD

Instrument (Lander)	Weight	Volume	Power Req'mts	Location	Sampling Schedule	Data Format
Mass Spectrometer	8 lbs	2 x 7 x 14 in.	7 watts	Internal near surface. Requires port through heat shield	Initiates near Mach 5 Terminates at impact	50 (8) bit words per sample (2 sec scan, 8 sec readout) 50 bits/sec readout
Resistance Thermometer	0.5 lb each	1 in. dia x 2 in. long	1 watt each	Two on base of vehicle	Initiates at Mach 5 Terminates at impact	1 sensor output channel 1 sample/sec
Variable Capacitor Pressure Transducers	0.5 lb each	2 in. dia x 2 in. long	1 watt each	Two on base of vehicle	Initiates at beginning of entry Terminates at impact	1 sensor output channels 1 sample/sec
Tri-Axial Accelerometer (1 Dual Scale)	2 lb	2.8 x 1.8 x 2 in.	4 watts	Located at body c.g. with one axis aligned to vehicle vertical axis	Initiates at beginning of entry Terminates impact	8 bits/sample/axis 10 samples/sec 72 bits/sec total Automatic scale switching
Water Vapor	1 lb (ducting only)	Detector located in surface science package	N/A	Ducting located same as mass spectrometer ducting	Initiates near Mach 5 Terminates at impact	1 sample/15 sec 2 seven bit (parallel) channels 1 eleven bit (parallel) channels

TABLE 3.5.2-1. ENTRY SCIENCE PAYLOAD (Concluded)

Instrument (Aeroshell)	Weight	Volume	Power Req'mts	Location	Sampling Schedule	Data Format
Stagnation Temperature Transducer (1)	0.5 lb	1 in. dia x 2 in. long	1 watt	See text	Initiates at beginning of entry Terminates at aeroshell ejection	1 sensor output 1 sample/sec
Stagnation Region Pressure Transducer (4)	0.5 lb each	2 in. dia x 2 in. long each	1 watt each	Behind nose of aeroshell (See text)	Initiates at beginning of entry Terminates at aeroshell ejection	1 sensor output 1 sample/sec

The other two thermometers are located on the base of the Lander system and are used during the subsonic region of flight primarily during parachute descent. Table 3.5.2-1 shows the physical and electrical characteristics of the resistance thermometers and its data collection profile. The exact configuration and design of the stagnation transducer will depend upon a large number of variables. The definition of the transducer design parameters will require preflight testing of the thermal characteristics of either scale model or prototype vehicles.

3.5.2.2.3 Pressure Transducers

Variable capacitance pressure transducers located on the aeroshell and on the base of the entry system measure atmospheric pressure profiles. The four transducers arrayed about the stagnation region perform the dual function of measuring pressure and angle-of-attack. These transducers are located just behind the heat shield and are exposed to the external environment via ducting leading through the beryllium cap of the heat shield. The pressure transducer located on the base of the Lander system measures base pressure from supersonic through subsonic flight regimes. Table 3.5.2-1 lists the characteristics of these transducers and also shows the sampling schedule and data format.

3.5.2.2.4 Mass Spectrometer

The measurement of atmospheric composition by mass spectrographic techniques requires acquisition of a sample from the atmosphere. This acquisition must be performed without exposure to contamination from gaseous materials exuded by the heat shield or other sources. The ducting leading from the mass spectrometer to the external environment terminates in the nose area that contains the beryllium plug which serves to minimize the probability of contamination from heat shield outgassing products. This same ducting also delivers atmospheric samples to the water vapor detector located in the entry payload and must be disconnected when the aeroshell is separated from the Lander at parachute deployment.

Table 3.5.2-1 shows the physical, electrical, and data collection characteristics of the mass spectrometer.

3.5.2.2.5 Water Vapor Detector

At present the chemical/radiological water detector is in the concept development stage. Since this device will also be used during landed operations it must be designed for high shock survival. Fig. 3.5.2-1 shows, in block diagram form, the design of the water vapor detector. Table 3.5.2-1 shows the physical and electrical characteristics of the detector. The ducting leading from the nose for entry data is disconnected at aeroshell separation and a second port is opened for landed operations.

The basic operating principle is that when calcium hydride comes in contact with water (in either liquid or vapor form) the following reaction takes place:

$$CaH_2 + 2HOH \longrightarrow Ca(OH)_2 + 2H_2$$

When the hydride is labelled with tritium, the gaseous effluence contains the radioactive tritium. This element may be quantitatively detected by its radiation and thus the amount of water entering into the reaction may be determined. Radiation shielding of this system will present no problems since tritium emits 18 kev beta particles that are stopped by the chamber walls. Present laboratory tests have demonstrated the device at 1 part/million with definite indications of feasibility for operation of 1 part/billion.

3.5.2.3 Surface Science Payload

3.5.2.3.1 Pressure Transducer

Unlike the pressure transducers included in the entry payload, the surface pressure transducer must be able to withstand high level shock loading. This requirement necessitates either an extension to the state-of-the-art in low pressure transducers or provisions for reducing impact loading much below 1000 g. The added weight and volume for this shock compatibility or attenuation is not included in the component weight or volume shown in table 3.5.2-2.

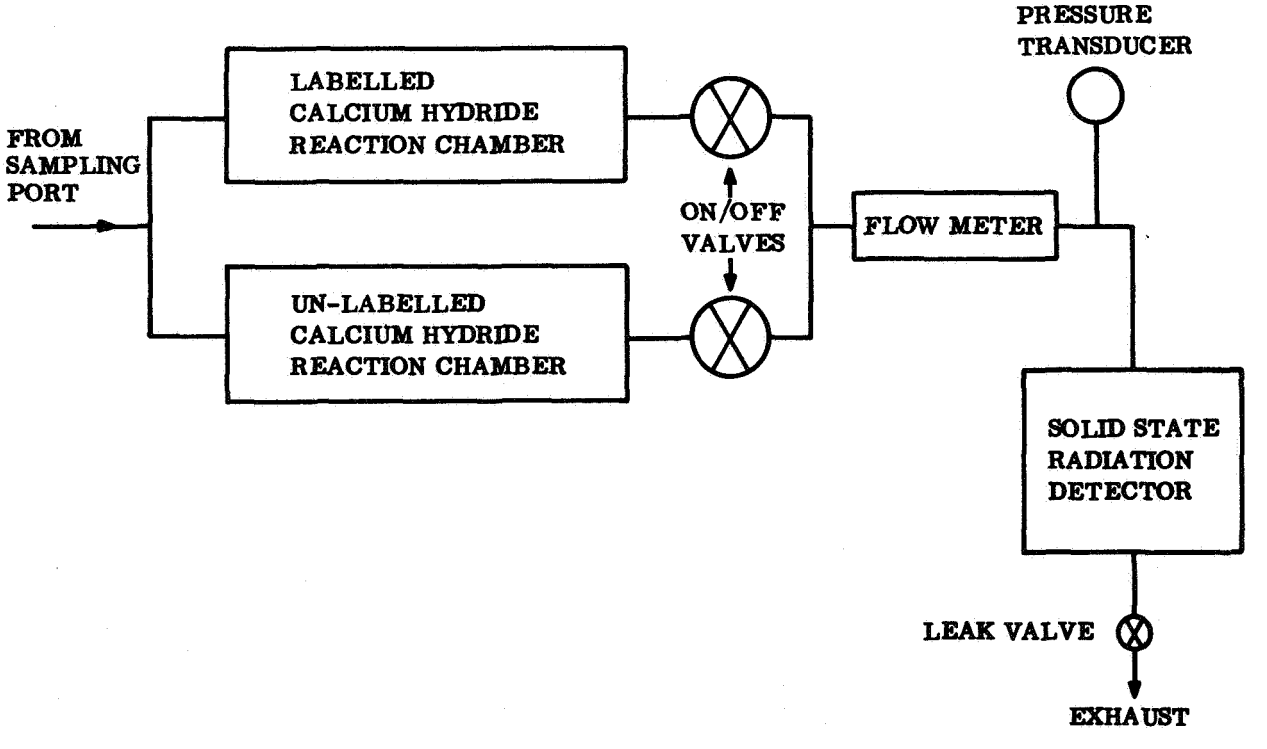


Figure 3.5.2-1. Water Vapor Detector, Block Diagram

TABLE 3.5.2-2. SURFACE SCIENCE PAYLOAD

Instrument (Lander)	Weight	Volume	Power	Location	Deployment/ Orientation	Mission Profile	Data Format/ Requirements
Pressure Transducer (2)	0.7 lb each	2 in. dia, 2 in. long each	1 watt each	Internal near skin of vehicle	Port through skin to ambient environment either top or bottom No deployment	Operates continuously after impact	3 samples hr each 1% accuracy Two channels total
Resistance Thermometer (4)	0.5 lb each	1 in. dia, 2 in. long each	1 watt each	One on each camera boom	Deployed above Lander on camera booms One on each boom	Same as above	3 samples/hr each 1% accuracy Four channels total
Wind Velocity Transducer (2)	2.5 lbs each	25 cubic in. prior to deployment each	3 watts each	One on each of two camera booms	Boom deployment above vehicle on camera booms	Same as above	3 samples/hr 6 channels Each channel consisting of 11 parallel bits Total of 66 bits/sample
Moisture Detector (1)	10 lb	60 $in.^3$	5 watts	Mounted internal to Lander	Pneumatic tubes deployed as part of camera booms	Same as above	3 samples/hr 2 seven bit (parallel) channels 1 eleven bit (parallel) channel

TABLE 3.5.2-2. SURFACE SCIENCE PAYLOAD (Concluded)

Instrument (Lander)	Weight	Volume	Power	Location	Deployment/ Orientation	Mission Profile	Data Format/ Requirements
Surface Composition (Alpha backscatter) (1)	9.5 lb	5.5 x 7.5 x 4.5 in.	5 watts	Internal to vehicle	Must be deployed so that sensor head rests on surface of planet top or bottom deployment controlled by clinometer	Deploy 3 hr after impact First readout 1 hr after impact 2nd readout 3 hr after impact then readouts every 3 hr thereafter	1 sample/3 hr 130 channels 14 bits (parallel) each 130 channels 12 bits (parallel) each 3 channels 7 bits (parallel) each
Photo-imaging (4)	4.8 lb total	1 to 2 in. dia 9 to 12 in. long each	6-10 watts total	One on each of four booms deployed above Lander	Boom deployment 36 in. Height > 18 in. One boom/ camera	4 frame sweeps on high resolution and 4 frame sweeps on low resolutions in sequence Operation time time coincident with transmissions	Flexible to meet maximum transmission capability of Lander. Period from 1 sec to 8 hr/ picture. Total bits between 10^7 and 10^8
Clinometer (2)	1.3 lb each	2 in. dia x 3 in. long	3 watts	Two internal to Lander mounted with long dimension parallel to vertical axis of Lander	N/A	Sampled immediately after impact then once every 3 hr	1 sample/3 hr 2 channels 7 bits (parallel) per channel

3.5.2.3.2 Temperature Transducer

Atmospheric temperature is measured by a set of platinum resistance thermometers. They are deployed following impact with the camera booms to obtain free stream data with minimum Lander induced perturbations. Such devices have been designed to withstand rather high g-loading and thus no serious problems are expected as a result of a rough landing. The ultimate physical design of the thermometers will deal with minimization of direct solar heating since this can be a serious measurement problem. A solar shield is required to accomplish the task of decoupling the resistance element from the solar flux. See table 3.5.2-2 for transducer characteristics.

3.5.2.3.3 Wind Velocity Sensor

Although an acoustic velocity sensor has not yet been built for planetary exploration application, the changes required to modify existing designs intended for terrestrial applications appears straightforward. The design approach used for point design evaluation consists of five magnetostrictive transducers (fig. 3.5.2-2) mounted on the boom supporting the TV camera system. A microminiaturized electronics package produces the necessary ultrasonic pulses that drive the transducers and also measures the transit time for each pulse to travel from one transducer to the next. No problem is foreseen in fabricating the required electronics and transducers to meet the sterilization and shock environment requirements. Care must be taken, however, to assure reasonably good rigidity in the transducer supporting arms during the measurement since motion of the transducers may be misinterpreted to signify motion of the medium (atmosphere). Table 3.5.2-2 shows the anticipated physical and electrical characteristics of the wind velocity sensor.

3.5.2.3.4 Water Vapor (Moisture) Detector

The chemical/radiological water vapor detector has not been hardened for the extreme environments that will be encountered during the entry and landing phases of the mission. However, since the design is inherently mechanically simple, it is expected that a device with the physical characteristics shown in table 3.5.2-2 can be developed and tested in time for a 1973 mission to Mars. Operating experience (laboratory) in the low parts/million and high parts/billion range has demonstrated that water vapor sorption-desorption by materials used in the sampling system could be the major factor toward limiting the response and detection sensitivity in this and lower concentration regions. This would also be of special importance for water detectors based on physical principles, especially at lower operating pressures, where sorption-desorption by the detector supporting hardware could contribute significantly to a non-representative water environment around the detector. It is felt that water sorption-desorption can be controlled by appropriate materials selection, by minimizing exposed surfaces, and by operating these surfaces at temperatures consistent with the level of water concentration to be sensed.

The device will remain in the Lander during operation and gas sampling will occur through a vent tube in a camera boom. The key interface requirements are shown in table 3.5.2-2.

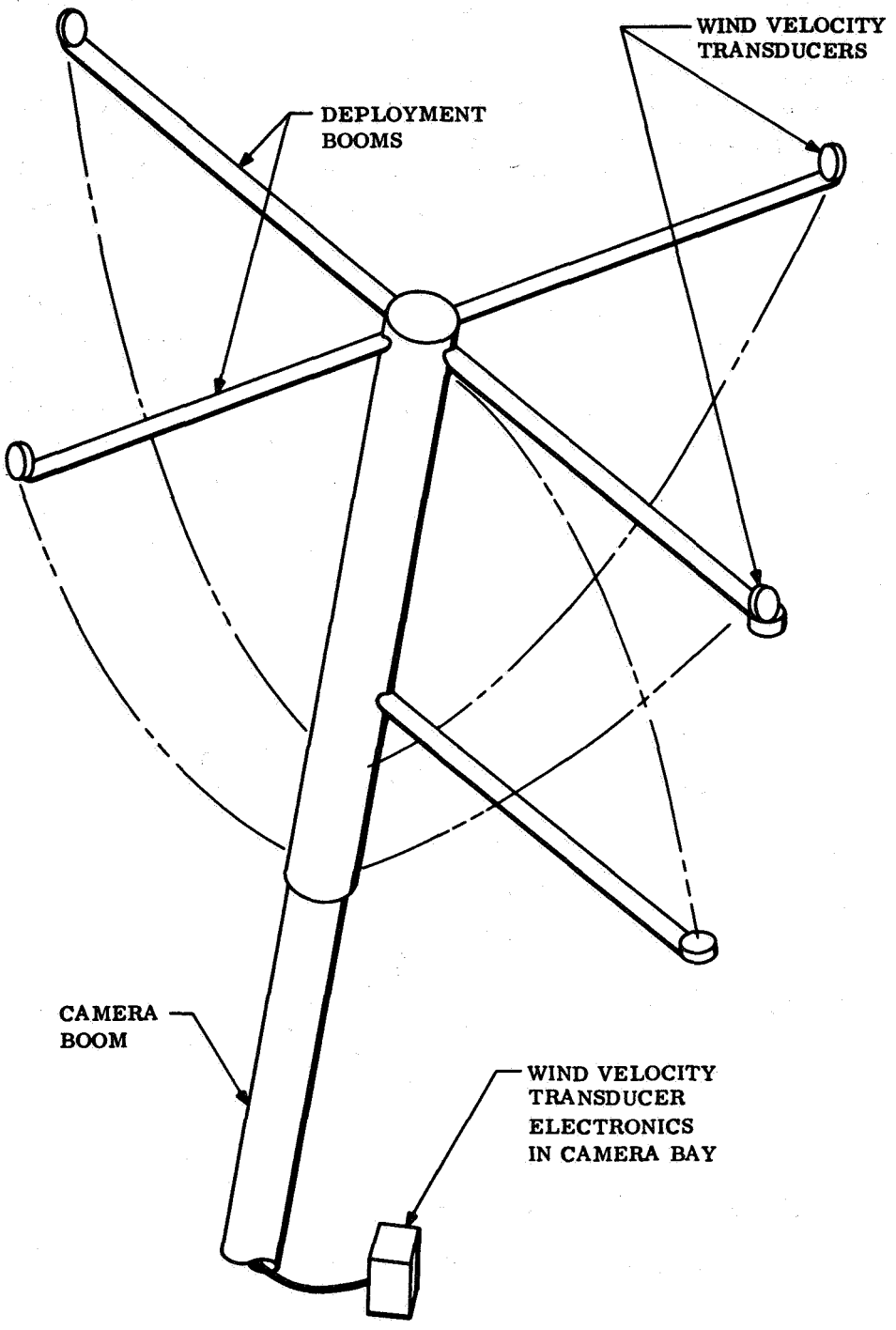
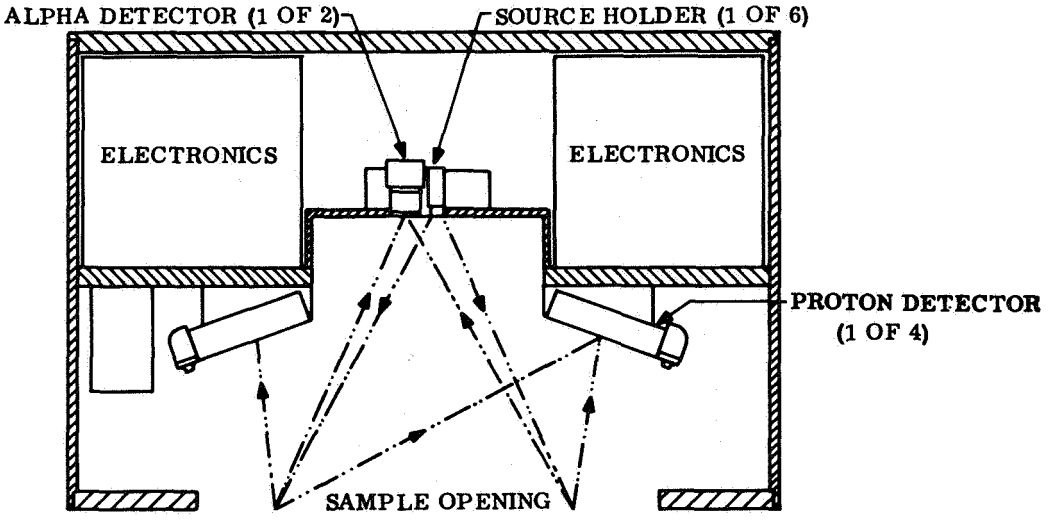


Figure 3.5.2-2. Wind Velocity Sensor

3.5.2.3.5 Alpha Back Scatter Spectrometer

An alpha back scatter spectrometer suitable for operation on Mars is being considered for development by the University of Chicago (Turkevitch). Such a device will most probably not use the isotope source (Cm^{242}) used in the Surveyor spectrometer and the source selection will be one of the prime considerations for any future designs. Mechanically, with the possible exception of the deployment mechanism, the spectrometer will probably be able to meet the requirements of a rough landing. Fig. 3.5.2-3 shows the Surveyor alpha-spectrometer for reference purposes. Reduction of the overall dimensions of the sensor head are anticipated since the Martian atmosphere will interfere with the measurement. This reduction will result in shorter particle path lengths and correspondingly smaller interference with the measurement.

The head, which must be deployed to come in contact with the surface of the planet, is mounted on a swivel bracket so that deployment either up or down will be possible. The existence of surface protuberances in the field of view will introduce errors. A calibration sample is exposed to the bottom of the sensor head when in the stowed position thus providing a reference source for data interpretation. Table 3.5.2-2 gives the physical and electrical parameter estimates for the proposed device. The deployment will be carried out in two stages; i.e., partial deployment toward surface for background counting and full deployment for composition measurements.



VERTICAL SECTION THROUGH THE CENTER

Figure 3.5.2-3. Alpha Back Scatter Instrument

3.5.2.3.6 TV Cameras

The high and low resolution cameras are installed on individual hinged masts although it may be possible to combine them within one casing. Fig. 3.5.2-4 shows the basic elements that each contains. Neither of the two versions shown contain the azimuthal drive motor. The high speed version (fig. 3.5.2-4) has a five-sided mirror that rotates unidirectionally. The preferred video rate for this version is not well defined and can be from 10 kHz to 100 kHz depending on circumstances. The incident light passes through the window and is reflected from the mirror onto the silicon cell detector. The solid state amplifier amplifies the resulting electrical signal to ± 5v maximum, the output signal leads from the camera housing carry this signal to the processing electronics. The slow speed version (that can take up to 4 hr for a full panoramic sweep) has a nodding mirror activated by a cam. The light beam is deflected via this mirror onto the silicon cell after being chopped by a small light chopper placed in front of the cell. This latter addition enables the same basic amplifier to be used for both the high speed and low speed versions. The silicon cell response is shown in fig. 3.5.2-5. The dimensions of the camera unit that contains all the mechanical drive mechanisms and all the electronics for the video and synchronizing signals varies with the full design specification; normally, however, these will be between 1 and 3 in. in diameter and between 6 and 16 in. long. Total weights of the cameras as described can again vary from 1/2 to 6-1/2 lb. (See table 3.5.2-3.)

3.5.2.3.7 Clinometer

The clinometer proposed for the 1973 Hard Lander will require development. Specifications for the design are not complete; however, the parameters shown in table 3.5.2-2 are based on engineering estimate for the conceptual design shown in fig. 3.5.2-6. The potentiometer housings could also include any electronics required to operate the system. Location of the instrument in the Lander is not critical.

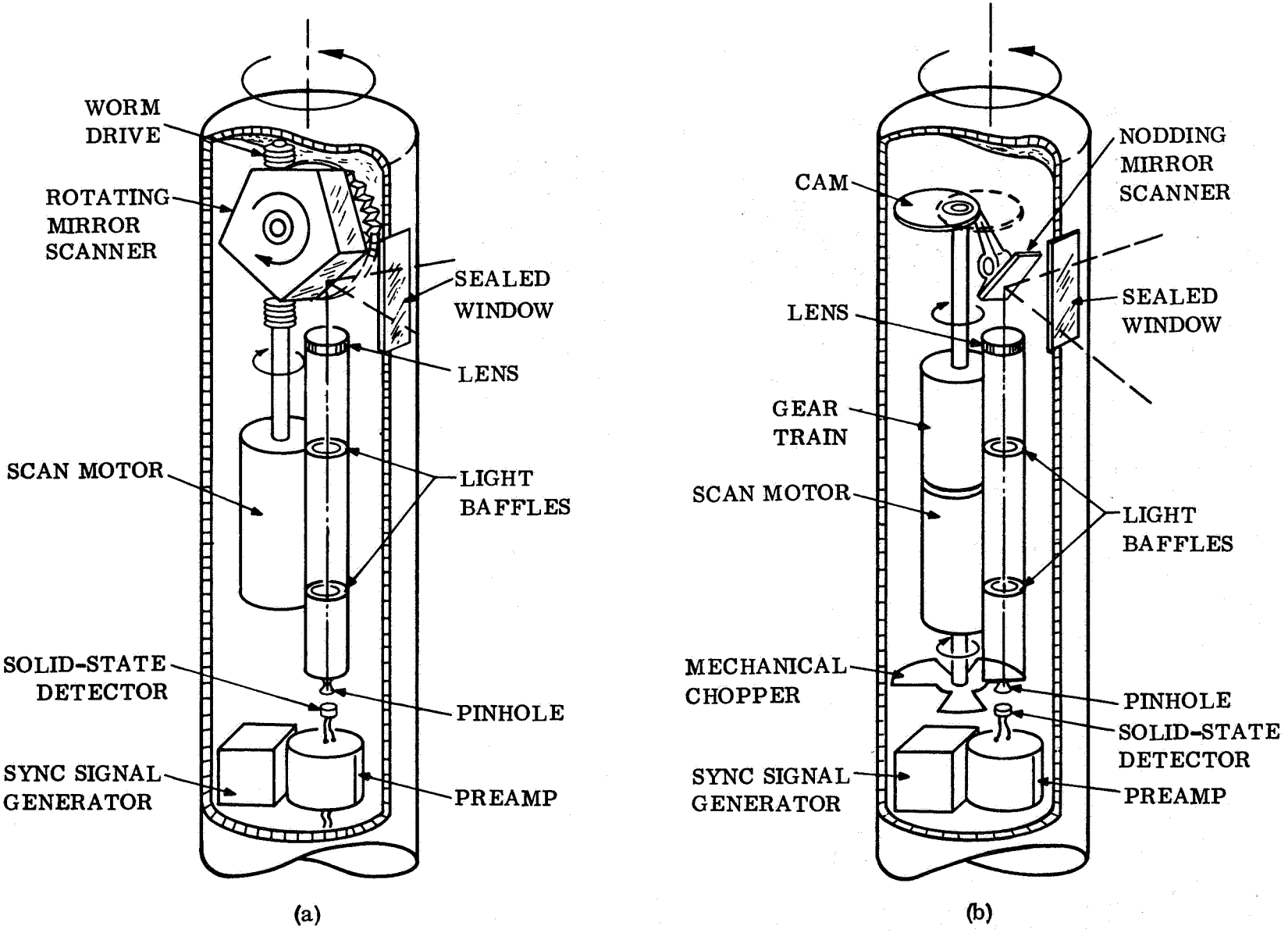


Figure 3.5.2-4. High and Low Speed TV Cameras

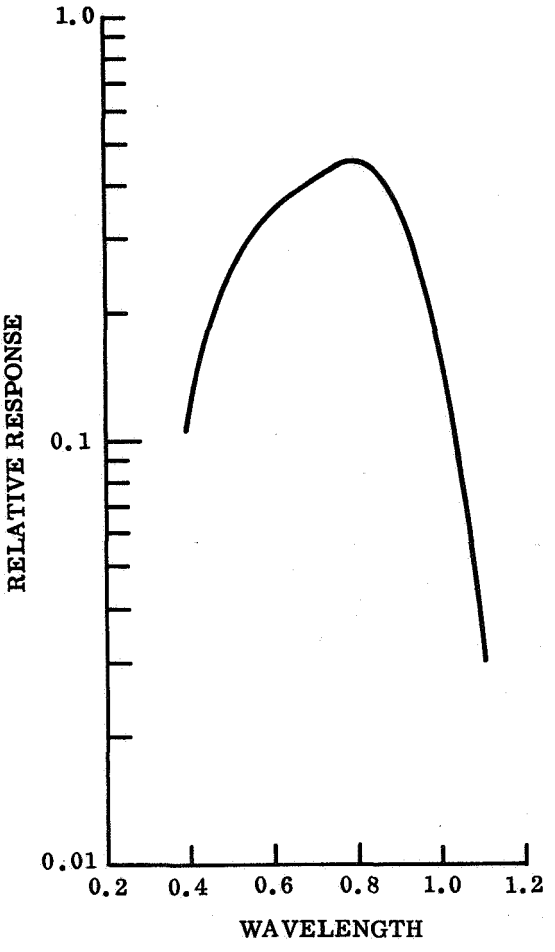


Figure 3.5.2-5. Silicon Photo-voltaic Cell Spectral Response

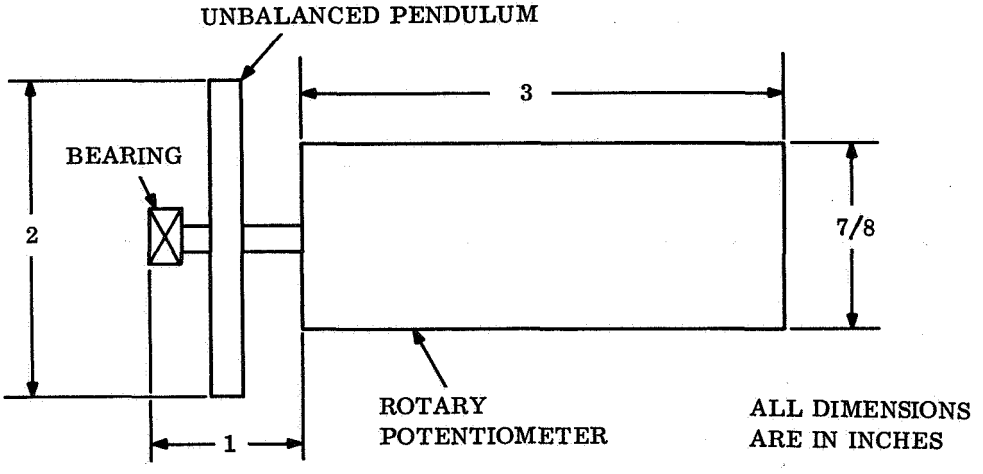


Figure 3.5.2-6. Rotary Potentiometer Clinometer

TABLE 3.5.2-3. TYPICAL CAMERA SPECIFICATIONS

Model Identification	CM	SL	NP	SS	SM
Special Feature	small size, small power	rugged	high speed	adjustable performance	high resolution
Field of view	9^{o} x 360^{o}	50^{o} x 360^{o}	25^{o} x 360^{o}	10^{o} x 10^{o} to 90^{o} x 360^{o}	1^{o} x 1^{o}
Resolution	0.1 in. @6 ft.	0.1 in. @6 ft	1 in. @100 ft	0.1 in. @1 ft to 0.1 in. @ 60 ft	1 micron @ 3/4 in.
Frame time	1/2 min	7 min	2 1/2 sec	30 sec to 10 hr	1 sec
Sensitivity range	0.1-1000 ft-L	0.3-3000 ft-L	1.5000 ft-L	0.001-5000 ft-L	10-10,000 ft-L
Size	1 in. dia x 6 in. long	1.5 in. dia x 10 in. long	2.5 in. dia 11 in. long	3 in. dia x 18 in. long	3 in. dia x 15 in. long
Weight	0.4 lb	3.5 lb	5.5 lb	6.5 lb	6 lb
Power	1 W	10 W	150 W	15 W	4W
Temperature (of the environment)	-10^{o}F to $+150^{o}$F	-40^{o}F to $+180^{o}$F	-10^{o}F to $+125^{o}$F	-45^{o}F to + 145^{o}F	-45^{o}F to + 145^{o}F
Pressure (external)	1 ATM	10^{-9} Torr	1000 psi	1 mb	1 mb
Shock and Vibration	1000 g	3500 g	100 g	300 g	50 g

3.5.3 TELECOMMUNICATIONS

3.5.3.1 Summary

The telecommunications subsystem consists of:

1. A hardwire data link for Lander/Capsule checkout prior to separation from the spacecraft

2. A relay communications link to provide Lander/Capsule entry data and high data rate imagery after landing

3. A UHF beacon link to detect Orbiter presence for relay communications.

A functional block diagram of the telecommunication subsystem is shown in fig. 3.5.3-1. The communication link characteristics are summarized in table 3.5.3-1.

To support the high data requirement for imagery, the data will be relayed to Earth via the Orbiter, with communication to the Orbiter taking place during a periapsis pass to take advantage of the relatively short line-of-sight range. All data except imagery is stored in the Orbiter and subsequently transmitted to Earth. Non-coherent frequency shift keying with Manchester coding is chosen for the modulation technique to minimize acquisition time. After landing, the link is designed to operate at a 160 kbps data rate, the optimum from the standpoint of achieving maximum total data transmission. At this rate, it is feasible to transfer 8.1×10^7 bits in a period of 8.5 min with maximum adverse link tolerance, 46° worst case Lander tilt, and reference Orbiter-Lander line-of-sight parameters. To accomplish this data transfer requires 50 watts of transmitter power, the maximum allowable to avoid antenna breakdown at Mars surface pressure. It is assumed that the Orbiter will be provided with the capability to record data at this high rate. If this is not the case, the total data transferable (and the transmitter power) scale down approximately proportional to the actual recording rate.

Data requirements prior to and during entry are relatively modest, but communication ranges are more severe. It was determined that the same transmitter and receiver used for imagery data after landing can be used at a lower data rate for entry data. This minimizes equipment and complexity on both the Orbiter and Lander.

Because of the widely varying communication parameters due to atmosphere uncertainty and possible vehicle tilt, the amount of data transferable immediately after

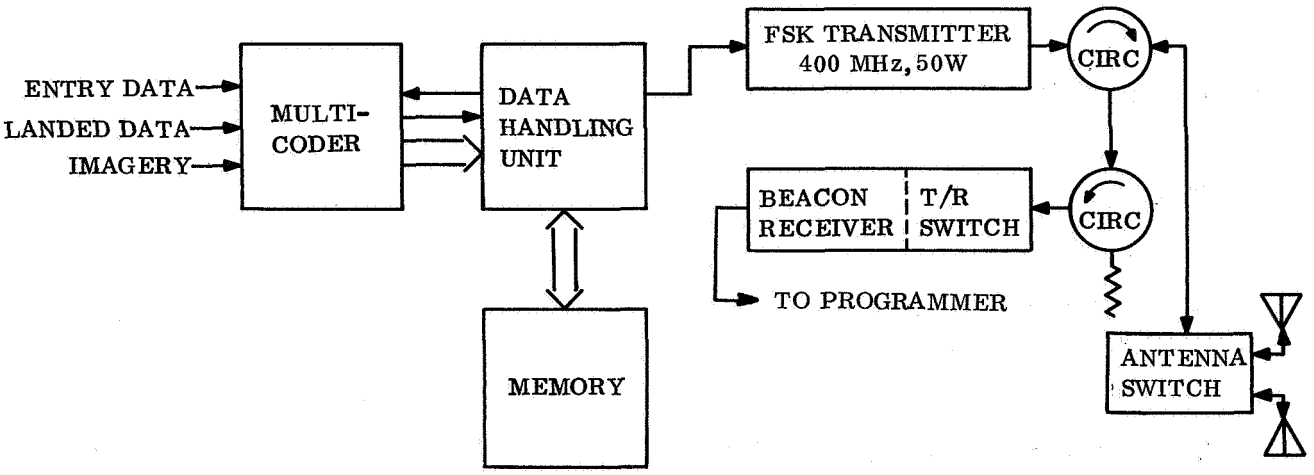


Figure 3.5.3-1. Telecommunications Subsystem, Functional Block Diagram

TABLE 3.5.3-1. DESIGN SUMMARY, POINT DESIGN 1

Phase	Link	Data Rate (bps)	Transmission Time	Total Data (bits)
Post-separation	400 MHz FSK, relay	1090	30 min	2.0×10^6
Entry	400 MHz FSK, relay	1090	460 to 1250 (1) sec	0.50 to 1.4×10^6 (1)
Post impact, set-up	400 MHz FSK, relay	1090	2.5 min (2)	0.16×10^6 (2)
Post impact, Orbiter pass	400 MHz FSK, relay	160×10^3	10.4 min	0 to 10.3×10^7 (4)
Periapsis pass	400 MHz FSK, relay	160×10^3	20.5 min (3)	8.1×10^7

(1) Atmosphere dependent.
(2) Data during this period may be lost because entry antenna may be underneath Lander.
(3) Includes maximum beacon turn-on time error of 12 min and 8.5 min minimum effective transmission interval for 46° tilt.
(4) Atmosphere and tilt dependent

impact varies widely. For the VM-9 atmosphere, communications at the high data rate cannot be established except in the improbable case of large negative in-plane tilt towards the Orbiter.

A beacon link is provided to detect Orbiter presence. The Orbiter beacon transmitter and Lander beacon receiver are turned on prior to nominal periapsis by the time of arrival uncertainty as indicated in Section 3.5.3. The beacon link then essentially measures received signal strength and initiates data transmission when link conditions capable of supporting the established data rate are indicated. By using the same antennas for the beacon and data links, much of the potential differences between beacon and data links are removed. The remaining uncertainty in the beacon link is 9.2 dB resulting in worst case early turn-on of 12 min when the beacon link is designed to trigger at the latest time possible as determined by worst case telemetry link performance.

3.5.3.2 Telecommunications Sequence

Prior to separation, Lander power is turned on for final checkout (table 3.5.3-2). Except for a momentary check of transmitter power, transmitter operation within the canister is avoided. During this interval, data is transferred via hardwire. Immediately after separation r-f transmission is initiated for event monitoring and engineering diagnostic measurements.

TABLE 3.5.3-2. TELECOMMUNICATIONS SEQUENCE

Phase	Duration	Communications
Pre-separation	15 min	Low rate/hardwire
Post-separation	30 min	Low rate
Entry	460 to 1250 sec	Low rate
Post-impact (Lander settling)	2.5 min	Low rate
Post-landing	(see table 3.5.3.7)	High rate
Orbit period	~ 25 hr	None
Beacon turn-on	Periapsis uncertainty	None
Beacon early trigger	0 to 12 min	High rate
Periapsis pass	8.5 min	High rate

During entry and for 2.5 min after impact, scientific and diagnostic data is transmitted at the low rate. The high data rate is then used to transmit imagery for a period dependent on the atmosphere characteristics, i.e., entry time. For the VM-9 atmosphere, the Orbiter is beyond the range of the high data rate, and no imagery can be relayed until the next periapsis pass.

The beacon receiver is turned on early by a time equal to the total Orbiter arrival time uncertainty. The beacon receiver, upon exceeding the threshold, triggers the high rate transmission of stored scientific and engineering data and imagery. The beacon link trigger occurs 0 to 12 min early because of link parameter tolerances.

3.5.3.3 Data Requirements

Table 3.5.3-3 is a list of measurements for the entry and landed mission phases. Table 3.5.3-4 gives the corresponding data transmission. During entry, real time data is interleaved with data delayed by 70 sec to avoid loss of data during blackout. The combined data dictates a 1.09 kbps data rate. Prior to entry, only engineering diagnostic data is transmitted. Immediately after landing, imagery is transmitted at the high data rate if the Orbiter is still in view. Imagery and surface science data are transmitted at the high data rate on subsequent periapsis passes. The period required to relay the total data of 8.1×10^7 bits is 506 sec, with surface science and engineering diagnostic data requiring approximately 0.4 sec and the rest of the period devoted to imagery. For the sake of redundancy, the stored surface science and engineering diagnostic data are read out of memory and transmitted at the beginning and middle of each 506 sec period.

TABLE 3.5.3-3. MEASUREMENTS LIST

	Pre-impact	Post-impact
Diagnostic Data (50 channels)	X	X
Scientific Data		
Pressure	X	X
Stagnation pressure	X	
Temperature	X	X
Stagnation temperature	X	
Water vapor	X	
Tri-axial accelerometer	X	
Wind velocity		X
Moisture		X
Surface composition		X
Clinometer		X
Imagery		X
Stored data	X	X

TABLE 3.5.3-4. DATA TRANSMITTED

Source	Entry	Landed
Science	194 2/3 bps	34.6 bits
Diagnostic	350 bps	26.25 kbits
Stored	544 2/3 bits (1)	100 kbits (2)
Imagery	---	$\sim 8.1 \times 10^7$
Total data/day	---	8.1×10^7
Data transmission time	460 to 1250 sec	8.5 min
Data rate	1.09 kbps	160 kbps

(1) Science and diagnostic data delayed by 70 sec

(2) Data stored during entry.

3.5.3.4 Link Designs

3.5.3.4.1 Landed

The fundamental constraints for the landed telemetry link are that maximum data is to be transferred, the transmitter power is to be kept below 50 watts to avoid antenna breakdown, and the maximum permissible bit error probability is 4×10^{-3} (Orbiter to Earth link is 1×10^{-3} giving an overall bit error probability of 5×10^{-3}). Additionally, the link must be tolerant of Lander attitude (tilt) uncertainty due to surface slopes and crush-up variance, and must also be tolerant of landing site uncertainty. Finally, the Lander size requires that the antenna be of minimum size.

These constraints are satisfied by the non-coherent frequency shift keyed (FSK), Manchester coded, 400 MHz link. The use of non-coherent FSK with Manchester coding minimizes acquisition time. The antenna size is minimized by sacrificing bandwidth with essentially no degradation in link performance. The need for pointing or steering mechanisms is avoided by using an antenna with sufficient beamwidth to accommodate Lander tilt uncertainties.

The data optimization is described in Volume III. Resulting available data rates vs time for the reference orbit are repeated in fig. 3.5.3-2 for worst case adverse link tolerances. These results do not consider possible antenna distortion resulting from ground reflections or specific Lander configuration. Fig. 3.5.3-3 is the relay/beacon block diagram, and table 3.5.3-5 contains the design control table. In this table, the 1000 km range and 0 dB transmitter antenna gain are reference values and yield an allowable data rate of 190 kbps with worst case adverse tolerances. For such high data rates relative to the frequency uncertainty, the available data rate is proportional to the gain over range squared ratio, G/R^2, which is the basis of fig. 3.5.3-2.

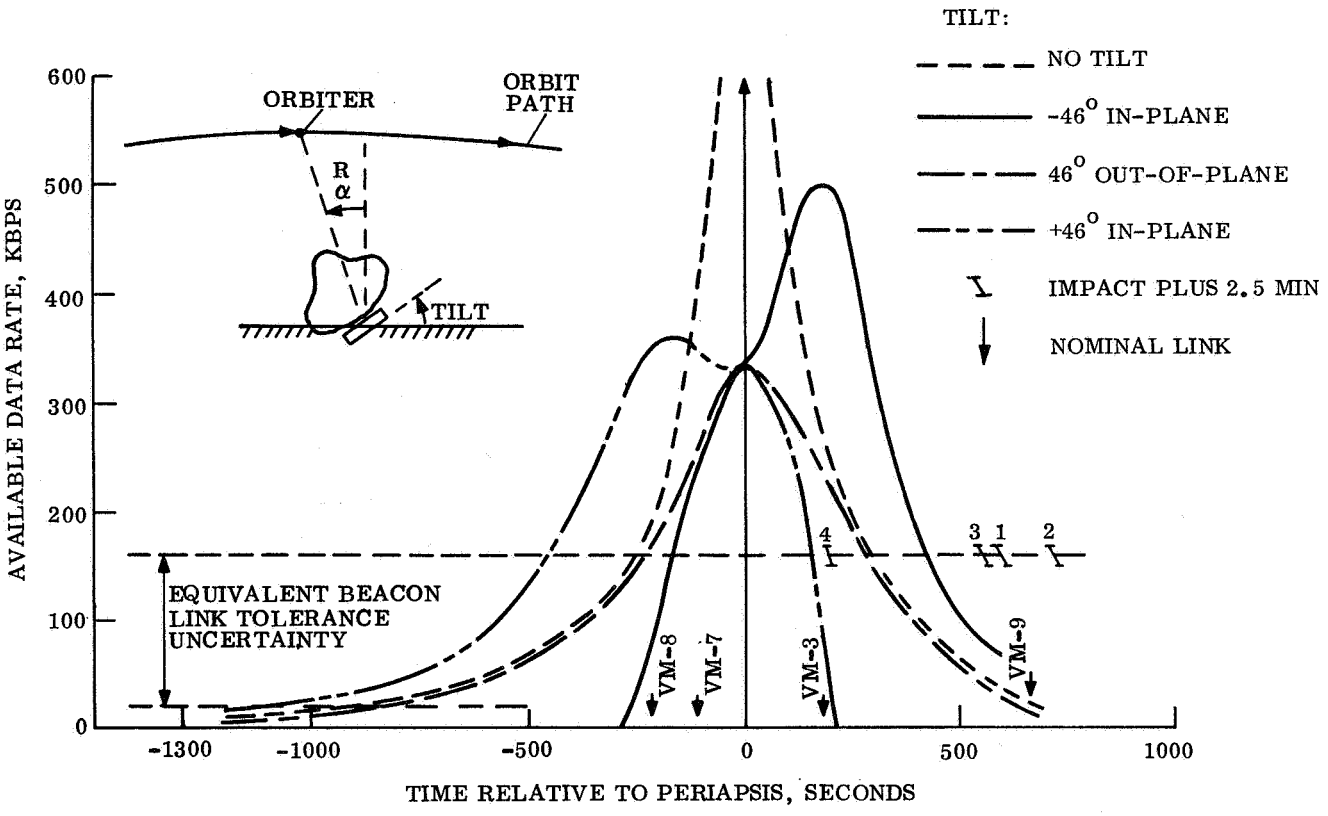


Figure 3.5.3-2. Available Data Rate vs Time With Adverse Tolerances

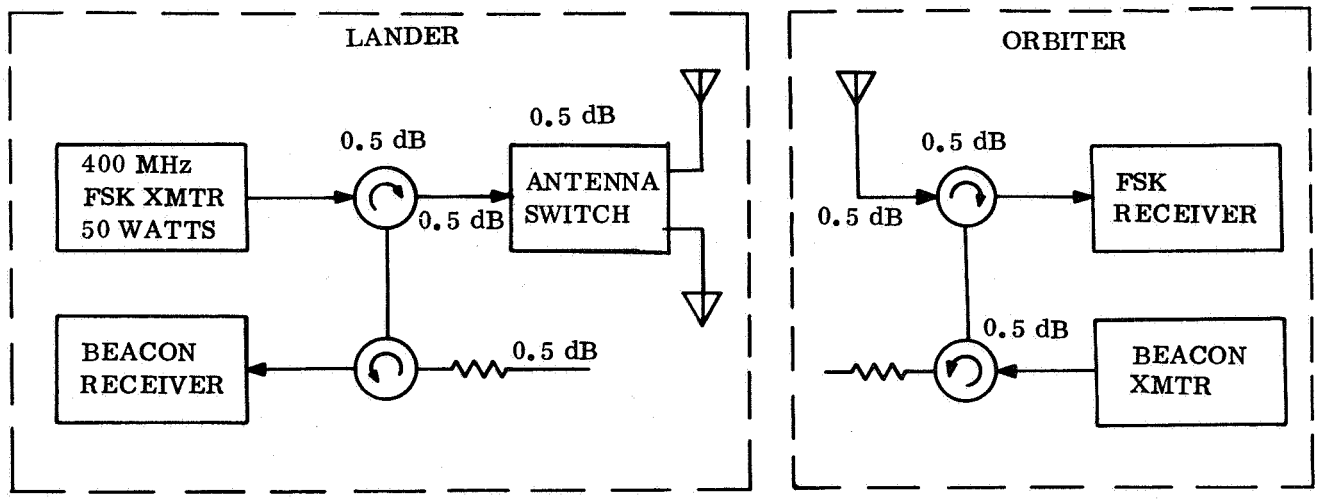


Figure 3.5.3-3. Relay and Beacon Link, Block Diagram

TABLE 3.5.3-5. DESIGN CONTROL TABLES - RELAY (LANDED) AND BEACON

Parameter	Nominal Values and Worst Case Tolerances					
	Relay (landed)			Beacon Link		
	Nominal	+ Tolerance	- Tolerance	Nominal	+ Tolerance	- Tolerance
Modulation technique	FSK	--	--	AM	--	--
Frequency (MHz)	400	--	--	400	--	--
Transmitter power (watts)	50	--	--	0.83	--	--
(dBm)	47.0	0.0	1.0	29.3	0.0	1.0
Transmit circuit loss	-1.5	0.2	0.4	-1.5	0.2	0.4
Transmit antenna gain	0.0(1)	0.5	0.5	2.0	0.0	0.5
Transmit antenna pointing loss	0.0	0.0	0.0	-1.0	1.0	0.0
Range (km)	1000(1)			1000(3)		
Space loss	-144.5	--	--	-144.5	--	--
Polarization loss	-1.0	1.0	0.5	-1.0	1.0	0.5
Receiving antenna gain	2.0	0.0	0.5	-0.8(3)	0.5	0.5
Receiving antenna pointing loss	-1.0	1.0	0.0	0.0	0.0	0.0
Receiving circuit loss	-1.0	0.2	0.4	-2.0	0.2	0.4
Total received power (S) (dBm)	-100.0	2.9	3.3	-117.7	2.9	3.3
Effective noise temperature (°K)	650	--	--	724	--	--
Receiver noise power spectral density (N/B)	-170.5	0.0	1.0	-170.0	0	1.0
Bit rate, 1/T (bps/dB)	190K/ 52.8	--	--	--	--	--
Frequency uncertainty (kHz)	20.0(4)	--	--	16.0(5)	--	--
I-F bandwidth (kHz)	780.0	--	--	25.0	--	--
Required S/N/B	64.2(6)	0.0	2.0(6)	47.0	1.0	1.0
Required ST/N/B	11.4(6)	0.0	2.0(6)	3.0(2)	1.0	1.0
Threshold data power (dBm)	-106.3	0.0	3.0	-123.0	1.0	1.0
Margin	6.3	2.9	6.3	5.3	3.9	5.3

(1) Reference values

(2) Signal-to-noise ratio in i-f bandwidth

(3) Values chosen correspond to G/R^2 ratio required by relay link to support 160 kbps data rate.

(4) Transmitter stability ±10 ppm; Receiver stability ±5 ppm; Doppler ±4 kHz

(5) Same as (4) except only positive doppler need be considered.

(6) Nominal signal-to-noise ratio is theoretical value. 2dB adverse tolerance is allowed to account for practical performance degradation, e.g., non-ideal bit sync. Required ST/N/B from Vol. III, Section 4.2.3.

Fig. 3.5.3-2 includes gain and range as determined from Lander to Orbiter line-of-sight range and look angle (fig. 3.5.3-4) and Lander tilt. Both positive and negative tilts in the Orbiter plane and tilt perpendicular to the Orbiter plane are considered. The reference condition of zero tilt shows a very sharp peak as the Orbiter passes overhead. This is the result of minimum communication range and maximum antenna gain. When the Lander is tilted in the orbit plane, the peak gain is pointed off vertical and tends to counteract the bit rate loss resulting from the increased range. The net effect of in-plane tilt is a lower peak data rate and longer available transmission time at near peak data rates. On the other hand, pure out-of-plane tilt lowers the gain and, hence, available data rate at all times.

Optimization is accomplished by examining the communication time as a function of bit rate for positive and negative in-plane tilt and for out-of-plane tilt. The maximum total data that can be transmitted with confidence at a specific bit rate is the product of bit rate and minimum communication time for the three tilt conditions considered. The bit rate yielding the largest maximum total data transmitted is the optimum bit rate.

The maximum data transferable per pass for the worst case tilt of 46° and the maximum adverse link tolerances is 8.1×10^7 bits at the optimum bit rate of 160 kbps. The effect of tilt on maximum data transferable is small, e.g., maximum data with zero tilt is 9.1×10^7 bits (at an optimum rate of 350 kbps) but 8.1×10^7 bits may be transferred at the optimum rate of 160 kbps in the case of 46° tilt.

In fig. 3.5.3-2, transmission at a given rate is allowable under maximum adverse link tolerances when the available data rate is equal to or greater than that rate. For 160 kbps the allowable transmission times for positive 46° in-plane tilt, 46° out-of-plane tilt, and negative 46° in-plane tilt are 610, 506, and 590 sec respectively. However, the three cases do not have a common 506 sec period requiring transmission for longer than 506 sec to assure coverage. Transmission must be initiated 506 sec before the end of allowable period for $+46^\circ$ in-plane tilt and continue 506 sec beyond the start of the allowable period for -46° tilt. Thus, transmission should begin 350 sec before overhead pass and continue until 340 sec after overhead pass, a total time of 690 sec which is about 3 min longer than the minimum time to transmit the data. Of course, if transmission is initiated by internal timing, the transmission time must be lengthened by the uncertainty in time of overhead pass.

3.5.3.4.2 Beacon Link

The beacon link consists of a beacon transmitter on the Orbiter and a beacon receiver on the Lander. To conserve weight and space on the Lander and to have as many elements as possible common to the data and beacon link, the beacon link uses the same antennas as the relay link. The narrowband antenna characteristic forces the beacon link to operate at essentially the same frequency as the relay link, which in turn dictates that the two links time share the antennas. To accomplish this the Orbiter beacon transmitter must transmit, for example, for an interval of 1 sec and then listen for 10 sec to see if the Lander is transmitting. When the Lander received signal strength is above a preset threshold level, data transmission will be initiated after a 1 sec delay. The Orbiter will sense Lander transmission and cease beacon transmission.

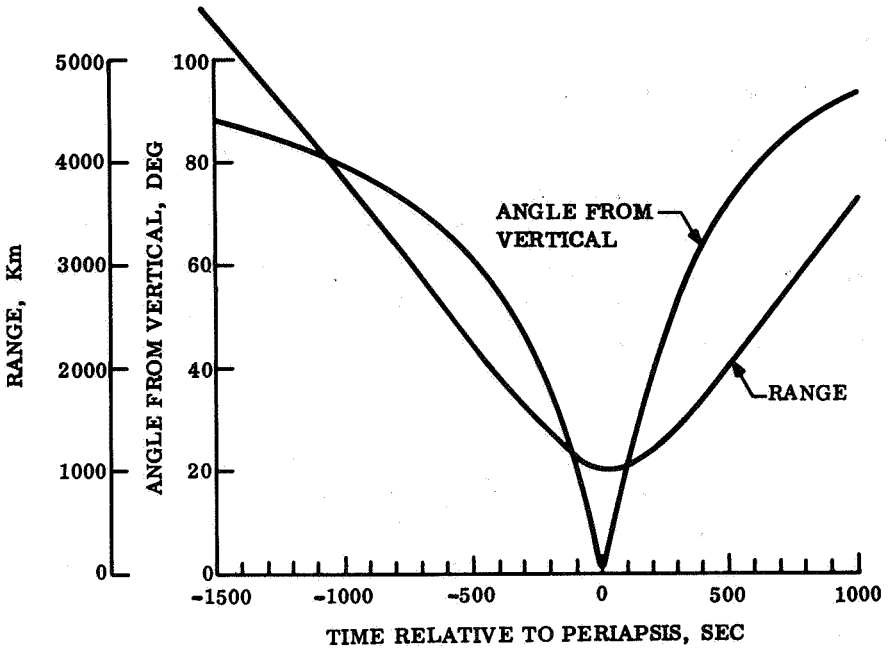


Figure 3.5.3-4. Reference Orbit Communications Parameters

The beacon link received signal strength is proportional to link antenna gain divided by range squared and, hence, is indicative of relay link available data rate. Ideally, the link can detect exactly when the 160 kbps data rate can be supported, which would lower the required transmission time to just that necessary to transmit the data (506 sec). However, the beacon link does have a range of performance which must be considered. To aid in minimizing the performance range, the beacon transmitter power will be closely controlled, i.e., within 1 dB, and its signal will be AM modulated to eliminate the noise bias uncertainty. The maximum beacon link uncertainty is 9.2 dB, a factor of 2.9 in range (see table 3.5.3-5). Since the link is designed such that transmission will be triggered in time to complete data transfer under worst case adverse tolerance conditions, worst case early turn-on will occur when the gain divided by the range squared is sufficient to support a data rate of 160/8.3 = 19.6 kbps. Using fig. 3.5.3-2, the early turn-on increment can be found as the difference between times that data rates of 19.6 kbps can be supported. The early turn-on intervals are indicated in table 3.5.3-6. (Possible antenna pattern distortion by ground reflections and specific Lander configuration is not considered.) Total transmission time is the early turn-on interval plus 8.5 min for data transmission.

3.5.3.4.3 Entry

Due to atmosphere uncertainty, there is a wide variation in the link parameters, e.g., line-of-sight range and look angle, during the entry phase. It is found for the

TABLE 3.5.3-6. EARLY TURN-ON INTERVALS

Tilt Condition	Interval (min)
No tilt	9.2
-46° in-plane (toward Orbiter set)	1.7
46° out-of-plane	10
+46° in-plane (toward Orbiter rise)	12

reference mission that communications can be maintained throughout entry. However, communications at the high data rate immediately after landing cannot be accomplished for the VM-9 atmosphere because the Orbiter is too far past periapsis.

To minimize weight and complexity, the entry data is transmitted via the same link as landed data is transmitted by keying at the low data rate, 1090 bits/sec. (This requires that the Orbiter receiver be capable of receiving either data rate.) The design control table for the entry link is shown in table 3.5.3-7. The link has a margin over adverse tolerance of 13.8 dB at the reference range, 1000 km, with 0 dB transmitter antenna gain. This indicates a worst case range limitation of 4890 km with 0 dB transmit antenna gain. The antenna provided has 0 dB or higher gain over a range of ± 80° with respect to the rear-looking Lander roll axis (effects of Lander configuration and aeroshell are not considered). The reference mission range and look angle profiles show a maximum range of 2480 km (VM-8 at parachute deployment) and maximum look angle of 74° (VM-9 at impact). (Look angle is the angle to Orbiter with respect to the velocity vector. Any variation between the velocity vector and roll axis, e.g., due to coning or swing on the parachute, will worsen the communication angle.) For the VM-3, -7 and -8 atmospheres the worst look angle is 63° at parachute deployment. Swing in excess of 17° at this time could cause the link margin to fall below the adverse tolerance level. As the Lander descends and the Orbiter begins to overtake the Lander, the look angle improves and more swing is allowable.

Times of impact plus 2.5 min for the VM-3, -7, -8 and -9 atmospheres are indicated in fig. 3.5.3-2. Table 3.5.3-8 gives the data that can be transferred at the high data rate with the worst case adverse tolerance and with nominal link parameters. The amount of data is the bit rate, 160 kbps, times the time remaining with allowable bit rates greater than 160 kbps.

During the entry phase, signals transmitted from the Lander may be reflected from the planetary surface toward the Orbiter. These multipath signals may interfere with the desired signal which is received on the line-of-sight path from the Lander. As shown in Volume III, Section 4.2.3, the slow fading environment is most detrimental to the communication link performance. The conditions for slow fading occur near impact. Based upon the maximum range during entry, the minimum margin over worst case tolerances is 5.9 dB. The tolerable signal-to-interference level to allow fading loss for less than 99 percent of the time is about 10.0 dB for the 5.9 dB margin. If this level proves to be a problem, another Orbiter receiver can be added with an i-f bandwidth to match the transmitted data rate yielding an additional margin of approximately 6 dB.

TABLE 3.5.3-7. ENTRY LINK DESIGN CONTROL TABLE

Parameter	Relay (Entry) Nominal	Adverse Tolerance
Modulation technique	FSK	--
Frequency (MHz)	400	
Transmitter power (watts)	50	
(dBm)	47.0	1.0
Transmit circuit loss	-1.5	0.4
Transmit antenna gain	0.0 (1)	0.5
Transmit antenna pointing loss	0.0	0.0
Reference range (km)	1000 (1)	
Space loss	-144.5	
Polarization loss	-1.0	0.5
Receiving antenna gain	2.0	0.5
Receiving antenna pointing loss	-1.0	0.0
Receiving circuit loss	1.0	0.4
Total received power (S) (dBm)	-100.0	3.3
Effective noise temperature (°K)	650°	
Receiver noise power spectral density (N/B)	-170.5	1.0
Modulation loss	N/A	
Data power (dBm) S_D	-100.0	3.3
Bit rate, 1/T (bps/dB)	1090/30.4	--
Frequency uncertainty	20.	--
IF bandwidth (kHz)	660. (3)	--
Required S/N/B	50.4 (2)	2.0 (2)
Required ST/N/B	20.0 (2)	2.0 (2)
Threshold data power (dBm)	-120.1	3.0
Margin	20.5 (4)	6.3

(1) Reference values.

(2) Nominal signal-to-noise ratio used is theoretical value. Two dB adverse tolerance is allowed to account for practical performance degradation, e.g., non-ideal bit sync. Required ST/N/B from Vol. III, Section 4.2.2.1.

(3) Bandwidth is same as required by high bit rate.

(4) This margin, less the adverse tolerances, is available as protection against multipath. At the maximum range during entry, the margin is reduced to 12.2 dB.

TABLE 3.5.3-8. DATA TRANSFERABLE AFTER IMPACT PLUS 2.5 MIN (BITS/10^7)

Atmosphere Model	No Tilt	-46° In-plane	46° Out-of-plane	+46° In-plane
Adverse tolerances				
VM-3	1.7	3.9	1.6	0
VM-7	6.5	8.4	6.2	4.3
VM-8	8.3	10.3	8.0	6.1
VM-9	0	0	0	0
Nominal parameters				
VM-3	6.7	8.4	6.1	0.4
VM-7	11.3	13.2	10.8	5.1
VM-8	13.2	15.0	12.6	7.0
VM-9	0	1.2	0	0

3.5.3.5 Equipment Descriptions

3.5.3.5.1 Antennas

The configuration of the wide beam 400 MHz antenna is that of a pill box 8 in. in diameter and 2 in. deep. The top surface of the box is flush with the vehicle outer surface and has two orthogonal slots, 2 in. wide and 8 in. long (dividing the top of the box into four quarters). The slots are tuned with capacitors to match the input and provide circular polarization. The bandwidth of this antenna is about 2 MHz. The estimated pattern is shown in fig. 3.5.3-5. Since the Lander diameter is on the order of a wavelength, the available ground plane is not large, indicating that the actual antenna pattern will vary somewhat from that shown.

3.5.3.5.2 400 MHz FSK Transmitter

A block diagram for the FSK transmitter is shown in fig. 3.5.3-6. The frequency shift keyed modulation is produced by switching between two stable crystal oscillators operating at 25.0375 MHz and 24.9625 MHz, respectively. Multiplying these signals by a factor of 16 produces transmitter output signals at 400.6 MHz and 399.4 MHz, respectively. The multiplier chain will be constructed at a low signal level in order that filtering and multiplier inefficiencies do not adversely affect the overall efficiency.

The power amplifier chain consists of amplifier stages to produce a total gain of about 47 dB; approximately 10 dB of this will be excess gain to be used for AGC. The

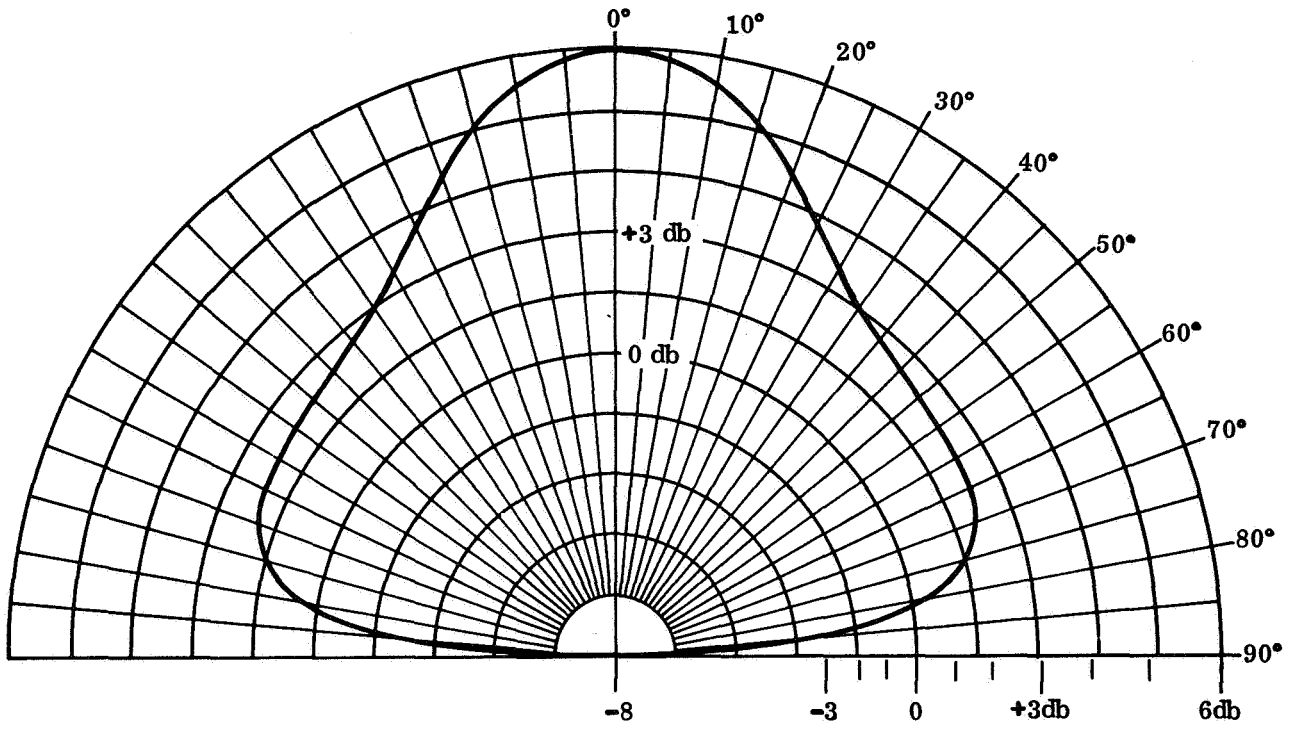


Figure 3.5.3-5. 400 MHz Antenna Pattern

final amplifier stage consists of two 2N5178's operating in push-pull; these transistors are each rated for 50 watts output at 500 MHz with a dissipation rating of 70 watts at 25°C.

The output power level of the transmitter will be controlled at 50 watts (+0, -1 dB) through the temperature environment by means of an AGC circuit consisting of a detector for output sampling, a high gain amplifier, and a voltage variable attenuator located at the low level input to the 400 MHz power amplifier chain.

The transmitter oscillator stability will be 10 ppm over a temperature range of -40°C to +70°C with negligible warmup time at any temperature. Aging will be 1 ppm per year. The state-of-the-art in temperature compensated crystal oscillators has reached a point where stabilities in the order of 1 ppm or better can be achieved for considerable periods of time; however, to account for degradation which may result from shock, such as deformation of the crystal structure or holder, a stability of 10 ppm is considered conservative.

No serious problems are anticipated in the sterilization of the transmitter or in the high shock levels expected. Several years ago GE-RS designed and constructed a VHF 50 watt transmitter which was successfully sterilized and subjected to multiple shock impacts at levels of 5000 g's for approximately 500 μsec. The transmitter was

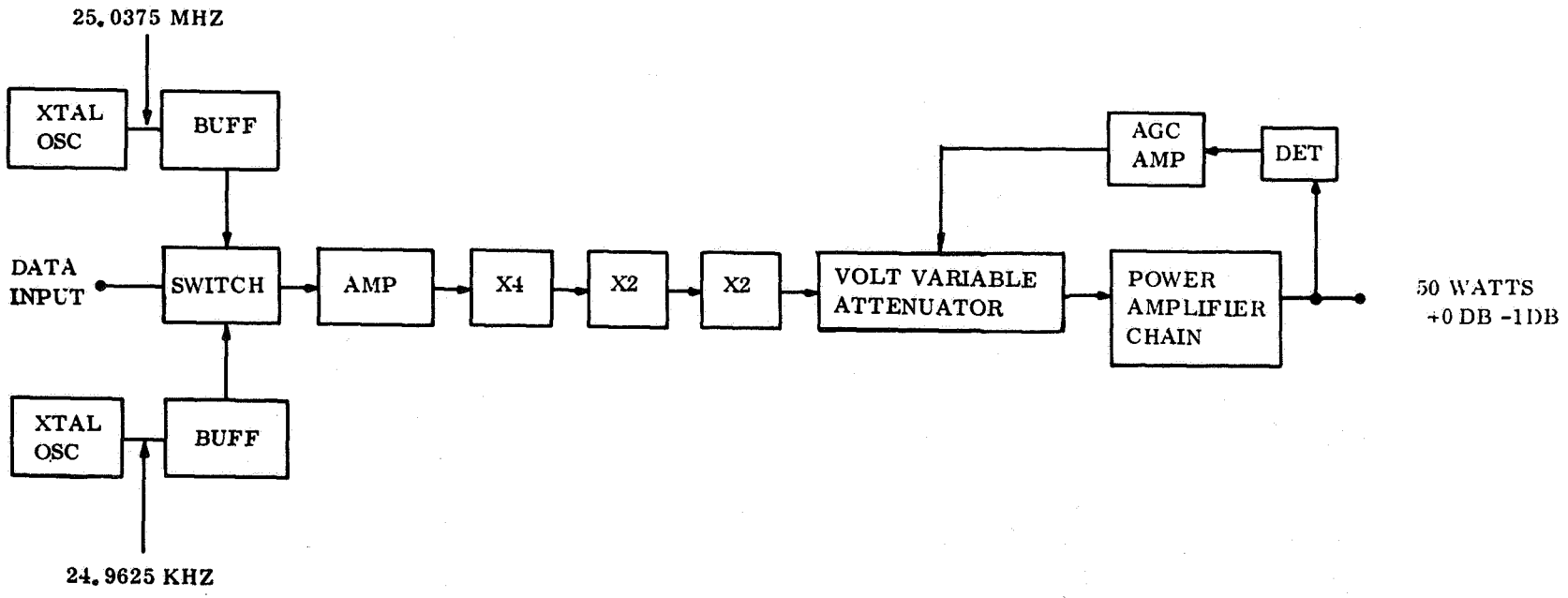


Figure 3.5.3-6. 400 MHz Transmitter, Block Diagram

potted with Dow Corning XR-6-3700 silicon potting compound. (The complete results of these tests are reported in GE, TIS 66SD2002 entitled "Fifty Watt Solid State FM Transmitter for Deep Space Communications", by Julius Shatas.)

3.5.3.5.3 Duplexing Circuit

The duplexing arrangement used for the 400 MHz transmitter and receiver, shown in fig. 3.5.3-7, consists of two circulators connected as a four-port circulator and a receiver T/R switch. The circulators protect the transmitter against large reflections and provide receiver isolation. In the normal receive mode the T/R switch is biased to pass the received signal. When the transmitter is turned on the circulator provides 20 dB receiver isolation, and the T/R switch is biased to reflect the leakage power back into the circulator where it is dissipated in a load. The T/R switch will be located in the receiver and the four-port circulator near the transmitter.

The T/R switch considered is a Hylelectronics model SU 175, and the circulators are similar to the Melabs HB 5 series.

The antenna terminal of the duplexing circuitry is connected to the antenna switch as shown in the block diagram. This solid state switch is used to select one of two antennas according to Lander orientation. A solid state switch is selected because of its reliability and potential to withstand the shock environment. The switch considered is Hylelectronics model SU 176.

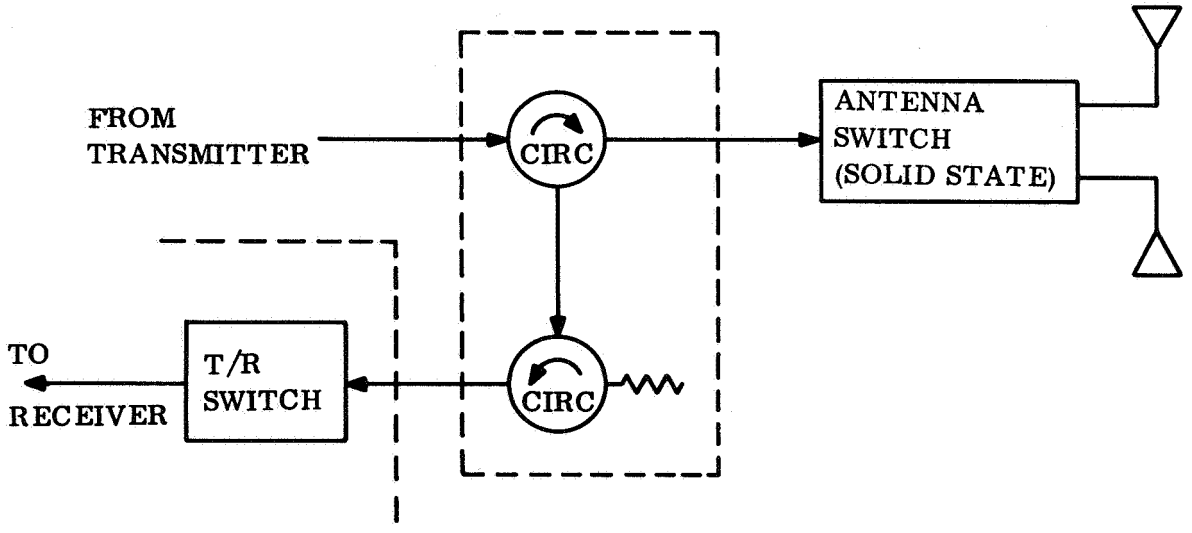


Figure 3.5.3-7. Duplexer and Antenna Selector

3.5.3.5.4 400 MHz Beacon Receiver

The purpose of the beacon receiver is to sense when the relay link can support the high data rate. This is accomplished by looking for reception of a preset signal level. When the expected signal level is detected the 400 MHz transmitter is energized after a 1 sec delay.

The receiver shown in fig. 3.5.3-8 receives an amplitude modulated signal of 400 MHz which is amplified in the low noise pre-amplifier and converted to the first i-f frequency. After amplification a second conversion takes place resulting in a second i-f signal at 3 MHz. The second mixer is fed to a band pass filter which reduces the overall noise level at that point to prevent limiting in the 3 MHz i-f amplifiers which follow. The signal is then filtered in a band pass filter with a noise bandwidth of about 25 kHz. The filter is a four-pole crystal filter with variations of not more than ±0.1 dB across the 18 kHz passband. After filtering the signal is detected and the demodulated signal is filtered in a tone filter with a pass band of about 100 Hz. At this point the signal is fed to a threshold detector.

The threshold is set for a nominal signal-to-noise ratio of 3 dB in the 25 kHz bandwidth which is equivalent to 27 dB in the 100 Hz final detection bandwidth. Allowing 3 dB for modulation loss and 6 dB for detection loss leaves a signal-to-noise ratio at threshold of 18 dB with a corresponding probability of false alarm on the order of 10^{-26}, implying false alarm is essentially impossible.

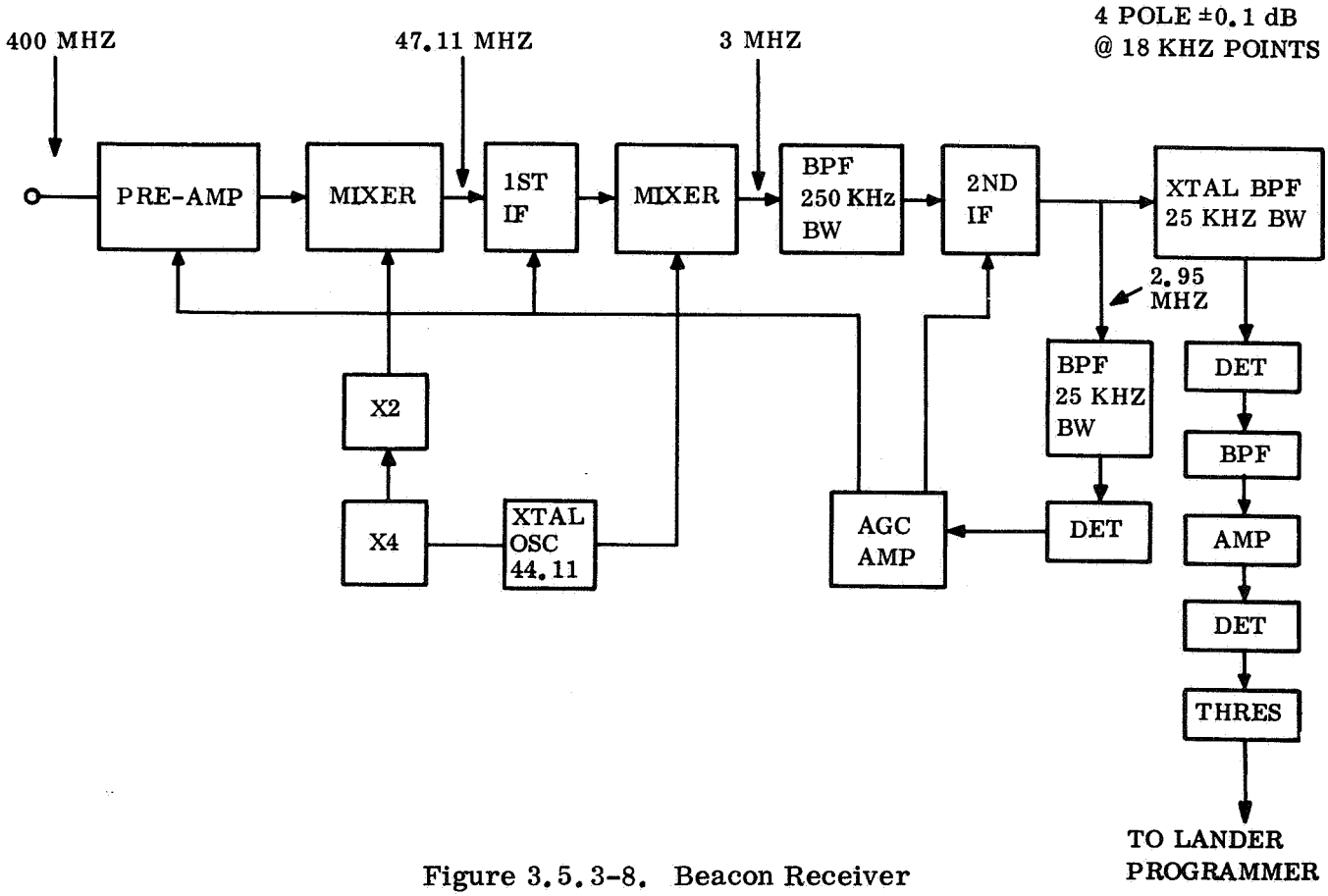


Figure 3.5.3-8. Beacon Receiver

In order for the receiver to provide indication of signal strength, the total gain of the receiver must be stable over a wide temperature range. This is achieved from the receiver front end to the output of the second i-f by means of an AGC circuit referenced to the receiver noise generated in the receiver front end. With a high gain AGC loop gain variations with temperature can be kept to ±0.5 dB, excluding effects of changes in the referenced noise level.

The remaining gain of the receiver which falls outside the AGC loop, that is, from the output of the second i-f to the threshold detector, must be kept within ±0.5 dB for a total receiver gain variation of ±1 dB. This includes ripple (±0.1 dB) in the pass band of the 25 kHz bandwidth crystal filter, changes in the detectors and threshold circuit and variations in gain of amplifiers outside the AGC loop.

The noise figure of the receiver is 5 dB referenced to the input of a pre-selector filter at the pre-amplifier front end. Since the receiver AGC circuit is referenced to front-end receiver noise, variations in noise figure will cause the receiver gain to vary. Thus the noise figure will be required to remain constant to within ±0.5 dB over the operating temperature range. The transistor anticipated for use in the pre-amplifier circuit is a KMC-K5001 specified at a noise figure of 1.4 dB at 400 MHz. If the noise figure of the transistor circuit is optimized at room temperature, the noise figure increases 0.4 dB at both temperature extremes. Since the optimum noise figure for this transistor is obtained with a 3:1 mismatch at the input, any temperature effects on the circuit affect the overall noise figure.

If the device noise figure changes from 1.4 to 1.8 dB, then 0.6 dB variation allowance remains for the rest of the front end circuit if the overall noise figure is to remain at a fixed value -0, +1 dB. This is accomplished by temperature compensating the front end circuitry and also by having sufficient gain at the front end to override noise contributed by the following stages such as the first mixer.

The effective receiver temperature is given by:

$$T_e = (N - 1)\, 290^\circ + \frac{T_a}{L} + \left(1 - \frac{1}{L}\right) T_L$$

where N is the receiver noise figure, T_a is the antenna noise temperature, T_L is the temperature of the receiving circuit loss components, and L is the numeric loss factor (greater than one). The receiver loss is 2 dB (two circulators at 0.5 dB, one antenna switch at 0.5 dB, and 0.5 dB of cable losses). Using an antenna temperature of 70°K, a loss temperature of 200°K, and N = 5 dB yields.

$$T_e = (3 - 1)\, 290 + \frac{70}{1.51} + \left(1 - \frac{1}{1.51}\right) 290^\circ = 724^\circ K.$$

3.5.3.5.5 Orbiter 400 MHz Radio Subsystem

Fig. 3.5.3-9 shows a simplified block diagram of the Orbiter UHF equipment. The duplexing circuitry, including the two circulators and T/R switch, is identical to that in the Lander vehicle.

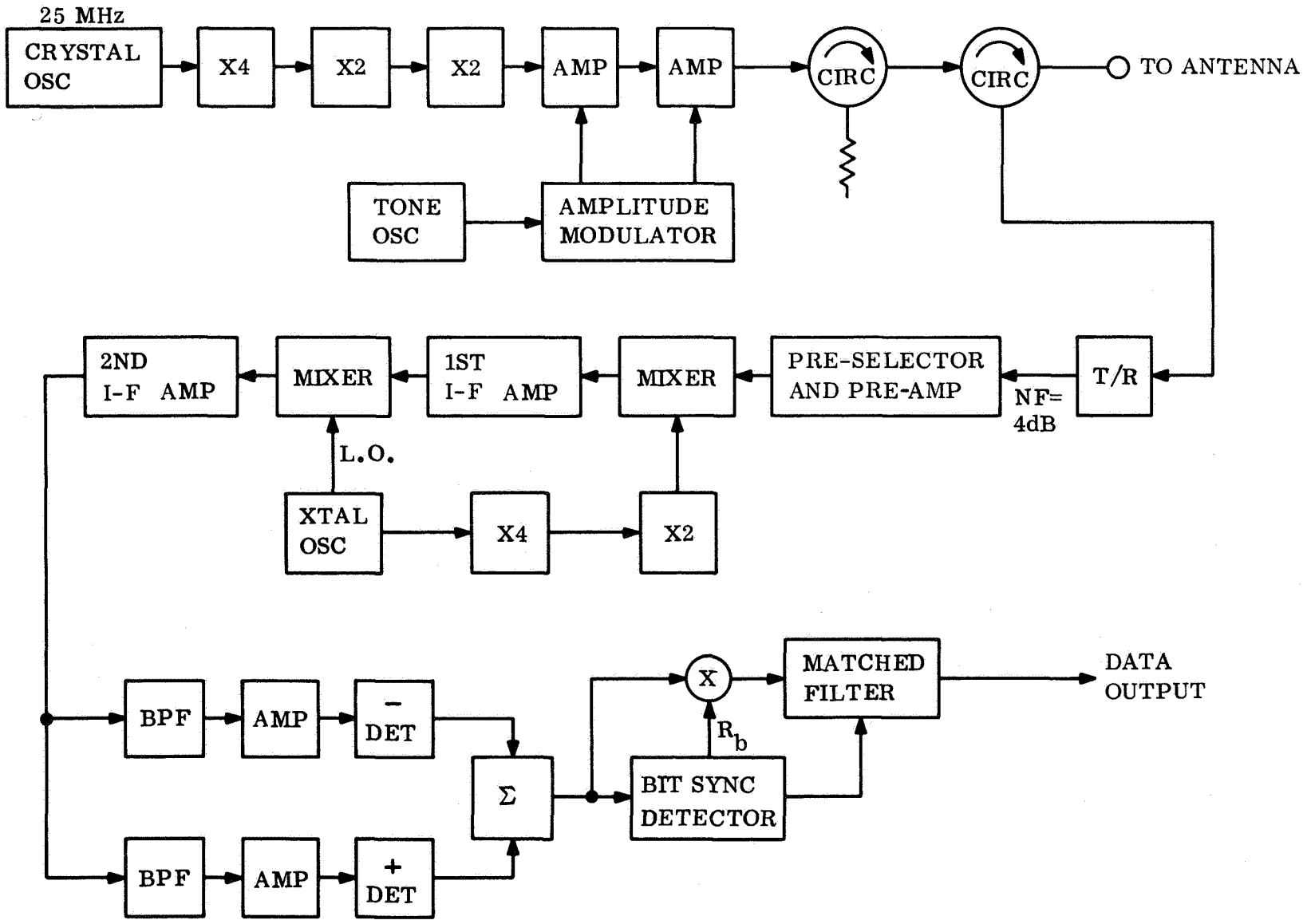


Figure 3.5.3-9. Orbiter 400 MHz Radio Subsystem

The beacon transmitter consists of a stable crystal oscillator operating at 25 MHz and a times 16 multiplier chain to 400 MHz, and amplifies to achieve the desired output level. The square wave tone oscillator 100 percent amplitude modulates the transmitter output.

The receiver, with an overall noise figure of 4 dB, is similar to the beacon receiver used on the Lander except for the output detectors. The second i-f output drives the FSK demodulator having two wideband filters followed by independent opposite polarity detectors which are summed to form the Manchester coded signal.

In the Lander transmitter, binary data having an NRZ format and bit rate R_b is bi-phase modulated on a square-wave subcarrier with frequency R_b to produce a Manchester coded signal; this signal modulates the frequency shift key (FSK) transmitter. The reconstructed signal (detected by the Orbiter FSK detector) is fed to the bit sync detector which generates a square-wave subcarrier at frequency R_b to convert the reconstructed signal back to the NRZ format. This signal is detected in a matched filter.

3.5.3.5.6 Data Handling System

A. Functions

The data handling and storage subsystem provides encoding, time multiplexing, sequencing information and storage of the Capsule's engineering and science data, and storage and execution of on-board command functions. The data handling and storage subsystem controls the data collection, formatting, and data transmission as a function of the mission phase from interplanetary cruise through post impact operations.

B. Summary Description

The functional block diagram of the data handling subsystem is presented in fig. 3.5.3-10. All analog signals (0 - 5 v), are multiplexed by the analog gates. The formatting of the data is determined by the data handling unit. The fixed formats are selected as a function of mission phase by a mode select command from the random access memory.

The analog to digital (A/D) encoders sample the analog signals and perform the digital conversion many times faster than the word rate. Using the fast conversion and a 9 bit analog-to-digital converter (ADC), the transmitted number of conversion bits per scientific data source can be made 9 bits or less depending on the source's accuracy requirements. The engineering signals are encoded to 7 bits.

Multicoder - The multicoder will have four modes of operation, each controlled by the data handling unit pulse lasting the duration of each mode. The number of data channels per mode are defined below: All analog inputs are high level (0 to +5 VDC).

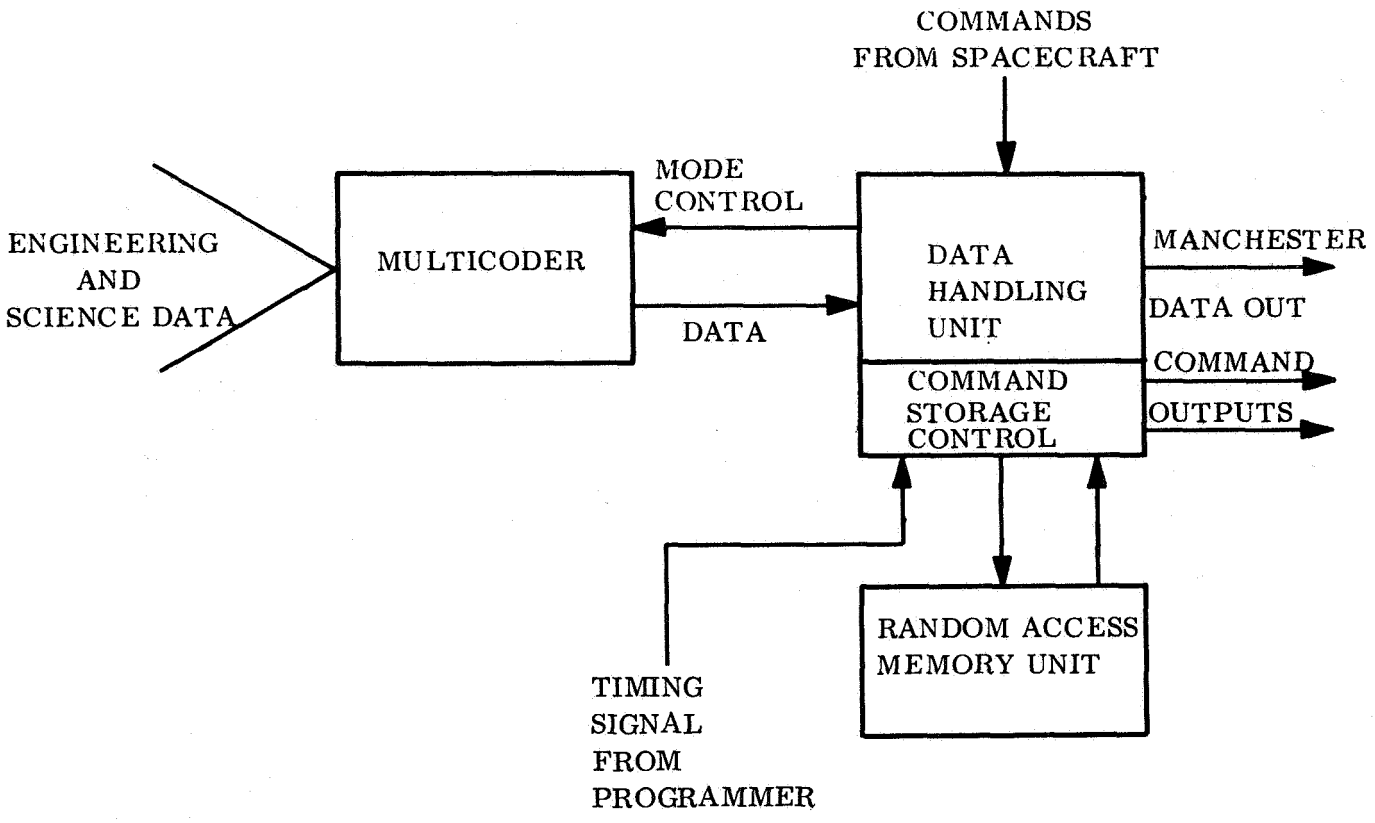


Figure 3.5.3-10. Data Handling System

1. Entry Mode

   a. 60 analog inputs, 9 bit resolution, 1 sample/sec

   b. 3 analog inputs, 9 bit resolution, 3 samples/sec

   c. 50 digital groups, 8 bit parallel occurring in 50 serial words on command from the multicoder at the rate of 5 groups/sec

   d. 2 digital words, 7 bit parallel, 1 sample/10 sec

   e. 1 digital word, 11 bit parallel occurring in two words, 1 sample/10 sec.

2. Landed Mode #1

   a. 58 analog inputs, 7 bit resolution, 1 sample 20 min

   b. 6 digital words, 11 bit parallel, 2 lines, 3 words/line. 1 sample/20 min

   c. 1 digital word, 11 bit parallel, 1 sample/20 min

   d. 130 digital words, 14 bit parallel sequential on multicoder command, 1 sample/20 min

   e. 130 digital words, 11 bit parallel sequential on multicoder command, 1 sample/20 min

f. 3 digital words, 7 bit parallel sequential on multicoder command, 1 sample/20 min

g. 2 digital words, 7 bit parallel, 1 sample/20 min.

3. Landed Mode #2

a. 14 analog inputs, 7 bit resolution, 1 sample/20 min

b. Digital inputs b, c, and g of Landed Mode #1.

4. Landed Mode #3

a. One of four TV inputs, 6 bit resolution, 27000 SPS (160 kbps).

Data Handling Unit - The data handling unit (DHU) accepts commands from the command storage control unit to determine in which mode the multicoder will operate, (fig. 3.5.3-10). It decodes these commands and controls the multicoder functions by supplying pulses on one of four mode lines. The data from the multicoder is routed by the DHU either to the random access memory unit to the VHF transmitter or to the S-band transmitter. During entry, data from the multicoder is interleaved with delayed data from the random access memory unit.

The DHU also conditions the signals from the multicoder and memory going to the transmitters.

Commands from the spacecraft via hardwire are routed through the DHU to the command storage unit and then to the memory.

Random Access Memory Unit - The random access memory unit (RAMU) is used to provide storage for digital words from the multicoder (7 bits/length) and to store command words (21 bits length).

The telemetry storage has two modes:

1. Store data serially and read out serially 70 sec later.

2. Store data and read out at a fixed rate at some later time.

Both of these modes are used in entry data collection as shown in fig. 3.5.3-13. Mode 2 is also used for collection of landed serial and engineering data and playback during Orbiter passes.

Data will be inputted and outputted in a 21 bit format. Read out will be destructive with a restore mode option for Mode 1 as required.

Command Storage Unit - The command storage unit (CSU) (part of the DHU) accepts commands from the spacecraft via hardwire. The commands and time labels are stored in the memory. The unit examines sequentially each command location in the memory. It does pass a command time word until that time agrees with the vehicle clock time.

When agreement occurs it jumps to the next location which should be a command and outputs it to the Lander programmer (see para 3.5.4.2).

The commands in the memory can also control the sequence of examination of the CSU. Thus, a fixed sequence of operations can be addressed by commanding the CSU to that memory location. At the end of this sequence (e.g., data gathering) a command would be present which would send the CSU back to the memory location following the jump command. By using auxiliary registers (part of the random access memory) and decoding functions to control the CSU, the CSU became a versatile general purpose program machine.

For a mission of 24 hr with experiments requiring data gathering every 20 min, 3 hr,and 6 hr, the specific actions at each sampling time need be stored only once with time increment and return commands at the end of these sequences.

The timing signals for the CSU are provided by the Lander programmer.

A program for operation after separation is stored in the memory. The commands are read out of the memory sequentially as the time for execution matches the present time in the vehicle. The command storage control unit will run continuously until 1 hr after impact. It will then control the landed operations until end of life.

Fig. 3.5.3-11 shows the command word format. Since there is no radio command system on this vehicle all the words will be stored program commands. These commands and the proper time labels will be loaded into the random access memory prior to separation from the spacecraft. The experiment routine on the surface will be controlled by these commands as the time labels associated with each sequence agrees with the time on the vehicle clock. This unit will be shut down to conserve power when the time between commands is more than 20 min. A separate set of registers will be used to store the time at which the data handling system shall begin functioning and also the memory location of the next command. The flow chart in fig. 3.5.3-12 shows how the command storage unit checks the time until next command execute and shuts the system down until this time is reached on the vehicle clock.

When the commands are loaded into the memory prior to separation from the spacecraft the presence of data on the command line causes a command interrupt in which the system acts as though it is in the dormancy subroutine. After memory updating is completed, the unit will again return to the last memory location and time and sequentially search the memory. Real time commands and generated commands at this time will both appear on the eight output lines which go to the programmer.

Table 3.5.3-9 shows the entry data measurements and table 3.5.3-10 shows the landed data measurements.

C. Data Handling vs Mission Phase

Interplanetary Cruise - The Capsule's data handling equipment is assumed de-energized during interplanetary cruise. Monitoring of thermal control and the Capsule's electrical power subsystem is performed by the spacecraft's data handling subsystem.

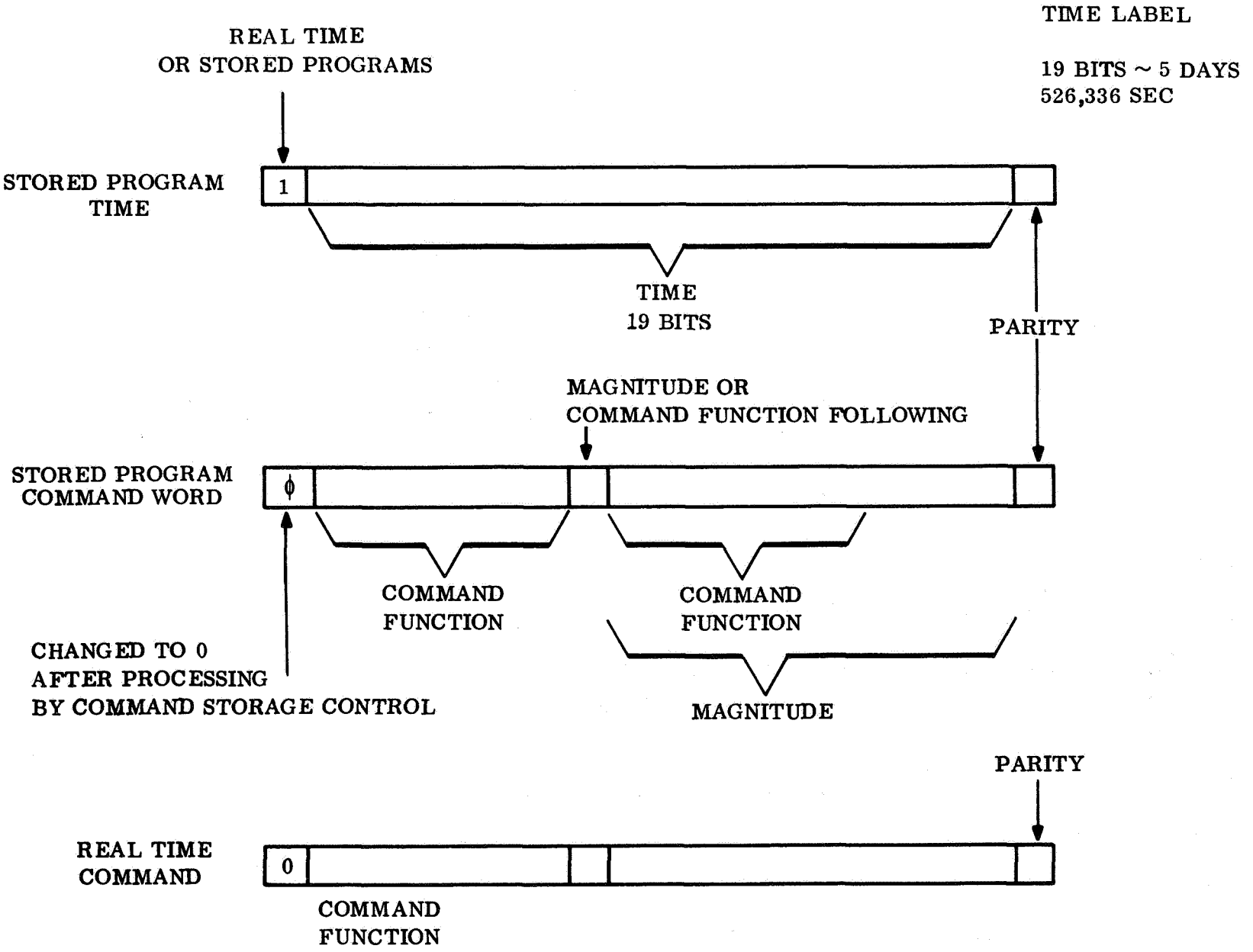


Figure 3.5.3-11. Command Word Format

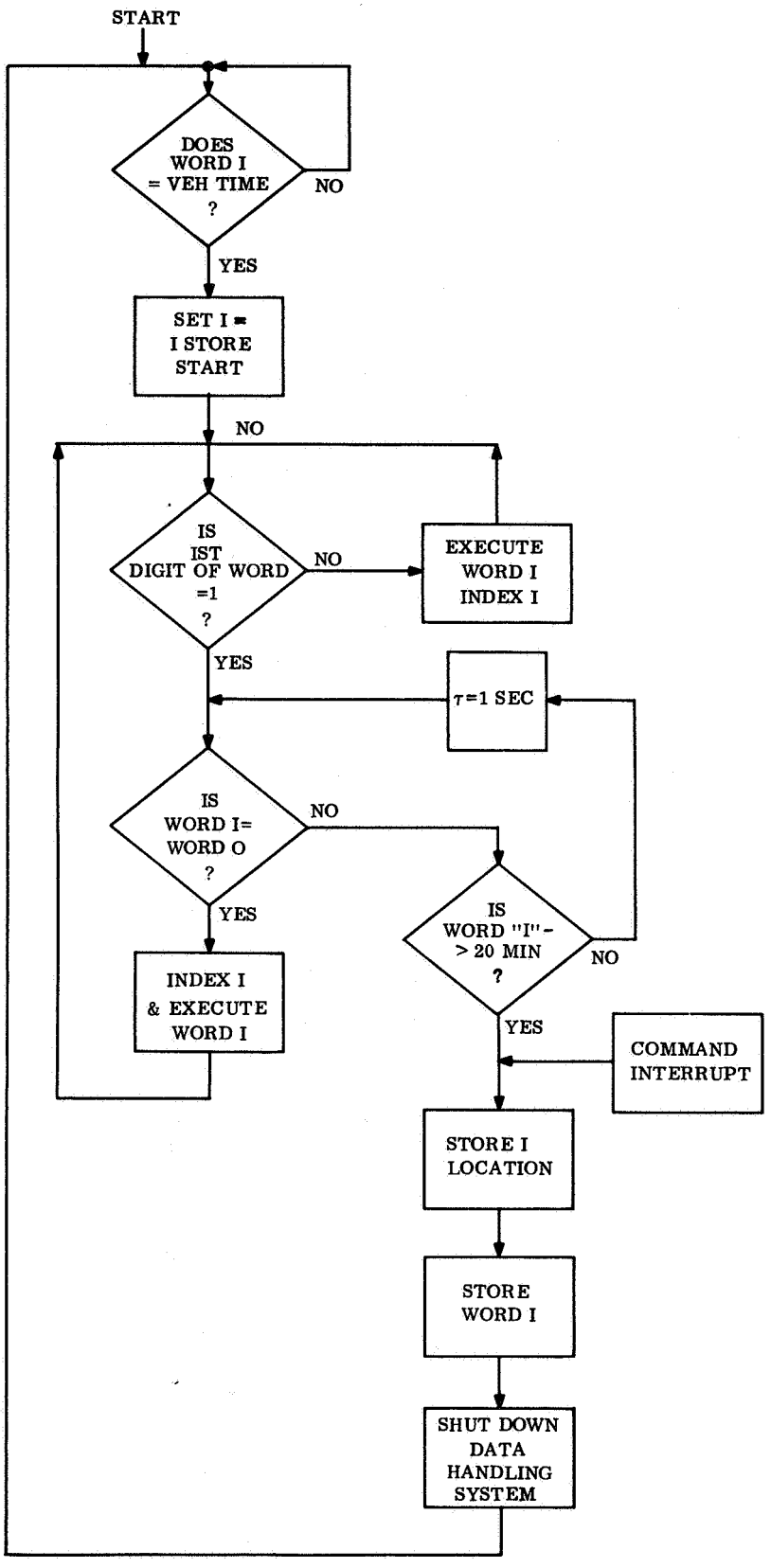


Figure 3.5.3-12. Operation of Command Storage Control Unit

TABLE 3.5.3-9. ENTRY DATA

Sensor	Accuracy (%)	Sampling Rate (SPS)	Bits/Sample	No. of Channels	bps	Time
Pressure transducer (2) 0 - 0.3 psia	1	1	9	2	18	Post chute deployment
Resistance thermometer (2) 100° - 300° K	0.2	1	9	2	18	
Mass spectrometer (readout 8 bits at a time)	—	N/A	8	N/A	40	1 hr before entry to impact
Accelerometer, triaxial (dual scale)	1	3	8	3	72	1 hr before entry to impact
Stagnation temperature	0.25	1	9	1	9	1 hr before entry to impact
Stagnation pressure (4)	0.25	1	9	4	36	1 hr before entry to impact
Water vapor	N/A	1/15	7 (parallel)	2	14/15	1 hr before entry to impact
		1/15	11 (parallel)	1	11/15	
Engineering measurement	—	1	7	50	350	1 hr before entry to impact

TABLE 3.5.3-10. LANDED SCIENCE (NON-IMAGING)

Sensor	Accuracy	Sampling Rate	Bits/ Sample	Number of Channels per Sensor	Number of Bits per Hour
Pressure transducer (2)	1%	3/hr	6	2	36
Thermometer	1%	3/hr	6	2	72
Wind velocity (2)	3%	3/hr	11 (P)	6	66
Moisture	--	3/hr	7 (P) 11 (P)	2 1	75
Surface composition	Less than 256 counts per energy slot in 3 hr	1/3 hr	14 (P) 12 (P) 7 (P)	130 130 3	1133
Clinometer (2)	1%	1/6 hr	7 (P)	2	14/6
Engineering measurements	--	3/hr	7	50	1050

(P) - Parallel

Capsule Checkout - The Capsule checkout mode is initiated sufficiently prior to separation to determine the status of the Capsule and its payload and to allow for corrective action. Under control of the programmer and command storage control unit, Capsule checkout is accomplished with data being transferred to the spacecraft via hard-wire.

Capsule Separation and Engine Fire - From Capsule separation to engine fire, the Capsule is transmitting at 1090 bps. Only engineering data is monitored. The received data on the spacecraft is detected and stored for delayed transmission to Earth over the high data rate link.

Capsule Entry - Upon initiation of entry, the data rate is 1090 bps. The entry data rate requirements are shown in table 3.5.3-9. Assuming 350 bps for engineering data, the total data rate required is 1090 bps. For a blackout time of less than 70 sec the storage required is approximately 50 kbits.

The data is stored in the random access memory. Essentially, the memory will act in two modes; one, as a delay line with a 70 sec delay, and two, as a memory in up to 100 kbits of entry data are stored. Each word in the memory is 7 bits. The operation of the random access memory during entry is shown in fig. 3.5.3-13.

Post Impact Relay - Upon impact the buffer readout is temporarily halted. The buffer will contain 100 kbits of entry data. Engineering data is continued to be read out at 1090 bps until completion of the setup period. Upon completion of the setup period, the imaging data collection and transmission begins. Stored engineering and scientific data are read out at the beginning and middle of each imaging cycle.

Landed Operations - The data presented in table 3.5.3-10 is collected and stored. The basic period between sampling is 20 min. Approximately 25 hr after impact the Orbiter will again be in view and all the stored data will be transmitted at 160 kbps at the beginning of the transmission period. Then video data will be generated and transmitted and after 4 min the stored Lander data will be repeated prior to resuming video transmission for the next approximately 4 min period. This procedure is repeated for the entire relay transmission interval.

3.5.3.5.7 Physical Characteristics

Table 3.5.3-11 summarizes the physical characteristics of telecommunications equipments. The key to development status is:

1. No modification required (off-the-shelf)
2. Modify (e.g., for high shock)
3. Redesign (basic equipment exists but redesign for new frequency, detection technique, etc.)
4. New design (specify new design using established techniques)
5. New development (employs near-future state-of-the-art techniques).

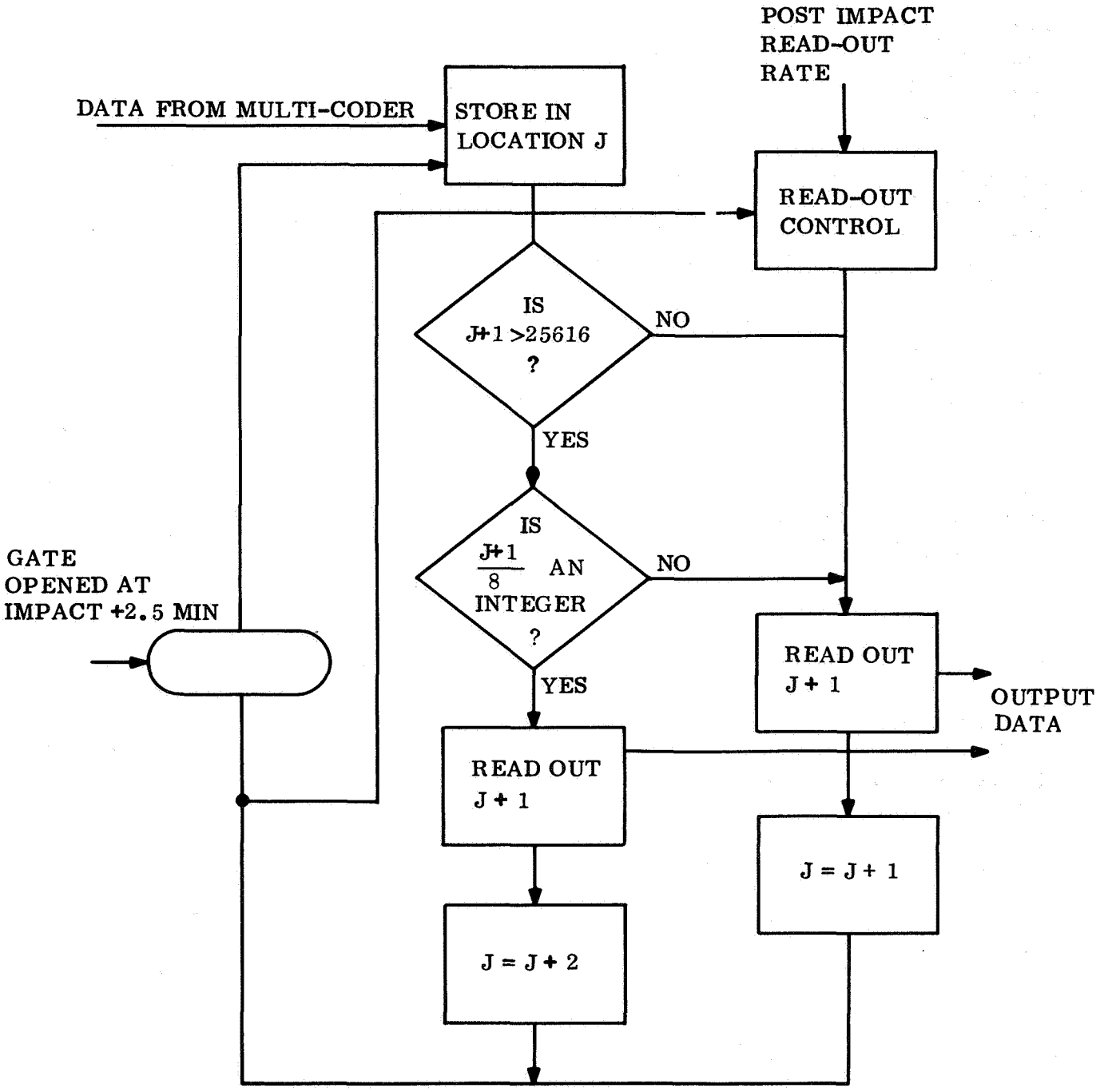


Figure 3.5.3-13. Entry Data Storage Routine

TABLE 3.5.3-11. PHYSICAL CHARACTERISTICS

Component and Quantity	Size (in.)	Weight (Based on 1000 g's)(lb)	Power	Sterilizable (125°C)	Minimum Shock (present information)	Development Status	Remarks
UHF transmitter	30 in.^{3} 1.5 x 4 x 5	2.5	150 watts	yes		4	
UHF antenna (2)	8 diameter x 2	1	--	yes		4	2 required 1 will be used
UHF circulators (2)	6 in.^{3} 2.5 x 2.5 x 1	0.4	--	yes		3	2 required in close proximity
UHF antenna switch	1.1 in.^{3} 2 x 1.5 x .375	1.0	0.25A @ 3.5v and 10 micro-A @ 28v	yes	3000 g's, 3 ms	1	Interchange voltages to switch antenna - Power required during xmt, and receive
Beacon receiver and T/R switch	21 in.^{3} 5.4 x 3.6 x 1/1	1.3	0.5 watts and 0.06A @ 1.2v	yes		4	0.06A @ 1.2v required during 400 MHz transmit periods
Multicoder	104 in.^{3} 3.5 x 4.3 x 7	5	15 watts	yes		3	Power required during data sampling periods only (see text)
Data handling unit	100 in.^{3} 4 x 5 x 5	4	3 watts	yes		4	
Thin film memory	88 in.^{3} 4 x 4 x 5.5	5	6 watts	yes		4	180 kbit capacity, random access
Signal conditioner	4 x 5 x 7	4	8 watts	yes		2	50 channels only
Three axis impact Accelerometer	1.3 x 1.3 x 0.8	0.6	--	yes	10,000 g's	1	
Charge amplifier (3)	1.25 x 2 x 3	0.5	1.2 watts each	yes	representative unit passed 2000 g test	1	2 required connected to impact accelerometer by coaxial cables

3.5.4 ELECTRICAL POWER EQUIPMENT

The power equipment provides electrical energy, power switching, charge control, voltage control and electrical distribution. Fig. 3.5.4-1 illustrates this equipment. Note that the electrical energy flow, power, signals and data which takes place between subsystems are shown in the Functional Block Diagram, Section 3.2.4.

3.5.4.1 Operation

Commands are received via hardwire connection to OSE for post sterilization check, via hardwire from the spacecraft through the telecommunications subsystem during interplanetary cruise and during Martian orbit, and from the telecommunications subsystem after landing. These commands enter the programmer as a 21 bit word where they are decoded into operational signals for the relays which switch the power feeder lines. The programmer also contains a multichannel hardwire program section which provides an additional independent operation of the spin, de-boost, and landing sequences for mission assurance. These programs have programmable start times and, once initiated, proceed with the execution of a fixed program sequence. A single command, regardless or origin, may signal the operation of either a single load or a group of loads as required.

All operation signals from the programmer go the power controller where power switching takes place. The components which require independent switching, such as the payload scientific instruments, have separate electrical power feeders. Other components which are always used as a group, such as the engineering diagnostic instrumentation, share a single feeder. The power controller can accept energy from the operational battery, from the high rate batteries, from the spacecraft or from ground power, and switch this power to the appropriate load or loads. The line contactor is used to select and control which of these power sources supplies the power controller.

The operational battery provides all Lander electrical energy except the high rate pyrotechnic and hot-wire initiations. This secondary silver-zinc battery is charged from raw spacecraft power prior to separation. Power from the operational battery feeds the unregulated loads directly. This battery is equipped with extra cells and semiconductor bypass for redundancy.

3.5.4.1.1 Battery Redundancy Considerations

To enhance reliability, three alternatives have been investigated.

If two batteries are flown, each capable of providing the minimum mission duration objectives, a considerable weight penalty would be suffered. An alternative route would be to provide two batteries which would each provide half the desired output. This method would increase the battery weight about 25 percent, because of the lower power-to-weight ratios of smaller batteries, and ensure that half the mission objective would be achieved even if one battery failed.

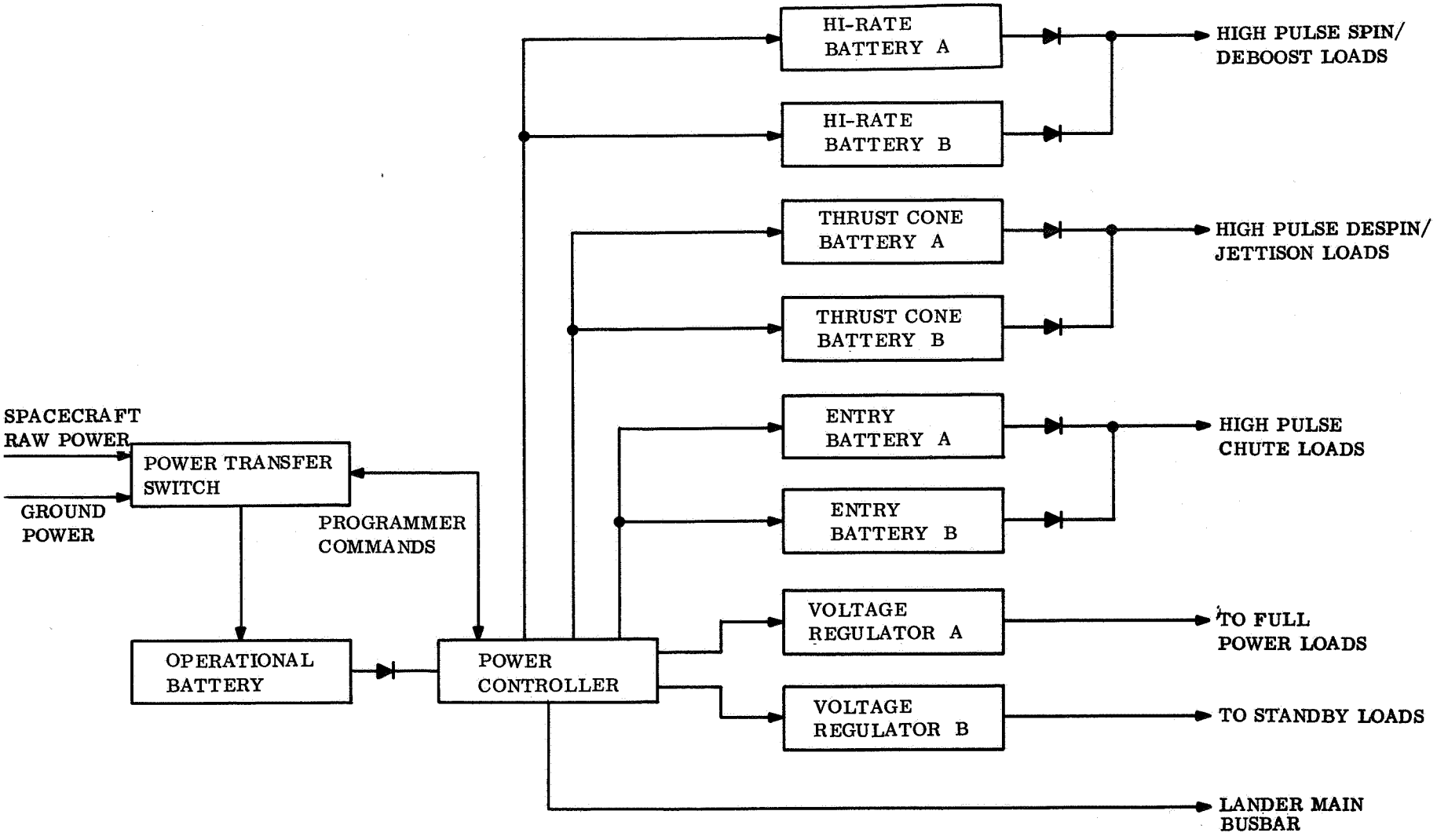


Figure 3.5.4-1. Electrical Power Subsystem Block Diagram, Point Design 1

The method adopted to provide adequate redundancy is to carry redundant cells. The logic in this approach is that it is ususal if failure should occur for only one, or at most two, cells to fail. If these can be replaced by reserve cells considerable savings will result.

The circuit shown in fig. 3.5.4-2 incorporates diodes on the charging side having a tightly controlled Zener regulating level, e.g., 2.05 v, and very low dynamic impedance. The diode on the discharge side of the circuit has a low forward voltage. Three redundant cells in the battery are connected through the controller to be added in series when needed as directed by the programmer.

If, during charge, a cell fails open circuit or high resistance, the Zener voltage of that cell will be exceeded. The cell will be bypassed. If the cell fails short circuit or low resistance then the cell will carry the charge current. A slight loss may result in charging a bad cell. Because each Zener protective voltage level will be equal to its cut-off voltage, the arrangement gives added protection against overcharging.

If a cell fails on discharge, the diode in the discharge circuit will conduct and bypass the failed cell, avoiding driving the cell negative. Whichever way the cell fails, it will always be bypassed.

Switching in new cells through the controller is achieved by low voltage sensing in the programmer. The low voltage is caused by the loss of a cell plus the diode drop as it switches in. Two cells would therefore be switched in for the first cell failure to compensate for diode voltage drop. A nominally higher voltage than the original battery would then result. If the second cell failed only one other cell would be switched.

A redundant system has been provided which allows for the failure of two cells in a battery. The additional weight approximates 20 percent of the original battery. This includes cells, diodes, programmer and controller modifications.

The need for high current capability during initiation operations is met by three pairs of thermal batteries. These provide power for spin/de-boost operations, despin/entry operation and parachute/aeroshell operations. In each case two batteries are available for redundancy. The batteries are activated separately from the canister or operational battery and the output is switched to the initiators via the power controller. These activation circuits are equipped with thermal relays to protect the operational battery.

The scientific payload, r-f equipment, diagnostic instrumentation, data processing equipment, and sequencing components will require voltage regulation. To minimize weight, to obtain the high efficiency needed on the extended mission and to permit noise control, a single central voltage regulator should be used. However, the high degree of energy conservation required would not permit standby losses of such a large regulator on a continuing basis. For this reason two regulators are used, a small unit for the timer and receiver, which are operated through the dormant periods,

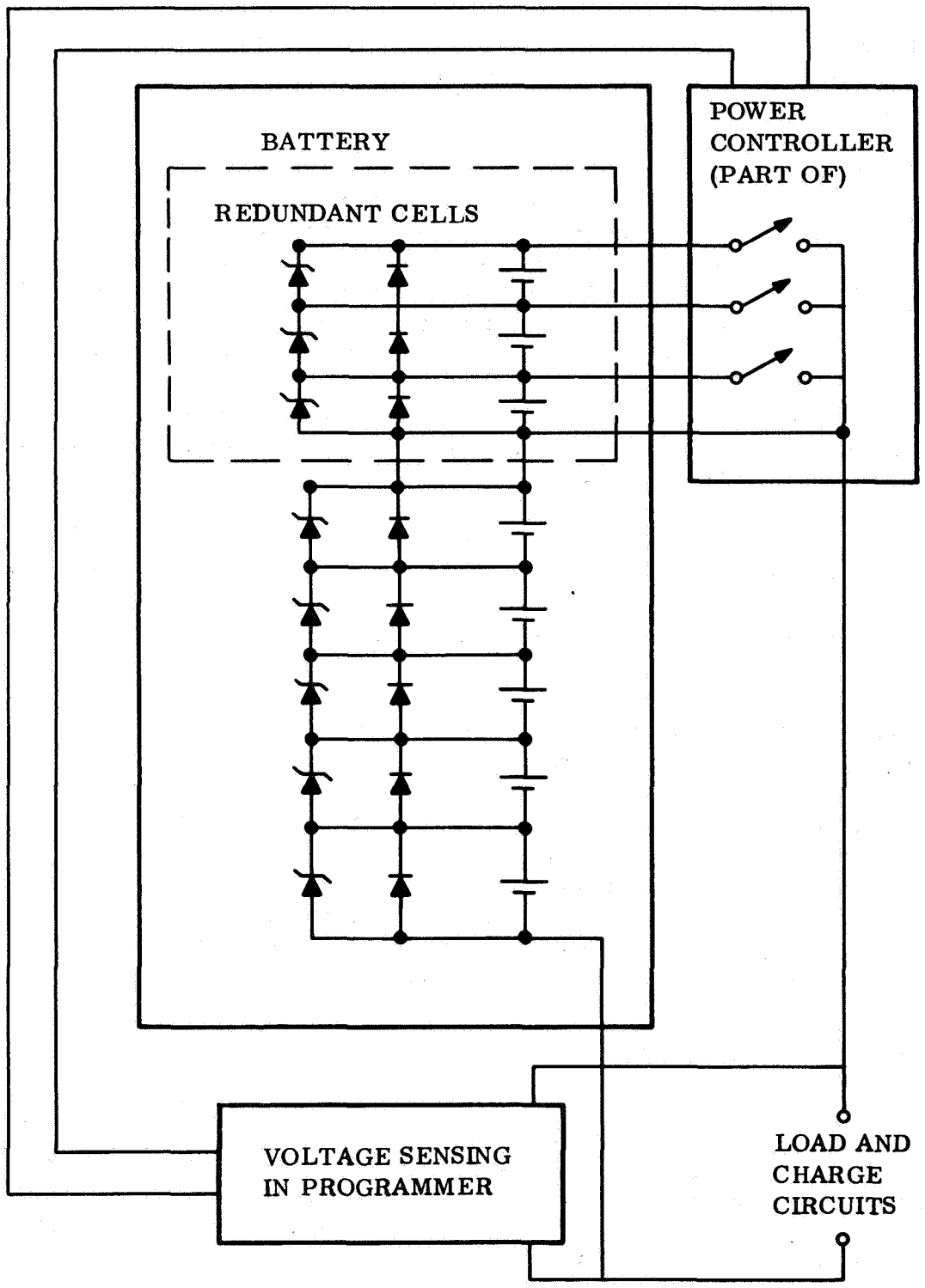


Figure 3.5.4-2. Battery Redundancy Circuit

and a larger unit which handles all other loads. In addition, it is recognized that selected small loads in the scientific instruments may require special high accuracy regulation.

Battery charging is controlled by redundant equipment located in the canister. This equipment uses solid-state switching circuitry with time ratio control for high efficiency.

The Mars Hard Lander electrical system utilizes direct current power sources and distribution as well as steady-state sensing of pressure and temperatures. Programming, sequencing and power switching are performed for durations of a minute or longer with synchronization accuracies in the order of 0.1 sec. Safing and arming are performed manually. Conditioned and regulated powers are processed at a low audio frequency. Initiation and electromechanical operations are performed with the application of electrical energy for durations of a few msec to a few hundred msec.

Electromagnetic compatibility equipment is designed to provide protection over a broad spectrum. This includes low repetition rate pulse-transients through the r-f frequencies used for telemetry.

Data processing, encoding, and multiplexing involve kilocycle and higher frequencies. The camera electronics with imagery represents the highest data bit rate.

UHF is used for telemetry, providing the highest frequency equipment aboard the probe system.

These needs describe the spectrum of electrical energy which must be distributed by the cables and harnessing.

Since the Lander will carry a number of different scientific equipments as payload, it is desirable to make arrangements permitting the mission to continue should electrical difficulties arise in a limited area. This feature is provided through a breaker and limiter unit which provides electrical protection to each payload item. Should an electrical fault develop, the load element is disconnected or current limited so that the remainder of the mission may continue.

3.5.4.2 Component Description

Each component is described in detail in this section. Table 3.5.4-1 lists the electrical equipment of Point Design 1 by name, location, weight, size, and power level, together with electrical reference designators. The equipment situation is indicated by capability to withstand 125°C sterilization temperature, prior shock level accomplished, and development status. The development status is shown by the same numerical code as defined in para 3.5.3.5.

TABLE 3.5.4-1. ELECTRICAL EQUIPMENT HARDWARE MATRIX, POINT DESIGN 1

Component	Size (in.)	Weight (based on 1000 g's) (lb)	Power (watts)	Sterilizable (125 C)	Maximum Shock (present information)	Development Status
Operational battery (A101)	9.0 × 5.5 × 9.0	29.8	Source	yes	2,000	5
Line contactor (A106)	2.5 × 2.5 × 5.0	2.0	5.6	yes	400	3
Lander programmer (A107)	8.8 × 7.7 × 3.5	7.2	12.0	yes	400	4
Voltage regulator (A108)	5.0 × 6.0 × 8.0	7.0	250.0	yes	1,000	3
Power controller (A110)	3.5 × 5.0 × 7.0	5.5	15.0	yes	700	5
High rate battery (A113, A114)	2.0 diameter × 3.0	0.5	Source	yes	15,000	1
EMC filter (A115)	3.0 × 3.75 × 5.5	1.9	--	yes	5,000	2
Diode blocking module (A121)	1.5 × 1.5 × 2.5	0.2	13.0	yes	20,000	2
Thermal relay module (A124)	1.5 × 1.5 × 2.5	0.15	3.0	yes	50	4
Hg Switch (A128, A129)	1.0 diameter × 2.5	0.1	--	yes	50	4

TABLE 3.5.4-1. ELECTRICAL EQUIPMENT HARDWARE MATRIX, POINT DESIGN 1 (Concluded)

Component	Size (in.)	Weight (based on 1000 g's) (lb)	Power (watts)	Sterilizable (125 C)	Maximum Shock (present information)	Development Status
Voltage regulator (A130)	2.5 × 3.0 × 4.0	0.9	27.0	yes	1,000	3
Breaker and limiter unit (A132)	2.0 × 2.0 × 3.0	0.6	1.0	yes	10,000	2
Aeroshell/Lander IFD (J2002)	1.83 diameter × 1.5	0.13	338.0	yes	2,000	3
Thrust Cone/Lander IFD (J2003)	2.5 diameter × 2.0	0.75	338.0	yes	2,000	3
Command cable assembly (WL1)	14C × 8 ft	2.1	3.0	yes	2,000	3
Power cable assembly (WL2)	16C × 28 ft	3.7	12.0	yes	2,000	3
Instrumentation cable assembly (WL3)	50C × 40 ft	3.0	0.3	yes	2,000	3
Shielded cable assembly (WL4)	1C × 24 ft	0.8	--	yes	2,000	3

3.5.4.2.1 A101, Operational Battery

Function: Provides energy source for all aeroshell and Lander electrically operated equipment, except high rate initiation loads, from the time of canister release through the mission completion.

Type: Manually activated heat-sterilizable silver-zinc secondary battery sealed with high pressure emergency rupture disk.

Rating: 511.1 watt-hours, 28v nom, ±18 percent
Load profile per Section 3.2.5.

3.5.4.2.2 A113, A114 High Rate Batteries

Function: Provide energy source for multiple high-rate initiation type loads.

Type: Remotely activated, electrically initiated, thermal type, primary battery.

Rating:

Peak power output	1000 watts
Maximum activated stand	3 min
Power profiles	later

3.5.4.2.3 A106 Line Contactor

Function: Power transfer of aeroshell Lander systems from ground power to spacecraft power to internal batteries.

Type: Electromechanical latch type line power contactor.

Rating:

Contact rating	20 amp
Interrupt capacity	250 amp
Pull-in time	100 msec maximum
Pull-in power	0.3 watt maximum
Contact configuration	later
Operating life	100,000 cycles
Dielectric withstand capability	1500 v for 1 min

3.5.4.2.4 A107 Lander Programmer

Function: Provide all sequencing, timing, signals, synchronization and clock functions within the Lander and aeroshell. Decode commands.

Type: Solid-state digital circuitry using majority logic or redundance back-up features.

Rating: Channels
In-flight check-out
Powered flight program
Diagnostics cycle
Maneuver mode control
Preseparation program
De-boost sequence
Entry sequence
Set-up mode control
Surface science sequence
Photography cycle
Vehicle clock

3.5.4.2.5 A108 Voltage Regulator

Function: Provide control and correction for electrical potential variations. Also, provide various potential levels required to operate aeroshell and Lander electronics

Type: D-C isolated solid-state inverter transformer-rectifier with time ratio control and feedback regulation.

Rating:		
	Output	250 watts
	Voltage levels	later
	Transient recovery time	later
	Regulation	later
	Input	23 to 33 vdc

3.5.4.2.6 A110 Power Controller (Lander)

Function: Provide distribution center equipment and all power switching for the aeroshell, thrust core, and Lander electrical loads. Receives commands with proper time sequences and synchronization from the Lander Programmer A107.

Type: Electromechanical relay, switch and contactor construction

Rating:		
	Number of switched loads	100
	Contract rating	40 amp maximum
	Pull-in time	10 to 100 msec
	Pull-in power	0.5 watt each
	Feeder buses	50

3.5.4.2.7 A121 Diode Blocking Module

Function: Prevent reverse power flow between various energy sources.

Type: Solid-state single crystal silicon semiconductor diode with redundancy.

Rating:	PIV	75 v
	Recovery time	NA
	Forward current	10 to 75 amp

3.5.4.2.8 A115 Electromagnetic Compatibility Filter

Function: Suppress spurious and conducted electromagnetic interference.

Type: Lumped parameter networks with non-linear and lossy type circuit elements.

Rating:	r-f band pass rejection	
	Number of bands	later
	Center frequencies	later (VHF)
	Attentuation	later
	Dielectric withstand	1500 v

3.5.4.2.9 A124 Thermal Relay Module

Function: Provide system protection against faulted squib firing circuits.

Type: Bimetallic heat operated latch type switching element.

Rating:	Interrupt capacity	10 amperes
	Trip level I^2 Rt	later

3.5.4.2.10 A128, A129 Switch, Hg

Function: Detect upwards direction and enable proper deployment circuits.

Type: Potted mercury switch, 3 pole

Rating:	Current rating	1 amp
	Voltage rating	250 vdc
	Dielectric withstand	1500 v, 1 min

3.5.4.2.11 A130 Voltage Regulator

Function: Provide control and correction for electrical potential variations at high efficiency for standby usage. Also, provide various potential levels required to operate the standby Lander electronics.

Type: DC isolated solid state inverter transformer-rectifier with time ratio control.

Rating:	Output	27 watts
	Input	23 to 33 vdc

3.5.4.2.12 A132 Breaker and Limiter Unit

Function: Protect the electrical system against non-essential functional faults.

Type: Circuit breaker, thermal relays, and limiting resistors in selected groups.

Rating:		
	Circuits	20
	Trip levels	30 ma to 2 amp

3.5.4.2.13 J2002, P2002 Inflight Disconnect Aeroshell-Lander (connector, electrical; electromechanically disconnected)

Function: Provide remotely operable, electrical disconnection between the aeroshell and the Lander vehicle during Martian entry flight.

Type: Hot-wire operated push-off type collet lock-unlock connectors with crimp insertable cuperic contacts and 360° RFI shielding.

Rating:		
	Circuits	10 pins
	Wire sizes	later
	Operate time	less than 100 msec
	Operated signal	3.5 amp for 50 msec
	Safe level	1 amp, 1 watt, for 5 min
	Release impulse	later
	Reliability	0.995 at 90% confidence, each device.

3.5.4.2.14 J2003, P2003 Inflight Disconnect - Thrust Cone/Lander (connector, electrical; electromechanically disconnected)

Function: Provides remotely operable/electrical disconnection between the thrust cone and the Lander vehicle during Martian entry flight.

Type: Hot-wire operated push-off type collet lock-unlock connectors with crimp insertable cuperic contacts and 360° RFI shielding.

Rating:		
	Circuits	50 pins
	Wire sizes	later
	Operate time	less than 100 msec
	Operated signal	3.5 amp for 50 msec
	Safe level	1 amp, 1 watt, for 5 min
	Release impulse	later
	Reliability	0.995 at 90% confidence, each device.

3.5.4.2.15 WL1 - Lander Command Cable Assembly

Function: Provides command and signal distribution from the Lander programmer to various receiving equipment.

Type: Copper conductor electrical cable insulated with Kaptan and teflon (HF + 1/2 T) in a wrapped construction. Cable connectors of NAS 1599 type and modified in selected cases to permit high density inserts and rear insertion construction.

Rating: Later

3.5.4.2.16 WL2 - Lander Power Cable Assembly

Function: Provide electrical power distribution throughout the Lander, from the power controller and batteries to the various loads.

Type: Copper conductor electrical cable insulated with Kaptan and teflon (HF + 1/2 T) in a wrapped construction. Cable connectors of NAS 1599 type and modified in selected cases to permit high density inserts and rear insertion construction.

Rating: Later

3.5.4.2.17 WL3 - Lander Instrumentation Cable Assembly

Function: Distributes data from sensors and payload instruments to data conditioners, encoders and telecommunication equipment in the Lander.

Type: Copper conductor electrical cable insulated with Kaptan and teflon (HF + 1/2 T) in a wrapped construction. Cable connectors of NAS 1599 type and modified in selected cases to permit high density inserts and rear insertion construction.

Rating: Later

3.5.4.2.18 WL4 - Shielded Lander Cable Assembly

Function: Provides coaxial transmission of signals and high frequency energy through the Lander.

Type: RG - 58

Rating: Z_c 50 ohms

3.5.5 ENVIRONMENTAL CONTROL

The mission weight and reliability constraints are such that the environmental control system complexity and design margins must be the minimum possible. In line with this objective, a semi-passive method of thermal control utilizing an insulated payload, optimum surface radiative coatings, and local electrical heaters was selected to safisfy the thermal control requirements.

The Lander configurations present an ideal approach for providing the necessary payload thermal insulation. The 1.5 in thick honeycomb container structure will be utilized, thereby eliminating any additional space requirements for the insulating material. A low thermal conductivity core material (phenolic glass) with foam insulation packed cells will be utilized to control the Lander temperature response. Detailed insulating trade-offs are presented in the parametric data (Volume III Section 4.4). By adding the foam insulation the heat transfer losses are reduced to a conduction mode only with a relatively high thermal resistance. This is desirable since the radiative and convective heat losses between the honeycomb face sheets could be considerable based on:

1. Radiation across the cell ends could be significant with a possible outside surface temperature of -60°F and an inside structural temperature of 50°F.

2. Although a reduced atmosphere exists, minimizing the heat transfer coefficient, some convection losses could be present in the air space thereby contributing to the overall heat loss.

This conceptual design produced a shell around the payload which has a thermal conductance value of 0.36 Btu/hr-°F-ft^2. Therefore, the payload has sufficient thermal isolation that its minimum temperature will not fall below -40°F, the lower allowable limit for all of the payload components except the battery. To maintain the battery at or above its minimum operation temperature of 50°F, it is thermally isolated from the payload with an insulated package which contains an electrical heater. This heater is thermostatically controlled to turn on when the battery falls below 50°F.

A transient solution was performed to determine the temperature response of an isothermal payload and battery in the Martian environment. Appropriate conduction and radiation was considered based on the Lander configuration. For minimum heat leak, a low surface emissivity of $E_{OS} = 0.1$ was assumed. Results of this analysis are shown in figs. 3.5.5-1, -2, -3 and -4. Figs. 3.5.5-1 and -2 show the battery temperature response and heater power necessary to maintain the battery at 50°F. The temperature response of the payload for the minimum and maximum environments are shown in figs. 3.5.5-3 and -4, respectively. These show that no heater power is required to maintain payload temperature above -40°F.

The transmitter temperature response was studied as a function of daily transmission power with the resulting analysis indicating that no protection in the form of thermal storage material is required to prevent overheating. The specified power level of 32.5 watt-hr/day will only produce an 18°F temperature rise resulting in a peak temperature of 138°F.

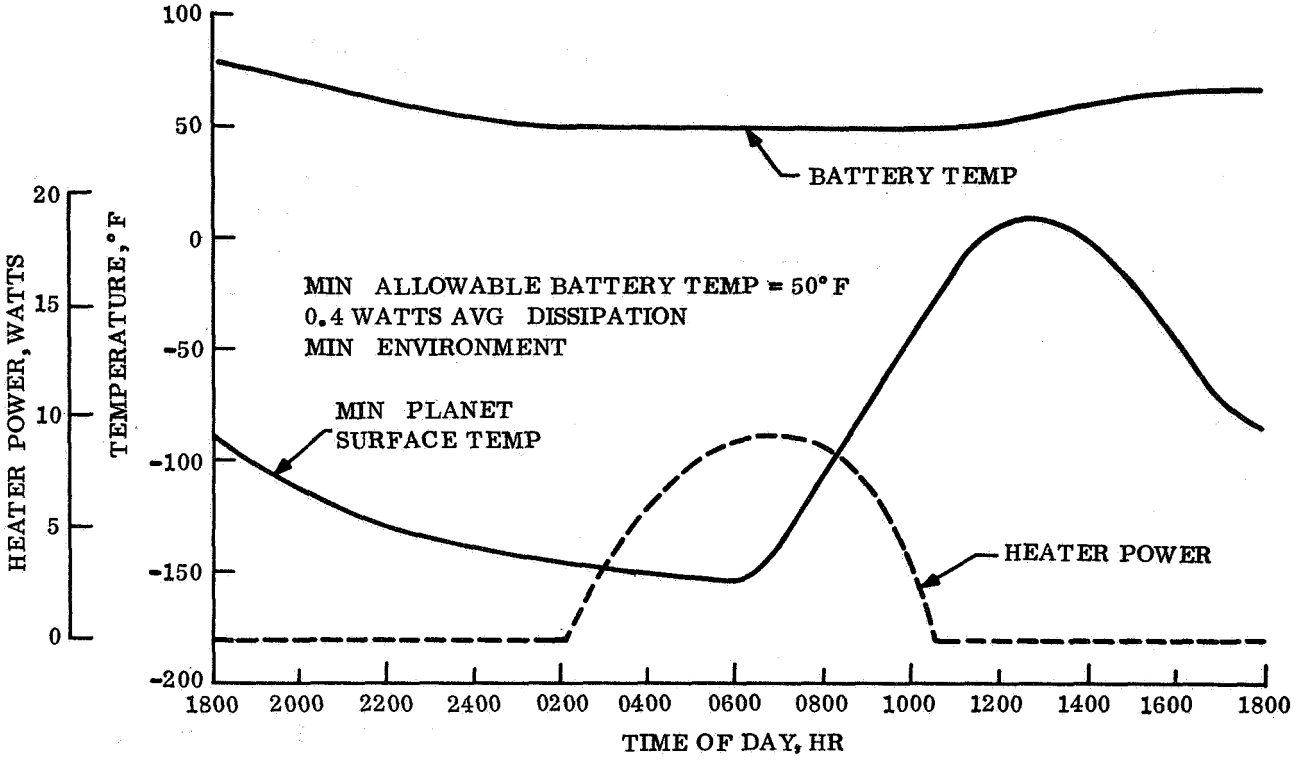


Figure 3.5.5-1. Battery Temperature Profile and Heater Power Requirements Minimum Environment

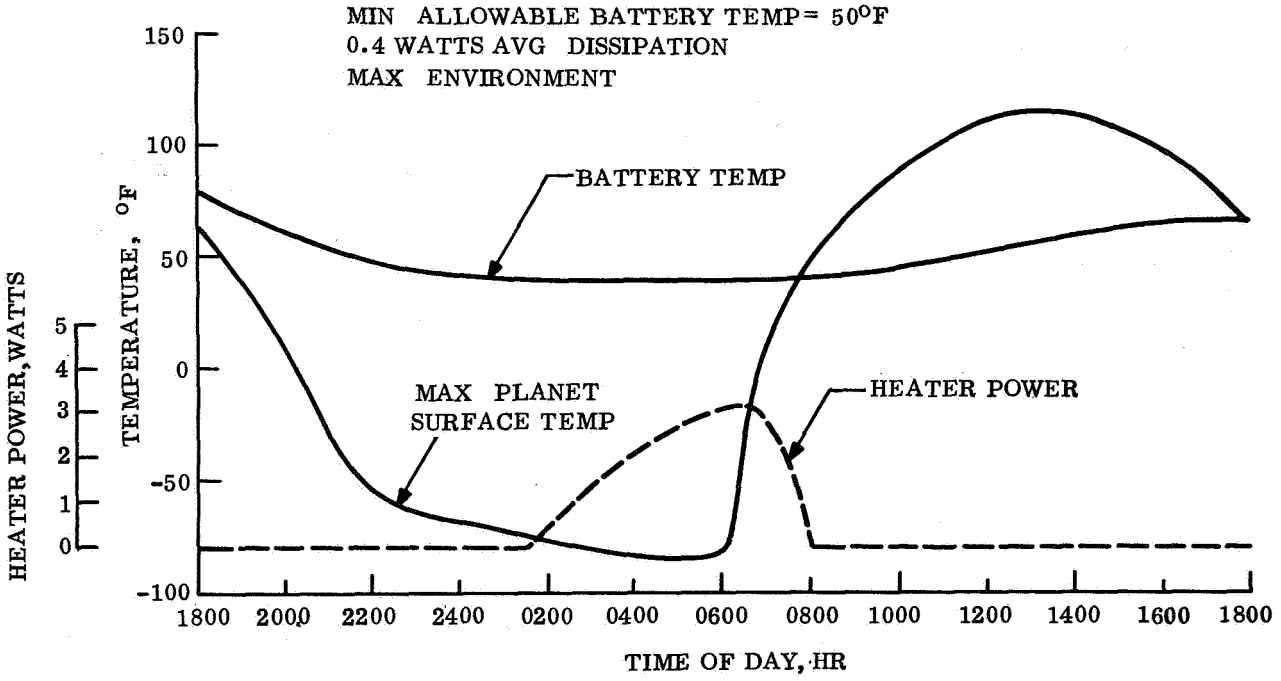


Figure 3.5.5-2. Battery Temperature Profile and Heater Power Requirements, Maximum Environment

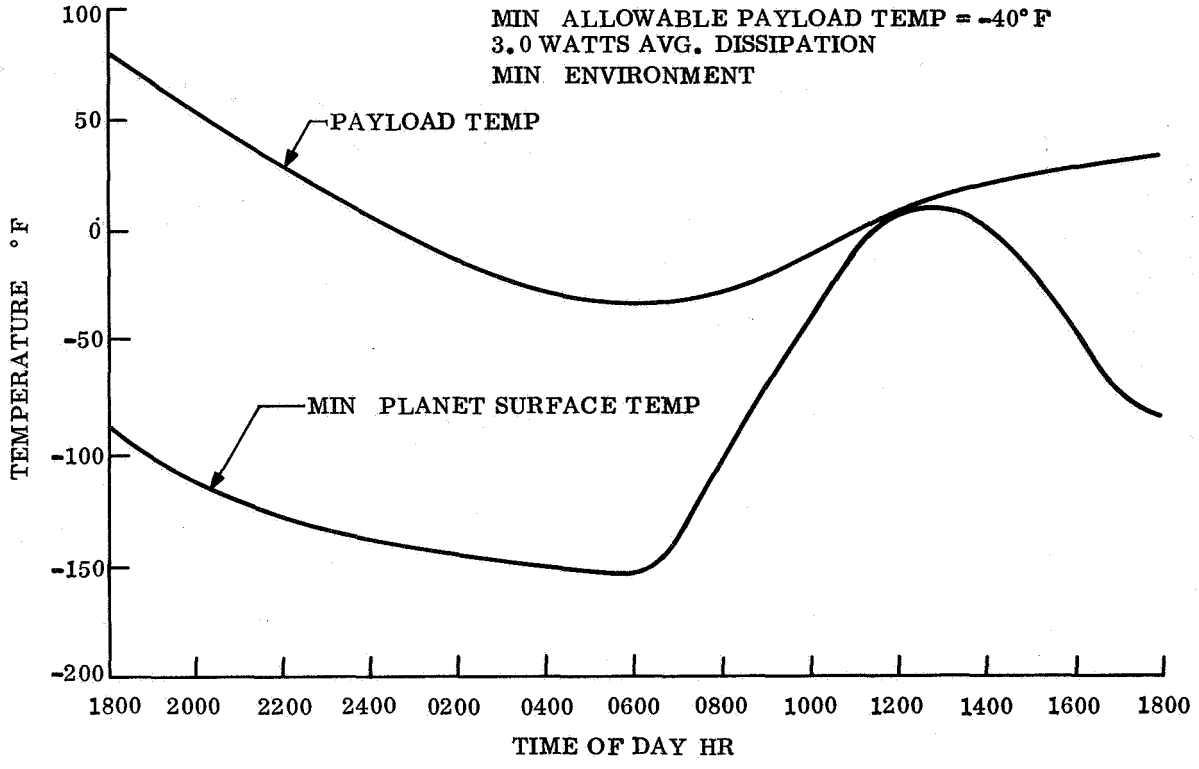


Figure 3.5.5-3. Payload Temperature Profile, Minimum Environment

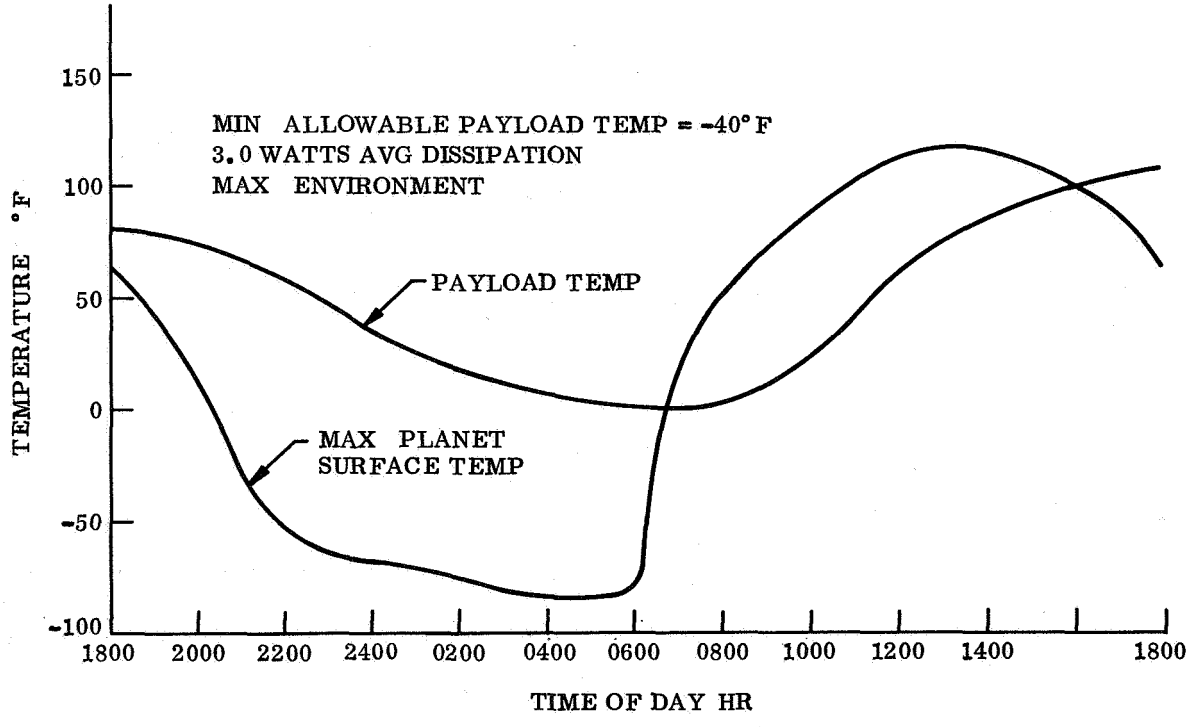


Figure 3.5.5-4. Payload Temperature Profile, Maximum Environment

3.5.6 DEPLOYMENT MECHANISMS

In the landed position, either side of the vehicle may be uppermost, so provision has been made for the deployment of instruments and equipment from both sides of the flat pack container. However, to avoid unnecessary duplication of the instruments, the actuating mechanisms have, in general, been designed for two way operation. A g-sensing device will determine the direction of deployment operation.

Instruments deployed in Point Design 1 are: four cameras (two high and two low resolution), ten wind velocity transducers (two sets of five), four temperature transducers and one surface composition (alpha back scatter) instrument head. All except the alpha back scatter are located in a central bay the full width and depth of the Lander container, as shown in fig. 3.5.1-1. The alpha back scatter is located in an individual full depth bay, also shown on the drawing.

3.5.6.1 Camera Installation, Deployment and Mechanism

The camera(s) and swinging boom(s) installation and associated mechanism is shown in detail in fig. 3.5.6-1.

Each of the four cameras is mounted on the free end of pivoted tubular booms. The booms are aluminum alloy material approximately 36 in. long and 2.0 in. outside diameter. They rotate through approximately 90° in either direction, as shown, from the installed horizontal position so that when erected, two are side by side at opposite edges of the Lander, one with a high and one with a low resolution camera. This arrangement of relatively short swinging booms, with the capability to erect four cameras on either side of the Lander and take pictures over the edge of the Lander in segments shown in the insert on the drawing, was selected as the most satisfactory compromise between the need for simple and stable erection devices and mechanism and the requirement for adequate azimuth and vertical angles of uninterrupted vision. Deployment design with telescoping (not hinged) tubes, cannot easily be made to work in two directions, and investigations proved that unless the number of cameras was doubled, the telescopes had to be many feet in length, to provide adequate vertical angles of vision over the edge of Lander impact attenuation system. Deployment booms of such length pose serious problems regarding camera stability. Stowed, the cameras and booms lie horizontally across the Lander in a block of four. Saddles on the inside of the jettisonable doors covering the camera bay, clamp the booms securely to withstand the g-forces imposed, in particular during the landing phase. The booms are spring-actuated to move through 90° in either direction from the stowed position, by a single torsion spring around the hinge pivot, which is restrained in a neutral setting when the bay doors are assembled. Release and jettison of the camera bay door from the uppermost exposed side of the Lander, unclamps the boom(s) and releases one end of the torsion spring to pick up a lever on the boom and effect its rotation. Thus boom operation is automatic once the appropriate cover door has been jettisoned. All four booms are individually operated by the same spring loaded principle, the two lying deepest in the Lander from the exposed side are restrained to move until the two uppermost ones are deployed and are unlocked by the final motion of the upper booms. This is a simple and automatic sequencing for the four boom arrangement. The cover door(s) are secured with bolts incorporating a hot-wire release and jettisoned by springs with sufficient force to ensure that they fall clear of the Lander.

3.5.6.2 Wind Velocity and Temperature Transducers

Five wind velocity transducers constitute a set necessary to obtain wind measurement data. Four are mounted in a plane at 90° to each other on a 2 ft pitch circle diameter, the fifth is mounted below one of the other four to provide a vertical reading. As stated in Section 3.5.2, the instruments are acoustic devices requiring unimpeded line of sight between each sensor. In the arrangement shown in fig. 3.5.6-1 the transducers are attached to the ends of spring-loaded arms, which are mounted on a telescoping extension of the camera booms and unfold when the boom triggers a release mechanism as it locks into the erected position.

The weight involved in the installation of a set of wind velocity transducers is very small and two sets have been provided on two camera booms for redundancy.

A temperature transducer is mounted directly on each of the four camera booms at the base of the camera.

3.5.6.3 Surface Composition (Alpha Back Scatter)

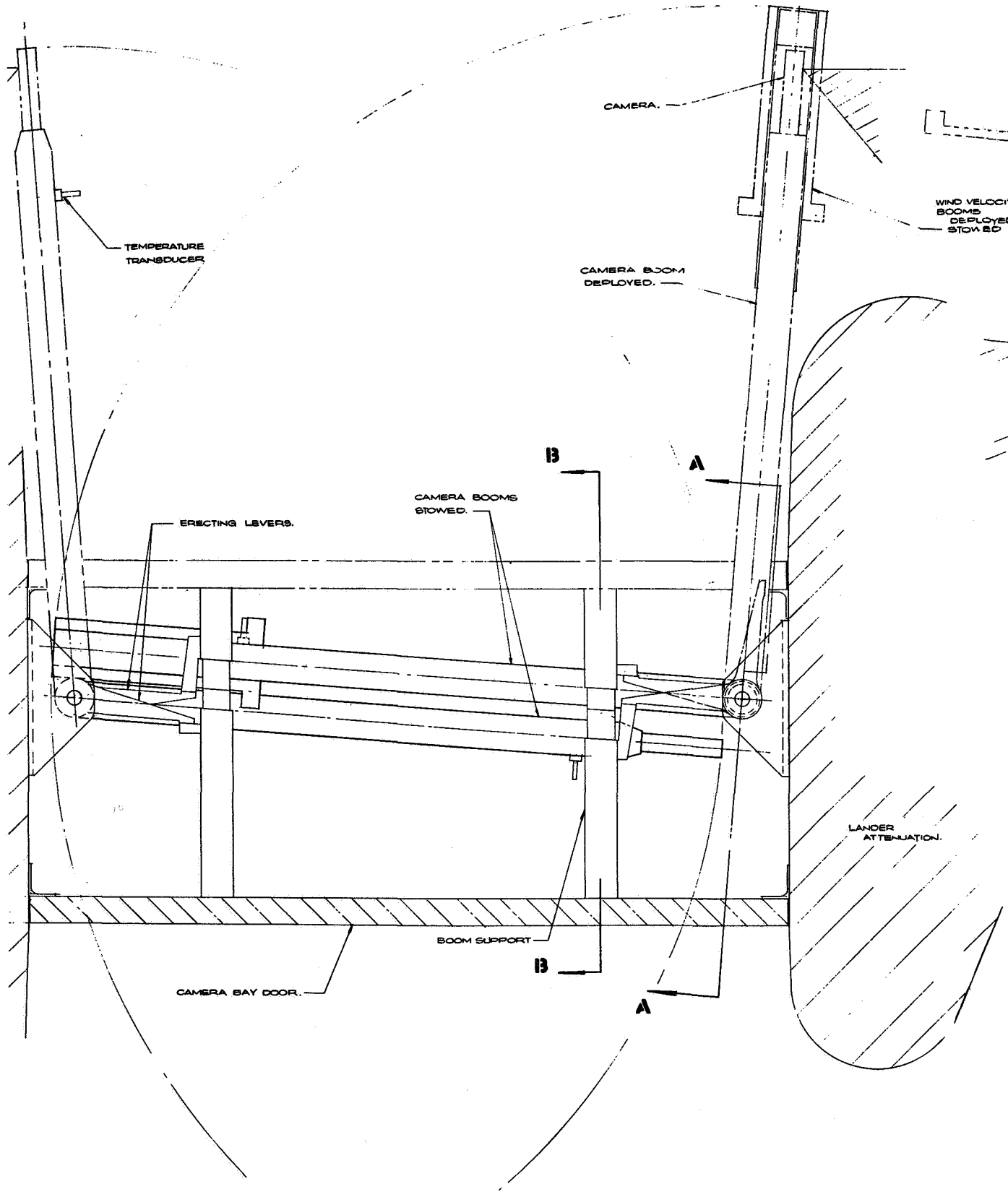
Although this instrument has not been completely designed, analysis has provided preliminary weight, volume, deployment and other requirements. The installation and deployment approach herein is based on a conceptual design illustrated in fig. 3.5.6-2. The Surveyor alpha back scatter instrument has been referred to and utilized to some extent.

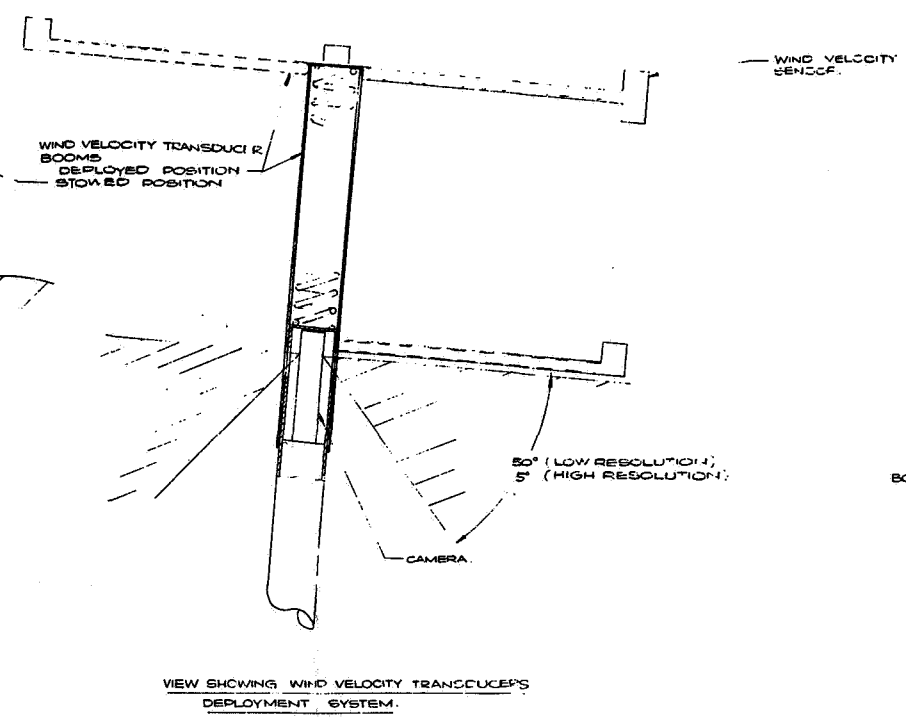
The instrument sensor head is installed on its side in the bay provided in the Lander container. The head will be firmly clamped against a pivot bar, in the stowed position, by a soil calibration sample holder extended across the bay and secured to the vertical side walls. When the calibration phase of the alpha back scatter instrument is completed the sample holder will be moved away from the back scatter instrument head either linearly along the bay or by rotation. The function will be performed by a pin pulling device and spring-loaded mechanism. The instrument head is now free to rotate through 90° due to its offset c.g. and the force of gravity and drop through the bottom side of the Lander attached by the control cord and wire bundle provided.

Low friction guides will be installed on either side of the instrument head from the bay sidewalls to ensure that the head rotates and exits from the Lander with a smooth controlled motion.

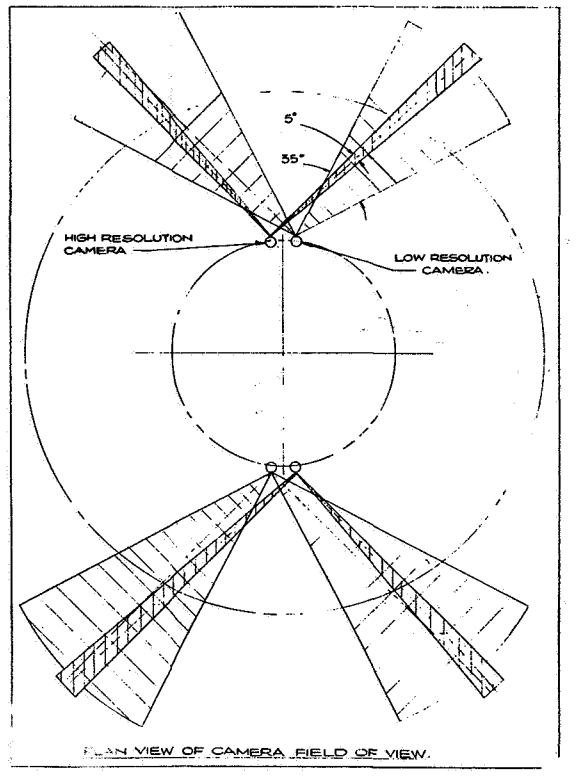
Assuming that the head is prevented from being lowered completely clear of the Lander, it can operate equally well within the bay provided the surface is in good contact with the ground.

Covers over the bay provided in the Lander have been studied, but jettisonable or sliding doors are not desirable because of possible interference with the instrument head or jamming in the event of landing damage. Consequently, two inward opening hinged doors will be provided on either side of the Lander.

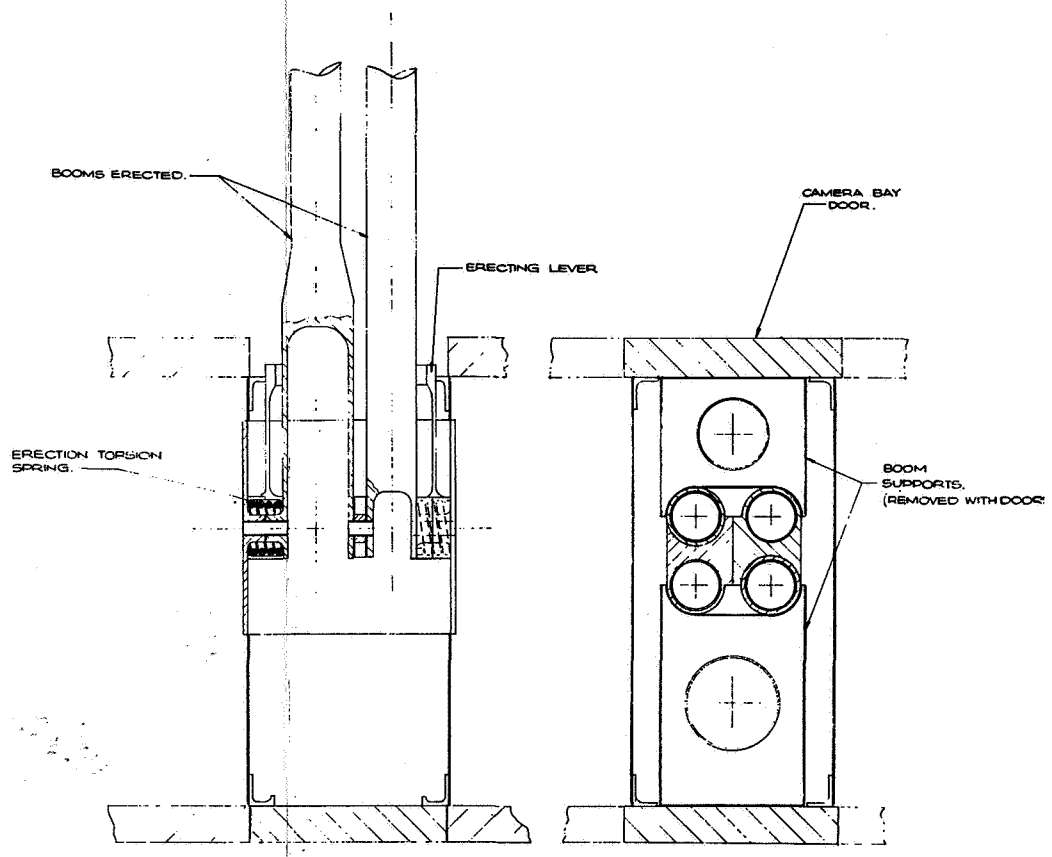




VIEW SHOWING WIND VELOCITY TRANSDUCERS DEPLOYMENT SYSTEM.



PLAN VIEW OF CAMERA FIELD OF VIEW.



SECTION A-A

SECTION B-B

Figure 3.5.6-1. Camera Deployment (Includes Wind Velocity and Temperature Transducers)

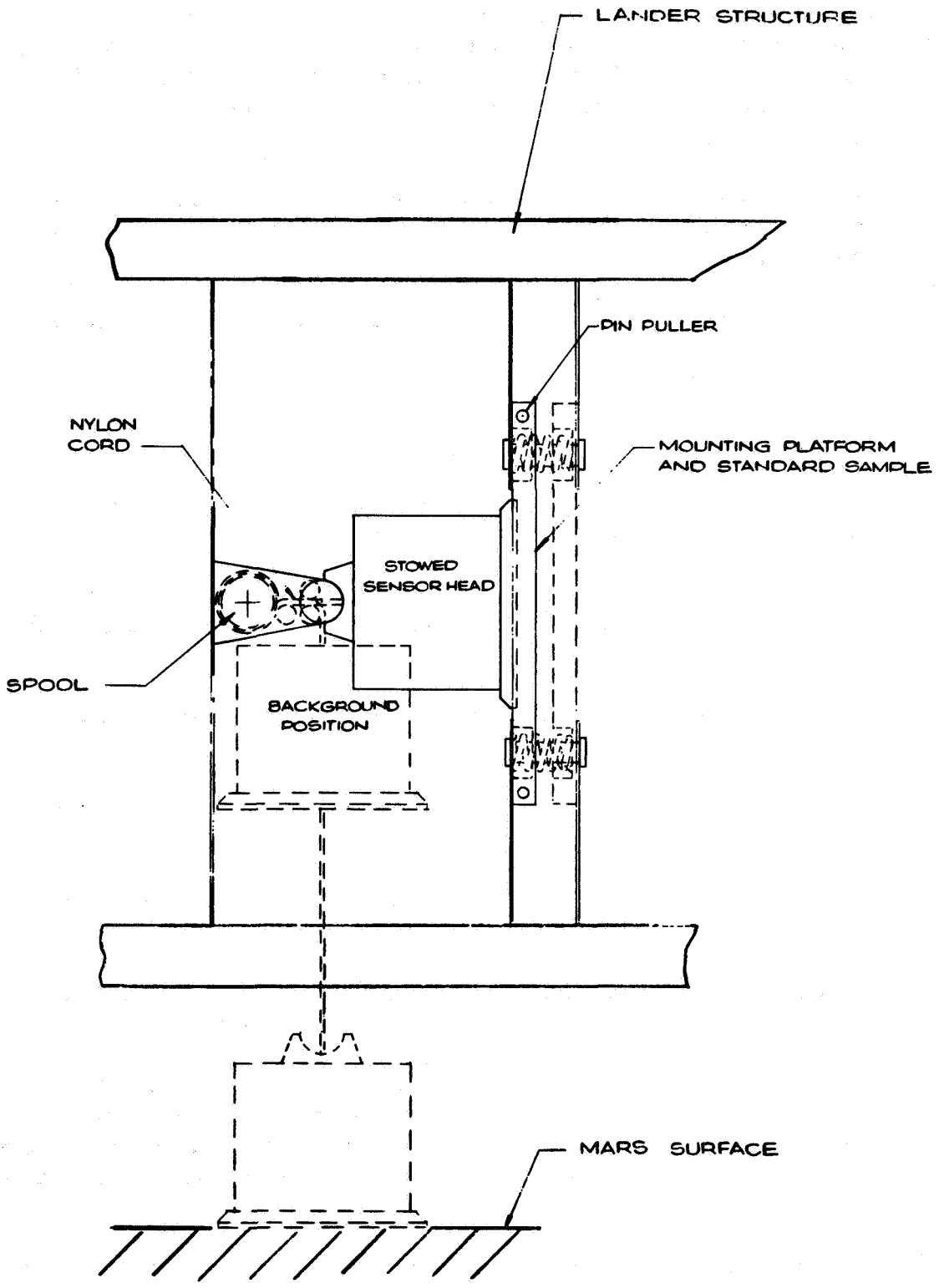


Figure 3.5.6-2. Operation of Alpha Back Scatter Deployment Mechanism

3.5.7 LANDER CONTAINER STRUCTURE

The flatpack configuration for the landed payload container illustrated in fig. 3.5.7-1, was selected on the basis that it offers a good compromise between structural efficiency and all other design constraints, notable packaging and deployment of experiments. The following requirements and criteria were imposed for the design of this structure:

1. Design weight - 900 lb. This is used for structural design purpose and is based on total Lander weight less the material which is crushed during primary impact

2. Local pressures and inertia loads resulting from impact up to 1000 g's

3. Limit design factor - 1.0

4. Ultimate design factor - 1.25

Based on the requirements and constraints which are present, a design has been evolved which has the following significant features:

1. A full-depth inner space frame module containing most instrumentation and subsystems. This module can be removed from or inserted into the flatpack as a bench subassembly.

2. Individual components can be added or removed from the top or bottom of the space frame while installed in the container.

3. Dual purpose space frame which acts as primary structure and component support.

4. Jettisonable and hinged doors for deployment of camera and alpha back scatter instrument, respectively.

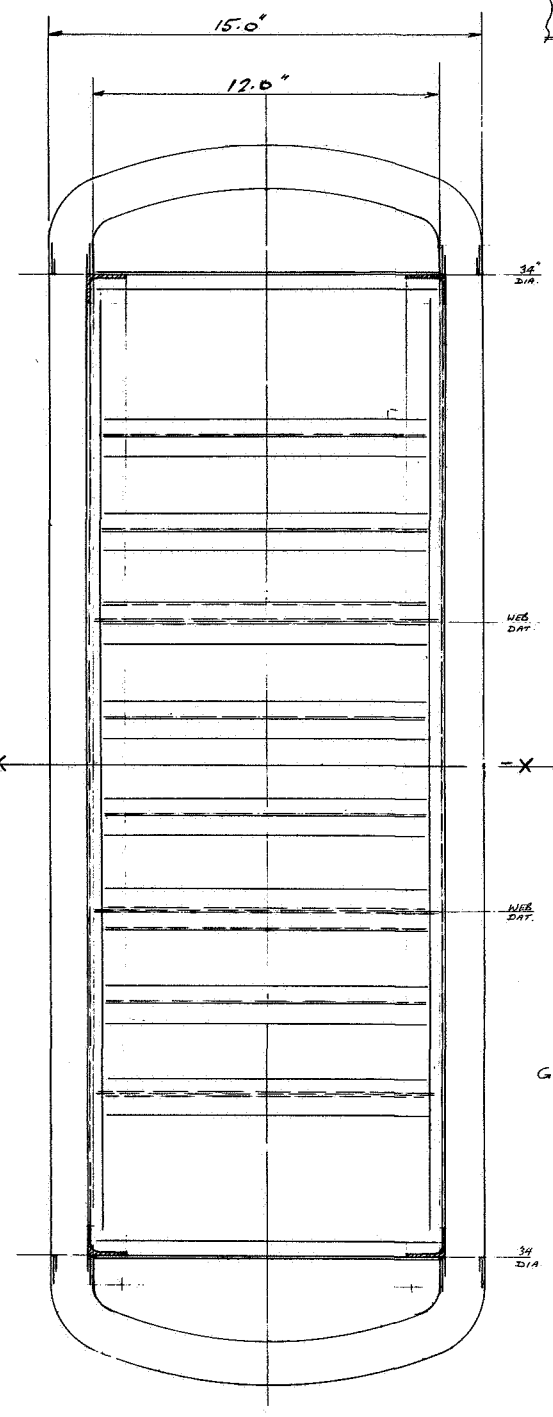
5. Primary structure consisting of a D-shaped toroid section supporting the impact attenuator, combined with the inner space frame.

The container consists of three basic elements: the D-shaped toroidal edge structure, the inner space frame, and the top and bottom covers and doors. (See fig. 3.5.7-1.) This complete assembly is designed to withstand the forces generated by initial impact at 1000 g's and any forces resulting from subsequent impact after rebound.

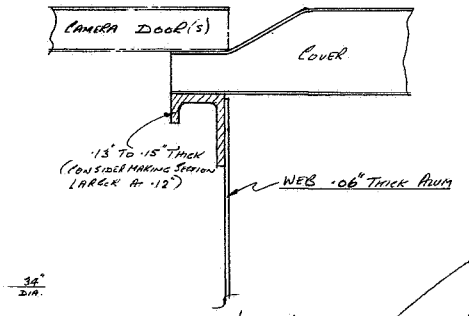
The D-shaped edge structure acts as a primary load path for distribution of impact attenuator loads. The outer shell of this section is tied to the cylindrical wall with radial aluminum sheet nose ribs, stiffened and spaced approximately every 5 in. around the circumference. These radial members transfer some of the loading to the internal cylindrical web and allow the section to act as a heavy ring frame,

FOLDOUT FRAME 1

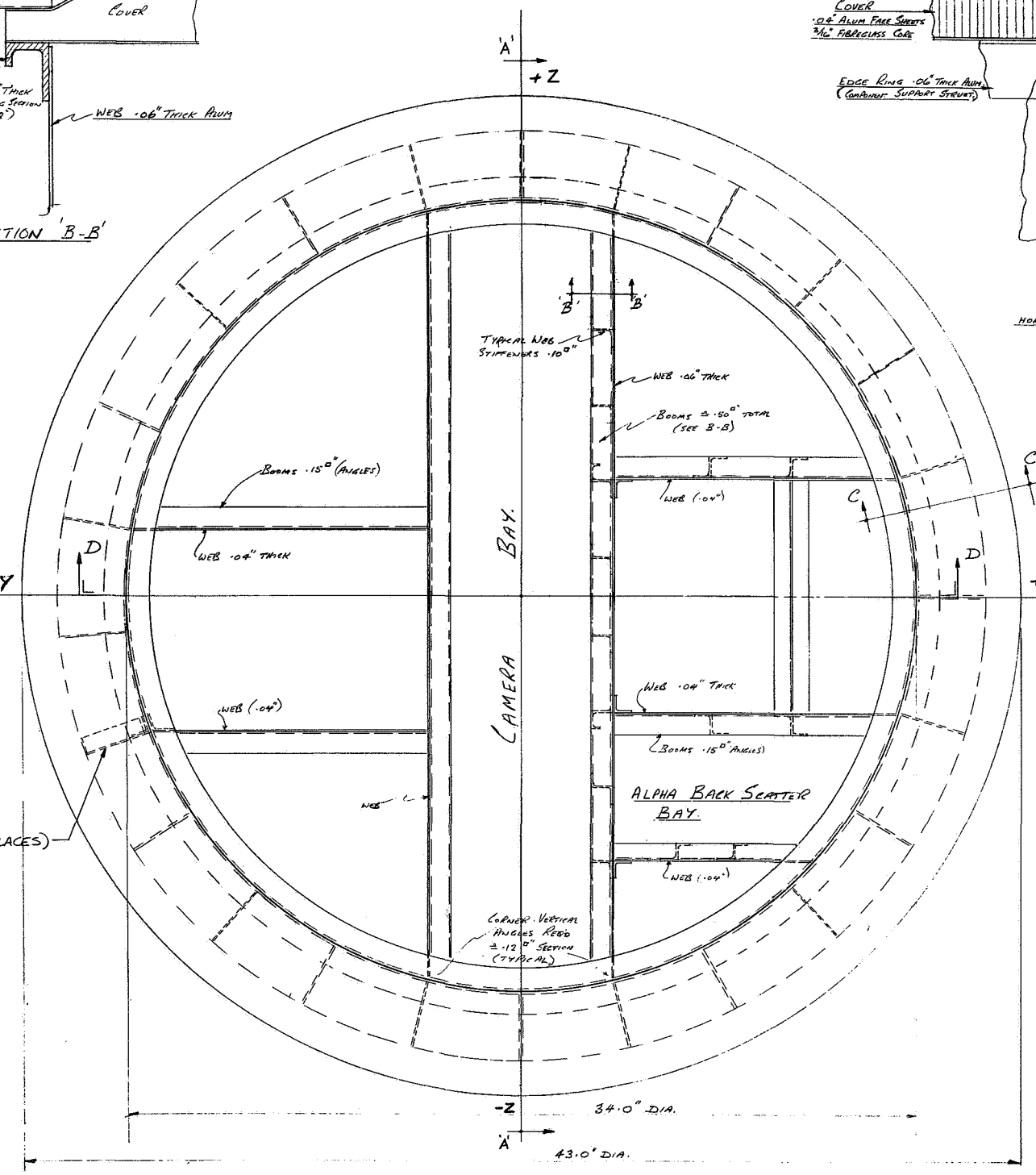
FOLDOUT FRAME 2



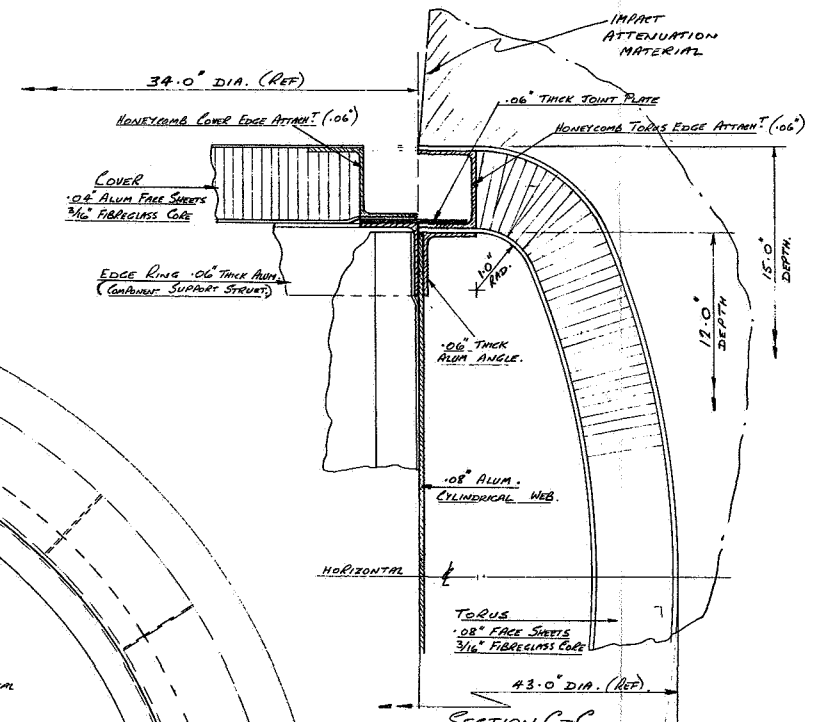
SECTION A-A



SECTION 'B-B'

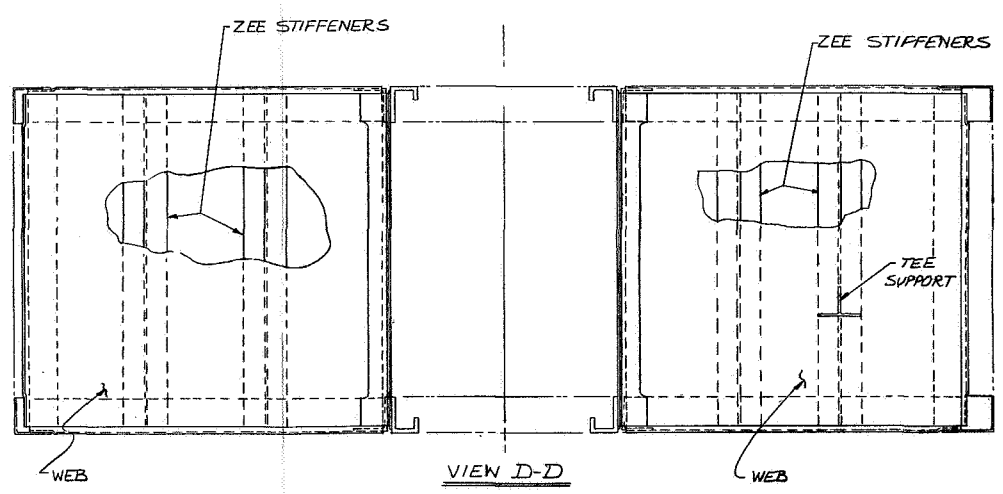


PLAN VIEW (COVERS REMOVED FOR CLARITY)



SECTION C-C

TYPICAL SECTION THRO' TOP EDGE OF CONTAINER. (BTM EDGE IDENTICAL)



VIEW D-D

Figure 3.5.7-1. Structure Assembly

transferring load into the upper and lower cylindrical edge rings. Local loading up to 925 psi imposed by the crushing honeycomb is resisted by the outer shell of the D-shaped section which is a 1-1/2 in. thick fiberglass honeycomb (3/16 in. cells) core with 0.08 in. aluminum face sheets. The cylindrical section is an 0.08 in. lightened and stiffened cylindrical shell. Except for items such as cable harnesses, it is not proposed to utilize the edge structure for packaging, and therefore some structural deformation is tolerable.

The full depth cross members of the inner space frame stiffen the container against deformation from the cylindrical shape and resist bending of the flatpack, as well as providing component support. Two main cross members form the camera bay. These beams have 0.06 in. aluminum alloy webs, extruded alloy channel beams, and section vertical stiffeners. There are five secondary cross beams at right angles to the main beams. These are of similar but lighter construction of aluminum alloy. Top and bottom angle rings, 0.06 in. thick, and vertical angles at the junctions of the main and secondary beams and at the free ends of these beams complete the assembly. The inner space frame is attached to the D-shaped section through the vertical flanges of top and bottom angles.

The top and bottom covers are considered secondary structure. They are 1.35 in. thick fiberglass honeycomb panels with 0.04 in. aluminum face sheets. A Z edge section is inserted for attachment. The edge members of the D-section, the inner space frame and covers, when bolted together form strong rings at the top and bottom surface of the container.

Thick honeycomb panels with fiberglass core have been selected for the construction of the outer shell of the container as a means of satisfying both structural and thermal requirements. A possible alternative for the container outer shell generally, could be reduced depth honeycomb panels with foam on the inner side. Additional investigation will consider fiberglass facing sheets for all honeycomb panels used as a strength-to-weight trade-off. Surfaces of the full depth cross beams, which are exposed when the camera and alpha back scatter bay doors are jettisoned, are thermally insulated with a layer of foam to the full depth of the beam vertical stiffeners. The foam is covered with plastic coating to maintain integrity on landing impact.

A preliminary analysis, for critical loading points of four conditions shown in fig. 3.5.7-2, has been made and used to formulate the estimated weight of the container. Typical torus cylinder interface loads, for the edge impact condition illustrated, are shown in figs. 3.5.7-3, -4, and -5.

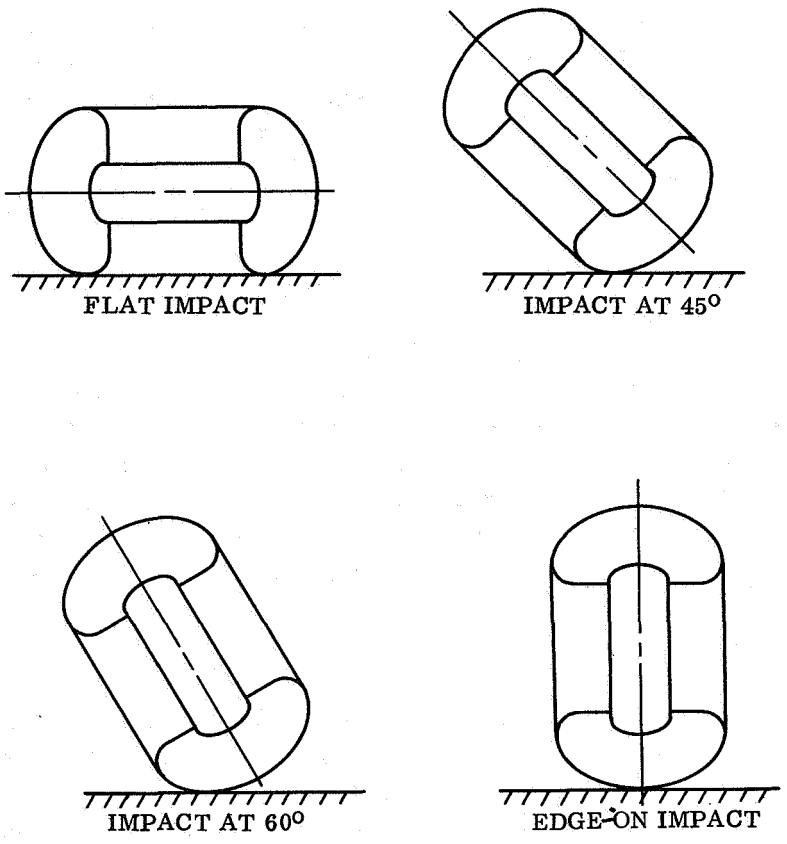


Figure 3.5.7-2. Four Conditions Used for Preliminary Loading Analysis

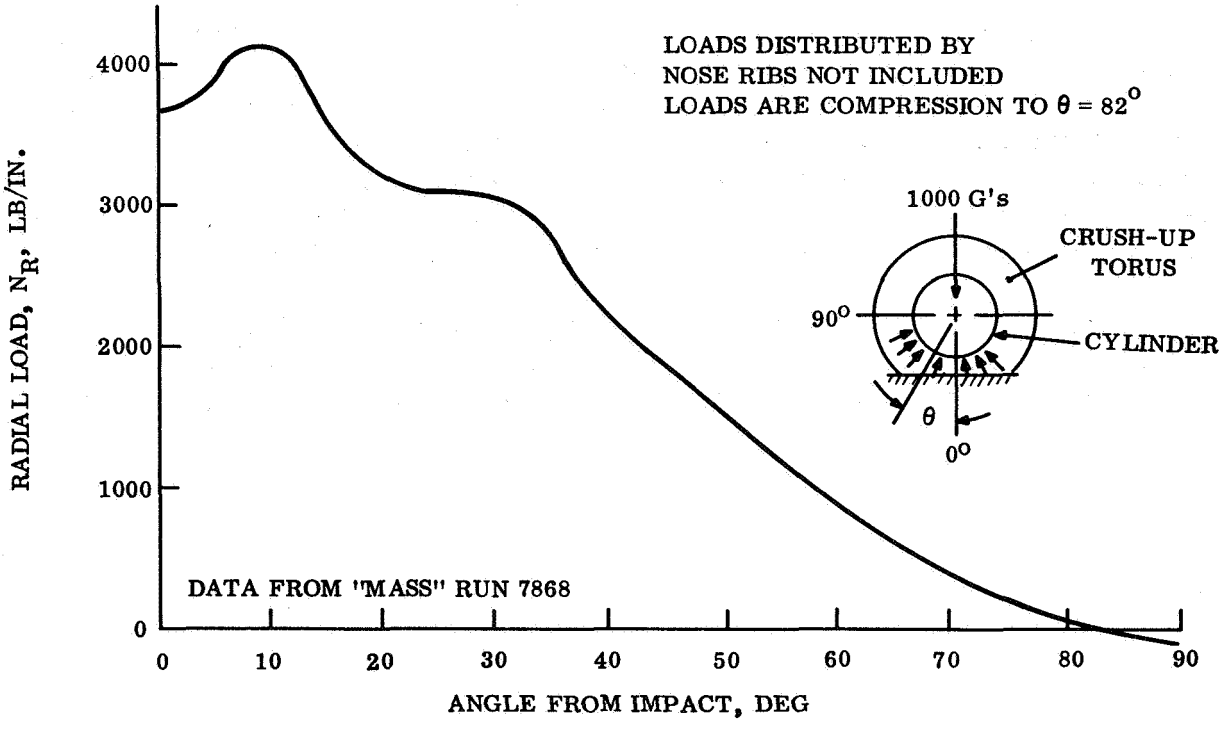


Figure 3.5.7-3. Typical Interaction Radial Loads Between Torus and Cylinder, Edge-on Condition

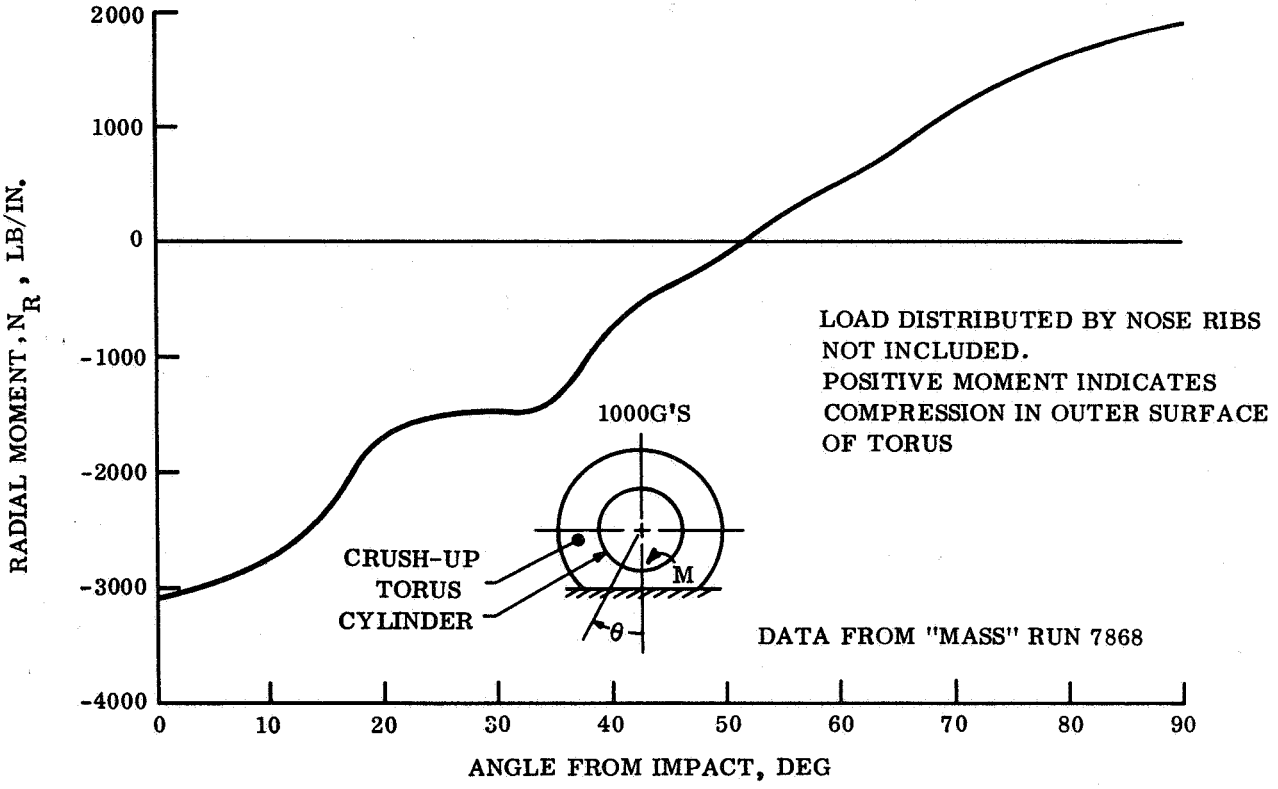


Figure 3.5.7-4. Typical Interaction Moment Between Torus and Cylinder, Edge-on Condition

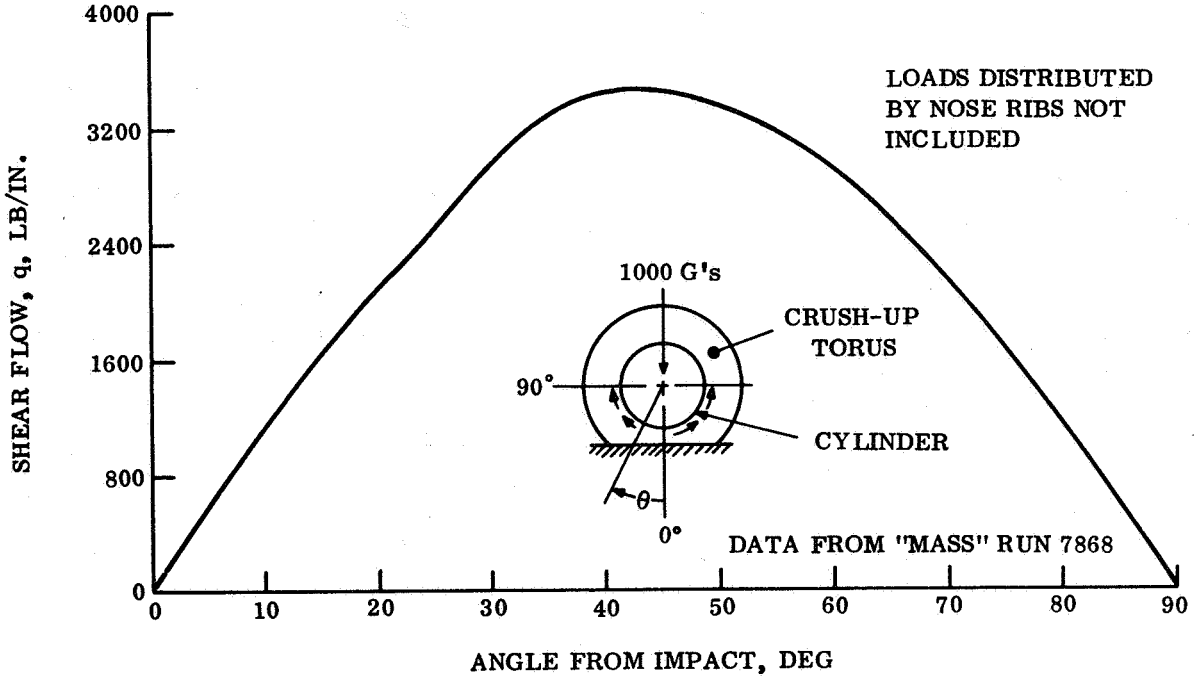


Figure 3.5.7-5. Typical Interaction Shear Flow Between Torus and Cylinder, Edge-on Condition

3.5.8 IMPACT ATTENUATION AND STRUCTURE

3.5.8.1 Attenuation Requirements and Criteria

3.5.8.1.1 Gross Vehicle Response

The mechanical crush-up impact attenuation system is designed to provide sufficient stopping distance to decelerate the Lander within the allowable g-limits while dissipating the impact kinetic energy. At the same time the acceleration pulse must have a sufficient rise time and be essentially broad and flat. The honeycomb phenolic fiberglass material inherently behaves in a manner which produces this behavior.

3.5.8.1.2 Response of Individual Components

Initial studies have been performed to determine the feasibility of further attenuating the impact acceleration levels experienced by individual components carried by the Lander. These are reported in Volume IV, Appendix A. The conclusions drawn from this appendix indicate that it does not appear feasible to obtain significant reductions with shock mounts or by component mounting stiffness tailoring. These devices are of primary use in minimizing g-level amplification effects.

3.5.8.1.3 Angular Accelerations: Their Effect on Components

It appeared that if the Lander impacts on one edge, there was the possibility that high angular accelerations might produce high loading on components located at the outer extremity of the container. This situation is studied in Appendix IV-A. The conclusion reached is that such high angular acceleration g's will not occur.

3.5.8.1.4 Selection of Phenolic Honeycomb as the Reference Material for Impact Attenuator Design

Phenolic honeycomb was selected as the reference material for this study for the following reasons. Both balsa wood and phenolic honeycomb are feasible materials for the size and weight vehicles being examined herein. Both materials can function at the operating g-levels anticipated with a Hard Lander System. However, the balsa wood can be adversely affected by exposure to the sterilization cycle. In past tests, balsa wood has split after being subjected to dry heat sterilization. Careful control of the wood moisture content can, however, probably eliminate this problem. Balsa wood has the added disadvantage that its material properties have been known to vary from ± 15 to ±50 percent. This is significant since balsa, being a natural material, cannot be further developed to a significant extent. Phenolic honeycomb, on the other hand, has been improved in the past and this trend can be expected to continue.

3.5.8.2 Environmental Definition and Interpretation

Appendix IV-B contains the detailed account of the specification used in the point design. Included are discussions of surface strength, friction, slopes and rocks. The wind specification for the point designs is also elaborated upon.

In brief, the point design is capable of impacting an infinitely hard surface with friction, 5 in. rocks and slopes up to and including 34° from the horizontal. The prevailing wind blowing against the surface slope is the extreme value of 220 fps. Should the surface strength be less than attenuator stress, some penetration will be experienced but this is estimated as a few inches by the analysis in Appendix IV-B.

The important effect of a parachute sway angle (of up to 40° from the local vertical) was also examined. The chief result is that the sway angle couples with the surface slopes to require higher angles of the Lander to be analyzed for the initial impact condition. The significance is that an increment in honeycomb attenuator thickness over that thickness necessitated by a non-swaying vehicle must be incorporated on the Lander sides to allow for the swaying effect on vehicle orientation at touchdown. Details are given in Appendix IV-B.

3.5.8.2.1 Secondary Impacts of the Lander Vehicle

The combined environmental conditions of extreme wind, parachute sway and varying surface slopes warranted an investigation of post impact vehicle motion. In particular, the probability and significance of secondary impacts were reviewed. Appendix IV-B contains the dynamic analysis for the secondary impact problem as well as an initial probability estimate of the likelihood of occurrence of this event.

Statistical analyses were performed for the purpose of ascertaining the probability of experiencing a secondary impact velocity less than or equal to a chosen value. In particular, the value of 100 fps was investigated because this was the velocity used to size the top side of the multi-directional Lander. Based upon the limited first order approximation used, the following trends are indicated. For the extreme wind velocity of 220 fps the Lander flips over about 92 percent of the time and hits the second time on its top side.

In light of the new Mars Mission Specification (1968) of a design wind velocity of 110 fps, another probability estimate may be made. For this wind velocity, (but the same slope and sway angle variations) the Lander will flip over only about 25 percent of the time. Given that the Lander does flip, the secondary velocity will be 100 fps or less 81 percent of the time. If the analysis were adjusted to account for the new definition of surface slope of 20° (as contained in the Mars Mission Specification - 1968) this 81 percent figure would improve considerably. The foregoing brief summary identifies the surface wind specification as a critical design parameter.

3.5.8.3 Effect on Point Design Due to Perturbation in the Design Parameters

Appendix IV-C delineates the effects on the impact attenuation system design due to variation in the reference condition. Those parameters in which perturbations are especially significant are also identified.

In general, lower wind and descent velocities, flatter slopes, softer surfaces, smaller rocks, lessened parachute sway, higher component g-tolerance and lower Lander weights than the corresponding design values enhance the point design integrity.

Increases in velocities, slopes and parachute sway angle tend to compromise the design integrity. Higher Lander weights than in the design condition and lower component g-tolerance tend to compromise the adequacy of the design.

Small increments in effective rock size are deleterious but, after a point, the rock becomes a large outcrop and is more of a hard surface than a penetrating hazard. It is noted that since the design is based on an infinitely hard surface no problem arises with an increase in surface hardness above that used in design computations.

Appendix IV-C also encompasses variations in honeycomb material properties. Specific comments identify the effects of variations in crushing density, specific energy, stroke efficiency, effective geometry and crush-up behavior.

3.5.8.4 Impact Attenuation Design Approach

The attenuation system design approach for Point Design 1 is now described. Fig. 3.5.8-1 is a sketch of the nominal deep ring geometry for the Point Design 1 omni-directional Lander. In the design, the attenuation material is phenolic fiberglass honeycomb (3/16 in. cell size) of the type developed by GE-MSD under contract to the JPL. This material is of the hexagonal cell variety with parallel cells which can be wrapped with (R/t) radius to thickness ratios of greater than five. It is the reference material selected for use in this study and is currently used in the JPL drop testing program. This material is readily available from Honeycomb Products Inc. in densities of 4 to 12 pcf. The particular density used in the point design will be determined by the design conditions, especially Lander weight and allowable rigid body g-level. The performance of this thin dipped phenolic material varies depending upon its axial orientation with respect to the impact load vector. This is a key design factor investigated in the point design computation. The requirement for omni-directionality results in analyses of the Lander for various cutting plane orientations ranging from forward-flat-on to aft-end-first. Requirements of omni-directionality lead to increased weight over multi-directional Landers since material which is fully effective in one touchdown orientation may be of less or no value when other orientations are examined. Past analyses and judicious application of the specifications have indicated that three critical crush-up conditions must be analyzed. These are 0^{o} (forward) impact, 90^{o} (side-on) impact, and an intermediate surface slope impact. The intermediate slope has been taken as 34^{o} for point design purposes. It is apparent that to adequately handle all of the highly probable impact conditions special attention must be directed toward the crush-up lay-up because of the materials variable effectiveness. For point designs this honeycomb lay-up is produced by cutting and segmenting the attenuator material to produce near-radial cell axis orientations with respect to the internal toroidal container structure. At the same time this segmented approach allows more efficient wrapping of the container. Refer to para 3.5.8.5 for details. The same varying effectivity is also complicated by a geometric effect produced by the curvature of the Lander as seen in plan. The net result is that the area-stroke characteristics are direction dependent in a complex relationship (refer to fig. 3.5.8-2). This means that the force stroke history is direction dependent and that, depending on the direction of impact, the stroke (and thus the thickness required) will be different.

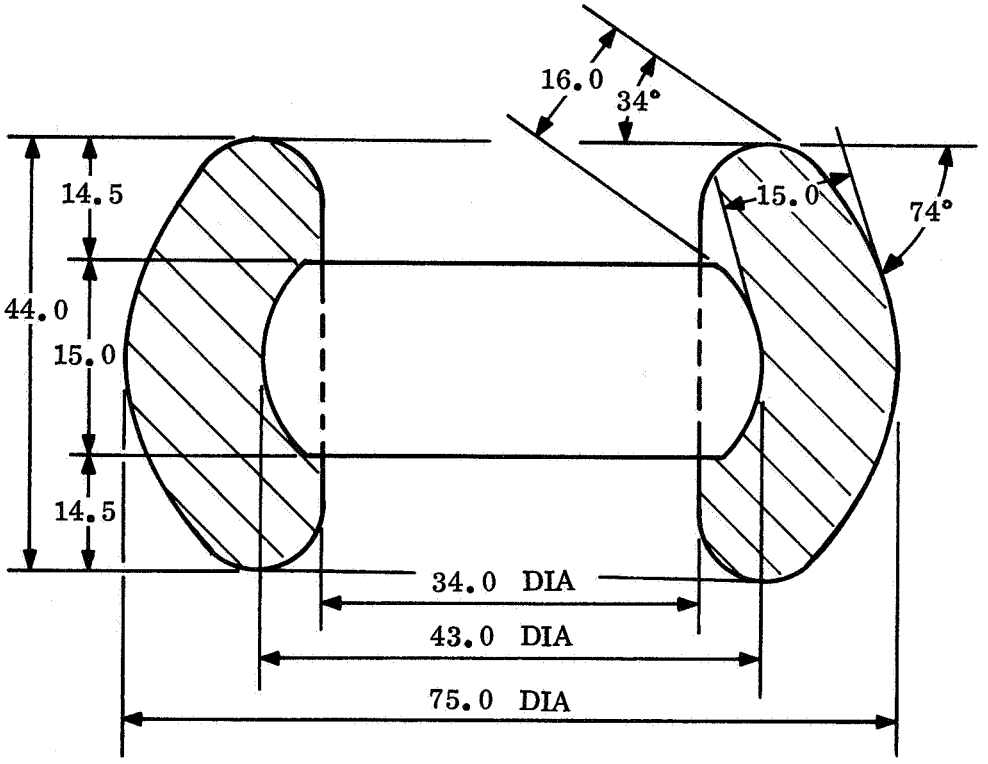


Figure 3.5.8-1. Lander Attenuation, Point Design 1

An additional geometric effect, distinct from that of crush-up directionality also enters the analysis. This is, for a given direction of impact a variable amount of honeycomb material is actively being crushed. Some material may be oriented in such a way that it experiences shearing forces. Because of this localized condition bond line shear failures can result with little or no crush-up action. Such failures could occur without providing sufficient stroke capability. For this effect detailed design must ensure that sufficient material is working in each specific direction. Finally, attention must be directed toward the location of crush-up propagation. It is desired that the fracturing progress from the outside in and not from the payload to the extremity of the attenuator. Design details of the container/honeycomb interface and slight precrushing of the attenuator can eliminate this problem.

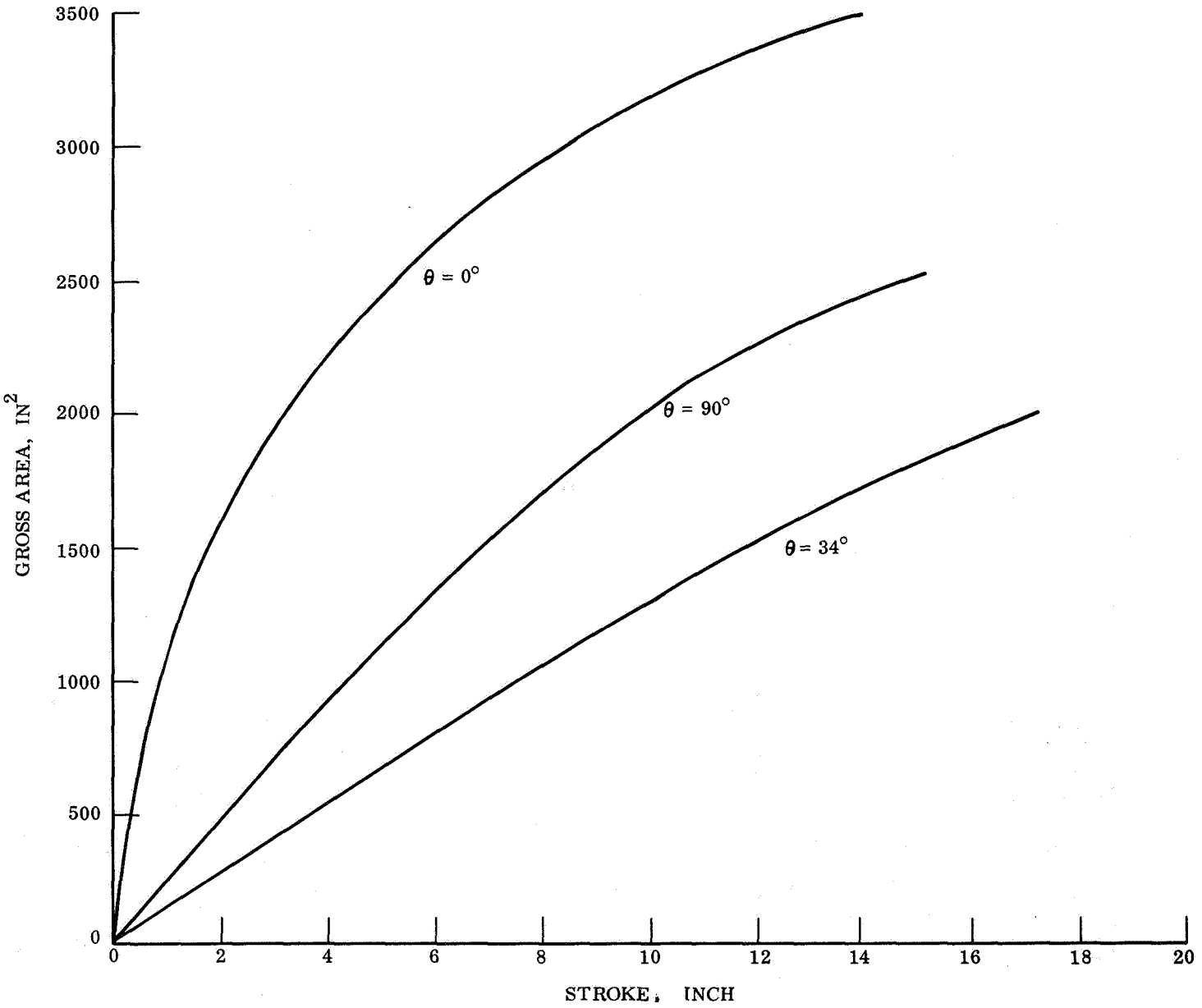


Figure 3.5.8-2. Gross Cross-sectional Area vs Stroke

3.5.8.4.1 Analytical Details

With the above background, point design analysis takes the following form. A series of CRUSH (geometrical program) runs were made for each prototype point design. The results were of the form of gross crushed cross-sectional area against stroke for various angles encompassing the operational map as defined in the specification. The geometric results were used to perform a direct graphical analysis of several prototype shapes. The conclusions drawn from this thorough study provide the underlying philosophy for a computer-assisted procedure to size the attenuator for point design purposes.

In fig. 3.5.8-2 plots of crushed area against stroke for a nominal deep ring omni-directional Lander are produced. It is emphasized that this figure is for gross area with no directionality effects included. In fig. 3.5.8-3 plots of effective sectional area are provided. These latter plots were generated in the following manner. The phenolic material loses 2 percent of its strength per degree of obliquity between the longitudinal cell axis and the normal to the crushing plane.

The design guide for this reduction is fig. 3.5.8-4. This design guide is based upon test results summarized in fig. 3.5.8-5.

The data to support this procedure are reported in ref. 3-1. In addition, a 20 percent reduction is incorporated to account for the effect of curvature (in plan). The analysis also assumes that the active area encompasses all cells lying within 30^{o} of the normal to the impacting plane examined and that all others are not actively crushed.

After examining various cutting planes for the Lander prototypes it was found that for the omni-directional Lander three principal strokes need be computed: dead-on, side-on and 45^{o} angular cutting plane. Actually for sizing purposes there is small difference by passing the cutting plane at 34^{o} or 45^{o}. This is shown in fig. 3.5.8-3.

From data in fig. 3.5.8-4 the principal strokes can now be computed by equating Lander normal kinetic energy to the absorbed energy due to crushing. For the prime (0^{o} impact) case,

$$\text{energy absorbed} = 1/2\ WGS + 1/4\ WG\ \frac{S}{2} + (1/2)\ (3/4)\ S\ \frac{WG}{2}$$

$$1/2\ \frac{W}{g}\ V_N^{\ 2} = \frac{13}{16}\ WGS$$

$$S_{(0^{o})} = \frac{0.62\ (V_N)^2}{gG}$$

where V_N is the impact velocity component normal to the plane, g is the gravitational constant and G is the allowable deceleration level in g-units. As described

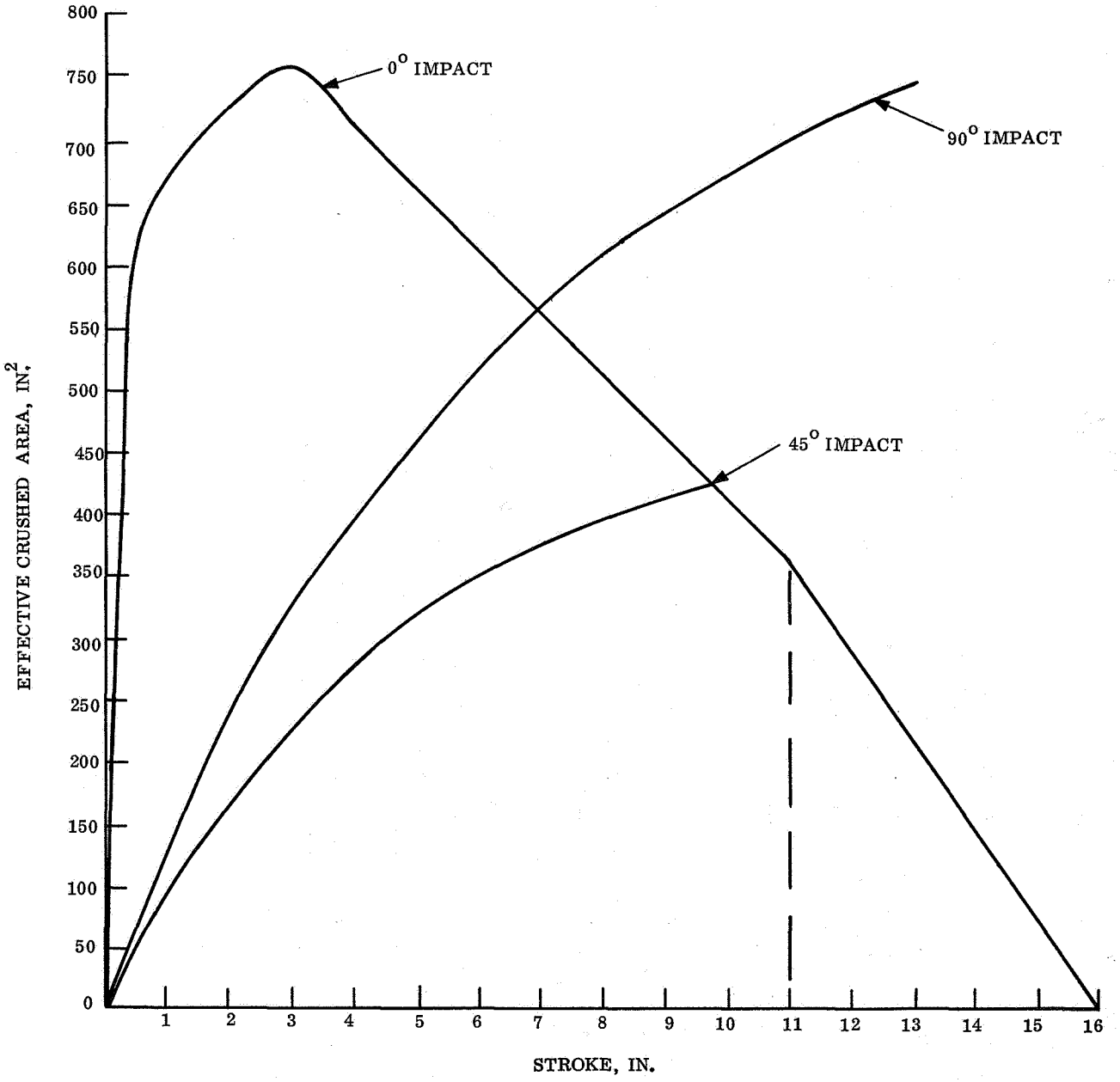


Figure 3.5.8-3. Effective Cross-sectional Area vs Stroke

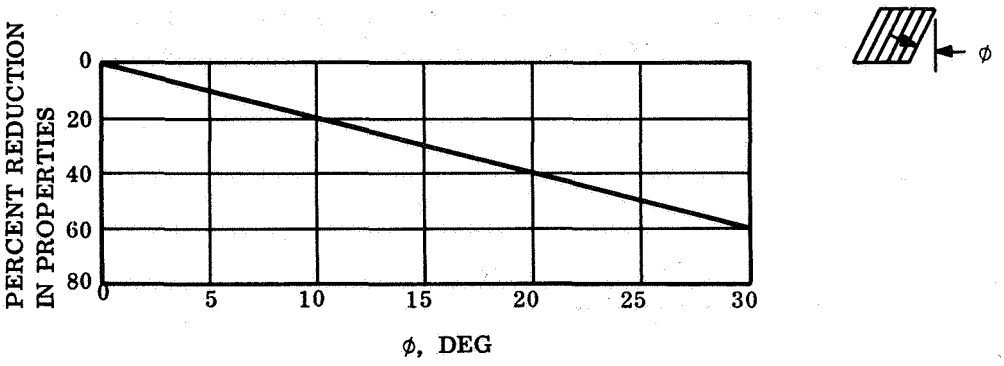


Figure 3.5.8-4. Design Guide for Reduction in Honeycomb Properties for Non-axial Impacts

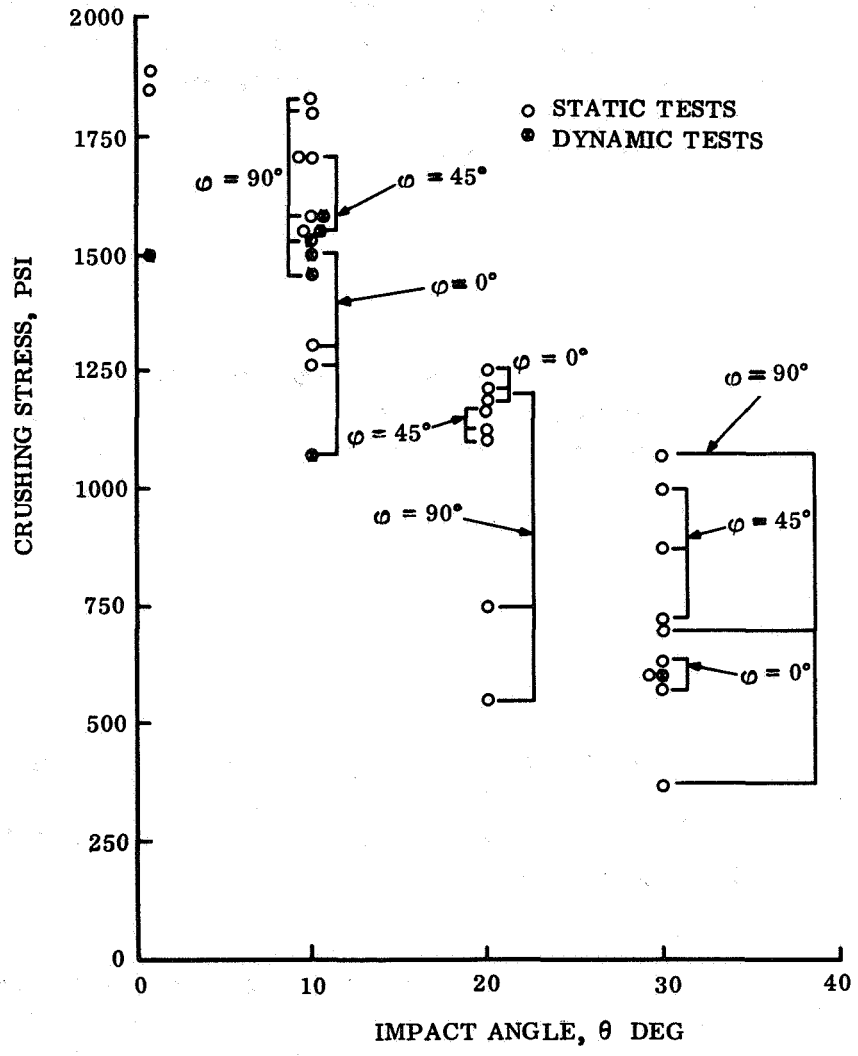


Figure 3.5.8-5. Comparison of Crushing Stress vs Angle-of-Impact for Static and Dynamic Loading

in Appendix IV-B it is assumed that the velocity component parallel to the plane is absorbed by surface sliding. This is why the normal velocity component is used in the stroke sizing computations. For the 45° and 90° side-on cases the same procedure yields

$$1/2 \frac{W}{g} (V_N)^2 = WGS \ (1/3 + 1/2 \times 2/3)$$

$$S_{45^o} = S_{90^o} = \frac{0.75 (V_N)^2}{gG} \approx \frac{0.7 (V_N)^2}{gG}$$

for design purposes. With the three principal strokes known, the principal contributing factors to the attenuator thickness computation are known. Provision must still be made for stroke efficiency, a factor of safety, and rock protection dimensions. These are handled as follows. Ref. 3-1 contains data on honeycomb stroke efficiency. For the point design this efficiency is about 0.8 (see fig. 3.5.8-6 for data). Stroke efficiency is defined as that fraction of total honeycomb thickness which will actually crush-up when impacted. This effect occurs because some of the total thickness provided is lost as accumulated crushed material builds up. (See fig. 3.5.8-7.) Therefore, corresponding to the three stroke values (S_i for i = 0°, 45°, 90°) just derived, one must provide associated thickness (t_i) of

$$t_i = \frac{S_i}{0.8}$$

However, due to the possibility of rock or other outcroppings, these thicknesses must be compared to S_i + 5 in. and the larger value used in design. Therefore, the design thickness is the greater of the following two expressions (ref. Appendix IV-B).

$$t_i = \frac{S_i}{0.8}$$

$$t_i = S_i + 5$$

With the three thicknesses known, the attenuation system may be sized and the volume of crush-up material computed. For omni-directional designs this was accomplished by fitting a smooth curve through the three key points and using the symmetry of the Lander body to completely define the attenuator.

Another design quantity is the material density to be used to limit the g-loading to the desired values. This density for the 3/16 phenolic honeycomb is related to the specific energy and crushing stress as shown in fig. 3.5.8-8. For minimum attenuator weight a density greater than 11.85 pcf should not be used since the maximum specific energy and crushing stress occur at this value. This establishes an upper limit on the useful density. A lower bound on the density is determined from previously

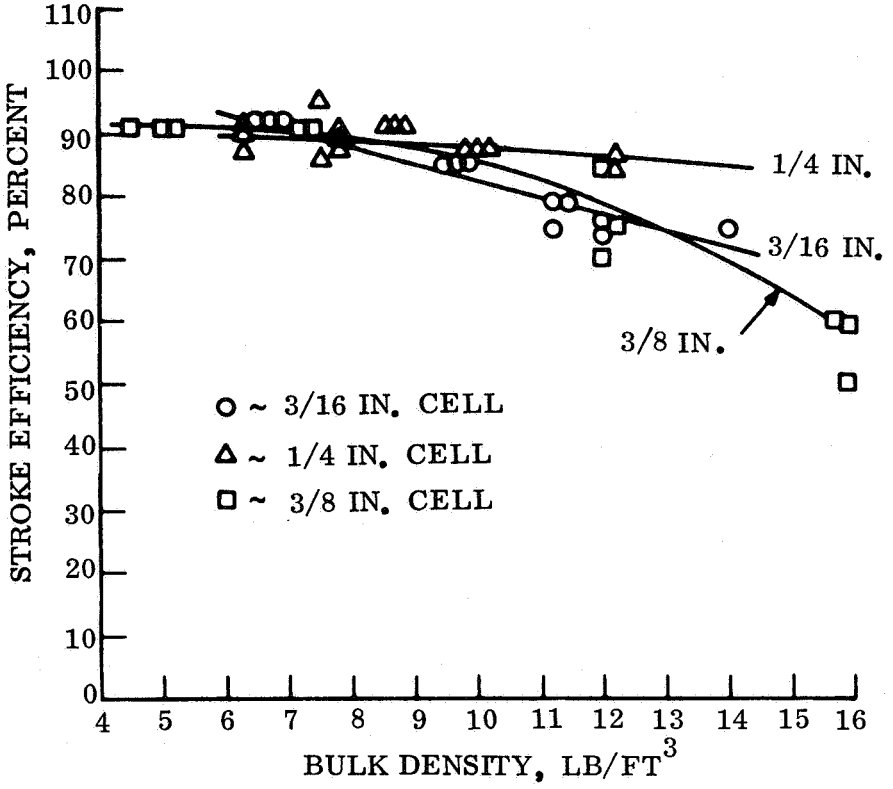


Figure 3.5.8-6. Stroke Efficiency vs Bulk Density

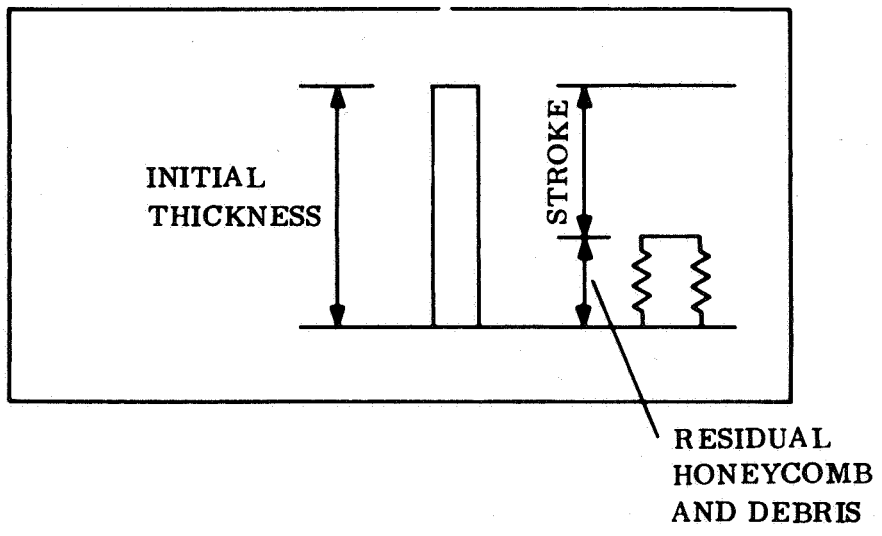


Figure 3.5.8-7. Stroke Efficiency

reported experimentation. It is shown that honeycomb densities below 4 pcf are erratic in behavior and this density is consequently a lower bound on the feasible materials for design use.

The density selection for use in point designs is made by selection of a crushing stress according to the formula

$$\sigma_{cr} = \frac{W\ G}{A}$$

where W is Lander weight, G is allowable deceleration level and A is the cross sectional area corresponding to the progression of the stroke to that point at which the peak g-loading is experienced. The area A is determined via a computer code and used to find the corresponding crushing stress. With this crushing stress the appropriate density from the relation in fig. 3.5.8-8 is read off and used in the attenuator design.

Options in the two different computer design codes were constructed based on this information. The codes allow one to input the point design conditions of touchdown velocity, size, landed subsystem weight, g-tolerance and surface rock specification in order to obtain attenuation sizing, volume and weight, crushing stress, and material density for a given point design. The computer-calculated volume and weight are then verified by planimeter computations using the exact cross sectional areas. The geometry used in the program is sketched in fig. 3.5.8-9. The input geometry includes interior and exterior diameters and inside container height. A program option yields complete sizing dimensions of the Lander as well as geometric checks for compatibility with aeroshells of different cone angles for initial installation feasibility computations.

3.5.8.4.2 Point Design 1 Particulars for Impact Attenuation System

When the foregoing criteria were applied to Point Design 1 the impact attenuation system was defined as 522 lb of 3/16 in. cell size phenolic fiberglass honeycomb. The honeycomb volume was 66 ft^3; the density was 7.9 pcf. The other conditions were:

V_D = 100 fps descent velocity

V_H = 220 fps wind velocity

omni-directional capability

clearance and protection for 5 in. rocks

1000 g (rigid body) limitation.

The honeycomb thicknesses are shown in outline form in fig. 3.5.8-1.

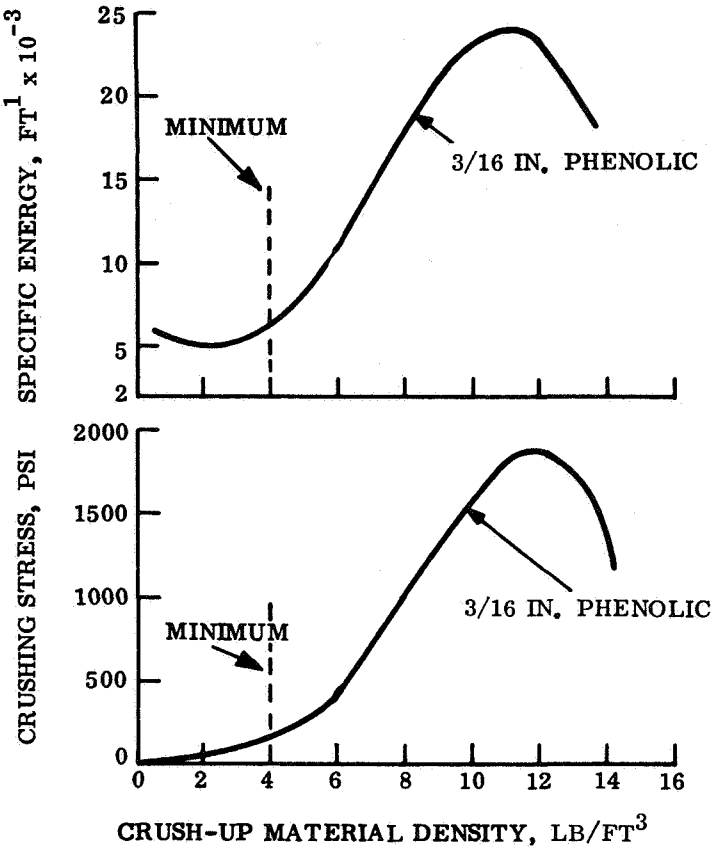
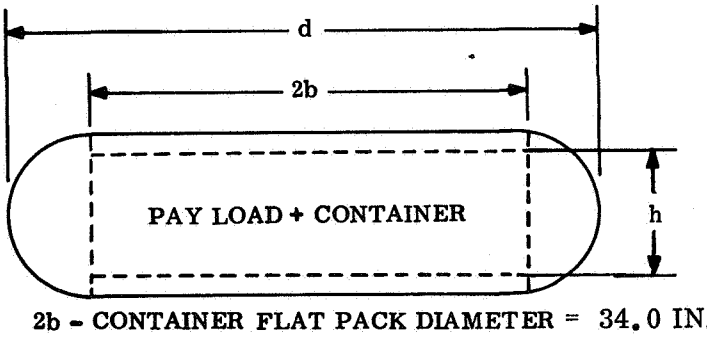


Figure 3.5.8-8. Crushable Honeycomb Properties



2b - CONTAINER FLAT PACK DIAMETER = 34.0 IN.

h - INTERNAL CONTAINER HEIGHT = 12.0 IN.

d - OVERALL CONTAINER DIAMETER INCLUDING ELLIPTICAL ENDS = 43.0 IN.

Figure 3.5.8-9. General Internal Geometry, Point Design 1

3.5.8.5 Detailed Design

Another detail in the point designs is the utilization of a face sheet over the honeycomb to encapsulate it. The factors which necessitate this facing are five:

1. Prevention of the honeycomb cells from filling with loose surface debris

2. Facilitation of sliding. The sliding mechanism is used to absorb the impact velocity component parallel to the surface

3. Enhancement of the structural integrity of the attenuator

4. Distribution of or spreading of concentrated loads produced by surface protrusions

5. Confinement of crush-up fragments which might provide an undesirable background for surface measurements.

Experimentation has shown that loose surface (sand, loam, dust, etc.) tend to fill up the impacting cells quite quickly. This filling will interfere with pure crushing action and for this reason is undesirable. However, for surfaces presenting this potential hazard, the major energy absorber is the ground, with a reduced amount of honeycomb attenuator crushing or no crush-up at all. From this viewpoint, therefore, the first consideration for a cover may not produce a compelling argument.

The smooth surface presented by a cover would certainly provide better sliding behavior than the exposed open cells of a honeycomb. On anything less than a very hard terrain of low relative roughness this is an important factor. Moreover, in the point design analyses lateral sliding motions are counted on to absorb the horizontal component of the impact velocity vector.

The structural strength of the attenuator is favorably affected by use of a facing plate. The facing lessens the tendency to shear off entire chunks of the attenuator, thereby thwarting the desired crush-up behavior. A wrap-around membrane also allows more of the attenuator to participate in the energy absorbing process than if no cohesive member was used.

More important than this last argument, however, a face sheet produces a spreading action of possible localized loads produced by rocks and other surface protrusions. This lessens the possibility of local punctures or intrusions which could circumvent the crush-up process. The spreading of loads is important if the design assumptions are to be reasonably accurate. Moreover, a thin cover protects the outermost cell edges and minimizes local shear deformations which could cause lateral failures produced by the surface friction.

Finally, encapsulation of the honeycomb prevents stray honeycomb fragments from reaching the surface and interfering with surface science measurements and other scientific experiments (alpha back scatter, for example).

If an encapsulation device is used, the determination of its thickness can be made as follows. Strength will not govern the design since the facing is not required to perform a major structural function. Instead the facing must be designed to be sufficiently thin so that it can be contoured to fit the doubly curved Lander geometry. The actual lay-up is a detailed design manufacturing problem. A piece-wise lay-up of extremely light gauge material is one possible design choice. The lower limit on gauge is determined by the criteria that the membrane itself must not be so light that it is easily punctured by surface abrasion.

Finally, two other design details remain. First, gross deformation effects are investigated for two conditions. The first is excessive stroke requirements which produce thickness sufficiently large (> 24 in.) to lead to impulsive buckling of the honeycomb cells without crushing behavior. If such strokes are indicated the attenuator is segmented further to eliminate buckling and promote crushing of the attenuator. Second, gross shear failures must also be considered. This possible mode involves the breaking off of an entire piece of material without crushing deformation. Where analysis indicates that gross shear is a possibility, radial metallic strips welded to the payload container can be used to take out the shear in excess of what can be carried laterally by the honeycomb cells. These elements, while resistant to shear, are sufficiently slender so that they buckle when impacted along their length and thereby crush-up with the phenolic honeycomb material.

Past experience indicates that the double curvature introduced in this Lander concept can be wrapped effectively by segmenting the honeycomb into pieces which are then bonded together. In this way the longitudinal axis of the honeycomb cells can be made near-radial with the payload contained structure. The wrapping proceeds around the Lander circumference and then outward until the desired thicknesses are provided.

3.5.8.6 Honeycomb Lander Fabrication

The principal operations involved in the fabrication of the honeycomb crush-up system include the segmenting and cutting of the honeycomb material so that it may be properly oriented as shown in fig. 3.5.8-10, the bonding of the honeycomb segments to one another, and the bonding of the honeycomb to the aluminum substructure and the external protective covering.

3.5.8.6.1 Adhesive Selection

For proper bond action suitable adhesives must be selected. Adhesive bond systems are required for two distinctly different joints; honeycomb-to-honeycomb and metal-to-honeycomb. While these configurations present separate joining problems the bonded joints must nevertheless have the same cure cycle. There are, however, modified epoxy-phenolic adhesives suitable for temperatures of -200°F to 900°F. A representative example of such a product is the HT 424 adhesive manufactured by the Bloomingdale Department of the American Cyanimid Corporation. These adhesives may be formulated to be RF transparent as required. The properties of this class of adhesive are such that the bonds formed are stronger than the weakest material

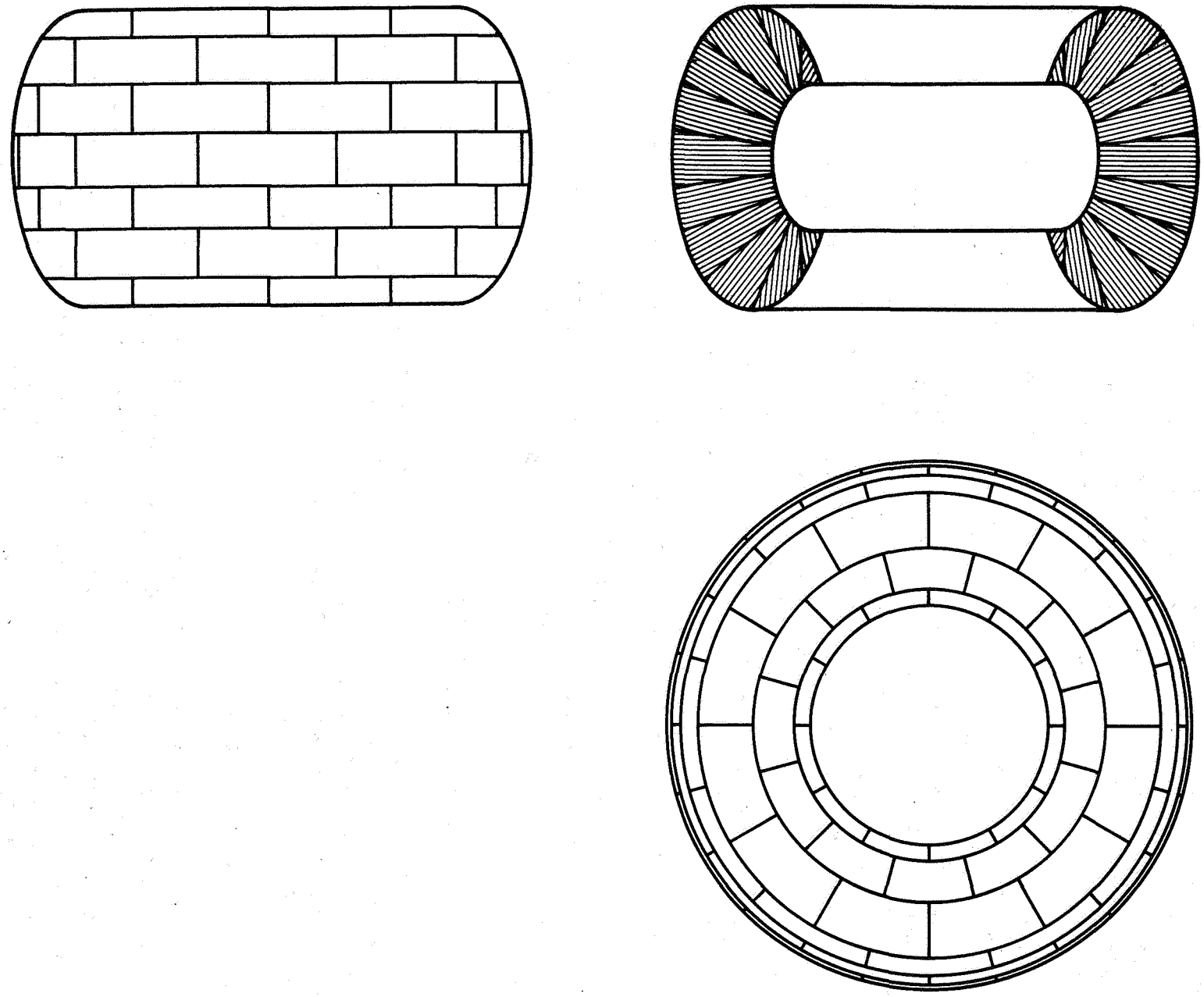


Figure 3.5.8-10. Layup of Honeycomb Attenuator

comprising the joint. In fact, shear and bending tests will fail the honeycomb interface of the bond.

3.5.8.6.2 Honeycomb-to-Honeycomb Joints

In fabricating the Lander, there are a large number of possible variations at the interface between the honeycomb segments. The selected desirable approach is to bond flat surfaces of honeycomb together utilizing a space-filling adhesive as needed to fill gaps between points contacts.

3.5.8.6.3 Honeycomb-to-Aluminum Joints

Previous development testing (ref. 3-2) has identified adhesives suitable for bonding phenolic fiberglass honeycomb to aluminum.

Previous GE-MSD efforts have, furthermore, identified adhesives for this bond which have cure cycles compatible with the adhesives used for honeycomb-to-honeycomb joints. As an example, adhesives of the H424 high-temperature resin family produced by the Bloomingdale Department of the American Cyanimid Corporation are feasible. (For aluminum-to-honeycomb joints HT 424 F, in particular, has been tested by GE-MSD as reported in ref. 3-2. For honeycomb-to-honeycomb bonds HT 424 is indicated.)

3.5.8.6.4 Tooling and Fixtures

Phenolic fiberglass honeycomb material of the densities used in this Lander point design can be cut to size and shape with moderate ease. Heavier or lighter densities should also work well. Standard shop equipment with metal cutting tools may be used throughout.

Tool steel routers and mills may be used; for rough cutting the honeycomb segments a carbide tipped band saw blade is preferred. For final thickness and taper large inertia sanding wheels are used. Specialized wood fixtures can be designed for many of the sizing and contour cutting operations. For curing operations a standard circulating air furnace provides a rotating spit fixture for the assembly cure cycle.

3.5.8.6.5 Lander Fabrication

The Lander fabrication sequence proceeds according to the following steps:

1. Preparation of container structure surface. This includes final finishing to produce proper dimensional tolerances and special treatment of apertures and holes. After all finishing the structure is surface-treated with a chemical reagent (such as Alodine 1200) to promote good adhesive bonding.

2. Preparation of exterior shell interior surface. This includes final shaping of the impact attenuator encapsulating structure (skin). This surface is also surface treated prior to adhesive bonding.

3. The raw honeycomb crush-up material is then rough cut to size with proper attention to the designed lay-up and resultant cell wall orientation.

4. The rough cut surface is then checked for dimensional accuracy and secondary trimming or sanding is performed.

5. A preliminary fit-up of the honeycomb to the subsystems container is made. This is done by using shims to allow for adhesive bond thicknesses.

6. The epoxy adhesive is then prepared according to the manufacturer's specifications.

7. The bonding of the honeycomb segments to the container structure and to one another is then begun. For this purpose a rotating spit device to hold the container, along with the associated jigs and fixtures for temporary support during curing are used. The exact fixture details must be determined during the manufacturing development period. However, in general, these are wooden forms which can be snapped in and out of position.

8. The assembly, which is now fully mated, is subjected to the proper cure cycle determined by the adhesive and the specified strength level to be attained. Refer to fig. 3.5.8-10 for lay-up details.

9. The exterior facing plate is now attached, held in position by jigs and cured. Because of the double curvature of this element it must be laid up in pieces in a manner comparable to the lay-up of conventional toroidal metallic shells.

3.5.9 MASS PROPERTY AND INERTIA DATA

Following is a summary weight statement for the complete Lander, table 3.5.9-1, and a detailed weight breakdown of the payload subsystems and components, table 3.5.9-2.

TABLE 3.5.9-1. WEIGHT SUMMARY

Lander Systems and Equipment Design Point 1	Weight (lb)	Total (lb)
Lander (complete)	--	(858.0)
Structure	160.0	
Attenuation	522.0	
Electrical power equipment	56.5	
Telecommunications	30.7	
Environmental control	10.0	
Scientific payload	48.3	
Interface equipment	0.9	
Cables and harness	9.6	
Deployment-cameras	10.0	
Deployment-alpha back scatter	10.0	
Total		858.0

C.G.s('X' CG Datum - apex of heat shield cone) (in.)			Gross Inertias in slug/ft^2		
X	Y	Z	Roll	Pitch	Yaw
38.0	-0.08	-0.42	92	61	60

TABLE 3.5.9-2. DETAILED WEIGHT BREAKDOWN, SUBSYSTEMS COMPONENTS

Lander Subsystems	Weight (lb)
Electrical Power Equipment	56.45
A101 Battery, Operational	29.80
A106 Switch, Power Transfer	2.00
A107 Programmer, Lander	7.20
A108 Regulator, Voltage	7.00
A130 Regulator, Voltage	0.9
A110 Controller, Power	5.50
A113 Battery, High Rate 'A'	0.50
A114 Battery, High Rate 'B'	0.50
A115 Filter, EMC 'C'	1.90
A121 Module, Diode Blocking	0.2
A124 Module, Thermal Relay	0.15
A128 Switch, Hg 'A'	0.10
A132 Breaker and Limiter Unit	0.60
Telecommunications	(30.7)
A602 Transmitter, UHF	2.50
A604 Conditioner, Signal Data	4.00
A605 Antenna, UHF Relay 'A'	1.00
A607 Unit, Memory	5.00
A608 Receiver, UHF Beacon	1.30
A609 Processor, Data Handling	4.00
A610 Circulator, UHF 'A'	0.40
A611 Circulator, UHF 'B'	0.40
A621 Switch, Antenna	1.00
A623 Antenna, UHF Relay 'B'	1.00
A676 Multicoder	5.00
Mach 2 Sensor	3.00
A682 Accelerometer, Impact	0.60
A683 Amplifier, Charge (3)	1.50

TABLE 3.5.9-2. DETAILED WEIGHT BREAKDOWN, SUBSYSTEMS COMPONENTS (Continued)

Lander Subsystems	Weight (lb)
Thermal Control Subsystem	(10.00)
Insulation, 1 in.	7.00
Hardware, Installation	3.00
Scientific Payload Subsystem	(48.30)
A807 Accelerometer, Tri-Axial	2.00
A808 Transducer, Temperature (2)	1.00
A809 Transducer, Pressure (2)	1.00
A810 Transducer, Pressure (2)	1.40
A817 Transducer, Temperature (2)	1.00
A822 Camera, Facsimile A	2.00
A823 Camera, Facsimile B	2.00
A824 Camera, Facsimile C	0.40
A825 Camera, Facsimile D	0.40
A829 Sensor, Wind Velocity A	0.50
A830 Sensor, Wind Velocity B	0.50
A831 Sensor, Wind Velocity C	0.50
A832 Sensor, Wind Velocity D	0.50
A833 Sensor, Wind Velocity E	0.50
A834 Sensor, Wind Velocity F	0.50
A835 Sensor, Wind Velocity G	0.50
A836 Sensor, Wind Velocity H	0.50
A837 Sensor, Moisture	10.00
A849 Detector, Water Vapor and Moisture	1.00
A838 Spectrometer, Mass	8.00

TABLE 3.5.9-2. DETAILED WEIGHT BREAKDOWN, SUBSYSTEMS COMPONENTS (Concluded)

Lander Subsystems	Weight (lb)
A841 Inclinometer (2)	2.60
A845 Sensor, Wind Velocity I	0.50
A846 Sensor, Wind Velocity J	0.50
A847 Transducer, Temperature	0.50
A848 Transducer, Temperature	0.50
A842 Instrument, Surface Composition	9.50
Interface Equipment	(0.88)
J2002 IFD, A/S Lander	0.13
J2003 IFD, T/C Lander	0.75
Cable Assembly	(9.60)
WL1 Cable, Assembly Command	2.10
WL2 Cable, Assembly Power	3.70
WL3 Cable, Assembly Instrument	3.00
WL4 Cable, Assembly Shielded	0.80

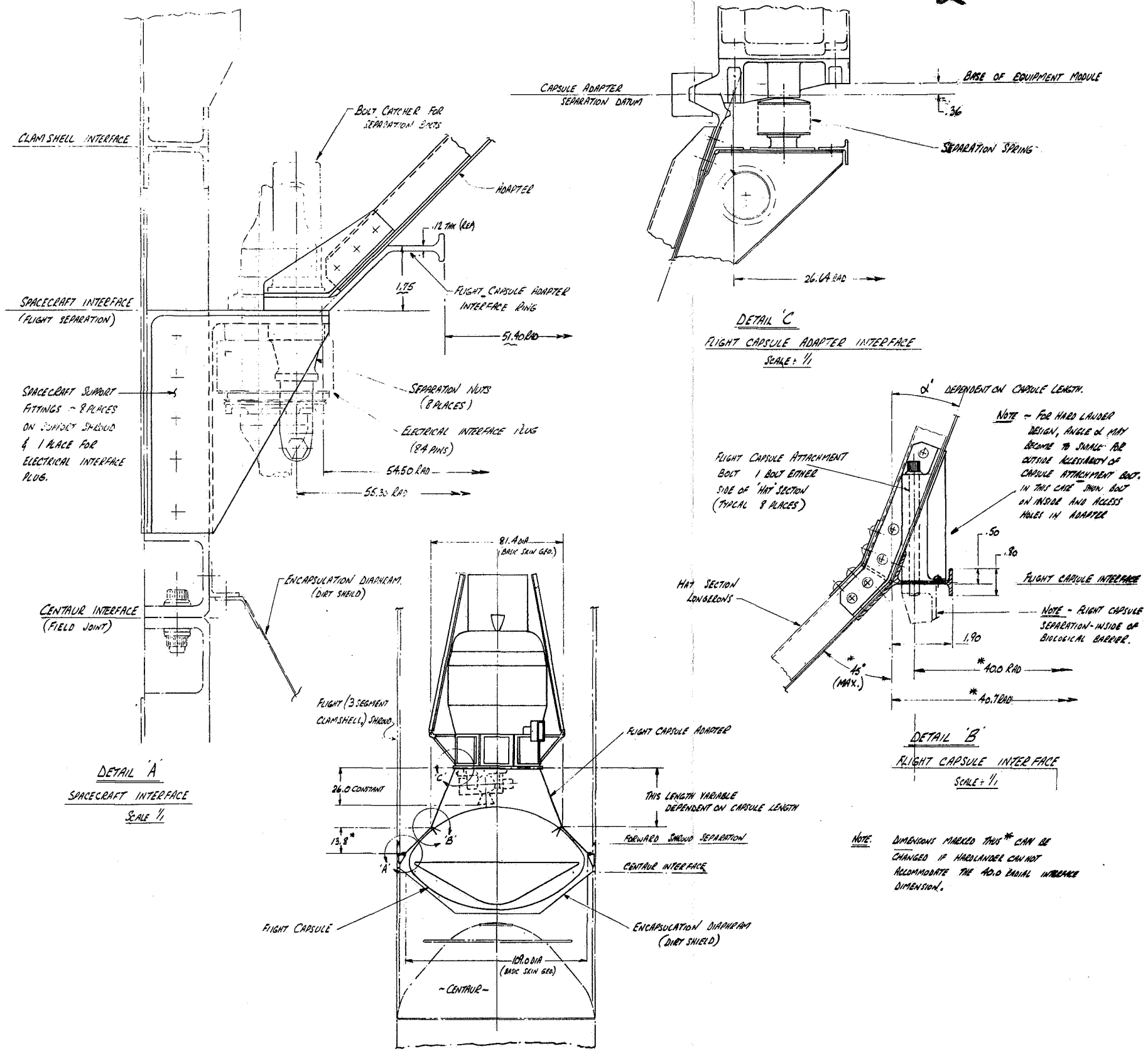
3.6 CONSTRAINTS IMPOSED ON ORBITER

The majority of constraints imposed by the Flight Capsule on the Orbiter are relatively independent of the mode of Capsule entry (direct or orbital) and the size or weight of the Capsule. Addition of the Flight Capsule, however, requires mechanical and electrical interfaces between the Orbiter and the Capsule. Fig. 3.6-1 shows the Capsule adapter which will provide the mechanical interface. In this study, it has been assumed that the Mariner Mars '71 Orbiter will be modified for the combined Orbiter and Hard Lander mission in 1973. MM '71 is itself an adaption of the Mariner Mars '69 flyby spacecraft. A complete description of the Mars '73 Orbiter is contained in Appendix D. Table 3.6-1, excerpted from the appendix, highlights the major changes required of the MM '69 subsystems for conversion to an Orbiter in '71, and then to a Capsule bus (as well) in '73.

In addition to the changes summarized in the table, the Orbiter propulsion tankage must be expanded to insert the entire spacecraft into a Mars orbit. The increased mass of the propulsion module, in turn, dictates that the rings, longerons, and shear panels of the MM '71 octagonal equipment module be increased in gauge to carry the increased loads. The details of the structural changes are discussed in detail in Appendix D. The details of the propulsion changes are tabulated in table 3.6-2.

FOLDOUT FRAME 1

FOLDOUT FRAME 2



DETAIL 'A'
SPACECRAFT INTERFACE
SCALE 1/1

DETAIL 'C'
FLIGHT CAPSULE ADAPTER INTERFACE
SCALE = 1/1

DETAIL 'B'
FLIGHT CAPSULE INTERFACE
SCALE = 1/1

NOTE: DIMENSIONS MARKED THUS * CAN BE CHANGED IF HARDLAUNCH CAN NOT ACCOMMODATE THE 40.0 RADIAL INTERFACE DIMENSION.

Figure 3.6-1. Capsule/Bus Interface

TABLE 3.6-1. MAJOR SUBSYSTEM CHANGES

MM '69 Subsystem	Change For '71 Orbiter	Change For '73 Capsule
Power	• Solar Array Increase	• Solar Array Increase
Radio	• New Maneuver Antenna • New High Gain Antenna • Modified Low Gain Antenna	• New Maneuver Antenna • New High Gain Antenna • New Relay Receiver • New Relay Antennas
Attitude Control	• Cold Gas and Jet Size Increase • Modification of Autopilot Electronics	• Cold Gas and Jet Size Increase • Modification of Autopilot Electronics • Relocated Sun Sensors • Possible Approach Guidance
Data Storage	• Additional Air • Additional DTR	• New Relay Recorders
Command	• Possible Decoder Expansion	• Probable Decoder Expansion
Telemetry		• Data Modes for Capsule Telemetry
Scan Control	• Removal of Mars Gates	
Science	• Passive Cooling of IRS • Possible TV Field of View Changes	No Estimate
Cabling		• Three Inflight Disconnects
Mechanical Devices	• High Gain and Maneuver Antenna Deployment • High Gain Antenna Articulation • Modified Separation Mechanics	• Spacecraft Separation Mechanics • Modified Orbiter Separation Mechanics • New High Gain Antenna Deployment
Propulsion	• New	• New Tanks and Supports for (Orbital Entry Capsule)
Structure	• Strengthened Adapter	• Capsule Adapter • Spacecraft Adapter • Strengthened Octagon for (Orbital Entry Capsule)

TABLE 3.6-2. ORBITER PROPULSION SUMMARY

ΔV (Total)	1525 mps
Weights -	
Capsule	1626 lb
Orbiter	963 lb
Adapter	70 lb
(1) Propulsion (dry)	317 lb
(2) Residuals	79 lb
(3) Total propellant and pressurant	2240 lb
(1) + (2) Burnout	396 lb
(1) + (3) Propulsion system	2557 lb
Volumes* -	
Propellant tank diameter	22 in.
Propellant tank length	46 in.
Pressurant tank diameter	17 in.
Burn time (insertion)	1983 sec
Spacecraft launch weight	5216 lb
*Based on four propellant and two pressurant tanks	

3.7 PROBABILITY OF SUCCESS

3.7.1 INTRODUCTION

A key factor in evaluating a design concept is the determination of the probability of success of the configuration. This determination is primarily beneficial at the early concept design state in performing trade-off evaluations of several potential design configurations. As the design evolves from conceptual towards final, the merit of the quantitative value shifts from comparative to predictive.

A probability of success determination was performed for the conceptual mission as defined by Point Design 1. Due to the early stage of the design, it was necessary to perform this determination based on many assumptions. These are listed below. In general, it can be stated that failure rate data was based on information known concerning components of similar generic or complexity definition. It was also assumed that the new development items required for this mission will be developed, tested, and qualified before being flown.

Due to these assumptions, and the uncertainty of sterilization influence on some of the components the predictive value of the determination may not be accurate. However, since the same assumptions and methodologies were used on all determinations during the study, the comparative value of the determinations are significant.

3.7.2 RESULTS

Probability of success values were determined for both the Capsule systems and for the booster and Orbiter systems of the mission. The procedures used in performing these determinations are presented in Sections 3.7.3 and 3.7.4 A summary of the determinations, by major mission phase, is shown by table 3.7.2-1.

This tabulation indicates that the value obtained, under the study ground rules stated in the preceding paragraph for the probability of success of the total mission is 0.616. This is the probability of obtaining proper functioning of all mission equipment, as required, for the duration of the mission from launch to completion of one full diurnal cycle on the Martian surface.

TABLE 3.7.2-1. MISSION SUCCESS PROBABILITY, POINT DESIGN 1

MISSION PHASE	BOOSTER AND ORBITER		CAPSULE		COMBINED	
	Phase	Cumulative	Phase	Cumulative	Phase	Cumulative
Launch/Cruise	.748	.748	.945	.945	.707	.707
Mars Orbit	.945	.707	---	.945	.945	.669
Separation and Entry	.999	.706	.958	.905	.957	.639
Landed Operation	.997	.704	.967	.875	.964	.616

3.7.3 CAPSULE ANALYSIS

This section presents the procedure followed in analyzing the Mars Hard Lander System Point Design for the probability of successfully accomplishing its intended functions.

3.7.3.1 Assumptions

The assumptions and ground rules used in the analysis were as follows:

1. A component would not fail under non-operating conditions.
2. The probabilities of success of all components were considered to be statistically independent. This permitted the use of the product rule for assessing the system and subsystem success probabilities. In the case of redundant application, the above ground rule applied to the component function.
3. The success probability of the structure, aeroshell and impact attenuation was assumed equal to unity (1.0).
4. The probability of success of the system or its components was defined as being equal to the probability of zero functional failures.
5. The mission phases and time of each phase upon which the analysis was based are as follows:

Phase		
Launch/Cruise	5,856	hr
Pre-entry	2	hr
Entry	0.36	hr
Landed Operation	24.6	hr

6. The assessment for the success probability of a component during any given phase reflects only the time during the phase in which it operates.
7. If any portion of a component operated during a particular phase the entire component was assessed for its success probability.
8. The success probability of the various system components was based on failure data of components which were similar or identical in function or of equivalent complexity.

3.7.3.2 Procedure

3.7.3.2.1 Component Success Probability

The probability of success of time (or cycle) sensitive components was obtained using the following expression:

$$R_c = e^{-\lambda t} \qquad (1)$$

where:

R = probability of success

λ = failure rate in failures/hr (or cycle)

t = operating time (hr) or cycles

For redundant application of a component the following expression was used to obtain the probability of success of the function:

$$R = [1 - (1 - R_c)^n] \quad (2)$$

where:

R = probability of success of the function

R_c = probability of success of the component

n = number of components in the redundant group.

For components which are not time (or cycle) sensitive, such as squib valves, the success probability reflects the results of successes versus trials using appropriate statistical techniques.

3.7.3.2.2 Subsystem Success Probability

The probability of success of a subsystem for any given phase was obtained using the following expression:

$$R\ (S/S)_p = \pi_i\ R_i \quad (3)$$

where:

$R\ (S/S)_p$ = probability of success of the subsystem in the phase

R_i = probability of success of the i^{th} component or function (for redundant application) for the phase being considered

π = symbol for product

The probability of success of a subsystem over its entire mission was obtained using the following expression.

$$R\ (S/S)_M = \pi_j\ R\ (S/S)_j \quad (4)$$

where:

$R\ (S/S)_M$ = probability of success of the subsystem over the mission.

$R\ (S/S)_j$ = probability of success of the subsystem for the j^{th} mission phase.

3.7.3.2.3 System Success Probability

The probability of success of the system for any given phase was obtained using the following expression.

$$R\ (System)_p = \pi_k\ R\ (S/S)_k \tag{5}$$

where:

$R\ (System)_p$ = probability of success of the system in the phase.

$R\ (S/S)_k$ = probability of success of the k^{th} subsystem for the phase being considered.

The probability of success of the system over the entire mission was obtained using the following expression.

$$R\ (System)_M = \pi_k\ R\ (S/S)_{M_k} \tag{6}$$

where:

$R\ (System)_M$ = probability of success of the system for the mission

$R\ (S/S)_{M_k}$ = probability of success of the k^{th} subsystem for the mission.

3.7.3.2.4 Orbiter Support Analysis

The probability of success of the Mars Hard Lander for the i^{th} mission phase, reflecting the success probability of the booster and spacecraft (in support of Capsule operations) and the Capsule system is given by:

$$R\ (MHL)_i = R\ (booster)_i\ R\ (spacecraft)_i\ R\ (Capsule) \tag{7}$$

The cumulative probability of success of the Mars Hard Lander for the i^{th} mission phase is given by:

$$R\ (MHL;\ cumulative) = \prod_{i-1}^{i} R\ (MHL) \tag{8}$$

where:

$R\ (MHL)_{i-1}$ = independent probability of success of the MHL for the $(i-1)^{th}$ phase as obtained from (7)

$R\ (MHL)_i$ = independent probability of success of the MHL for the i^{th} phase as obtained from (7)

The cumulative success probability for each of the systems are similarly obtained from (8).

3.7.3.3 Results

3.7.3.3.1 Component Success Probabilities

The success probability for the components (or functions in the case of redundant applications) comprising Point Design 1 for the Mars Hard Lander System is summarized in table 3.7.3-1 for each of the mission phases.

The values appearing in the table were computed using expressions (1) or (2), described in para 3.7.3.2 as applicable for time (or cycle) sensitive components. These values reflect failure rate data from the sources indicated in the table. Non-time (or cycle) sensitive component success probabilities were obtained directly from the indicated source.

3.7.3.3.2 System and Subsystem Success Probabilities

The success probabilities for the subsystems and system which define Point Design 1 are summarized in table 3.7.3-2 for each of the phases described in para 3.7.3.1 and the total mission. The values appearing in the table were obtained using expressions (3), (4), (5) and (6) described in 3.7.3.2.

3.7.3.4 Redundancy Considerations

A failure mode effects analysis (FMEA) was performed as part of the Capsule analyses. Due to the conceptual state of the mission design this was performed on a qualitative rather than a quantitative basis. The primary purpose of this analysis was to point out potential problem areas for redundancy considerations.

During the FMEA it was learned that the items that had the greatest criticality and risk of failure were the canister heater and thermostat and the operational battery. The former were of high risk due to the long duty cycle during the interplanetary cruise. The latter was critical due to its requirement to perform all Capsule operations. Redundancy inclusions were provided for these items; a standby parallel thermal control system and internal cell redundancy in the battery.

TABLE 3.7.3-1. RELIABILITY ESTIMATES, POINT DESIGN 1 COMPONENTS

Description	Reliability				Data Source
	Launch and Cruise	De-orbit	Entry	Landed Operation	
EP&D Subsystem					
Battery, Operational (1)	-	.9999	.9997	.9993	ERSR-TT Program
Battery, Entry (Dual)	-	.9999	-	-	
Battery, T/C (Dual)	-	.9999	-	-	
Programmer, Lander (1)	-	.9999	.9995	.9942	REA-MBRV Program
Voltage Regulator, A (1)	-	.9999	.9999	.9999	RFMA-MK12 Program
Voltage Regulator, B (1)	-	.9999	.9999	.9999	
Voltage Regulator, C (1)	.9999	.9999	-	-	
Regulator, Charge (1)	.9999	-	-	-	REA-Voyager Study
Module, Diode Block (2)	-	.9998	-	-	RFMA-TT Program
Module, Diode Block (1)	-	-	.9999	-	
Battery, H.R. (Dual)	-	-	.9999	.9999	ERSR-TT Program
Module, Power Distribution	-	.9999	-	-	REA-MK12 Program
Filter, EMC, A (1)	-	.9999	-	-	RFMA-TT Program
Filter, EMC, B (1)	-	.9999	-	-	
Filter, EMC, C (1)	-	-	.9999	.9999	
Module, Thermal Relay (2)	-	.9998	-	-	
Module, Thermal Relay (1)	-	-	.9999	.9999	
Battery, Dual	.9999	.9999	-	-	ERSR-TT Program
Control, Power-C	.9999	.9999	-	-	REA-MK12 Program
Control, Power-L	-	.9999	.9999	.9999	
Programmer, Dual-C	-	.9999	-	-	RFMA-TT Program
Switch, Hg (Dual)	-	-	-	.9999	FARADA
Switch, Breaker and Limit	-	.9999	-	-	FARADA
Switch, Power Transformer	.9999	-	-	-	REA-MBRV Program
Pressurization and Venting Subsystem					
Valve, Vent	.9999	-	-	-	FARADA
Separation Subsystem					
Release, Hot-Wire (4)	-	.9996	-	-	RFMA-MK12 Program
Nut, Explosive (4)	-	.9894	-	-	FARADA
Nut, Explosive (4)	-	.9894	-	-	FARADA
Scientific Payload Subsystem					
Transducer, Temperature -A (4)	-	-	.9997	-	FARADA
Transducer, Temperature -L (4)	-	-	-	.9981	
Transducer, Pressure -A (6)	-	-	.9996	-	
Transducer, Pressure -L (2)	-	-	-	.9940	
Accelerometer, Tri-Axial (1)	-	-	.9983	-	
Release, Hatch Cover (1)	-	-	-	.9999	
Solenoid, Camera Release (4)	-	-	-	.9987	
Camera, Facsimile (4)	-	-	-	.9996	
Sensor, Wind Velocity (10)	-	-	-	.9972	
Sensor, Moisture (1)	-	-	.9999	.9997	
Spectrometer, Mass (1)	-	-	.9997	-	
Inclinometer (1)	-	-	-	.9996	
Comp, Surface (1)	-	-	-	.9960	FARADA
Attitude Control and Propulsion					
Tank, N_2	.9995	.9999	-	-	FARADA
Valve, Squib	-	.9999	-	-	
Valve, Fill	.9994	.9999	-	-	
Tank, Hydrazine	.9995	.9997	-	-	
Disc, Burst	.9999	.9999	-	-	FARADA

Legend
- RFMA - Reliability Figure of Merit Analysis
- REA - Reliability Estimate Analysis
- ERSR - Equipment Reliability Status Report

TABLE 3.7.3-1. RELIABILITY ESTIMATES, POINT DESIGN 1 COMPONENTS (Concluded)

Description	Reliability				Data Source
	Launch and Cruise	De-orbit	Entry	Landed Operation	
Attitude Control and Propulsion (Cont'd)					
Valve, Solenoid (12)	-	.9999	-	-	FARADA
Gyro, Rate	-	.9993	-	-	
Amplifier	-	.9997	-	-	
Detector, Threshold	-	.9994	-	-	
Driver, Pneumatic	-	.9993	-	-	
Generator, R.R.	-	.9996	-	-	
Switch	-	.9995	-	-	
Rocket, Retro	-	.9999	-	-	
Ejector, Nozzle	-	.9975	-	-	FARADA
Retardation Subsystem					
G-Switch	-	-	.9991	-	MBRV Program
Mortar, Drogue	-	-	.9999	-	
Fitting, Main Release (3)	-	-	.9997	-	
Fitting, Drogue Release	-	-	.9999	-	
Switch, Impact	-	-	.9999	-	
Parachute Assembly	-	-	.9999	-	MBRV Program
Telecommunication Subsystem					
Transmitter, VHF	-	.9998	.9999	.9999	RFMA-MK12 Program
Conditioner, Signal Data	-	.9999	.9999	.9997	
Antenna, VHF (2)	-	.9999	.9999	.9999	FARADA
Core, Memory	-	.9999	.9999	.9996	
Processor, Data	-	.9999	.9999	.9999	RFMA-MK12 Program
Diplexer (2)	-	-	.9999	.9999	FARADA
Communicator, Cruise	.9999	-	-	-	
Switch, Microwave (2)	-	-	-	.9989	
Receiver, Beacon VHF	-	-	-	.9940	RFMA-MK12 Program
Sensor, Temperature (18)	.9961	.9982	-	-	FARADA
Sensor, Pressure (8)	.9982	.9992	-	-	
Sensor, Linear Velocity (12)	.9988	.9988	-	-	
Conditioner, Firing Checkout (1)	.9999	.9999	-	-	RFMA-MK12 Program
Sensor, Power Supply	.9999	.9999	-	-	MIL HDBK-217A
Conditioner, Signal-C	.9999	.9999	-	-	RFMA- MK12 Program
Sensor, Voltage Regulator	.9999	-	-	-	MIL HDBK-217A
Detector, Separation Load (2)	-	.9999	-	-	Accelerometer est.
Indicator, A/S Rel (2)	-	.9999	-	-	Sep. Switch est.
Conditioner, Linear Velocity Data	.9999	-	-	-	RFMA-MK12 est.
Multicoder	-	.9999	.9999	.9999	PCM est.- MBRV
Sensor, Link Tensile (4)	.9996	-	-	-	Strain Gage est.
Accelerometer, Impact	-	-	.9999	-	FARADA
Processor, Impact Data	-	-	.9999	-	Computer est.
Electrical Interface					
IFD, Capsule-Spacecraft	.9988	-	-	-	MIL-HDBK-217A MK12 RFMA
IFD, A/S-Lander	.9988	.9999	.9999	-	
IFD, T/C-Lander	.9988	.9999	-	-	
Safe-Arm, Lander	.9988	.9999	.9999	.9999	
Safe-Arm, Aeroshell	.9988	.9999	-	-	
Safe-Arm, Canister	.9988	-	-	-	
Fitting, Coaxial Data	.9988	-	-	-	
Fitting, Coaxial Interface	.9988	-	-	-	
Fitting, Coaxial VHF	.9988	-	-	-	MIL-HDBK-217A MK12 RFMA
Thermal Control Subsystem					
Heater	.9988	.9999	-	-	FARADA
Thermostat	.9988	.9999	-	-	FARADA

Legend

RFMA - Reliability Figure of Merit Analysis
REA - Reliability Estimate Analysis
ERSR - Equipment Reliability Status Report

In addition to these items many other redundancy inclusions are provided in the Capsule design. A typical listing of some of these inclusions together with the type of redundancy used is shown in the following. Other redundancy provisions, such as back-up gate or switching signals and back-up time signals, are also provided but not included in the listing.

Item	Type of Redundancy
Operational Battery	Internal
Canister Heater and Thermostat	Parallel
Dual Battery	Internal
Thermal Batteries	Parallel
Lander Programmer	Internal
Charge Regulator	Internal
Blocking Module	Internal
Power Distribution Module	Internal
Thermal Relay Module	Internal
Dual Programmer	Internal
Hg. Switch	Parallel
Breaker and Limiter Unit	Internal
Spin Initiator	Parallel Squibs
De-spin Initiator	Parallel Squibs
Rocket Initiator	Parallel Squibs
Temperature Transducers	Parallel
Pressure Transducers	Parallel
UHF Antenna	Parallel

TABLE 3.7.3-2. RELIABILITY SUMMARY, POINT DESIGN 1
CAPSULE SYSTEM AND SUBSYSTEM

Subsystem	Mission Phase				
	Launch and Cruise	De-orbit	Entry	Landed Operation	$R_M = \pi R_p$
EP &D	.9995	.9981	.9985	.9928	.9889
Attitude Control and Propulsion	.9883	.9934	-	-	.9917
Pressure and Venting	.9999	-	-	-	.9999
Separation	-	.9784	-	-	.9784
Telecommunications	.9921	.9950	.9991	.9917	.9780
Thermal Control	.9619	.9998	-	-	.9617
Scientific Payload	-	-	.9972	.9828	.9800
Retardation	-	-	.9984	-	.9984
Electrical I/F	.9924	.9996	.9998	.9999	.9917
$R_p = \pi R$ (S/S)	.9448	.9646	.9930	.9675	.8755

3.7.4 ORBITER SUPPORT ANALYSIS

3.7.4.1 Introduction

Probability of success determinations for the booster and Orbiter systems were performed for those functions which support and/or contribute to the success of the Capsule and its mission. Flight operations were based on an out-of-orbit reference mission with a flight time of 244 days.

3.7.4.2 Assumptions

The assumptions made and the ground rules followed in the analysis were as follows:

1. Only those functions required for the success of the Capsule missions were included.
2. The Orbiter is assumed to use 1971 equipment hardware with only minor modifications.
3. For the orbital entry mode, up to 30 days of orbital operations plus a trim maneuver have been assumed prior to Capsule release.
4. The spacecraft support is required for a one day landed mission.
5. The reliability of criticality of the ground support functions have not been included in the study.

3.7.4.3 Procedure and Data Sources

In arriving at the reliability estimates, the tools and failure rate data bases developed during the Voyager Task C redundancy and Task D Design studies conducted for JPL as modified by more recent studies, were used. These procedures are described in detail in the reference documents shown in Section 3.8. In summary these can be stated as follows:

a. Minuteman level parts and Minuteman and Apollo failure rates were used to the greatest extent possible.

b. Curves developed during the studies showing the projected reliability growth for inertial components and integrated circuits were used.

c. Factors to reflect (1) parts reliability growth and (2) upgrading to a high reliability status were used to obtain failure rates for sources other than Minuteman and Apollo.

d. Where failure rate data was lacking, or inadequate, failure rates were derived by comparing the part in question with another part of similar construction or performance for which reliability information was available.

3.8 REFERENCES

3-1 RF Transparent, Energy Absorbing, Structural Elements. Phase II Final Report, Prepared for JPL under Contract No. 950964, Aug. 1964, GE-MSD, Doc. No. 64SD4329.

3-2 Development of Energy Dissipating Plastic Honeycomb, Quarterly Progress Report Nos. 7 and 8, Contract No. 951172, JPL. GE-MSD, Doc. No. 66SD4390.

3-3 Failure Rate Data Base for Spacecraft Redundancy Study, VOY-C3-TR8.

3-4 Reliability Characteristics of Voyager Components - Voyager Spacecraft Redundancy Study, VOY-C3-TR7.

3-5 Voyager Final Report, Phase IA, Task C, Volume 4, Application of Redundancy Study, July 28, 1967, VOY-CO-FR, prepared for JPL under contract 951112.

3-6 Voyager Spacecraft Final Report, Phase B, Task D. Volume II (Book 1 of 5), Systems Description, October 2, 1967, under contract NAS 8-22603.

4. POINT DESIGN 2

4. POINT DESIGN 2

4.1 MISSION SEQUENCE

A sequence of events from launch to mission completion for this mission is shown in table 4.1-1. This is a direct entry mission with a nominal interplanetary flight time of 164 days before separation. Flight sequence from start of separation to impact is illustrated by fig. 4.1-1. The landed sequence is illustrated by fig. 4.1-2.

Separation occurs 24 hr prior to entry. The Lander Capsule is stabilized after separation of a spin/de-spin and roll control system. Deceleration is accomplished by parachute whose deployment is actuated by a g-switch at Mach 2. After separation, the spacecraft will go into synchronous orbit for one full diurnal cycle to support the Lander Capsule. Entry and surface science and surface imaging is performed at the beginning of the cycle with data transmitted real time to the Orbiter for relay to Earth. Surface composition and meteorology measurements will continue for the full diurnal cycle and the data is stored until the Orbiter is within communication range at periapsis. When the Orbiter returns to range it will signal the Lander and the stored data plus an additional complete set of real time data will be sent to the Orbiter for relay to the Earth.

TABLE 4.1-1. MISSION SEQUENCE OF EVENTS, POINT DESIGN 2

Item	Event	Time
A.	Launch to Impact	
1.	Launch	TL
2.	First mid course maneuver (if required)	TL + 30 days
3.	Second mid course maneuver (if required)	TL + 154 days
4.	Mars arrival	TL + 164 days
5.	Start final Capsule diagnostic checkout	To (entry - 48 hr)
6.	Complete diagnostic checkout	To + 120 min
7.	Update programmers complete	To + 20 hr
8.	Turn on Lander power, T/M, sequencer and diagnostic data	T1 (To + 23.8 hr)
9.	Canister separation	T2 (T1 + 5 min)
10.	Spacecraft maneuvers to Capsule separation attitude	T2 + 10 min
11.	Capsule separates from spacecraft	T3 (T2 + 10.1 min)
12.	Initiate spin stabilization	T3 + 0.5 sec
13.	Ignite deflection propulsion	T3 + 30 min
14.	Terminate deflection propulsion	T3 + 30.3 min
15.	Initiate de-spin	T3 + 30.5 min

TABLE 4.1-1. MISSION SEQUENCE OF EVENTS, POINT DESIGN 2 (Continued)

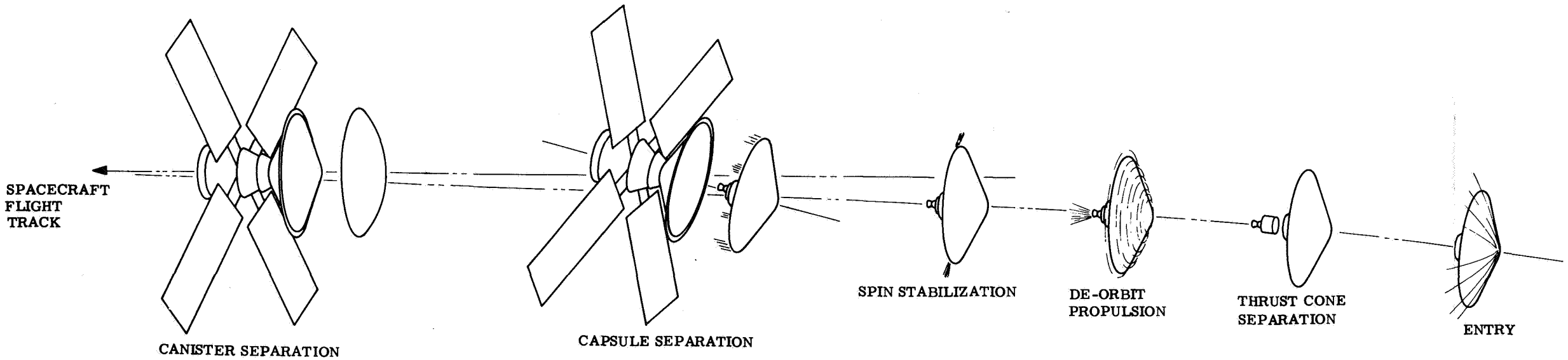
Item	Event	Time
16.	Separate thrust cone	T3 + 30.6 min
17.	Turn power and T/M off	T3 + 30.7 min
18.	Turn on mass spectrometer for warm-up	T4 - 15 min
19.	Turn on T/M (low data rate), initiate accelerometer and pressure sensor readings	T4 - 60 sec
20.	Entry	T4 (T3 + 24 hr, 8.3 min)
21.	Mach 5 - initiate mass spectrometer, water vapor, and temperature sensor readings	VM-8: T4+107 sec; VM-9: T4+97 sec
22.	Mach 2 - deploy parachute	T4+121 sec T4+118 sec
23.	Aeroshell separation	T4+131 sec T4+128 sec
24.	Jettison parachute	T4+350 sec T4+1216 sec
25.	Impact - force sensed and transmitted to spacecraft (with redundant storage)	T5 (T4+351 sec) T5(T4+1217 sec)
B.	Landed Operations	
1.	Diagnostic and stored entry data transmitted to Orbiter (low data rate)	T5 + 0.1 min
2.	Lander comes to rest, up direction sensed	T5 + 2 min
3.	Initiate hatch cover and boom deployments	T5 + 2.1 min
4.	Switch to high data rate transmission mode	T6 (T5 + 2.5 min)
*5.	Initiate stored diagnostic, entry, and impact data transmission to Orbiter	T6 + 0.1 min
*6.	Initiate imagery, meteorology, and inclinometer measurements and transmit to Orbiter for relay to Earth	T6 + 0.2 min
*7.	Repeat items 5 and 6	T6 + 8.5 min
8.	Turn off imagery and T/M systems	T6 + 20 min
9.	Repeat surface science measurements (excluding imagery) at 20 min intervals and store data	----

*If impact occurs too late for relay to Orbiter (VM-9), gate switch delays function until Item 14.

TABLE 4.1-1. MISSION SEQUENCE OF EVENTS, POINT DESIGN 2 (Concluded)

Item	Event	Time
10.	Initiate surface composition (alpha back scatter) measurement cycle and store data	T7 (T5 + 1 hr)
11.	Complete initial surface composition cycle	T7 + 5 hr
12.	Repeat surface composition measurements every 3 hr	----
13.	Receive signal that Orbiter is returning to range	T8 (T6 + 24.5 hr)
14.	Turn on T/M system (high data rate) and transmit stored science data to Orbiter	T9 (T6 + 24.6 hr)
15.	Perform imagery and surface science measurements and transmit data to Orbiter for relay to Earth	T9 + 0.1 min
16.	Repeat items 14 and 15	T9 + 8.5 min

FOLDOUT FRAME



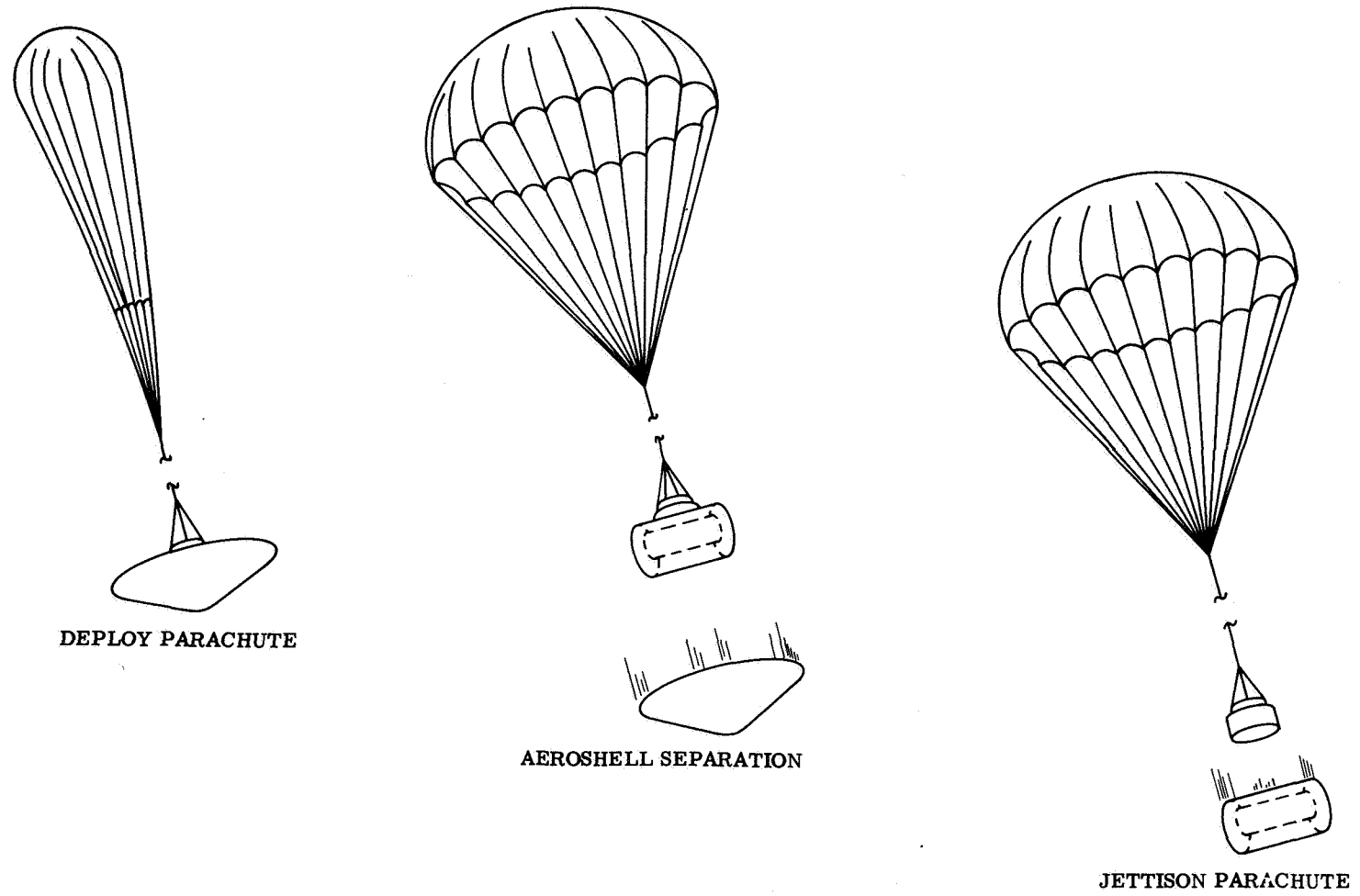
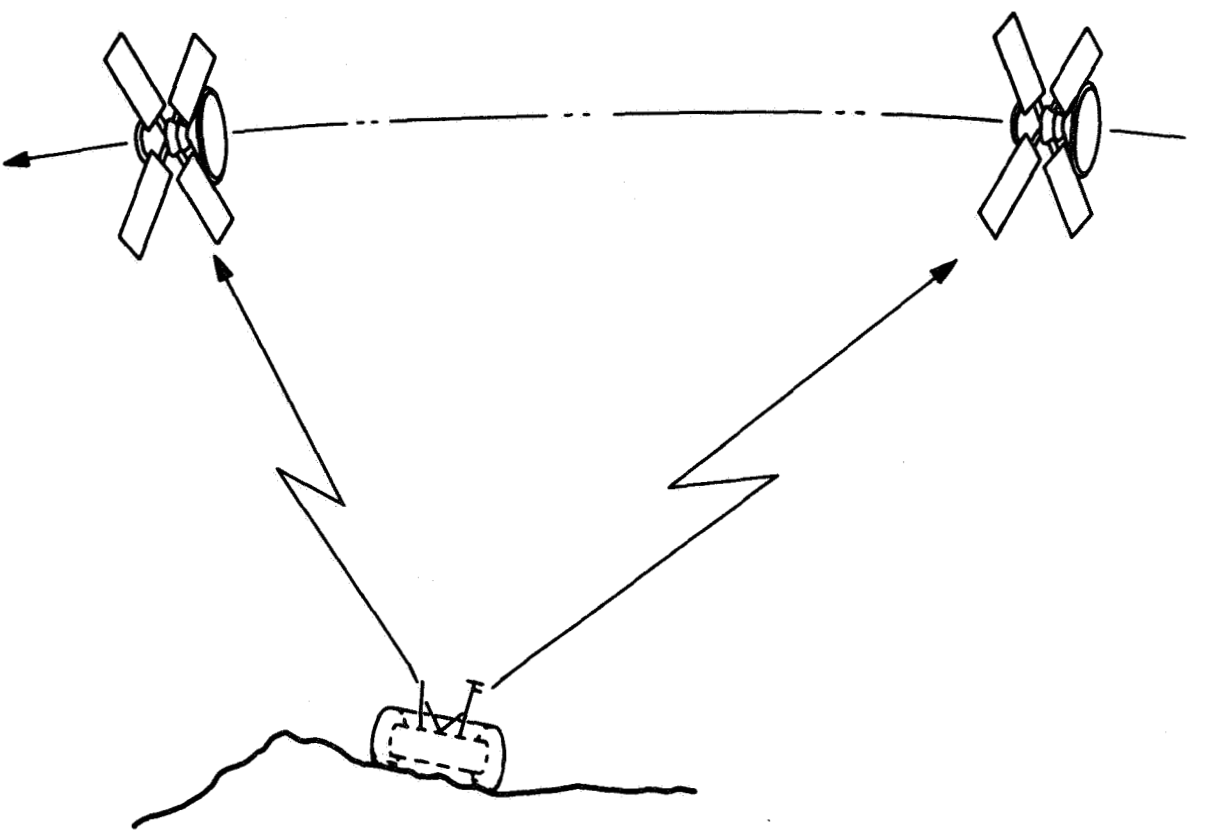


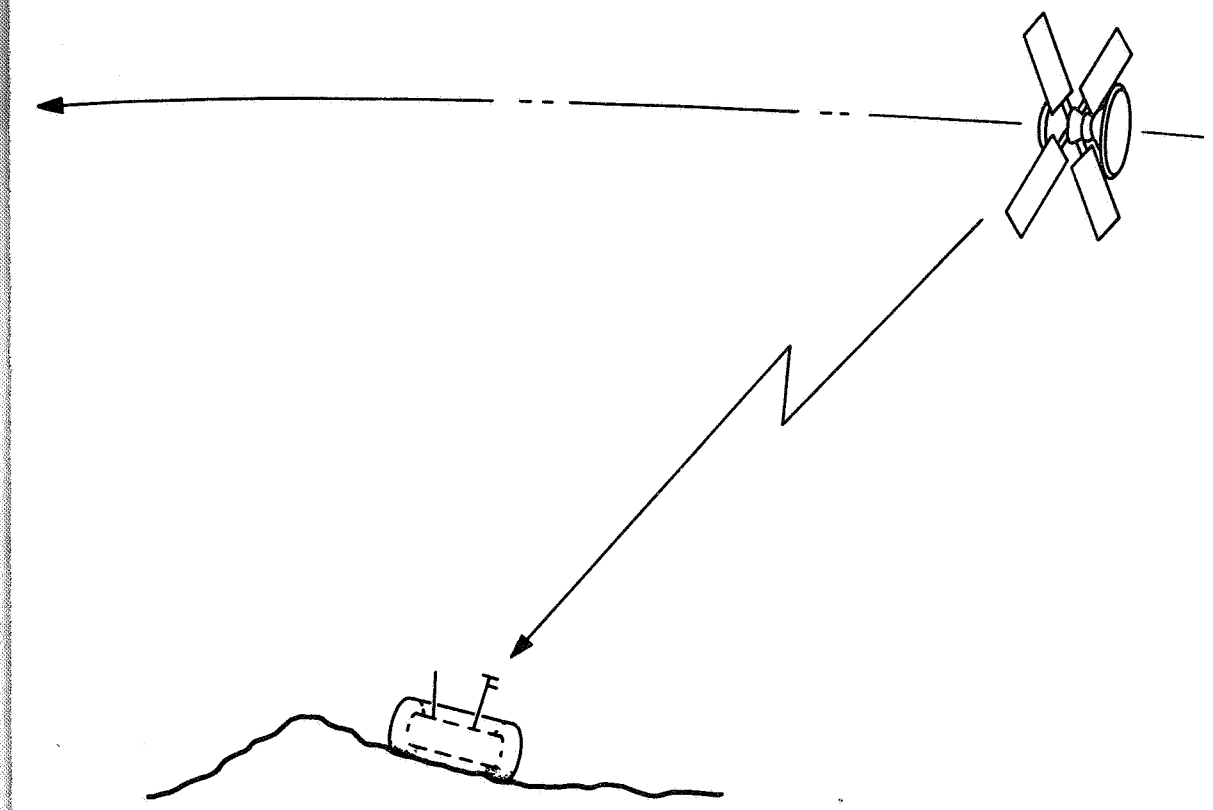


Figure 4.1-1. Operational Flight Sequence from Separation to Impact



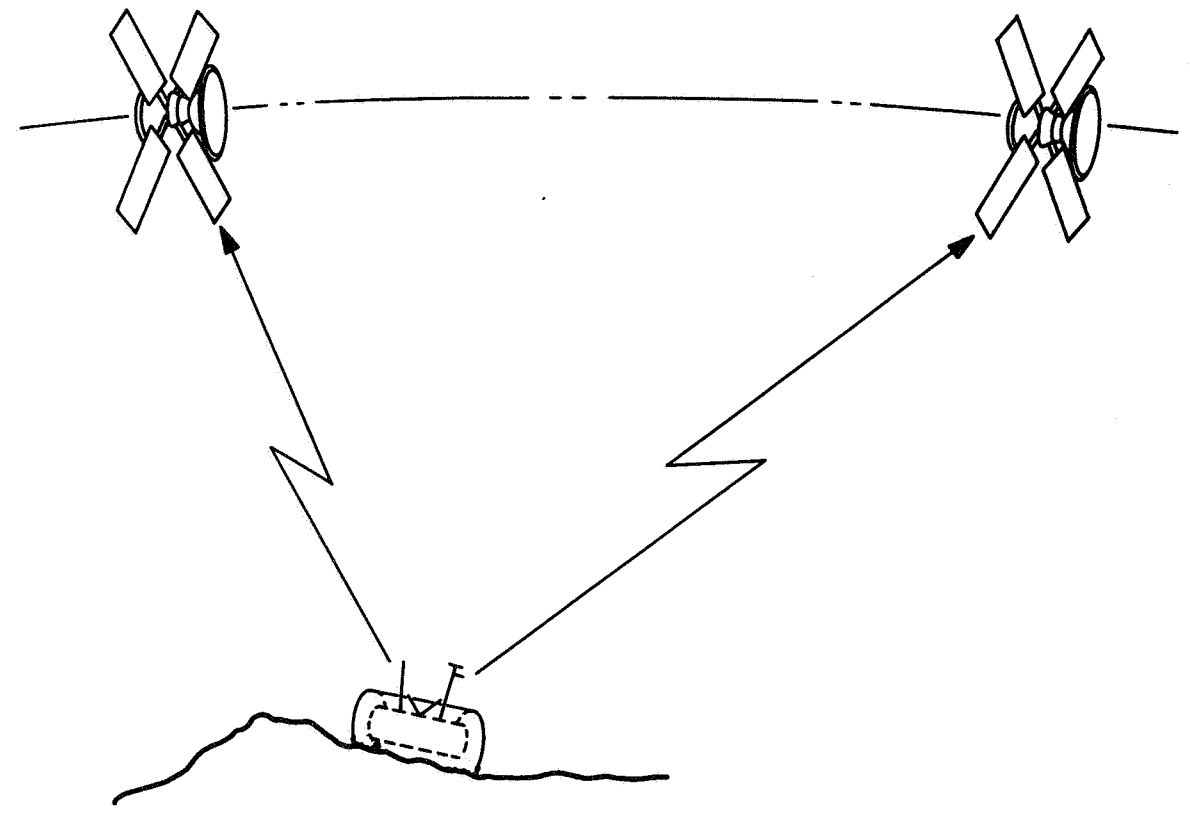
DATA TRANSMITTED TO SPACECRAFT

FOLDOUT FRAME 2



LANDER RECEIVES SIGNAL THAT
SPACECRAFT IS RETURNING
(24.5 HRS LATER)

FOLDOUT FRAME



STORED DATA, TRANSMITTED TO SPACECRAFT

Figure 4.1-2. Landed Operation

4.2 CAPSULE SYSTEM DESIGN DESCRIPTION

A basic difference in the direct entry system and the out-of-orbit entry system in a given point design pair is that the ballistic entry parameter (W/C_DA) for the direct entry vehicle (20.8 kft/sec entry velocity and 25° path angle) is approximately 0.75 the value appropriate for the out-of-orbit entry system (15 kft/sec and 16° at entry). Direct entry systems entering at a path angle increased to 40° require a ballistic parameter about 0.4 times smaller than the out-of-orbit vehicle.

The allowable or limiting ballistic coefficient is determined for the different entry mission modes by selecting the best combination of aeroshell drag area, parachute deployment, size, and landing load attenuation in the deceleration profile to Lander touchdown. The entry system velocity must be reduced to Mach 2 before parachutes are deployed and this deceleration increment must occur at a sufficiently high altitude that the Capsule Lander system can be decelerated by parachute to the acceptable touchdown velocity increment. In this study, the ballistic entry parameter limit is determined for each entry mode base on parachute deployment in the VM-8 Mars model atmosphere (lower altitude at Mach 2) and parachute sizing for descent in the VM-7 atmosphere, the model having the lowest atmospheric density at the surface.

The effect of the limiting ballistic coefficient is that the direct entry Capsules are designed with considerably larger base diameter and heavier aeroshells than the slower entry, out-of-orbit vehicle of the point design pair. The design approach taken for each vehicle in the particular design pair is the same and the system weight difference in the launch configuration, separation, and entry is primarily due to the entry shell size because it directly affects the weight of aeroshell structure and heat shield and the Canister (larger size and inertial loading).

The aeroshell designs selected for each of the six Capsule point designs incorporate blunt body, sphere cone shell structures with ablative heat shields using formulations such as GE's ESM 1004X at 16 lb/ft^3 density for the out-of-orbit vehicles and ESM 1004 AP at 35 lb/ft^3 density for the direct entry vehicles. The selected entry system structure and shield design is an extension of ICBM technology and the integrity of the approach in either soft bonded shields or film adhesive shields has been proved. The shield materials referenced are typical of the application but the exact formulation required would be specified in a more detailed engineering phase of a Mars mission program.

The Lander system of the Capsule is retained within the aeroshell by a tension strap arrangement and released by burning the wire wrap of the hot-wire bolts with 30 msec of 10 to 15 amp current. It is separated from the aeroshell by the parachute drag differential. The preferred release, separation and deceleration sequence is initiated with an altimeter. A g-level switch and timing units as well as an axial g-level and base pressure measurements approach have been considered for the parachute deployment device. The altimeter approach is preferred because it can be used to delay parachute opening (below Mach 2) to match the descent time of the Lander to the view time available for communication with the Orbiter before and after landing. The requirement for shortening the descent time is most necessary if the flight is made in a VM-9 type atmosphere.

The Lander contains the instruments, power, sequencing, telemetry, and communication equipment to perform the surface science operations. The equipment is contained within a toroidal rim-stiffened cylinder equipped with a deep ring of phenolic glass honeycomb structure sized and positioned to attenuate the landing loads by mechanical crush-up of the honeycomb material. The first point design pair developed for the minimum surface lifetime mission were prepared with both omni-directional and multi-directional Landers to develop the weight and size difference in the out-of-orbit and direct entry vehicles due to the design approach taken for impact attenuation. The difference in the weight of attenuation material between omni-directional and multi-directional landing (522 and 287 lb, respectively) is the difference in the omni-directional and multi-directional Lander total weights (weight suspended on parachute) of 858 and 623 lb. The following weight statement (table 4.2-1) summarizes the comparison of the out-of-orbit and direct vehicles and the influence of Lander type for the minimum lifetime mission. The comparison is based on the first design pair data but the results are typical of like comparison studies of the other design pairs.

TABLE 4.2-1. COMPARATIVE WEIGHT SUMMARY OF MINIMUM MISSION SYSTEMS

Aeroshell base diameter	Out-of-Orbit Entry		Direct Entry	
	8.3 ft	8.3 ft	12.7 ft	11.4 ft
Lander type - weight (lb)	Omni-858	Multi-623	Omni-858	Multi-623
Retardation weight (lb)	228	172	228	172
Aeroshell and propulsion (lb)	329	329	465	389
	---	---	---	---
Capsule weight at separation from spacecraft (lb)	1415	1124	1551	1184
Capsule weight at entry (lb)	1246	955	1480	1127
Ballistic entry coefficient $\frac{(lb)}{ft^2}$	15.2	11.7	7.9	7.3
Capsule weight at launch (lb)	1626	1335	1882	1463

The pre-entry systems of the Capsule consist of the sterilization canister and its internal adapter, attitude control and the de-orbit maneuver hardware. The prime function of the canister is to encapsulate the Capsule system and maintain a physical, biological barrier to prevent contamination of the Capsule during:

1. Terminal sterilization cycle

2. Post sterilization operations in the ground environment

3. Launch and powered flight

4. Cruise and up to the sequence for Capsule-Orbiter separation.

The canister design approach for the six capsule designs is a semi-monocoque construction in minimum manufacturing gauge (0.012), 7075 aluminum. The rear shell of the canister assembly contains the internal adapter within the sterilized envelope and connections to the Orbiter are made outside this envelope.

The forward shell is released by applying 24 amp for 30 msec to the four hot-wire bolts of the V-ring type clamp segments. The shell is separated by two mechanical springs with a velocity of 2 ft/sec.

The internal adapter provides the structural transition between Capsule and the Orbiter and contains the equipment for separating the flight systems. The Capsule is released by applying 48 amp to four explosive nuts and is separated at approximately 1 ft/sec by four springs.

Both spin/de-spin and three axis control systems were studied for Capsule attitude control for the de-orbit maneuver, for entry path angle control and for vehicle control up to Lander separation from the aeroshell. The six point designs have been detailed with spin/de-spin for pre-entry flight and roll control during entry. The final system would be selected after more detailed error analyses are made and the principle trade-offs in landing site location, data communication and trajectory design are completed.

Based on the baseline missions data, the out-of-orbit entry vehicles require a velocity increment of 235 meters/sec and the direct vehicles 45 meters/sec. Both solid propellant systems and liquid propulsion systems have been detailed in the point designs. The liquid systems are more easily adapted to the de-orbit maneuver changes as weight and velocity requirements are modified. In the low impulse requirements range, the liquid systems have disproportionate weights for the propulsion hard parts compared to the total and, generally, the liquid systems applicable to these study vehicles are about three times heavier and require considerably larger packaging volumes than the solids. Both systems have been designed into the Capsule and the pertinent trades and the engineering details in each design application are given in the following section of this volume. In all six design applications the de-orbit maneuver system is arranged to be jettisoned before entry by release of preloaded, hot-wire bolts of the thrust cone and separation by mechanical springs.

The following sections give engineering details and analyses of the direct entry Capsule with a surface lifetime goal of one diurnal cycle. A design approach with an omni-directional Lander (Point Design 2A) and with a multi-directional Lander (Point Design 2B) were prepared. This Capsule is shown as Point Design 2 of the six Capsules prepared.

4.2.1 SCIENCE DATA REFERENCE

The weight of the sensors selected and a baseline reference of the atmospheric data acquired from entry to impact in the maximum flight time range of atmospheres is shown on table 4.2-2. Pressure and temperature readings are taken at both the stagnation and the base region of the aeroshell. The atmospheric density profile is determined from the vehicle aerodynamic data and the measured deceleration profile of the Capsule.

TABLE 4.2-2. SCIENCE WEIGHT SUMMARY

Entry Science	Weight (lb)	Data Load (bits)	
		VM-8*	VM-9*
Pressure	3.0	1.0×10^4	2.6×10^4
Temperature	1.5	4.4×10^3	2.0×10^4
Composition	8.0	6.6×10^3	10×10^3
Density	2.0	0.8×10^5	2.0×10^5
Water vapor (ducting)	1.0	5.7×10^1	3.7×10^2
	15.5	1.01×10^5	2.56×10^5
Landed Science			
Pressure	1.4	1.35×10^3	
Temperature	2.0	2.7×10^3	
Wind	5.0	4.9×10^3	
Moisture	10.0	1.77×10^3	
Photo imaging	4.8	1.02×10^7	
Clinometer	2.6	7.0×10^1	
Soil sampler	9.5	3.0×10^4	
	35.3	1.02×10^7	

*Time from entry to impact in VM-8 = 351 sec
in VM-9 = 1217 sec

The landed science consists of meteorological data and surface imagery taken with (Philco) facsimile cameras that take four scenes of low resolution data and four nested scenes of high resolution data. The low resolution scenes are each 35° x 50° segments imaged with 1/10° Instantaneous Field of View (IFOV) and the high resolution scenes are 5° x 5° segments imaged with 1/100° IFOV. The total data acquired in four high and four low scenes (63 gray shades) is $6 \times 10^6 + 4.2 \times 10^6$ or 1.02×10^7 bits. A typical data summary for the surface operations is included in table 4.2-2.

The surface imagery data is transmitted real time to the Orbiter after impact and again at periapsis passage. The meteorological data is readout from the magnetic core storage unit at both opportunities, with the first readout including entry science data. To preclude possible data loss from plasma sheath blocking, the entry data is interleaved for two transmissions with the readout portion delayed approximately 70 sec.

In the Mission Analysis, Volume II, the results of trajectory design analyses show that the Lander delivered with an out-of-orbit entry mode has two times the relay data transmission quantity capability of the same Lander delivered with a direct entry system.

4.2.2 CAPSULE SYSTEM CONFIGURATION

Two Capsule configurations have been designed for the direct entry version Lander containing the minimum surface science with a one diurnal cycle surface lifetime. Configuration 2A incorporates the same omni-directional Lander used in Point Design 1. Configuration 2B depicts a multi-directional Lander with the minimum capability. Both configurations employ a UHF telecommunication relay to the Orbiter, solid propellant propulsion system and Mach 2 sensed parachute deployment. Fig. 4.2.2-1 shows the Capsule configuration for Point Design 2A and fig. 4.2.2-2 shows Point Design 2B.

4.2.3 CAPSULE SYSTEMS WEIGHT

The weight and inertias of the minimum mission life, direct entry Capsule with an omni-directional Lander is given in Table 4.2-3. The weight and inertias of the direct entry comparison system with a multi-directional Lander is given in table 4.2-4. The basic composition of each Capsule design, the weights and inertias are given for the key mission events of launch, separation, entry and landing. The detailed weight, balance and inertia statements for the pre-entry system are given in Section 4.3, the entry systems in Section 4.4 and the Lander in Section 4.5.

TABLE 4.2-3. WEIGHT AND INERTIA COMPOSITION, POINT DESIGN 2A

Capsule Systems	Weight (lb)	Roll	Pitch	Yaw
		(slug ft^2)		
Lander	858			
Aeroshell	394			
Retardation	228			
Propulsion (Solid)	71			
Canister and thermal blanket	331			
Capsule at launch	1882	454	381	381
Capsule at separation	1551	319	246	246
Capsule at entry	1480	318	197	197
Landed system	858	92	61	60

TABLE 4.2-4. WEIGHT AND INERTIA COMPOSITION, POINT DESIGN 2B

Capsule Systems	Weight (lb)	Roll	Pitch	Yaw
		(slug ft^2)		
Lander	623			
Aeroshell	332			
Retardation	172			
Propulsion (solid)	57			
Canister and thermal blanket	279			
Capsule at launch	1463	338	277	278
Capsule at separation	1184	215	135	136
Capsule at entry	1127	214	134	135
Landed system	623	39	25	26

4.2.4 FUNCTIONAL BLOCK DIAGRAMS

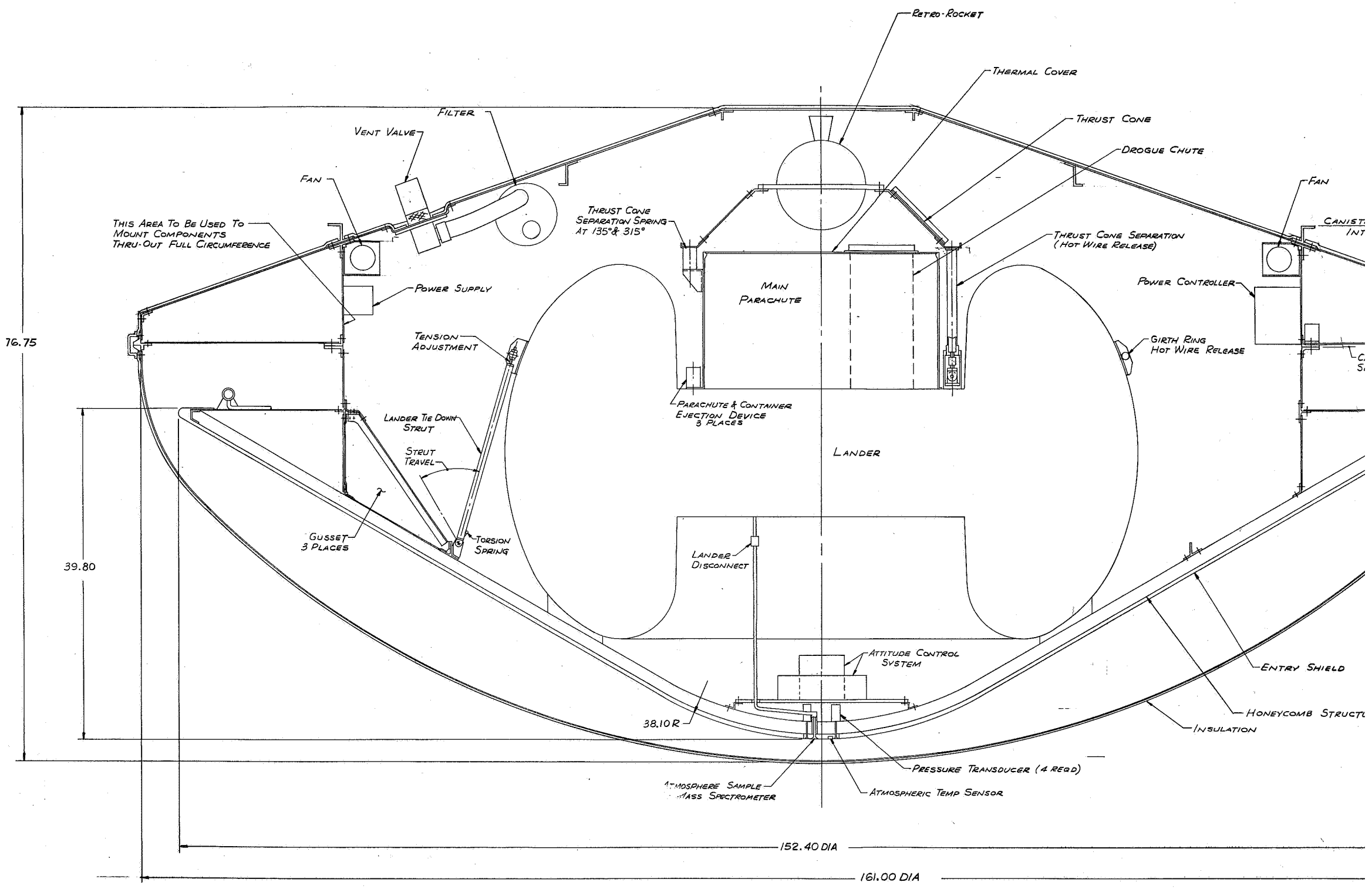
The Functional Block Diagram, fig. 4.2.4-1 is the complete system delineation of events from launch until the end of the mission. Each functional component is located with respect to functional criteria.

The horizontal axis can be considered a relative time axis with each mission phase occupying a discrete time segment. Each segment, however, does not represent a linear time scale since the total cumulative length would become unreasonable. The time axis then, indicates the sequence of events rather than the time at which they occur. Whenever components operate in multiple events, either the primary event or the typical mode of operation is indicated. Although the component location indicates the relative beginning of the event, the duration, repetitive rate or the stop time of the event is not indicated.

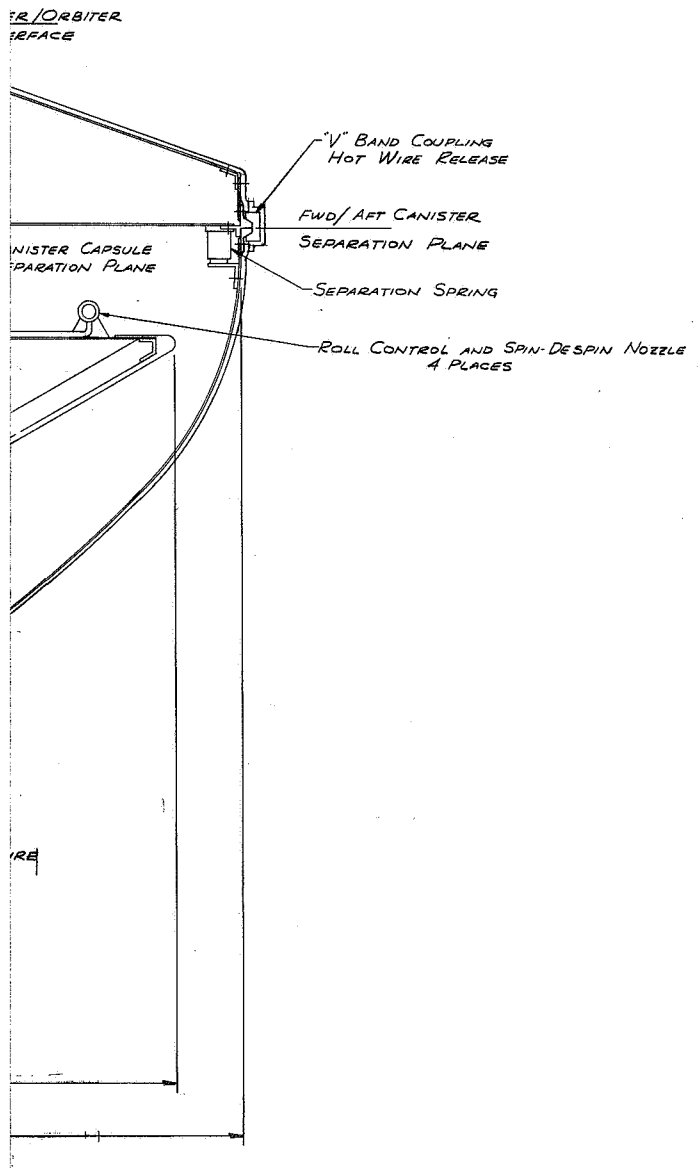
The vertical axis is used to group the components by subsystem. The subsystem groupings, indicated on both the right and left hand borders, is maintained throughout the drawing. Therefore, for any given event, all components within the system used to perform that event will be shown within the same vertical time boundaries designated at the borders, and the components within a given subsystem are aligned from top to bottom in order of the first function of operation.

The interrelationship of the components has been separated into four classifications as indicated on the drawing: (1) unregulated power; (2) regulated power; (3) signals; and (4) data. For clarity, components are shown with the most meaningful functions indicated. For example, On/Off signals are often considered to originate by correct power switching and are thus designated by a power flow line rather than a signal line. Furthermore, each individual line may carry one or more similar functions, such as different power levels.

FOLDOUT FRAME 1



SECTION A1-A1
SCALE 1/4



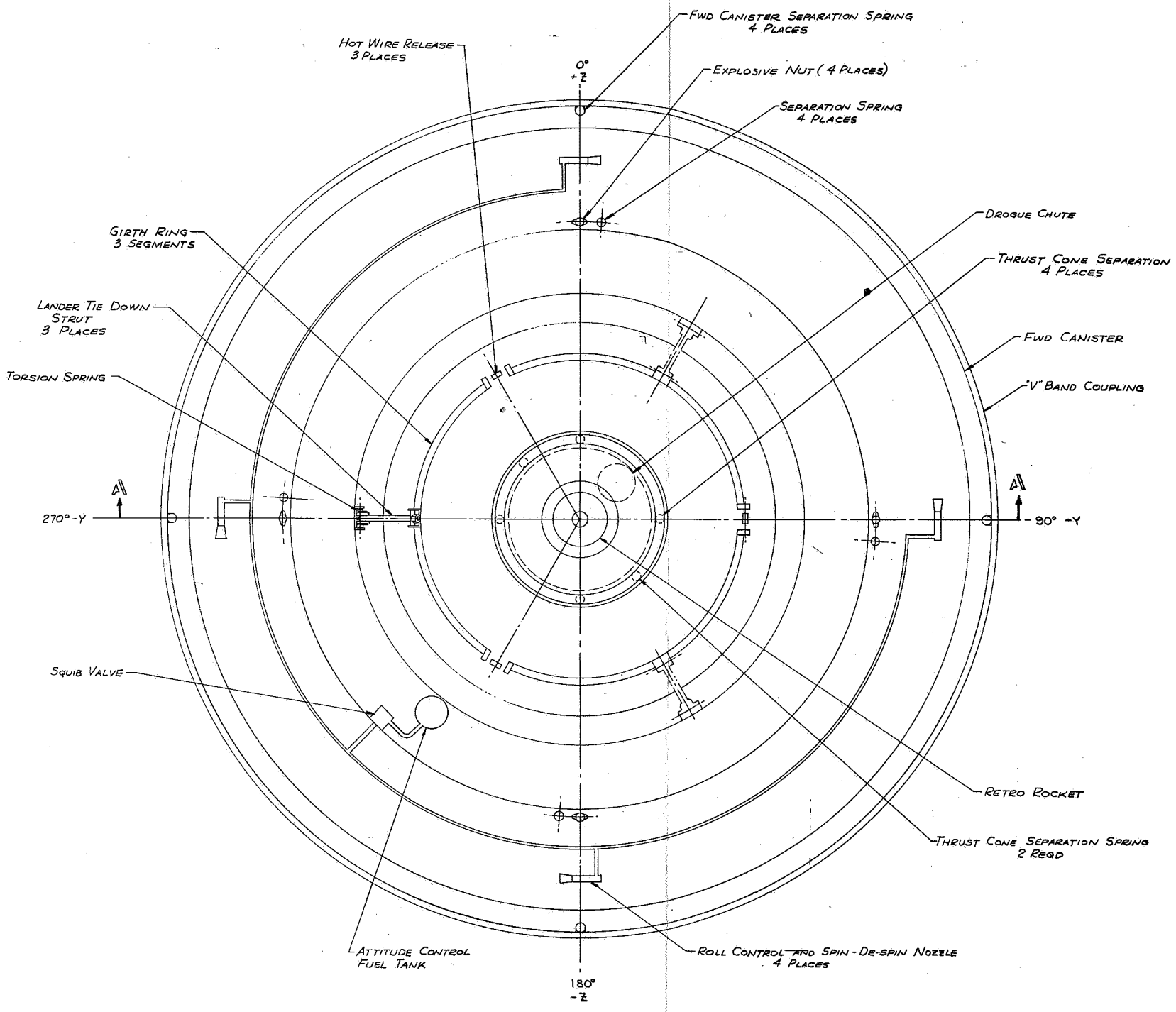
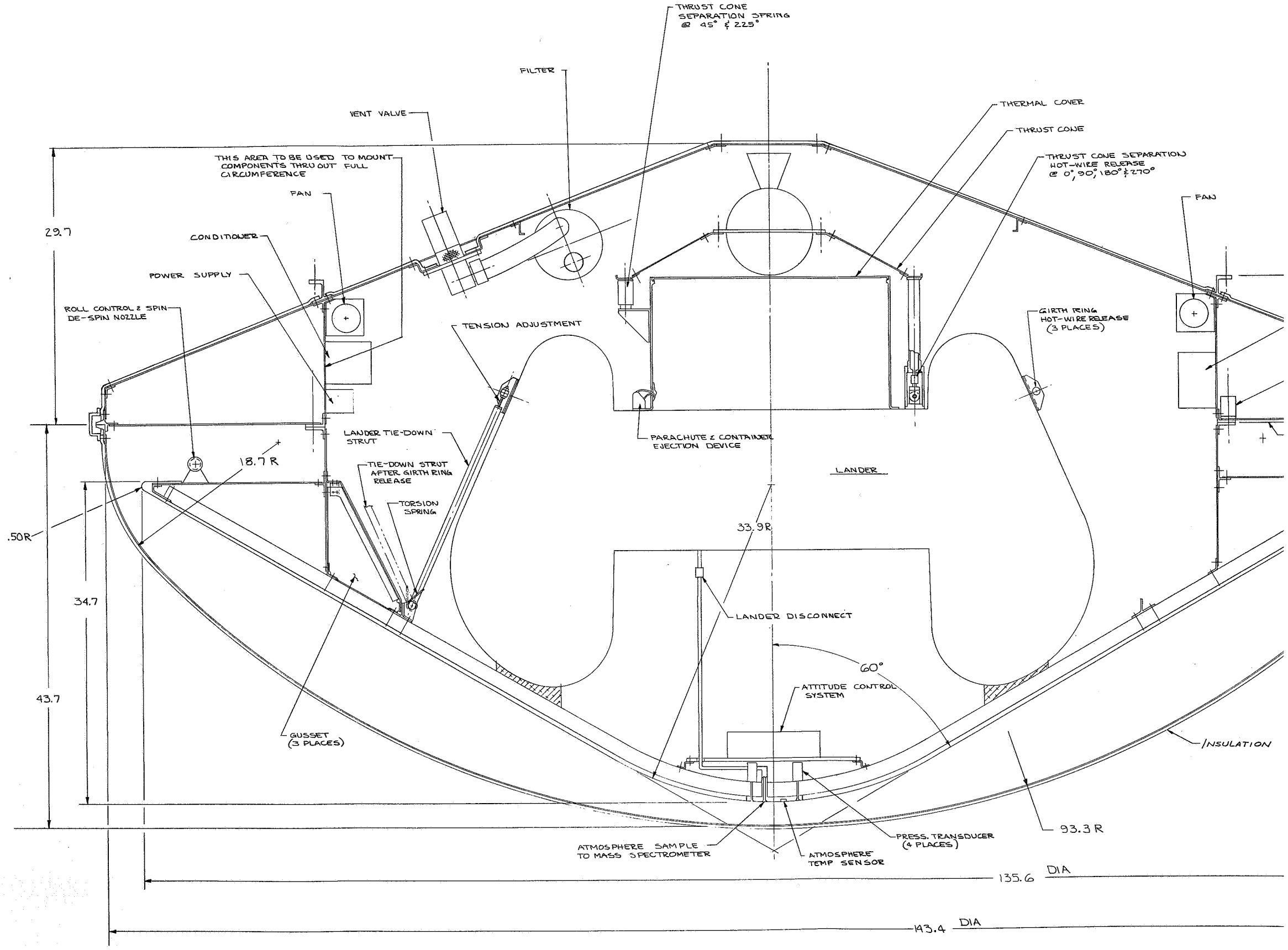


Figure 4.2.2-1 Mars Hard Lander, Point Design 2A

FOLDOUT FRAME 1



FOLDOUT FRAME 2

FOLDOUT FRAME

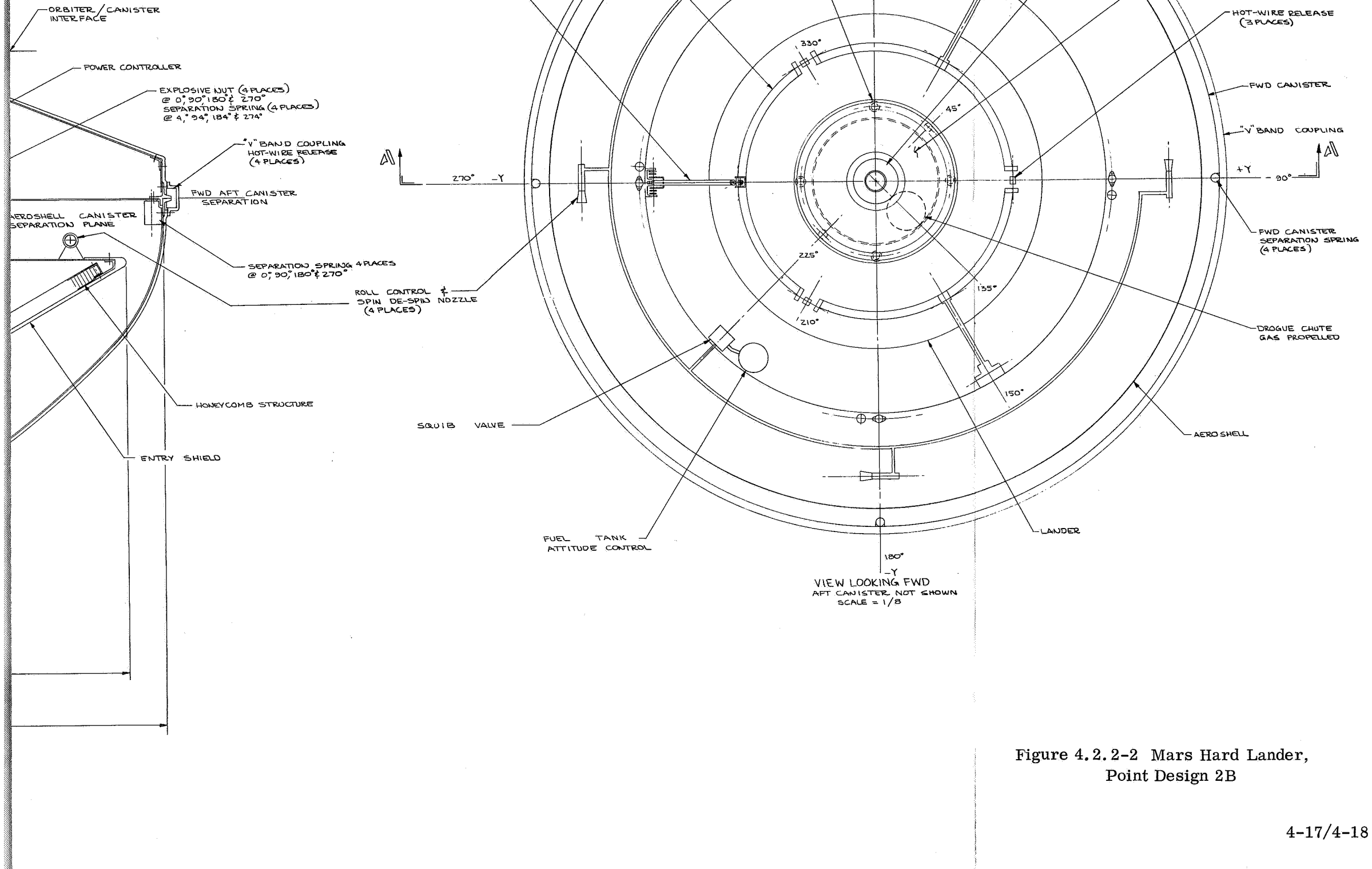


Figure 4.2.2-2 Mars Hard Lander, Point Design 2B

FOLDOUT FRAME

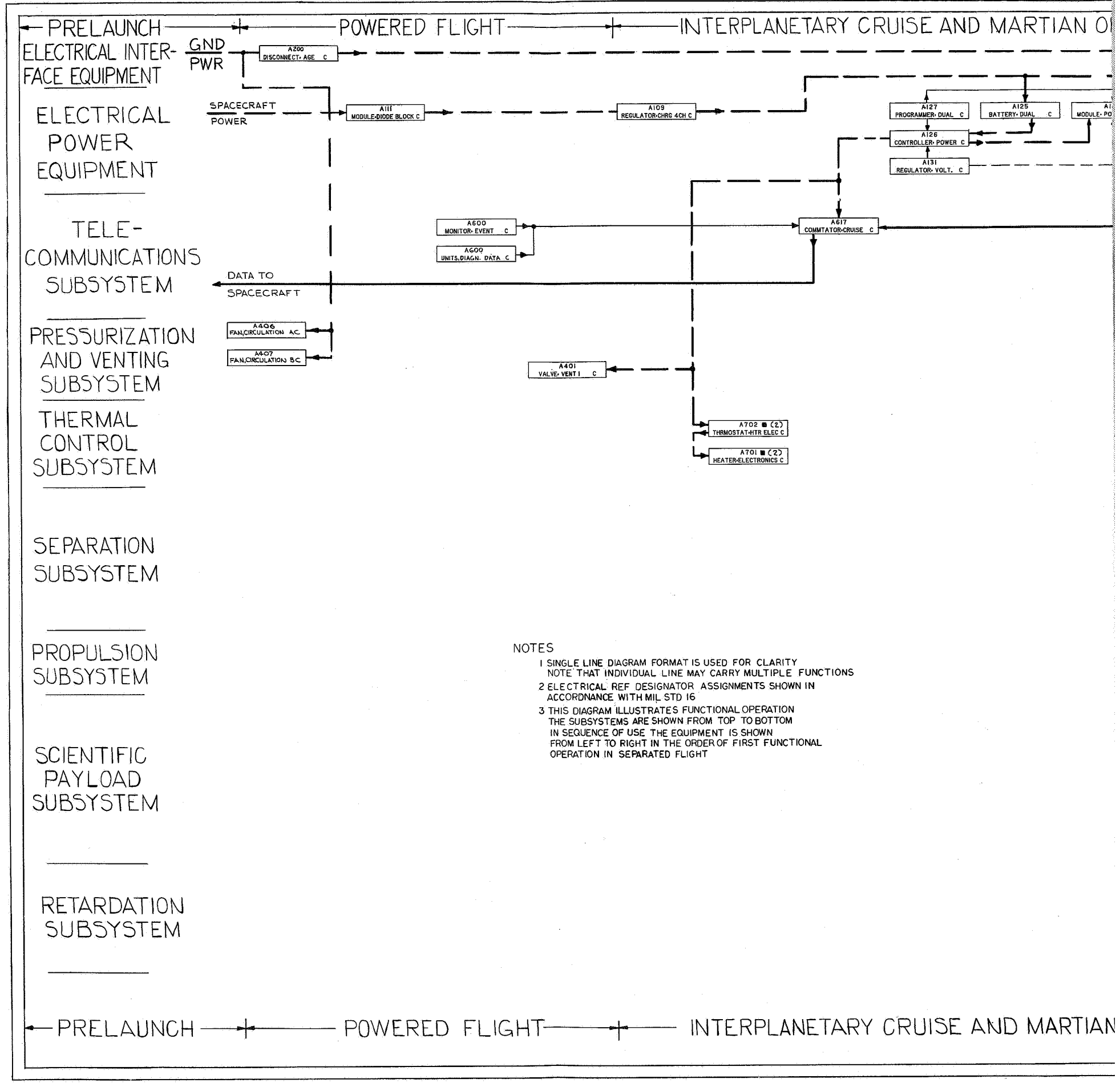


Figure 4.2.4-1. Electrical System Signal and Power, Functional Block Diagram, Point Design 2 (Sheet 1 of 2)

FOLDOUT FRAME 2

ORBITAL FLIGHT — SEPARATION PHASE — DEBOOST PHASE

A107 PROGRAMMER- LANDER L
A101 BATTERY-OPERATNL L
A110 CONTROLLER-POWER L
A106 SWITCH-PWR TRANSFR L
A130 REGULATOR- VOLT. B L
A157 A CONTROLLER, PRE-ENTRY
A108 REGULATOR-VOLTA L
A117 FILTER, EMC B C
A156 A BATTERY, PRE- ENTRY
A132 UNIT- BRKR + LIMT L
A158 A MODULE, DIODE, BLCK A
A116 FILTER-EMC A C
A605 ANTENNA-UHF RELY A L
A602 TRANSMITTER- UHF L
A611 CIRCULATOR, UHF B L
A610 CIRCULATOR, UHF A L
A623 B L ANTENNA, UHF RELAY
A621 SWITCH, ANTENNA AL
A681 ANTENNA, PARASITIC C
A515 ■ (4) RELEASE, HT WIRE C
A509 ■ (4) NUT, EXPL. A C
A518 GYRO, RATE A
A519 VALVE, SQUIB A
A520 ■ (2) VALVE, SOLENOID A
A200 IFD- CAP-S/C A
A103 BATTERY- ENTRY B T
A119 MODULE, DIODE, BLK A T
A102 BATTERY- ENTRY A T
A122 MODULE, THRM. RLY. A T
A105 BATTERY- THRST CN B T
A120 MODULE, DIODE, BLK B T
A104 BATTERY- THRST CN A T
A123 MODULE, THRM. R'LY B T
A600 MONITOR- EVENT L
A600 UNITS, DIAGN., DATA L
A307 INITIATOR, ROCKET T
A309 IGNITER PELLET T

LEGEND

■ ADDITIONAL. UNITS NOT SHOWN
UNREGULATED POWER FLOW
REGULATED POWER FLOW
SIGNAL PATH
DATA PATH

ORBITAL FLIGHT — SEPARATION PHASE — DEBOOST PHASE

FOLDOUT FRAME

ENTRY PHASE

A200
IFD, TC-LANDER L

A200
IFD A/S-LANDER L

IMF

A113
BATTERY, HI RATE A L

A121
MODULE, DIODE, BLKCA L

A124
MODULE, THRM. RLY C L

A114
BATTERY, HI RATE B L

A609
PROCESR-DATA HNDLG L

A604
CONDITIONR-SIGDATA L

A607
UNIT MEMORY L

A676
MULTICODER L

A501 ■ (4)
RELEASE, HT WIRE A T

A505 ■ (5)
RELEASE, HT WIRE A A

A324
UNIT, THRUST TERM T

A838
SPECTROMETER, MASS L

A807
ACCELEROMTR-TRI AX L

A801
TRANSDUCER-TEMP, S A

A802 ■ (2)
TRANSDUCER-TEMP, B A

A804 ■ (4)
TRANSDUCER-PRESS, S A

A805 ■ (2)
TRANSDUCER-PRESS, B A

A808 ■ (4)
TRANSDUCER-TEMP, I L

A809 ■ (2)
TRANSDUCER-PRES AT L

AG82
ACCELEROMTR-IMPC

AG83 ■ (3)
AMPLIFIER, CHARG

A501
"G" SWITCH ASSEMB L

A905
FITTING-DROGUE REL L

A902
MORTAR-DROGUE EJEC A

A903 ■ (3)
FITTING-MAIN REL A L

IMF

ENTRY PHASE

FOLDOUT FRAME 2

FOLDOUT FRAME

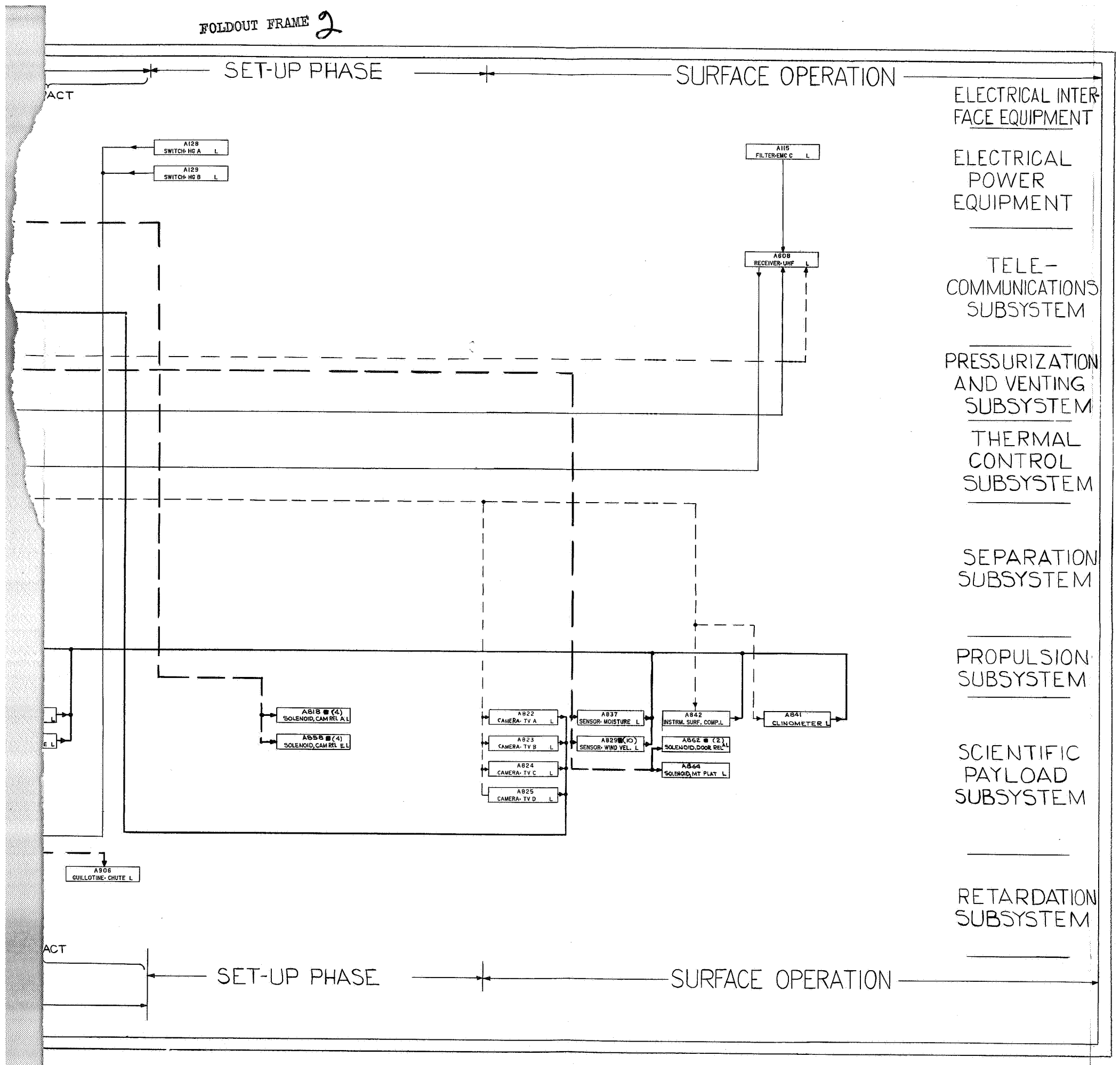


Figure 4.2.4-1. Electrical System Signal and Power, Functional Block Diagram, Point Design 2 (Sheet 2 of 2)

The components are represented by uniform blocks with a common notation. The electrical reference designator is assigned in accordance with MIL-STD-16. The component's name is listed below and the location of the component is noted by the appropriate letter abbreviation at the extreme right of the block.

The electrical connections between individual components and between subsystems is designed such that it allows the appropriate operations to be performed. By referring to Point Design 2 Block Diagram, fig. 4.2.4-1, it can be seen that for a particular event, such as UHF transmission, there exists a specific group of components that must operate. These components are linked by several of the function lines. The sequence of events and flow data can be traced as shown below. The appropriate type of power is switched through the power controller. This signal is supplied by the Lander programmer which initiates the power controller switching of all components required for the transmission of the data, whether in the electrical, telecommunication or scientific payload subsystem. The correct interconnections then allow data flow from the science subsystem to the telemetry subsystem.

Although other events require a different series of components, the relationship of component functional line designations to events is similar. A separation event is preceded by the Lander programmer signalling the power controller which turns on the stepping switch and connects the capacitor discharge circuit. These then supply the pulse loads as required.

Similar interconnections exist for all other events and the same scheme of functional operations is carried throughout the drawing. These component/subsystem relationships then become the foundation for the harnesses that physically supply the required electrical interconnections.

4.2.5 POWER PROFILES, POINT DESIGN 2

The power profiles, as illustrated in fig. 4.2.5-1, represent the power demand sequence on the operational and pre-entry batteries. By relating these demands to the event times, the curves reflect the mission sequence of events since each pulse is the power required by all the components operating at the event.

Superimposed on a continuous level of power are the various events. The operational battery is activated prior to Capsule/spacecraft separation. It then supplies the required power for telemetry transmission during de-orbit and entry. In addition, entry science data is transmitted until impact.

After impact, the UHF relay link transmits the stored data with a real time imagery period. The meteorological sampling period begins at 20 min intervals with clinometer readings every 6 hr. The surface composition instrument represents the relatively high continuous power level during the first day. The diurnal day concludes with another UHF relay transmission of stored transmission data and real time imagery.

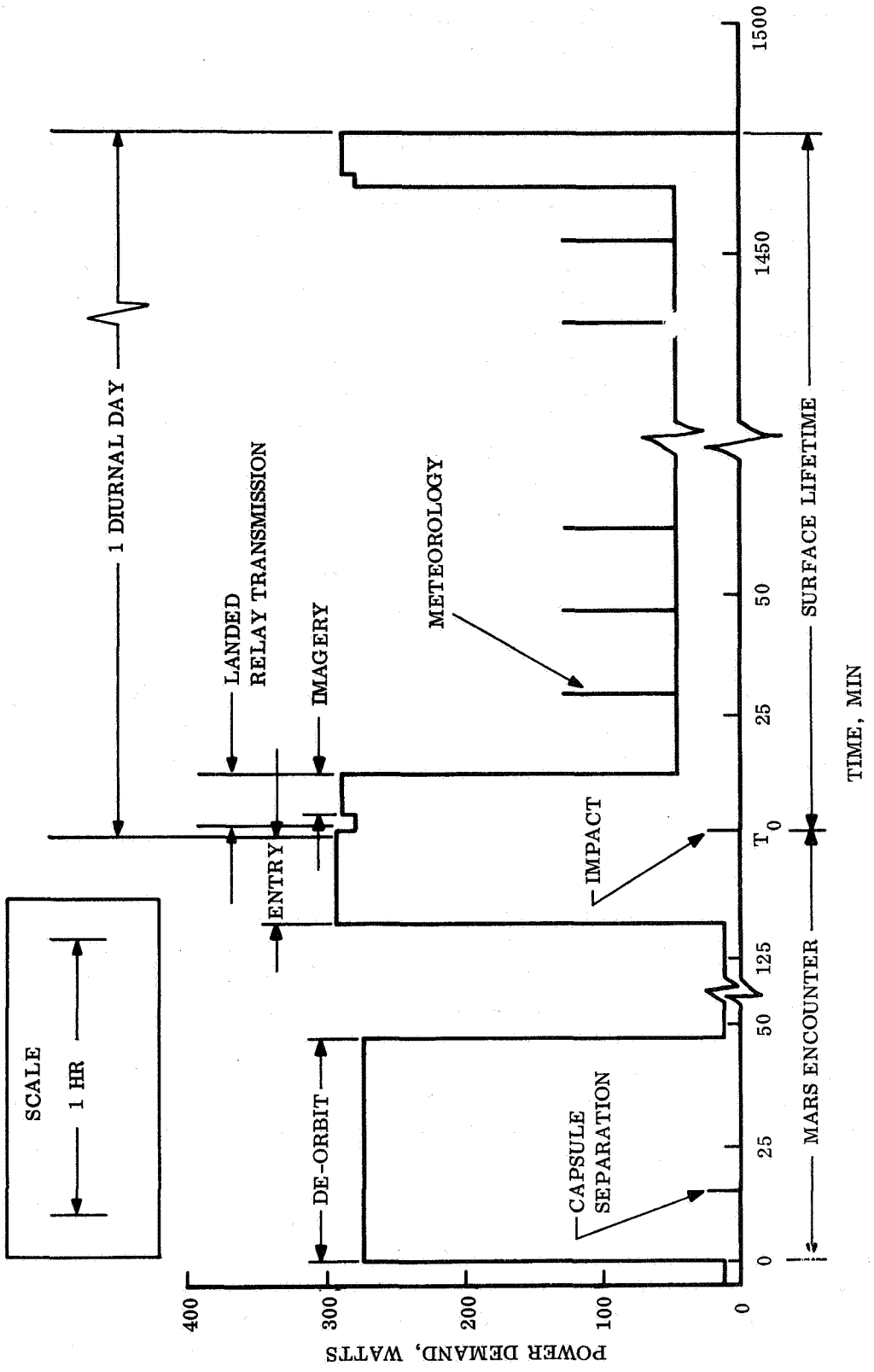


Figure 4.2.5-1. Power Profile, Point Design 2 (Nominal Mission)

4.3 PRE-ENTRY SYSTEMS

4.3.1 CANISTER

4.3.1.1 Design Constraints

Canister design constraints for Point Designs 2A and 2B were as follows:

1. Maximum diameter less than specified in Section 2.3.1 (175.6 in.)
2. Withstand an internal pressure
3. Withstand the inertial loads of launch and powered flight
4. Provide adequate clearance between the aeroshell heat shield and canister
5. Provide a separation and field joint as one and the same joint
6. Provide support for the entry system.

Diameter constraints on the maximum allowable canister diameter were fully described in Section 2.3.1 and were imposed by the internal envelope available for the Capsule system installation.

Due to the requirement to maintain biological integrity within the internal portion of the canister it was necessary to evaluate the effects of an internal pressure on the shape, material and construction of both the forward and aft canisters. Inertial loading of the canister during flight and handling conditions, including equipment loadings on the aft canister, was a constraint which was traded off against the differential pressure to determine the more severe loading environment for the canister structure.

A driving influence on the canister size was the allowance necessary for clearances between the entry system and canister. This clearance has been estimated to be 2.0 in. as shown in fig. 4.3.1-1, to allow for Capsule system dynamic excursions.

The field joint for the canister could be combined with the device used for inflight separation or it could be entirely separated. Maximum leak tightness was an overriding criteria in either case.

The entry system must be supported within the Capsule system and a means of support had to be designed. This design also considered that in addition to support it must have the capability of withstanding and transfering the entry system inertia loads through the structure and to the Capsule bus interface to the bus adapter ring.

4.3.1.2 Canister Structural Description

The forward canister for Point Designs 2A and 2B is a hemispherically shaped minimum gauge aluminum shell making a tangent at its maximum diameter through a quarter torus section, figs. 4.3.1-2 and -3. This structure has been designed to

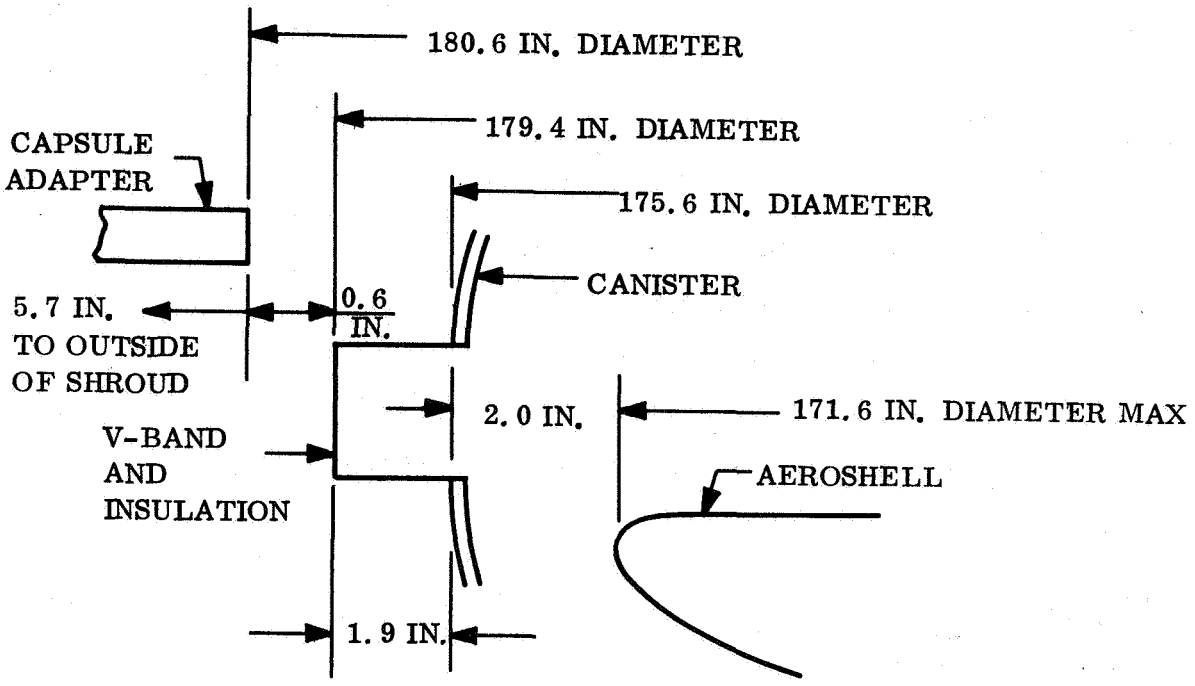


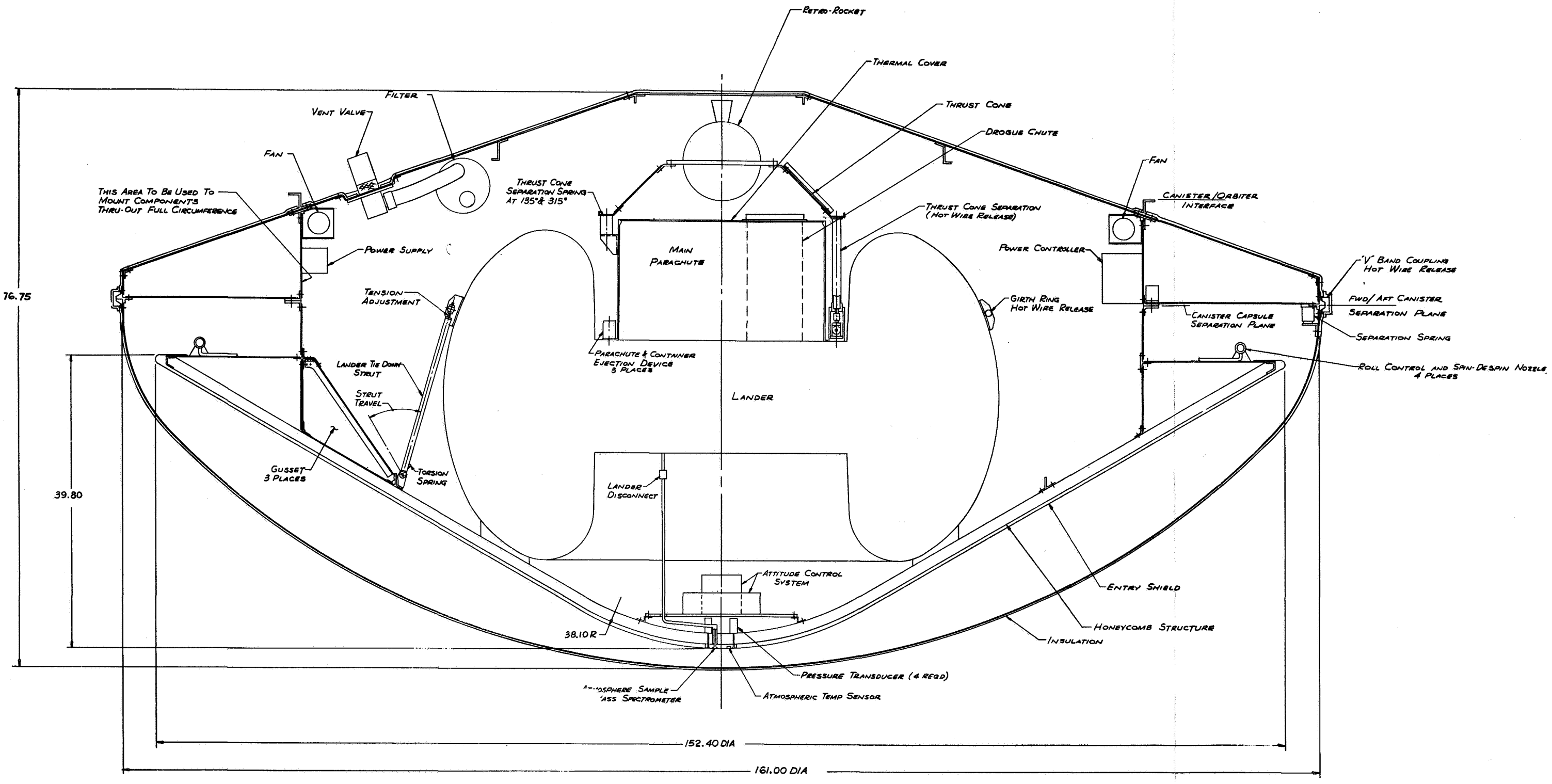
Figure 4.3.1-1. Aeroshell/Canister Clearances

act as a pressure vessel and the torus section provided to eliminate the inboard kick loads and minimize shell bending at the field joint ring due to the internal pressure. The minimum gauge aluminum material is more than adequate to withstand the pressurization and inertial loads imposed on it. The hemispherical shape has been proven in previous analyses (Voyager Phase B Study) to be considerably stiffer from a dynamic standpoint than a conical shape.

The forward canister has been designed such that there will be no yielding under design load conditions and no failure under ultimate design load conditions. This includes the transient and steady state loads encountered under the conditions of handling, transportation, sterilization, pre-flight, powered flight, transit and separation.

Inertial loading conditions were determined to be less severe than the internal pressurization condition in the design of the canister and the field joint ring. This can be seen in table 4.3.1-1 where the running loads on the interface ring are tabulated for both inertial and pressure loading conditions. As a result, the pressure loading condition determined the desired construction, material and thicknesses to be used in the structural design of both the forward and aft canister.

FOLDOUT FRAME



SECTION A-A
SCALE 1/4

Figure 4.3.1-2. Inboard Profile, Point Design 2A

FOLDOUT FRAME

FOLDOUT FRAME

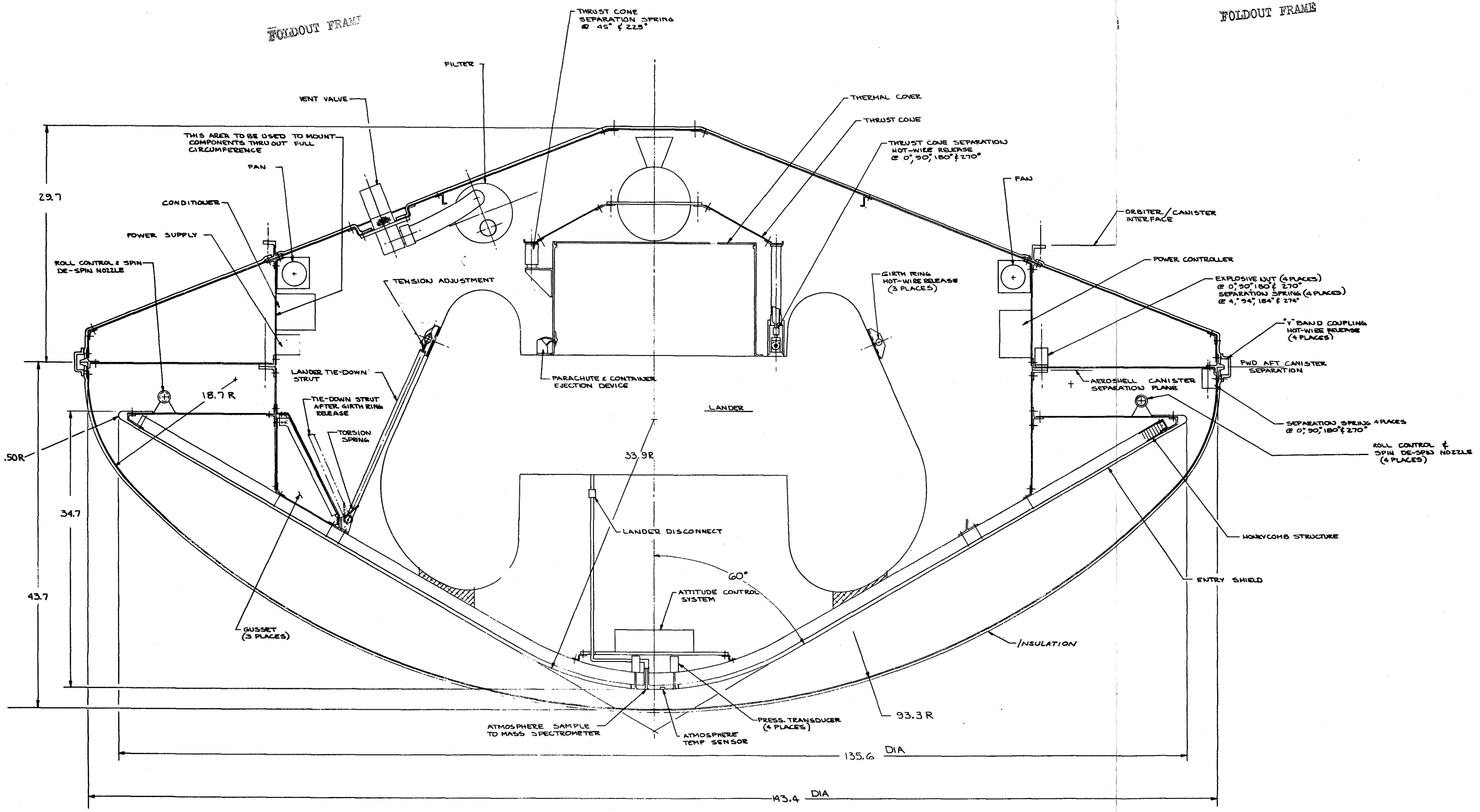


Figure 4.3.1-3. Inboard Profile, Point Design 2B

TABLE 4.3.1-1. INTERFACE RING LOADS

Load Condition	Vertical Load W_V (lb/in.)		Inboard (horizontal) Load W_H (lb/in.)		
	2A	2B	2A	2B	
C	1.59	1.42	0.57	0.51	
E	2.87	2.57	0	0	
F	0.45	0.40	2.87	2.51	
C & F	4.46	4.0	0.57	0.51	
C & F	2.06	1.85	3.39	3.04	
M	41.65	37.65	0	0	0.5 psi skin pressure
N	83.30	74.56	0	0	1.0 psi skin pressure

Minimum sheet gauges were the over-riding constraints on the thicknesses selected for the canister design. Stiffeners to rigidize the shell for dynamic and ground handling loads have been provided. The limit pressure condition for the canister is 1.0 psid internal pressure and the structure is adequate to withstand a 1.7 psi burst pressure which results in a safety factor of 1.7 on the limit pressure.

The field joint rings for the forward and aft canisters provide a seat for the band clamp, which holds the canister halves together, resist the loads imposed by the internal pressure and the band clamp and provide for the pressure-tight sealing of the canister assembly. The aft canister ring slides under the forward mating ring and has an internal leg, as shown in fig. 4.3.1-4, which is connected to a bulkhead joining the ring with the internal adapter. This arrangement provides a torque box in the aft canister increasing both its stiffness and structural load carrying capability.

The combined inertia of the forward ring, aft rings and bulkhead is more than adequate to insure structural stability of the field joint under the critical load condition. Figure 4.3.1-5 shows a plot of the required inertias for ring stability as a function of critical load in lb/in.

Structurally the aft canister is sized for the internal pressure which dictates the same minimum sheet gauge as the forward canister. The aft canister is essentially conical in shape, with the forward end a quarter torus making a tangent with the maximum diameter and the conical afterbody as shown in figs. 4.3.1-2 and -3. Stiffening members are located between the adapter to canister ring and the end bulkhead ring. These members also act as supports for the electrical equipment and venting system equipment in the aft canister.

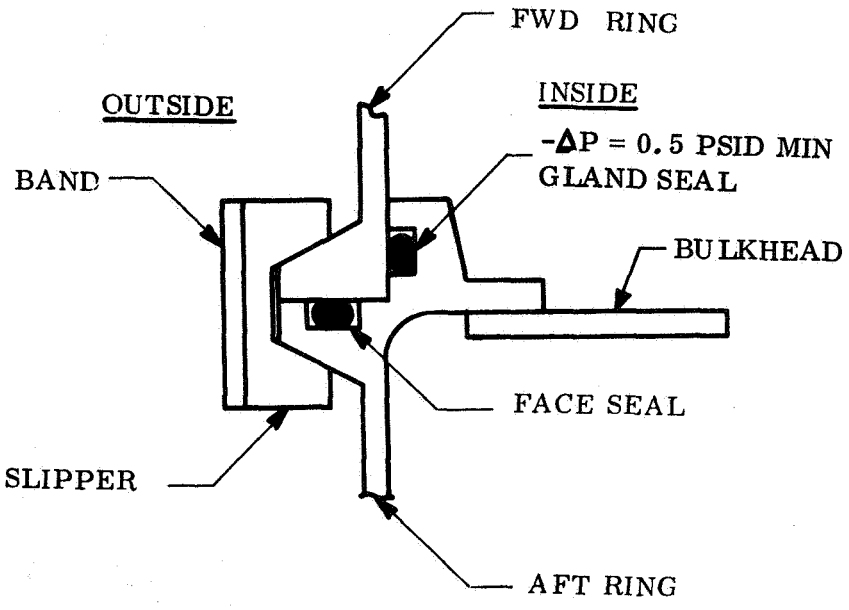


Figure 4.3.1-4. Canister Field Joint

4.3.1.3 Internal Adapter

The adapter for Point Designs 2A and 2B is designed to support the entry system and transfer loads introduced by the entry system to the Capsule bus inter-ring. This adapter is internal to the sterilization canister and interfaces with it at the aft canister ring. The adapter picks up the entry system at four points and attaches to the Capsule bus interface ring through the canister skin.

Structurally the internal adapter is a cylindrical aluminum shell with longitudinal stiffeners as shown in fig. 4.3.1-2. The shell and stiffeners have been sized such that the section modulus and working area are more than adequate to withstand bending moment and axial loads which the structure will experience. The inertial loads used in determining the necessary section properties of the cylindrical skin and stiffeners were 6 g's limit in the axial direction and 2 g's limit in the lateral direction.

The forward ring, at the entry vehicle interface, attaches to a lateral interconnection to the aft canister interface ring. Lightening holes have been placed in the cylindrical structure to allow for free passage of heated gases between the canister and adapter during heat sterilization cycles. The lateral interconnection or bulkhead provides support for the aft canister ring as well as the adapter.

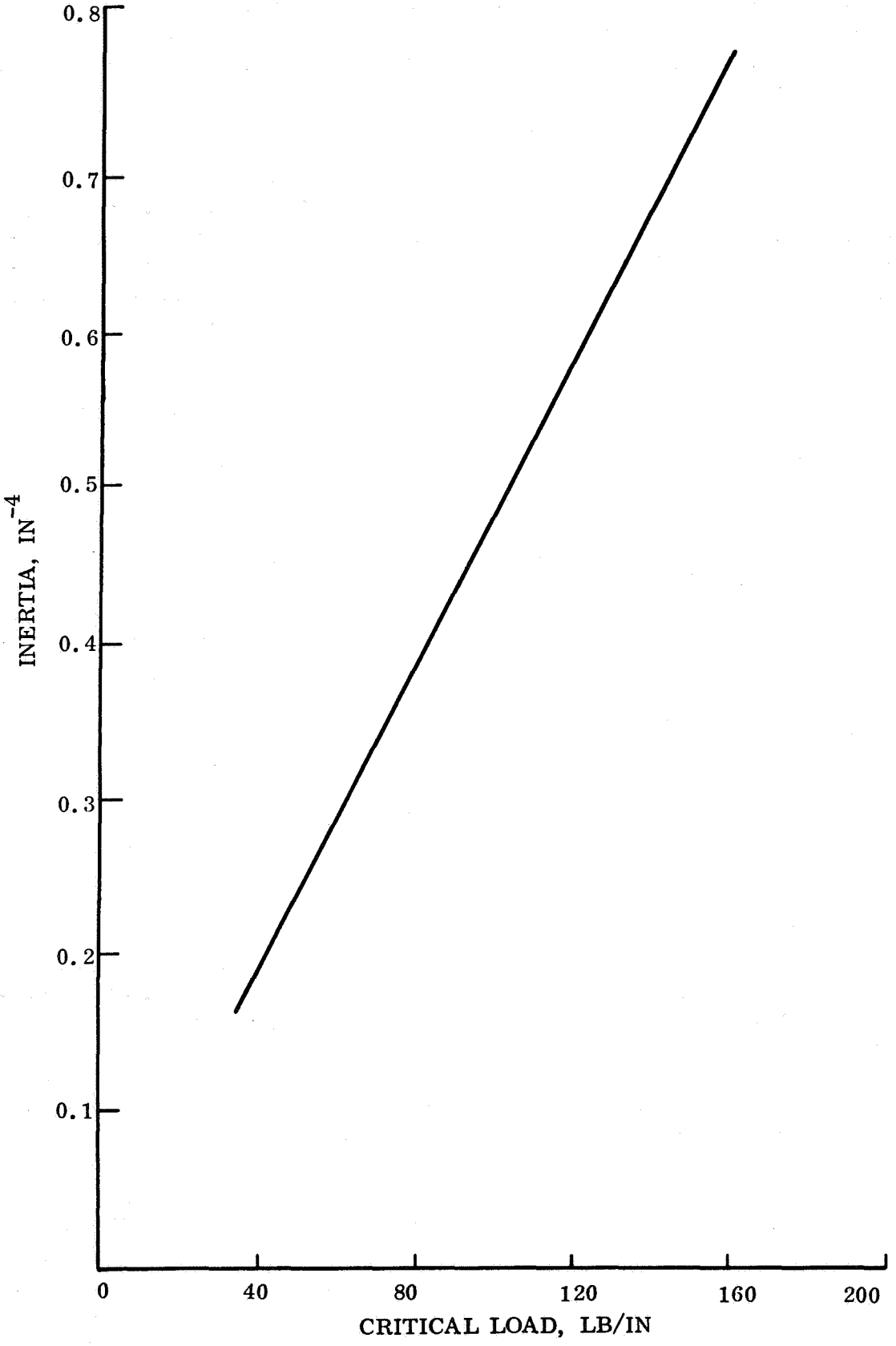


Figure 4.3.1-5. Required Ring Inertia for Stability as a Function of Critical Load

The spring-pusher housing is located on the inside of the adapter at the interface with the entry system. This device provides the separation force necessary to eject the entry system from the bus. Separation forces are reacted through the adapter skin and stiffeners.

4.3.2 PRESSURE AND VENTING SYSTEM

The basic function of the pressure and venting (P&V) system for Point Design 2 is to prevent recontamination of the Capsule by maintaining a minimum specified differential pressure (ΔP) between the canister and the ambient environment. This positive ΔP is maintained from sterilization until prior to canister separation.

4.3.2.1 Design Constraints

The P&V system has been designed to meet the following design constraints:

1. Provide inlet and outlet ports into the canister for sterilization
2. Provide circulation of air during sterilization
3. Provide pressure relief - due to temperature variations
4. Maintain a positive ΔP between 0.5 and 1.0 lb/in.^{2} differential (psid) between the canister and ambient atmosphere from sterilization until exit from Earth's atmosphere.
5. Vent 350 ft^3 of internal air during ascent for Point Design 2A and 220 ft^3 of internal air for Point Design 2B
6. Evacuate all entrapped gases to ambient space vacuum.

4.3.2.2 System Description

The primary function of the P&V system is to vent the internal canister during sterilization, after sterilization, and during flight to prevent the internal pressure from exceeding 1 psid. This is accomplished using a combination relief valve with a solenoid override which opens at a nominal pressure of 15.6 psia with increasing pressure and closes at a nominal pressure of 15.3 psia with decreasing pressure. A biological filter is installed upstream of the valve to filter out any bacteria flowing upstream. Relief of a pressure buildup to a temperature increase is accomplished using the same valve described above.

The block diagram for Point Design 2 is shown in fig. 4.3.2-1. During sterilization, the P&V system provides for inlet and exit of sterilized gas (and decontaminating gases if used) by using a manually operated inlet valve connected to the sterile, filtered air supply, and electrically opening the vent valve for use as the outlet port. Since the gas will pass through the biological filter, it must be pre-filtered to prevent clogging of the prime flight filter. Two circulating fans are used to speed up the

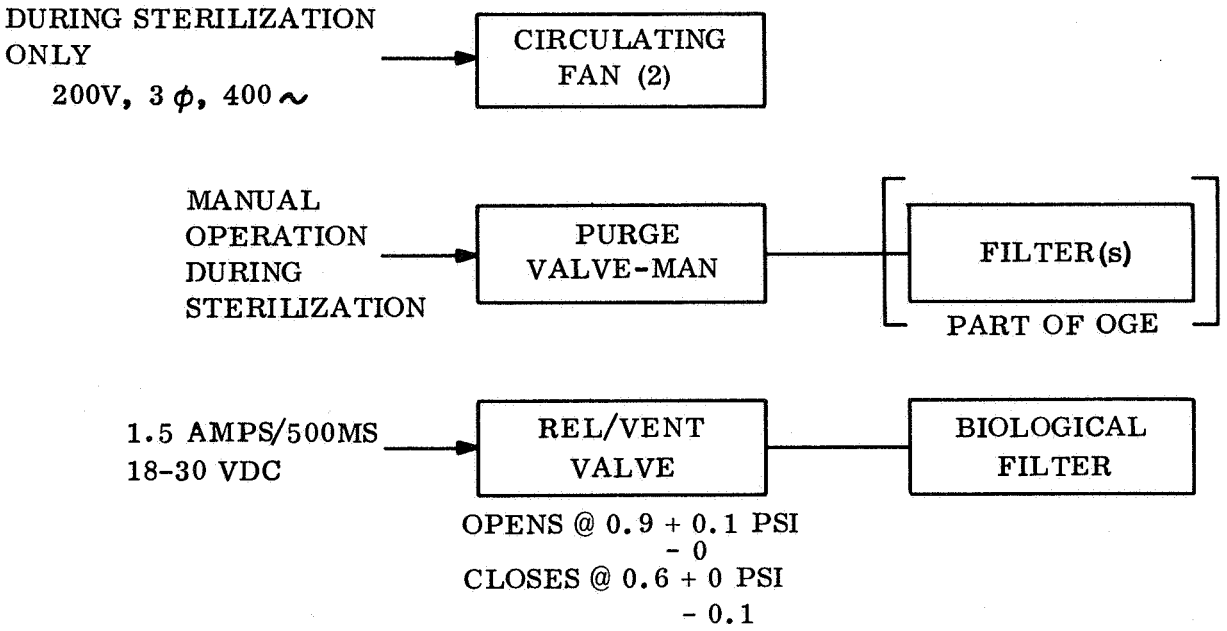


Figure 4.3.2-1. Pressure and Venting System, Block Diagram

heating and cooling cycles and to eliminate hot spots. These fans are used only during sterilization and their power will be provided by GSE. After sterilization, the makeup gas supply is connected to the manually operated valve. The canister is vented after launch and throughout powered flight until the canister reaches 0.5 psia.

The canister remains pressurized at ~0.5 psia less leakage, after exiting the Earth's atmosphere until prior to canister separation; at which time the vent valve will be electrically opened to evacuate to near space vacuum.

To minimize the possibility of backflow during venting, the exit port from the canister is shaped as a convergent nozzle. It has been shown that in a convergent nozzle flow separation does not occur. Thus, the possibility of gas flow upstream during venting is almost nil. This fact would preclude the entry of bacteria during the venting process when the valve is open.

4.3.2.2.1 Canister Venting

The vent valve is used to vent the canister during power flight. It's size is determined by the amount of gas and maximum permissible ΔP. For Point Design 2A there is an initial volume of 350 ft^3 of air while Point Design 2B has a volume of 220 ft^3 of air and the maximum allowable ΔP is 1 psid. The nominal fill pressure will

be 15.45 psia at 70°F. From the P&V parametric study, the vent area required for 350 ft^3 of air is 4.0 $in.^2$ and for 220 ft^3 of air is 2.4 $in.^2$; and assuming a C_D for the valve of 0.7, gives a required valve aperture equivalent to a 5.72 $in.^2$ circular orifice for Point Design 2A and a 3.43 $in.^2$ circular orifice for Point Design 2B.

The valve is a spring-loaded, pilot operated relief valve with a latching, override solenoid, and a position indicating switch. This valve design permits its use for relief, venting, purging and evacuation. The proposed design will be similar to Sterer P/N 19260, Pneumatic and Pressure Control Valve Assembly. The basic changes required to the valve relate to operating pressure and orifice area. The reference valve weighed 3.0 lb and it is estimated that the proposed valve will weigh 6.0 lb for 2A and 5.0 lb for 2B. Electrical power required for the solenoid is 1.5 amp at 30 vdc at 70°F for 1/2 sec maximum.

The outline of the proposed valve is:

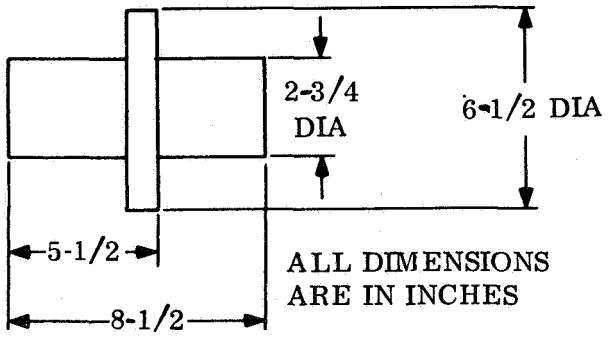


Fig. 4.3.2-2 shows the approximate ΔP time history for a valve that opened and remained opened. Obviously, this method will not meet the requirement for maintaining the $\Delta P > 0.5$ psid. The relief valve will act as a controller and it is expected that the valve will close in the cross-hatched portion of the curve. The valve will be set to open at $0.9\ ^{+0.1}_{-0}$ psid on increasing pressure and to close at $0.6\ ^{+0}_{-0.1}$ psid on decreasing pressure. The valve will most likely cycle several times during the first 20 sec and remain open until L.O. +90, after which time will remain closed until opened prior to canister separation.

The biological filter is used to prevent bacteria migration into the Capsule through the vent valve. The filter is installed in series with the valve and upstream of it. The filter is required then, to filter bacteria (0.3 microns) in the backward direction while presenting a low pressure drop to the air being vented. The filter size is governed by the maximum flow, the pressure drop and the differential pressure (ΔP). The maximum calculated flow for Point Design 2A is (350 ft^3 of air) 0.53 lb/sec or 425 scfm. For the 1 psid ΔP system and a specified pressure drop of 0.1 psi, a filter area of approximately 12 ft^2 is required. Using Pall Corporation's Ultipor 0.9 medium, an element size of 9.0 in. long x 6.2 in. diameter is obtained. The filter assembly will be 10.25 in. long x 7.5 in. diameter and would weigh approximately 4.0 lb. The maximum calculated flow for Point Design 2B (220 ft^3 of air) was 0.36 lb/sec or 282 scfm. For 1 psid ΔP system and a specified pressure drop of 0.1 psi, a filter area

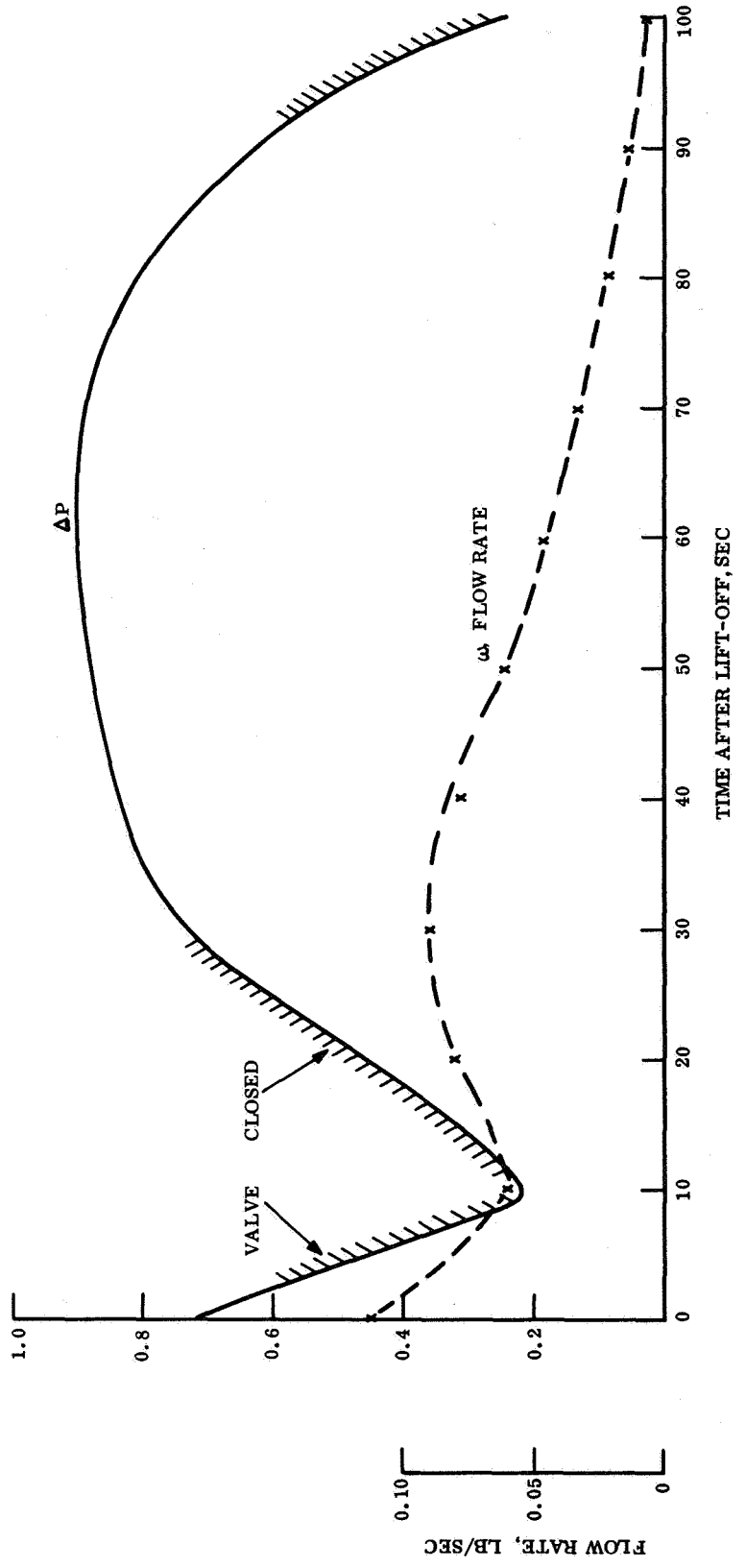


Figure 4.3.2-2. Flow Rate and Differential Pressure vs Time after Lift-off

of 8 ft^2 is required. Using Pall Corporation's Ultipor 0.9 medium, an element size of 5.5 in. long x 6.2 in. diameter is obtained. The filter assembly will be 6.75 in. long x 7.2 in. diameter and would weigh approximately 2.6 lb.

The choice of Ultipor 0.9 was made because it presents a lower pressure drop than Ultipor 0.15, while satisfying the filtering requirements. It has a catalog rating of 100 percent removal of -0.08 micron particles in dry air. The filter can be decontaminated with ETO and has a temperature rating of 350°F in air.

To maintain the necessary flow, the filter housing required 2-1/2 in. ports for 2A and 2 in. ports for 2B and will be connected to the vent valve with 2-1/2 in. aluminum tubing for 2A and 2 in. aluminum tubing for 2B.

4.3.2.2.2 Canister Sterilization

During canister sterilization, air will be introduced into the canister to speed up heating or cooling through the manually operated valve. Using 1-3/8 in. tubing for 2A and 1 in. tubing for 2B and a valve with an area of 1.25 $in.^2$ for 2A and 0.80 $in.^2$ for 2B, 27 cfm of air for 2A and 17.3 cfm of air for 2B can be introduced at 1 psid (15.7 psia), thus the canister air will be changed 4 + times in 1 hr.

Two fans, Rotron Manufacturing Co. type AXIMAX 3 for 2A and AXIMAX 2 for 2B, with a delivery of 150 cfm and 50 cfm respectively at 1 in. H_2O SP will be used to circulate air during sterilization for Point Designs 2A and 2B, thus reducing warm-up times, eliminating hot spots, and insuring that the entire Capsule reaches sterilization temperature.

Power required for the fans will be provided by OGE and shall be as follows: 200v, 3ϕ, 400~, 0.41 amp line current per motor for 2A and 200v, 3ϕ, 400~, 0.14 amp line current per motor for 2B.

Fan size is 3.0 in. diameter 2-5/16 in. long and weight 14 oz for 2A and 2.0 in. diameter by 1.5 in. long with a weight of 4.5 oz for 2B.

4.3.3 SEPARATION SUBSYSTEM

4.3.3.1 Design Constraints, Functions and Requirements

The separation subsystem performs the following pre-entry functions:

1. Separation of the forward canister
2. Separation of the Capsule assembly
3. Separation of the thrust cone assembly
4. Separation of the aeroshell.

The subsystem has been designed to meet the following requirements in addition to the usual environmental criteria:

1. Provide field and separation joints for the canister

2. Eject the canister at 2.5 ± 0.3 fps

3. Maintain a pressure-tight joint from sterilization through exit from the earth's atmosphere for a maximum internal pressure of 1.67 psid. Pressure tight is defined as leakage which results in less than 0.002 psi drop/hr at $70^{\circ}F$

4. Maintain maximum attainable pressure tightness during space cruise where outside temperature may be as low as $-300^{\circ}F$

5. Maintain sterility of Capsule

6. Separation shall not produce debris or loose objects

7. Attach the Capsule at four points

8. Eject the Capsule at 1.5 ± 0.25 fps separation velocity from a bus with tip-off rates of $< 0.5^{\circ}$/sec to the Capsule. Bus pitch inertia is equal to the Capsule's

9. Separation shall not cause collision with any of the remaining payload

10. Attach and separate the thrust cone at 1.0 fps minimum

11. Attach and release the aeroshell

12. Provide electrical separation as required

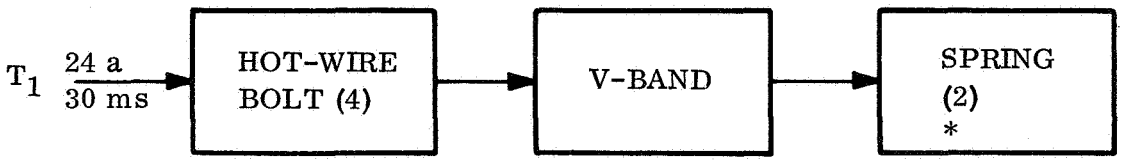
13. Optimum reliability and subsystem performance is paramount to mission success. Use proven concepts.

Other system constraints - electrical power, distribution, timing, and signal lockout shall be provided by the EP&D S/S.

4.3.3.2 General Subsystem Description (See Block Diagram, fig. 4.3.3-1)

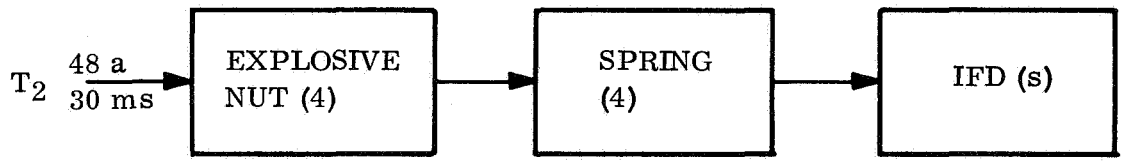
The canister halves of both Point Designs 2A and 2B are joined by a V-band assembly consisting of independent slippers attached to a strap. The band is made in four equal segments joined by hot-wire tension bolts. The hot-wire bolt is a non-pyrotechnic, mechanical device consisting of a turnbuckle coupling which separates when an electrical signal is applied to a hot-wire element which kept the turnbuckle together. The forward canister is ejected using four helical coil compression springs. The rings, to which the V-band clamps, perform double duty by providing the groove

FWD CANISTER SEPARATION

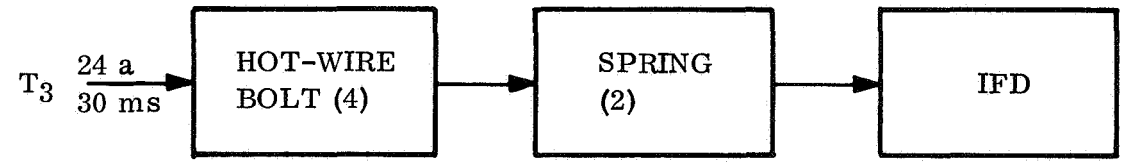


* 4 SPRINGS FOR POINT DESIGNS 2A, 2B, 4, 6

CAPSULE SEPARATION



THRUST CONE SEPARATION



AEROSHELL SEPARATION

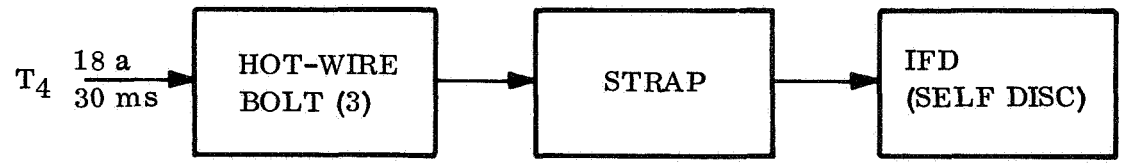


Figure 4.3.3-1. Separation Subsystem, Block Diagram

and sealing surfaces for the O-ring type pressure seal. After separation, the V-band segments remain attached to the aft canister via springs and lanyards. The canister is completely evacuated by the P&V S/S prior to separation.

The Capsule assembly is separated from the Orbiter approximately 10 min after canister separation. The Capsule is attached to the adapter at four points by explosive nuts, but a hot-wire type of coupling is also being investigated. The Capsule is ejected at 1.4 fps for 2A and 1.6 fps for 2B nominally, by four helical coil compression springs.

The thrust cone assembly is attached to the Lander/aeroshell assembly by four hot-wire tension bolts, identical to the ones used on the V-band. Two helical coil compression springs identical to the ones used for canister ejection are used to eject the thrust cone at 3.3 fps nominally for 2A and 3.5 fps nominally for 2B. The thrust cone is separated after the de-orbit function is completed.

The aeroshell is attached to the Lander by a strap assembly retained by three hot-wire tension bolts and released after parachute deployment. This system is described in Volume IV, Section 4.4.5.

The weight of the subsystem as described above based on an 13.6 ft diameter canister for 2A and a 12.2 ft diameter canister for 2B are:

	Point Design 2A	Point Design 2B
Canister		
V-band assembly	14.3	11.7
4 hot-wire bolts	0.8	0.8
4 springs	0.4	0.4
4 spring housings, adjustable	1.4	1.4
Capsule		
4 explosive nuts	1.0	1.0
4 springs	0.8	0.8
4 spring housings, adjustable	1.4	1.4
Thrust Cone		
4 hot-wire bolts	1.0	1.0
2 springs	0.2	0.2
Aeroshell		
1 strap	1.2	1.2
3 hot-wire bolts	0.6	0.6
TOTAL	23.1 lb	20.5 lb

The following sections discuss the detail designs.

4.3.3.2.1 Canister Separation

The selection of the separation method for the canister is governed by the requirement for a sterile, pressure-tight joint for a large, flexible structure. This basic requirement limits the separation joint design to one that can apply a continuously distributed force, such as flexible shape charge, various types of MDC or primer cord, V-bands, closely spaced bolted joint, pyro fuze joint system or a thermal heat pad system. The V-band system was selected because of its simplicity, reliability, low separation shock, lack of debris, tolerance to temperature environment, elimination of the need for a field joint, and presentation of a tortuous path for microbial access to the separation interface.

The band must meet the following specific requirements:

1. Contain proof pressure without yielding

2. Provide the necessary clamping force without yielding

3. Contain the burst pressure without breaking

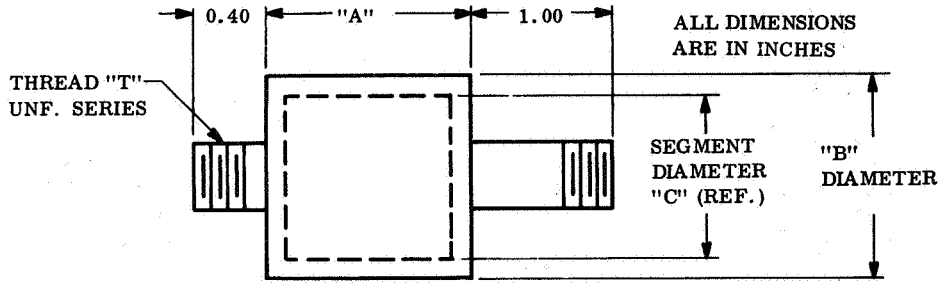
4. Make allowance for creep at low temperature over a 9 month period.

The V-band assembly is made in four segments, with the strap material being 2024T86 Aluminum, 1 in. wide x 0.072 in. thick for 2A and 0.064 in. thick for 2B. The slippers, which are attached to the band by clips, are made of 7075T73 aluminum. The band is preloaded to 2360 lb ± 10 percent for 2 A and 1980 lb ± 10 percent for 2 B in order to sustain all loads, allow for creep during cruise, and allow for tension variations during assembly. (See Volume III, Appendix B for load and stresses in band.)

The V-band segments are held in tension by the four hot-wire* bolt assemblies. The choice of four points for attaching and torquing was made to maintain nearly uniform tension on the entire band and to facilitate band disengagement. The hot-wire bolt is a mechanical separation device which utilizes the reduction of tensile strength property of a material upon heating to actuate. Upon application of 6 amp for 30 msec the hot-wire element breaks and separation occurs. The hot-wire bolt consists of two separate studs connected by a segmented coupling. The coupling is held together by the hot-wire element, so that tension can be carried by the mechanism.

The required preload can be applied through 1/2 in. diameter thread and a 1.30 in. O.D. coupling (see fig. 4.3.3-2) made of 17-4 PH, Cond 1050, with an ultimate load capacity of 19,000 lb tension. Nine turns of .014 in. diameter 302 stainless wire form the hot-wire element. The segments of the coupling are retained so that there is no debris. This unit is ideal for long service in space because of its all metal design. The band will separate if any of the four bolts operate.

* The hot-wire bolt is a GE-RS proprietary design.



MAX LOAD (LB)	PHYSICAL DATA				HOT WIRE DATA				
	A	B	T	C	WIRE DIA	NOTCH DIA	NO. OF TURNS	A.F. CURRENT	WT LB
8000	0.90	1.00	3/8	0.69	0.014	0.0040	9	6.0	0.20
12,000	1.15	1.32	7/16	1.00	0.020	0.0660	11	9.0	0.44
19,000	1.40	1.62	1/2	1.30	0.025	0.0075	13	12.0	0.81

Figure 4.3.3-2. Hot-wire Tension Bolt

The forward canister is ejected by four helical coil compression springs. The springs provide 35 lb of initial force each and have a working stroke of 2 in. They will impart a velocity of 2.5 ± 0.25 fps to the 2A canister and 2.7 ± 0.25 fps to the 2B canister. The springs are of 302 stainless steel, stressed at 90 kpsi and are retained with the aft canister, in an adjustable subassembly. (See fig. 4.3.3-3.) Tip-off rates will be less than 2.0 deg/sec about any axis. Center-of-gravity offsets are expected to be minimal since the forward canister is of symmetric construction.

The canister separation joint seal utilizes two silicone rubber O-rings to attain a pressure-tight seal. The O-rings are used in two different modes to enhance sealing capabilities, one O-ring being a face seal and the other a gland seal (see fig. 4.3.1-4). This arrangement utilizes the axial and radial clamping forces of the V-band and closes off the clearances resulting from manufacturing tolerances, while retaining a machineable and structurally sound ring design. The basic cross-section is depicted in figs. 4.3.3-4 and -5 for the Point Design 2 ring. The face seal O-ring is nominally 0.139 in. diameter and is compressed from 0.014 to 0.041 in. The force necessary to compress this O-ring using 50 durometer silicone is from 1.2 to 12.0 lb/linear in. The gland seal is nominally 2.10 in. diameter and is compressed from 0.015 to 0.045 in. or 7 to 22 percent. The radial force to compress this ring is from 1 to 16 lb/linear in. The radial clamping force available if the nominal axial clamping force of 45.1 lb/in. for 2A is attained is,

$$FR = FN\,(TAN) = 45.1\ (TAN\ 20^{\circ}) = 16.4 \text{ lb/in.}$$

which is adequate for both point designs.

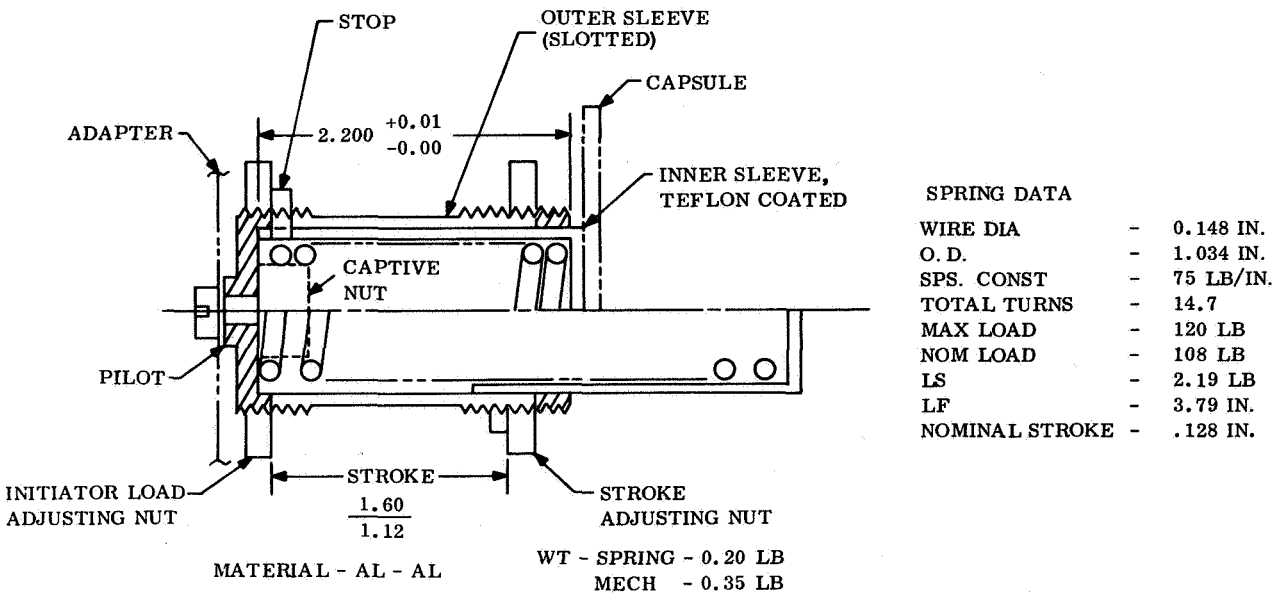


Figure 4.3.3-3. Capsule Separation Adjustable Spring Assembly

Silicone rubber material was selected because it has the best low temperature properties -- rated to -80°F for seals, but doesn't harden until -150 to -180° F. Therefore, it is expected that the seal will degrade during the space cruise. If it is mandatory that a seal be maintained, thermal insulation could be applied to the band to keep the temperature about -150° F.

The ability of the separation joint to inhibit the penetration of bacteria is further enhanced by the tortuous path which they must follow to gain entry into the Capsule. The slipper is in full contact with the ring except for a 1/4 in. gap between the 5-3/4 in. long slippers, or a total of 96 percent of the circumference is covered by the slippers. The band, of course, covers the entire circumference except at openings for the hot-wire bolts, which probably will be about 1-1/2 in. long each, or 94.5 percent band coverage.

4.3.3.2.2 Capsule Separation

The main consideration for Capsule separation and ejection was the stringent tip-off rate requirement. To meet this requirement, it is necessary that the impulse generated by the separation device be either very low or nearly the same at all points. Likewise, the ejection system must have controlled force and energy, with low variances; and lastly, c.g. offsets and ejection system force axes must be controlled.

Separation devices that meet the above needs are ball locks, collet releases, and explosive nuts. The later were chosen because of compactness and ease of use and installation. All of the above utilize pressure cartridges for operation, and for high reliability, dual cartridges will be used. This introduces the problem of wide impulse variance as a function of gas pressure (a function of cartridge design, simultaneity, and number of cartridges firing).

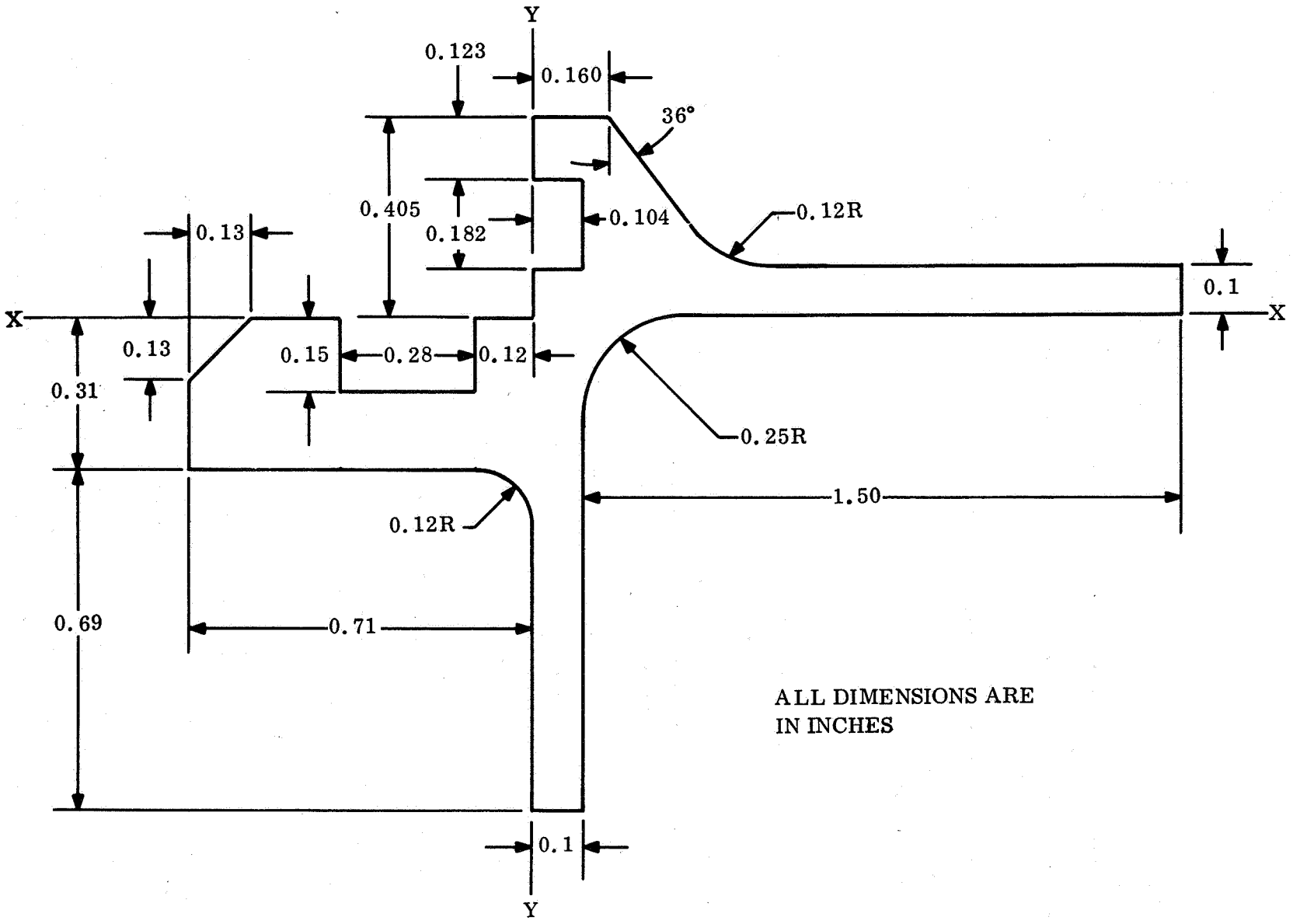


Figure 4.3.3-4. Aft Canister Ring

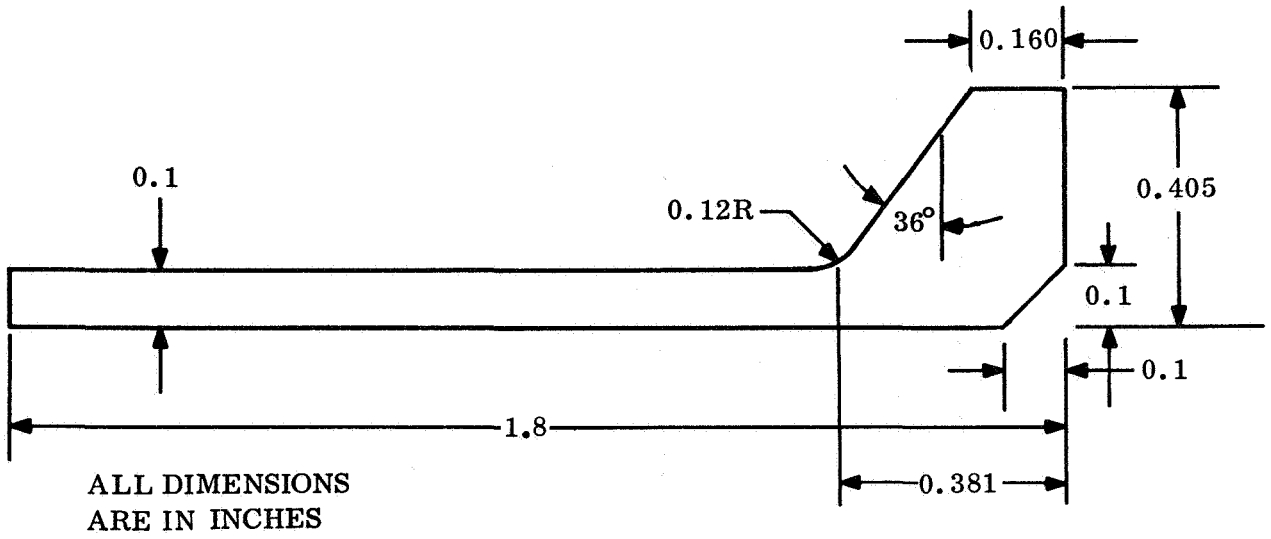


Figure 4.3.3-5. Forward Canister Ring

A non-pyrotechnic device, similar to the hot-wire tension bolt previously discussed, will be very seriously considered, because of obvious advantages. The main draw-back is that it is new and needs further development.

The ejection systems available are pneumatic pistons, pyrotechnic thrusters, reaction systems and springs. Springs were selected for their obvious simplicity. To minimize tip-off rates, the energy and force of the ejection system must be controlled. A guide/roller system may also be required if rates are too high. The proposed solution uses preset springs in an energy package, with selective assembly and gives a maximum tip-off rate of 0.20°/sec for 2A and 0.32°/sec for 2B when the maximum and minimum spring forces are combined with the worst case c.g. offset.

The Capsule is attached to the adapter by four 1/4 in. explosive nuts, each having dual cartridges. The explosive nut is of the captive type, with all loose pieces contained within the unit. The gas generated by the squibs is also contained. The choice of an explosive nut was made because of its reliability, capability for dual squib initiation, low weight, and high load carrying ability. The 1/4 in. size nut can carry the full load of a 1/4 in. 160,000 psi UTS bolt, which is 3600 lb. The applied limit load is 2800 lb for 2A and is 2200 lb for 2B and therefore there is ample margin. Four nuts were selected based on the four pick-up points on the structure.

Capsule ejection is accomplished by four helical coil compression springs. The springs exert a 108 lb force each, and have a working stroke of 1.28 in. The springs are stable ($L/D < 5$) and will impart a separation velocity of 1.4 ± 0.15 fps to the 2A Capsule and a velocity of 1.6 ± 0.15 fps to the 2B Capsule. Thus, the Capsule will

acquire a positive ΔV of 0.70 fps for 2A and 0.80 fps for 2B, whereas the forward canister was ejected at 2-1/2 fps for 2A and 2.7 fps for 2B. Tip-off imparted to the Capsule for 2A will be 0.24°/sec and 0.32°/sec for 2B obtained by trimming and selecting the springs. The Orbiter will acquire a negative or retrograde ΔV of 3/4 fps and a tip-off rate from 2A of 0.24°/sec and from 2B of 0.32°/sec as a result of Capsule separation. It was assumed that this small motion was not detrimental to the mission. (See Volume III, Appendix B for tip-off analysis.)

The spring assembly is shown in fig. 4.3.3-3. It provides for adjustment of initial load - one turn of the adjustment nut gives approximately a 2 lb load change - it provides for adjustment of total stroke, it retains the spring at the end of the stroke and provides a locating pilot. The inner sleeve is coated with teflon on both inner and outer surfaces to reduce friction. Operation of the spring over the inner 80 percent of its total possible stroke assures nearly constant spring rate.

The following summarize the recommended spring design (see table 4.3.3-1 for spring detail data).

Spring material - National Standard NS355 stainless steel

Ultimate tensile strength = 330,000 psi for up to 0.159 in. wire

Torsional shear - 45 percent x UTS = 148,000 psi

Initial load - 108 lb at 0.16 in. from solid

Final load - 12 lb at 1.44 in. from solid

Maximum load - 120 lb at solid height

Maximum stroke, Xm - 1.60 in.

Operating stroke - 1.60 - 20 percent (1.60) = 1.28:

Energy Required - 25.5 ft-lb

Energy Available - $\frac{(108 + 12)}{2} \frac{(1.28)}{12}$ (4 springs) = 25.6 ft-lb

Control spring rate to 75 (± 3 percent) lb/in

Adjust spring to 108 (± 2) lb initial load

Install springs, so that diametrically opposite springs have an initial load within 0.5 lb.

IFD's for electrical separation will be self disconnect type or electrically actuated, hot-wire type depending on size and location on the vehicle.

TABLE 4.3.3-1. SEPARATION SPRING DATA

	Canister	T/C	Capsule
Wire diameter (in.)	0.107	0.107	0.148
Mean coil diameter (in.)	1.07	1.07	1.034
Number of springs	2	2	4
Component length (in.)	1.29	1.29	2.35
Solid height (in.)	1.09	1.09	2.19
Free length (in.)	3.29	3.29	3.79
Total weight (lb)	0.17	0.17	0.80
Number of active coils	8.4	8.4	12.7
Stress ($lb/in.^2$)	90,000	90,000	110,000
Nominal ΔV (fps)	2.5	2.5	1.5

4.3.2.3 Thrust Cone Separation

The thrust cone for 2A and 2B is attached to the aeroshell/Lander by four 3/8 in. hot-wire tension bolts similar to those used in the V-band. The thrust cone is ejected at 3.5 fps using two helical coil compression springs identical to the ones used for canister separation. The springs remain with the thrust cone. IFD's for electrical separation will be of the spring self-disconnect type.

4.3.4 ENVIRONMENTAL CONTROL

Thermal control of the Lander components during interplanetary travel will be accomplished by insulating the Lander from the space environment and using heater power from the spacecraft to control the Lander temperatures. The insulated blanket will be a multi-radiation barrier type composed of a number of layers of either aluminized mylar or aluminum foils separated by an insulating material. An effective thermal conductivity of 1×10^{-4} Btu/hr-ft-°R was selected for this type of insulation. Definition of the insulation details and heater power requirements will be dependent on the surface radiative properties, payload allowable temperatures and canister surface area. A low emissivity coating (EoS = 0.1) on the outside insulation surface will be utilized to maintain minimum heat loss through the canister. From fig. 4.3.4-1, insulation and heater power requirements can be determined on a unit surface area basis for a compartment temperature requirement of 310°R. Total heater power can be evaluated from fig. 4.3.4-2 at the design values.

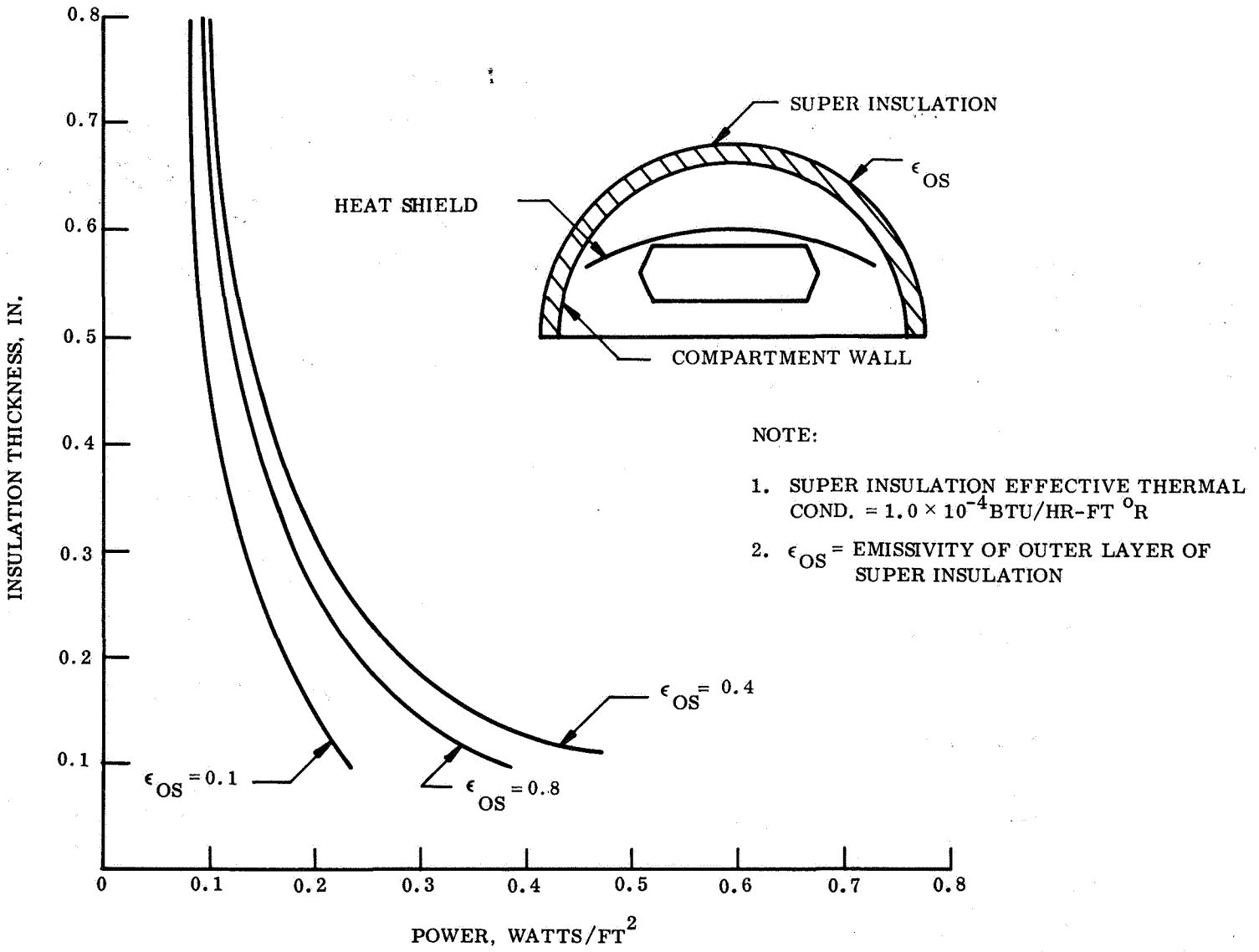


Figure 4.3.4-1. Super Insulation Requirements to Maintain 310°R on Compartment Wall and Heat Shield

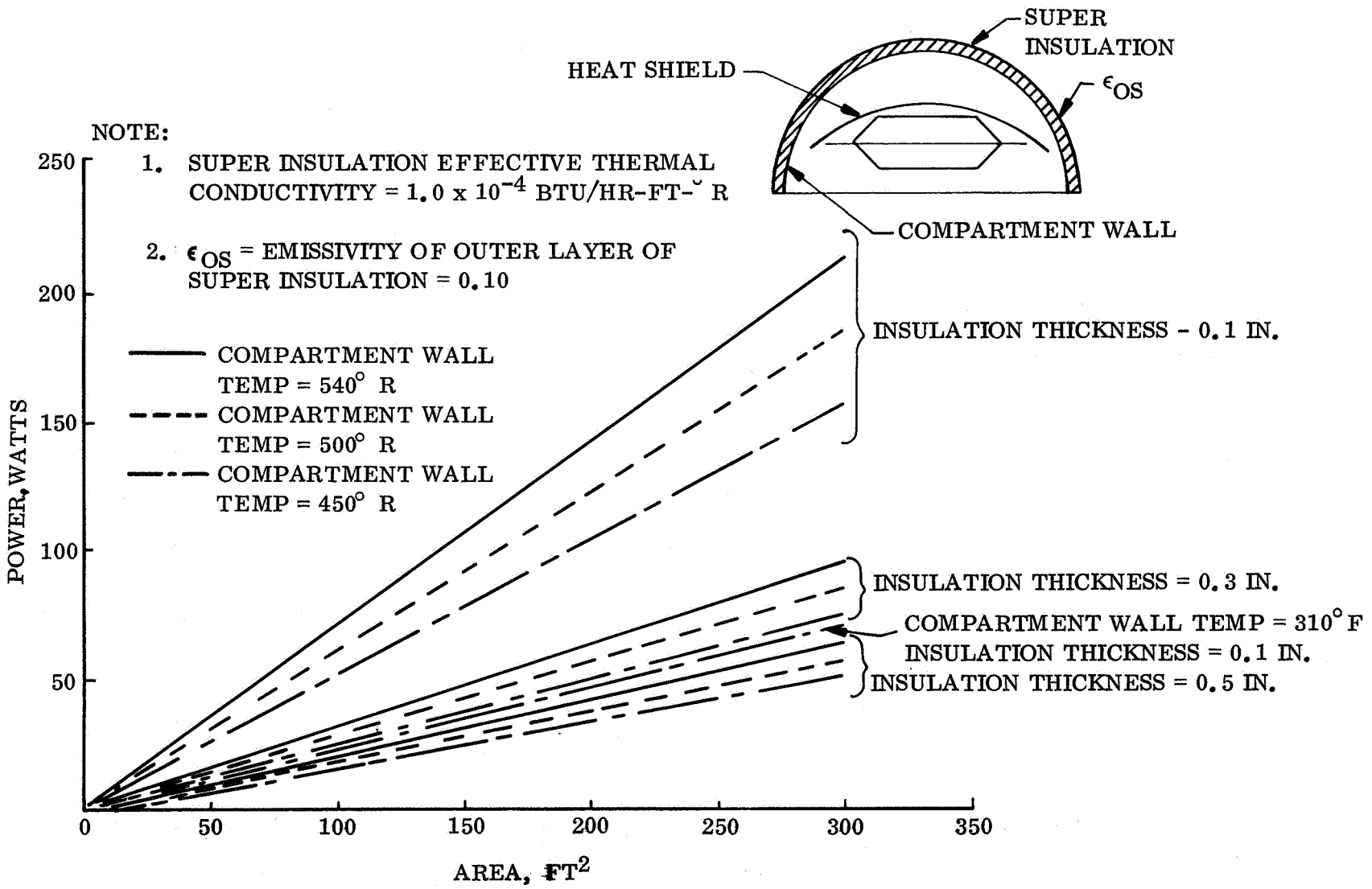


Figure 4.3.4-2. Transit Mode Power and Insulation Requirements for Various Canister Areas

4.3.5 DE-ORBIT PROPULSION SYSTEM

4.3.5.1 Design Constraints

The design constraints for the de-orbit propulsion system for Point Design 2 were as follows:

1. De-orbit weight of 1200 and 1560 lb (less propulsion)
2. Velocity increment 45 meters/sec
3. Motor burn time 20 to 30 sec
4. Solid propellant system.

4.3.5.2 Systems Description

4.3.5.2.1 De-orbit Propulsion Design Description

The selected propulsion equipment for Point Design 2 is a solid propellant system conforming to the requirements presented below. This portion of the report presents the performance data and system description of the selected de-orbit propulsion equipment.

The de-orbit propulsion system must impart a velocity increment of 45 meters/sec to a 1560 lb vehicle for 2A and a 1200 lb vehicle for 2B for direct planet entry at 20,000 ft/sec and 25° path angle. The vehicle weight does not include the propulsion system weight. Thrust termination is required and the system must be aligned to within ± 2° with respect to the principal axis. Motor burn time is to be approximately 20 to 30 sec.

The performance, weight, and basic envelope data is presented in table 4.3.5-1. The propellant weight shown in the table is useful propellant weight. Inert weights consist of the case, liner, insulation, nozzle, igniter, and thrust termination mechanism for the solid system. The velocity increment variation for the solid system has been estimated not to exceed plus or minus one meter/sec. Using statistical data obtained primarily from Minuteman motor firings, the variation in specific impulse was estimated at ± 0.338 percent (3-sigma). Propellant and inert weight variations can be held to limits approaching weighing system accuracies of ± 0.05 percent (3-sigma). Therefore, assuming no variation in payload weight, the resulting velocity increment variation is ± 0.34 percent (3-sigma), or less than plus or minus one meter/sec.

A representative solid propellant propulsion system as designed by Aerojet-General is shown in fig. 4.3.5-1. Major components include a case bonded, saturated, hydroxy terminated polybutadiene sterilizable propellant grain with a stress relief boot; a titanium alloy case; a single, fixed, semi-submerged nozzle, an epoxy-cured, saturated, polybutadiene insulation system, a BPN pellet igniter, and a shaped charge thrust termination unit which allows jettisoning the nozzle.

All materials and component configurations, except the propellant, have been used successfully for other solid rocket motors and the manufacturing and assembly techniques

TABLE 4.3.5-1. PERFORMANCE, WEIGHT, AND ENVELOPE DATA, POINT DESIGNS 2A AND 2B

	2A	2B
ΔV, meters/sec	45	45
Payload weight (lb) (less propulsion)	1560	1200
Total propulsion system weight (lb)	37.1	28.6
Propellant weight (lb)	29.3	22.5
Propulsion inert weight (lb)	7.8	6.1
Mass fraction (propellant weight/ total weight)	0.79	0.79
Propellant	ANB 3289-2	ANB 3289-2
I_{sp} vacuum (sec)	247.9	247.9
Nozzle expansion ratio	40	40
Total impulse (lb-sec)	7259	5584
Burn time (sec)	23.2	23.2
Thrust (total) (lb)	313	241
Approximate dimensions; case (spherical diameter in.)	10.2	9.3
Throat area	0.24	0.19

are well established. State-of-the-art inert materials and procedures will be used to fabricate and process the motor. The propellant is an 85 percent solid loaded propellant with a saturated hydrocarbon binder and stabilized ammonium perchlorate oxidizer recently developed by Aerojet-General for use in sterilizable motors.

ANB-3289-2 is a heat sterilizable propellant manufactured by Aerojet-General Corporation. It is formulated from stabilized ammonium perchlorate and a binder based on saturated hydroxy terminated polybutadiene binder cured with an isocyanate. Only slight changes in mechanical properties (with respect to a conventional propellant) were detected when 3 x 3 x 5 in. blocks of this propellant were exposed to six successive 53 hr exposures at 275° F in air.

Achievement of satisfactory heat sterilization performance requires the use of (1) a stable propellant formulation with good high temperature strength and stress relaxation properties and good flow and pot-life characteristics, and (2) controlled processing procedures which minimize defects in the cured grain or specimen.

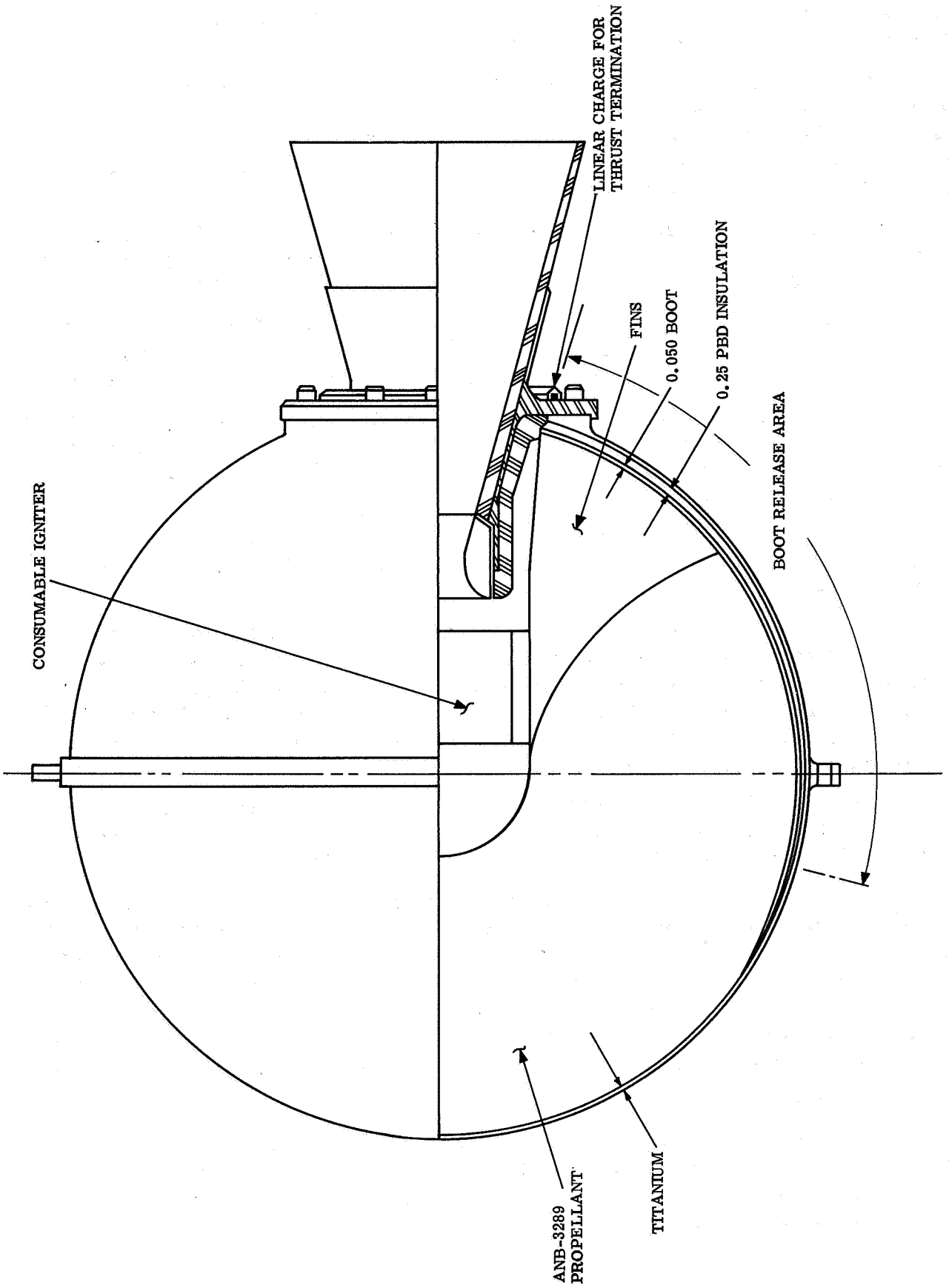


Figure 4.3.5-1. Solid Propellant System

The combination of the ANB-3289-2 binder system formulated at a high cross link density and a process based on vacuum stripped prepolymer, very dry oxidizer, high vacuum mixing and bayonet casting appears to satisfy all requirements.

The propellant grain configuration is designed to minimize stresses during sterilization heat cycling. The forward portion of the grain is case bonded and the aft end is released from the chamber by the release boot. Fins in the aft portion of the grain neutralize the progressive burning surface nature of the grain and provide a grain with low inner bore strains.

The selection of SD-850-2 liner was made on the basis of tests of the effect of heat sterilization on the bond strength of a saturated HTPB/aromatic isocyanate propellant. The bond strength appeared good and was not degraded by heat sterilization.

The motor case will be insulated with IBT insulation, a filled epoxy-cured, saturated, polybutadiene insulation system, developed by Aerojet-General especially for sterilization requirements. The propellant release boots are made of the same material.

The case is made of 6A1-4V titanium alloy, spun in halves and welded together. An increased thickness is provided in the weld area to compensate for reduced strength. A single aft opening is provided for attaching the nozzle and tabs are located at the equator for mounting the motor.

Since no opening is available at the forward end of the case, a phenolic boss is bonded to the center of the forward dome to act as a guide for locating the insulation installation tooling.

The nozzle consists of a forged titanium housing, graphite throat insert, silica-phenolic exit cone and IBT insulation on the outside of the submerged portion of the expansion cone. A circular shaped charge is mounted on the nozzle flange to release the nozzle when the thrust termination device is actuated. The angular displacement of the nozzle centerline with respect to the motor centerline is plus or minus 10 min and the radial displacement shall not exceed 0.030 in.

A consumable BPN pellet igniter will be used. The igniter, inserted into the bore of the propellant grain and bonded in place before the nozzle is installed, consists of a BPN pellet charge and an initiator in a foamed plastic housing.

Thrust termination is accomplished by releasing the nozzle from the chamber when the shaped charge is actuated to cut the nozzle flange. (This well-proven technique is currently used on the third stage Minuteman III to release the head end thrust termination ports.) The resultant vent area increase will be approximately 17 times the throat area. A case blowdown analysis shows that the motor will extinguish itself by a $\dot{P}$ extinguishment phenomena (rapid depressurization) in 18 msec when 50 percent of the propellant is consumed and in 28 msec when 99 percent of the propellant is consumed.

4.3.5.2.2 De-orbit Structure

The de-orbit propulsion system for Point Designs 2A and 2B is supported by an aluminum sheet metal thrust cone which is attached to the Lander cover by means of four tubular struts. Fig. 4.3.5-2 depicts the complete assembly and the associated attachments for both point designs.

FOLDOUT FRAME

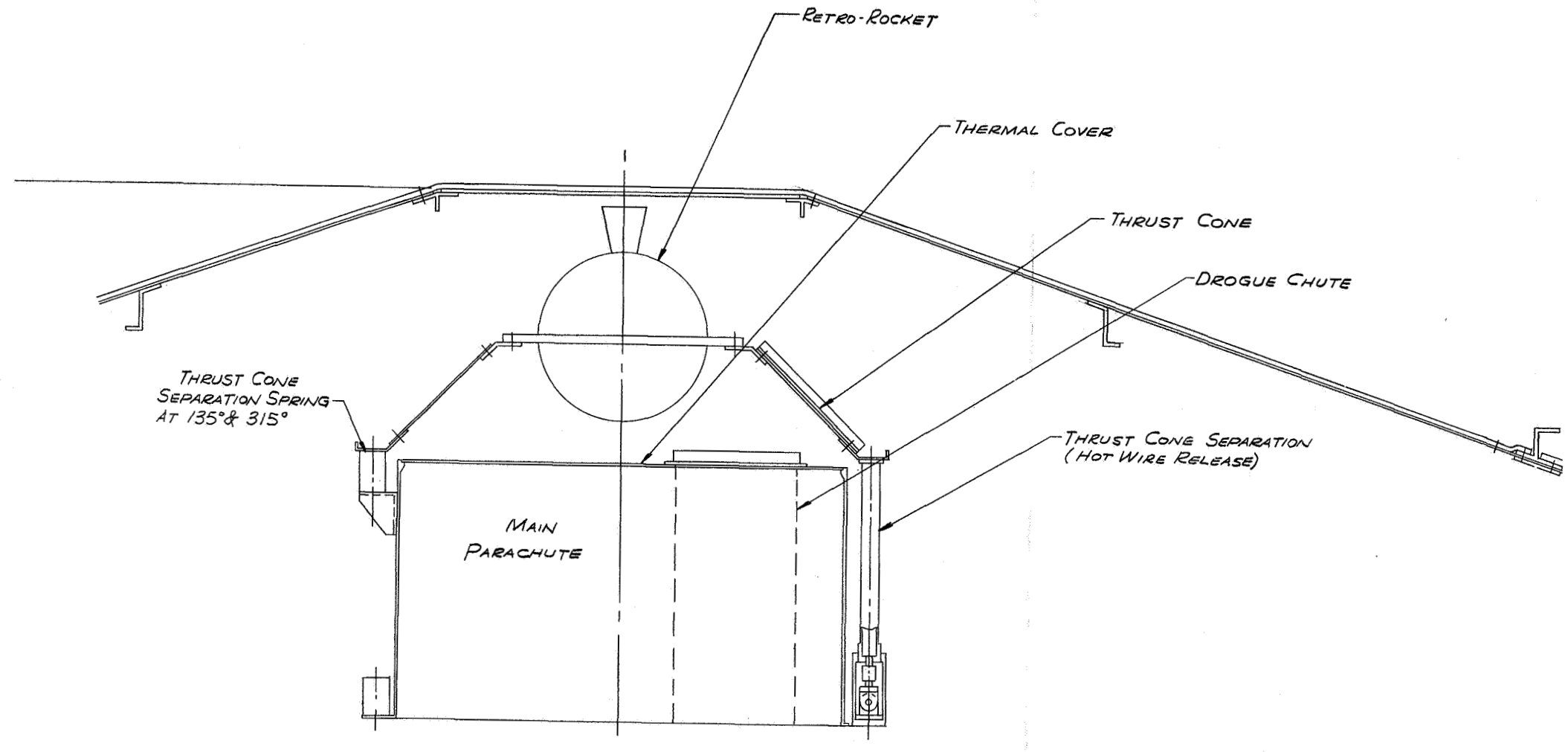


Figure 4.3.5-2. De-orbit Propulsion Installation, Point Designs 2A and 2B

An aluminum ring provides the interconnection between the engine and a conical aluminum adapter or thrust cone. The thrust cone is of aluminum sheet metal construction with longitudinal stiffeners to aid in taking the axial and bending loads introduced during flight conditions and during de-orbit engine burn. Another aluminum ring at the larger diameter end of the thrust cone provides the attachment for the main support members. This ring takes the shear loads due to lateral loading conditions and redistributes them to the tubular struts. The ring also tends to stiffen the cone for torsional forces which occur during spin and de-spin.

The four struts are aluminum tubes which act as short columns, taking the loads introduced by the cone structure and propulsion engine and redistributing them as four point loads into the Lander structure. The struts are attached to the Lander, as shown in fig. 4.3.5-3, through a hot-wire bolt to a male fitting which fits into and is pinned to a female fitting on the Lander cover. The lower end of the column is threaded to match a threaded pre-load sleeve which when tightened puts tension in the hot-wire bolt. The de-orbit engine and all of the structure is released when the hot-wire separates.

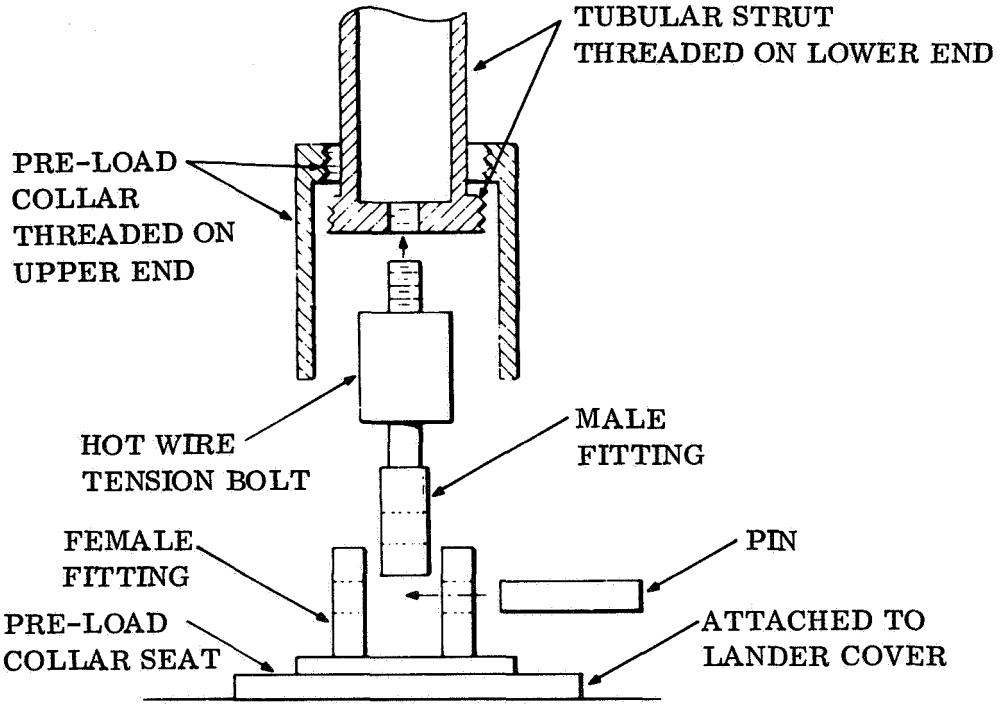


Figure 4.3.5-3. Thrust Cone Separation

4.3.6 ELECTRICAL EQUIPMENT, PRE-ENTRY

The canister is equipped with electrical/electronic equipment which provides status monitoring during cruise, preseparation, check-out, arming, electrical disconnection, separation initiations and separation event monitoring.

Commands from the Orbiter CC&S are sent to the canister via hardwire where decoding takes place in the dual canister programmer. Signals from the programmer operate the power controller which contains redundant capacitor discharge energy storage units. Energy from these capacitors provides electrical initiation.

All canister equipment is powered from a sterilized dual silver-zinc secondary battery. This battery is similar in design to the Lander battery and its development is described in section 4.3.1 of Volume III. This provides an independent energy source for operation when the Orbiter solar arrays are pointed away from the Sun, e.g., maneuver and separation attitude, for separation event monitoring after Lander disconnection, and to avoid sending initiation energy across an interface.

The aeroshell for direct entry designs is also equipped with a pre-entry silver-zinc battery which provides all power during the 24 hr coast period between separation and the onset of entry.

Thermal batteries located on the thrust cone provide high level currents for the electrical initiation events associated with spin, de-boost and de-spin. These are ignited from the Lander or pre-entry battery through thermal relay modules which protect the operational battery against initiation circuit faults. The thermal batteries are used in redundant pairs with diode blocking for isolation.

4.3.7 DE-ORBIT SYSTEM

4.3.7.1 Spin Control Subsystem

The subsystem configuration described here for Point Design 2 performs attitude control for the de-orbit system and roll control for the entry system. By combining these functions, the overall equipment design is simpler, weighs less, and, since fewer components are needed, is more reliable. In the following discussion, reference will be made to the entry system description, Section 4.4.7, where appropriate.

4.3.7.1.1 Spin Requirements

The most important requirement for the spin control subsystem is to control the Capsule attitude during firing of the propulsion system so that the error in direction of the velocity increment (ΔV) will not cause excessive entry path angle or downrange dispersions. Errors will be caused by thrust misalignment of the propulsion engine, center-of-mass offset of the Capsule, separation tip-off rates, and by other sources to be discussed later. The spin control subsystem provides a combination of gyroscopic stability and cyclical averaging to reduce the effect of these error sources to less than 2.1^{o}, 3-sigma error on the ΔV orientation.

Another requirement for the subsystem is to control the Capsule attitude at the beginning of entry into the atmosphere so that a large initial angle-of-attack, or even backward entry, is avoided. Since the initial angle-of-attack can be as large as 40°, the requirement is met by maintaining until entry the same inertial orientation established for de-orbit propulsion firing. Again, the gyroscopic stability of the spin control performs this function.

The requirements for roll control during entry are discussed in Section 4.4.7 under entry systems.

Additional requirements and constraints for the spin control for both Point Designs 2A and 2B are summarized in table 4.3.7-1. These requirements determine the required torque level and impulse.

TABLE 4.3.7-1. SPIN AND ROLL CONTROL REQUIREMENTS, POINT DESIGN 2

	Units	Point Design	
		2A	2B
Capsule weight	lb	1636	1270
Roll inertia	sl-ft^2	319	215
P/Y inertia	sl-ft^2	242	135
Moment arm	in.	72	64
Separation rate	deg/sec	0.5	0.5
CM offset	in.	0.3	0.3
Nozzle alignment error	deg	0.5	0.5
Velocity increment	ft/sec	147.5	147.5
Separation to entry time	sec	86,400	86,400
Entry spin rate	rpm	5	5
Entry roll torque	ft-lb	125	90
Entry roll impulse	ft-lb-sec	1,000	720

4.3.7.1.2 Description of the Spin Control Subsystem

The spin control subsystem consists of a small monopropellant hydrazine reaction control, a single rate gyro, and an electronic assembly. A block diagram is shown in fig. 4.3.7-1 which applies to both 2A and 2B. The rate gyro measures Capsule roll rate which is compared with the output of the roll rate generator. When the spin command is given, the high rate (50 rpm) mode is used for spin-up for engine firing. When the de-spin command is given, the low rate (5 rpm) mode is used for both de-spin and entry roll control. When the error voltage is larger than the preset threshold, the valve drivers operate the appropriate valve to generate corrective roll torques.

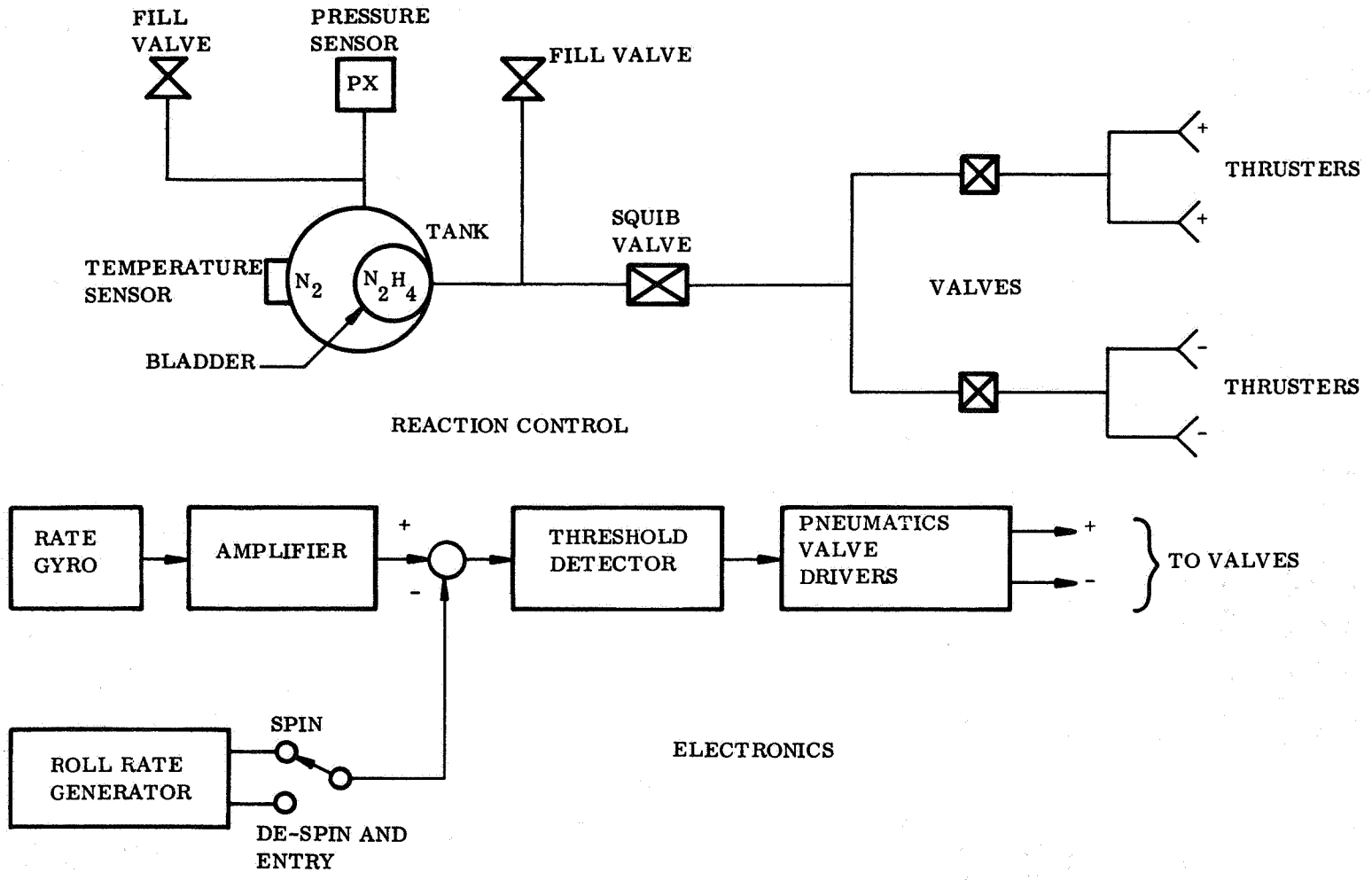


Figure 4.3.7-1. Spin and Roll Control Subsystem, Block Diagram.

Reaction control is provided by a blow-down hydrazine system using nitrogen as a pressurant. An aluminum tank less than 8 in. in diameter is used and its size is chosen so that the initial gas pressure of 400 psi is reduced to 300 psi when all of the hydrazine has been expelled. This limits the thrust decrease to approximately 25 percent. All control torques are provided as couples. The system is sealed off until Capsule separation by the explosive squib shown in fig. 4.3.7-1.

Power requirement for the gyros and electronic assembly is 5 watts. When one of the valves is energized, an additional 2 watts is required. The size of the combined gyro and electronics is 5 x 6 x 3 in.

The operational sequence of the subsystem is as follows:

1. The spacecraft orients the Capsule in the proper direction for firing the de-orbit propulsion engine. The gyros and electronics are energized just prior to separation. The high rate mode of operation is commanded.

2. At 1.5 sec after separation, the explosive squib is fired, initiating spin-up.

3. A spin rate of 50 rpm is reached at 25 sec after spin-up is started. This rate is maintained during propulsion firing.

4. After propulsion firing, and prior to entry, the low rate mode of operation is commanded. The subsystem remains in this mode throughout entry.

4.3.7.1.3 Spin Control Subsystem Performance

The pointing accuracy of the spin control subsystem is, of course, directly dependent on the accuracy with which the spacecraft orients the Capsule prior to separation. Two major additional errors are introduced by the Capsule separation subsystem and the spin control subsystem. These errors are the tip-off error and the coning error during propulsion firing.

The tip-off error is caused by the Capsule angular rate uncertainty at separation from the Capsule. This rate produces an attitude deviation from the separation spacecraft attitude proportional to the time interval from separation to spin-up command. It is estimated that the separation tip-off rate can be held to less than 0.5°/sec. For spin-up occurring 1.5 sec from separation, this creates an angular error of 0.75° 3-sigma.

The coning error is caused by the upsetting torque created by the propulsion thrust not acting through the Capsule center-of-mass. Gyroscopic action reacts to the torque by producing a spiralling increase in the attitude error. To maintain a required ΔV orientation error, the spin rate must be increased as the propulsion thrust level is made larger. For the selected spin rate of 50 rpm, the ΔV orientation error will be held to less than 0.75°, 3-sigma.

An error analysis, including these and other error sources, was described in Volume III, para 5.2.5.3. The overall error in ΔV orientation is estimated to be 2.1°, 3-sigma.

The attitude error of the Capsule at entry is dependent on the stability of the spinning Capsule from the time of propulsion burnout to entry. To use spin stabilization during this period, the problem of energy dissipation which could lead to attitude divergence must be considered. Since a vehicle is stable about the axis of maximum moment of inertia, even with energy dissipation, this point design will present no problem since its roll (spin) axis inertia is larger than that of the pitch/yaw axes.

4.3.8 PRE-ENTRY SYSTEMS WEIGHT

The weights of those items contained within the pre-entry systems for Point Designs 2A and 2B are listed in table 4.3.8-1. (The attitude control system is carried in the entry system weight summary, table 4.4.8-1.) Total pre-entry system weight for Point Design 2A is 401.6 lb and for Point Design 2B is 336.5 lb.

TABLE 4.3.8-1. PRE-ENTRY SYSTEMS WEIGHT SUMMARY, POINT DESIGNS 2A AND 2B

Item	Weight (lbs) 2A		Weight (lbs) 2B	
Thrust Cone Assembly		70.8		57.3
Structure	25.0		20.0	
Propulsion system (less propellant)	7.8		6.1	
Propellant	29.3		22.5	
Separation system	1.2		1.2	
Electrical	7.5		7.5	
Canister		330.8		279.2
Shell	81.4		61.8	
Internal structure	59.5		51.4	
Separation rings	39.1		34.4	
Separation system	20.1		17.5	
P&V system	13.7		9.3	
EP&D	53.4		53.4	
Thermal blanket	33.6		26.0	
Hardware and miscellaneous	30.0		25.4	
Pre-entry system total		401.6		336.5

4.4 ENTRY SYSTEMS

4.4.1 CONFIGURATION

4.4.1.1 Constraints

Constraints for Point Designs 2A and 2B were placed on the following parameters:

1. Ballistic coefficient
2. Entry system weight
3. Maximum aeroshell diameter
4. Entry angle and velocity
5. Payload weight and volume
6. Powered flight and entry loads
7. Materials and construction techniques.

The design goal was to achieve a direct entry vehicle design with a ballistic coefficient of 7 lb/ft^2. This had to be achieved within the envelope constraints discussed in Section 2.3.1, which limited the Capsule system maximum diameter to 175.6 in. and the entry system diameter to 171.6 in., as was shown in fig. 4.3.1-1.

Entry system weight was an important parameter since along with the half cone angle and base diameter it determined the final ballistic coefficient achieved for a given design. It must be pointed out that the ballistic coefficient was the overriding criteria,because it was this factor that had the most effect on heating rates, trajectories, and loading and determined the retardation system deployment regime. Table 4.4.1-1 shows a tabulation from the Configuration Selection Program (CONSEP) for Point Design 2A. It can be seen from looking at this table that for a fixed base radius of 76 in. and a varying half cone angle of 50 to 70^{o}, the ballistic coefficient varies from 10.78 down to 7.12 for a change of greater than 25 percent while the weight change is only 60 lb (less than 4 percent). This points out the fact that the ballistic coefficient is the important factor and must be held constant.

Internal clearances between the canister and the aeroshell limit the aeroshell diameter to 171.6 in. Additionally, the aeroshell could not be so small as to adversely affect the packaging of the Lander system. Working with both the 171.6 in. diameter and the packaging volume necessary for the Lander, Point Designs 2A and 2B configurations were evolved.

The entry angle and entry velocity along with the ballistic coefficient, base diameter and bluntness ratio were important factors in determining the thickness of heat shield material necessary for this direct entry mission.

TABLE 4.4.1-1. CONSEP PROGRAM RESULTS - POINT DESIGN 2A

Half Cone Angle (deg)	Ballistic Parameter (lb/ft^2)	Entry Weight (lb)	Base Radius (in.)
50	10.78	1585	76
60	8.45	1549	76
65	7.69	1535	76
70	7.12	1524	76

The payload weight was an important factor for determining internal shell loads and for sizing the retardation system because it was this weight which contributed greatly to the total deceleration load.

The critical loading conditions for the entry system in the out-of-orbit mode were conditions J, K, O and P as shown in table 4.4.1-2. It was based on these conditions and the entry-heating environment that the aeroshell structure was selected. Also important in selection of the material and construction of the aeroshells was ease of fabrication, cost and light weight.

4.4.1.2 Description

Geometrically, Point Design 2A is a blunt sphere cone vehicle with a bluntness ratio (R_N/R_B) of 0.5. The spherically shaped nose has a radius of 38.1 in. making a tangent with a frustum of a cone with a half angle of 60^o and a base diameter of 152.4 in. as shown in fig. 4.4.1-1.

Point Design 2B is also a blunt sphere cone (bluntness ratio of 0.5) with a nose radius of 33.9 in. making a tangent with a frustum of a cone with a half angle of 60^o and a base diameter of 135.6 in. This configuration is shown in fig. 4.4.1-2.

The heat shield for both 2A and 2B is an elastomeric shield material (ESM) 1004 AP with a tapering thickness from the stagnation region to the end of the skirt. Density of this selected heat shield material is 35 lb/ft^3. Corner heating effects were accounted for in the design and protection has been provided in the form of a peripheral edge protection. To protect against the possibility of backface heating around edge of the entry vehicle, the backface is coated for a short distance with a heat shield material.

The aeroshell structure is an aluminum honeycomb shell with a core thickness of 1.50 in. and facing sheets 0.025 in. thick to form a total shell thickness of 1.55 in. In the aft end of the aeroshell is a torque box structure made up of webs and rings with periodic ribs to provide internal stiffness. This structure tends to stiffen the

TABLE 4.4.1-2. POINT DESIGN LOADS

Letter	Condition	Limit Load (Gx)	Acceleration (Gn)	Remarks
A	Ground handling	2.0	2.0	
B	Band clamp	N/A	N/A	83 lb/in radial
C	First stage burnout	5.2	2.0	
D	Second stage burnout	4.0	2.0	
E	Axial vibration	+6.0 -3.0	---	
F	Lateral vibration	---	±2.0	
G	Canister separation	Negligible	Negligible	
H	Entry systems separation	Negligible	Negligible	
I	Thrust cone separation	Negligible	Negligible	
J	Entry (max Gx)	5.5	Negligible	Out-of-Orbit 320° interface
		12.7	Negligible	Out-ofOrbit 200°F interface
		48.0	Negligible	Direct Entry 200°F interface
K	Parachute opening	10.0	---	
L	Impact	1000.0	---	
M	Canister pressure	N/A	N/A	ΔP = 0.5 psi at 275°F
N	Canister pressure	N/A	N/A	ΔP = 1.0 psi at Ambient
O	Spin	N/A	N/A	50
P	Sterilization	N/A	N/A	

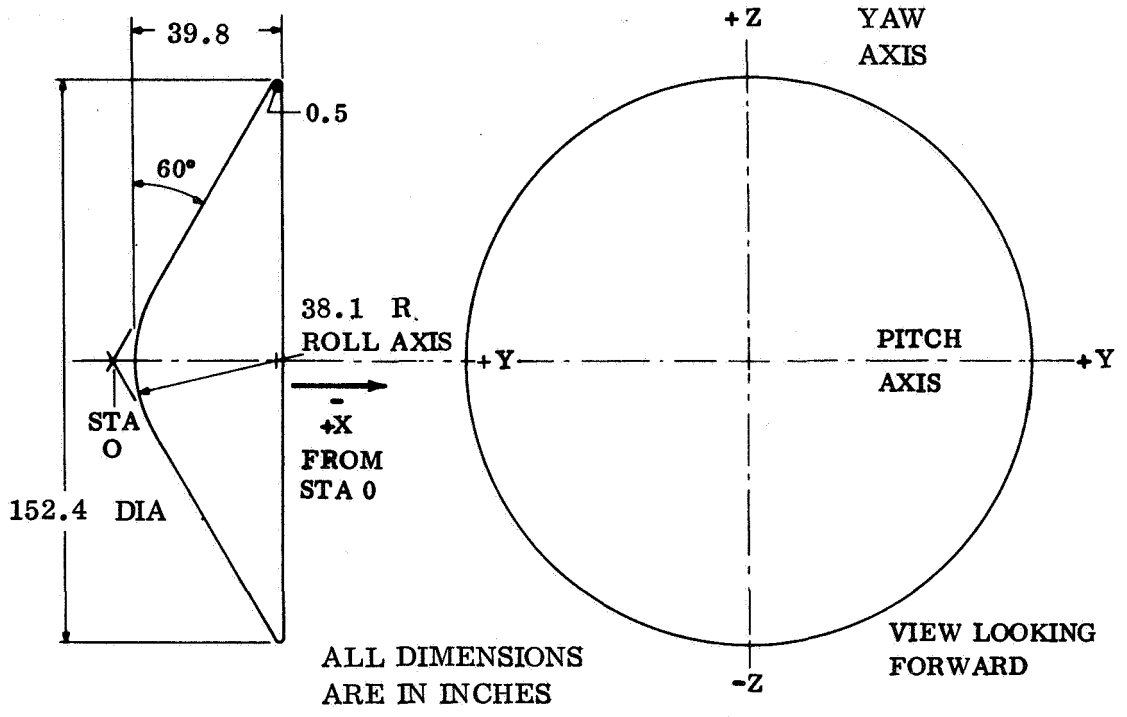


Figure 4.4.1-1. Aeroshell Geometry, Point Design 2A

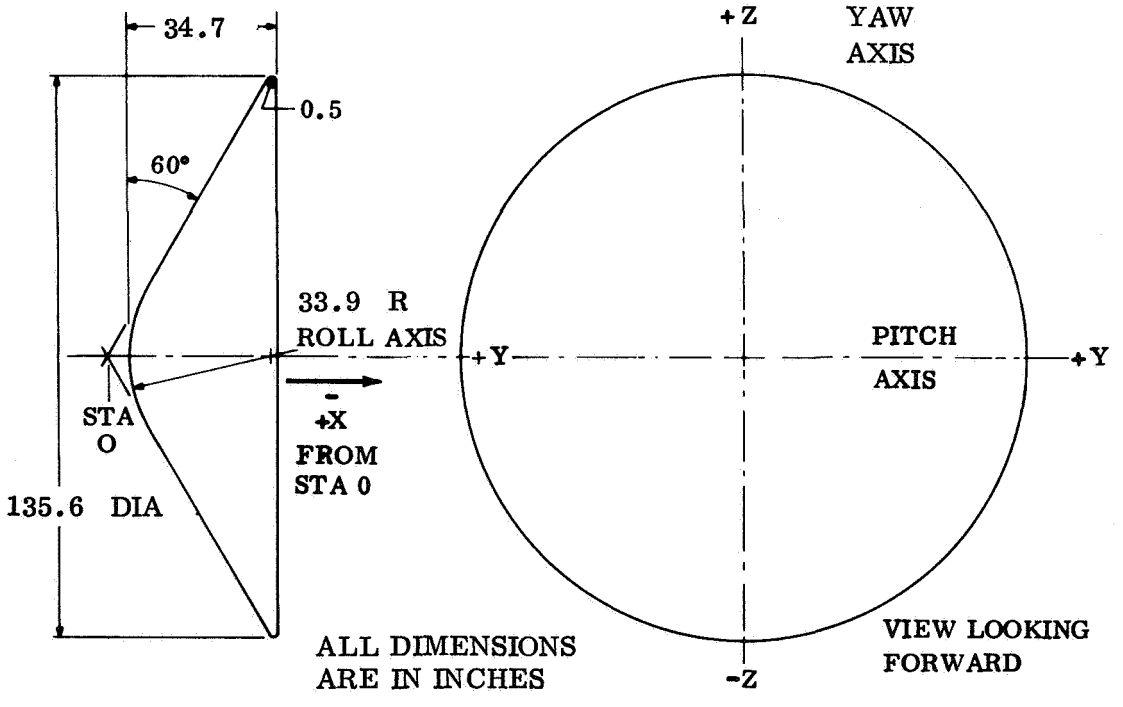


Figure 4.4.1-2. Aeroshell Geometry, Point Design 2B

shell and minimize local shell bending and rotation as well as provide a load path for the Lander loads introduced by securing the Lander into the aeroshell. The combined spin, de-spin and roll control nozzles are mounted on the aft web of the torque box. Separation forces, which occur at separation from the adapter and at Lander release, are taken in the longitudinal web of the box.

The Lander is held in by a strap arrangement which consists of a strap or bellyband, which runs completely around the Lander (see figs 4.3.1-2 and -3), hot-wire device, T-bolt, tie-down strap and torsion spring. The load in the tie-down strap is sufficient to overcome the rotational forces due to spin and de-spin and thus restrain the Lander from moving during these events.

The forward portion of the Lander sits in a phenolic glass honeycomb saddle, which has a teflon lining between it and the Lander to eliminate the possibility of the Lander and saddle from adhering to each other during the long space flight while under the tie-down load.

Pressure sensors, a temperature sensor, and an air intake for the mass spectrometer located in the Lander, are located in the nose of the aeroshell. Also located in the nose of both 2A and 2B are the electronics, rate gyro, and gas tank necessary for the attitude control system.

4.4.2 HEAT SHIELD

At the heating rates expected for the direct entry Point Design 2 mission described in table 4.4.2-1, the most efficient materials on a weight basis are, in general, members of the low density charring ablator class. Thus, because of the relatively mild Martian entry environment where total surface recession is small in most cases and thermal insulation is of prime importance, the low density charring ablator, ESM 1004 AP, was selected to be a design solution for the Mars Hard Lander heat protection system for direct entry modes.

The basis for selection of this material was:

1. Minimum system weight
2. Maximum flexibility to accommodate non-design conditions
3. Fewer anticipated fabrication and development problems than with other approaches
4. Sensitivity to the sterilization/decontamination and low temperature hard vacuum environments can be circumvented by proper material formulation.

For the direct entry mission where steep angle entry into the VM-8 atmosphere 25^{o} Nom (+ 7) results in ESM surface melting, ESM 1004 AP (35 lb/ft ^{3} density) is the preferred approach due to its good performance in relatively mild melting regimes.

TABLE 4.4.2-1. ENTRY CONDITIONS AND GEOMETRY OF POINT DESIGNS 1 THROUGH 6

Point Design	Mission Entry Mode	Entry Velocity (kft/sec)	Entry Angle (deg)	Ballistic Coefficient (lb/ft^2)	Aeroshell Base Diameter (ft)	Half Cone (deg)	R_N/R_B
1	Out-of-Orbit	15.3	14	14	8.33	60	0.5
2A	Direct	20.8	16	7	12.7	60	0.5
2B	Direct	20.8	16	7	11.4	60	0.5
3	Out-of-Orbit	15.3	14	14	8.33	60	0.5
4	Direct	20.8	16	7	12.7	60	0.5
5	Out-of-Orbit	15.3	14	14	10.0	60	0.5
6	Direct	20.8	16	7	14.0	60	0.5

It has been shown in Volume III, Section 3 that the maximum heat shield thickness requirement is dictated by the shallowest path entry angle attainable. The heating histories which include both convective heating and equilibrium and non-equilibrium radiative heating for Point Design 2B are shown in fig. 4.4.2-1 for the stagnation point and end of skirt locations.

Employing the thermo-physical properties described in table 4.4.2-2 and the convective and radiative heat-flux histories shown in fig. 4.4.2-1, the heat shield thickness requirements were generated using the techniques described in Volume III, Section 3 and are shown for Point Design 2B in fig. 4.4.2-2. The shield thickness requirements are those required to hold the design bondline temperature to 600°F with a safety factor of 1.0. In lieu of a detailed evaluation to justify a statistical safety margin, it is suggested that a safety factor of 1.2 be applied to the shield thickness requirements presented for Point Design 2. This would result in a margin of about 200°F on the backface temperature. Analysis has shown that one of the most significant factors that affects the estimation of the shield thickness is the tolerance on the entry path angle. Designing the heat shield thickness to the lower limit on entry angle results in a safety margin of about 10 percent for Point Design 2 when compared to the nominal entry condition.

The backface and frontface temperature histories of the shield material for Point Design 2B are shown in fig. 4.4.2-3. Fig. 4.4.2-4 shows the thermal gradients through the ESM material at selected times in the Martian entry corresponding to peak surface temperature and peak bondline temperature. These results are presented for entry into the VM-3 atmosphere. Shield thickness requirements for Point Design 2A and 2B are shown in table 4.4.2-3.

Since the entry conditions and shield requirements for Point Design 2A are very similar to those of Point Design 2B, the thermal gradients and temperature histories presented for Point Design 2B in figs. 4.4.2-3 and -4 are representative for direct entry Point Design 2A.

Since the total heat load on the afterbody of the sphere cone is expected to be small compared with the forebody, an ablating material for thermal protection is unnecessary, and a high emissivity coating would be an adequate protection. An analysis* indicated that for Voyager the peak cold wall heat flux on the afterbody was small, the resultant temperature rise being only 256°F.

The current design for the ESM 1004AP heat shield allows for ease of fabrication, handling and final assembly. The heat shield material is designed to be fabricated in panel sections of approximately 10 ft^2. Additional advantages of the segmented shield are that it allows for 100 percent inspection, does not require the aeroshell during shield manufacturing operations, and allows for finish machining prior to its being bonded to the aeroshell.

Design considerations were also taken into account for the steps developed between the segmented panels both longitudinally and circumferentially. These steps were determined by both the bond and heat shield thickness tolerances.

*McDonnell Astronautics Voyager Capsule Phase B, final report F694, Vol. II Part B, 31 August 1967 (On the Voyager Lander Studies)

TABLE 4.4.2-2. THERMOPHYSICAL PROPERTIES OF ESM MATERIALS

		ESM 1004X	ESM 1004AP
Virgin density (P_v lb/ft^3)		16.6	35.0
Char density (P_c lb/ft^3)		6.7	14.0
Pyrolysis gas specific heat (Cpg Btu/lb$^\circ$P)		.4	0.384
Molecular weight of injected species (Mg)		24.5	24.5
Order of reaction (N)		2	2
Pre-exponential factor (A sec^{-1})		15000	30000
Activation Energy (E Btu/lb mole)		44700	47500
Heat Decomposition (HGF) (Btu/lb gas generated)	1335°R	0	50
	1460°R		45
	1710°R		1000
	1960°R		2610
Specific Heat (Cp) (Btu/lb °R)	600°R	0.31	0.305
	710°R	0.33	0.360
	1210°R	0.44	0.44
	2075°R	0.44	0.44
Conductivity (k) Virgin (Btu/ft - sec°R)	610°R	0.0000115	0.0000237
	800°R	0.0000170	0.0000220
	1335°R	0.0000220	0.0000210
	1710°R	0.0000260	0.0000231
Char	1335°R	0.0000740	0.0000777
	1710°R	0.0000850	0.0000855
	2210°R	0.0001000	0.000104

For the decomposition reaction described by the following Arrhenius type equation:

$$\frac{1}{W_o}\frac{dw}{dt} = \frac{(W - Wf)^N}{(Wo)} Ae^{-\delta E/RT}$$

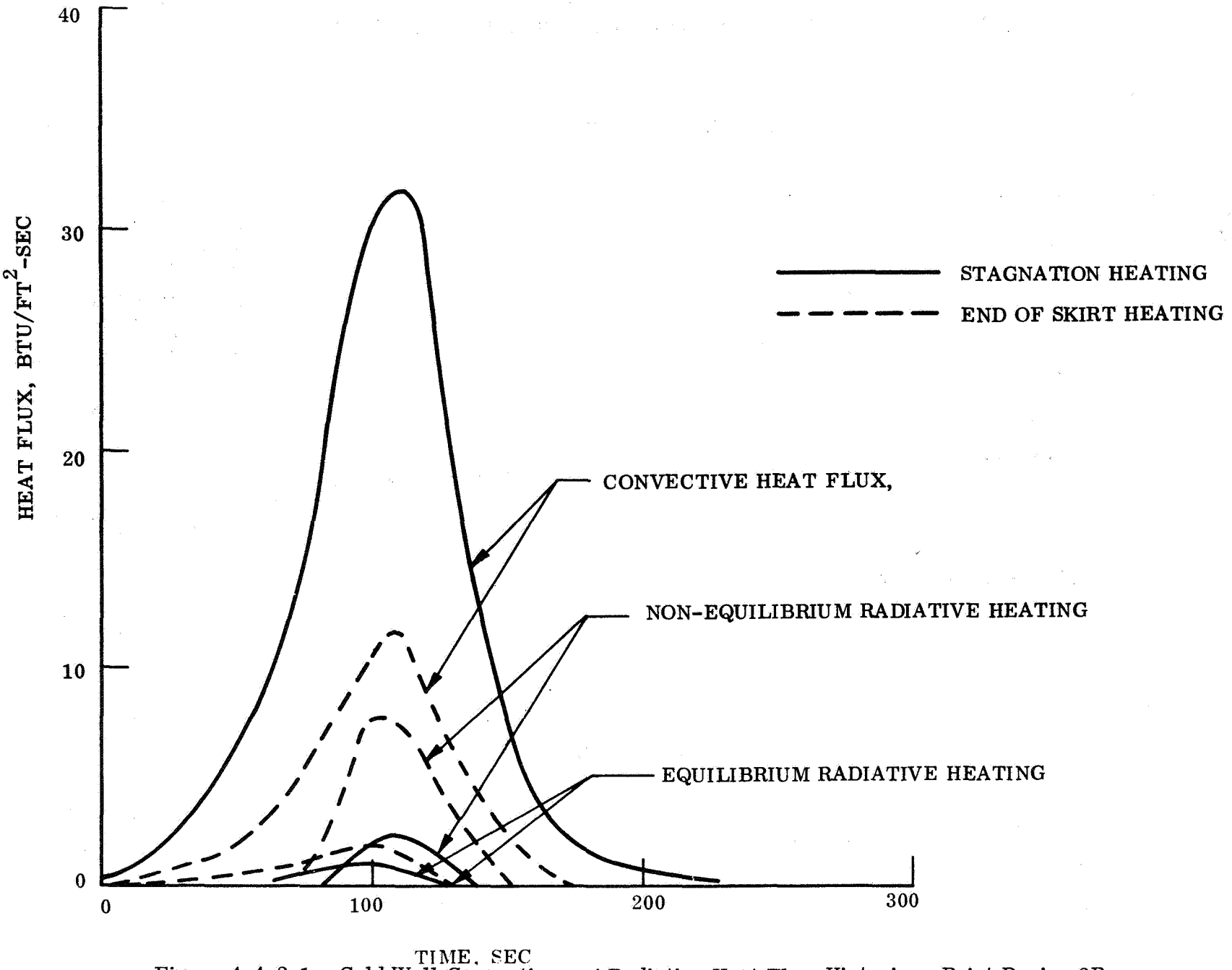


Figure 4.4.2-1. Cold Wall Convective and Radiative Heat Flux Histories, Point Design 2B

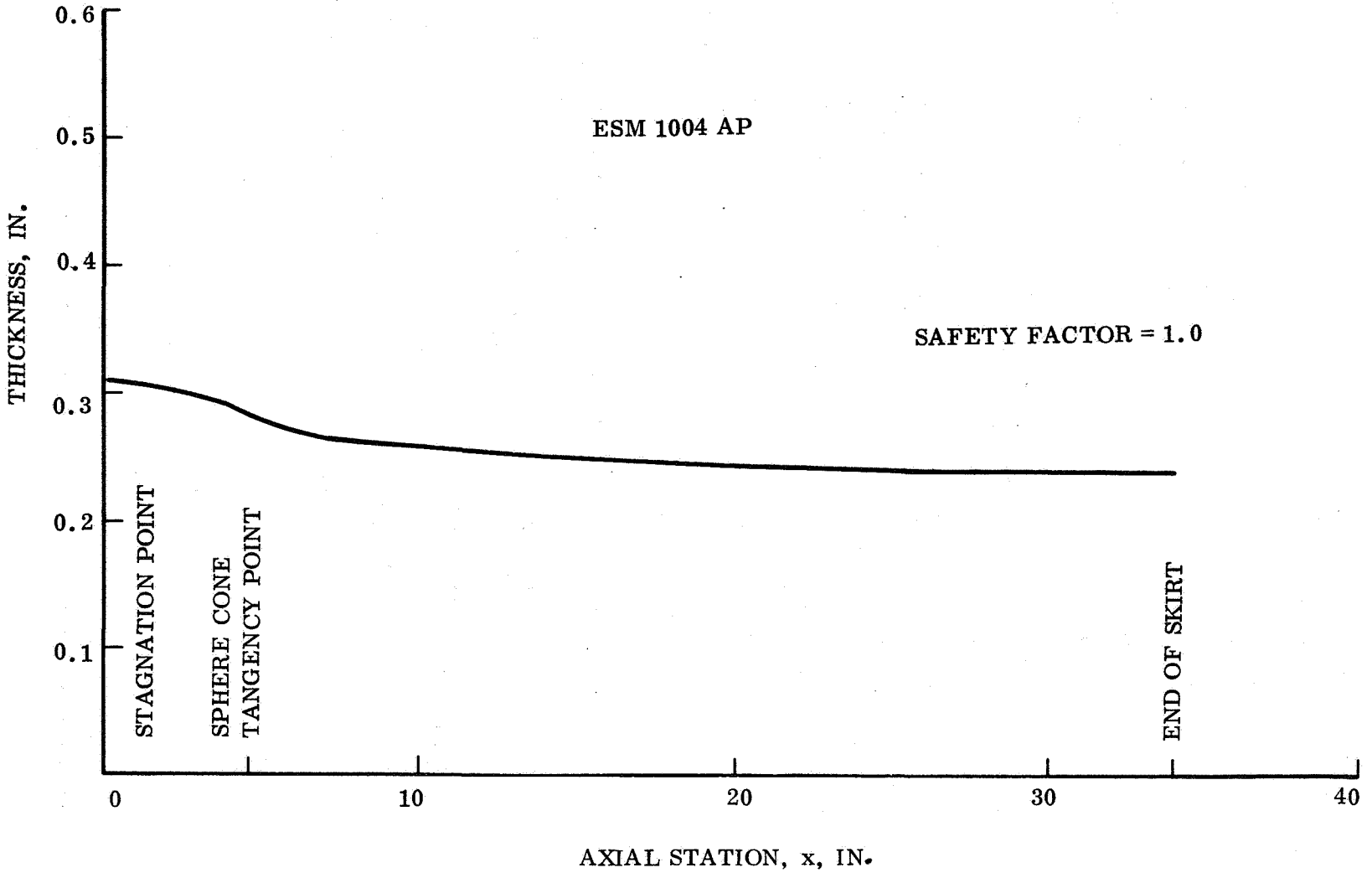


Figure 4.4.2-2. Heat Shield Thickness Requirements, Point Design 2B

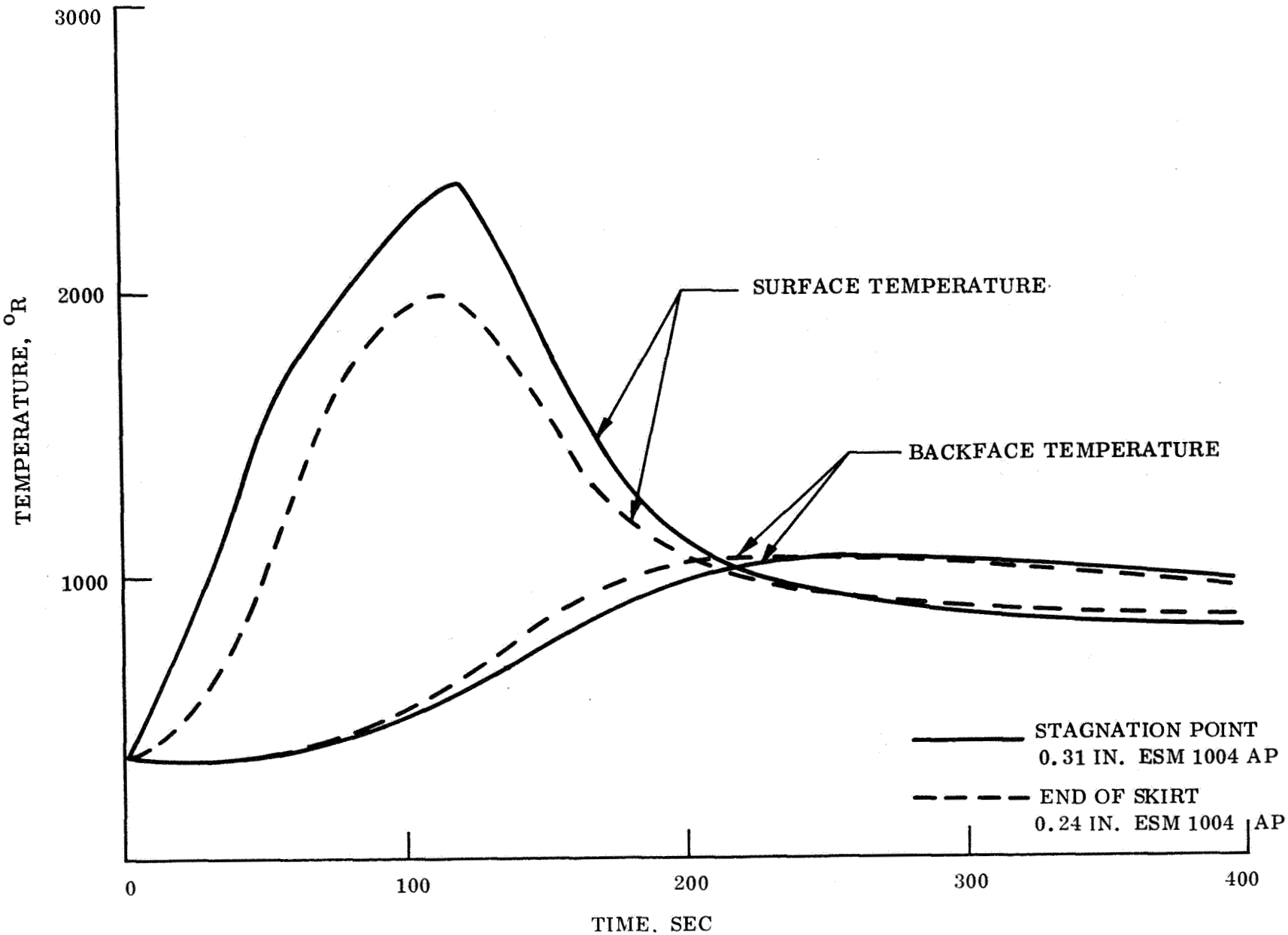


Figure 4.4.2-3. Surface and Backface Temperature Histories, Point Design 2B

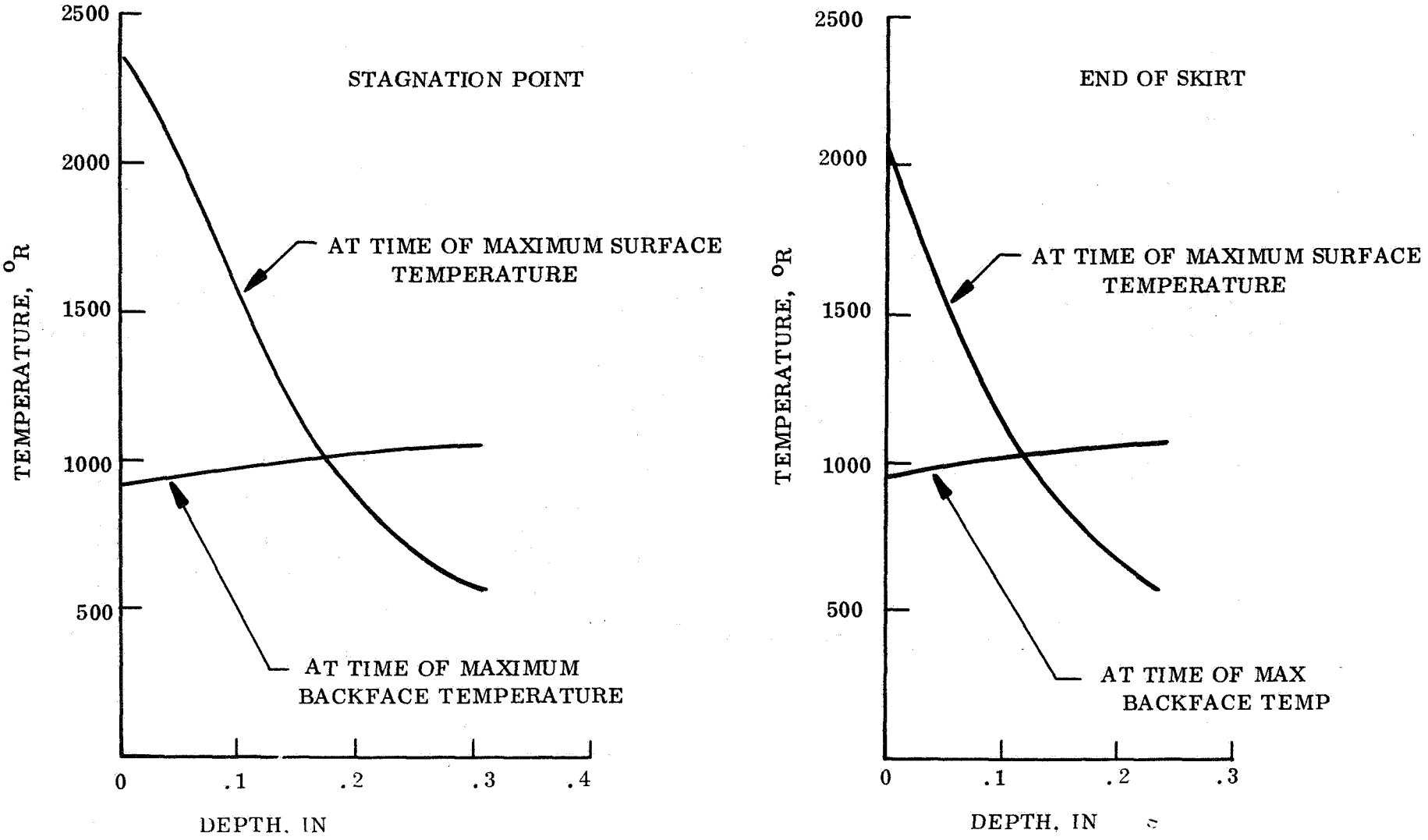


Figure 4.4.2-4. Temperature Gradients through the Shield, Point Design 2B

TABLE 4.4.2-3. SHIELD THICKNESS REQUIREMENTS FOR POINT DESIGNS 1 THROUGH 6

Point Design	Mission Entry Mode	Shield Material	Shield Thickness Requirements with 1.2 Safety Factor	
			Stagnation Point	End of Skirt
1	Out-of-Orbit	ESM 1004X	0.624	0.415
2A	Direct	ESM 1004 AP	0.367	0.275
2B	Direct	ESM 1004 AP	0.372	0.288
3	Out-of-Orbit	ESM 1004X	0.624	0.415
4	Direct	ESM 1004 AP	0.367	0.275
5	Out-of-Orbit	ESM 1004X	0.617	0.407
6	Direct	ESM 1004 AP	0.360	0.263

Corner heating effects were taken into consideration at the base of the entry vehicle and a peripheral edge protection of ESM 1004AP is provided at the base of the aeroshell. To protect against the possibility of backface heating around the edge of the entry vehicle, the exposed aeroshell structure at the base and inboard on the vehicle is coated with ESM 1004AP.

4.4.3 AEROSHELL AND STRUCTURE

The aeroshell for Point Designs 2A and 2B is an aluminum honeycomb shell 1.55 in. thick. It is comprised of a lb/ft^3 core 1.50 in. thick with 0.025 in. thick 7075 aluminum facing sheets bonded on with HT 424 bond. This shell material was selected for its light weight, ease of fabrication and the lower cost than other types of honeycomb materials. It was designed to take the axial, bending and shear loads encountered during powered flight and planetary entry.

The detailed analysis of the aeroshell to withstand the entry inertial loads and aerodynamic pressure loadings was performed by MULTISHELL, a GE computer program. The inputs to this program to perform the analysis consist of the entire aeroshell configuration upon which are imposed the inertia and pressure loadings. Output from the program consists of the shell internal stresses, moments, shear, in-plane shell loads and, in addition, the complete shell deformations. These deformations include all local discontinuity deformations of the shell. Figs. 4.4.3-1 through -5 present the deflection, moment, shear, in-plane load and stress distribution for Point Design 2A. The general distributions for Point Design 2B are similar.

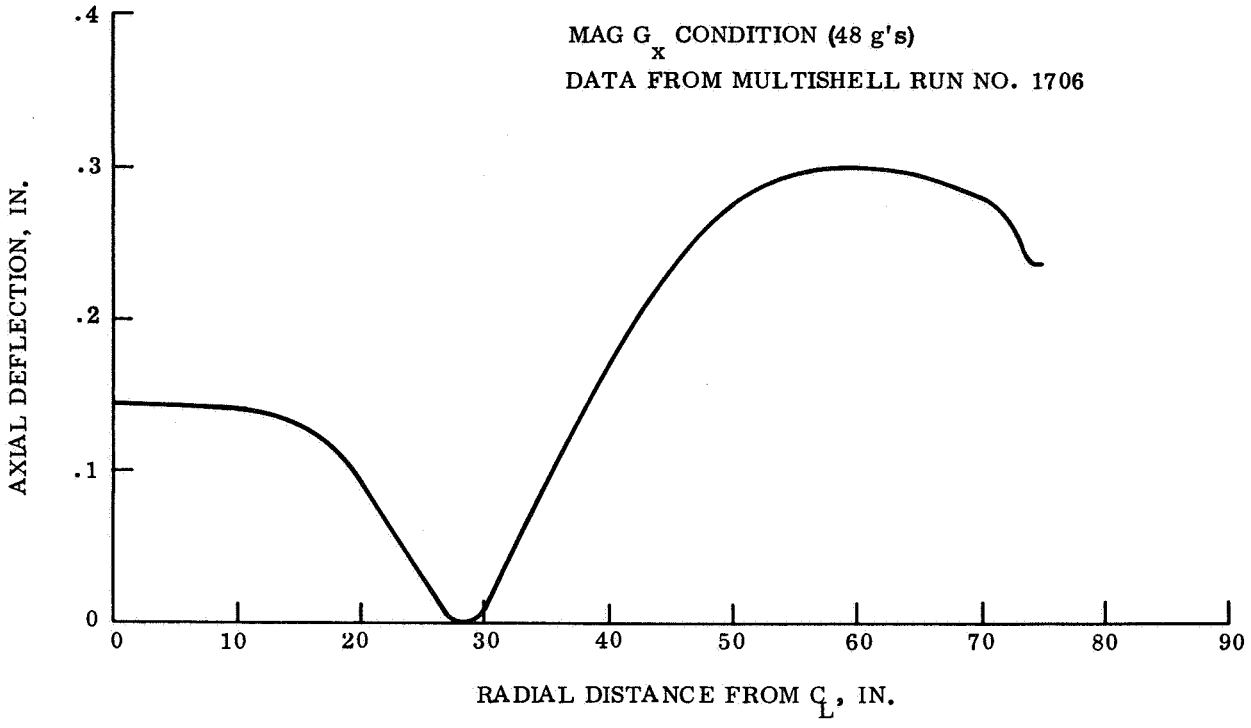


Figure 4.4.3-1. Axial Deflection-Aeroshell 2A Versus Radial Distance

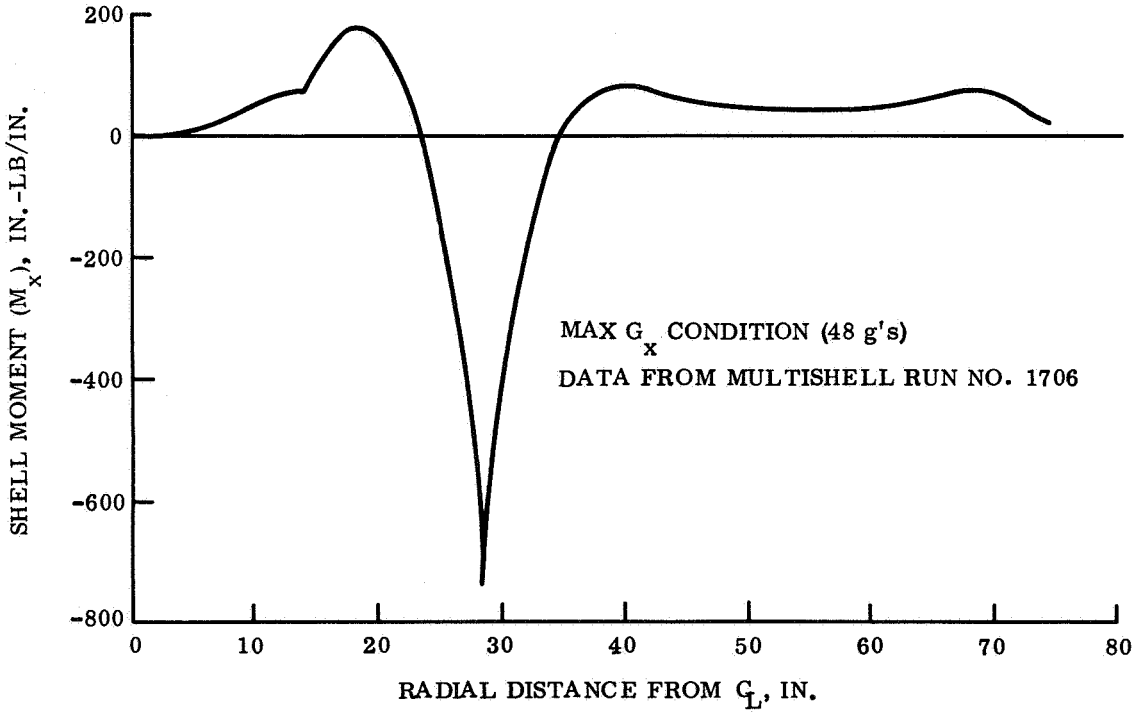


Figure 4.4.3-2. Axial Bending Moment (M_x) - Aeroshell 2A Versus Radial Distance

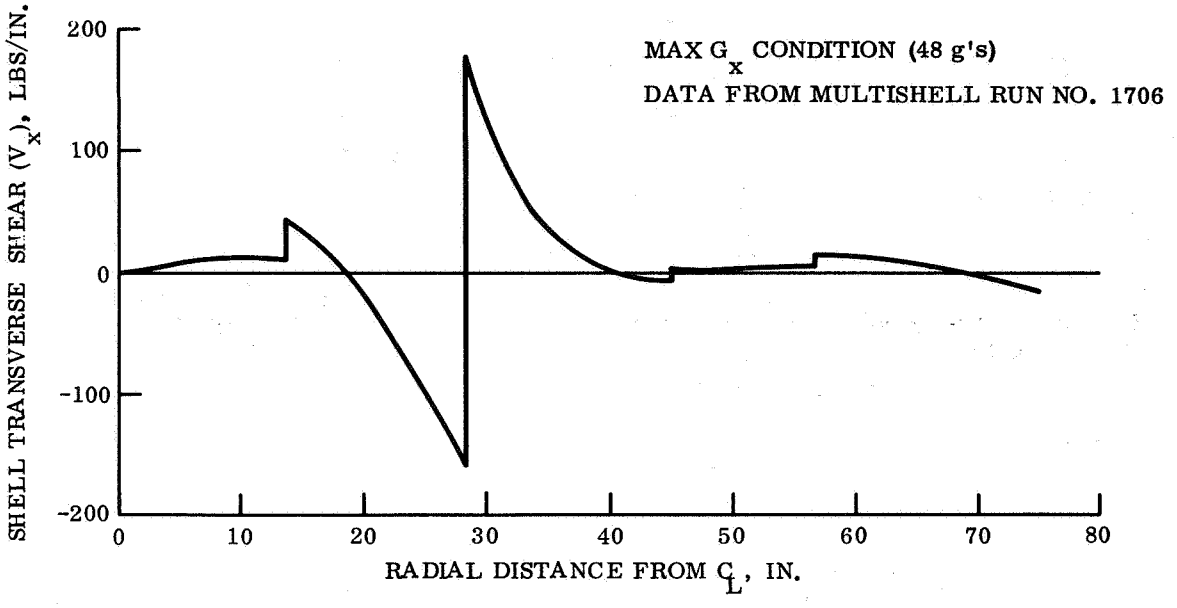


Figure 4.4.3-3. Shell Transverse Shear-Aeroshell 2A Versus Radial Distance

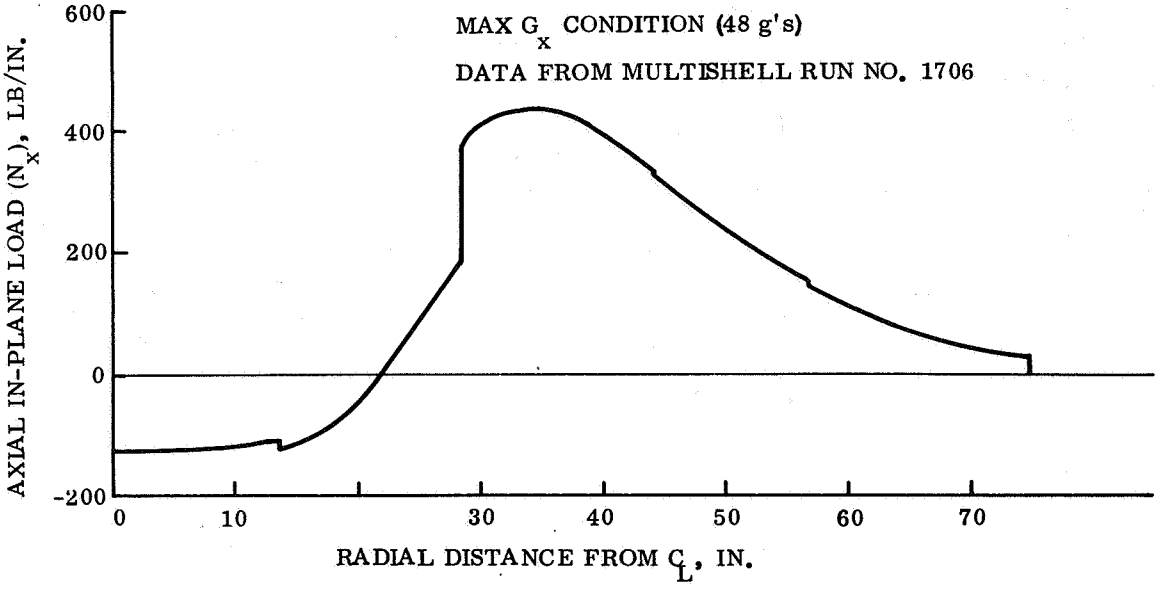


Figure 4.4.3-4. Axial In-Plane Load-Aeroshell 2A Versus Radial Distance

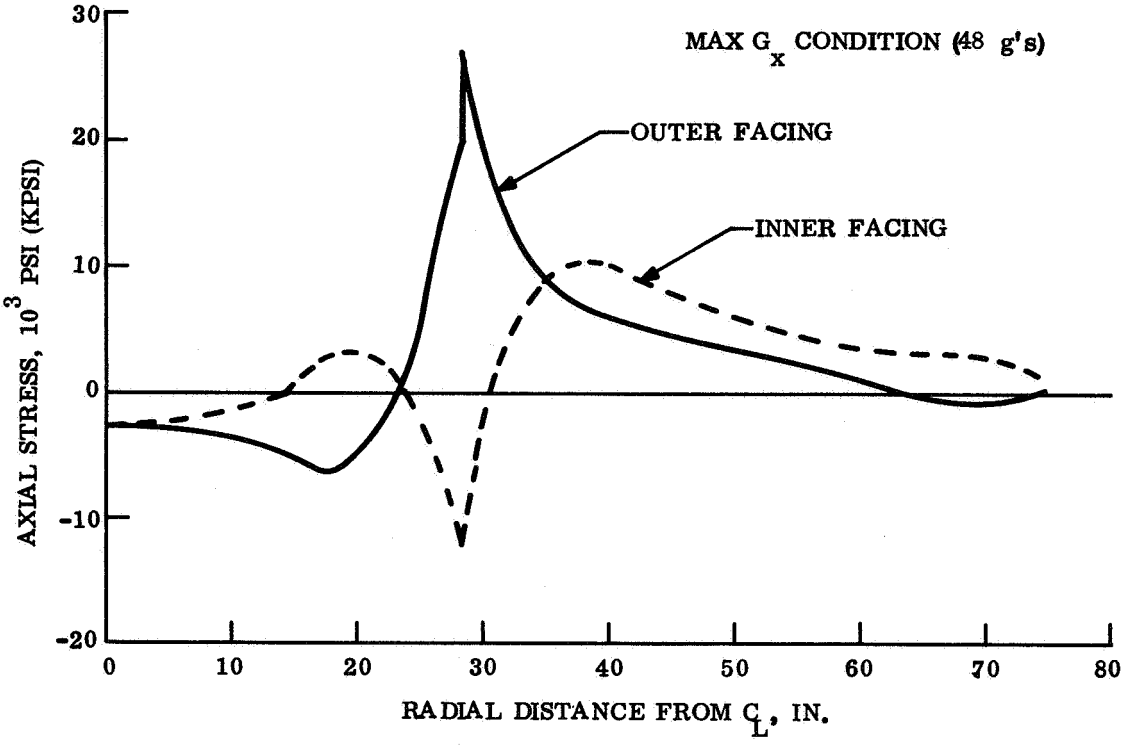


Figure 4.4.3-5. Axial Honeycomb Facing Stress - Aeroshell 2A Versus Radial Distance

Approximate structural analysis was performed to determine the initial core and facing thicknesses to be used in the computer program. Upon completion of the first MULTISHELL analysis, any necessary changes to the structural material gages are made to result in small positive margins of safety for all of the elements of the shell as shown in table 4.4.3-1.

TABLE 4.4.3-1. FINAL ALUMINUM HONEYCOMB REQUIREMENTS FOR AEROSHELLS

Point Design	Honeycomb		Minimum Safety Margin	Facing Material
	Facing Thickness	Core Thickness		
1	0.020	0.75	0.50	2024-T4
2A	0.025	1.50	0.09	7075-T6
2B	0.025	1.50	0.15	7075-T6
3	0.020	0.75	0.65	2024-T4
4	0.025	1.50	0.09	7075-T6
5	0.020	0.75	0.21	2024-T4
6	0.030	1.50	0	7075-T6

Analysis of Point Design 2A and 2B indicates that the shell bending is critical and that aluminum honeycomb is just as efficient as titanium honeycomb, lighter than stainless steel honeycomb, and easier to fabricate than both materials. The aluminum honeycomb is just as efficient as the titanium or steel honeycomb because local shell bending is the critical loading condition and the minimum gage is no longer the controlling factor. This local shell bending is induced by the loading of the aeroshell internally by the Lander and the aerodynamic pressure externally.

The heat shield structure interface temperature is less than 200°F at the time of maximum loading (48.0 g's limit) and the loadings are lower at times of higher temperatures. The temperature at parachute deployment at the heat shield structure interface can be 600°F, since at this time the loading on the aeroshell is negligible.

Figure 4.4.3-6 shows the time of maximum load imposed on the aeroshell and the interface temperature as a function of time from entry for the VM-3 environment. The maximum load occurs when the heat shield structure interface temperature is 103°. When parachute deployment occurs (230 sec from entry), the load has reduced to zero while the interface temperature has increased to 600°F. The total time at elevated temperature, prior to parachute deployment, is 125 sec or 2.0 min. It is assumed that the temperature gradients are negligible until the load has reduced to zero but for conservatism, the allowable honeycomb strength has been reduced to one half the actual.

Point Designs 2A and 2B configuration parameters are presented in table 4.4.3-2. The honeycomb core and facing thickness requirements and minimum margins of safety are presented in table 4.4.3-1.

TABLE 4.4.3-2. POINT DESIGN ENTRY DATA

Point Design	Entry Weight (lb)	Diameter (in.)	Radius To Bearing Load (in.)	Radius To Box Structure A (in.)
1 (out-of-orbit)	1246	100.0	27.0	41.5
2A (direct)	1480	152.4	32.0	44.0
2B (direct)	1127	135.6	27.0	37.0
3 (out-of-orbit)	1324	100.0	31.0	41.5
4 (direct)	1558	152.4	31.0	44.0
5 (out-of-orbit)	1530	120.0	32.5	42.5
6 (direct)	1766	168.0	31.0	46.5

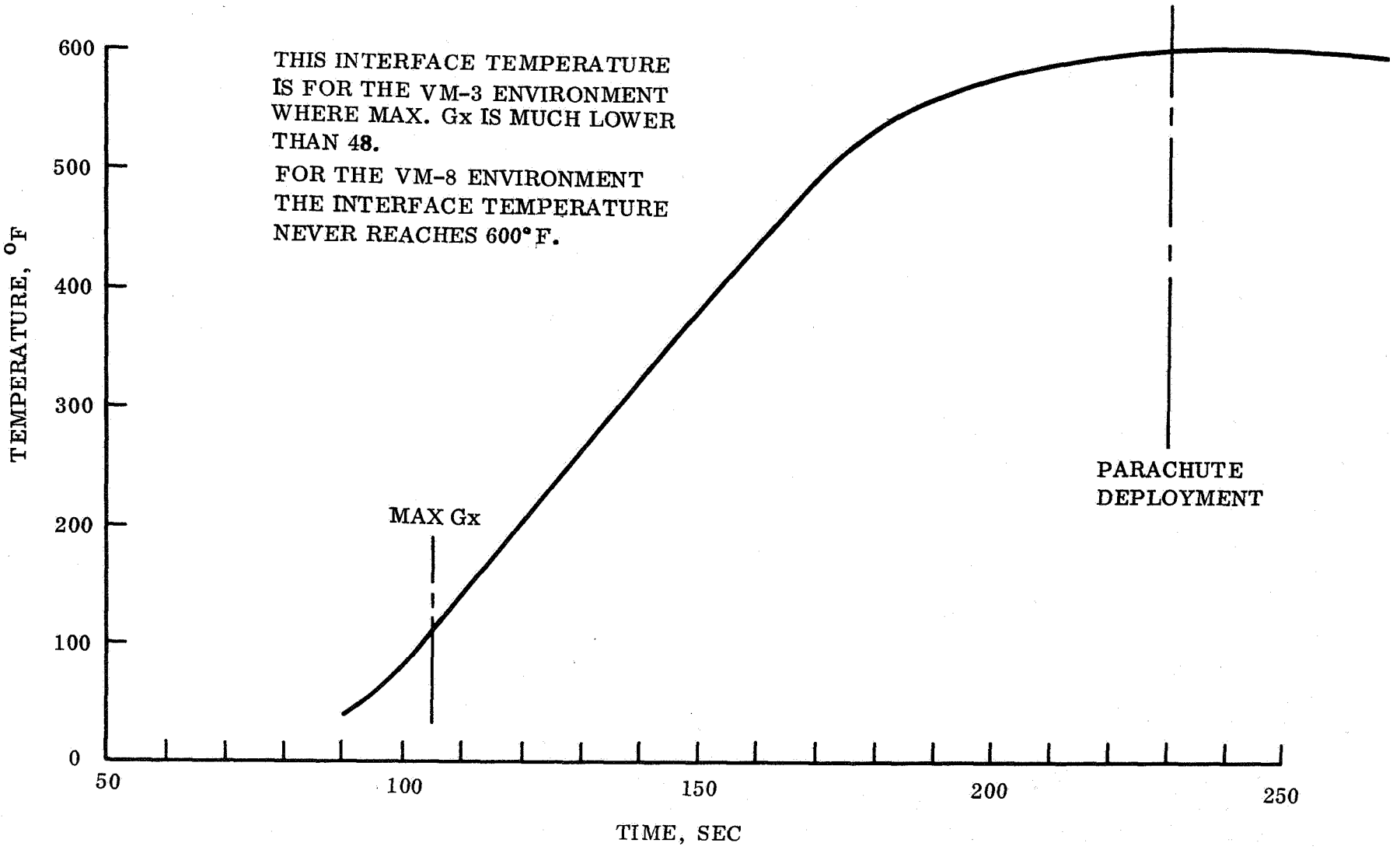


Figure 4.4.3-6. Shield-Structure Interface Temperature, Point Design 2A

The aluminum honeycomb weight is 1.15 lb/ft^2 of surface area (including bond) compared with 0.98 lb/ft^2 for titanium honeycomb and 1.25 lb/ft^2 for stainless steel honeycomb.

At the maximum base diameter is a box structure which extends forward into the aeroshell. This box structure is made up of a circular radial web and a cylindrical longitudinal web with periodic ribs joined together by a ring at the base and tied into the aft ring of the aeroshell and a frustum ring internal and forward in the aeroshell. The cylindrical longitudinal web extends beyond the maximum base diameter of the aeroshell to provide a support for the entry system separation device. At this point is the mating interface with the internal adapter.

This box-like outer structure of the aeroshell acts as a torque box and restrains the rotation of the outer edge of the aeroshell. The construction of this torque box structure and the radial distance from the point of application of the load due to the payload bearing against the honeycomb shell determines the magnitude of the shell bending loads. With the torque box structure made very stiff to allow very little torsional rotation, the maximum honeycomb shell bending moments and highest facing stresses would occur in the outer portions of the aeroshell. A reduction in the torsional box stiffness resulted in the maximum shell bending moments shifting to the center portion of the aeroshell. The ideal situation occurs when some rotation is allowed such that the shell bending is reduced over the entire shell and the moments are of the same order of magnitude in the center and outer portions.

4.4.4 LANDER/AEROSHELL SEPARATION

The Lander is attached to the aeroshell by a strap assembly retained by three hot-wire tension bolts. The strap assembly, shown in fig. 4.4.4-1, consists of a strap or bellyband which runs completely around the Lander. Part of the strap are cushioning pads and a teflon spacer to eliminate the possibility of damage to the crush-up material. The strap is in three segments connected by three hot-wire tension bolts. In the middle of each segment is a fitting which is retained by a T-bolt to the tie-down strap. The tie-down strap is attached to a fitting on the box structure in the aft end of the aeroshell. A torsion (or mousetrap) spring is also attached to this fitting and fits around the tie-down strap. Tension is placed in the entire assembly to obtain the required restraining loads for the Lander by torquing the T-bolt to a predetermined torque.

In order to separate the system, which occurs after parachute deployment, a current of 6 amps for 30 msec is fed to the hot-wire bolts causing them to separate. At this instant the torsion springs snap the tie-down strap and attached segments of the bellyband outboard and clear of the Lander which is extracted from the aeroshell by the parachute.

4.4.5 ENTRY SYSTEM EQUIPMENT

With the exception of the four pressure and one temperature transducers for stagnation region measurements, all of the entry science instruments and support equipment (13.0 lb of the basic 15.5 lb package of instruments) is incorporated in the Lander module (fig. 4.4.5-1).

4.4.6 RETARDATION SUBSYSTEM

The retardation subsystem requirements are so similar for all of the point designs that a single subsystem design approach appears to be adequate. The design evolved for Point Design 2 will permit deployment and proper landing impact velocity to meet the required conditions of the mission. These conditions are deployment at speeds not greater than Mach 2, terminal velocity on main parachute at altitude not less than 6,000 ft; and a vertical descent velocity in least dense atmosphere (VM-7) of 100 fps.

4.4.6.1 Retardation Performance

4.4.6.1.1 Mortared Pilot Parachute Selection

The use of a mortared pilot extraction parachute was selected over direct mortar ejection of the main parachute. The size of mortar required to directly eject such a large mass from the decelerating vehicle would take more weight than the selected arrangement. Furthermore, a more orderly deployment of the large diameter main parachute is ensured by using the pilot parachute extraction technique.

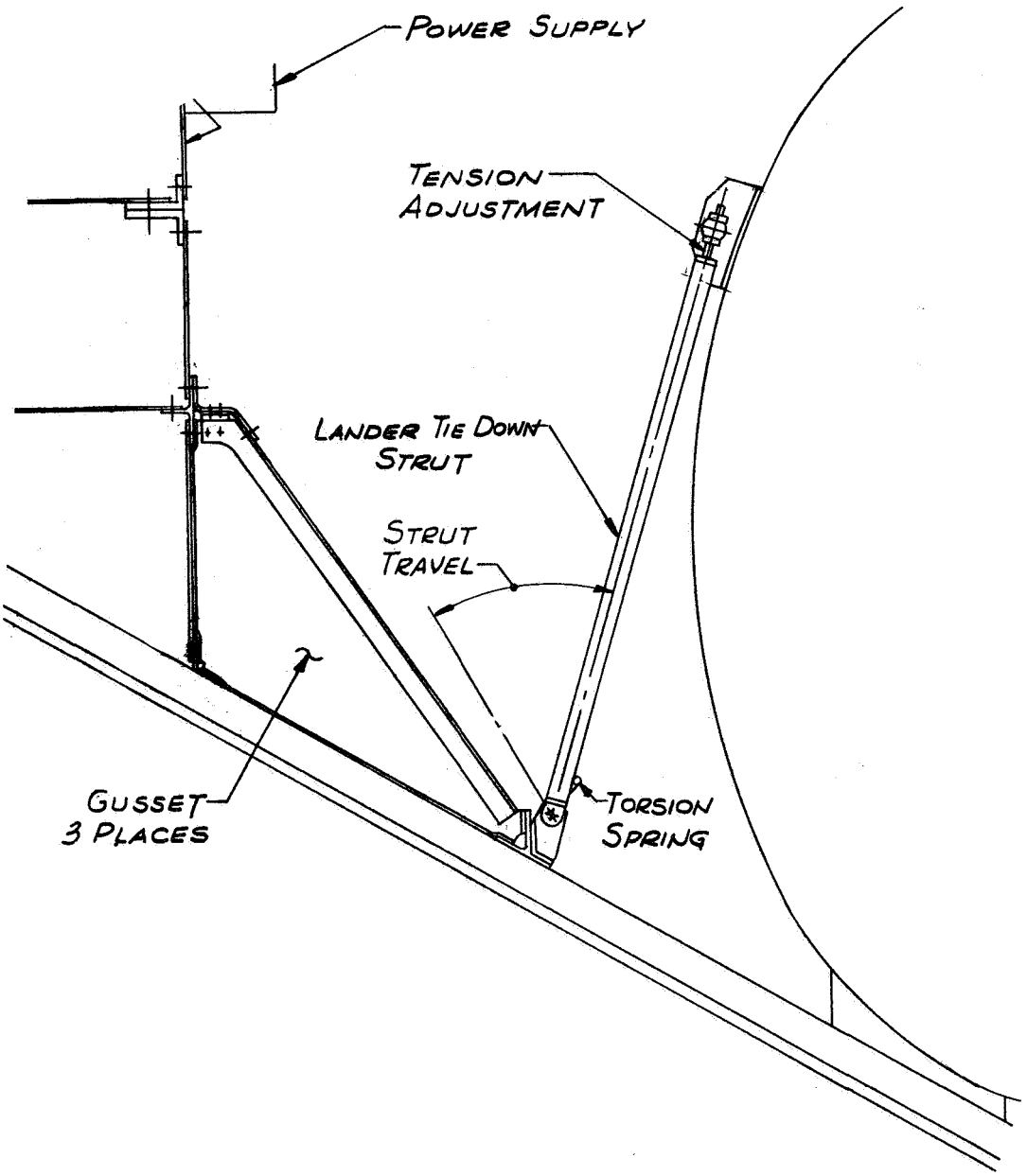


Figure 4.4.4-1. Lander Installation into Aeroshell, Point Designs 2A and 2B

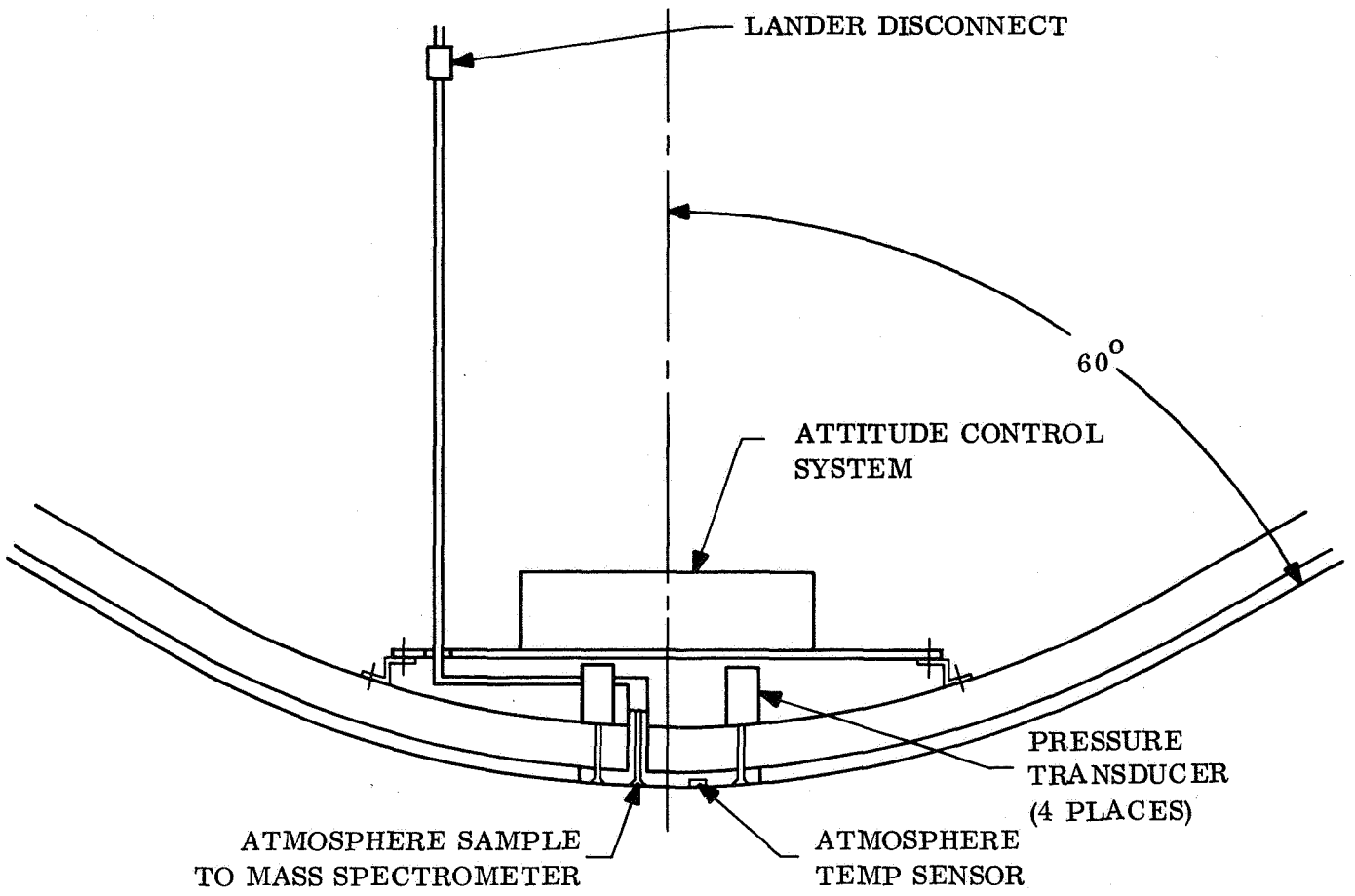


Figure 4.4.5-1. Entry Systems Instrumentation

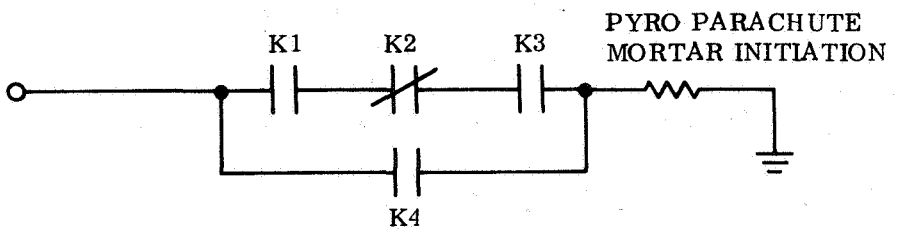
4.4.6.1.2 Trajectory Considerations

It is desired to minimize descent time on the main parachute while insuring that the main parachute will be at equilibrium terminal velocity at the time of its separation for Lander impact. Deployment based on sensing altitude alone would not be optimum. For the case where Mach 2 occurs at 11 kft in the VM-8 atmosphere, deploying at 11 kft in the VM-7 or VM-1 atmospheres would result in reaching terminal velocity on the main parachute at a lower altitude than in the VM-8 case, even though the initial deployment would be below Mach 2.

Deploying on Mach number alone would therefore produce high altitude deployment, and a long descent time on the main parachute if the atmosphere is dense (i.e., VM-9). If the deployment sensing coupled a Mach 2 gate with a time gate and an altitude gate, deployment below Mach 2 and minimum descent time would be assured. The logic for this arrangement would probably be as discussed below. Further trajectory investigations would be necessary for any particular point design for optimization.

Parachute deployment will be programmed to occur between 11 kft and 20 kft. A 20 kft signal from the radar altimeter would enable parachute deployment. On receipt of the Mach 2 signal, the timer would be started. If the 20 kft signal were received until the preset time-out, parachute deployment would occur. This would indicate a rare atmosphere. If Mach 2 did not occur before the receipt of the 11 kft signal from the radar altimeter, this would indicate very rare atmosphere such as VM-8. If the Mach 2 signal were received and time-out of the timer occurred prior to the 20 kft signal from the altimeter, this would indicate a dense atmosphere such as VM-9 or -10. In this case, parachute deployment initiation is delayed until the 11 kft signal from the altimeter. In any case, deployment would be initiated at 11 kft.

The following schematic clarifies this deployment logic:



K1 - Closes at Mach 2 signal
K2 - Opens at end of timer time-out
K3 - Closes at 20 kft signal
K4 - Closes at 11 kft signal

4.4.6.2 Parachute Design

The modified Ringsail parachute configuration, as tested in the PEPP Program, was selected for the parachute design. To assure reliable deployment, a single large diameter main canopy deployed by an extraction pilot parachute was selected. The main parachute will be deployed with one stage of reefing to minimize opening loads and parachute weight. The technique of reefing is a proven and commonly used method

of controlling parachute inflation and loads. It has been used in numerous applications in the past with complete success in all sizes of parachutes including Ringsail parachutes of the size that would be required for the Hard Lander of this study.

The single large diameter main canopy was selected over a cluster of smaller parachutes. More complexity is involved in deploying clustered canopies. The use of a cluster would increase the development risk for this application. Providing reefing with clustered canopies is much more complex than in the case of a single canopy because of the interactions of the clustered canopies. This interaction problem created a great deal of difficulty in applying reefing to the clustered parachutes used in the Apollo development. None of the inflation problems encountered in the Apollo development should be experienced in applying reefing to a single main parachute design investigated here.

With a reefed stage, the deployment loads experienced by the main canopy will be low enough to allow the use of light weight parachute construction. Analyses substantiating the materials and construction selected are presented in Volume III under Parachute Deceleration. The parachute system weights used were calculated using the RESEP program, which is described in Volume III, Appendix A. 4.

Parachute design drag performance was based on results obtained in the PEPP program. A constant value for C_D of 0. 52 was used. Other test data on Ringsail parachutes indicates a higher value for C_D should be obtainable. This would cause a reduction in parachute size, weight and opening loads. The use of $C_D = 0.52$ should therefore be conservative.

Available test data indicates that the Ringsail parachute inflation will follow the performance curve of figures 4-49 and 4-50 of "Performance of and Design Criteria for Deployable Aerodynamic Decelerators", ASD-TR-61-579 (referred to as the parachute handbook). This data was used for this preliminary design analysis. The parachute inflation characteristic was assumed to be linear with time for each stage of deployment, i. e., $C_D S$ increases linearly with filling time. This is a good assumption for a first cut design analysis and is fairly representative of test data.

4. 4. 6. 3 Design Trajectory Example

The purpose of the trajectory study was to verify that the selected point design could function under the worst case deployment conditions and meet the established design requirements of parachute deployment at Mach $\leq$ 2. 0 and reach main parachute full open terminal velocity at approximately 6 kft.

In some of the worst case point design trajectories investigated, the main parachute does not reach terminal velocity until altitude is down to almost 4 kft. When further work is done to finalize a planned vehicle design and re-entry trajectory, the deployment altitude of the parachute system can be adjusted to reach terminal velocity at 6 kft.

The worst design conditions for the parachute occur in the rarest atmosphere represented by VM-8. The trade-off studies indicate that the vehicle will not decelerate to Mach 2 until approximately 11 kft altitude. For all other atmospheres, Mach 2 occurs at a higher altitude. Parachute performance was designed to meet the worst case deployment conditions of the VM-8 deployment. The study made included the extraction and deployment of the main parachute by the pilot parachute.

The pilot parachute deployment occurred at 11kft, Mach 2, and q = 20 psf. The trajectory of pilot parachute extracting the main parachute was examined and compared to the trajectory of the vehicle now minus the weight of parachutes. This study was used to determine the point of start of main parachute reefed inflation where the main parachute skirt has been deployed. The results of this study are shown in fig. 4.4.6-1 for Point Design 2A and fig. 4.4.6-2 for Point Design 2B. The parameters selected for use in Point Design 2 are listed in table 4.4.6-1.

TABLE 4.4.6-1. PILOT PARACHUTE DESIGN PARAMETERS

	Design 2A	Design 2B
Atmosphere	VM-8	VM-8
Initial deployment altitude	11 kft	11 kft
Weight being decelerated by pilot parachute	193 lb	144.7 lb
Vehicle weight minus the parachutes	893 lb	650 lb
Path angle below horizontal	40°	40°
Pilot parachute fill time	0.24 sec	0.18 sec
Linear pilot parachute inflation with time assumed		
Pilot parachute D_o	15.7 ft	12.64 ft
Pilot parachute C_D	0.52	0.52
Pilot parachute C_DS	101. ft	65.3 ft
Pilot parachute opening shock factor	2.0	2.0
Average wake reduction effect during pilot parachute extraction	0.85	0.85
Aeroshell D_o	12.7 ft	11.4 ft
Aeroshell C_D	1.46	1.46

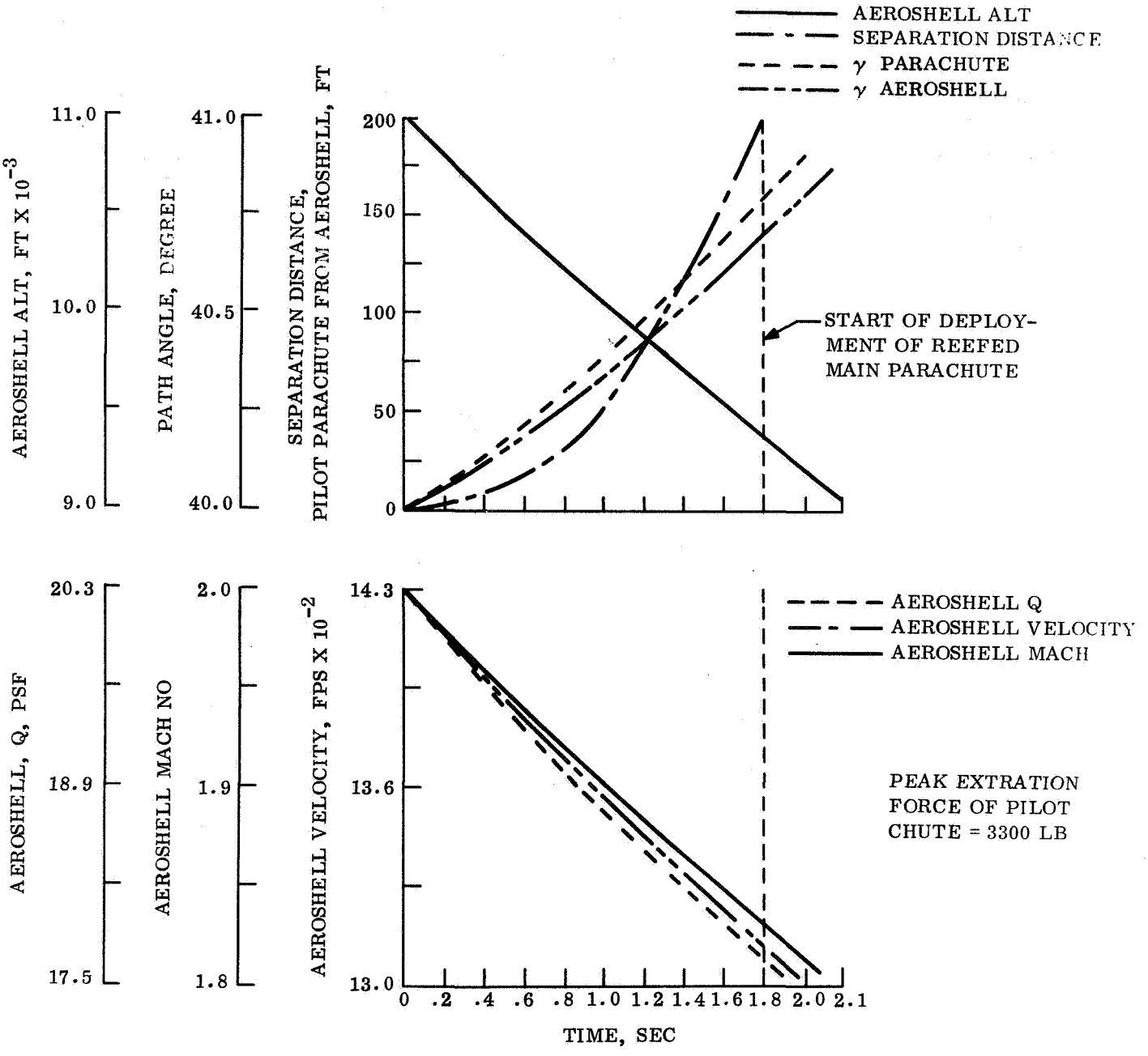


Figure 4.4.6-1. Pilot Deployment Trajectory Study, Point Design 2A

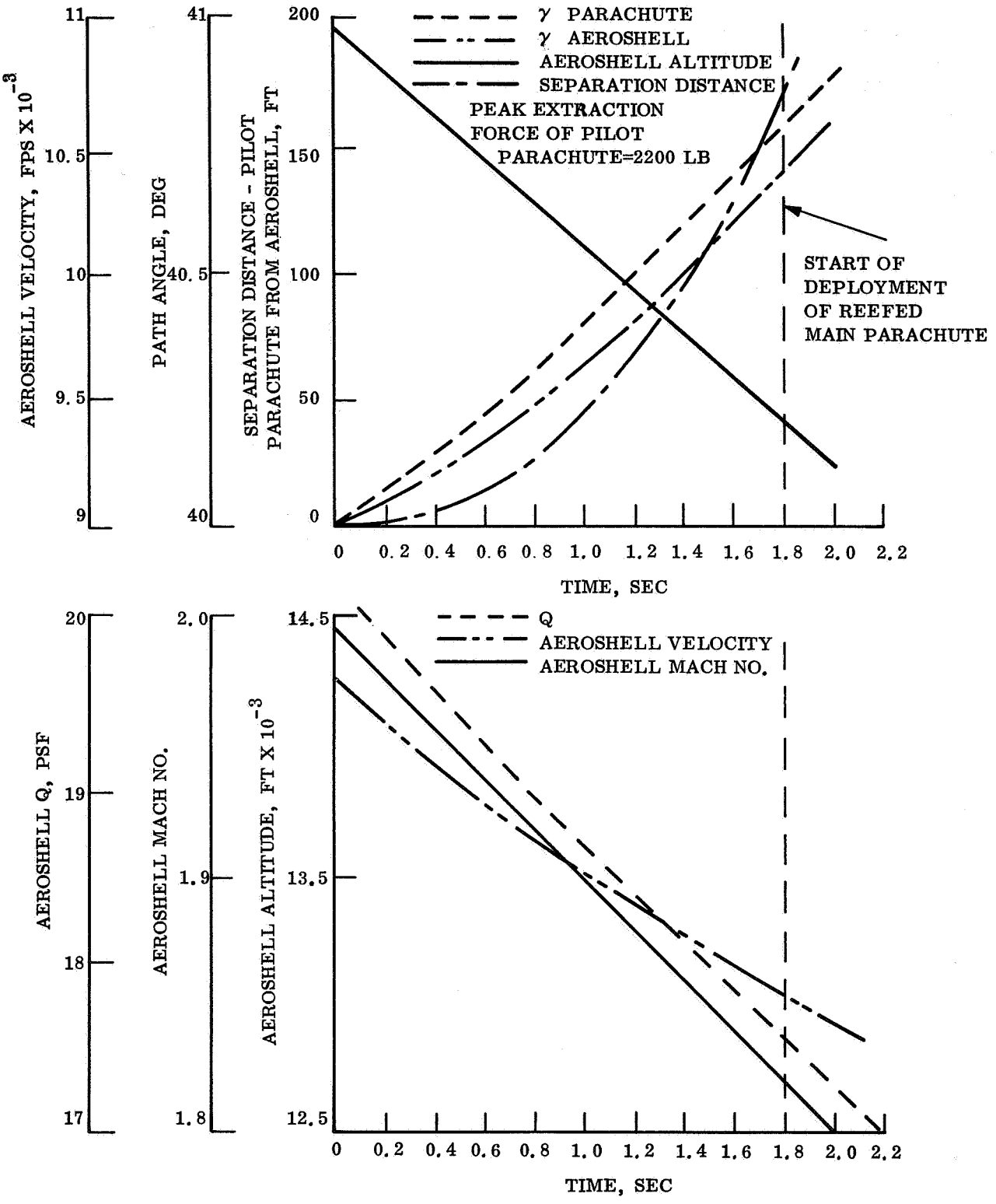


Figure 4. 4. 6-2. Pilot Deployment Trajectory Study, Point Design 2B

4.4.6.3.1 Parachute Staging Design and Trajectory

Parachute reefing and duration of the reefed stage were determined using existing computer programs to produce opening loads for both main parachute stages to be within the strength capability of the suspension lines and minimize altitude loss during deployment.

The analysis to establish reefing ratio is based on a simultaneous solution of the following equations for the two stage main parachute deployment.

$$F_1 = C_D S_1 \cdot X_1 \cdot q_1$$

$$F_2 = C_D S_2 \cdot X_2 \cdot q_2$$

$$q_2 = \frac{W_1 \cdot LF_1}{C_D A_1}$$

Where:

$C_D S$ = effective drag - ft^2

F = opening force - lb

X = opening shock factor

q = dynamic pressure - psf

W = weight in local gravity - lb

LF = force along Z axis in local gravity - g's

Subscripts:

1 = stage one

2 = stage two

The quantities $C_D S_2$, q_1, X_1, X_2, LF_1 and W_1 must be known. Without accurate performance data on a given design, assumptions must be made for X_1, X_2, and LF_1. If the correct characteristics are used, the performance can be verified in a computer trajectory analysis with a program designed to vary the $C_D S$ during parachute inflation.

Optimum reefing should produce equal opening load peaks for both stages. However, a reefed design can be satisfactory if other objectives are met and the peak loads are not balanced. In this case, if the opening forces are within the structural capability of the parachute and the total altitude loss during deployment is not excessive, the performance will meet the requirements.

In the staging study below values were selected based on past experience and data. Reefing ratio was selected, using the approach described above, to produce equal stage loads. In the trajectory study, fill time was based on data from the parachute handbook (ASD-TR-61-579) and C_DS growth was assumed to be linear with time. The disreef opening force from the trajectory analysis (shown on figure 3.4.6-2) came out lower than the reefed opening force. By iteration, the opening forces in the reefing ratio selection analysis and the trajectory analysis could be made to come out equal. However, at this point, the exercise would be academic. Slight changes in the disreef fill time, or some non-linearity in C_DS growth, or a combination of the two could significantly affect the resulting disreef open force. At this point, there is higher confidence that the reefed opening force is correct than there is in the disreef opening force.

In the hardware development program, the reefing line length to produce the desired reefing ratio will be selected based on the best existing data available. After first test data is obtained necessary adjustments would be made to obtain the desired reefed performance based on data from the actual system. There is high confidence that required reefed performance can be achieved with little difficulty.

The PEPP program demonstrated satisfactory inflation characteristics in Mach 2 deployment in a rare atmosphere. With reefing, inflation will proceed in the same manner as without reefing until the point where the reefing line restricts and delays full inflation. In all cases, a reefing design must be verified in the parachute development test program.

The parameters selected for the staging study are shown in table 4.4.6-2 for Point Design 2.

The parachute trajectory was calculated by computer using the established or calculated parameters shown in table 4.4.6-3.

The results of this trajectory study are shown in fig. 4.4.6-3 for Point Design 2A and in fig. 4.4.6-4 for 2B. These calculations are conservative inasmuch as the aeroshell or Lander drag area is not considered as part of retardation drag area after main parachute deployment.

4.4.6.4 Hardware Description and Function

The basic hardware concepts selected for Point Designs 2A and 2B have been previously used, tested and proven in other programs. The mortared parachute deployment is a commonly used, proven technique and the thermal cover concept and deployment arrangement were used by GE on the 698 BJ program and the MBRV program. The method of main parachute release has also been demonstrated on these programs using explosive nuts. The parachute designs are based on the designs and results to date of the NASA PEPP program. The aeroshell release and fall-away is similar to the re-entry heat shield separation used by GE in the A-45 program.

TABLE 4.4.6-2. MAIN PARACHUTE DESIGN PARAMETERS

	Design 2A	Design 2B
Main parachute full open C_DS	6587 ft^2	4897 ft^2
Initial reefed deployment q	17.74 psf	17.75 psf
Reefed stage opening shock factor	2.0	2.0
Disreef opening shock factor	0.5	0.5
Axial deceleration at disreef, Martian	7 g's	7 g's
Total weight being decelerated	1086 lb	795 lb
Main parachute C_D	0.52	0.52

TABLE 4.4.6-3. PARACHUTE TRAJECTORY PARAMETERS, POINT DESIGN 2

	Design 2A	Design 2B
Atmosphere	VM-8	VM-8
Total weight being decelerated	1086 lb	795 lb
Initial deployment altitude	9397 ft	9485 ft
Initial velocity, reefed deployment	1312 fps	1314 fps
Initial path angle	40.7°	40.7°
Linear reefed opening inflation with time assumed		
Reefing ratio	8.06%	8.07%
Reefed filling time	0.16 sec	0.14 sec
Total time of reefed stage	4.0 sec	4.0 sec
Main parachute D_o	127 ft	109.5 ft
Main parachute C_D	0.52	0.52
Main parachute full open C_DS	6587	4897
Main parachute full open fill time	3.16 sec	2.72 sec
Linear full opening inflation with time assumed.		

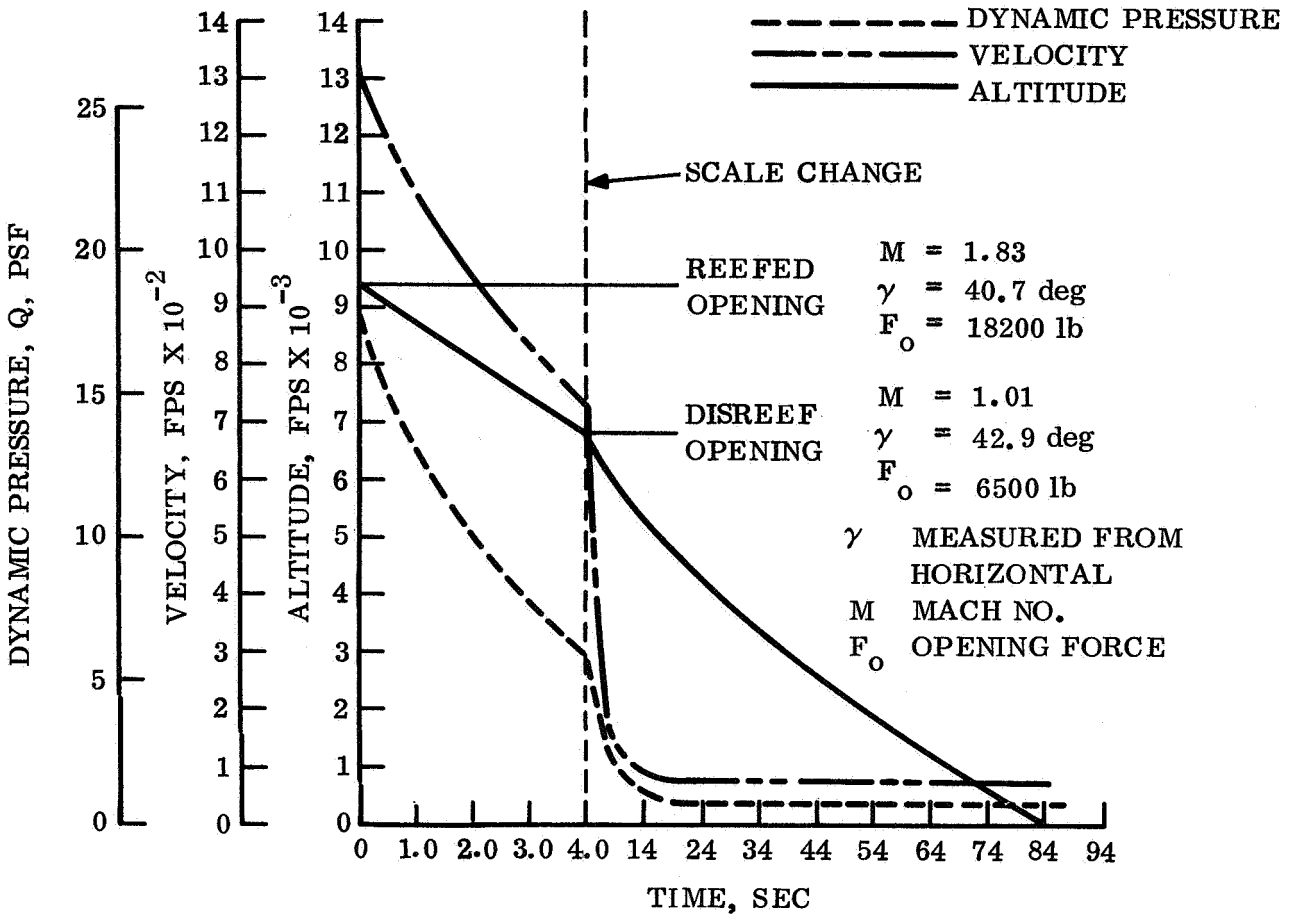


Figure 4.4.6-3. Main Parachute Trajectory in VM-8 Atmosphere, Point Design 2A

4.4.6.4.1 Pilot Parachute Mortar Thermal Cover

The thermal cover provides the means for securing the pilot extraction parachute in the mortar prior to mortar deployment. It also anchors one end of the main parachute thermal cover and provides thermal protection from wake heating to the pilot parachute, mortar gas source and the pull-away electrical disconnect. The cover will be secured to the mortar tube by a break cord or shear pins until mortar firing. A bag handle on the pilot parachute deployment bag will be secured to the thermal cover in a recess within the cover. Thus, the thermal cover will also provide a mass to assist in stripping the deployment bag from the pilot parachute during deployment.

4.4.6.4.2 Pilot Extraction Parachute

The pilot extraction parachute will be similar in design to modified Ringsails tested in the NASA PEPP Program. All parachute lines and materials will be sterilizable dacron. Presently, lightweight construction is envisioned using 1.1 oz cloth and 300 lb suspension lines. In a development program, an investigation would be made to determine the suitability of utilizing 0.8 oz material in the lower panels near the skirt to save weight. The pilot parachute will be pressure packed to a 40 lb/ft^3 density or slightly higher.

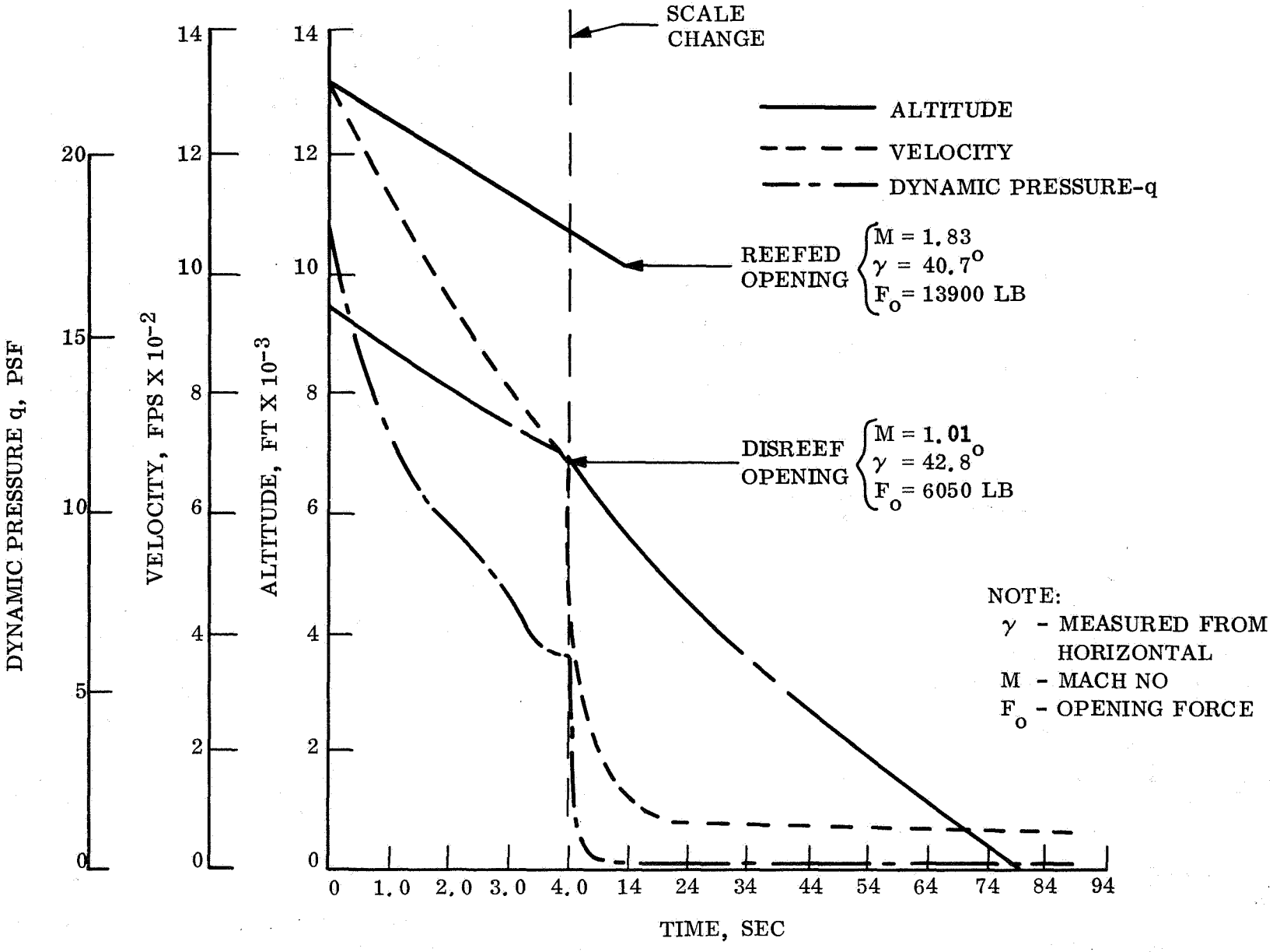


Figure 4.4.6-4. Main Parachute Trajectory in VM-8 Atmosphere, Point Design 2B

4.4.6.4.3 Pilot Parachute Riser Line

The pilot extraction parachute will be provided with a riser line to provide a minimum length of six aeroshell base diameters to the skirt at parachute inflation. This line will also be used to provide a mouth lock for the pilot parachute bag and to extract the main parachute bag for main deployment. It will be attached to two fittings, one at each end of the main parachute thermal cover, for extraction and deployment of this cover. The end of this line, at the main parachute bag, will be used to form a tuck bight through a locking loop of the three tie-down straps securing the main parachute in its compartment.

4.4.6.4.4 Main Parachute Compartment Thermal Cover

The main compartment thermal cover provides thermal protection for the main parachute pack from re-entry wake heating. It is deployed by the pilot extraction parachute and permanently attached to the pilot parachute riser. This cover can also serve as a mounting point for spring pushers to jettison the de-orbit propulsion and thrust structure. The cover will be made of aluminum with necessary reinforcement to sustain the loads of deployment. All edges will be rounded to prevent damage to the pilot riser line. The outside surface will be covered with a thermal protective coating to preserve the cover's structure and control main parachute temperature from re-entry wake heating.

4.4.6.4.5 Main Parachute, Two Stage Deployment, Modified Ringsail - 15 Percent Geometric Porosity

The main parachute will be a single large diameter parachute with one stage of reefing. Existing design hermetically-sealed reefing line cutters, manufactured by Technical Ordnance Products Co., will be used. The parachute will be made of sterilizable dacron material, which is a light weight construction similar to the constructions tested in the PEPP Program. At present, the parachute would be made of 1.1 oz cloth with 300 lb suspension lines because deployment 'q' will be 20 psf or less. In a development program to further reduce weight and volume, the use of 0.8 oz cloth in the lower panels near the skirt would be investigated. A higher weight, lower mechanical porosity material is needed in the crown area to facilitate initial reefed deployment. 1.6 oz material will be used in the crown area if added strength is required. The main parachute will be pressure packed to 38 to 40 lb/ft^3 density. Parachute reefing will be established to produce approximately equal opening loads at each stage of deployment to a level that utilizes the full structural strength capability of the suspension lines, considering appropriate design derating factors. The reefed stage time will be set as short as possible to minimize altitude loss during this stage and provide a high opening velocity for rapid full open inflation. The trajectory in the VM-8 atmosphere, where Mach 2 occurs at the lowest altitude, will be used to determine staging time and reefing ratio. The opening loads in any other atmosphere will be lower than those for the VM-8 atmosphere as the deployment is presently envisioned.

4.4.6.4.6 Main Parachute Attachment Riser

The attachment risers will connect the main parachute at the suspension line confluence to the three tie-down fittings at the bottom of the parachute compartment. As the main parachute releases, the parachute compartment including the mortar will remain with the main parachute.

4.4.6.4.7 Parachute Compartment Including Mortar

The parachute compartment will be an aluminum sheet metal fabrication to confine the parachute and provide thermal protection from re-entry wake heating. The outside surface of the compartment will be provided with the required thermal protective coating. The attachment and tie-down fittings will be attached to the rim at the bottom of the compartment. The pilot parachute mortar will be built into one side of the compartment. It will consist of a mortar tube and a sabot for the pilot parachute to seat against. The gas for mortar ejection will enter through tubing at the bottom of the mortar under the sabot. The area on each side of the mortar will be used for mounting the gas source for mortaring and the pull-apart electrical disconnect to separate the power supply from the mortar pyrotechnic. The side of the parachute compartment opposite the mortar will provide a slotted projection to receive a tang on the main thermal cover that secures that end of the thermal cover.

4.4.6.4.8 Parachute Attachment and Tie-down Fittings

Three fittings, one for each of three risers, are attached to the parachute compartment at the bottom flange and will be provided with two pins for webbing attachment. One pin will attach the main parachute risers (3), and the second pin will attach tie-down straps that secure the main parachute in a position such that it does not put a load on the main parachute thermal cover by pressing against it. The three tie-down straps will secure the main parachute using a locking loop and a tuck bight formed by the pilot parachute riser.

4.4.6.4.9 Mortar Pyro Gas Generator or Compressed Gas Supply

The gas for mortar ejection can be provided by either a pyro gas generator or a compressed gas supply. The compressed gas supply can be provided at a slight weight increase over the gas generator. Standard components are available from Conax Corporation (Conax Eager Paks) for the compressed gas supply. It would consist of a small hermetic cylinder (10 to 15 $in.^3$ capacity) containing compressed nitrogen at 3000 psi and a pyro valve that fires, piercing the cylinder allowing flow out through a connecting tube. This arrangement offers several advantages. There is no hot gas that could damage fabrics or components used for mortaring. There will be less problem of pyro development for the Mars mission in that the valve uses a standard squib and does not need the special gas generating materials. Reaction forces and performance will be more predictable. The compressed gas can be readily sterilized where this may be a problem with the gas generator materials.

4.4.6.4.10 Pull-apart Electrical Disconnect

This component consists of an electrical connector, half of which is mounted captive to the main parachute compartment. As the main parachute releases, i.e., the parachute compartment is pulled away, the two halves of the connector are separated. This component has been used successfully in a number of GE vehicle designs in the past.

4.4.6.4.11 Parachute Compartment Separation

The parachute compartment will be secured to the payload by three explosive nuts, each having dual cartridges, attached to bolts passing through the attachment and tie-down fittings.

These will be similar to the explosive nuts used for Capsule separation and described in Section 4.3.3. The main parachute tie-down and deployment loads will be carried by these separation devices and fittings.

4.4.6.4.12 Mach 2 Sensor

This device will sense Mach number as a function of vehicle base pressure divided by axial acceleration. The weight of the Mach 2 sensor is excluded from the retardation weight tables but is included in the entry systems weights. (Point Designs 3, 4, 5, and 6 incorporate an altitude marking radar for parachute deployment and release.)

4.4.6.5 Sequence of Retardation Subsystem Events

The series of deployment events described are depicted in fig. 4.4.6-5.

On receipt of the signal for parachute system deployment, power from the vehicle power supply will be applied to the mortar pyro initiation. Mortar firing will release and deploy the pilot parachute thermal cover and the pilot parachute. After stripping off the pilot parachute, the pilot parachute deployment bag and attached thermal cover free-fall away.

As the pilot parachute is being deployed, the main compartment thermal cover will be deployed by the snatch force of the pilot parachute. One end of the main thermal cover is released by the pilot parachute cover separation. The main cover is attached to the pilot parachute riser at two points for deployment and retention to the riser. As the cover is rotated out by the pull from the pilot parachute, the hold-down tang on the edge of the cover opposite the mortar will rotate out of a slot in the main parachute compartment, completely releasing the cover.

The snatch force of the main compartment thermal cover on the pilot parachute riser will pull out the tuck bight securing the main parachute tie-down straps. This releases the main parachute pack for deployment. Further pull force on the pilot parachute riser will be applied to the main parachute bag handles for main parachute extraction and deployment.

The aeroshell release devices would be delayed until the mortar is fired. The main parachute is extracted and deployed in a reefed condition by the pilot parachute. During this deployment, the mechanically initiated pyro time delay reefing line cutters are actuated. As the drag of the reefed main parachute develops, the aeroshell is released and allowed to free-fall away. After time-out of the redundant reefing line cutters, the cutters actuate severing the reefing line. This event permits main parachute full open deployment.

A 150 ft long drop line is used to sense the touchdown surface. Power is applied to the separation devices that cause release of the parachute compartment/mortar assembly from the Lander. The Lander will free fall to surface impact. The jettisoned main parachute will collapse and spill to one side due to the sudden release of loading from the suspension lines while the parachute was fully inflated. (Point Designs 3, 4, 5, and 6 incorporate a radar altimeter for this purpose.)

4.4.6.6 Retardation Subsystem Weight

The subsystem equipment weight for Point Designs 2A and 2B is tabulated in table 4.4.6-4.

TABLE 4.4.6-4. RETARDATION SYSTEM WEIGHT BREAKDOWN

	Design 2A	Design 2B
Pilot parachute mortar thermal cover	1.5	1.2
Pilot extraction parachute (modified Ringsail)	7.0	6.0
Main parachute compartment thermal cover	7.0	5.0
Main parachute, two stage deployment (modified Ringsail)	188.0	140.2
Main parachute attachment riser (3 legs)	2.0	1.5
Parachute compartment including mortar	15.0	12.0
Parachute attachment and tie-down fittings (3)	2.0	1.5
Mortar pyro gas generator or compressed gas supply	3.0	2.5
Pull-apart electrical disconnect	0.2	0.2
Explosive nuts (3)	2.5	2.2
Total subsystem weight	228.2	172.3

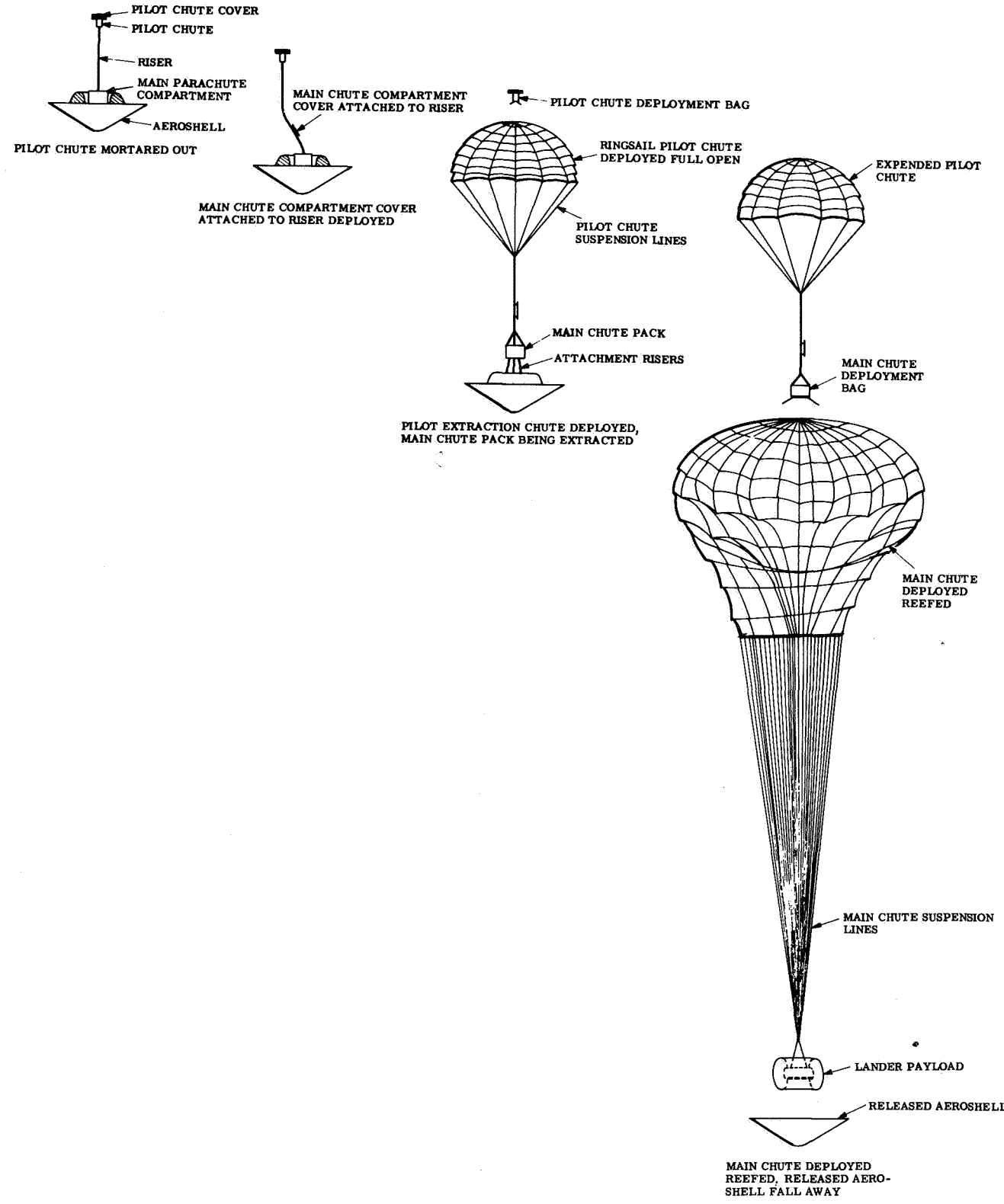


Figure 4.4.6-5. Retardation System Sequence of Events

4.4.7 ROLL CONTROL SUBSYSTEM

The roll control function for Point Designs 2A and 2B is performed by the deorbit equipment described in Section 4.3.7. A single monopropellant hydrazine control is used, in conjunction with a rate gyro, to perform both the functions of spin and entry roll control.

4.4.7.1 Roll Control Requirements

At very low dynamic pressures, blunt bodies can be made unstable at zero angle-of-attack by spin, contrary to the generally accepted trend. This phenomenon occurs after peak pressure where the pressure is decreasing with time. The effect here is that in the terminal steady state condition the vehicle will diverge to a trim angle-of-attack (dependent on configuration, spin rate, ballistic coefficient, and inertia properties) and follow a helical flight path.

The effects of this divergence may or may not be significant depending on requirements. Specific items that would be affected are base pressure measurements, radar altimeter measurements, vehicle ballistic coefficient (increases at angle-of-attack), and communication aspect angle.

In order to insure stability in this region a maximum roll rate must not be exceeded. However, roll torques will develop during entry due to built-in and ablation induced asymmetries. An estimate of this roll torque and the total roll impulse during entry was listed in table 4.3.7-1.

The Capsule will tend to spin up under the action of this roll torque and it is necessary to provide sufficient roll control torque and impulse to prevent Capsule roll rate from exceeding a maximum limit. Note, however, that it is not necessary to provide roll control torque greater than the peak disturbance torque because there is no requirement for roll attitude control in a non-lifting vehicle and the peak torque occurs for a very short period. The list of fixed hardware is given in table 4.4.7-1 for a total fixed weight of 10.7 lb for 2A and 10.3 lb for 2B. The weight of the remainder of the subsystem (hydrazine, pressurant, and tankage) for the two point designs is included in the design data shown in table 4.4.7-2. The control torque and impulse provided for roll control is listed in table 4.4.7-2.

TABLE 4.4.7.1. SPIN AND ROLL CONTROL SUBSYSTEM FIXED HARDWARE WEIGHT, POINT DESIGNS 2A and 2B

Component	Quantity	Weight (lb)	
		2A	2B
Rate gyro	1	1.0	1.0
Spin electronics	1	2.4	2.4
Fill valve	2	0.5	0.5
Squib valve	1	0.5	0.5
Pressure sensor	1	0.5	0.5
Temperature sensor	1	0.25	0.25
Valves	2	0.6	0.6
Thrusters	4	1.0	1.0
Tubing, fittings	-	1.05	1.05
Supports	-	2.9	2.5
Total weight		10.7	10.3

TABLE 4.4.7-2. SPIN AND ROLL CONTROL SUBSYSTEM, POINT DESIGN 2 PARAMETERS

	Units	Point Design	
		2A	2B
Separation to spin-up time	sec	1.5	1.5
Spin rate	rpm	50	50
Spin-up time	sec	25	25
Roll thrust	lb	5.6	4.2
Roll torque	ft-lb	67.2	44.8
Impulse requirements			
spin/de-spin	lb-sec	529	391
roll control	lb-sec	167	135
Weight of Hydrazine			
spin/de-spin	lb	2.3	1.7
roll control	lb	0.7	0.6
Tank weight	lb	2.7	2.1
Pressurant weight	lb	0.6	0.4
Fixed hardware weight	lb	10.7	10.3
Total subsystem weight	lb	17.0	15.1

4.4.8 ENTRY SYSTEMS WEIGHT

A summary weight statement for the items comprising the entry system weight (less Lander and pre-entry systems weight) for Point Designs 2A and 2B is shown in table 4.4.8-1. Total entry system weight for Point Design 2A is 622 lb and for Point Design 2B is 504.2 lb.

TABLE 4.4.8-1. ENTRY SYSTEM WEIGHT SUMMARY, POINT DESIGNS 2A AND 2B

Item	Weight (lb)	
	2A	2B
Aeroshell skin	116.0	90.0
Miscellaneous structure	52.0	40.0
Heat shield	182.0	160.0
Separation system	1.8	1.8
Attitude control	17.0	15.1
Retardation	228.2	172.3
Harness and cabling	19.5	19.5
Entry science	2.5	2.5
Mach 2 sensor	3.0	3.0
Total entry system weight	662.0	504.2

4.5 LANDER SYSTEMS

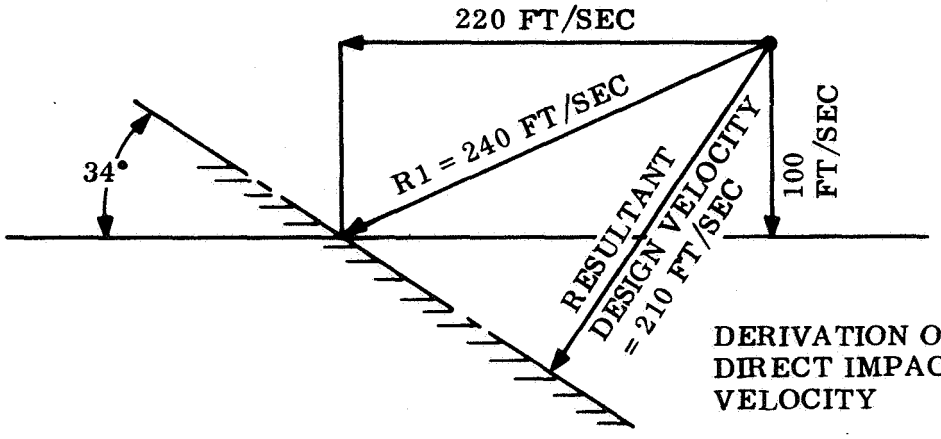
4.5.1 CONFIGURATION CONSTRAINTS AND DESCRIPTION

4.5.1.1 Constraints and Design Parameters for Point Design 2

1. Maximum horizontal velocity of Lander at impact due to winds: 220 ft/sec.

2. Maximum vertical velocity of Lander at impact: 100 ft/sec. This was selected based on the optimization of the deceleration and impact attenuation subsystems.

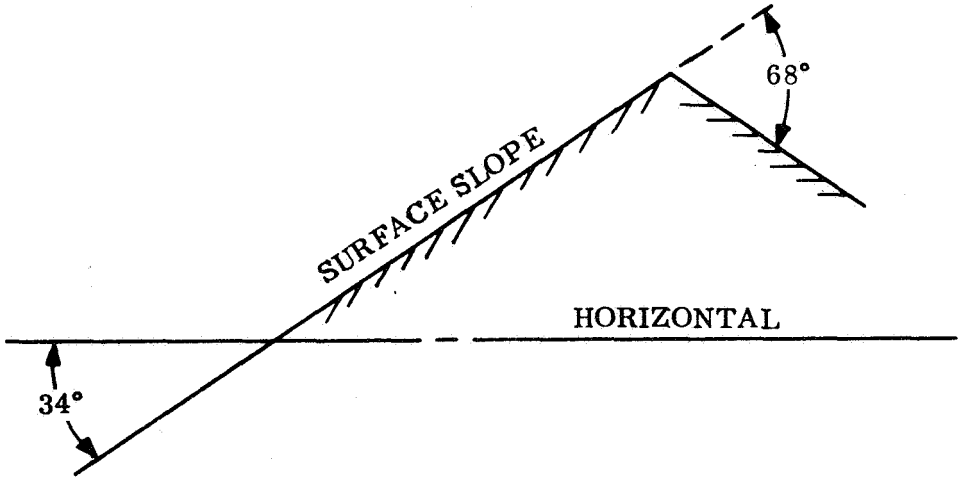
3. Maximum resultant direct impact design velocity: 210 ft/sec.



DERIVATION OF DIRECT IMPACT DESIGN VELOCITY

4. Surface characteristics (to NASA/LRC requirements)

   a. Surface slopes: zero to $\pm 34^{\circ}$ relative to horizontal, with abrupt slope changes of $\pm 68^{\circ}$ forming hills (or valleys), as shown in the following sketch:



b. Continuous slopes: as long or longer than the base diameter of the Lander.

c. Maximum surface rock diameter: 5.0 in.

5. Maximum total Lander design g-level: 1000. Selected for point design, as a compromise between conflicting influences of structure and impact attenuation system design, volume for aeroshell packaging and weight.

6. Vehicle attitude and impact system design

a. Vehicle 2A. Omni-directional full attenuation capability for maximum design velocity and g-level.

b. Vehicle 2B. Multi-directional design with attenuation capability for the maximum design velocity and g-level on the prime impact side and around the edge to approximately 70°. The remainder of the impact attenuation system on the backface and edges has been designed for 100 ft/sec impact velocity at maximum g-level. The geometry of the system is shown in Section 4.5.8.

7. Landed temperature conditions assumed for environmental control design

a. Ambient: -152° F to $+114^{\circ}$ F (to specification*)

b. Component tolerance (non operating): -40° F to $+160^{\circ}$ F except for battery where the allowable temperature range is $+50^{\circ}$ F to $+80^{\circ}$ F.

8. Surface mechanical properties

a. Bearing capacity: 6 psi to infinity

b. Coefficient of friction: up to 1.0

(Infinite strength surface assumed as the limiting design case for impact attenuation).

9. Geometrical, weight, and c.g. constraints

a. Packaging objective: approximately 40 lb/ft^3 in central cylinder of payload container.

b. Center-of-gravity: on or forward of horizontal center line of Lander container.

*Mars Engineering Model Parameters for Mission and Design Studies. Langley Research Center, May 1968.

4.5.1.2 Lander Description

4.5.1.2.1 Configuration

The Lander concept is a doughnut shaped vehicle, with a central circular flat pack payload container. Either side of the vehicle may be face up after landing. It utilizes a completely passive landing system. The configuration of Point Design 2, illustrated in fig. 4.5.1-1, general assembly of Lander, shows the layout of and the volume required for a solid core memory and dual multicoder telecommunication system. A thin film memory and single multicoder system was evolved during the Point Design 3 effort and has been included in Point Design 2 performance and weight descriptions without revising the Lander general assembly.

The central container, a short, large diameter cylinder with a D-shaped edge structure, houses all the science and supporting subsystem equipment. A deep ring phenolic glass impact attenuation system is bonded to the edge structure of the payload container. Provision is made for science instruments and other equipment to be deployed from the Lander. The degree and type of deployment necessary varies between point designs and is discussed in detail in deployment Section 4.5.6 for Point Design 2.

Depending upon the vehicle mission, electrical power and telecommunication subsystem vary between point designs. These subsystems and other vehicle equipment for Point Design 2 are discussed in detail in the following Lander sections.

Point Design 2 is the smallest and simplest Lander system with a minimum payload and the shortest operational surface lifetime. It is designed with an omni-directional landing capability in its 2A configuration, illustrating the penalties paid for this capability over the the 2B multi-directional Lander; in weight and volume in the impact attenuation system, in vehicle packaging in the aeroshell and, to some extent, added complexity in the required instrument deployment.

4.5.1.2.2 Science Payload

Science instrument payload installed is the specified minimum listed and discussed in Section 4.5.2. The Lander carries the majority of the entry science as well as the surface science, to avoid duplication of supporting subsystems and instruments and for flexibility of data acquisition and storage.

Provision is made for deployment of cameras, wind measuring instruments, temperature transducers and the alpha back scatter instrument head. The cameras, wind velocity and temperature instruments are housed in a central bay, which is the full width and depth of the Lander payload container. They are mounted on short spring-loaded swinging booms primarily provided for camera deployment. The wind velocity instrumentation requires secondary spring-loaded arms, which unfold at right angles to a spring-loaded extension of the camera booms when the booms are deployed, to provide correct relative location. Deployment of equipment from this bay is substantially automatic following selection and jettison of the bay door on the uppermost and exposed side of the Lander.

With the current provision of four separate cameras and deployment booms and the capability to deploy all four from either side of the Lander for high and low resolution imaging, some boom deployment sequencing will be necessary, but can be kept relatively simple.

A gravity-sensing device determines the uppermost side of the Lander and releases the upper door. Doors are spring-loaded and secured with bolts incorporating hot-wire devices.

The alpha back scatter instrument is located in a separate full depth bay and the instrument head can be deployed downward onto the planet surface through whichever side of the Lander constitutes the underside. To facilitate this operation with a minimum of rotational movement of the instrument head, the alpha back scatter instrument is installed on its side in the bay. Sensing for operation of inward hinging doors enclosing the alpha back scatter bay is by the gravity device provided for the camera bay doors. A full detailed description of the deployable instrument installation and mechanical operations, with illustrations, is given in Section 4.5.6.

The remainder of the payload (science and supporting subsystems) is housed in other compartments formed by the inner framework of the payload container. Access to this equipment is available through either the top or bottom bolted covers of the container, or by removal of the inner framework from the Lander, complete with all equipment. The installation is compact to achieve low weight and volume, but consistent with requirements for assembly, service and operational functions.

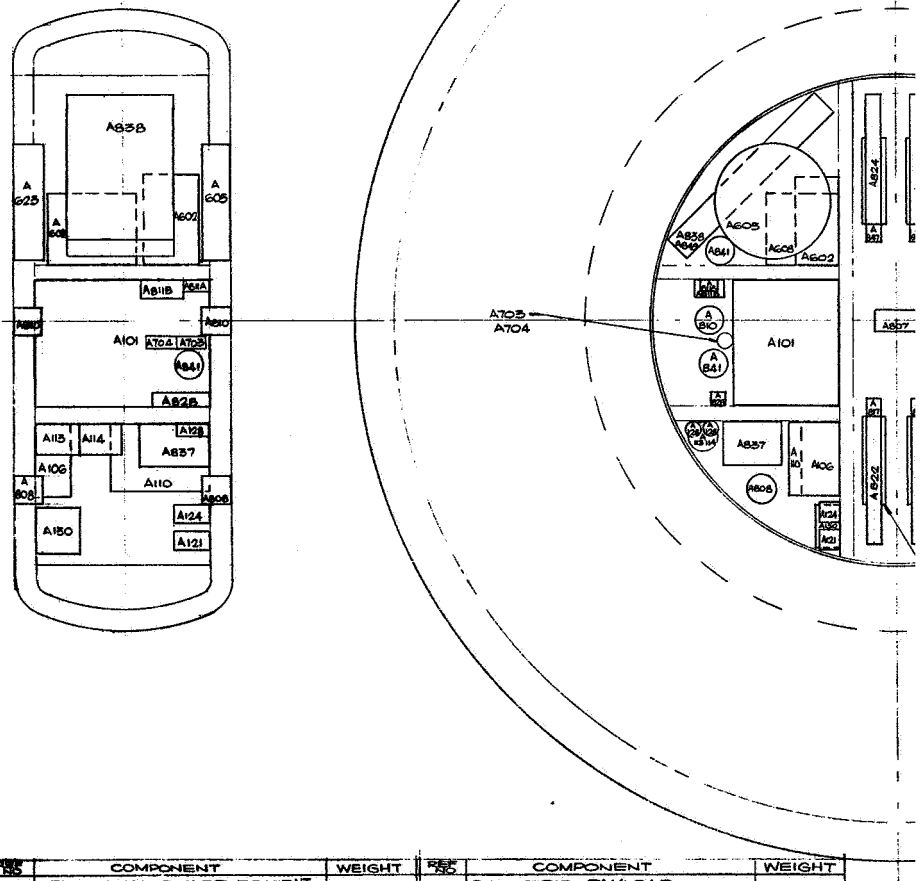
4.5.1.2.3 Lander Support Subsystems

To perform the one diurnal cycle mission of Point Design 2, the telecommunications link is designed to provide a relay link for transmission of imagery data for the periapsis passage of the Orbiter immediately after impact on the surface of the planet and at the end of each succeeding diurnal period. The telecommunications system consists of a 400 MHz transmitter with a dual power amplifier output stage, memory with 180 kbit storage capacity, and the appropriate signal condition and data handling equipment.

The electrical power and distribution equipment located in the Lander provides all the primary power required of the Lander and the appropriate programming and sequencing functions. The main power source for this mission is a silver-zinc battery of approximately 30 lb. This battery was sized based on a 30 watt-hr/lb rating.

As stated, surface science equipment consists of the minimum science package including equipment to measure wind velocity, surface temperature and pressure, alpha back scatter, imagery, a clinometer and moisture detector. Imagery data will be taken and transmitted to the Orbiter during the periapsis passage for each of the four available transmission periods, and will be transmitted real-time. Additionally, stored entry and surface science data, diagnostic, and real-time surface science data is alternately transmitted between the picture taking sequence.

FOLDOUT FRAME 1



REF NO	COMPONENT	WEIGHT
	ELECTRICAL POWER EQUIPNT.	
A101	BATTERY OPERATIONAL	5.5
A106	SWITCH PWR TRANSFER	2.0
A107	PROGRAMMER LANDER	7.2
A108	REGULATOR VOLTAGE	7.0
A110	CONTROLLER POWER	5.5
A115	BATTERY HI-RATE A	0.5
A114	BATTERY HI-RATE B	0.5
A115	FILTER EMC. C.	1.9
A121	MODULE DIODE BLOCK	0.18
A124	MODULE . THRM . RLY C.	0.18
A128	SWITCH . HG A	0.1
A129	SWITCH . HG B	0.1
A150	REGULATOR VOLTAGE	1.0
	TELECOMMUNICATIONS	
A602	TRANSMITTER VHF	9.0
A604	CONDITIONR. SIG. DATA (2)	9.0
A605	ANTENNA , VHF RLY. A	5.0
A607	UNIT CORE STORAGE	25.0
A608	RECEIVER VHF BEACON	7.5
A609	PROCESR . DATA . HANDLING	4.5
A610	DIPLEXER VHF A	.75
A611	DIPLEXER VHF B	.75
A623	ANTENNA VHF RELAY B	5.0
A670	MULTICODER (2)	9.0
A811B	IMPACT 'G' METER	2.2
WU104	CABLE ASSYS	10.0
	THERMAL CONTROL	
A703	HEATER ELECTRONICS	0.1
A704	THERMOSTAT HTR. ELEC	0.1
	INSULATION	10.0

REF NO	COMPONENT	WEIGHT
	SCIENTIFIC PAYLOAD	
A807	ACCELEROMETER TRI-AX	2.0
A808	TRANSDUCER TEMP. (2)	1.0
A809	TRANSDUCER PRESS (2)	1.0
A810	TRANSDUCER PRESS (2)	1.4
A817	TRANSDUCER TEMP (2)	2.0
A822	CAMERA A	2.0
A823	CAMERA B	2.0
A824	CAMERA C	.4
A825	CAMERA D	.4
A828	ACCELEROMETER LONGE	.5
A829	SENSOR WIND VEL.	.5
A830	SENSOR WIND VEL.	.5
A831	SENSOR WIND VEL.	.5
A832	SENSOR WIND VEL.	.5
A833	SENSOR WIND VEL.	.5
A834	SENSOR WIND VEL.	.5
A835	SENSOR WIND VEL.	.5
A836	SENSOR WIND VEL	.5
A837	SENSOR MOISTURE	10.0
A838	SPECTROMETER MASS	8.0
A841	INCLINOMETER (2)	2.6
A842	INSTRUM. SURF. COMPOSITION	9.5
A845	SENSOR WIND VEL	.5
A846	SENSOR WIND VEL	.5
A847	TRANSDUCER TEMP	.5
A848	TRANSDUCER TEMP	.5
A849	WATER VAPOR DETECTOR (DUCT)	1.0

FOLDOUT FRAME 2

FOLDOUT FRAME

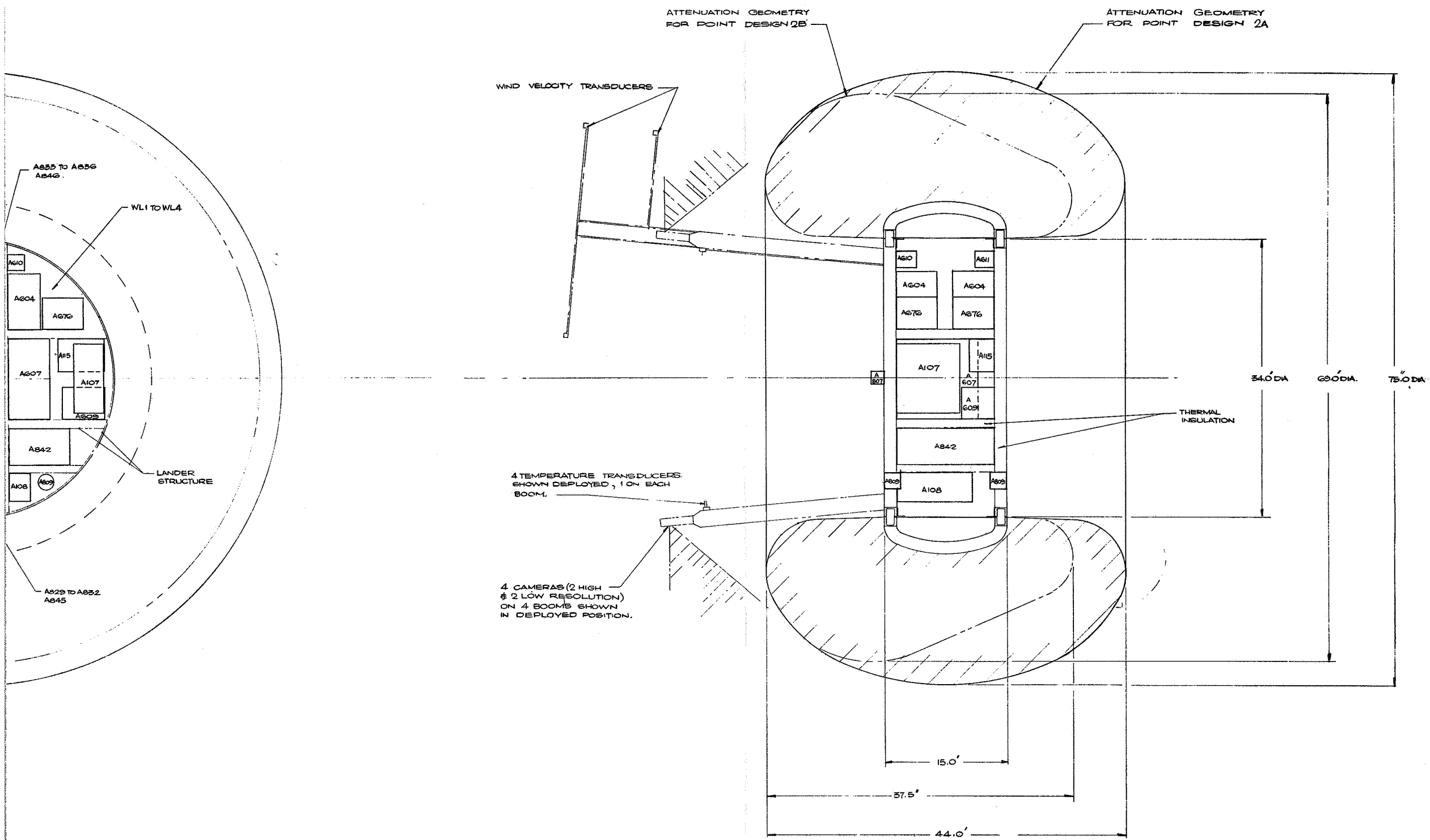


Figure 4.5.1-1. General Assembly Point Design 2

Environmental control, primarily an insulation problem, is achieved by the use of honeycomb panels with fiberglass core for the outer shell of the Lander container; coupled with the application of thick layers of foam on exposed surfaces, such as the sidewalls of the camera bay. Batteries, which are the components most sensitive to the cold environment, are maintained at a working temperature by a combination of heat dissipated from other components and an individual electric heater.

A complete description of science and Lander subsystems including structural and mechanical components is given in the following sections, together with detailed weight information.

4.5.2 SCIENCE PAYLOAD EQUIPMENTS

4.5.2.1 General

The various instruments carried by the Hard Lander to Mars may be classified into two general categories. They are the entry phase instruments, which require no special compatibility with unusually high deceleration loading, and the landed phase instruments, which must survive the extreme loads and shocks encountered during impact and maintain their calibration and state of operability. In most cases, the entry phase instrumentation can be rather well defined in terms of the state-of-the-art; however, certain devices, such as the water vapor detector, will require some development before a device is available that will fulfill the scientific requirements of measurement. The landed phase instrumentation includes a minimum science payload and certain other devices that may feasibly be carried by the Lander. In this group of instruments there are several devices that do not physically exist at the present. Others in this group are at some point in their development that provides sufficient confidence in their design to consider them in this mission even though serious doubts exist concerning their ability to withstand the high 'g' impact of the Hard Lander. For these designs, additional shock attenuation can be considered for isolating the instrument from the extreme environment. However, this additional weight and volume appears prohibitive at the present time.

The section provides a brief summary of the scientific instrumentation selected for inclusion in the point designs. Detailed descriptions of the equipment and the studies performed in their selection have been given in previous sections (2.3.3 and 2.3.4) of this volume. Considerations used for identifying the implementation approaches best suited for the missions have been discussed in Volume II, Section 4.

4.5.2.2 Entry Science Payload

4.5.2.2.1 Tri-axial Accelerometer

The tri-axial accelerometer is mounted at the entry system c.g. Several varieties are currently available, however the magnetic force balance type seems to have the most desirable characteristics. Table 4.5.2-1 shows the mechanical and electrical characteristics of an accelerometer that is currently being used on various military programs. Also shown are the sequencing, sampling and data format requirements for the accelerometer. No significant problems are foreseen in sterilizing the device.

TABLE 4.5.2-1. ENTRY SCIENCE PAYLOAD

Instrument (Lander)	Weight	Volume	Power Req'mts	Location	Sampling Schedule	Data Format
Mass spectrometer	8 lbs	2 x 7 x 14 in.	7 watts	Internal near surface. Requires port through heat shield	Initiates near Mach 5. Terminates at impact	50 (8) bit words per sample (2 sec scan, 8 sec readout) 50 bits/sec readout
Resistance thermometer	0.5 lb each	1 in. dia x 2 in. long	1 watt each	Two on base of vehicle	Initiates at Mach 5. Terminates at impact	1 sensor output channel 1 sample/sec
Variable capacitor pressure transducers	0.5 lb each	2 in. dia x 2 in. long	1 watt each	Two on base of vehicle	Initiates at beginning of entry. Terminates at impact	1 sensor output channels 1 sample/sec
Tri-axial accelerometer (1 Dual Scale)	2 lb	2.8 x 1.8 x 2 in.	4 watts	Located at body c.g. with one axis aligned to vehicle vertical axis	Initiates at beginning of entry. Terminates impact	8 bits/sample/axis 10 samples/sec 72 bits/sec total Automatic scale switching
Water vapor detector	1 lb (ducting only)	Detector located in surface science package	N/A	Ducting located same as mass spectrometer ducting	Initiates near Mach 5. Terminates at impact	1 sample/15 sec 2 seven bit (parallel) channels 1 eleven bit (parallel) channels

TABLE 4.5.2-1. ENTRY SCIENCE PAYLOAD (Concluded)

Instrument (Aeroshell)	Weight	Volume	Power Req'mts	Location	Sampling Schedule	Data Format
Stagnation temperature transducer (1)	0.5 lb	1 in. dia x 2 in. long	1 watt	See text	Initiates at beginning of entry. Terminates at aeroshell ejection	1 sensor output 1 sample/sec
Stagnation Region pressure transducer (4)	0.5 lb each	2 in. dia x 2 in. long each	1 watt each	Behind nose of aeroshell (See text)	Initiates at beginning of entry. Terminates at aeroshell ejection	1 sensor output 1 sample/sec

4.5.2.2.2 Temperature Transducers

Atmospheric temperature measurements during the entry phase are performed by three temperature transducers. These are platinum resistance thermometers. One is located in the stagnation region of the aeroshell and measures the stagnation temperature from the beginning of entry down to aeroshell ejection. The other two thermometers are located on the base of the Lander system and are used during the subsonic region of flight primarily during parachute descent. Table 4.5.2-1 shows the physical and electrical characteristics of the resistance thermometer and its data collection profile. The exact configuration and design of the stagnation transducer will depend upon a large number of variables. The definition of the transducer design parameters will require preflight testing of the thermal characteristics of either scale model or prototype vehicles.

4.5.2.2.3 Pressure Transducers

Variable capacitance pressure transducers located on the aeroshell and on the base of the entry system measure atmospheric pressure profiles. The four transducers arrayed about the stagnation region perform the dual function of measuring pressure and angle-of-attack. These transducers are located just behind the heat shield and are exposed to the external environment via ducting leading through the beryllium cap of the heat shield. The pressure transducer located on the base of the Lander system measures base pressure from supersonic through subsonic flight regimes. Table 4.5.2-1 lists the characteristics of these transducers and also shows the sampling schedule and data format.

4.5.2.2.4 Mass Spectrometer

The measurement of atmospheric composition by mass spectrographic techniques requires acquisition of a sample from the atmosphere. This acquisition must be performed without exposure to contamination from gaseous materials exuded by the heat shield or other sources. The ducting leading from the mass spectrometer to the external environment terminates in the nose area that contains the beryllium plug which serves to minimize the probability of contamination from heat shield outgassing products. This same ducting also delivers atmospheric samples to the water vapor detector located in the entry payload and must be disconnected when the aeroshell is separated from the Lander at parachute deployment.

Table 4.5.2-1 shows the physical, electrical, and data collection characteristics of the mass spectrometer.

4.5.2.2.5 Water Vapor Detector

At present the chemical/radiological water detector is in the concept development stage. Since this device will also be used during landed operations it must be designed for high shock survival. Figure 4.5.2-1 shows, in block diagram form, the design of the water vapor detector. Table 4.5.2-1 shows the physical and electrical characteristics of the detector. The ducting leading from the nose for entry data is disconnected at aeroshell separation and a second port is opened for landed operations.

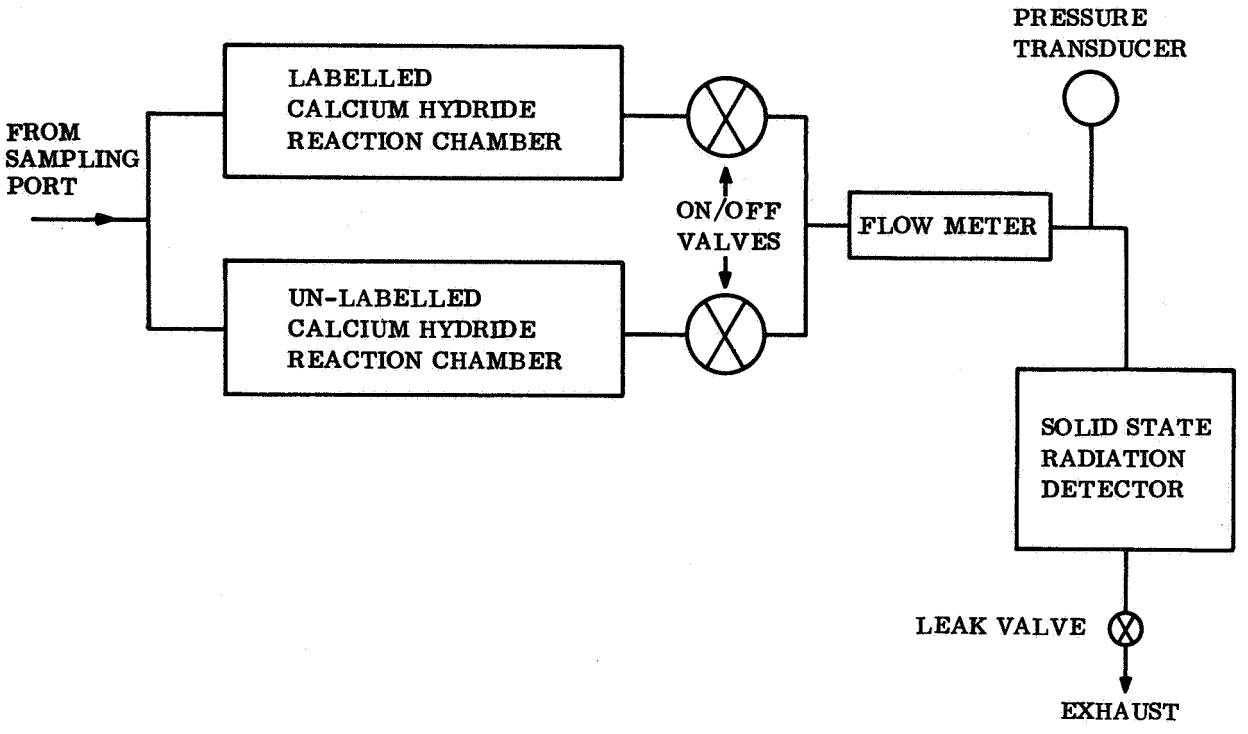


Figure 4.5.2-1. Water Vapor Detector, Block Diagram

The basic operating principle is that when calcium hydride comes in contact with water (in either liquid or vapor form) the following reaction takes place:

$$CaH_2 + 2HOH \longrightarrow Ca(OH)_2 + 2H_2$$

When the hydride is labelled with tritium, the gaseous effluence contains the radioactive tritium. This element may be quantitatively detected by its radiation and thus the amount of water entering into the reaction may be determined. Radiation shielding of this system will present no problems since tritium emits 18 kev beta particles that are stopped by the chamber walls. Present laboratory tests have demonstrated the device at 1 part/million with definite indications of feasibility for operation of 1 part/billion.

4.5.2.3 Surface Science Payload

4.5.2.3.1 Pressure Transducer

Unlike the pressure transducers included in the entry payload, the surface pressure transducer must be able to withstand high level shock loading. This requirement necessitates either an extension to the state-of-the-art in low pressure transducers or provisions for reducing impact loading much below 1000 g's. The added weight and volume for this shock compatibility or attenuation is not included in the component weight or volume shown in table 4.5.2-2.

TABLE 4.5.2-2. SURFACE SCIENCE PAYLOAD

Instrument (Lander)	Weight	Volume	Power	Location	Deployment/ Orientation	Mission Profile	Data Format/ Requirements
Pressure Transducer (2)	0.7 lb each	2 in. dia, 2 in. long each	1 watt each	Internal near skin of vehicle	Port through skin to ambient environment either top or bottom No deployment	Operates continuously after impact	3 samples hr each 1% accuracy Two channels total
Resistance Thermometer (4)	0.5 lb each	1 in. dia, 2 in. long each	1 watt each	One on each camera boom	Deployed above Lander on camera booms One on each boom	Same as above	3 samples/hr each 1% accuracy Four channels total
Wind Velocity Transducer (2)	2.5 lbs each	25 cubic in. prior to deployment each	3 watts each	One on each of two camera booms	Boom deployment above vehicle on camera booms	Same as above	3 samples/hr 6 channels Each channel consisting of 11 parallel bits Total of 66 bits/sample
Moisture Detector (1)	10 lb	60 in.^{3}	5 watts	Mounted internal to Lander	Pneumatic tubes deployed as part of camera booms	Same as above	3 samples/hr 2 seven bit (parallel) channels 1 eleven bit (parallel) channel

TABLE 4.5.2-2. SURFACE SCIENCE PAYLOAD (Concluded)

Instrument (Lander)	Weight	Volume	Power	Location	Deployment/ Orientation	Mission Profile	Data Format/ Requirements
Surface Composition (Alpha backscatter) (1)	9.5 lb	5.5 x 7.5 x 4.5 in.	5 watts	Internal to vehicle	Must be deployed so that sensor head rests on surface of planet top or bottom deployment controlled by clinometer	Deploy 3 hr after impact First readout 1 hr after impact 2nd readout 3 hr after impact then readouts every 3 hr thereafter	1 sample/3 hr 130 channels 14 bits (parallel) each 130 channels 12 bits (parallel) each 3 channels 7 bits (parallel) each
Photo-imaging (4)	4.8 lb total	1 to 2 in. dia 9 to 12 in. long each	6-10 watts total	One on each of four booms deployed above Lander	Boom deployment 36 in. Height > 18 in. One boom/ camera	4 frame sweeps on high resolution and 4 frame sweeps on low resolutions in sequence Operation time time coincident with transmissions	Flexible to meet maximum transmission capability of Lander. Period from 1 sec to 8 hr/ picture. Total bits between 10^7 and 10^8
Clinometer (2)	1.3 lb each	2 in. dia x 3 in. long	3 watts	Two internal to Lander mounted with long dimension parallel to vertical axis of Lander	N/A	Sampled immediately after impact then once every 3 hr	1 sample/3 hr 2 channels 7 bits (parallel) per channel

4.5.2.3.2 Temperature Transducer

Atmospheric temperature is measured by a set of platinum resistance thermometers. They are deployed following impact with the camera booms to obtain free stream data with minimum Lander-induced perturbations. Such devices have been designed to withstand rather high g-loading and thus no serious problems are expected as a result of a rough landing. The ultimate physical design of the thermometers will deal with minimization of direct solar heating since this can be a serious measurement problem. A solar shield is required to accomplish the task of decoupling the resistance element from the solar flux. See table 4.5.2-2 for transducer characteristics.

4.5.2.3.3 Wind Velocity Sensor

Although an acoustic velocity sensor has not yet been built for planetary exploration application, the changes required to modify existing designs intended for terrestrial applications appears straightforward. The design approach used for point design evaluation consists of five magnetostrictive transducers (fig. 4.5.2-2) mounted on the boom supporting the TV camera system. A microminiaturized electronic package produces the necessary ultrasonic pulses that drive the transducers and also measures the transit time for each pulse to travel from one transducer to the next. No problem is foreseen in fabricating the required electronics and transducers to meet the sterilization and shock environment requirements. Care must be taken, however, to assure reasonably good rigidity in the transducer supporting arms during the measurement since motion of the transducers may be misinterpreted to signify motion of the medium (atmosphere). Table 4.5.2-2 shows the anticipated physical and electrical characteristics of the wind velocity sensor.

4.5.2.3.4 Water Vapor (Moisture) Detector

The chemical/radiological water vapor detector has not been hardened for the extreme environments that will be encountered during the entry and landing phases of the mission. However, since the design is inherently mechanically simple, it is expected that a device with the physical characteristics shown in table 4.5.2-2 can be developed and tested in time for a 1973 mission to Mars. Operating experience (laboratory) in the low parts/million and high parts/billion range has demonstrated that water vapor sorption-desorption by materials used in the sampling system could be the major factor toward limiting the response and detection sensitivity in this and lower concentration regions. This would also be of special importance for water detectors based on physical principles especially at lower operating pressures, where sorption-desorption by the detector supporting hardware could contribute significantly to a non-representative water environment around the detector. It is felt that water sorption-desorption can be controlled by appropriate materials selection, by minimizing exposed surfaces, and by operating these surfaces at temperatures consistent with the level of water concentration to be sensed.

The device will remain in the Lander during operation and gas sampling will occur through a vent tube in a camera boom. The key interface requirements are shown in table 4.5.2-2.

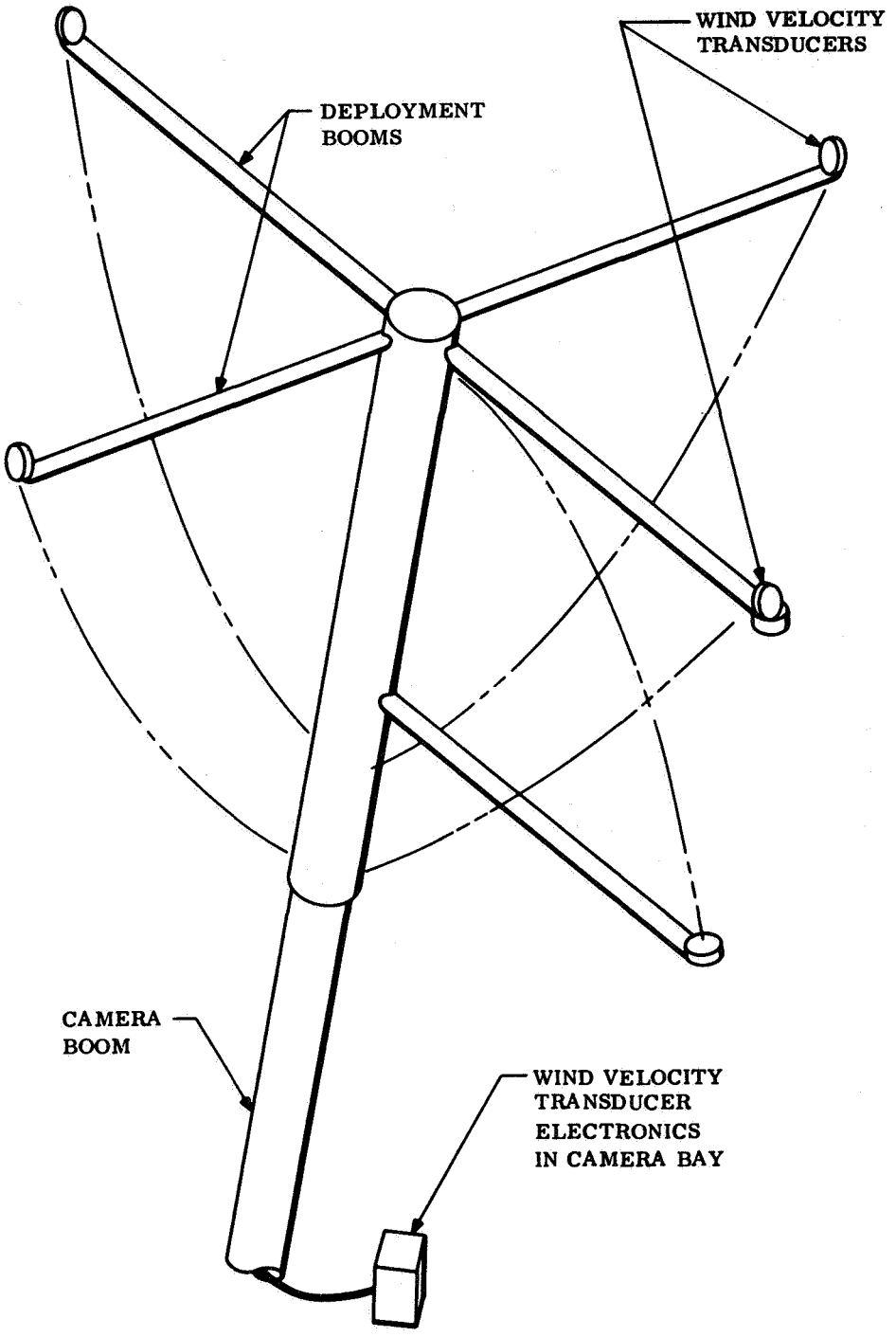


Figure 4.5.2-2. Wind Velocity Sensor

4.5.2.3.5 Alpha Back Scatter Spectrometer

An alpha back scatter spectrometer suitable for operation on Mars is being considered for development by the University of Chicago (Turkevitch). Such a device will most probably not use the isotope source (Cm^{242}) used in the Surveyor spectrometer and the source selection will be one of the prime considerations for any future designs. Mechanically, with the possible exception of the deployment mechanism, the spectrometer will probably be able to meet the requirements of a rough landing. Fig. 4.5.2-3 shows the Surveyor alpha-spectrometer for reference purposes. Reduction of the overall dimensions of the sensor head are anticipated since the Martian atmosphere will interfere with the measurement. This reduction will result in shorter particle path lengths and correspondingly smaller interference with the measurement.

The head, which must be deployed to come in contact with the surface of the planet, is mounted on a swivel bracket so that deployment either up or down will be possible. The existence of surface protuberances in the field of view will introduce errors. A calibration sample is exposed to the bottom of the sensor head when in the stowed position, thus providing a reference source for data interpretation. Table 4.5.2-2 gives the physical and electrical parameter estimates for the proposed device. The deployment will be carried out in two stages; i.e., partial deployment toward surface for background counting and full deployment for composition measurements.

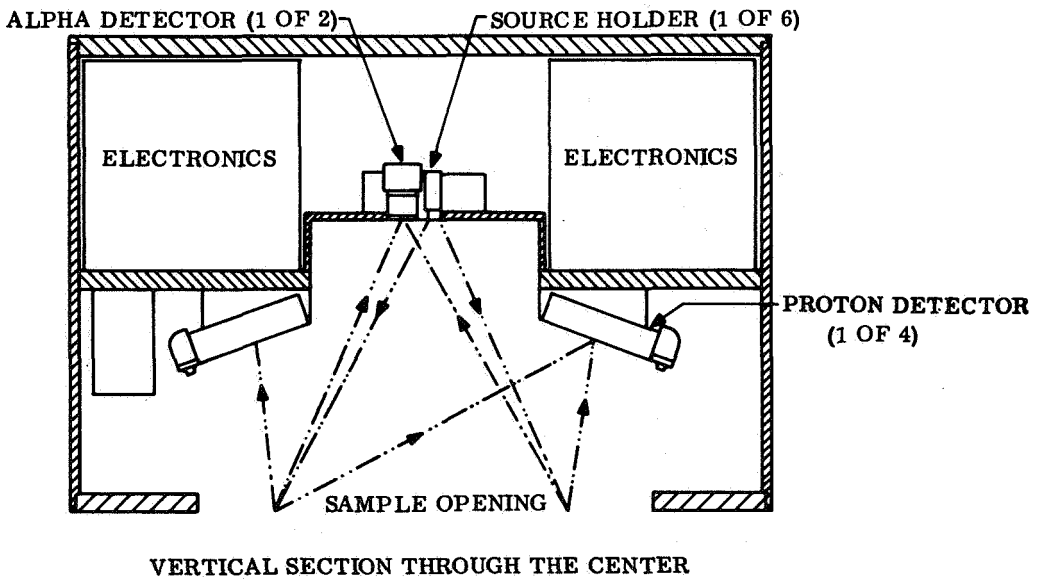


Figure 4.5.2-3. Alpha Back Scatter Instrument

4.5.2.3.6 TV Cameras

The high and low resolution cameras are installed on individual hinged masts although it may be possible to combine them within one casing. Figure 4.5.2-4 shows the basic

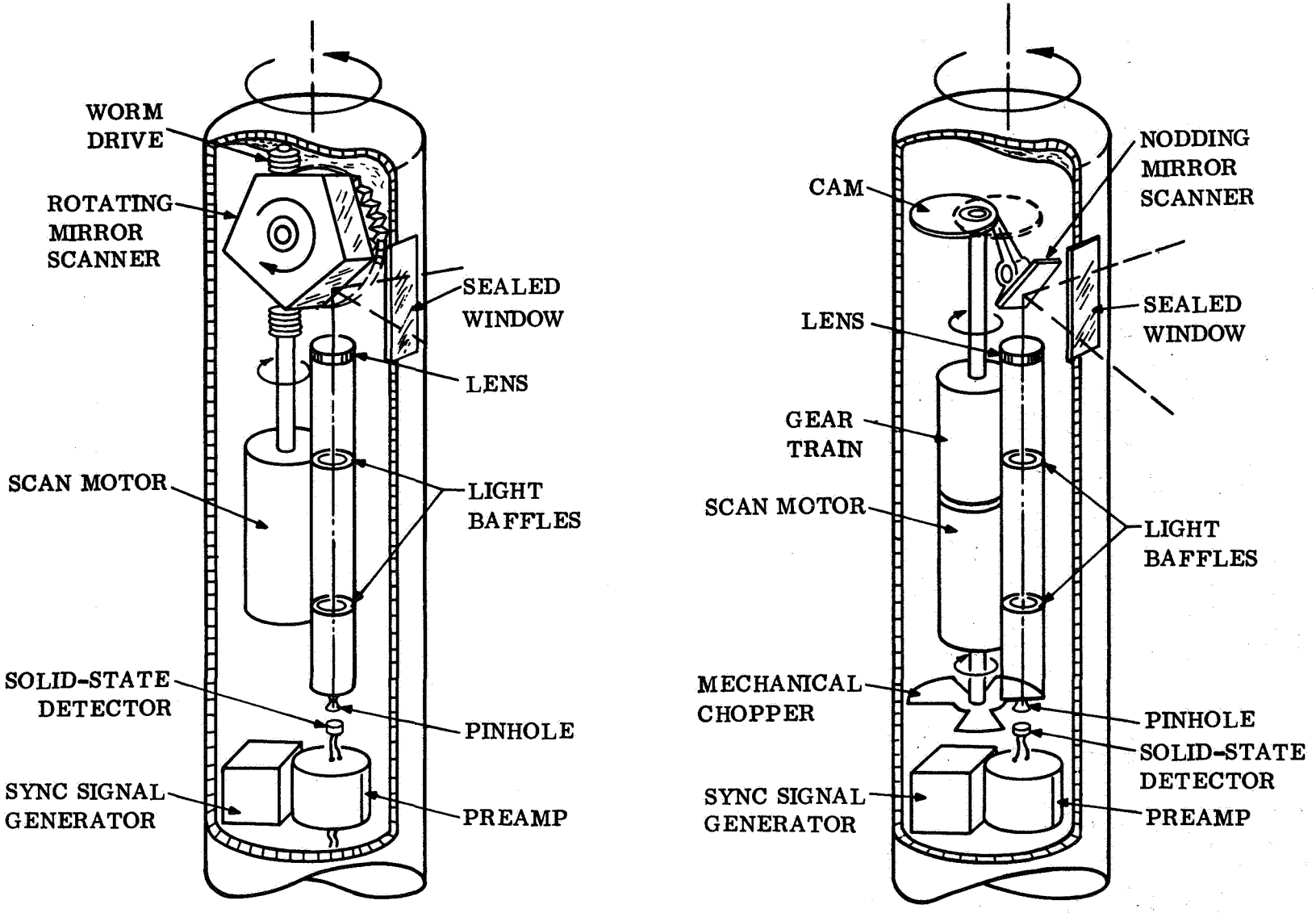


Figure 4.5.2-4. High and Low Speed TV Cameras

elements that each contains. Neither of the two versions shown contain the azimuthal drive motor. The high speed version (fig. 4.5.2-4) has a 5-sided mirror that rotates unidirectionally; the preferred video rate for this version is not well defined and can be from 10 kHz to 100 kHz depending on circumstances. The incident light passes through the window and is reflected from the mirror onto the silicon cell detector. The solid state amplifier amplifies the resulting electrical signal to +5v maximum, the output signal leads from the camera housing carry this signal to the processing electronics. The slow speed version (that can take up to 4 hr for a full panoramic sweep) has a nodding mirror activated by a cam. The light beam is deflected via this mirror onto the silicon cell after being chopped by a small light chopper placed in front of the cell. This latter addition enables the same basic amplifier to be used for both the high speed and low speed versions. The silicon cell response is shown in fig. 4.5.2-5. The dimensions of the camera unit that contains all the mechanical drive mechanisms and all the electronics for the video and synchronizing signals varies with the full design specification; normally, however, these will be between 1 and 3 in. in diameter and between 6 and 16 in. long. Total weights of the cameras as described can again vary from 1/2 to 6-1/2 lb (See table 4.5.2-3).

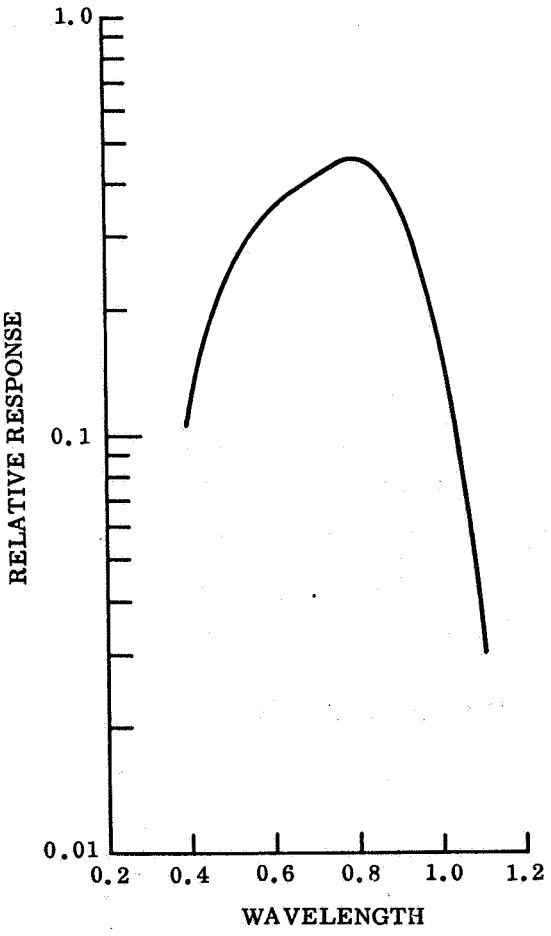


Figure 4.5.2-5. Silicon Photo-Voltaic Cell Spectral Response

TABLE 4.5.2-3. TYPICAL CAMERA SPECIFICATIONS

Model Identification	CM	SL	NP	SS	SM
Special Feature	small size, small power	rugged	high speed	adjustable performance	high resolution
Field of view	9^{o} x 360^{o}	50^{o} x 360^{o}	25^{o} x 360^{o}	10^{o} x 10^{o} to 90^{o} x 360^{o}	1^{o} x 1^{o}
Resolution	0.1 in. @6 ft	0.1 in. @6 ft	1 in. @100 ft	0.1 in. @1 ft to 0.1 in. @ 60 ft	1 micron @ 3/4 in.
Frame time	1/2 min	7 min	2 1/2 sec	30 sec to 10 hr	1 sec
Sensitivity range	0.1-1000 ft-L	0.3-3000 ft-L	1.5000 ft-L	0.001-5000 ft-L	10-10,000 ft-L
Size	1 in. dia x 6 in. long	1.5 in. dia x 10 in. long	2.5 in. dia 11 in. long	3 in. dia x 18 in. long	3 in. dia x 15 in. long
Weight	0.4 lb	3.5 lb	5.5 lb	6.5 lb	6 lb
Power	1 W	10 W	150 W	15 W	4W
Temperature (of the environment)	-10^{o}F to $+150^{o}$F	-40^{o}F to $+180^{o}$F	-10^{o}F to $+125^{o}$F	-45^{o}F to + 145^{o}F	-45^{o}F to + 145^{o}F
Pressure (external)	1 ATM	10^{-9} Torr	1000 psi	1 mb	1 mb
Shock and Vibration	1000 g	3500 g	100 g	300 g	50 g

4.5.2.3.7 Clinometer

The clinometer proposed for the 1973 Hard Lander will require development. Specifications for the design are not complete; however, the parameters shown in table 4.5.2-2 are based on engineering estimates for the conceptual design shown in fig. 4.5.2-6. The potentiometer housing could also include any electronics required to operate the system. Location of the instrument in the Lander is not critical.

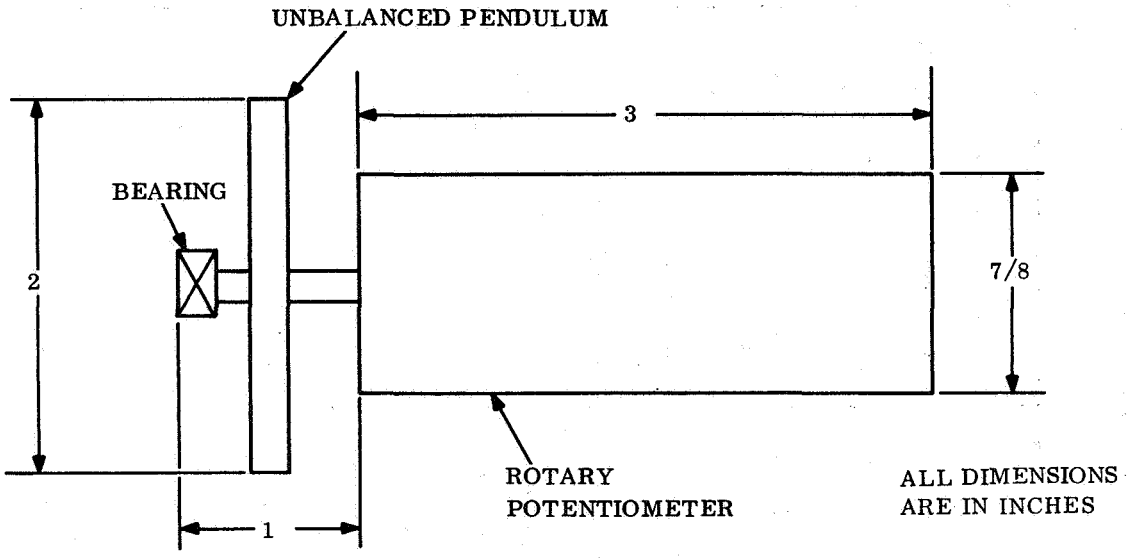


Figure 4.5.2-6. Rotary Potentiometer Clinometer

4.5.3 TELECOMMUNICATIONS

4.5.3.1 Summary

The telecommunications subsystem consists of:

1. a hardwire data link for Lander/Capsule checkout prior to separation from the spacecraft

2. a relay communications link to provide Lander/Capsule entry data and high data rate imagery after landing

3. a UHF beacon link to alert the Lander of the approaching Orbiter for relay communications.

A functional block diagram of the telecommunication subsystem is shown in fig. 4.5.3-1. The communication link characteristics are summarized in table 4.5.3-1.

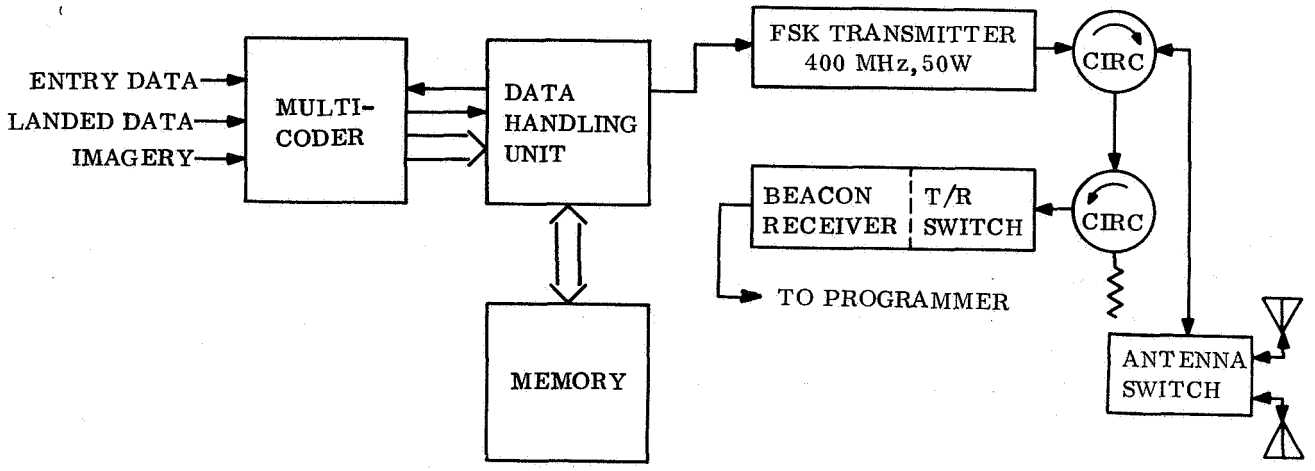


Figure 4.5.3-1. Telecommunications Subsystem, Functional Block Diagram

To support the high data requirement for imagery, the data will be relayed to Earth via the Orbiter, with communication to the Orbiter taking place during a periapsis pass to take advantage of the relatively short line-of-sight range. Data is stored in the Orbiter and subsequently transmitted to Earth. Non-coherent frequency shift keying with Manchester coding is chosen for the modulation technique to minimize acquisition time. After landing (for the entry and first Orbiter pass) the link is designed to operate at a 31 kbps data rate. The performance under maximum adverse tolerances, 46° worst case Lander tilt and worst case Orbiter-Lander line-of-sight parameters, is shown in table 4.5.3-1. To accomplish this data transfer requires 50 watts of transmitter power, the maximum allowable to avoid antenna breakdown at Mars surface pressure. It is assumed that the Orbiter will be provided with the capability to record data at this high rate. If this is not the case, the total data transferable (and the transmitter power) scale down approximately proportional to the actual recording rate.

TABLE 4.5.3-1 DESIGN SUMMARY

Phase	Link	Data Rate (bps)	Transmission Time	Total Data (bits)
Post-separation	400 MHz FSK, relay	1090	30 min	2.0×10^6
Entry	400 MHz FSK, relay	1090	350 to 1220 (1) sec	0.38 to 1.3×10^6(1)
Post impact, set-up	400 MHz FSK, relay	1090	2.5 min (2)	0.16×10^6(2)
Post impact	400 MHz FSK, relay	31×10^3	---	See table 4.5.3-6
1st orbiter pass	400 MHz FSK, relay	31×10^3	800 sec(3)	2.5×10^7
2nd orbiter pass	400 MHz FSK, relay	1090	1400 sec	1.5×10^6
3rd orbiter pass	400 MHz FSK, relay	---	---	No communication in extreme case.

(1) Atmosphere dependent
(2) Data during this period may be lost because entry antenna may be underneath Lander.
(3) Minimum effective transmission internal.

Data requirements prior to and during entry are relatively modest, but communication ranges are more severe. It was determined that the same transmitter and receiver used for imagery data after landing can be used at a lower data rate for entry data. This minimizes equipment and complexity on both the Orbiter and Lander.

Because of the widely varying communication parameters due to atmosphere uncertainty and possible vehicle tilt, the amount of data transferable immediately after impact varies widely. For the VM-9 atmosphere, communications at the high data rate cannot be established except in the improbable case of large negative in-plane tilt towards the Orbiter.

The turn-on of the data link is complicated by the large period uncertainties in the direct entry mission. The approaches considered in the out-of-orbit mission, the internal programmed time and the beacon-link operating continuously, can result in early turn-on of about 6.8 hr and 2 hr, respectively. From an energy consideration, these early turn-on times are unacceptable. By utilizing the command link to the Orbiter and controlling the beacon transmitter turn-on in order to account for the period error, as obtained from tracking the Orbiter, the early turn-on can be considerably reduced. The beacon link is used to initiate the data transmission.

4.5.3.2 Telecommunications Sequence

Prior to separation, Lander power is turned-on for final checkout (table 4.5.3-2). Except for a momentary check of transmitter power, transmitter operation within the canister is avoided. During this interval, data is transferred via hard wire. Immediately after separation r-f transmission is initiated for event monitoring and engineering diagnostic measurements.

TABLE 4.5.3-2. TELECOMMUNICATIONS SEQUENCE

Phase	Duration	Communications
Pre-separation	15 min	Low rate/hardwire
Post-separation	30 min	Low rate
Entry	351 - 1216 sec	Low rate
Post-impact (Lander set-up)	2.5 min	Low rate
Post-impact, Orbiter pass	See table 4.5.3-6	High rate
Orbit period	~ 25 hr	None
Beacon turn-on	Periapsis uncertainty	None
Beacon early trigger	0 - 12 min	High rate
Periapsis pass	8.5 min	High rate

During entry and for 2.5 min after impact, scientific and diagnostic data are transmitted at the low rate. The high data rate is then used to transmit imagery.

The beacon receiver is turned on prior to nominal Orbiter pass by a time interval equal to the Orbiter arrival time uncertainty. The beacon transmitter turn-on is initiated upon command to include updated orbit period information. The beacon link will trigger high rate transmission of stored scientific and engineering data and imagery.

4.5.3.3 Data Requirements

Table 4.5.3-3 is a list of measurements for the entry and landed mission phases, and table 4.5.3-4 gives the corresponding data accumulation. During entry real time data is interleaved with data delayed by 70 sec to avoid loss of data during blackout. The combined data dictates a 1.09 kbps data rate. Prior to entry, only engineering diagnostic data is transmitted. Immediately after landing, imagery is transmitted at the high data rate. Imagery and surface science data are transmitted at the high data rate on subsequent Orbiter passes if the Orbiter is within range.

TABLE 4.5.3-3. MEASUREMENTS LIST

	Pre-impact	Post-impact
Diagnostic Data (50 channels)	X	X
Scientific Data		
Pressure	X	X
Stagnation pressure	X	
Temperature	X	X
Stagnation temperature	X	
Water vapor	X	
Tri-axial accelerometer	X	
Wind velocity		X
Moisture		X
Surface composition		X
Clinometer		X
Imagery		X
Stored data		X

TABLE 4.5.3-4. DATA TRANSMISSION

	Entry	Landed Relay
Science	194 - 2/3 bps	34.6 kbits
Diagnostic	350 bps	26.25 kbits
Stored	544 - 2/3 bps(1)	100 kbits(2)
Imagery	---	2.5×10^7
Total data/day	---	2.5×10^7
Data transmission time	351 - 1216 sec	800 sec
Data rate	1.09 kbps	31 kbps

(1) Science and diagnostic data delayed by 70 sec
(2) Data stored during entry

4.5.3.4 Link Designs

4.5.3.4.1 Landed

The fundamental constraints for the landed telemetry link are that maximum data is to be transferred, transmitter power is to be kept below 50 watts to avoid antenna breakdown, and the maximum permissible bit error probability is 4×10^{-3} (Orbiter to Earth link is 1.0×10^{-3} giving an overall maximum bit error probability of 5×10^{-3}). Additionally, the link must be tolerant of Lander attitude (tilt) uncertainty due to surface slopes and crush-up variance, and must also be tolerant of landing site uncertainty. Finally, the Lander size constraint necessitates that the antenna be of minimum size.

These constraints are satisfied by the non-coherent, frequency shift keyed (FSK), Manchester coded, 400 MHz link. The use of non-coherent FSK with Manchester coding minimizes acquisition time. The antenna size is minimized by sacrificing bandwidth with essentially no degradation in link performance. The need for pointing or steering mechanisms is avoided by using an antenna with beamwidth wide enough to accommodate Lander tilt uncertainties.

The data optimization procedure is related in Volume III and summarized here. Resulting available data rates vs time for the nominal Orbiter/Lander line of sight parameters for the first Orbiter pass, fig. 4.5.3-2, are repeated in fig. 4.5.3-3 for worst case adverse link tolerances. Figs. 4.5.3-4 and -5 relate the available data rates vs time for the 3σ orbiter period errors, $\pm$ 3.4 hr. These results do not consider possible antenna distortion resulting from ground reflections or specific Lander configuration. Fig. 4.5.3-6 is the relay/beacon block diagram, and table 4.5.3-5 contains the design control table. In this table, 300 km range and 2 dB transmit antenna gain are reference values and yield an allowable data rate of 31 kbps with worst case adverse tolerance. For such high data rates relative to the frequency uncertainty, the available data rate is proportional to the gain over range squared ratio, G/R^2, which is the basis of figs. 4.5.3-3, -4, and -5. Figs. 4.5.3-3, -4, and -5 include gain and range as determined from Lander to Orbiter line-of-sight range and look angle and Lander tilt. Tilts in the direction of Orbiter set and Orbiter rise and tilt perpendicular to the Orbiter plane are considered. The reference condition of zero tilt (nominal case) shows a very sharp peak as the orbiter passes overhead. This is the result of minimum communication range and maximum antenna gain. When the Lander is tilted towards Orbiter rise (set), the peak gain is pointed off vertical and tends to counteract the bit rate loss resulting from increasing range. The net effect of in-plane tilt is a lower peak data rate and longer available transmission time at near peak data rates. On the other hand, pure out-of-plane tilt lowers the gain and, hence, available data rate at all times.

Optimization is accomplished by examining the communication time as a function of bit rate for positive and negative in-plane tilt and for out-of-plane tilt. The maximum total data that can be transmitted with confidence at a specific bit rate is the product of bit rate and minimum communication time for the three tilt conditions considered. The bit rate yielding the largest maximum total data transmitted is the optimum bit rate.

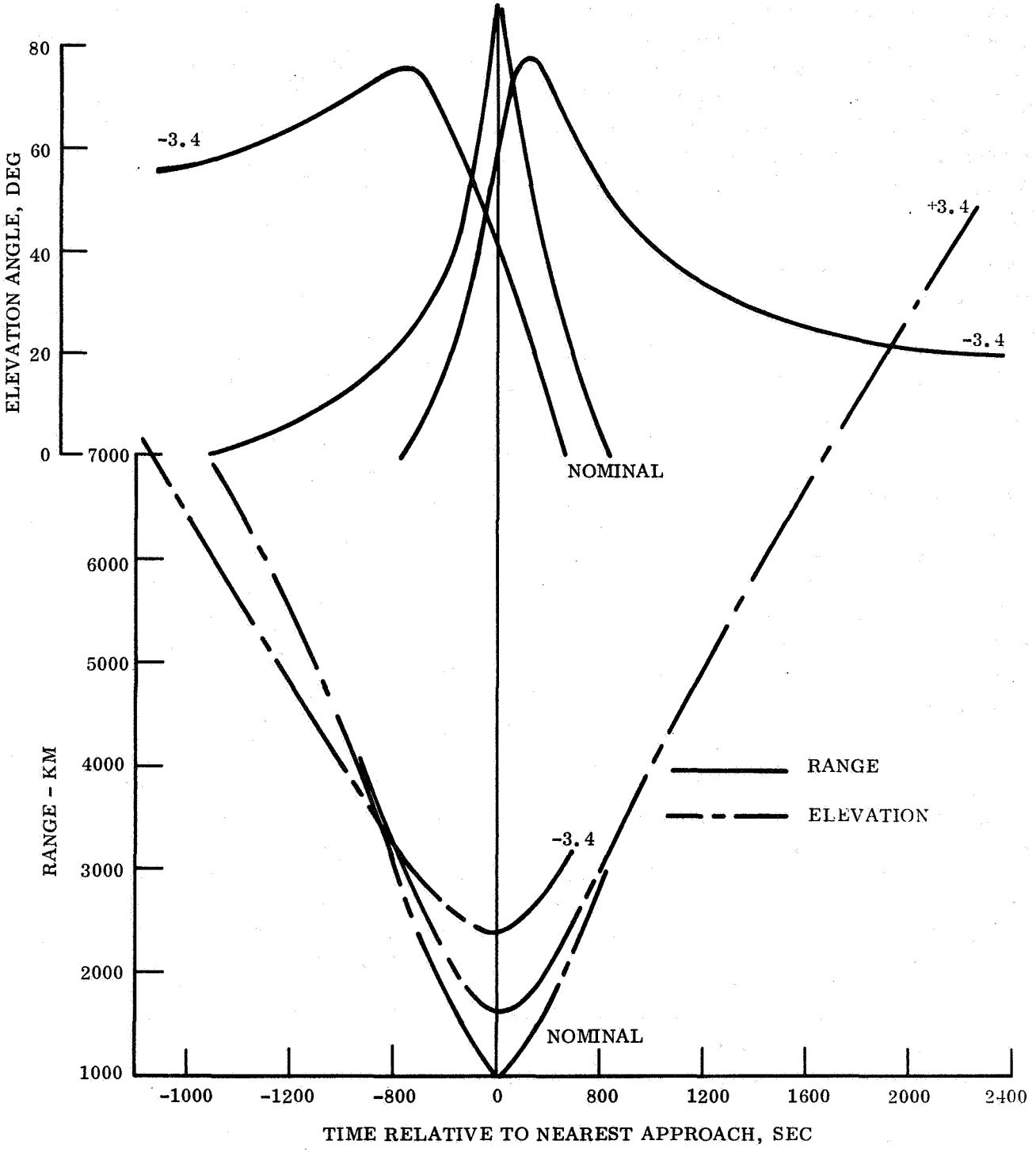


Figure 4.5.3-2. First Orbit Pass Communication Parameters

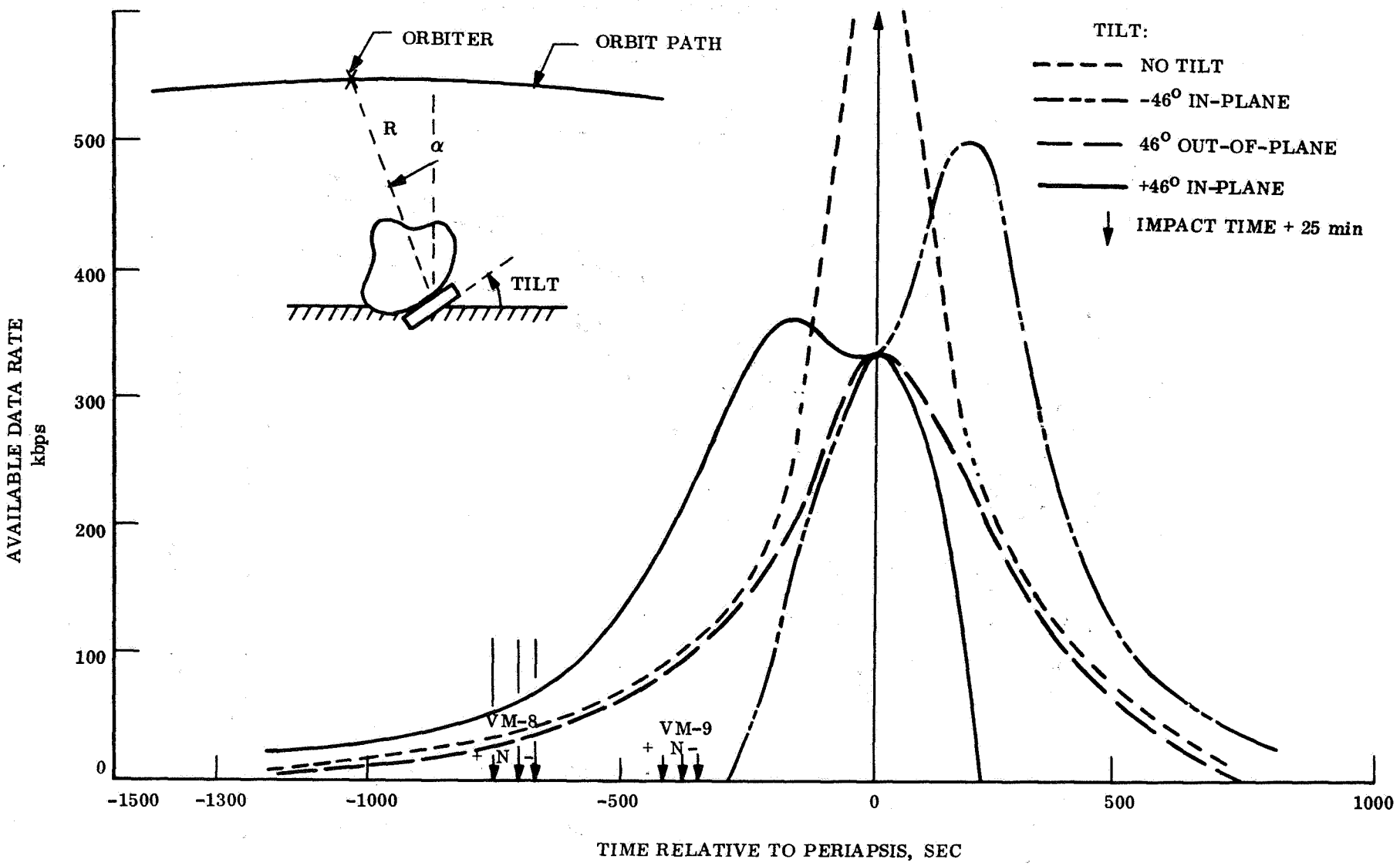


Figure 4.5.3-3. Available Data Rate vs Time with Adverse Tolerances, Entry Pass and Nominal Orbital Passes

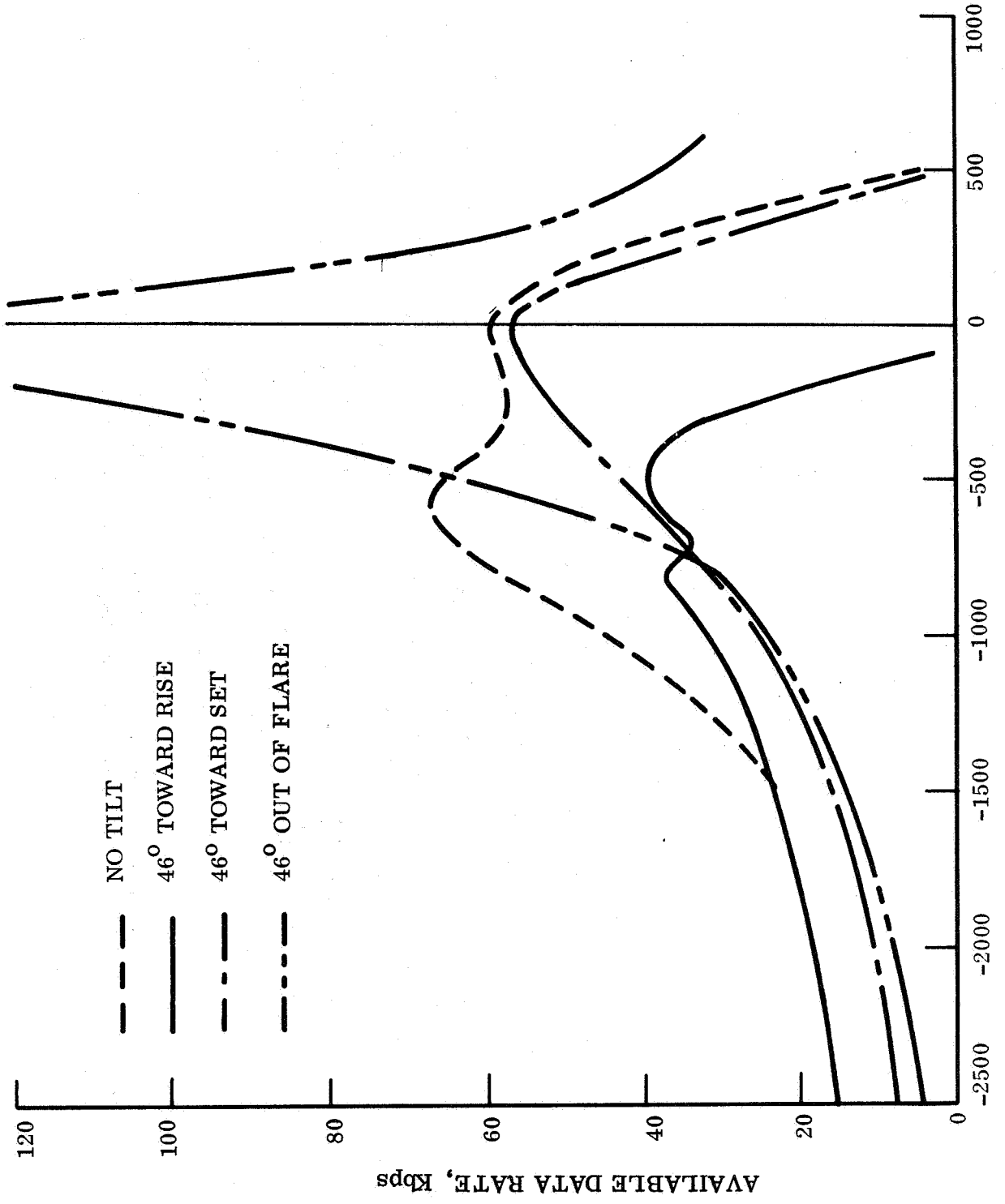


Figure 4.5.3-4. Available Data Rate vs Time with Adverse Tolerances, First Orbiter Pass, -3.4 hr Period Error

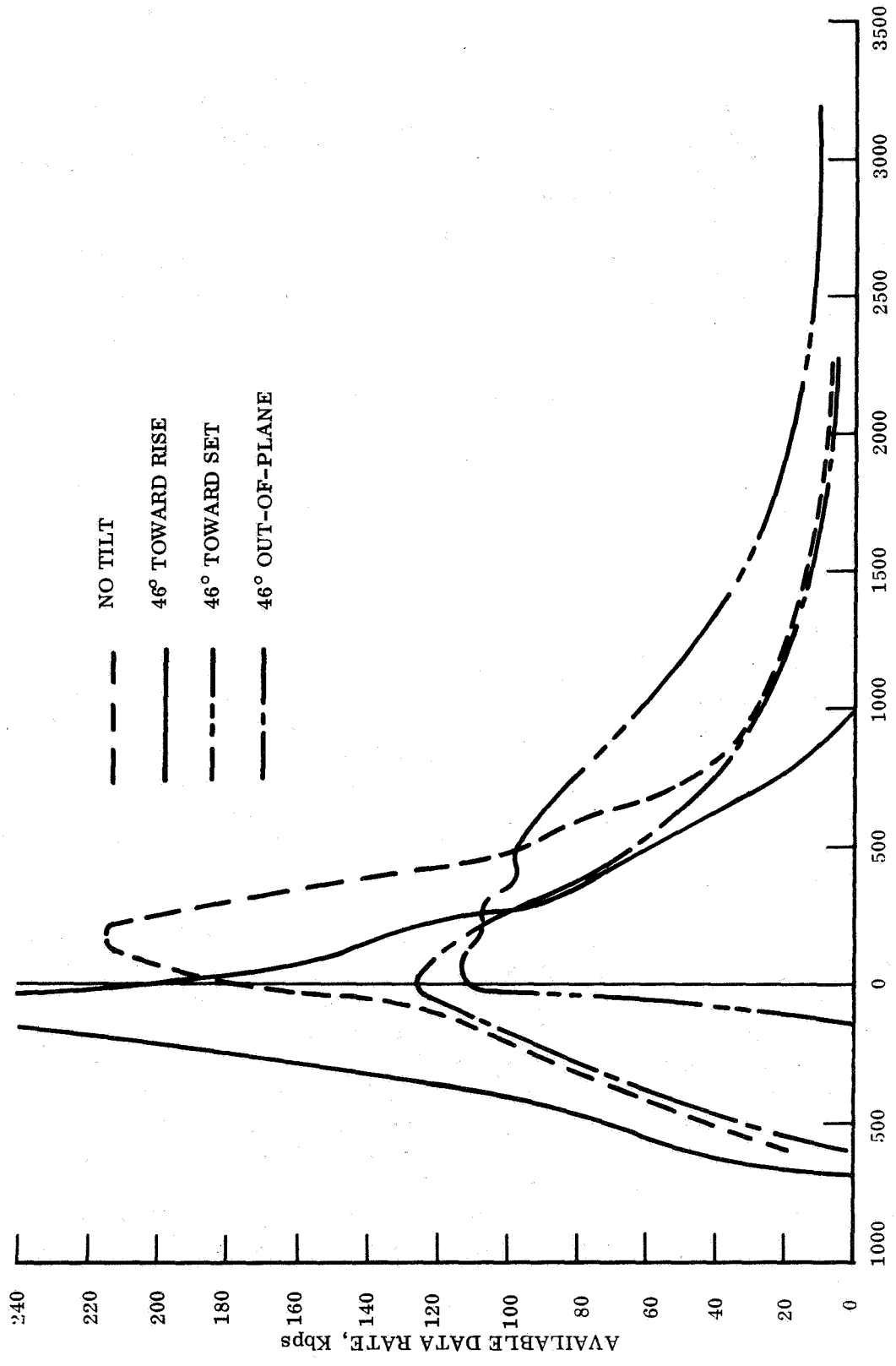


Figure 4.5.3-5. Available Data Rate vs Time with Adverse Tolerances, First Orbiter Pass, +3.4 hr Period Error

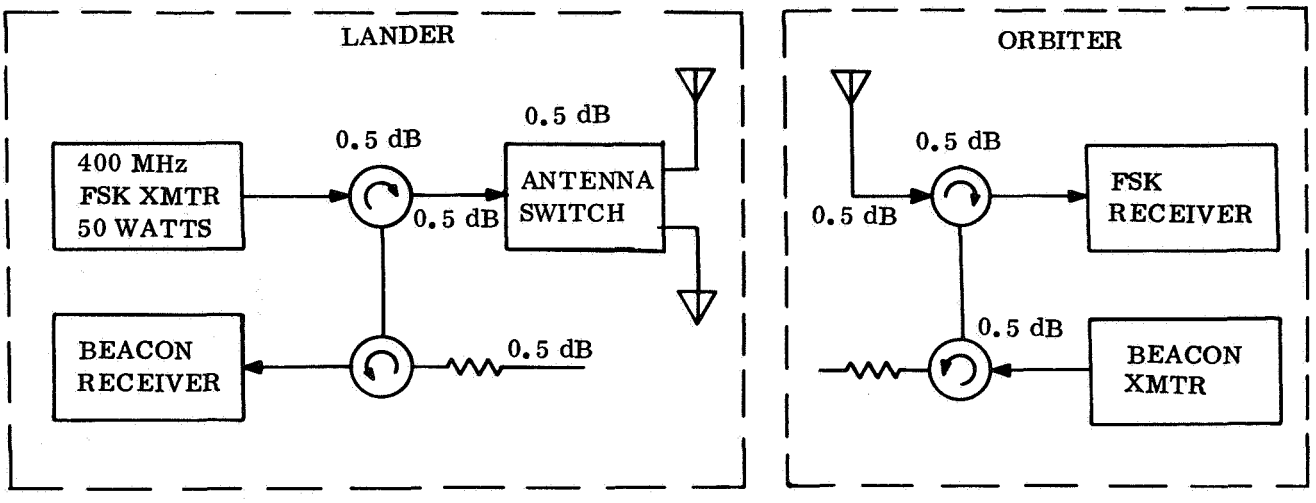


Figure 4.5.3-6. Relay and Beacon Link, Block Diagram

Times (relative to time of nearest Orbiter approach) of impact plus 2.5 min for the extreme atmospheres, VM-8 and VM-9, are indicated in fig. 4.5.3-2 for trajectory uncertainties leading to nominal and ± 3.4 hr Orbiter period errors. The data transferable after impact of a specific bit rate is the product of the bit rate and the time available at that bit rate. In this case the Lander is not within view of the Orbiter at impact for the 46° tilt toward Orbiter rise, otherwise a data rate of approximately 50 kbps can be supported. Requirements for transmission during the first Orbiter pass and the desire to use a single data rate for entry and first Orbiter passes will constrain the data rate to a lower value.

For the nominal Orbiter period, the maximum data transferable for worst case tilt of 46° and maximum adverse link tolerances is 8.1×10^7 bits at an optimum bit rate of 160 kbps. When Orbiter period errors are considered, the data transferable during the first Orbiter pass is significantly reduced. In fact, for the 3 σ case of a -3.4 hr period error, the maximum data rate that can be supported for all tilt considerations is about 40 kbps and the optimum is 21 kbps, yielding a total data of 3.1×10^7 bits. A data rate of 31 kbps is recommended as a compromise with the entry pass communications and to be consistent with the electrical system described in this report. At 31 kbps, the worst case data transferable during the first Orbiter pass is 2.4×10^7 bits, i.e., at least 800 sec or more transmission time at this rate is available. For the entry pass, the data transferable at 31 kbps during the entry pass is indicated in table 4.5.3-6.

TABLE 4.5.3-5. DESIGN CONTROL TABLES,
RELAY (LANDED) AND BEACON

Parameter	Nominal Values and Worst Case Tolerances					
	Relay (Landed)			Beacon Link		
	Nom	+tol	-tol	Nom	+tol	-tol
Modulation technique	FSK	--	--	AM	--	--
Frequency (MHz)	400	--	--	400	--	--
Transmitter power (watts)	50	--	--	4.1w	--	--
(dBm)	47.0	0.0	1.0	36.1	0.0	1.0
Transmit circuit loss	-1.5	0.2	0.4	-1.5	0.2	0.4
Transmit antenna gain (dB)	2.0(5)	0.5	0.5	2.0(5)	0.0	0.5
Transmit antenna pointing loss	0.0	0.0	0.0	-1.0	1.0	0.0
Range (km)	3000(5)			3000(5)		
Space loss	-154.1	--	--	-154.1	--	--
Polarization Loss	-1.0	1.0	0.5	-1.0	1.0	0.5
Receiving antenna gain	2.0(5)	0.0	0.5	2.0(5)	0.5	0.5
Receiving antenna pointing loss	-1.0	1.0	0.0	0.0	0.0	0.0
Receiving circuit loss	-1.0	0.2	0.4	-2.0	0.2	0.4
Total received power (S) (dBm)	-107.6	2.9	3.3	-117.7	2.9	3.3
Effective noise temperature (°K)	650	--	--	724	--	--
Receiver noise power spectral density (N/B)	-170.5	0.0	1.0	-170.0	0	1.0
Bit rate, 1/T (bps/dB)	31 k 44.9	--	--	--	--	--
Frequency uncertainty (kHz)	20.0(3)	--	--	16.0(4)	--	--
I-F bandwidth (kHz)	145.0	--	--	25.0	--	--
Required S/N/B	56.3(3)	0.0	2.0(3)	47.0	1.0	1.0
Required ST/N/B	11.7(3)	0.0	2.0(3)	3.0(1)	1.0	1.0
Threshold data power (dBm)	-113.9	0.0	3.0	-123.0	1.0	2.0
Margin	6.3	2.9	6.3	5.3	3.9	5.3

(1) Signal-to-noise ratio in i-f bandwidth.

(2) Transmitter stabilizer ±10 ppm; Receiver stability ±5 ppm; Doppler ±4 kHz.

(3) Nominal signal-to-noise ratio is theoretical value. 2 dB adverse tolerance is allowed to account for practical performance degradation, e.g., non-ideal bit sync. Value from Volume III, Section 4.2.2.

(4) Same as (2) except only one sided doppler shift needs to be considered.

(5) Values shown are typical and correspond to the G/R^2 ratio required to support the 31 kbps data rate.

TABLE 4.5.3-6. DATA TRANSFERABLE AFTER IMPACT PLUS 2.5 MIN[1] (BITS/10^7)

Atmosphere (Adverse Link Tolerances)	No Tilt	-46° Tilt[2]	46° Out-of-Plane[3]	+46° Tilt[4]
VM-8	3.3	3.7	3.2	2.3
VM-9	0.5	0.8	0.33	0

(1) Data shown is for nominal Orbiter parameters. Data transferable for 3σ tolerances in Orbiter parameters is within ± 0.3 x 10^7 bits.

(2) Lander tilted 46° in direction of Orbiter set.

(3) Lander tilted 46° perpendicular to and away from the Orbiter plane.

(4) Lander tilted 46° in direction of Orbiter rise.

In figs. 4.5.3-3, -4, and -5 transmission at a given rate is allowable when the available data rate is equal to or greater than that rate. To be certain of transmitting the 2.5 x 10^7 bits the transmission interval must include at least 800 sec having allowable rates greater than 31 kbps for each and every tilt and period error conditions. The minimum period is 1040 sec to cover tilt uncertainties. An additional 360 sec is required because of atmospheric uncertainty. Thus, the transmission interval must be 1400 sec (about 23.5 min), plus the uncertainty in Orbiter time of arrival.

For the second Orbiter pass the extreme period uncertainties have drastic effects on communication parameters. For example, with -3.4 hr period error, the minimum range of about 5100 km occurs at 0° elevation and the range at 34° set is about 6300 km. A reasonable approach is to reduce the bit rate to the entry value of 1090 bits/sec. From table 4.5.3-8, the margin over adverse tolerances is 18.6 db at 1000 km range, indicating a range limitation of 8500 km. To get a feel for communication capability, data transferable was completed by finding the time between the 8900 km range and 34° rise or set. For -3.4 hr period error 0.15 x 10^7 bits can be transferred (1400 sec). For +3.4 hr period error, 0.33 x 10^7 bits can be transferred (3000 sec available). (These data capacities do not consider battery energy limitations). The command capability could be used to transmit at higher rates in the case of near nominal Orbiter period.

For the third Orbiter pass with extreme period errors, the Orbiter appears only at less than 6° elevation angle. Clearly no communication is feasible under these conditions.

4.5.3.4.2 Beacon Link

The beacon link consists of a beacon transmitter on the Orbiter and a beacon receiver on the Lander. To conserve weight and space on the Lander and to have as many elements as possible common to the relay and beacon link, the beacon link uses the same antennas as the relay link. The narrowband antenna characteristic forces the beacon link to operate at essentially the same frequency as the relay link which in turn dictates that the two links time share the antennas. To accomplish this the Orbiter beacon transmitter must transmit, for example, for an interval of 1 sec and then listen for 10 sec to see if the Lander is transmitting. When the Lander received signal strength is above a preset threshold level, data transmission will be initiated after a 1 sec delay. The Orbiter will sense Lander transmission and cease beacon transmission.

The beacon link received signal strength is proportional to link antenna gain divided by range squared and hence, is indicative of relay link available data rate. Ideally the link can detect exactly when the high data rate can be supported which would lower the required transmission time to just that necessary to transmit the data. However, the beacon link does have a range of performance which must be considered. To aid in minimizing the performance range, the beacon transmitter power will be closely controlled, i.e., within 1 dB, and its signal will be AM modulated to eliminate the noise bias uncertainty. The maximum beacon link uncertainty is 9.2 dB, a factor of 2.8 in range (see table 4.5.3-5). This uncertainty would normally cause the transmitter to turn on early since the link is designed such that transmission will be triggered in time to complete data transfer under worst case adverse tolerance conditions.

If the beacon link was allowed to operate continuously, serious early turn-on, on the order of 2 hr, could occur for the -3.4 hr period uncertainty. This possibility is eliminated by inhibiting beacon transmitter turn-on until the Orbiter is near the Lander. This function is controlled from Earth. The beacon transmitter turn-on time is updated to reflect the orbit period as determined from tracking information.

4.5.3.4.3 Entry

Due to atmosphere uncertainty, there is a wide variation in the possible link parameters, viz., line-of-sight range and look angle, during the entry phase. It is found for the reference mission that communications can be maintained throughout entry.

To minimize weight and complexity, the entry data is transmitted via the same link as landed data is transmitted by keying at the low data rate, 1090 bits/sec (this requires that the Orbiter receiver be capable of receiving either data rate). The design control table for the entry link is shown in table 4.5.3-7. The link has a margin over adverse tolerance of 18.6 dB at the reference range, 1000 km, with 2 dB transmitter antenna gain. This indicates a worst case range limitation of 8500 km with the 2 dB transmitter antenna gain. The antenna provided has a gain greater than zero dB over a range of $\pm 70^{\circ}$ with respect to the rear-looking Lander roll axis (effects of Lander configuration and aeroshell are not considered). The reference

TABLE 4.5.3-7. ENTRY LINK DESIGN CONTROL TABLE

Parameter	Relay (entry) nominal	Adverse Tolerance
Modulation technique	FSK	--
Frequency (MHz)	400	
Transmitter power (watts)	50	
(dBm)	47.0	1.0
Transmit circuit loss	-1.5	0.4
Transmit antenna gain	2.0(1)	0.5
Transmit antenna pointing loss	0.0	0.0
Reference range (km)	1000(1)	
Space loss	-144.5	
Polarization loss	-1.0	
Receiving antenna gain	2.0	0.5
Receiving antenna pointing loss	-1.0	0.0
Receiving circuit loss	1.0	0.4
Total received power (S), dBm	-98.0	3.3
Effective noise temperature (^{o}K)	650	
Receiver noise power spectral density (N/B)	-170.5	1.0
Modulation loss	N/A	
Data power (dBm) S_D	-98.0	3.3
Bit rate, 1/T (bps/dB)	1090/30.4	--
Frequency uncertainty	20.	--
I-F bandwidth (kHz)	145.0(3)	--
Required S/N/B	47.6 (2)	2.0(2)
Required ST/N/B	17.2 (2)	2.0(2)
Threshold data power (dBm)	-122.9	3.0
Margin	24.9 (4)	6.3

(1) Reference values.

(2) Nominal signal-to-noise ratio used is theoretical value. 2 dB adverse tolerance is allowed to account for practical performance degradation, e.g., non-ideal bit sync.

(3) Bandwidth required for high bit rate.

(4) This margin, less the adverse tolerances, is available as protection against multipath. At the maximum range during entry, this margin is reduced to 4.3 dB.

mission range and look angle profiles show maximum range of about 5200 km and maximum look angle of about 60° (at parachute deployment). (Look angle is the angle to Orbiter with respect to the velocity vector. Any variation between the velocity vector and roll axis, e.g., due to coning or swing on the parachute, will worsen the communication angle.) Swing in excess of 20° at this time could cause the link margin to fall below the adverse tolerance level. As the Lander descends and the Orbiter begins to overtake the Lander, the look angle improves and more swing is allowable.

During the entry phase, signals transmitted from the Lander may be reflected from the planetary surface toward the Orbiter. These multipath signals may interfere with the desired signal which is received on the line-of-sight path from the Lander. As shown in Volume III, Section 4.2.2, the slow fading environment is most detrimental to the communication link performance. The conditions for slow fading occur near impact. Based upon the maximum range during entry, the minimum margin over worst case tolerances is about 4.3 dB. The tolerable signal-to-interference level to allow fading loss for less than 99 percent of the time is about 12.0 dB for the 4.3 dB margin. If this level proves to be a problem, another Orbiter receiver can be added with an i-f bandwidth to match the transmitted data rate yielding an additional margin of approximately 3 dB.

4.5.3.5 Equipment Descriptions

4.5.3.5.1 Antennas

The configuration of the wide beam 400 MHz antenna is that of a pill box 8 in. in diameter and 2 in. deep. The top surface of the box is flush with the vehicle outer surface and has two orthogonal slots, 2 in. wide and 8 in. long (dividing the top of the box into four quarters). The slots are tuned with capacitors to match the input and provide circular polarization. The bandwidth of this antenna is about 2 MHz. The estimated pattern is shown in fig. 4.5.3-7. Since the Lander diameter is on the order of a wave-length, the available ground plane is not large, indicating that the actual antenna pattern will vary somewhat from that shown.

4.5.3.5.2 400 MHz FSK Transmitter

A block diagram for the FSK transmitter is shown in fig. 4.5.3-8. The frequency shift keyed modulation is produced by switching between two stable crystal oscillators operating at 25.0375 MHz and 24.9625 MHz respectively. Multiplying these signals by a factor of 16 produces the transmitter output signals at 400.6 MHz and 399.4 MHz, respectively. The multiplier chain will be constructed at a low signal level in order that filtering and multiplier inefficiencies do not adversely affect the overall efficiency.

The power amplifier chain consists of amplifier stages to produce a total gain of about 47 dB; approximately 10 dB of this will be excess gain to be used for AGC. The final amplifier stage consists of two 2N5178's operating in push-pull. These transistors are each rated for 50 watts output at 500 MHz with a dissipation rating of 70 watts at 25° C.

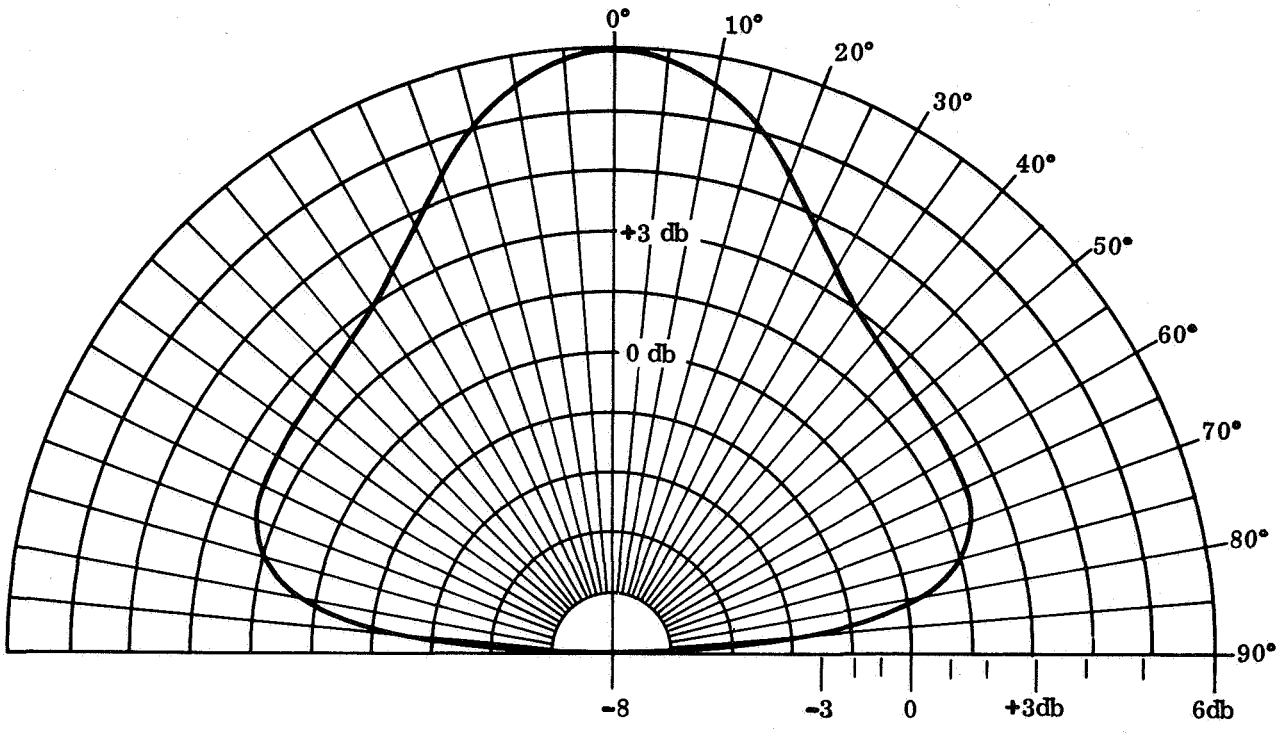


Figure 4.5.3-7. 400 MHz Antenna Pattern

The output power level of the transmitter will be controlled at 50 watts (+0, -1 dB) throughout the temperature environment by means of an AGC circuit, consisting of a detector for output sampling, a high gain amplifier, and a voltage variable attenuator located at the low level input to the 400 MHz power amplifier chain.

The transmitter oscillator stability will be 10 ppm over a temperature range of -40° C to + 70° C with negligible warmup time at any temperature. Aging will be 1 ppm/year. The state-of-the-art in temperature compensated crystal oscillators has reached a point where stabilities in the order of 1 ppm or better can be achieved for considerable periods of time, however, to account for degradation which may result from shock such as deformation of the crystal structure or holder, a stability of 10 ppm is considered conservative.

No serious problems are anticipated in the sterilization of the transmitter or in the high shock levels expected. Several years ago GE/RSD designed and constructed a VHF 50 watt transmitter which was successfully sterilized and subjected to multiple shock impacts at levels of 5000 g's for approximately 500 μsec. The transmitter was potted with Dow Corning XR-6-3700 silicon potting compound. (The complete results of these tests are reported in GE TIS 66SD2002 entitled "Fifty Watt Solid State FM Transmitter for Deep Space Communications", by Julius Shatas.)

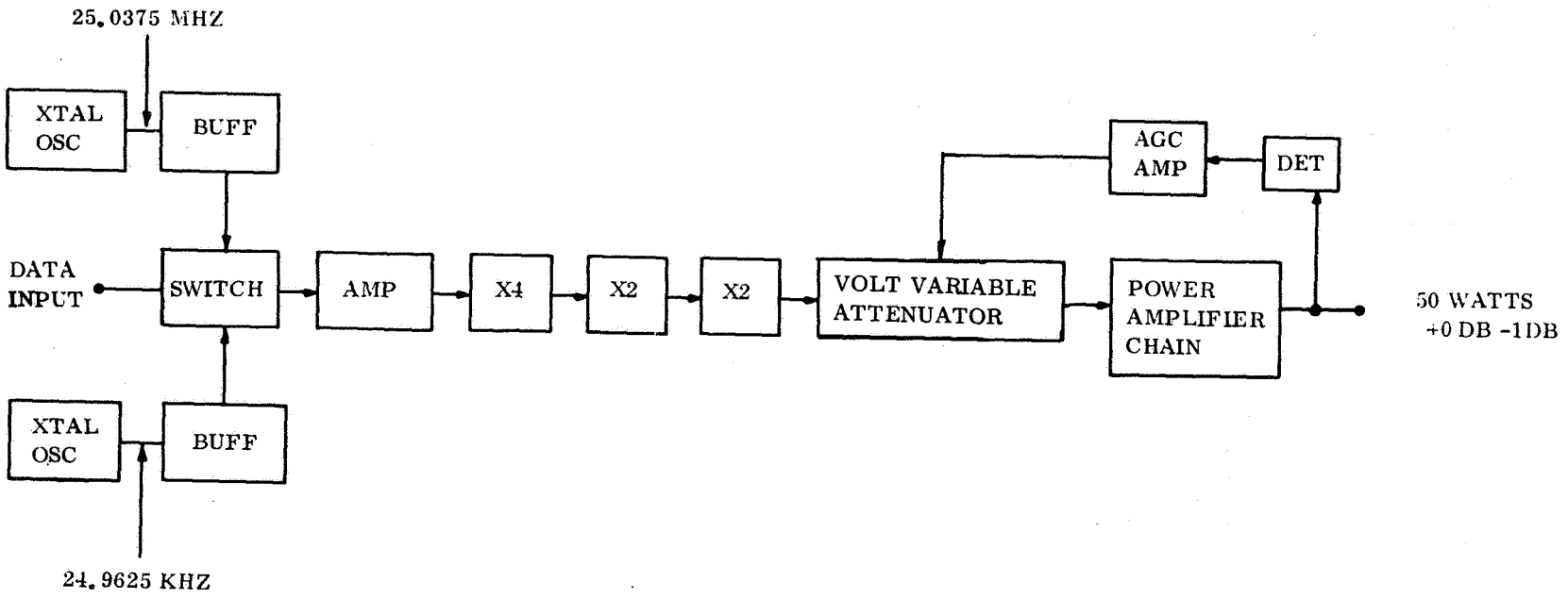


Figure 4.5.3-8. 400 MHz Transmitter, Block Diagram

4.5.3.5.3 Duplexing Circuit

The duplexing arrangement used for the 400 MHz transmitter and receiver, shown in fig. 4.5.3-9, consists of two circulators connected as a four-port circulator and a receiver T/R switch. The circulators protect the transmitter against large reflections and provide receiver isolation. In the normal receive mode the T/R switch is biased to pass the received signal. When the transmitter is turned on the circulator provides 20 dB receiver isolation, and the T/R switch is biased to reflect the leakage power back into the circulator where it is dissipated in a load. The T/R switch will be located in the receiver and the four-port circulator near the transmitter.

The T/R switch considered is a Hylelectronics model SU175, and the circulators are similar to the Melabs HB5 series.

The antenna terminal of the duplexing circuitry is connected to the antenna switch as shown in the block diagram. This solid state switch is used to select one of two antennas according to Lander orientation. A solid state switch is selected because of its reliability and potential to withstand the shock environment. The switch considered is Hylelectronics model SU176.

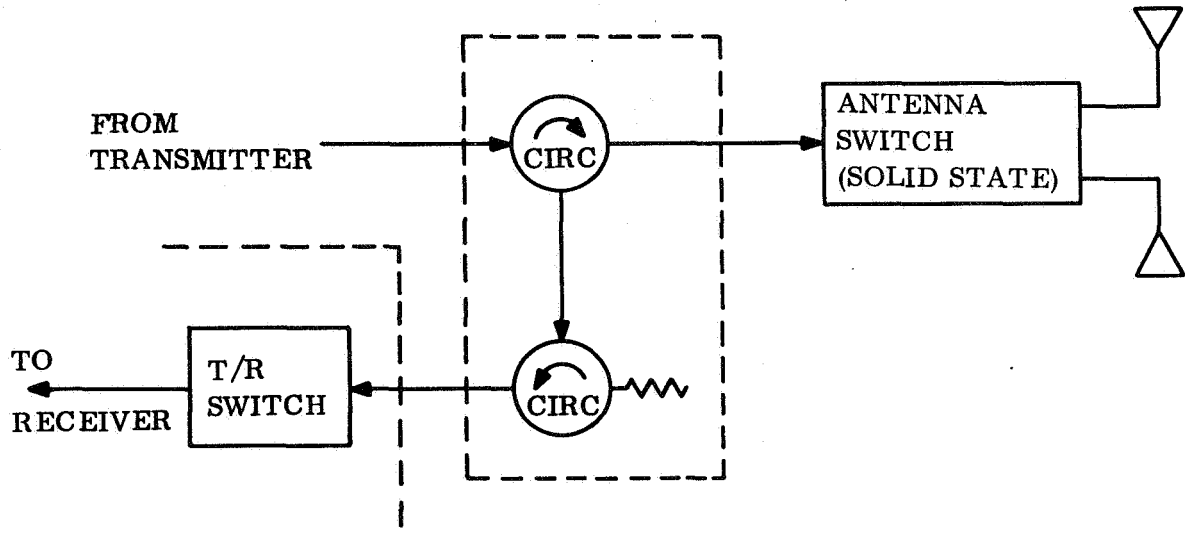


Figure 4.5.3-9. Duplexer and Antenna Selector

4.5.3.5.4 400 MHz Beacon Receiver

The purpose of the beacon receiver is to sense when the relay link can support the high data rate. This is accomplished by looking for reception of a preset signal level. When the expected signal level is detected the 400 MHz transmitter is energized after a 1 sec delay.

The receiver shown in fig. 4.5.3-10 receives an amplitude modulator signal of 400 MHz which is amplified in the low noise pre-amplifier and converted to the first i-f frequency. After amplification a second conversion takes place resulting in a second i-f signal at 3 MHz. The second mixer is fed to a bandpass filter which reduces the overall noise level at that point to prevent limiting in the 3 MHz i-f amplifiers which follow. The signal is then filtered in a bandpass filter with a noise bandwidth of about 25 kHz. The filter is a four-pole crystal filter with variations of not more than ±0.1 dB across the 18 kHz passband. After filtering the signal is detected and the demodulated signal filtered in a tone filter with a passband of about 100 Hz. At this point the signal is fed to a threshold detector.

The threshold is set for a nominal signal-to-noise ratio of 3 dB in the 25 kHz bandwidth which is equivalent to 27 dB in the 100 Hz final detection bandwidth. Allowing 3 dB for modulation loss and 6 dB for detection loss leaves a signal to noise ratio at threshold of 18 dB with a corresponding probability of false alarm on the order of 10^{-26}, implying false alarm is essentially impossible.

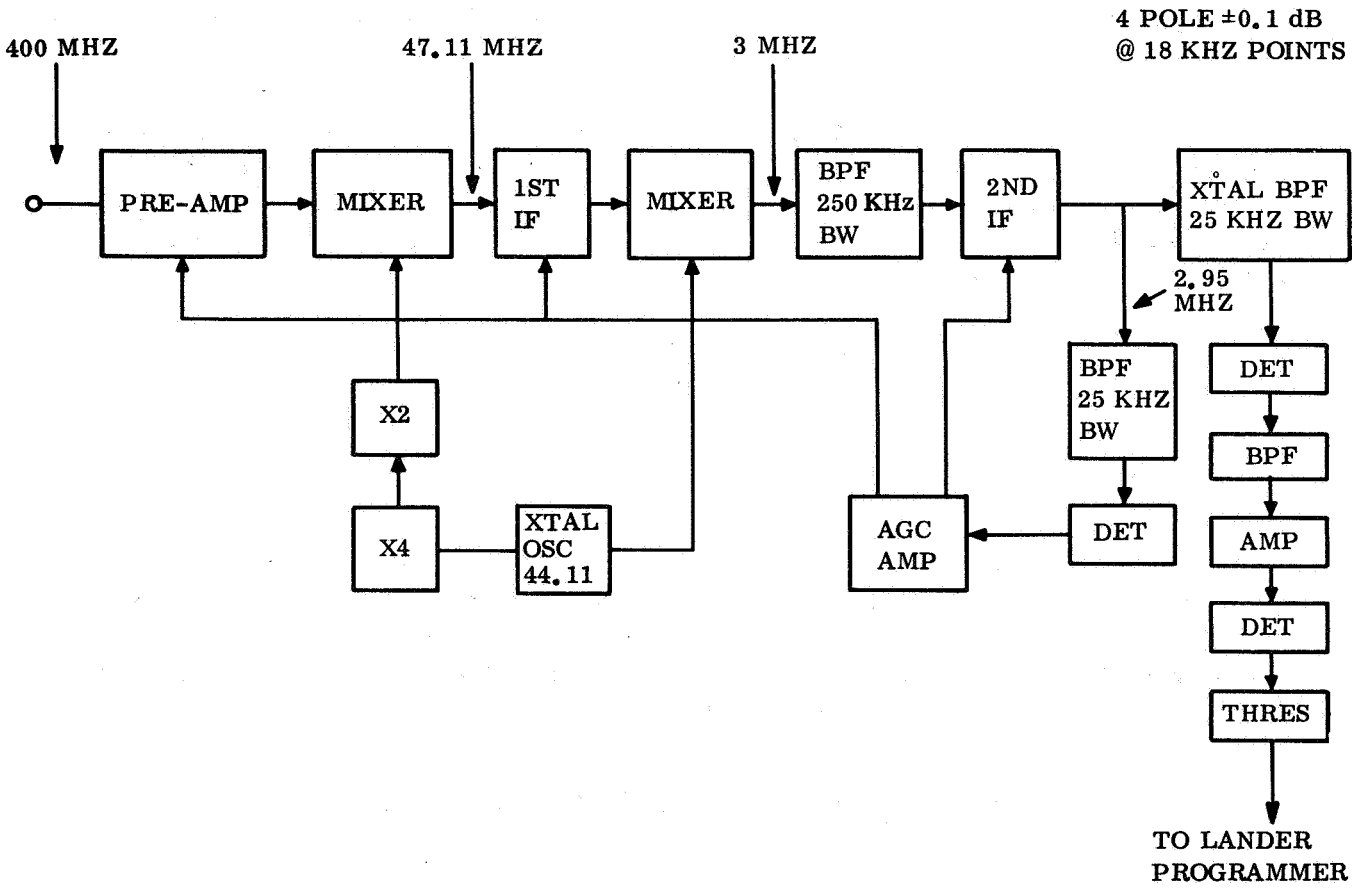


Figure 4.5.3-10. Beacon Receiver

In order for the receiver to provide indication of signal strength, the total gain of the receiver must be stable over a wide temperature range. This is achieved from the receiver front end to the output of the second i-f by means of an AGC circuit referenced to the receiver noise generated in the receiver front end. With a high gain AGC loop, gain variations with temperature can be kept to ±0.5 dB excluding effects of changes in the referenced noise level.

The remaining gain of the receiver which falls outside the AGC loop, that is, from the output of the second i-f to the threshold detector, must be kept within ±0.5 dB for a total receiver gain variation of ± 1 dB. This includes ripple (±0.1 dB) in the passband of the 25 kHz bandwidth crystal filter, changes in the detectors and threshold circuit and variations in gain of amplifiers outside the AGC loop.

The noise figure of the receiver is 5 dB referenced to the input of a preselector filter at the pre-amplifier front end. Since the receiver AGC circuit is referenced to front-end receiver noise, variations in noise figure will cause the receiver gain to vary. Thus the noise figure will be required to remain constant to within ±0.5 dB over the operating temperature range. The transistor anticipated for use in the pre-amplifier circuit is a KMC-K5001 specified at a noise figure of 1.4 dB at 400 MHz. If the noise figure of the transistor circuit is optimized at room temperature, the noise figure increases 0.4 dB at both temperature extremes. Since the optimum noise figure for this transistor is obtained with a 3:1 mismatch at the input, any temperature effects on the circuit affect the overall noise figure.

If the device noise figure changes from 1.4 to 1.8 dB, then 0.6 dB variation allowance remains for the rest of the front end circuit if the overall noise figure is to remain at a fixed value -0, +1 dB. This is accomplished by temperature compensating the front-end circuitry and also by having sufficient gain at the front end to over-ride noise contributed by the following stages such as the first mixer.

The effective receiver temperature is given by:

$$T_e = (N-1)\ 290^\circ + \frac{T_a}{L} + (1 - \frac{1}{L})\ T_L$$

where N is the receiver noise figure, T_a is the antenna noise temperature, T_L is the temperature of the receiving circuit lossy components, and L is the numeric loss factor (greater than one). The receiver loss is 2 dB (two circulators at 0.5 dB, one antenna switch at 0.5 dB, and 0.5 dB of cable losses). Using an antenna temperature of 70°K, a loss temperature of 200°K, and N = 5 db yields

$$T_e = (3-1)\ 290 + \frac{70}{1.51} + (1 - \frac{1}{1.51})\ 290^\circ = 724^\circ K.$$

4.5.3.5.5 Orbiter 400 MHz Radio Subsystem

Fig. 4.5.3-11 shows a simplified block diagram of the UHF equipment. The duplexing circuitry including the two circulators and T/R switch is identical to that in the Lander vehicle.

The beacon transmitter consists of a stable crystal oscillator operating at 25 MHz and a times 16 multiplier chain to 400 MHz, and amplifies to achieve the desired output level. The square wave tone oscillator 100 percent amplitude modulates the transmitter output.

The receiver, with an overall noise figure of 4 dB, is similar to the beacon receiver used on the Lander except for the output detectors. The second i-f output drives the FSK demodulator, having two wideband filters followed by independent opposite polarity detectors which are summed to form the Manchester coded signal.

In the Lander transmitter binary data having an NRZ format and bit rate R_b is bi-phase modulated on a square-wave subcarrier with frequency R_b to produce a Manchester coded signal; this signal modulates the frequency shift key (FSK) transmitter. The reconstructed signal (detected by the Orbiter FSK detector) is fed to the bit sync detector which generates a square-wave subcarrier at frequency R_b to convert the reconstructed signal back to the NRZ format. This signal is detected in a matched filter.

4.5.3.5.6 Data Handling System

A. Functions

The data handling and storage subsystem provides encoding, time multiplexing, sequencing and storage of the capsule's engineering and science data, and storage and execution of on-board command functions. The data handling and storage subsystem controls the data collection, formatting, and data transmission as a function of the mission phase from interplanetary cruise through post impact operations.

B. Summary Description

The functional block diagram of the data handling subsystem is presented in fig. 4.5.3-12. All analog signals, (0-5v), are multiplexed by the analog gates. The format of the data is determined by the data handling unit. The fixed formats are selected, as a function of mission phase, by a mode select command from the random access memory.

The analog to digital (A/D) encoders sample the analog signals and perform the digital conversion many times faster than the word rate. Using the fast conversion and a 9 bit analog to digital converter (ADC), the transmitted number of conversion bits per scientific data source can be made 9 bits or less depending on the source's accuracy requirements. The engineering signals are encoded to 7 bits.

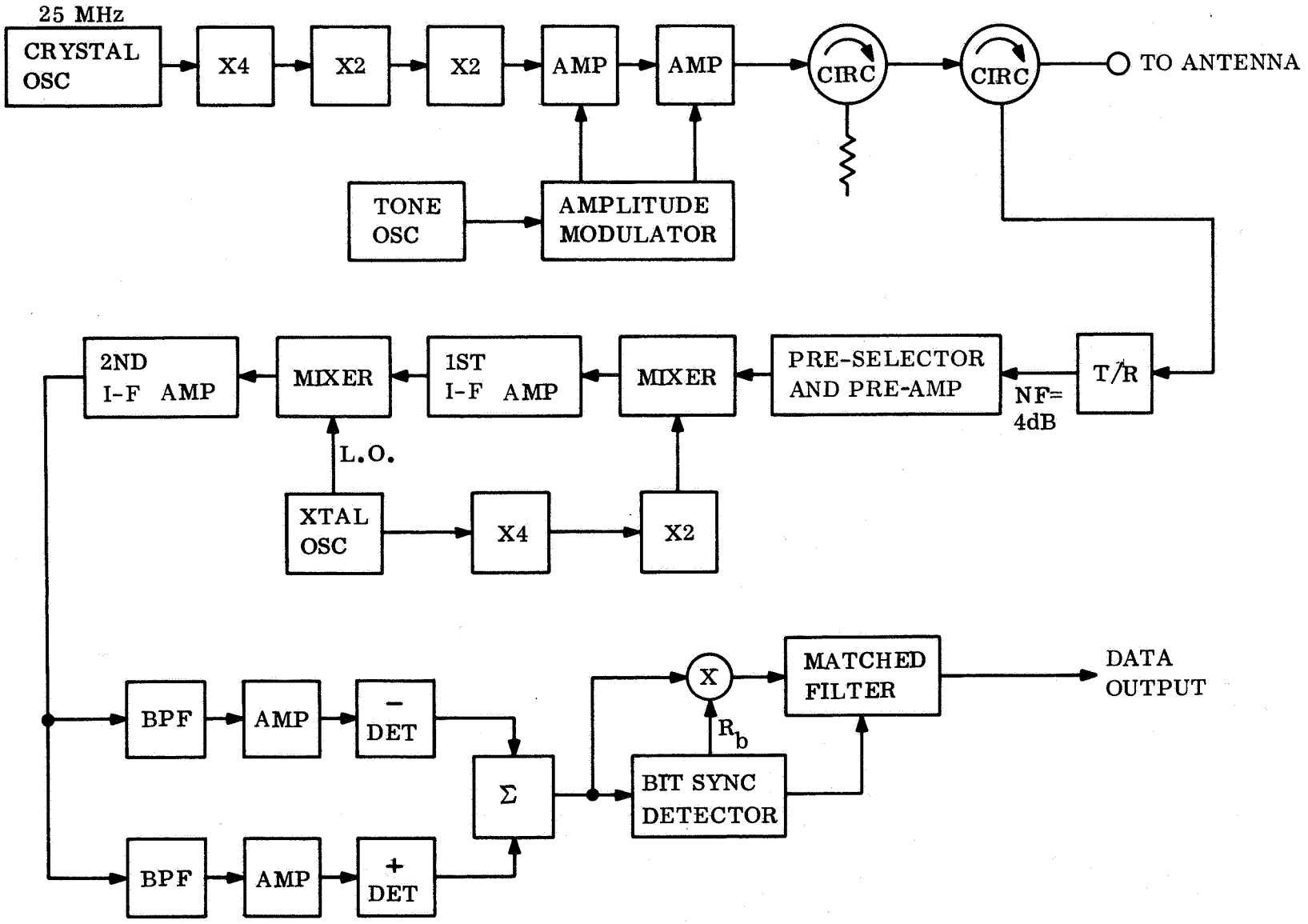


Figure 4.5.3-11. Orbiter 400 MHz Radio Subsystem

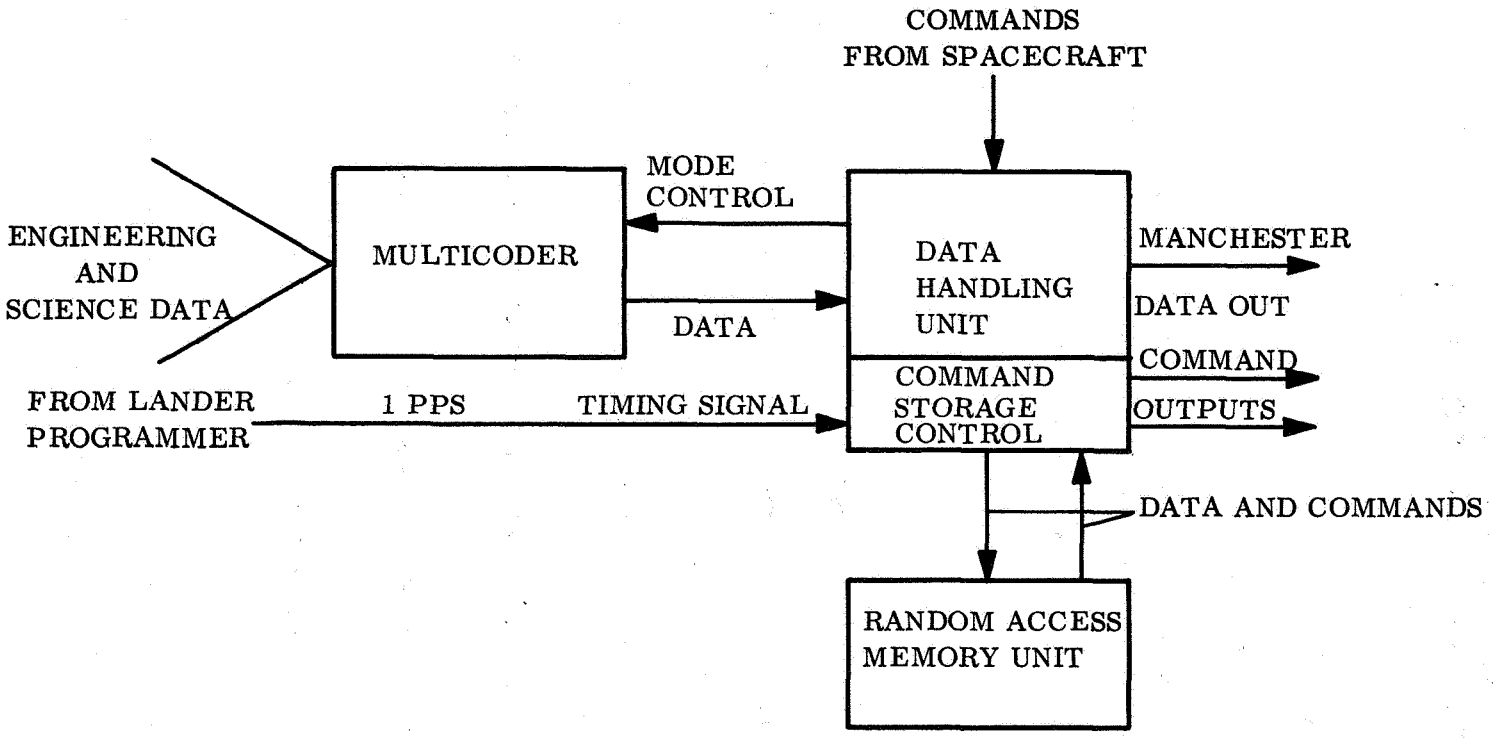


Figure 4.5.3-12. Data Handling System

Multicoder - The multicoder will have four modes of operation, each controlled by the data handling unit pulse lasting the duration of each mode. The number of data channels per mode are defined below. All analog inputs are high level (0 to +5 vdc).

1. Entry Mode

   a. 60 analog inputs, 9 bit resolution, 1 sample/sec

   b. 3 analog inputs, 9 bit resolution, 3 samples/sec

   c. 50 digital groups, 8 bit parallel occurring in 50 serial words on command from the multicoder at the rate of 5 groups/sec

   d. 2 digital words, 7 bit parallel, 1 sample/10 sec

   e. 1 digital word, 11 bit parallel occurring in two words, 1 sample/10 sec.

2. Landed Mode No. 1

   a. 58 analog inputs, 7 bit resolution, 1 sample/20 min

   b. 6 digital words, 11 bit parallel, 2 lines, 3 words/line. 1 sample/20 min

   c. 1 digital word, 11 bit parallel, 1 sample/20 min

   d. 130 digital words, 14 bit parallel sequential on multicoder command, 1 sample/20 min

   e. 130 digital words, 11 bit parallel sequential on multicoder command, 1 sample/20 min

   f. 3 digital words, 7 bit parallel sequential on multicoder command, 1 sample/20 min

   g. 2 digital words, 7 bit parallel, 1 sample/20 min.

3. Landed Mode No. 2

   a. 14 analog inputs, 7 bit resolution, 27000 SPS (160 kbps).

   b. digital inputs b, c and g of Landed Mode 1.

4. Landed Mode No. 3

   a. One of four TV inputs, 6 bit resolution, 27000 SPS (160 kbps).

Data Handling Unit - The data handling unit (DHU) accepts commands from the command storage control unit to determine in which mode the multicoder will operate fig. 4.5.3-12. It decodes these commands and controls the multicoder functions by supplying pulses on one of four mode lines. The data from the multicoder is routed by the DHU either to the random access memory unit or to the UHF transmitter. During entry, data from the multicoder is interleaved with delayed data from the random access memory unit.

The DHU also conditions the signals from the multicoder and memory going to the transmitters.

Commands from the spacecraft via hard-wire are routed through the DHU to the command storage unit and then to the memory.

Random Access Memory Unit - The random access memory unit (RAMU) is used to provide storage for digital words from the multicoder (7 bits/length) and to store command words (21 bits length).

The telemetry storage has two modes:

1. Store data serially and read out serially 70 sec later.

2. Store data and read out at a fixed rate at some later time.

Both of these modes are used in entry data collection as shown in fig. 4.5.3-15. Mode 2 is also used for collection of landed serial and engineering data and playback during Orbiter passes.

Data will be inputted and outputted in a 21 bit format. Read out will be destructive with a restore mode option for Mode 1 as required.

Command Storage Unit - The command storage unit (CSU) (part of the DHU) accepts commands from the spacecraft via hard-wire. The commands and time labels are stored in the memory. The unit examines sequentially each command location in the memory. It does pass a command time word until that time agrees with the vehicle clock time. When agreement occurs it jumps to the next location which should be a command and outputs it to the Lander programmer (see para 4.5.4.2).

The commands in the memory can also control the sequence of examination of the CSU. Thus, a fixed sequence of operations can be addressed by commanding the CSU to that memory location. At the end of this sequence (e.g., data gathering) a command would be present which would send the CSU back to the memory location following the jump command. By using auxiliary registers (part of the random access memory) and decoding functions to control the CSU, the CSU became a versatile general purpose program machine.

For a mission of 24 hr with experiments requiring data gathering every 20 min, 3 hr, and 6 hr, the specific actions at each sampling time need be stored only once with time increment and return commands at the end of these sequences.

The timing signals for the CSU are provided by the Lander programmer.

A program for operation after separation is stored in the memory. The commands are read out of the memory sequentially as the time for execution matches the present time in the vehicle. The command storage control unit will run continuously until 1 hr after impact. It will then control the landed operations until end of life.

Fig. 4.5.3-13 shows the command word format. Since there is no radio command system on this vehicle all the words will be stored program commands. These commands and the proper time labels will be loaded into the random access memory prior to separation from the spacecraft. The experiment routine on the surface will be controlled by these commands as the time labels associated with each sequence agree with the time on the vehicle clock. This unit will be shut down to conserve power when the time between commands is more than 20 min. A separate set of registers will be used to store the time at which the data handling system shall begin functioning and also the memory location of the next command. The flow chart in fig. 4.5.3-14 shows how the command storage unit checks the time until next command execute and shuts the system down until this time is reached on the vehicle clock.

When the commands are loaded into the memory prior to separation from the spacecraft the presence of data on the command line causes a command interrupt in which the system acts as though it is in the dormancy subroutine. After memory updating is completed, the unit will again return to the last memory location and time and sequentially search the memory. Real time commands and generated commands at this time will both appear on the eight output lines which go to the programmer and in the data handling unit to control data flow and mode.

Table 4.5.3-8 shows the entry data measurements and table 4.5.3-9 shows the landed data measurements.

C. Data Handling vs Mission Phase

Interplanetary Cruise - The Capsule's data handling equipment is assumed de-energized during interplanetary cruise. Monitoring of thermal control and the Capsule's electrical power subsystem is performed by the spacecraft's data handling subsystem.

Capsule Checkout - The Capsule checkout mode is initiated sufficiently prior to separation to determine the status of the Capsule and its payload and to allow for corrective action. Under control of the programmer and command storage control unit, Capsule checkout is accomplished with data being transferred to the spacecraft via hard-wire. At this time the memory can be updated, if necessary.

Capsule Separation and Engine Fire - From Capsule separation to engine fire, the Capsule is transmitting at 1090 bps. Only engineering data is monitored. The received data on the spacecraft is detected and stored for delayed transmission to Earth over the high data rate link.

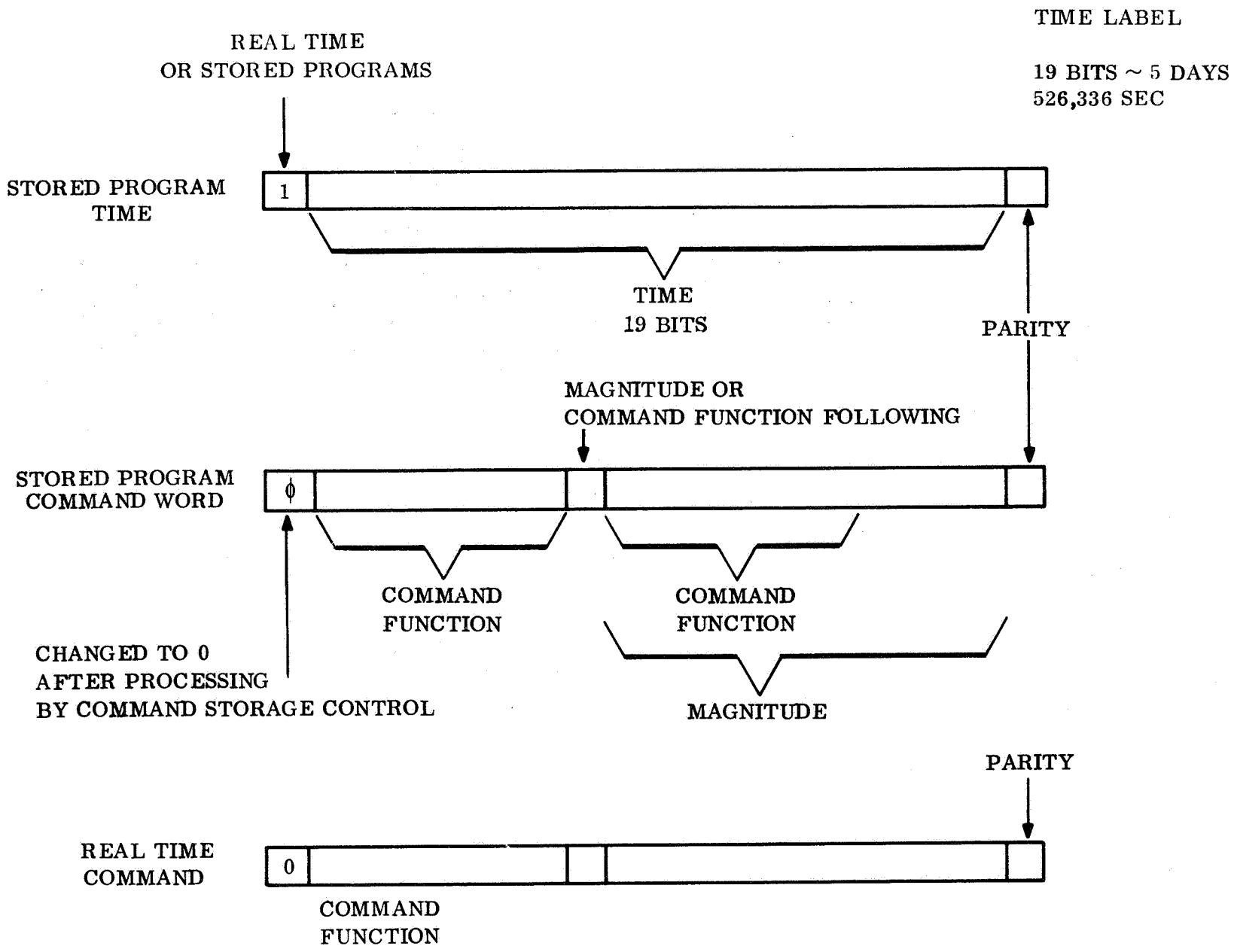


Figure 4.5.3-13. Command Word Format

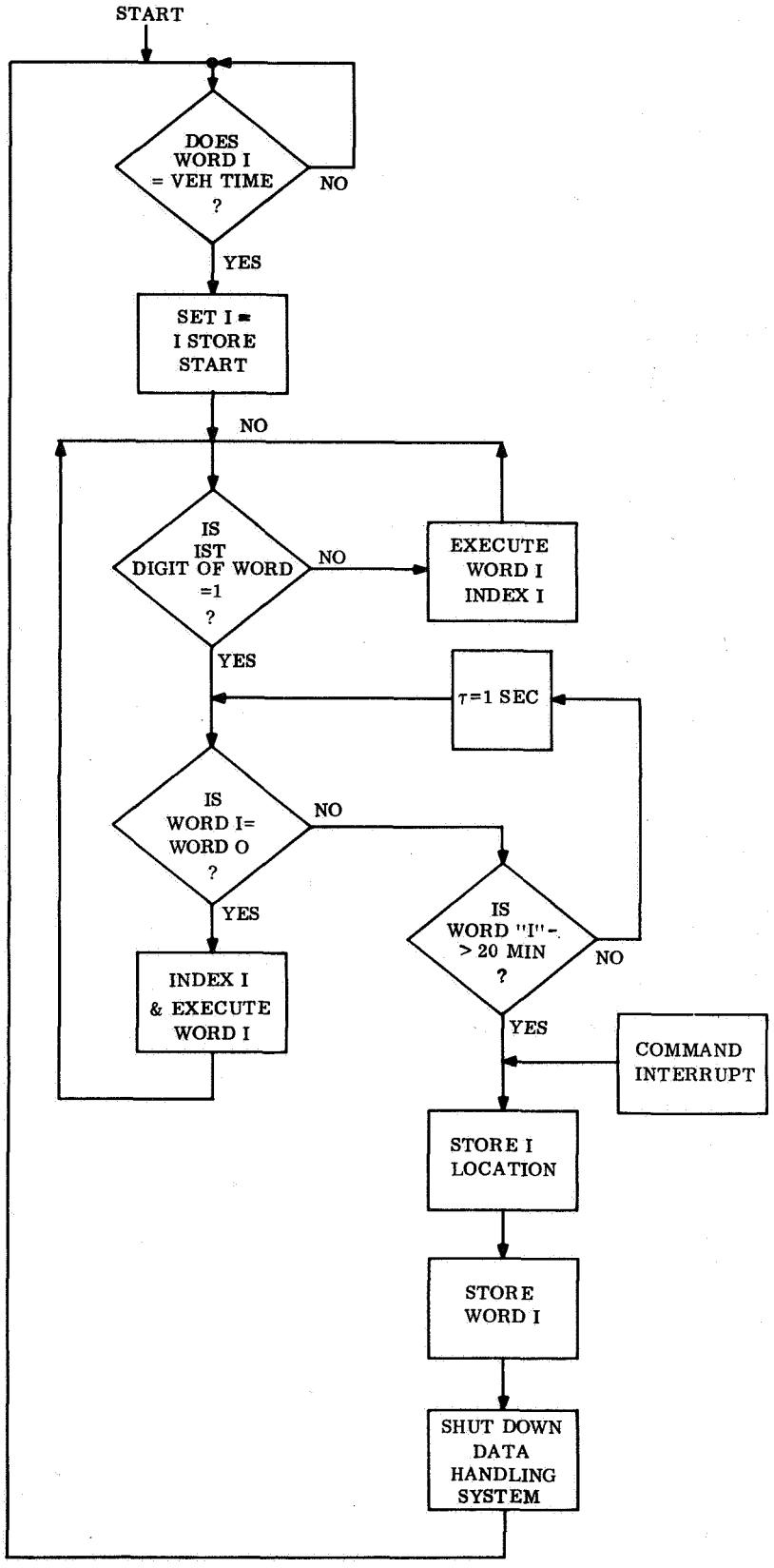


Figure 4.5.3-14. Operation of Command Storage Control Unit

TABLE 4.5.3-8. ENTRY DATA

Sensor	Accuracy (%)	Sampling Rate (sps)	Bits/Sample	No. of Channels	BPS	Time
Pressure transducer (2) 0 -0.3 psia	1	1	9	2	18	Post parachute deployment
Resistance thermometer (2) 100° - 300°K	0.2	1	9	2	18	
Mass spectrometer (readout 8 bits at a time)	---	N/A	8	N/A	40	1 hr before entry to impact
Triaxial accelerometer (dual scale)	1	3	8	3	72	1 hr before entry to impact
Stagnation temperature	0.25	1	9	1	9	1 hr before entry to impact
Stagnation pressure (4)	0.25	1	9	4	36	1 hr before entry to impact
Water vapor	N/A	1/15	7 (parallel)	2	14/15	1 hr before entry to impact
		1/15	11 (parallel)	1	11/15	1 hr before entry to impact
Engineering measurement	---	1	7	50	350	

TABLE 4.5.3-9. LANDED SCIENCE (NON-IMAGING)

Sensor	Accuracy	Sampling Rate	Bits/ Sample	Number of Channels per Sensor	Number of Bits per Hour
Pressure transducer (2)	1%	3/hr	6	2	36
Thermometer	1%	3/hr	6	2	72
Wind velocity (2)	3%	3/hr	11 (P)	6	66
Moisture	--	3/hr	7 (P) 11 (P)	2 1	75
Surface composition	Less than 256 counts per energy slot in 3 hr	1/3 hr	14 (P) 12 (P) 7 (P)	130 130 3	1133
Clinometer (2)	1%	1/6 hr	7 (P)	2	14/6
Engineering measurements	--	3/hr	7	50	1050

(P) - Parallel

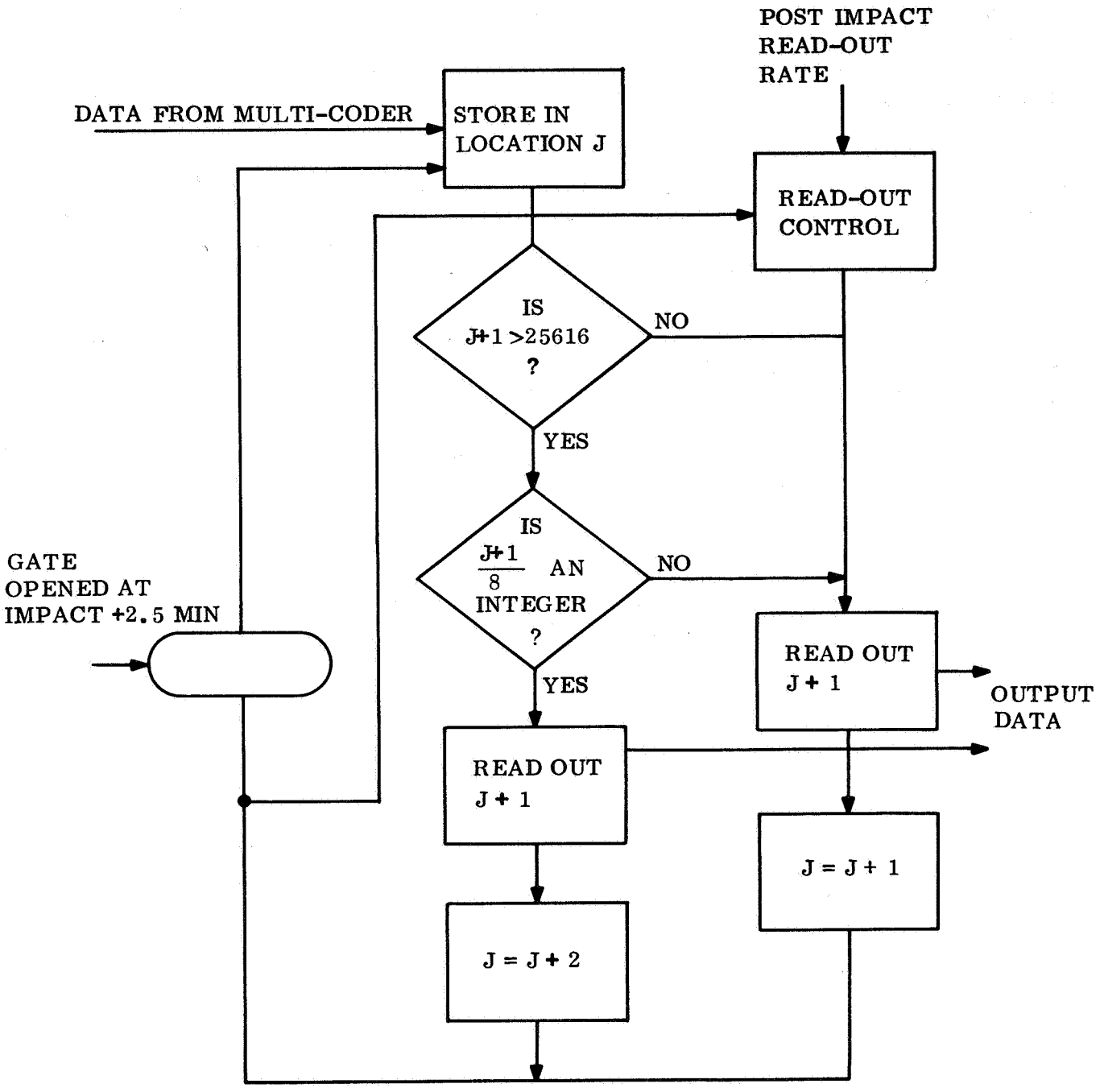


Figure 4.5.3-15. Entry Data Storage Routine

Capsule Entry - Upon initiation of entry the data rate is 1090 bps. The entry data rate requirements are shown in table 4.5.3-8. Assuming 350 bps for engineering data, the total data rate required is 1090 bps. For a blackout time of less than 70 sec the storage required is approximately 50 kbits.

The data is stored in the random access memory. Essentially, the memory will act in two modes; one as a delay line with a 70 sec delay, and two, as a memory in which up to 100 kbits of entry data are stored. Each word in the memory is 7 bits. The operation of the random access memory during entry is shown in fig. 3.5.3-15.

Post Impact Relay - Upon impact the buffer readout is temporarily halted. The buffer will contain 100 kbits of entry data. Engineering data is continued to be read out at 1090 bps until completion of the setup period. Upon completion of the setup period, the imaging data collection and transmission begins. Stored engineering and scientific data are read out at the beginning and middle of the imaging cycle.

Landed Operations - The data presented in table 4.5.3-9 is collected and stored. The basic period between sampling is 20 min. Approximately 25 hr after impact the Orbiter will again be in view and all the stored data will be transmitted at 31 kbps at the beginning of the transmission period. Then video data will be generated and transmitted video transmission for the next approximately 4 min period. This procedure is repeated for the entire relay transmission interval.

4.5.3.5.7 Physical Characteristics

Table 4.5.3-10 summarizes the physical characteristics of telecommunications equipments. The key to development status is:

1. No modification required (off-the-shelf)
2. Modify (e.g., for high shock)
3. Redesign (basic equipment exists but redesign for new frequency, detection technique, etc.)
4. New design (specify new design using established techniques)
5. New development (employs near-future state-of-the-art techniques).

TABLE 4.5.3-10. PHYSICAL CHARACTERISTICS

Component and Quantity	Size (in.)	Weight (Based on 1000 g's)(lb)	Power	Sterilizable (125°C)	Minimum Shock (present information)	Development Status	Remarks
UHF transmitter	30 $in.^3$ 1.5 x 4 x 5	2.5	150 watts	yes		4	
UHF antenna (2)	8 diameter x 2	1	--	yes		4	2 required 1 will be used
UHF circulators (2)	6 $in.^3$ 2.5 x 2.5 x 1	0.4	--	yes		3	2 required in close proximity
UHF antenna switch	1.1 $in.^3$ 2 x 1.5 x .375	1.0	0.25A @ 3.5v and 10 micro-A @ 28v	yes	3000 g's, 3 ms	1	Interchange voltages to switch antenna - Power required during xmt, and receive
Beacon receiver and T/R switch	21 $in.^3$ 5.4 x 3.6 x 1/1	1.3	0.5 watts and 0.06A @ 1.2v	yes		4	0.06A @ 1.2v required during 400 MHz transmit periods
Multicoder	104 $in.^3$ 3.5 x 4.3 x 7	5	15 watts	yes		3	Power required during data sampling periods only (see text)
Data handling unit	100 $in.^3$ 4 x 5 x 5	4	3 watts	yes		4	
Thin film memory	88 $in.^3$ 4 x 4 x 5.5	5	6 watts	yes		4	180 kbit capacity, random access
Signal conditioner	4 x 5 x 7	4	8 watts	yes		2	50 channels only
Three axis impact Accelerometer	1.3 x 1.3 x 0.8	0.6	--	yes	10,000 g's	1	
Charge amplifier (3)	1.25 x 2 x 3	0.5	1.2 watts each	yes	representative unit passed 2000 g test	1	2 required connected to impact accelerometer by coaxial cables

4.5.4 ELECTRICAL POWER EQUIPMENT

The power equipment provides electrical energy, power switching, charge control, voltage control and electrical distribution. Fig. 4.5.4-1 illustrates this equipment. Note that the electrical energy flow, power, signals, and data which takes place between subsystems is shown in the Functional Block Diagram, Section 4.2.4.

4.5.4.1 Operation

Commands are received via hardwire connection to OSE for post sterilization check via hardwire from the Spacecraft through the telecommunications subsystem during interplanetary cruise and Martian orbit and from the telecommunications subsystem after landing. These commands enter the programmer as a 21 bit word where they are decoded into operation signals for the relay which switch the power feeder lines. The programmer also contains a multichannel hardwire program section which provides an additional independent operation of the spin, de-boost, and landing sequences for mission assurance. These programs have programmable start times and, once initiated, proceed with the execution of a fixed program sequence. A single command, regardless of origin, may signal the operation of a single load or a group of loads as required.

All operation signals from the programmer go to the power controller where power switching takes place. The components which require independent switching, such as the payload scientific instruments, have separate electrical power feeders. Other components which are always used as a group, such as the engineering diagnostic instrumentation, share a single feeder. The power controller can accept energy from the operational battery, from the high rate batteries, from the Spacecraft or from ground power, and switch this power to the appropriate load or loads. The line contactor is used to select and control which of these power sources supplies the power controller.

The operational battery supplemented by the pre-entry battery during post separation coast provides all Lander electrical energy except the high rate pyrotechnics and hot-wire initiations. This secondary silver-zinc battery is charged from raw Spacecraft power prior to separation. Power from the operational battery feeds the unregulated loads directly. This battery is equipped with extra cells and semiconductor bypass for redundancy.

4.5.4.1.1 Battery Redundancy Considerations

To enhance reliability three alternatives have been investigated.

If two batteries were flown, each capable of providing the minimum mission duration objectives, a considerable weight penalty would be suffered. An alternative route would be to provide two batteries which would each provide half the desired output. This method would increase the battery weight, about 25 percent because of the lower power-to-weight ratios of smaller batteries, and ensure that half the mission objective would be achieved even if one battery failed.

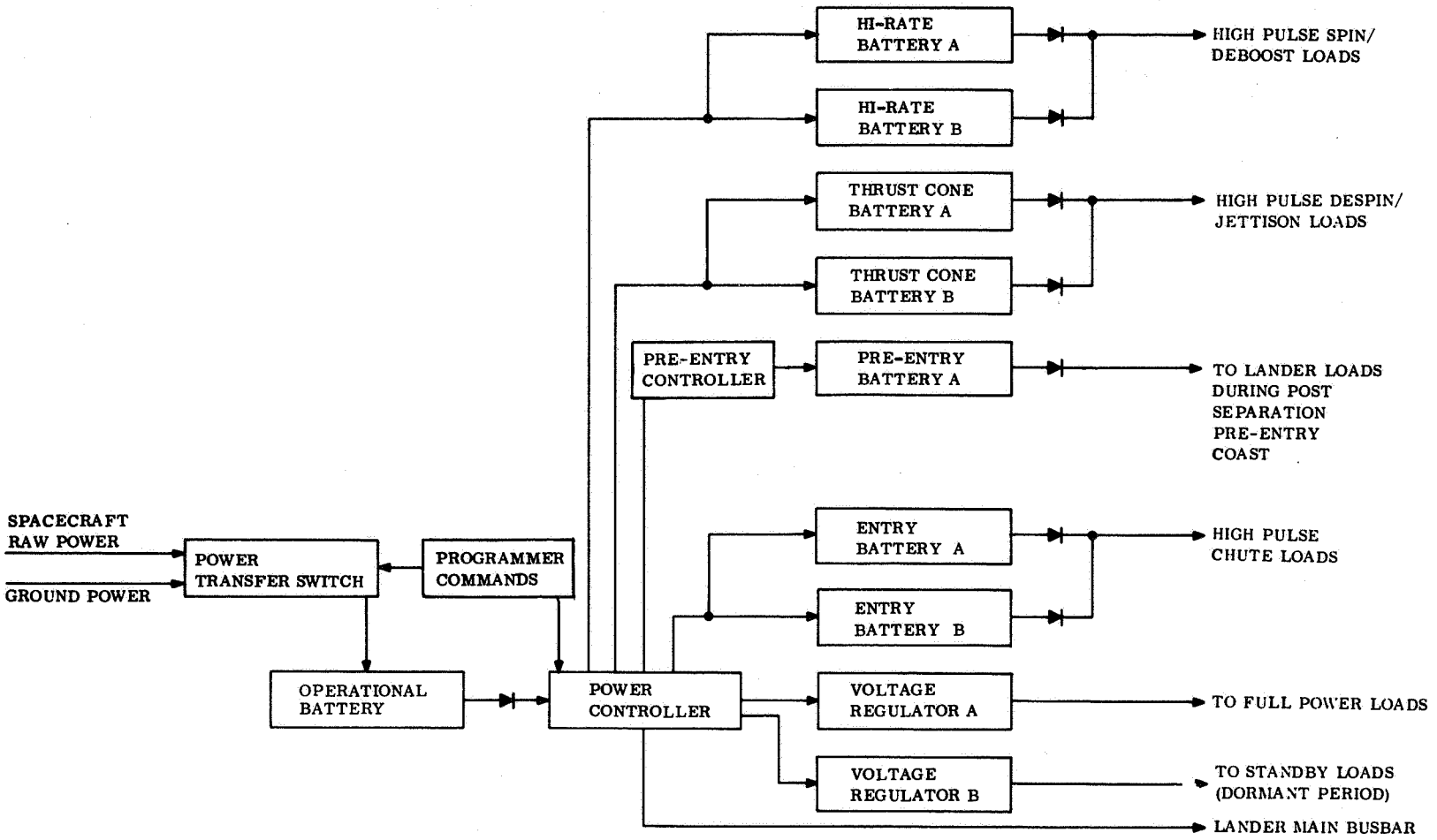


Figure 4.5.4-1. Electrical Power Subsystem, Point Design 2, Block Diagram

The method adopted to provide adequate redundancy is to carry redundant cells. The logic in this approach is that it is usual if failure should occur for only one or at most two cells to fail. If these can be replaced by reserve cells considerable savings will result.

The circuit shown in fig. 4.5.4-2 incorporates diodes on the charging side having a tightly controlled Zener regulating level, e.g., 2.05 v, and very low dynamic impedance. The diode on the discharge side of the circuit has a low forward voltage. Three redundant cells in the battery are connected through the controller to be added in series when needed as directed by the programmer.

If, during charge, a cell fails open circuit or high resistance, the Zener voltage of that cell will be exceeded. The cell will be bypassed. If the cell fails short circuit or low resistance the cell will carry the charge current. A slight loss may result in charging a bad cell. Because each Zener protective voltage level will be equal to its cut-off voltage, the arrangement gives added protection against overcharging. If a cell fails on discharge, the diode in the discharge circuit will conduct and bypass the failed cell, avoiding driving the cell negative. Whichever way the cell fails it will always be bypassed.

Switching in new cells through the controller is achieved by low voltage sensing in the programmer. The low voltage is caused by the loss of a cell plus the diode drop as it switches in. Two cells would therefore be swtiched in for the first cell failure to compensate for diode voltage drop. A nominally higher voltage than the original battery would then result. If the second cell failed only one other cell would be switched.

A redundant system has been provided which allows for the failure of two cells in a battery. The additional weight approximates 20 percent of the original battery. This includes cells, diodes, programmer and controller modifications.

The need for high current capability during initiation operations is met by three pairs of thermal batteries. These provide power for spin/de-boost operations, de-spin/entry operation and parachute/aeroshell operations. In each case two batteries are available for redundancy. The batteries are activated separately from the canister or operational battery and the output is switched to the initiators via the power controller. These activation circuits are equipped with thermal relays to protect the operational battery.

The scientific payload, r-f equipment, diagnostic instrumentation, data processing equipment, and sequencing components will require voltage regulation. To minimize weight, to obtain the high efficiency needed on the extended mission and to permit noise control, a single central voltage regulator should be used. However, the high degree of energy conservation required would not permit the standby losses of such a large regulator on a continuing basis. For this reason two regulators are used, a small unit for the timer and receiver, which are operated through the dormant periods, and a larger unit which handles all other loads. In addition, it is recognized that selected small loads in the scientific instruments may require special high accuracy regulation.

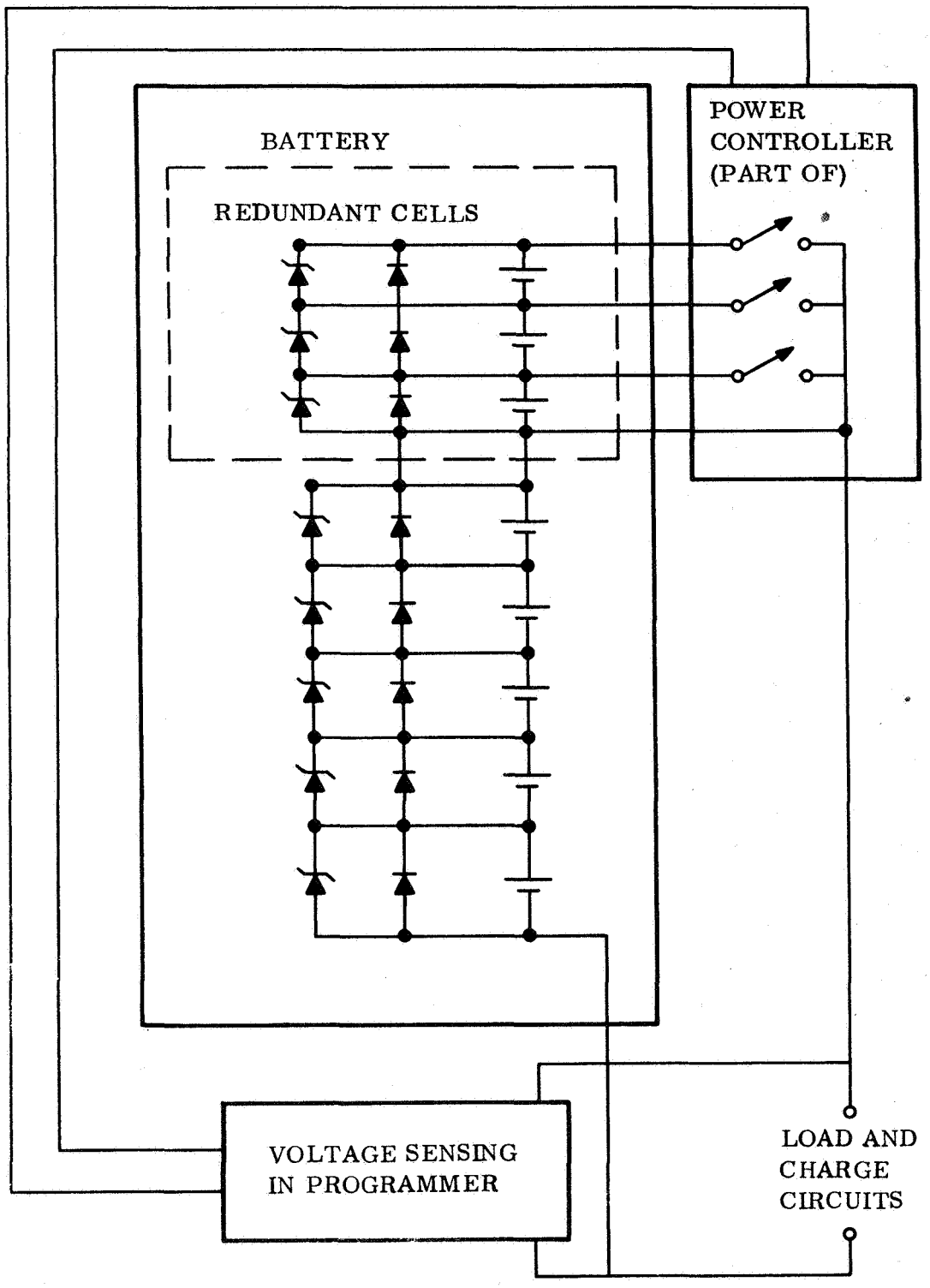


Figure 4.5.4-2. Battery Redundancy Circuit

Battery charging is controlled by redundant equipment located in the canister. This equipment uses solid state switching circuitry with time ratio control for high efficiency.

The Mars Hard Lander electrical system utilizes direct current power sources and distribution as well as steady-stage sensing of pressure and temperatures. Programming, sequencing and power switching are performed for durations of a minute or longer with synchronization accuracies in the order of 0.1 sec. Safing and arming are performed manually. Conditioned and regulated power are processed at a low audio frequency. Initiation and electromechanical operations are performed with the application of electrical energy for durations of a few msec to a few hundred msec.

Electromagnetic compatibility equipment is designed to provide protection over a broad spectrum. This includes low repetition rate pulse-transients through the r-f frequencies used for telemetry.

Data processing, encoding, and multiplexing involve kilocycle and higher frequencies. The camera electronics with imagery represents the highest data bit rate.

UHF is used for telemetry, providing the highest frequency equipment aboard the probe system.

These needs describe the spectrum of electrical energy which must be distributed by the cables and harnessing.

Since the Lander will carry a variety of scientific equipment as payload, it is desirable to make arrangements permitting the mission to continue should electrical difficulties arise in a limited area. This feature is provided through a breaker and limiter unit which provides electrical protection to each payload item. Should an electrical fault develop, the load element is disconnected or current limited so that the remainder of the mission may continue.

4.5.4.2 Component Description

Each component is described in detail in this section. Table 4.5.4-1 lists the electrical equipment of Point Design 2 by name, location, weight, size and power level, together with electrical reference designators. The equipment situation is indicated by capability to withstand 125°C sterilization temperature, prior shock level accomplished, and development status. The development status is shown by the same numerical code as defined in para 4.5.3.5.

4.5.4.2.1 A101, Operational Battery

Function: Provides energy source for all aeroshell and Lander electrically operated equipment, except high rate initiation loads, from the time of canister release through the mission completion.

Type: Manually activated heat-sterilizable silver-zinc secondary battery sealed with high pressure emergency rupture disk.

Rating: 561.1 watt-hours, 28V nom, ±18 percent, Load profile per Section 4.2.5.

TABLE 4.5.4-1. ELECTRICAL EQUIPMENT HARDWARE MATRIX, POINT DESIGN 2

Component	Size (in.)	Weight (based on 1000 g's) (lb)	Power (watts)	Sterilizable (125 C)	Maximum Shock (present information)	Development Status
Operational battery (A101)	9.0 × 5.5 × 9.0	29.8	Source	yes	2,000	5
Line contactor (A106)	2.5 × 2.5 × 5.0	2.0	5.6	yes	400	3
Lander programmer (A107)	8.8 × 7.7 × 3.5	7.2	12.0	yes	400	4
Voltage regulator (A108)	5.0 × 6.0 × 8.0	7.0	250.0	yes	1,000	3
Power controller (A110)	3.5 × 5.0 × 7.0	5.5	15.0	yes	700	5
High rate battery (A113, A114)	2.0 diameter × 3.0	0.5	Source	yes	15,000	1
EMC filter (A115)	3.0×3.75×5.5	1.9	--	yes	5,000	2
Diode blocking module (A121)	1.5 × 1.5 × 2.5	0.2	13.0	yes	20,000	2
Thermal relay module (A124)	1.5 × 1.5 × 2.5	0.15	3.0	yes	50	4
Hg Switch (A128, A129)	1.0 diameter × 2.5	0.1	--	yes	50	4

TABLE 4.5.4-1. ELECTRICAL EQUIPMENT HARDWARE MATRIX, POINT DESIGN 2 (Concluded)

Component	Size (in.)	Weight (based on 1000 g's) (lb)	Power (watts)	Sterilizable (125 C)	Maximum Shock (present information)	Development Status
Voltage regulator (A130)	2.5 × 3.0 × 4.0	0.9	27.0	yes	1,000	3
Breaker and limiter unit (A132)	2.0 × 2.0 × 3.0	0.6	1.0	yes	10,000	2
Aeroshell/Lander IFD (J2002)	1.83 diameter × 1.5	0.13	338.0	yes	2,000	3
Thrust Cone/Lander IFD (J2003)	2.5 diameter × 2.0	0.75	338.0	yes	2,000	3
Command cable assembly (WL1)	14C × 8 ft	2.1	3.0	yes	2,000	3
Power cable assembly (WL2)	16C × 28 ft	3.7	12.0	yes	2,000	3
Instrumentation cable assembly (WL3)	50C × 40 ft	3.0	0.3	yes	2,000	3
Shielded cable assembly (WL4)	1C × 24 ft	0.8	--	yes	2,000	3

4.5.4.2.2 A113, A114 High Rate Batteries

Function: Provide energy source for multiple high rate initiation type loads.

Type: Remotely activated, electrically initiated, thermal type primary battery.

Rating:

Power output	1000 watts
Maximum activated stand	3 min
Power profiles	later

4.5.4.2.3 A106 Line Contactor

Function: Power transfer of aeroshell Lander systems from ground power to Spacecraft power to internal batteries.

Type: Electromechanical latch type line power contactor.

Rating:

Contact rating	20 amp
Interrupt capacity	250 amp
Pull-in time	100 msec maximum
Pull-in power	0.3 watt maximum
Contact configuration	later
Operating life	100,000 cycles
Dielectric withstand capability	1500 v for 1 min

4.5.4.2.4 A107 Lander Programmer

Function: Provide all sequencing, timing, signals, synchronization and clock functions within the Lander and aeroshell. Decode command.

Type: Solid-state digital circuitry using majority logic or redundancy back-up features.

Rating:

Channels
In-flight check-out
Powered flight program
Diagnostics cycle
Maneuver mode control
Preseparation program
Coast sequence
De-boost sequence
Entry sequence
Set-up mode control
Surface science sequence
Photography cycle
Vehicle clock

4.5.4.2.5 A108 Voltage Regulator

Function: Provide control and correction for electrical potential variations. Also, provide various potential levels required to operate aeroshell and Lander electronics

Type: D-c isolated solid-state inverter transformer-rectifier with time ratio control and feedback regulation.

Rating:		
	Output	250 watts
	Voltage levels	later
	Transient recovery time	later
	Regulation	later
	Input	23 to 33 vdc

4.5.4.2.6 A110 Power Controller (Lander)

Function: Provide distribution center equipment and all power switching for the aeroshell, thrust cone, and Lander electrical loads. Receives commands with proper time sequences and synchronization from the Lander programmer A107.

Type: Electromechnical relay, switch and contactor construction

Rating:		
	Number of switched loads	100
	Contract rating	40 amp maximum
	Pull-in time	10 to 100 msec
	Pull-in power	0.5 watt each
	Feeder buses	50

4.5.4.2.7 A121 Diode Blocking Module

Function: Present reverse power flow between various energy sources.

Type: Solid-state single crystal silicon semiconductor diode with redundancy.

Rating:		
	PIV	75 v
	Recovery time	NA
	Forward current	10 to 75 amp

4.5.4.2.8 A115 Electromagnetic Compatibility Filter

Function: Suppress spurious and conducted electromagnetic interference.

Type: Lumped parameter networks with non-linear and lossy type circuit elements.

Rating:		
	Number of bands	later
	Center frequencies	later (UHF)
	Attenuation	later
	Dielectric withstand	1500 v

4.5.4.2.9 A124 Thermal Relay Module

Function: Provide system protection against faulted squib firing circuits.

Type: Bimetallic heat operated latch type switching element.

Rating:		
	Interrupt capacity	10 amp
	Trip level I^2 Rt	later

4.5.4.2.10 A128, A129 Switch, Hg

Function: Detect upwards direction and enable proper deployment circuits.

Type: Potted mercury switch, 3 pole.

Rating:		
	Current rating	1 amp
	Voltage rating	250 vdc
	Dielectric withstand	1500 v, 1 min

4.5.4.2.11 A130 Voltage Regulator

Function: Provide control and correction for electrical potential variations at high efficiency for standby usage. Also, provide various potential levels required to operate the standby Lander electronics.

Type: D-c isolated solid state inverter transformer-rectifier with time ratio control

Rating:		
	Output	27 watts
	Input	23 to 33 vdc

4.5.4.2.12 A132 Breaker and Limiter Unit

Function: Protect the electrical system against non-essential functional faults.

Type: Circuit Breaker, thermal relays, and limiting resistors in selected groups.

Rating:		
	Circuits	25
	Trip levels	30 ma to 2 amp

4.5.4.2.13 J2002, P2002 Inflight Disconnect Aeroshell-Lander (connector, electrical; electromechanically disconnected)

Function: Provide remotely operable, electrical disconnection between the aeroshell and the Lander vehicle during Martian entry flight.

Type: Hot-wire operated push-off type collet lock-unlock connectors with crimp insertable cuperic contacts and 360° RFI shielding.

Rating:

Circuits	15 pins
Wire sizes	later
Operate time	less than 100 msec
Operated signal	3.5 amp for 50 msec
Safe level	1 amp, 1 watt, for 5 min
Release impulse	later
Reliability	0.995 at 90% confidence each device.

4.5.4.2.14 J2003, P2003 Inflight Disconnect - Thrust Cone/Lander (connector, electrical; electromechanically disconnected)

Function: Provides remotely operable/electrical disconnection between the thrust cone and the Lander vehicle during Martian entry flight.

Type: Hot-wire operated push-off type collet lock-unlock connectors with crimp insertable cuperic contacts and 360° RFI shielding.

Rating:

Circuits	50 pins
Wire sizes	later
Operate time	less than 100 msec
Operated signal	3.5 amp for 50 msec
Safe level	1 amp, 1 watt, for 5 min
Release impulse	later
Reliability	0.995 at 90% confidence each device.

4.5.4.2.15 WL1 - Lander Command Cable Assembly

Function: Provides command and signal distribution from the Lander programmer to various receiving equipment.

Type: Copper conductor electrical cable insulated with Kaptan and teflon (HF + 1/2 T) in a wrapped construction. Cable connectors of NAS 1599 type and modified in selected cases to permit high density inserts and rear insertion construction.

Rating: Later

4.5.4.2.16 WL2 - Lander Power Cable Assembly

Function: Provide electrical power distribution throughout the Lander, from the power controller and batteries to the various loads.

Type: Copper conductor electrical cable insulated with Kaptan and teflon (HF + 1/2 T) in a wrapped construction. Cable connectors of NAS 1599 type and modified in selected cases to permit high density inserts and rear insertion construction.

4.5.4.2.17 WL3 - Lander Instrumentation Cable Assembly

Function: Distributes data from sensors and payload instruments to data conditioners, encoders and telecommunication equipment in the Lander.

Type: Copper conductor electrical cable insulated with Kaptan and teflon (HF + 1/2 T) in a wrapped construction. Cable connectors of NAS 1599 type and modified in selected cases to permit high density inserts and rear insertion construction.

Rating: Later

4.5.4.2.18 WL4 - Shielded Lander Cable Assembly

Function: Provides coaxial transmission of signals and high frequency energy through the Lander.

Type: RG-58
Zc 50 ohms

4.5.5 ENVIRONMENTAL CONTROL

The mission weight and reliability constraints are such that the environmental control system complexity and design margins must be the minimum possible. In line with this objective, a semi-passive method of thermal control utilizing an insulated payload, optimum surface radiative coatings, and local electrical heaters was selected to satisfy the thermal control requirements.

The Lander configurations present an ideal approach for providing the necessary payload thermal insulation. The 1.5 in. thick honeycomb container structure will be utilized thereby eliminating any additional space requirements for the insulating material. A low thermal conductivity core material (phenolic glass) with foam insulation packed cells will be utilized to control the Lander temperature response. Detailed insulating trade-offs are presented in the parametric data (Volume III, Section 4.4). By adding the foam insulation the heat transfer losses are reduced to a conduction mode only with a relatively high thermal resistance. This is desirable since the radiative and convective heat losses between the honeycomb face sheets could be considerable based on:

1. Radiation across the cell ends could be significant with a possible outside surface temperature of -60°F and an inside structural temperature of 50°F.

2. Although a reduced atmosphere exists, minimizing the heat transfer coefficient, some convection losses could be present in the air space thereby contributing to the overall heat loss.

This conceptual design produced a shell around the payload which has a thermal conductance value of 0.36 Btu Hr-°F-ft^2. Therefore, the payload has sufficient thermal isolation that its minimum temperature will not fall below -40°F, the lower allowable limit for all of the payload components except the battery. To maintain the battery at or above its minimum operation temperature of 50°F, it is thermally isolated from the payload with an insulated package which contains an electrical heater. This heater is thermostatically controlled to turn on when the battery falls below 50°F.

A transient solution was performed to determine the temperature response of an isothermal payload and battery in the Martian environment. Appropriate conduction and radiation was considered based on the Lander configuration. For minimum heat leak, a low surface emissivity of $E_{OS} = 0.1$ was assumed. Results of this analysis are shown in figs. 4.5.5-1, -2, -3 and -4. Figs. 4.5.5-1 and -2 show the battery temperature response and heater power necessary to maintain the battery at 50°F. The temperature response of the payload for the minimum and maximum environments are shown in figs. 4.5.5-3 and -4, respectively. These show that no heater power is required to maintain payload temperature above -40°F.

The transmitter temperature response was studied as a function of daily transmission power with the resulting analysis indicating that no protection in the form of thermal storage material is required to prevent overheating. The specified power level of 32.5 watt-hr/day will only produce an 18°F temperature rise resulting in a peak temperature of 138°F.

4.5.6 DEPLOYMENT MECHANISMS

In the landed position, either side of the vehicle may be uppermost, so provision has been made for the deployment of instruments and equipment from both sides of the flat pack container. However, to avoid unnecessary duplication of the instruments, the actuating mechanisms have, in general, been designed for two way operation. A g-sensing device will determine the direction of deployment operation.

Instruments deployed in Point Design 2 are: four cameras (two high and two low resolution), ten wind velocity transducers (two sets of five), four temperature transducers and one surface composition (alpha back scatter) instrument head. All except the alpha back scatter instrument are located in a central bay the full width and depth of the Lander container, as shown in fig. 4.5.1-1. The alpha back scatter instrument is located in an individual full depth bay, also shown on the drawing.

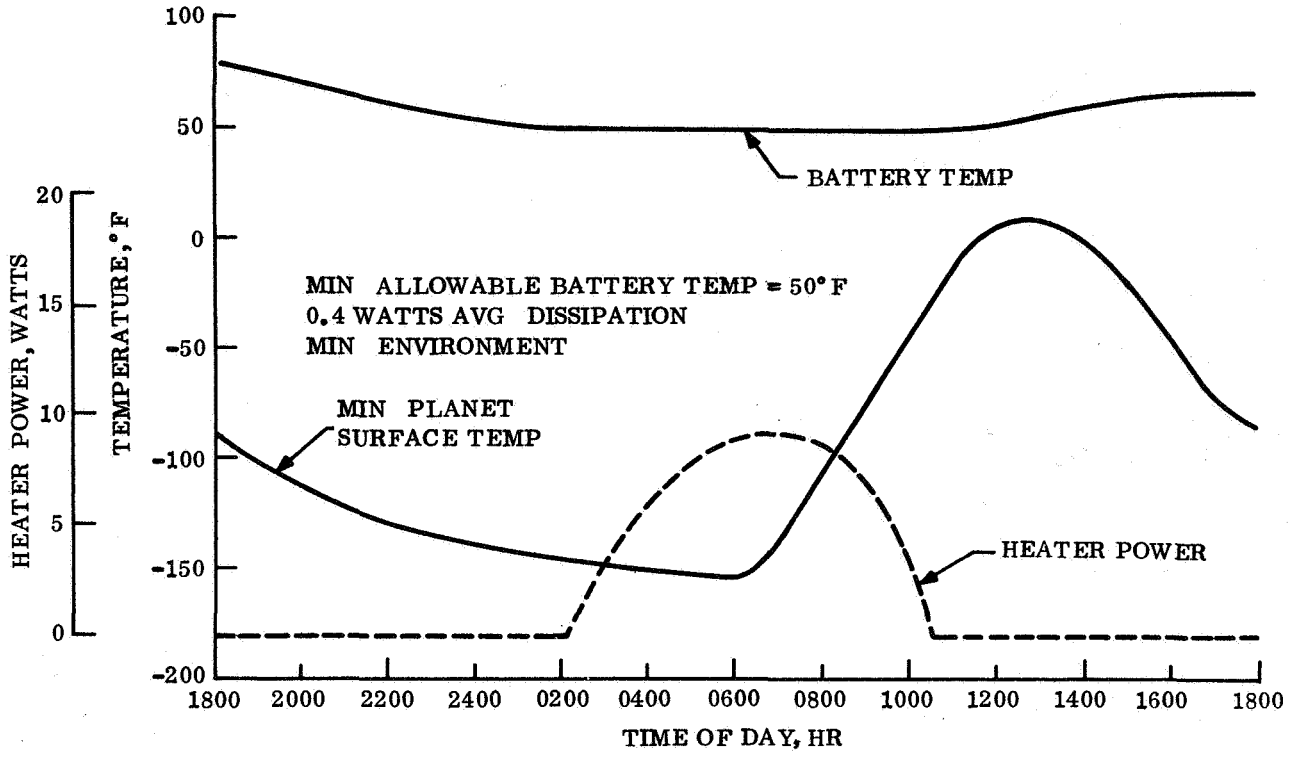


Figure 4.5.5-1. Battery Temperature Profile and Heater Power Requirements, Minimum Environment

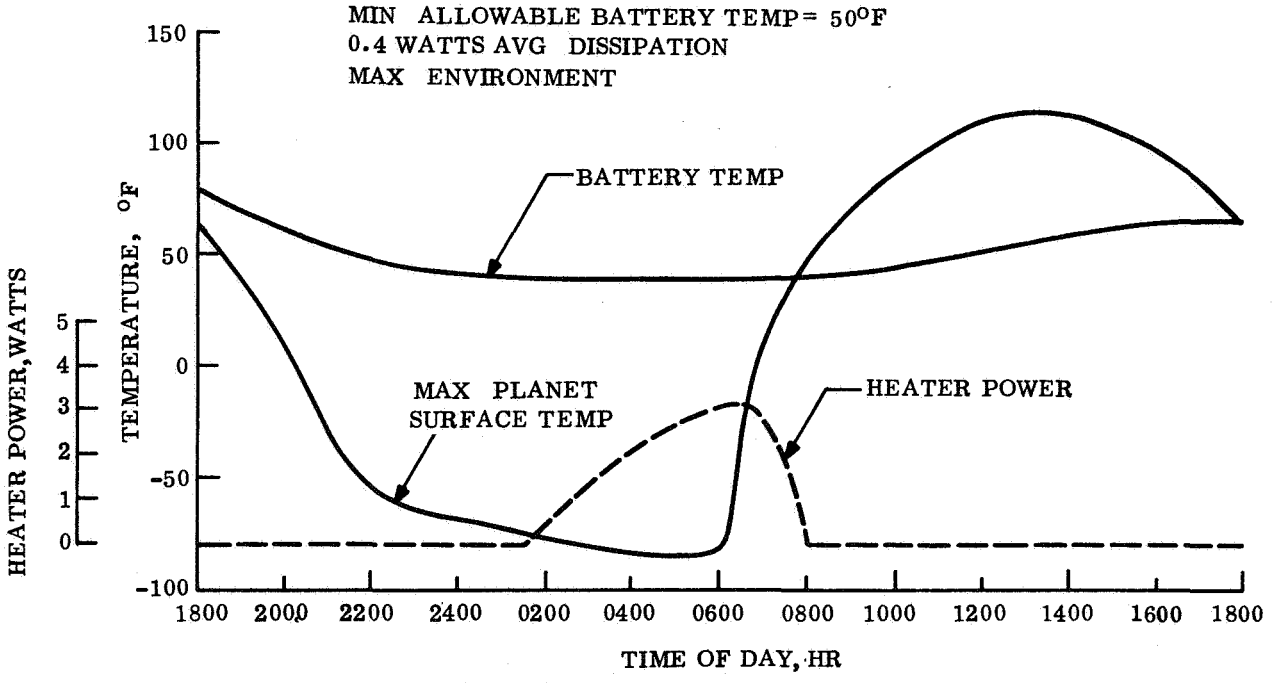


Figure 4.5.5-2. Battery Temperature Profile and Heater Power Requirements, Maximum Environment

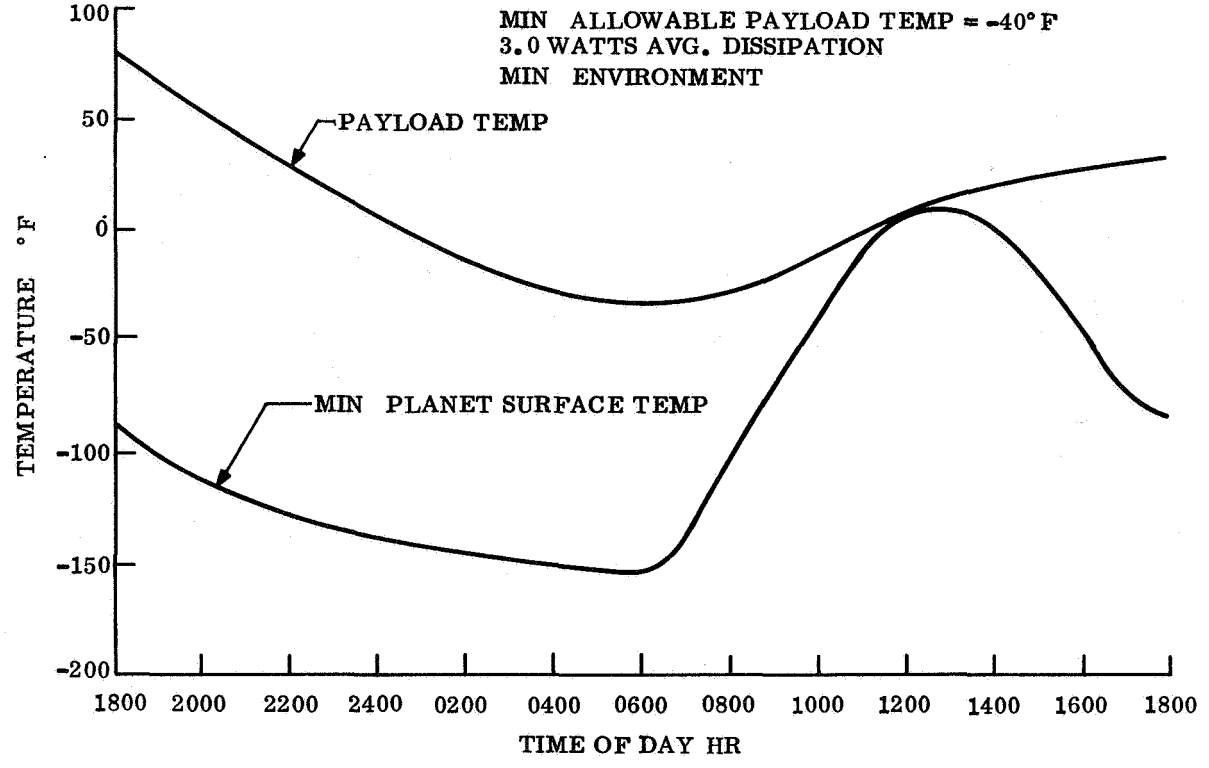


Figure 4.5.5-3. Payload Temperature Profile, Minimum Environment

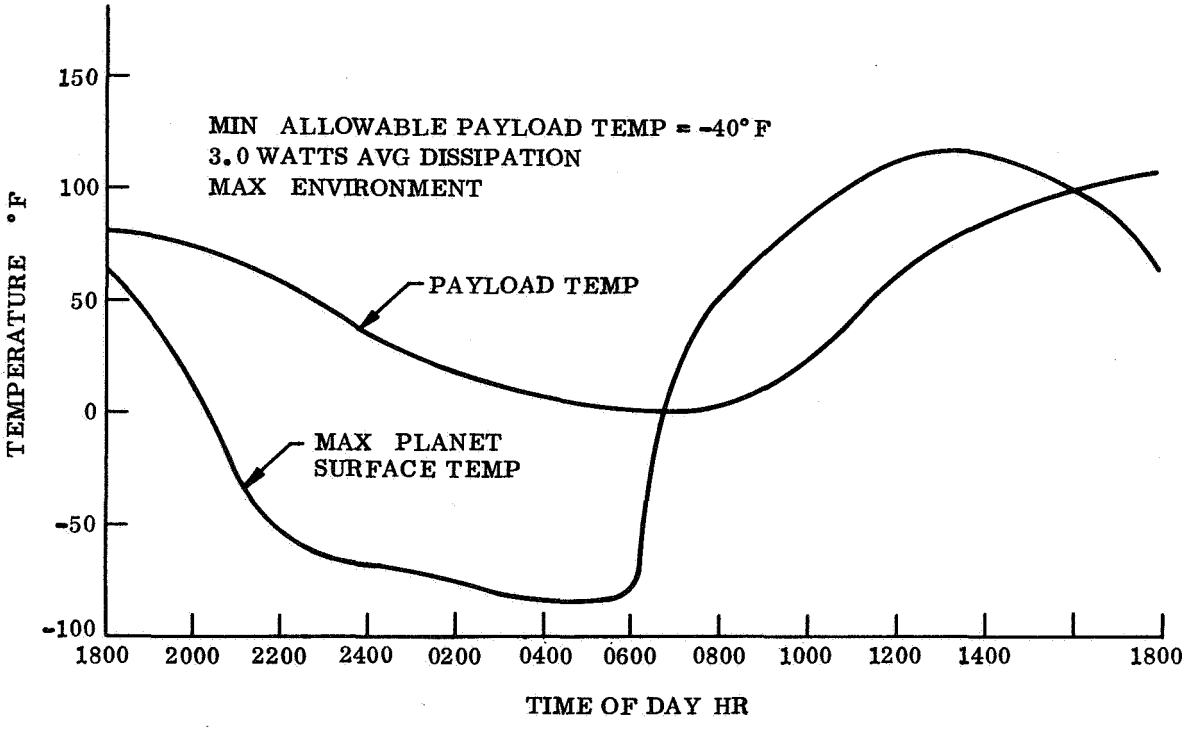


Figure 4.5.5-4. Payload Temperature Profile, Maximum Environment

4.5.6.1 Camera Installation, Deployment and Mechanism

The camera(s) and swinging boom(s) installation and associated mechanism is shown in detail in fig. 4.5.6-1.

Each of the four cameras is mounted on the free end of pivoted tubular booms. The booms are aluminum alloy material approx. 36.0 in. long and 2.0 in. outside diameter. They rotate through approximately 90^{o} in either direction, as shown, from the installed horizontal position so that when erected, two are side by side at opposite edges of the Lander, one with a high and one with a low resolution camera. This arrangement of relatively short swinging booms, with the capability to erect four cameras on either side of the Lander and take pictures over the edge of the Lander in segments shown in the insert on the drawing, was selected as the most satisfactory compromise between the need for simple and stable erection devices and mechanism and the requirement for adequate azimuth and verticle angles of uninterrupted vision. Deployment design with telescoping (not hinged) tubes, cannot easily be made to work in two directions, and investigations proved that unless the number of cameras was doubled, the telescopes had to be many feet in length, to provide adequate vertical angles of vision over the edge of Lander impact attenuation system. Deployment booms of such length pose serious problems regarding camera stability. Stowed, the cameras and booms lie horizontally across the Lander in a block of four. Saddles on the inside of the jettisonable doors covering the camera bay, clamp the booms securely to withstand the 'g' forces imposed, in particular during the landing phase. The booms are spring actuated to move through 90^{o} in either direction from the stowed position, by a single torsion spring around the hinge pivot, which is restrained in a neutral setting when the bay doors are assembled. Release and jettison of the camera bay door from the uppermost exposed side of the Lander, unclamps the boom(s) and releases one end of the torsion spring to pick up a lever on the boom and effect its rotation. Thus boom operation is automatic once the appropriate cover door has been jettisoned. All four booms are individually operated by the same spring loaded principle, the two lying deepest in the Lander from the exposed side are restrained to move until the two uppermost ones are deployed and are unlocked by the final motion of the upper booms. This is a simple and automatic sequencing for the four boom arrangement. The cover door(s) are secured with bolts incorporating a hot-wire release and jettisoned by springs with sufficient force to ensure that they fall clear of the Lander.

4.5.6.2 Wind Velocity and Temperature Transducers

Five wind velocity transducers constitute a set necessary to obtain wind measurement data. Four are mounted in a plane at 90^{o} to each other on a 2 ft pitch circle diameter, the fifth is mounted below one of the other four to provide a vertical reading. As stated in Section 4.5.2, the instruments are acoustic devices requiring unimpeded line of sight between each sensor. In the arrangement shown in fig. 4.5.6-1 the transducers are attached to the ends of spring-loaded arms, which are mounted on a telescoping extension of the camera booms and unfold when the boom triggers a release mechanism as it locks into the erected position.

The weight involved in the installation of a set of wind velocity transducers is very small and two sets have been provided on two camera booms for redundancy.

A temperature transducer is mounted directly on each of the four camera booms at the base of the camera.

4.5.6.3 Surface Composition (Alpha Back Scatter)

Although this instrument has not been completely designed, analysis has provided preliminary weight, volume, deployment and other requirements. The installation and deployment approach herein is based on a conceptual design which is illustrated in fig. 4.5.6-2. The Surveyor alpha back scatter instrument has been referred to and utilized to some extent.

The instrument sensor head is installed on its side in the bay provided in the Lander container. The heat will be firmly clamped against a pivot bar, in the stowed position, by a soil calibration sample holder extended across the bay and secured to the vertical side walls. When the calibration phase of the alpha back scatter instrument is completed the sample holder will be moved away from the instrument head either linearly along the bay or by rotation. The function will be performed by a pin pulling device and spring-loaded mechanism. The instrument head is now free to rotate through 90° due to its offset c.g. and the force-of-gravity and drop through the bottom side of the Lander attached by the control cord and wire bundle provided.

Low friction guides will be installed on either side of the instrument head from the bay sidewalls to ensure that the head rotates and exits from the Lander with a smooth controlled motion.

Assuming that the head is prevented from being lowered completely clear of the Lander, it can operate equally well within the bay provided the surface is in good contact with the ground.

Covers over the bay provided in the Lander have been studied, but jettisonable or sliding doors are not desirable because of possible interference with the instrument head or jamming in the event of landing damage. Consequently, two inward opening hinged doors will be provided on either side of the Lander.

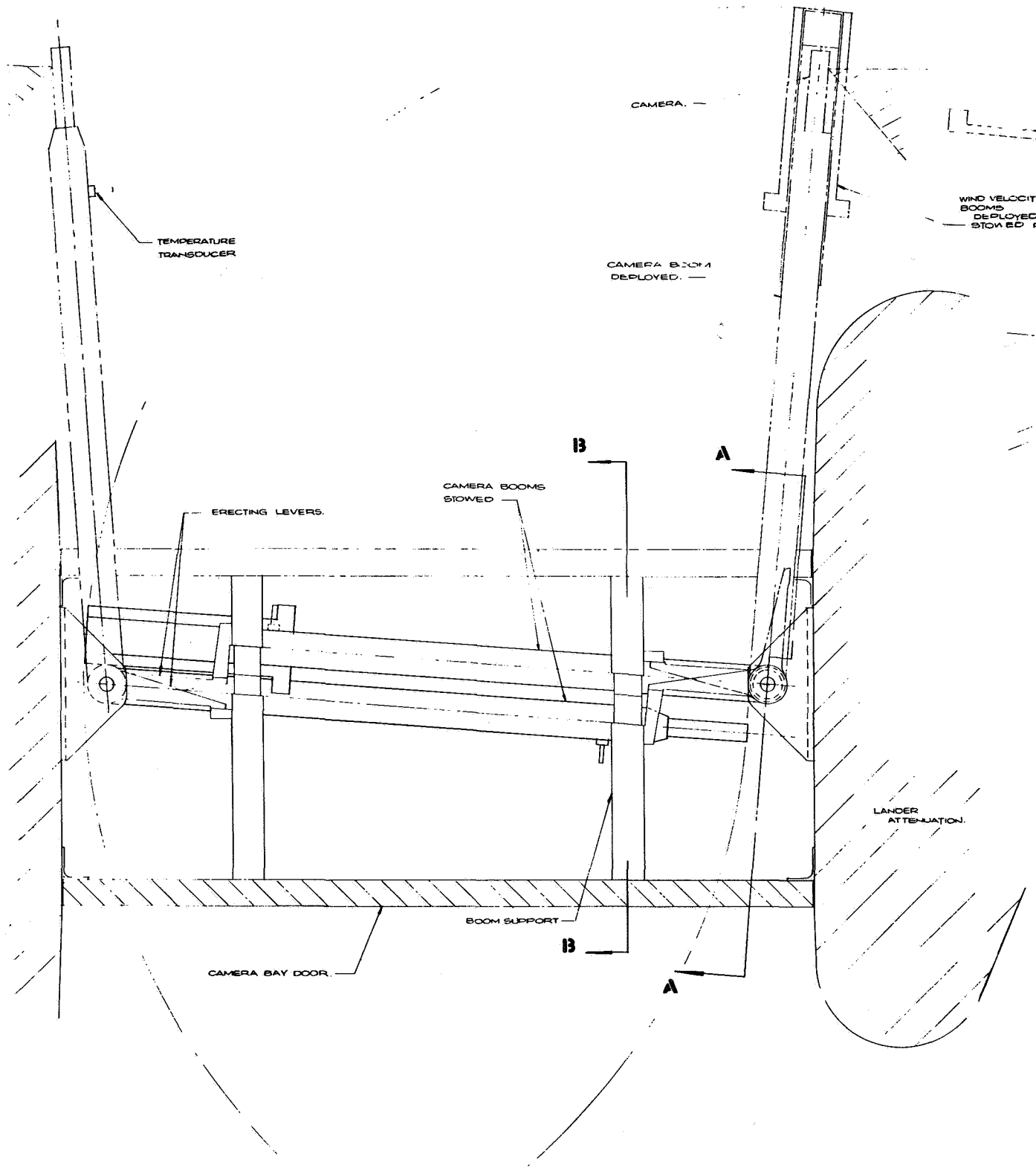
4.5.7 LANDER CONTAINER STRUCTURE

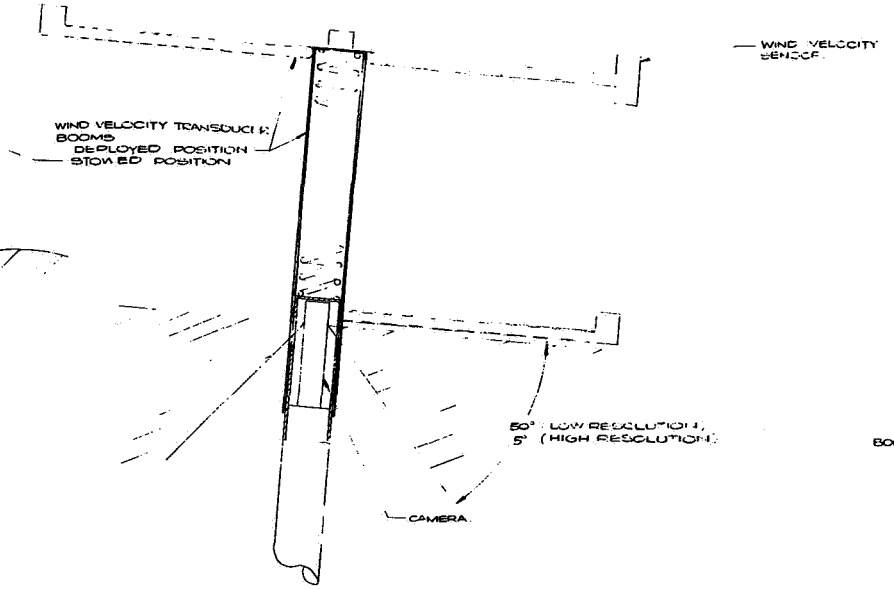
The flatpack configuration for the landed payload container illustrated in fig. 4.5.7-1, was selected on the basis that it offers a good compromise between structural efficiency and all other design constraints, notably packaging and deployment of experiments. The following requirements and criteria were imposed for the design of this structure:

1. Design weight - 900 lb. This is used for structural design purpose and is based on total Lander weight less the material which is crushed during primary impact.

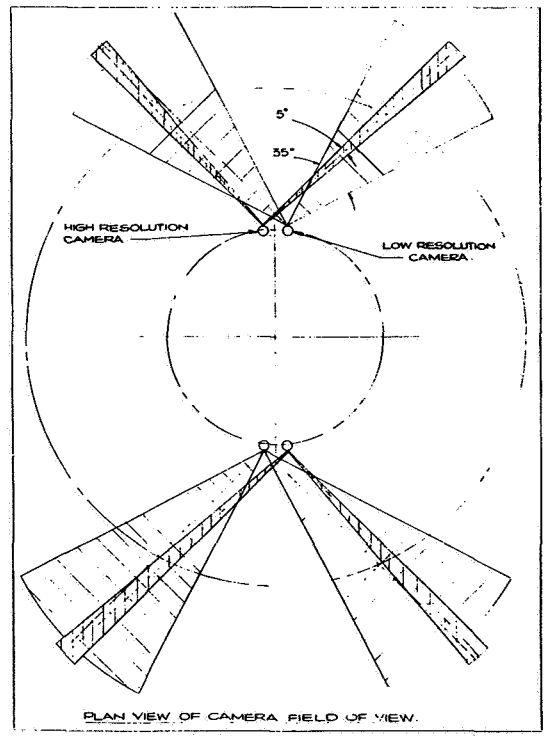
2. Local pressures and inertia loads resulting from impact up to 1000 g's.

FOLDOUT FRAME



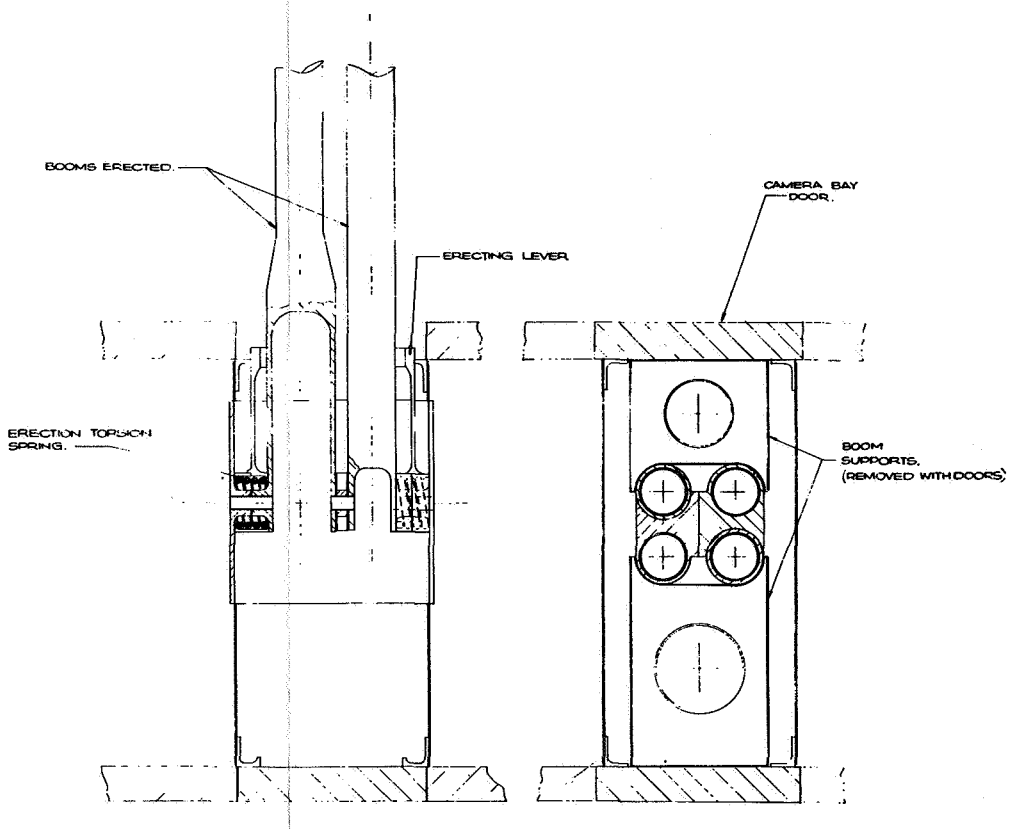


VIEW SHOWING WIND VELOCITY TRANSDUCER'S DEPLOYMENT SYSTEM.



PLAN VIEW OF CAMERA FIELD OF VIEW.

FOLDOUT FRAME



SECTION A-A

SECTION B-B

Figure 4.5.6-1. Camera Deployment, Includes Wind Velocity and Temperature Transducers

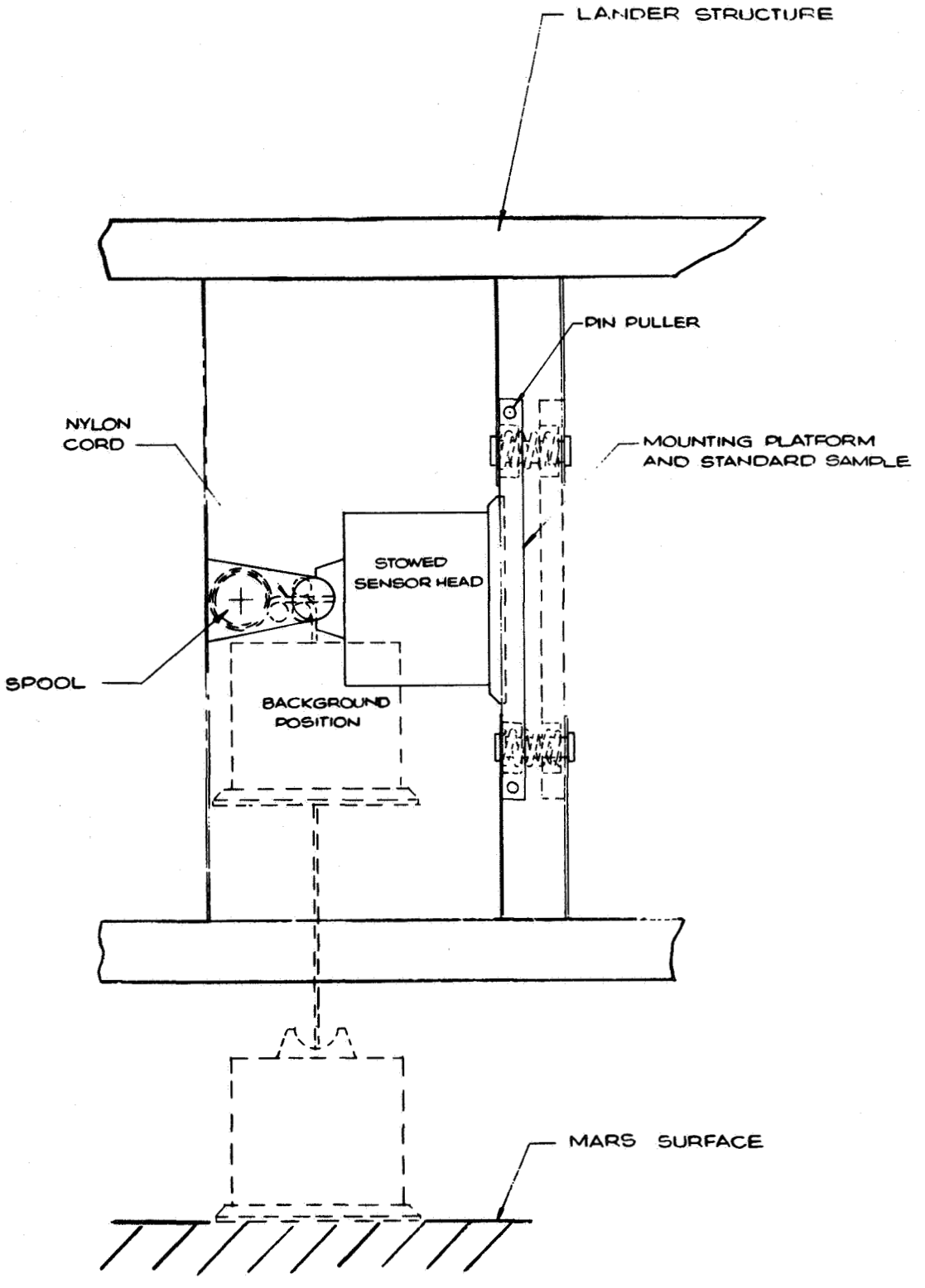


Figure 4.5.6-2. Operation of Alpha Back Scatter Deployment Mechanism

3. Limit design factor - 1.0

4. Ultimate design factor - 1.25.

Based on the requirements and constraints which are present, a design has been evolved which has the following significant features:

1. A full-depth inner space frame module containing most instrumentation and subsystems. This module can be removed from or inserted into the flatpack as a bench subassembly.

2. Individual components can be added or removed from the top or bottom of the space frame while installed in the container.

3. Dual purpose space frame which acts as primary structure and component support.

4. Jettisonable and hinged doors for deployment of camera and alpha back scatter instrument respectively.

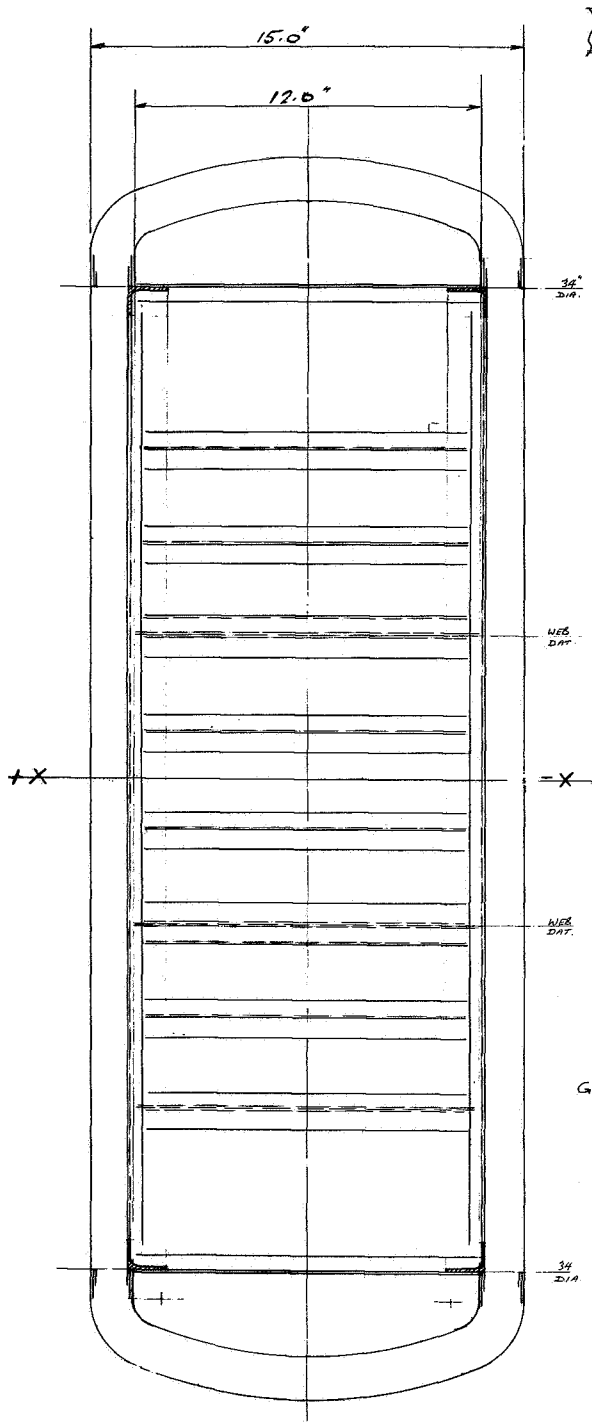
5. Primary structure consisting of a D-shaped toroid section supporting the impact attenuator, combined with the inner space frame.

The container consists of three basic elements: the D-shaped toroidal edge structure, the inner space frame, and the top and bottom covers and doors. (See fig. 4.5.7-1.) This complete assembly is designed to withstand the forces generated by initial impact at 1000 g's and any forces resulting from subsequent impact after rebound.

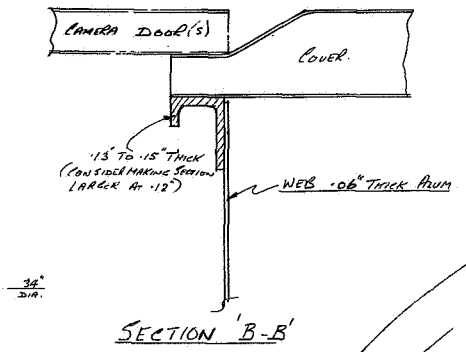
The D-shaped edge structure acts as a primary load path for distribution of impact attenuator loads. The outer shell of this section is tied to the cylindrical wall with radial aluminum sheet nose ribs, stiffened and spaced approximately every 5 in. around the circumference. These radial members transfer some of the loading to the internal cylindrical web and allow the section to act as a heavy ring frame, transferring load into the upper and lower cylindrical edge rings. Local loading up to 925 psi imposed by the crushing honeycomb is resisted by the outer shell of the D-shaped section which is a 1-1/2 in. thick fiberglass honeycomb (3/16 in. cells) core with 0.08 in. aluminum face sheets. The cylindrical section is an 0.08 in. lightened and stiffened cylindrical shell. Except for items such as cable harnesses, it is not proposed to utilize the edge structure for packaging, and therefore some structural deformation is tolerable.

The full depth cross members of the inner space frame stiffen the container against deformation from the cylindrical shape and resist bending of the flatpack, as well as providing component support. Two main cross members form the camera bay. These beams have 0.06 in. aluminum alloy webs, extruded alloy channel beams, and section vertical stiffeners. There are five secondary cross beams at right angles to the main beams. These are of similar but lighter construction in aluminum alloy.

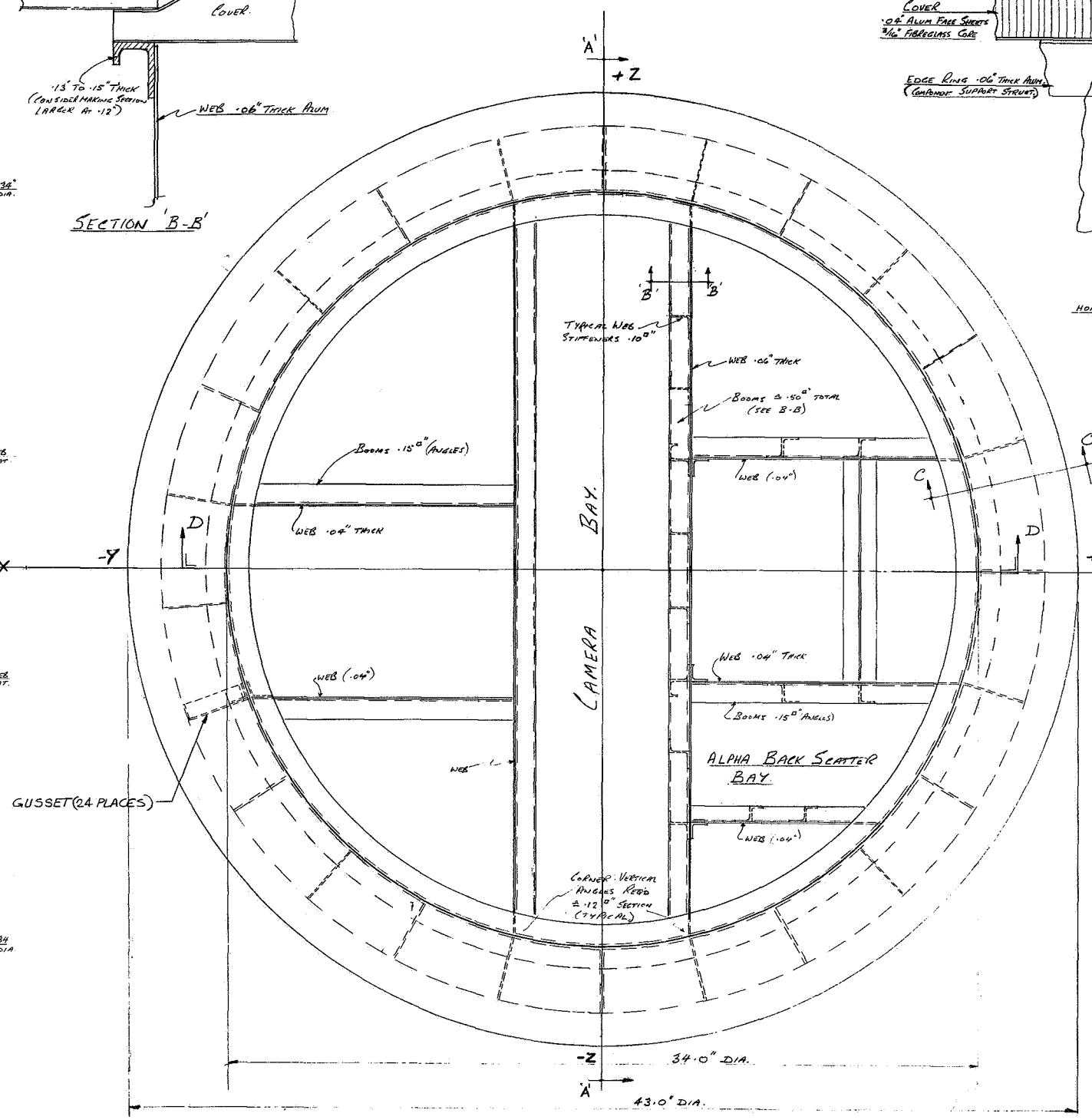
FOLDOUT FRAME



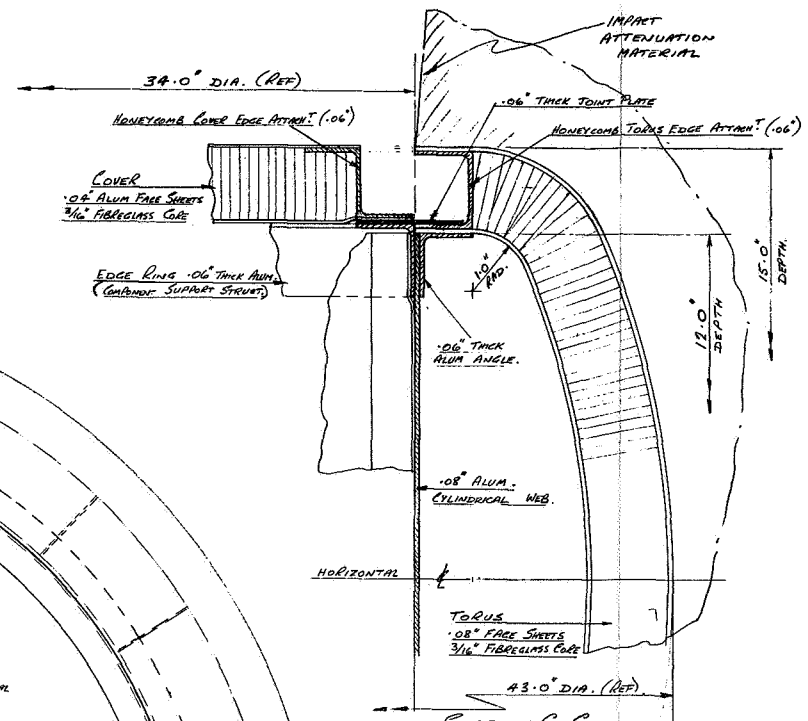
SECTION A-A



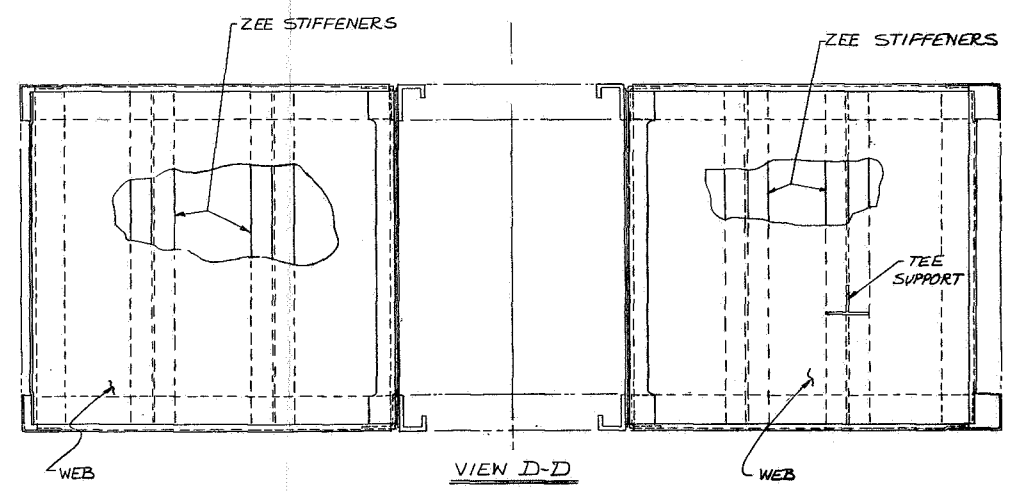
SECTION B-B



PLAN VIEW (COVERS REMOVED FOR CLARITY)



SECTION C-C
TYPICAL SECTION THRU TOP EDGE OF CONTAINER.
(BTM EDGE IDENTICAL)



VIEW D-D

Figure 4.5.7-1. Structure Assembly

Top and bottom angle rings, 0.06 in. thick, and vertical angles at the junctions of the main and secondary beams and at the free ends of these beams complete the assembly. The inner space frame is attached to the D-section through the vertical flanges of top and bottom angles.

The top and bottom covers are considered secondary structure. They are 1.35 in. thick fiberglass honeycomb panels with 0.04 in. aluminum face sheets. A Z edge section is inserted for attachment. The edge members of the D-section, the inner space frame, and covers, when bolted together form strong rings at the top and bottom surface of the container.

Thick honeycomb panels with fiberglass core have been selected for the construction of the outer shell of the container as a means of satisfying both structural and thermal requirements. A possible alternative for the container outer shell generally could be reduced depth honeycomb panels with foam on the inner side. Additional investigation will consider fiberglass facing sheets for all honeycomb panels used as a strength-to-weight trade-offs. Surfaces of the full depth cross beams, which are exposed when the camera and alpha back scatter bay doors are jettisoned, are thermally insulated with a layer of foam to the full depth of the beam vertical stiffeners. The foam is covered with plastic coating to maintain integrity on landing impact.

A preliminary analysis, for critical loading points for four conditions shown in fig. 4.5.7-2, has been made and used to formulate the estimated weight of the container. Typical torus cylinder interface loads, for the edge impact condition illustrated, are shown in figs. 4.5.7-3, -4, and -5.

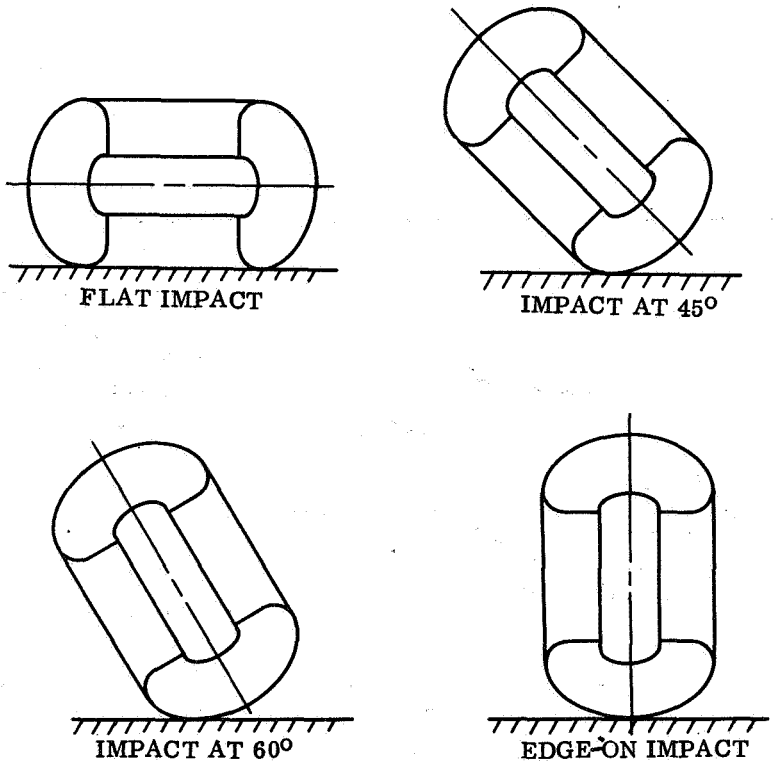


Figure 4.5.7-2. Four Conditions Used for Preliminary Loading Analysis

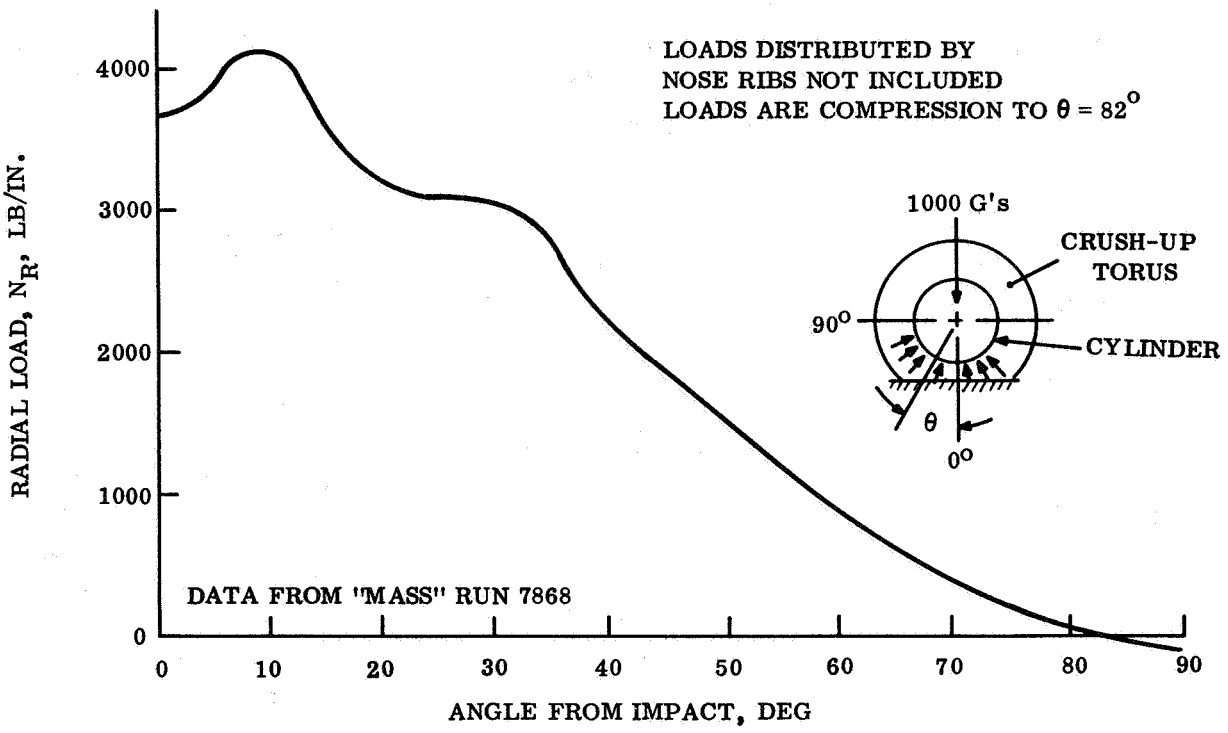


Figure 4.5.7-3. Typical Interaction Radial Loads Between Torus and Cylinder, Edge-on Condition

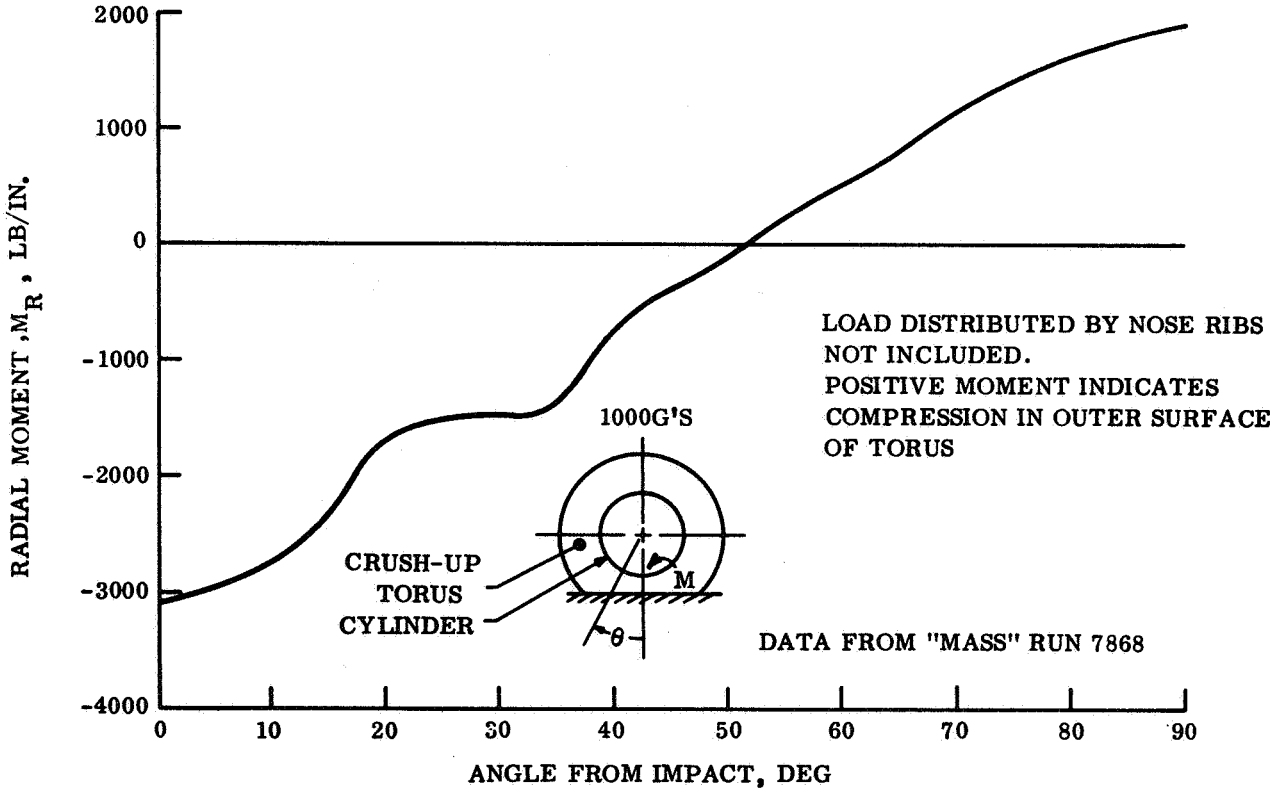


Figure 4.5.7-4. Typical Interaction Moment Between Torus and Cylinder, Edge-on Condition

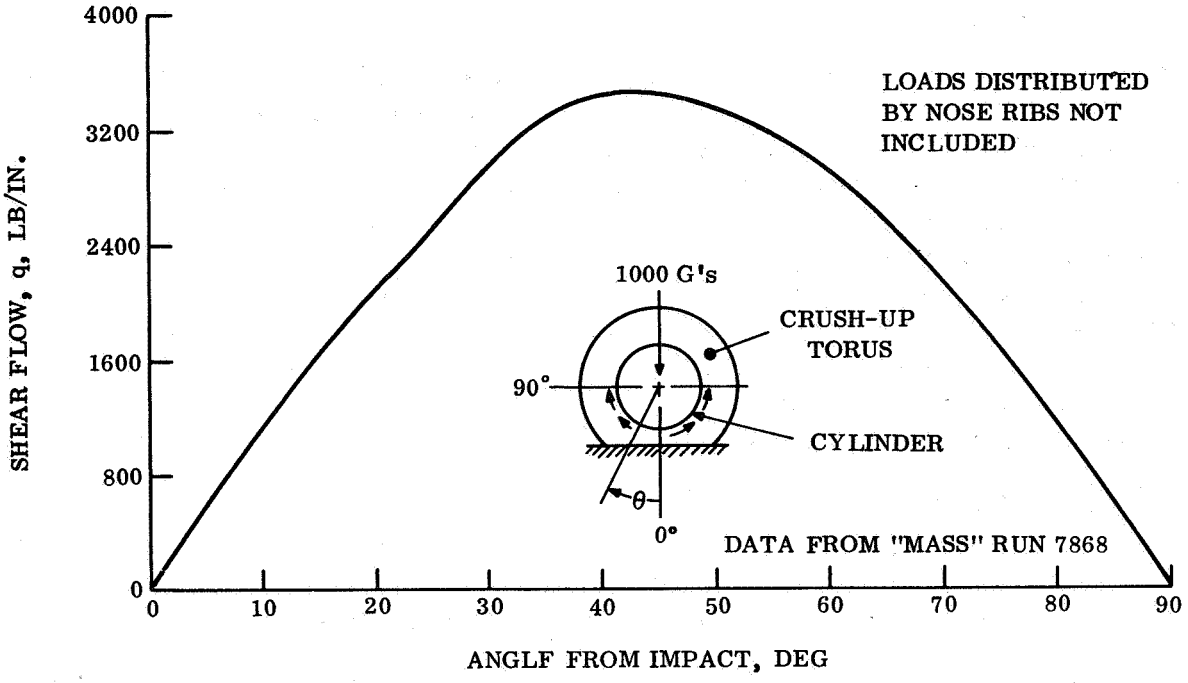


Figure 4.5.7-5. Typical Interaction Shear Flow Between Torus and Cylinder, Edge-on Condition

4.5.8 IMPACT ATTENUATION AND STRUCTURE

4.5.8.1 Attenuation Requirements and Criteria

4.5.8.1.1 Gross Vehicle Response

The mechanical crush-up impact attenuation system is designed to provide sufficient stopping distance to decelerate the Lander within the allowable g-limits while dissipating the impact kinetic energy. At the same time the acceleration pulse must have a sufficient rise time and be essentially broad and flat. The honeycomb phenolic fiberglass material inherently behaves in a manner which produces this behavior.

4.5.8.1.2 Response of Individual Components

Initial studies have been performed to determine the feasibility of further attenuating the impact acceleration levels experienced by individual components carried by the Lander. These are reported in Volume IV, Appendix A. The conclusions drawn from this appendix indicate that it does not appear feasible to obtain significant reductions with shock mounts or by component mounting stiffness tailoring. These devices are of primary use in minimizing g-level amplification effects.

4.5.8.1.3 Angular Accelerations: Their Effect on Components

It appeared that if the Lander impacts on one edge, there was the possibility that high angular accelerations might produce high loading on components located at the outer extremity of the container. This situation is studied in Appendix IV-A. The conclusion reached is that such high angular acceleration g's will not occur.

4.5.8.1.4 Selection of Phenolic Honeycomb as the Reference Material for Impact Attenuator Design

Phenolic honeycomb was selected as the reference material for this study for the following reasons. Both balsa wood and phenolic honeycomb are feasible materials for the size and weight vehicles being examined herein. Both materials can function at the operating g-levels anticipated, with a Hard Lander system. However, the balsa wood can be adversely affected by exposure to the sterilization cycle. In past tests, balsa wood has split after being subjected to dry heat sterilization. Careful control of the wood moisture content can, however, probably eliminate this problem. Balsa wood has the added disadvantage that its material properties have been known to vary from ± 15 to ± 50 percent. This is significant since balsa, being a natural material, cannot be further developed to a significant extent. Phenolic honeycomb, on the other hand, has been improved in the past and this trend can be expected to continue.

4.5.8.2 Environmental Definition and Interpretation

Appendix IV-B contains the detailed account of the specification used in the point design. Included are discussions of surface strength, friction, slopes and rocks. The wind specification for the point designs is also elaborated upon.

In brief, the point design is capable of impacting an infinitely hard surface with friction, 5 in. rocks and slopes up to and including 34^{o} from the horizontal. The prevailing wind, blowing against the surface slope is the extreme value of 220 fps. Should the surface strength be less than attenuator stress, some penetration will be experienced but this is estimated as a few inches by the analysis in Appendix IV-B.

The important effect of a parachute sway angle (of up to 40^{o} from the local vertical) was also examined. The chief result is that the sway angle couples with the surface slopes to require higher angles of the Lander to be analyzed for the initial impact condition. The significance is that an increment in honeycomb attenuator thickness over that thickness necessitated by a non-swaying vehicle must be incorporated on the Lander sides to allow for the swaying effect on vehicle orientation at touchdown. Details are given in Appendix IV-B.

4.5.8.2.1 Secondary Impacts of the Lander Vehicle

The combined environmental conditions of extreme wind, parachute sway and varying surface slopes warranted an investigation of post impact vehicle motion. In particular, the probability and significance of secondary impacts was reviewed. Appendix IV-B contains the dynamic analysis for the secondary impact problem as well as an initial probability estimate of the likelihood of occurrence of this event.

The statistical analyses were performed for the purpose of ascertaining the probability of experiencing a secondary impact velocity less than or equal to a chosen value. In particular, the value of 100 fps was investigated because this was the velocity used to size the top side of the multi-directional Lander. Based upon the limited first order approximation used, the following trends are indicated. For the extreme wind velocity of 220 fps the Lander flips over about 92 percent of the time and hits the second time on its top side.

In light of the new Mars Mission Specification (1968) of a design wind velocity of 110 fps, another probability estimate may be made. For this wind velocity, (but the same slope and sway angle variations) the Lander will flip over only about 25 percent

of the time. Given that the Lander does flip, the secondary velocity will be 100 fps or less 81 percent of the time. If the analysis were adjusted to account for the new definition of surface slope of 20^{o} (as contained in the Mars Mission Specification - 1968) this 81 percent figure would improve considerably. The foregoing brief summary identifies the surface wind specification as a critical design parameter.

4.5.8.3 Effect on Point Design Due to Perturbation in the Design Parameters

Appendix IV-C delineates the effects on the impact attenuation system design due to variations in the reference condition. Those parameters in which perturbations are especially significant are also identified.

In general, lower wind and descent velocities, flatter slopes, softer surfaces, smaller rocks, lessened parachute sway, higher component g-tolerance and lower Lander weights than the corresponding design value enhance the point design integrity. Increases in velocities, slopes and parachute sway angle tend to compromise the design integrity. Higher Lander weights than in the design condition, lower component g-tolerance tend to compromise the adequacy of the design.

Small increments in effective rock size are deleterious but, after a point, the rock becomes a large outcrop and is more of a hard surface than a penetrating hazard. It is noted that since the design is based on an infinitely hard surface no problem arises with an increase in surface hardness above that used in design computations.

Appendix IV-C also encompasses variations in honeycomb material properties. Specific comments identify the effects of variations in crushing density, specific energy, stroke efficiency, effective geometry and crush-up behavior.

4.5.8.4 Impact Attenuation Design Approach

The attenuation system design approach for Point Designs 2A and 2B is now described. It should be noted that the approach described in detail is pertinent to the omni-directional impact attenuator of Point Design 2A. This Lander is drawn as fig. 4.5.8-1. The general line of argument is similar for design 2B which is multi-directional. However, some of the individual design constants are different. To avoid repetition the multi-directional design approach will not be elaborated upon in this section. Section 5.5.8 may be consulted for complete details of a typical multi-directional impact attenuation system design procedure. The configuration of Point Design 2B is presented as fig. 4.5.8-2.

In the design, the attenuation material is phenolic fiberglass honeycomb (3/16 in. cell size) of the type developed by GE-MSD under contract to the JPL. This material is of the hexagonal cell variety with parallel cells which can be wrapped with (R/t) radius to thickness ratios of greater than five. It is the reference material selected for use in this study and is currently used in the JPL drop testing program. This material is readily available from Honeycomb Products Inc. in densities of 4 to 12 pcf. The particular density used in the point design will be determined by the

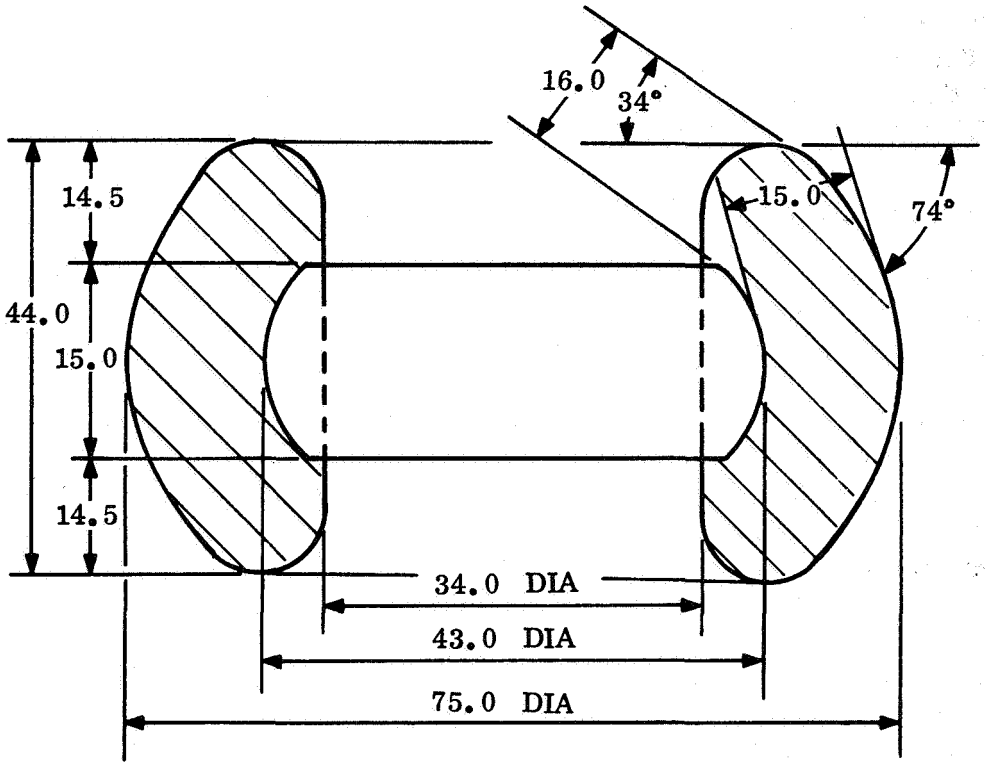


Figure 4.5.8-1. Lander Attenuation, Point Design 2A

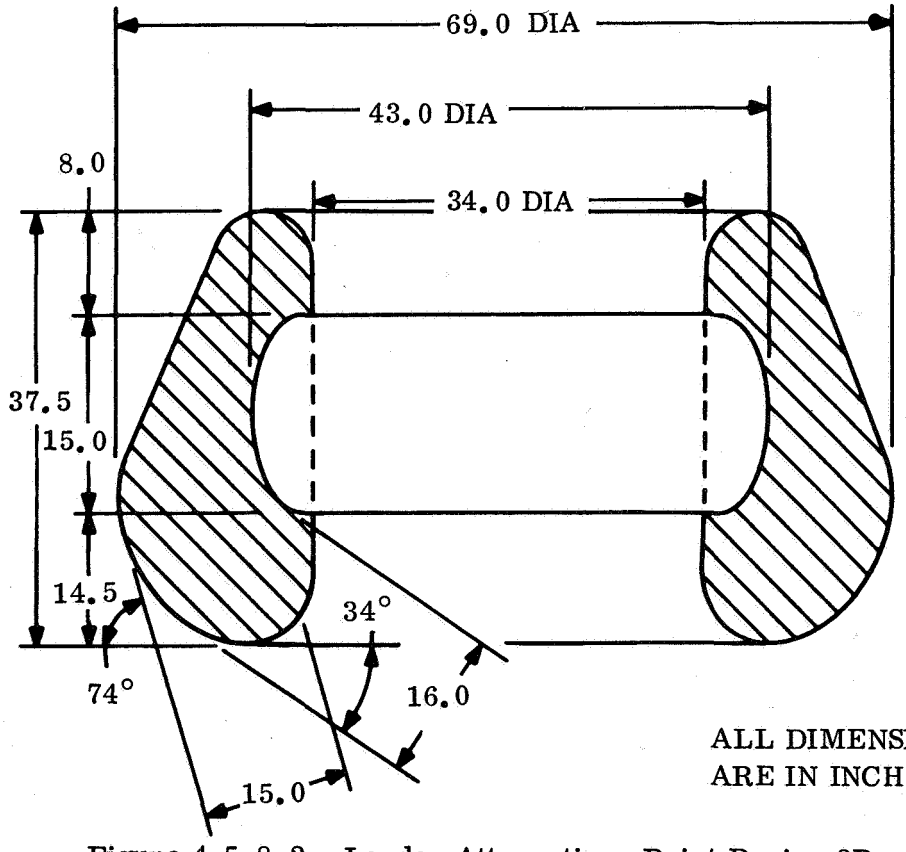


Figure 4.5.8-2. Lander Attenuation, Point Design 2B

design conditions, especially Lander weight and allowable rigid body g-level. The performance of this thin dipped phenolic material varies depending upon its axial orientation with respect to the impact load vector. This is a key design factor investigated in the point design computation. The requirements of omni-directionality results in analyses of the Lander for various cutting plane orientations ranging from forward-flat-on to aft-end-first. Requirements of omni-directionality lead to increased weight over multi-directional Landers since material which is fully effective in one touchdown orientation may be of less or no value when other orientations are examined. Past analyses and judicious application of the specifications have indicated that three critical crush-up conditions must be analyzed. There are 0^{o} (forward) impact, 90^{o} (side-on) impact, and an intermediate surface slope impact. The intermediate slope has been taken as 34^{o} for point design purposes. It is apparent that to adequately handle all of the highly probable impact conditions special attention must be directed toward the crush-up layup because of the material's variable effectiveness. For point designs this honeycomb layup is produced by cutting and segmenting the attenuator material to produce near-radial cell axis orientations with respect to the internal toroidal container structure. At the same time this segmented approach allows more efficient wrapping of the container. Refer to the para 4.5.8.5 for details.

The same varying effectivity is also complicated by a geometric effect produced by the curvature of the Lander as seen in plan. The net result is that the area-stroke characteristics are direction dependent in a complex relationship (refer to fig. 4.5.8-3). This means that the force stroke history is direction dependent and that, depending on the direction of impact the stroke (and thus the thickness required) will be different.

An additional geometric effect, distinct from that of crush-up directionality also enters the analysis. This is, for a given direction of impact a variable amount of honeycomb material is actively being crushed. Some material may be oriented in such a way that it experiences shearing forces. Because of this localized condition bond line shear failures can result with little or no crush-up action. Such failures could occur without providing sufficient stroke capability. For this effect detailed design must ensure that sufficient material is working in each specific direction. Finally, attention must be directed toward the location of crush-up propagation. It is desired that the fracturing progress from the outside in and not from the payload to the extremity of the attenuator. Design details of the contained/honeycomb interface and slight precrushing of the attenuator can eliminate this problem.

4.5.8.4.1 Analytical Details

With the above background, point design analysis takes the following form. A series of CRUSH (geometrical program) runs were made for each prototype point design. The results were of the form of gross crushed cross-sectional area against stroke for various angles encompassing the operational map as defined in the specification. The geometric results were used to perform a direct graphical analysis of several prototype shapes. The conclusions drawn from this thorough study provide the underlying philosophy for a computer-assisted procedure to size the attenuator for point design purposes.

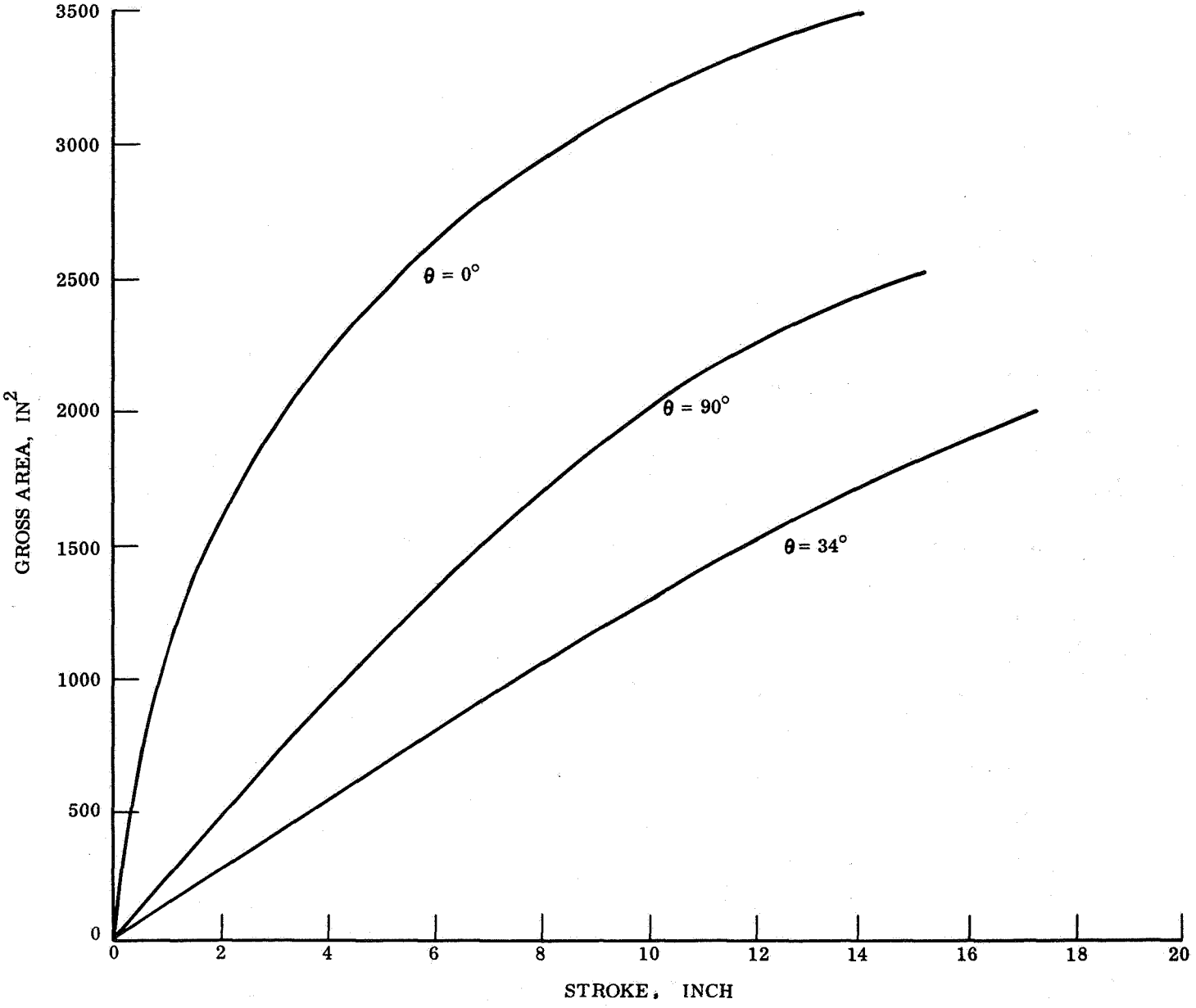


Figure 4.5.8-3. Gross Cross-sectional Area vs Stroke

In fig. 4.5.8-3, plots of crushed area against stroke for a nominal size deep ring omni-directional Lander are produced. It is emphasized that this figure is for gross area with no directionality effects included. In fig. 4.5.8-4, plots of effective sectional area are provided. These latter plots were generated in the following manner. The phenolic material loses 2 percent of its strength per degree of obliquity between the longitudinal cell axis and the normal to the crushing plane.

The design guide for this reduction is fig. 4.5.8-5. This design guide is based upon test results summarized in fig. 4.5.8-6.

The data to support this procedure are reported in ref. 4-1. In addition, a 20 percent reduction is incorporated to account for the effect of curvature (in plan). The analysis also assumes that the active area encompasses all cells lying within 30^{o} of the normal to the impacting plane examined and that all others are not actively crushed.

After examining various cutting planes for the Lander prototypes it was found that for the omni-directional Lander three principal strokes need be computed: dead on, side-on, and 45^{o} angular cutting plane. Actually, for sizing purposes there is small difference by passing the cutting plane at 34^{o} or 45^{o}. This is shown in fig. 4.5.8-3. From data in fig. 4.5.8-5 the principal strokes can now be computed by equating Lander normal kinetic energy to the absorbed energy due to crushing. For the prime (0^{o} impact) case,

$$\text{energy absorbed} = \frac{1}{2}\,WGS + \frac{1}{4}\,WG\,\frac{S}{2} + \frac{1}{2}\,\frac{3}{4}\,S\,\frac{WG}{2}$$

$$\frac{1}{2}\,\frac{W}{g}\,\left(V_N\right)^2 = \frac{13}{16}\,WGS$$

$$S_{(0^{o})} = 0.62\,\frac{\left(V_N\right)^2}{gG}$$

where V_N is the impact velocity component normal to the plane, g is the gravitational constant and G is the allowable deceleration level in g-units. As described in Appendix IV-B, it is assumed that the velocity component parallel to the plane is absorbed by surface sliding. This is why the normal velocity component is used in the stroke sizing computations. For 45^{o} and 90^{o} side-on cases the same procedure yields

$$\frac{1}{2}\,\frac{W}{g}\,\left(V_N\right)^2 = WGS\,\left(\frac{1}{3} + \frac{1}{2}\times\frac{2}{3}\right)$$

$$S = \frac{0.75\left(V_N\right)^2}{gG} \approx \frac{0.7\left(V_N\right)^2}{gG}$$

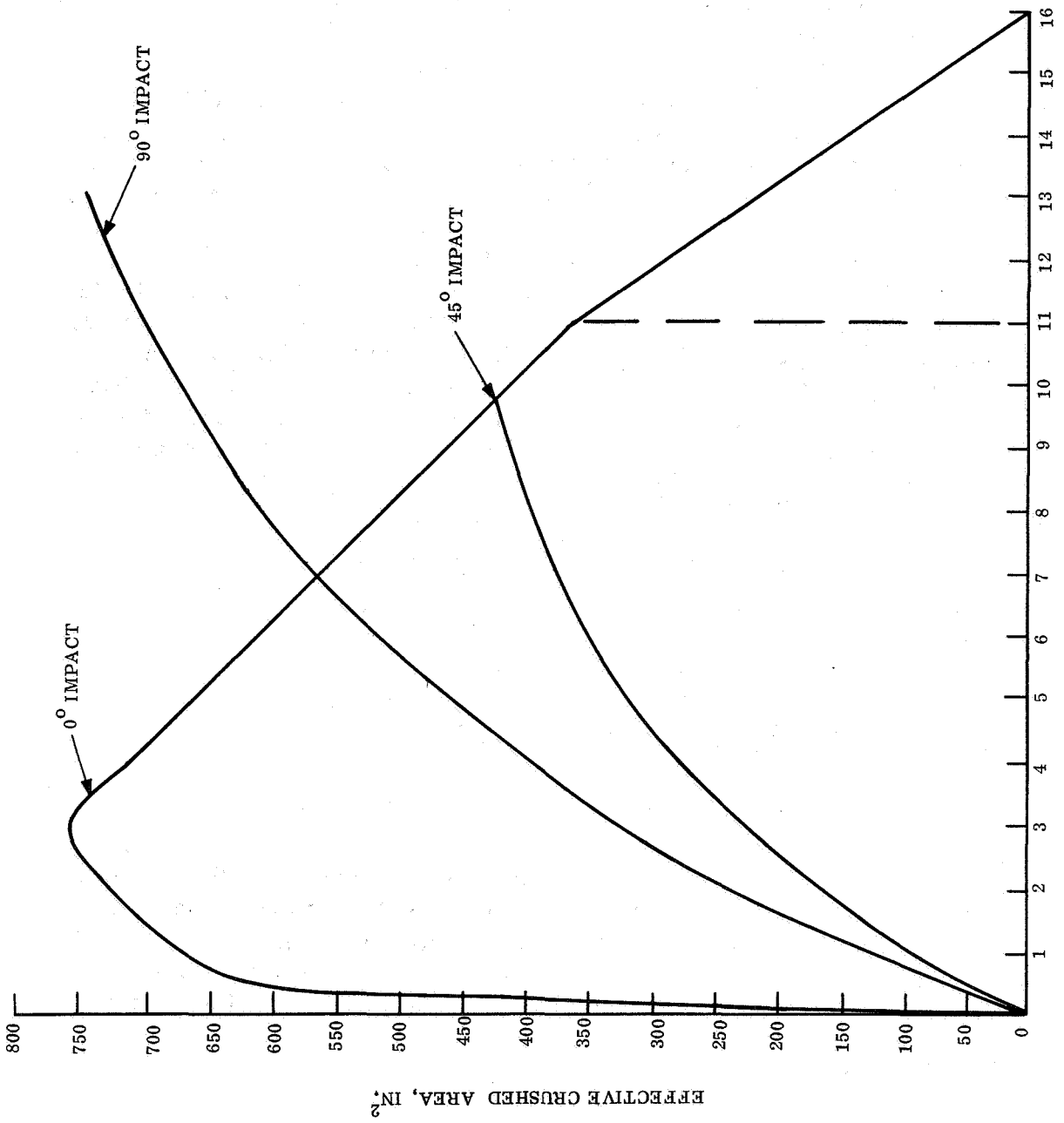


Figure 4.5.8-4. Effective Cross-sectional Area vs Stroke

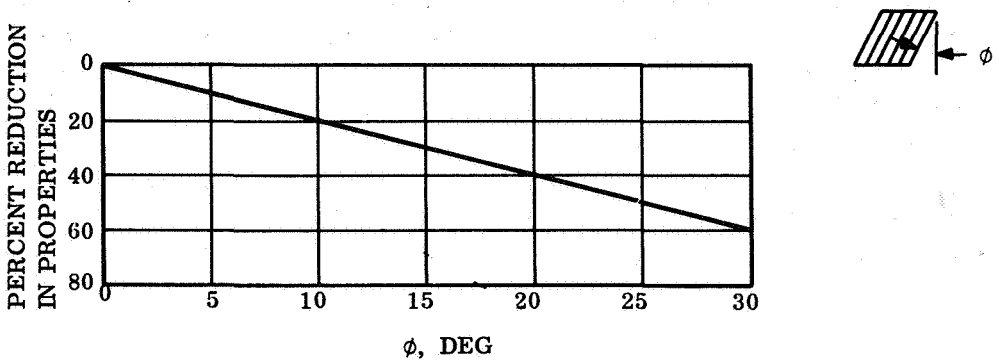


Figure 4.5.8-5. Design Guide for Reduction in Honeycomb Properties for Non-axial Impacts

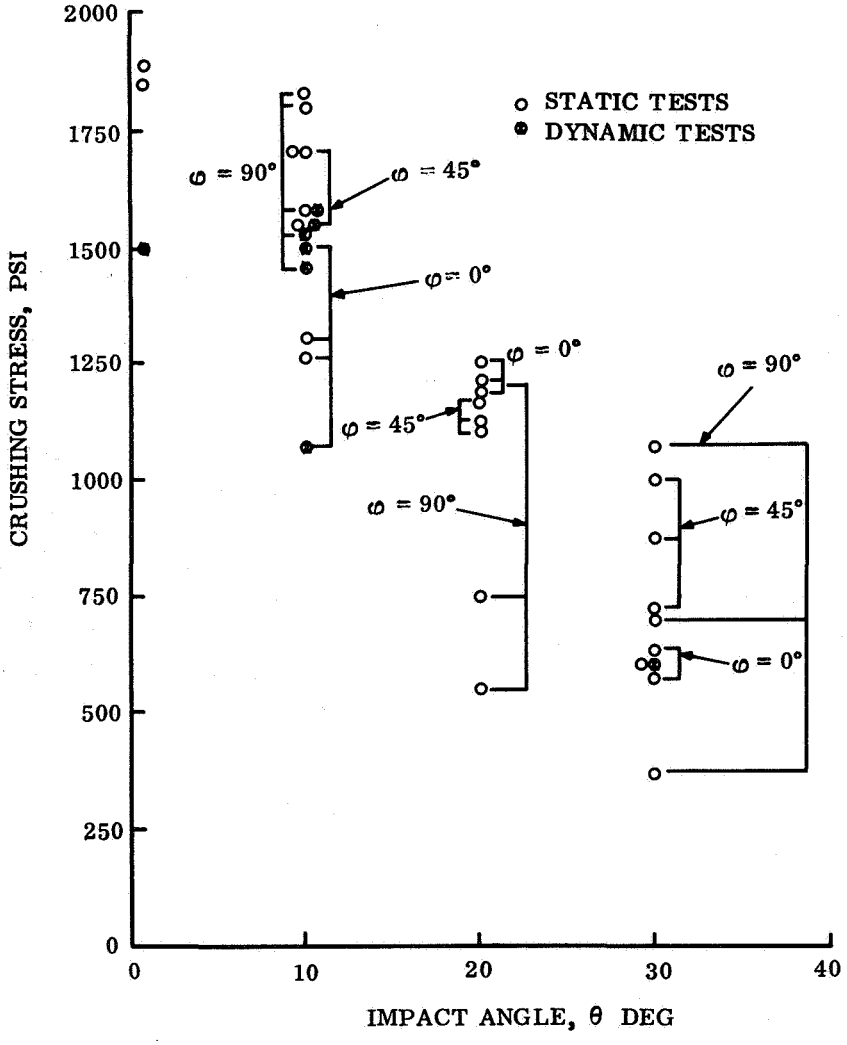


Figure 4.5.8-6. Comparison of Crushing Stress vs Angle of Impact for Static and Dynamic Loading

for design purposes. With the three principal strokes known one has the principal contributing factors to the attenuator thickness computation. Provision must still be made for stroke efficiency, a factor of safety, and rock protection dimensions. These are handled as follows. Ref. 4-1 contains data on honeycomb stroke efficiency. For the point design this efficiency is about 0.8 (see fig. 4.5.8-7 for data). Stroke efficiency is defined as that fraction of total honeycomb thickness which will actually crush up when impacted. This effect occurs because some of the total thickness provided is lost as accumulated crushed material builds up (see fig. 4.5.8-8). Therefore, corresponding to the three stroke values (S_i for $i = 0^o, 45^o, 90^o$) just derived one must provide associated thicknesses (t_i) of

$$t_i = \frac{S_i}{0.8}$$

However, due to the possibility of rock or other outcroppings these thicknesses must be compared to $S_i + 5$ in. and the larger value used in design. Therefore the design thickness is the greater of the following two expressions. (ref. Appendix IV-B.)

$$t_i = \frac{S_i}{0.8}$$

$$t_i = S_i + 5$$

With the three thicknesses known, the attenuation system may be sized and the volume of crush-up material computed. For omni-directional designs this was accomplished by fitting a smooth curve through the three key points and using the symmetry of the Lander body to completely define the attenuator.

Another design quantity is the material density to be used to limit the g-loading to the desired values. This density for the 3/16 phenolic honeycomb is related to the specific energy and crushing stress as shown in fig. 4.5.8-9. For minimum attenuator weight a density greater than 11.85 pcf should not be used since the maximum specific energy and crushing stress occur at this value. This establishes an upper limit on the useful density. A lower bound on the density is determined from previously reported experimentation in ref. 4-1. It is shown that honeycomb densities below 4 pcf are erratic in behavior and this density is consequently a lower bound on the feasible materials for design use.

The density selection for use in point designs is made by selection of a crushing stress according to the formula

$$\sigma_{cr} = \frac{W\,G}{A}$$

where W is Lander weight, G is allowable deceleration level, and A is the cross-sectional area corresponding to the progression of the stroke to that point at which the peak g-loading is experienced. The area (A) is determined via a computer code and

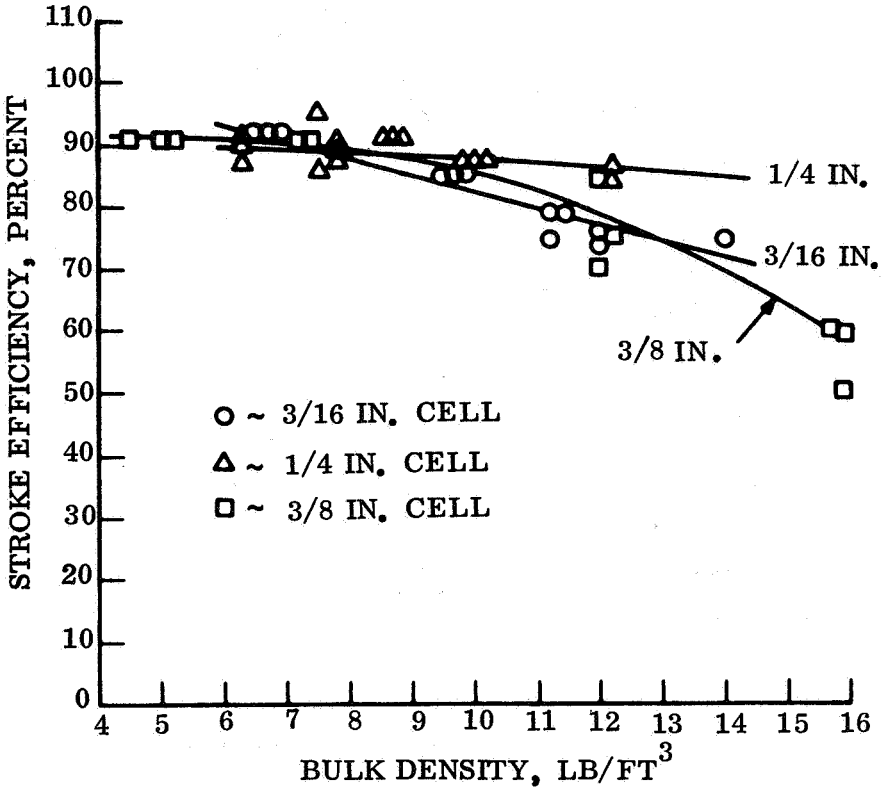


Figure 4.5.8-7. Stroke Efficiency vs Bulk Density

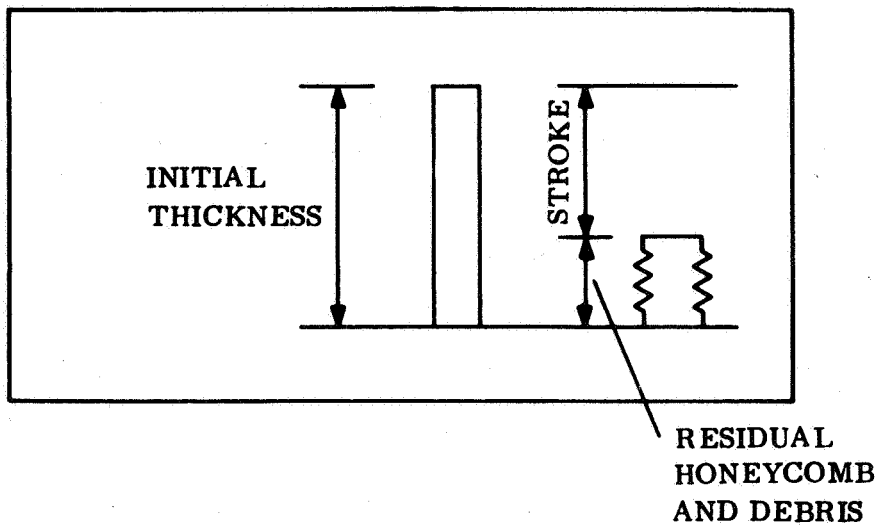


Figure 4.5.8-8. Residual Honeycomb and Debris

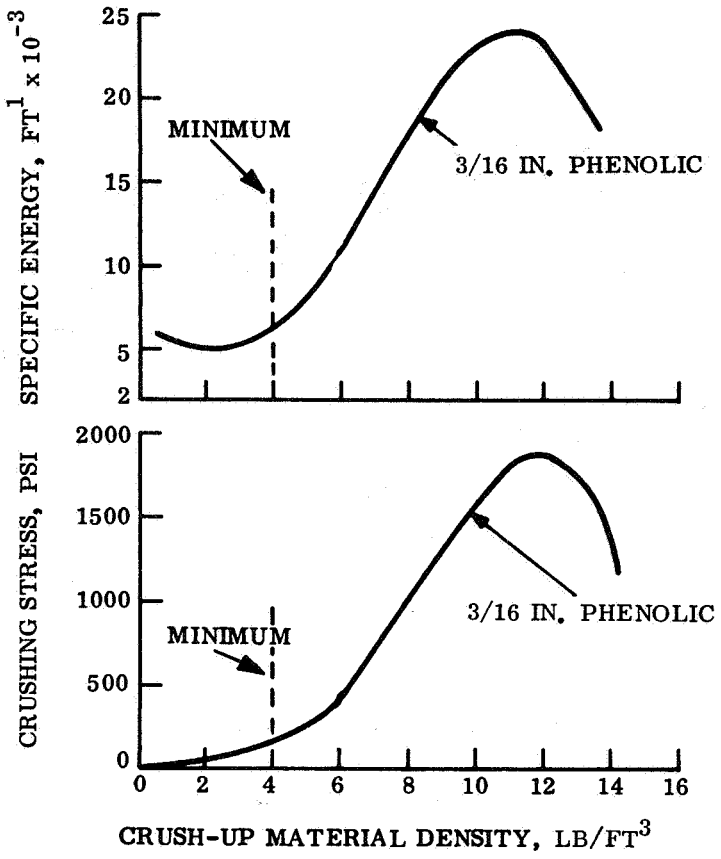


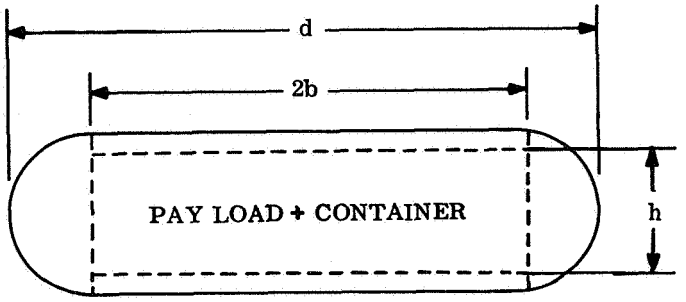
Figure 4.5.8-9. Crushable Honeycomb Properties

used to find the corresponding crushing stress. With this crushing stress the appropriate density from the relation in fig. 4.5.8-9 is read off and used in the attenuator design.

Options in the two different computer design codes were constructed based on this information. The codes allow one to input the point design conditions of touchdown velocity, size, landed subsystem weight g-tolerance and surface rock specification in order to obtain attenuation sizing, volume and weight, crushing stress and material density for a given point design. The computer calculated volume and weight are then verified by planimeter computations using the exact cross-sectional areas. The geometry used in the program is shown in fig. 4.5.8-10. The input geometry includes interior and exterior diameter and inside container height. A program option yields complete sizing dimensions of the Lander as well as geometric checks for compatibility with aeroshells of different cone angles for initial installation feasibility computations.

4.5.8.4.2 Particulars for Impact Attenuation System, Point Design 2A

When the foregoing criteria were applied to Point Design 2A the impact attenuation system was defined as 522 lb of 3/16 in. cell size phenolic fiberglass honeycomb. The honeycomb volume was 66 ft^3; the density was 7.9 pcf. The other conditions were:



2b - CONTAINER FLAT PACK DIAMETER = 34.0 IN.

h - INTERNAL CONTAINER HEIGHT = 12.0 IN.

d - OVERALL CONTAINER DIAMETER
INCLUDING ELLIPTICAL ENDS = 43.0 IN.

Figure 4.5.8-10. General Internal Geometry, Point Design 2A

V_D = 100 fps descent velocity

V_H = 220 fps wind velocity

omni-directional capability

clearance and protection for 5 in. rocks

1000 g (rigid body) limitation

The honeycomb thicknesses are shown in outline form in fig. 4.5.8-1.

4.5.8.4.3 Design Particulars for the Impact Attenuation System, Point Design 2B

When the appropriate criteria for a multi-directional Lander were applied to Point Design 2B the impact attenuation system was defined as 287 lb of 3/16 in. cell size phenolic fiberglass honeycomb. The honeycomb volume was 41 ft^3; the honeycomb density was 7 pcf. The other design conditions were:

V_D = 100 fps descent velocity

V_H = 220 fps wind velocity

multi-directional capability

clearance and protection for 5 in. rocks

1000 g (rigid body) limitation

The honeycomb thicknesses are shown in outline form in fig. 4.5.8-2.

4.5.8.5 Detailed Design

Another detail in the point designs is the utilization of a face sheet over the honeycomb to encapsulate it. The factors which necessitate this facing are five:

1. Prevention of the honeycomb cells from filling with loose surface debris.

2. Facilitation of sliding. The sliding mechanism is used to absorb the impact velocity component parallel to the surface.

3. Enhancement of the structural integrity of the attenuator.

4. Distribution of or spreading of concentrated loads produced by surface protrusions.

5. Confinement of crush-up fragments which might provide an undesirable background for surface measurements.

Experimentation has shown that loose surface (sand, loam, dust, etc.) tend to fill up the impacting cells quite quickly. This filling will interfere with pure crushing action and for this reason is undesirable. However, for surfaces presenting this potential hazard, the major energy absorber is the ground with a reduced amount of honeycomb attenuator crushing or no crush-up at all. From this viewpoint, therefore, the first consideration for a cover may not produce a compelling argument.

The smooth surface presented by a cover would certainly provide better sliding behavior than the exposed open cells of a honeycomb. On anything less than a very hard terrain of low relative roughness this is an important factor. Moreover, in the point design analyses lateral sliding motions are counted on to absorb the horizontal component of the impact velocity vector.

The structural strength of the attenuator is favorably affected by use of a facing plate. The facing lessens the tendency to shear off entire chunks of the attenuator, thereby thwarting the desired crush-up behavior. A wraparound membrane also allows more of the attenuator to participate in the energy absorbing process than if no cohesive member was used.

More important than this last argument, however, a face sheet produces a spreading action of possible localized loads produced by rocks and other surface protrusions. This lessens the possibility of local punctures or intrusions which could

circumvent the crush-up process. The spreading of loads is important if the design assumptions are to be reasonably accurate. Moreover, a thin cover protects the outermost cell edges and minimizes local shear deformations which could cause lateral failures produced by the surface friction.

Finally, encapsulation of the honeycomb prevents stray honeycomb fragments from reaching the surface and interfering with surface science measurements and other scientific experiments (alpha back scatter, for example).

If an encapsulation device is used, the determination of its thickness can be made as follows. Strength will not govern the design since the facing is not required to perform a major structural function. Instead the facing must be designed to be sufficiently thin so that it can be contoured to fit the doubly curved Lander geometry. The actual layup is a detailed design manufacturing problem. A piece wise layup of extremely light gauge material is one possible design choice. The lower limit on gauge is determined by the criteria that the membrane itself must not be so light that it is easily punctured by surface abrasion.

Finally, two other design details remain. First, cross deformation effects are investigated for two conditions. The first is excessive stroke requirements which produce thickness sufficiently large (> 24 in.) to lead to impulsive buckling of the honeycomb cells without crushing behavior. If such strokes are indicated the attenuator is segmented further to eliminate buckling and promote crushing of the attenuator. Second, gross shear failures must also be considered. This possible mode involves the breaking off of an entire piece of material without crushing deformation. Where analysis indicates that gross shear is a possibility, radial metallic strips welded to the payload container can be used to take out the shear in excess of what can be carried laterally by the honeycomb cells. These elements, while resistant to shear, are sufficiently slender so that they buckle when impacted along their length and thereby crush-up with the phenolic honeycomb materials.

Past experience indicates that the double curvature introduced in this Lander concept can be wrapped effectively by segmenting the honeycomb into pieces which are then bonded together. In this way the longitudinal axis of the honeycomb cells can be made near-radial with the payload contained structure. The wrapping proceeds around the Lander circumference and then outward until the desired thicknesses are provided.

4.5.8.6 Honeycomb Lander Fabrication

The principal operations involved in the fabrication of the honeycomb crush-up system include the segmenting and cutting of the honeycomb material so that it may be properly oriented, as shown in fig. 4.5.8-11 for Point Design 2A and fig. 4.5.8-12 for Point Design 2B, the bonding of the honeycomb segments to one another, and the bonding of the honeycomb to the aluminum substructure and the external protective covering.

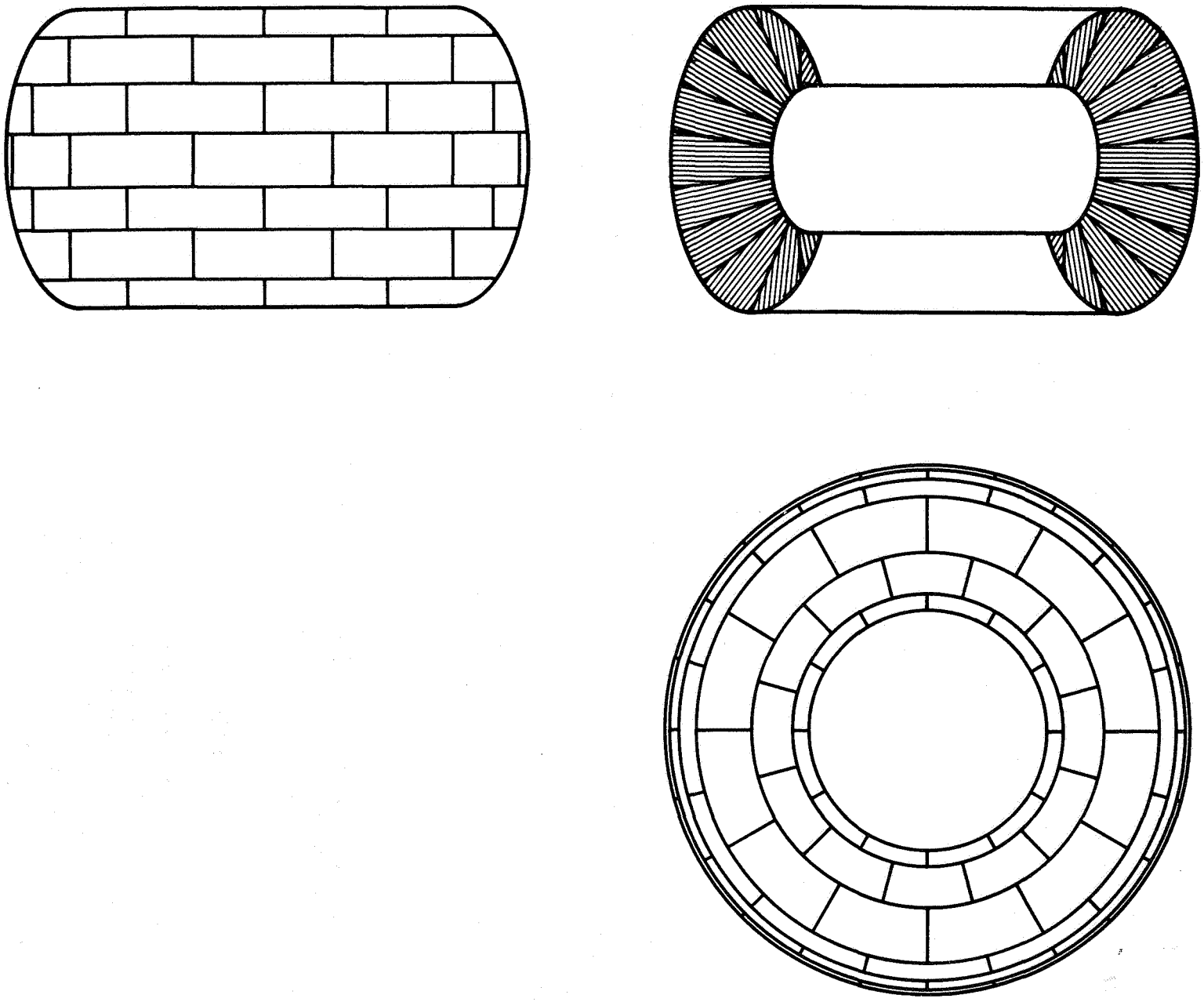


Figure 4.5.8-11. Layup of Honeycomb Arrangement (Omni-direction)

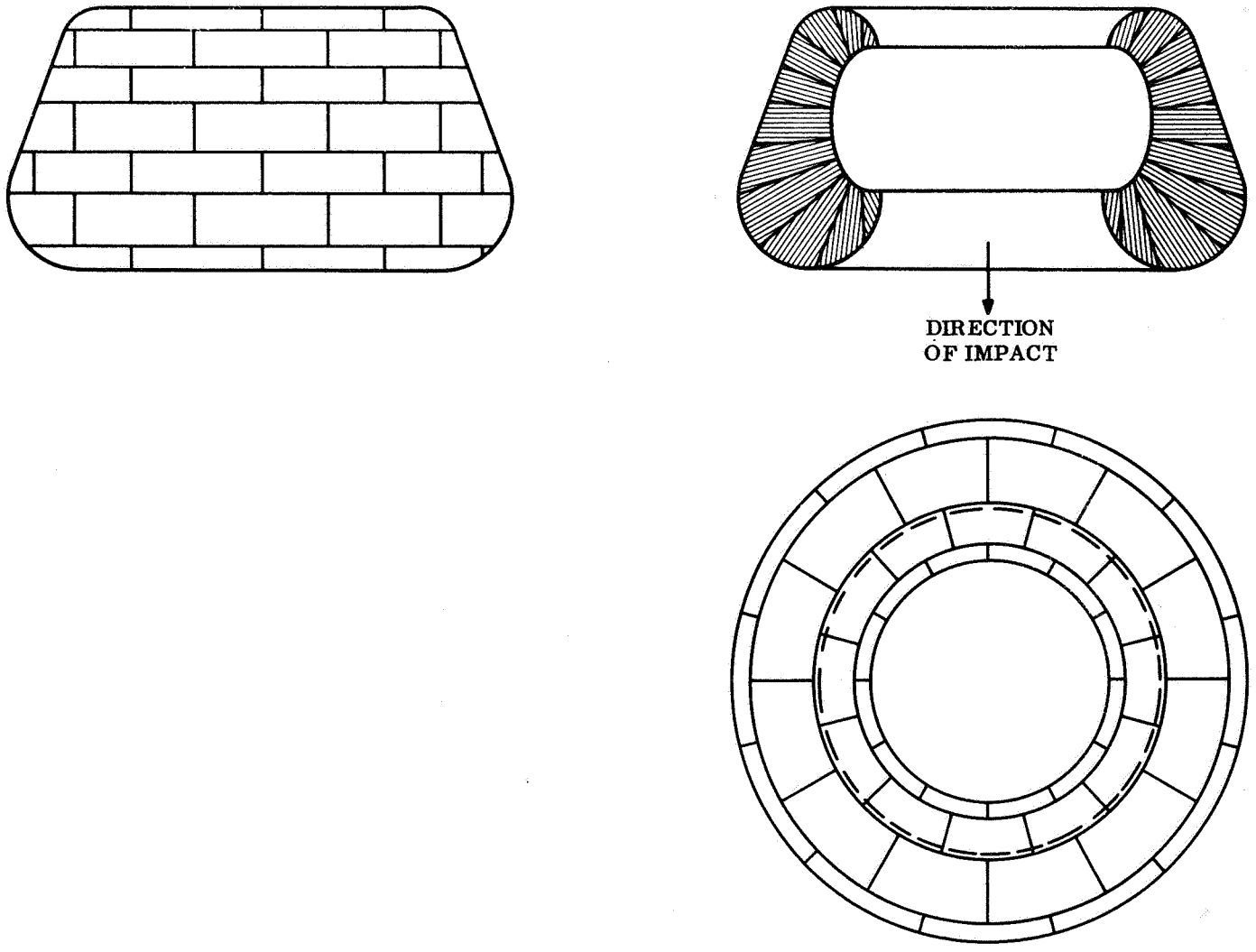


Figure 4.5.8-12. Layup of Honeycomb Attenuator (Multi-direction)

4.5.8.6.1 Adhesive Selection

For proper bond action suitable adhesives must be selected. Adhesive bond systems are required for two distinctly different joints: honeycomb-to-honeycomb and metal-to-honeycomb. While these configurations present separate joining problems the bonded joints must nevertheless have the same cure cycle. There are, however, modified epoxy-phenolic adhesives suitable for temperatures of -200°F to 900°F. A representative example of such a product is the HT 424 adhesive manufactured by the Bloomingdale Department of the American Cyanamid Corporation. These adhesives may be formulated to be r-f transparent as required. The properties of this class of adhesive are such that the bonds formed are stronger than the weakest material comprising the joint. In fact, shear and bending tests will fail the honeycomb interface of the bond.

4.5.8.6.2 Honeycomb-to-Honeycomb Joints

In fabricating the Lander, there are a large number of possible variations at the interface between the honeycomb segments. The selected desirable approach is to bond flat surfaces of honeycomb together utilizing a space-filling adhesive as needed to fill gaps between contact points.

4.5.8.6.3 Honeycomb-to-Aluminum Joints

Previous development testing (ref. 4-2) has identified adhesives suitable for bonding phenolic fiberglass honeycomb to aluminum.

Previous GE-MSD efforts have, furthermore, identified adhesives for this bond which have cure cycles compatible with the adhesives used for honeycomb-to-honeycomb joints. As an example, adhesives of the H424 high-temperature resin family produced by the Bloomingdale department of the American Cyanamid Corporation are feasible. (For aluminum-to-honeycomb joints HT 424 F, in particular, has been tested by GE-MSD as reported in ref. 4-2. For honeycomb-to-honeycomb bonds HT 424 is indicated).

4.5.8.6.4 Tooling and Fixtures

Phenolic fiberglass honeycomb material of the densities used in this Lander point design can be cut to size and shape with moderate ease. Heavier or lighter densities should also work well. Standard shop equipment with metal cutting tools may be used throughout.

Tool steel routers and mills may be used. For rough cutting the honeycomb segments a carbide tipped band saw blade is preferred. For final thickness and taper large inertia sanding wheels are used. Specialized wood fixtures can be designed for many of the sizing and contour cutting operations. For curing operations a standard circulating air furnace provides a rotating spit fixture for the assembly cure cycle.

4.5.8.6.5 Lander Fabrication

The Lander fabrication sequence proceeds according to the following steps:

1. Preparation of container structure surface. This includes final finishing to produce proper dimensional tolerances and special treatment of apertures and holes. After all finishing the structure is surface-treated with a chemical reagent (such as Alodine 1200) to promote good adhesive bonding.

2. Preparation of exterior shell interior surface. This includes final shaping of the impact attenuator encapsulating structure (skin). This surface is also surface treated prior to adhesive bonding.

3. The raw honeycomb crush-up material is then rough cut to size with proper attention to the designed layup and resultant cell wall orientation.

4. The rough cut surface is then checked for dimensional accuracy and secondary trimming or sanding is performed.

5. A preliminary fit of the honeycomb to the subsystems container is made. This is done by using shims to allow for adhesive bond thicknesses.

6. The epoxy adhesive is then prepared according to the manufacturer's specifications.

7. The bonding of the honeycomb segments to the container structure and to one another is then begun. For this purpose a rotating spit device to hold the container, along with the associated jigs and fixtures for temporary support during curing are used. The exact fixture details must be determined during the manufacturing development period. However, in general, these are wooden forms which can be snapped in and out of position.

8. The assembly, which is now fully mated, is subjected to the proper cure cycle determined by the adhesive and also the specified strength level to be attained. Refer to figs. 4.5.8-11 and -12 for layup details.

9. The exterior facing plate is now attached, held in position by jigs, and cured. Because of the double curvature of this element it must be laid up in pieces in a manner comparable to the layup of conventional toroidal metallic shells.

4.5.9 MASS PROPERTY AND INERTIA DATA

Following are summary weight statements for the complete Lander, table 4.5.9-1 for Point Design 2A and table 4.5.9-2 for Point Design 2B, and a detailed weight breakdown of the payload subsystem and components, table 4.5.9-3 for both Point Design 2A and Point Design 2B.

TABLE 4.5.9-1. WEIGHT SUMMARY, POINT DESIGN 2A

Lander Systems and Equipment	Weight (lb)	Total (lb)
Lander (Complete)	--	(858.0)
Structure	160.0	
Attenuation	522.0	
Electrical power equipment	56.5	
Telecommunications	30.7	
Environmental control	10.0	
Scientific payload	48.3	
Interface equipment	0.9	
Cables and harness	9.6	
Deployment-cameras	10.0	
Deployment-alpha back scatter	10.0	
Total	--	858.0

C.G.'s ('X' CG Datum - Apex of Heat Shield Cone) (in.)		
X	Y	Z
38.0	-0.08	-0.42

Gross Inertias (slug/ft^2)		
Roll	Pitch	Yaw
92	61	60

TABLE 4.5.9-2. WEIGHT SUMMARY, POINT DESIGN 2B

Lander Systems and Equipment	Weight (lb)	Total (lb)
Lander (Complete)	--	(623.0)
Structure	160.0	
Attenuation	287.0	
Electrical power equipment	56.5	
Telecommunications	30.7	
Environmental control	10.0	
Scientific payload	48.3	
Interface equipment	0.9	
Cables and harness	9.6	
Deployment-cameras	10.0	
Deployment-alpha back scatter	10.0	
Total	--	623.0

C.G's ('X' CG Datum - Apex of Heat Shield Cone) (in.)			Gross Inertias (slug/ft^2)		
X	Y	Z	Roll	Pitch	Yaw
35.7	-0.11	-0.19	39	25	26

TABLE 4.5.9-3. DETAILED WEIGHT BREAKDOWN, SUBSYSTEMS COMPONENTS

Lander Subsystems	Weight (lb)
Electrical Power Equipment	56.45
A101 Operational Battery	29.80
A106 Switch Power Transfer	2.00
A107 Programmer Lander	7.20
A108 Regulator Voltage	7.00
A130 Regulator Voltage	0.9
A110 Controller Power	5.50
A113 Battery High Rate 'A'	0.50
A114 Battery High Rate 'B'	0.50
A115 Filter EMC 'C'	1.90
A121 Module Diode Block	0.2
A124 Module Therm. Relay	0.15
A128 Switch Hg 'A'	0.10
A132 Breaker and Limiter Unit	0.60
Telecommunications	(30.7)
A602 Transmitter UHF	2.50
A604 Conditioner Signal Data	4.00
A605 Antenna UHF Relay 'A'	1.00
A607 Unit Memory	5.00
A608 Receiver UHF Beacon	1.30
A609 Processor Data Handling	4.00
A610 Circulator UHF 'A'	0.40
A611 Circulator UHF 'B'	0.40
A621 Switch Antenna	1.00
A623 Antenna UHF Relay 'B'	1.00
A676 Multicoder	5.00
Mach 2 Sensor	3.00
A682 Accel Impact	0.60
A683 Amplifier Charge (3)	1.50

TABLE 4.5.9-3. DETAILED WEIGHT BREAKDOWN, SUBSYSTEMS COMPONENTS (Continued)

Lander Subsystems	Weight (lb)
Thermal Control Subsystem	(10.00)
1 in. Insulation	7.00
Installation Hardware	3.00
Scientific Payload Subsystem	(48.30)
A807 Accelerometer Tri. Ax	2.00
A808 Transducer Temperature (2)	1.00
A809 Transducer Pressure (2)	1.00
A810 Transducer Pressure (2)	1.40
A817 Transducer Temperature (2)	1.00
A822 Camera Facsimile A	2.00
A823 Camera Facsimile B	2.00
A824 Camera Facsimile C	0.40
A825 Camera Facsimile D	0.40
A829 Sensor-Wind Velocity A	0.50
A830 Sensor-Wind Velocity B	0.50
A831 Sensor-Wind Velocity C	0.50
A832 Sensor-Wind Velocity D	0.50
A833 Sensor-Wind Velocity E	0.50
A834 Sensor-Wind Velocity F	0.50
A835 Sensor-Wind Velocity G	0.50
A836 Sensor-Wind Velocity H	0.50
A837 Sensor Moisture	10.00
A849 Detector (Water Vapor and Moisture)	1.00
A838 Spectrometer Mass	8.00

TABLE 4.5.9-3. DETAILED WEIGHT BREAKDOWN
SUBSYSTEMS COMPONENTS (Concluded)

Lander Subsystems	Weight (lb)
A841 Inclinometer (2)	2.60
A845 Sensor-Wind Velocity I	0.50
A846 Sensor-Wind Velocity J	0.50
A847 Transducer-Temperature	0.50
A848 Transducer-Temperature	0.50
A842 Instrument, Surf Comp	9.50
Interface Equipment	(0.88)
J2002 IFD A/S Lander	0.13
J2003 IFD T/C Lander	0.75
Cable Assembly	(9.60)
WL1 Cable Assembly Command	2.10
WL2 Cable Assembly Power	3.70
W13 Cable Assembly Instrument	3.00
WL4 Cable Assembly Shld	0.80

4.6 CONSTRAINTS IMPOSED ON ORBITER

The majority of constraints imposed by the Flight Capsule on the Orbiter are relatively independent of the mode of Capsule entry (direct or orbital) and the size or weight of the Capsule. Addition of the Flight Capsule however, requires mechanical and electrical interfaces between the Orbiter and the Capsule. Fig 4.6-1 shows the Capsule adapter which will provide the mechanical interface. In this study, it has been assumed that the Mariner Mars '71 Orbiter will be modified for the combined Orbiter and Hard Lander mission in 1973. MM '71 is itself an adaption of the Mariner Mars '69 flyby spacecraft. A complete description of the MM '73 Orbiter is contained in Appendix D. Table 4.6-1, excerpted from the appendix, highlights the major changes required of the MM '69 subsystems for conversion to an Orbiter in '71, and then to a Capsule bus (as well) in '73. No other changes are required of the Orbiter to accommodate this specific Capsule point design. Tables 4.6-2 and -3 show the Orbiter propulsion summary for Point Designs 2A and 2B.

FOLDOUT FRAME

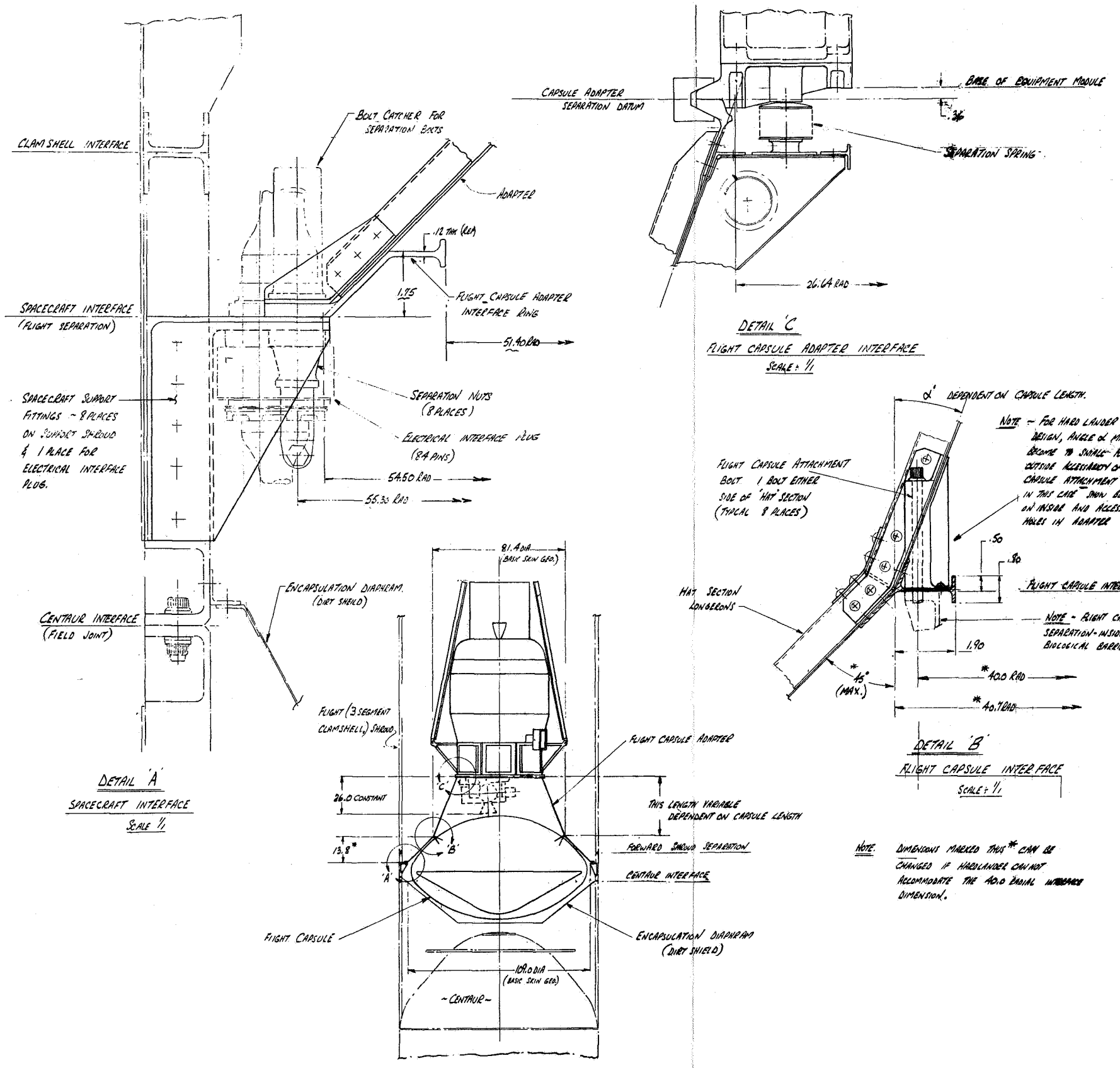


Figure 4.6-1. Capsule/Bus Interface

TABLE 4.6-1. MAJOR SUBSYSTEM CHANGES

MM '69 Subsystem	Change For '71 Orbiter	Change For '73 Capsule
Power	• Solar Array Increase	• Solar Array Increase
Radio	• New Maneuver Antenna • New High Gain Antenna • Modified Low Gain Antenna	• New Maneuver Antenna • New High Gain Antenna • New Relay Receiver • New Relay Antennas
Attitude Control	• Cold Gas and Jet Size Increase • Modification of Autopilot Electronics	• Cold Gas and Jet Size Increase • Modification of Autopilot Electronics • Relocated Sun Sensors • Possible Approach Guidance
Data Storage	• Additional Air • Additional DTR	• New Relay Recorders
Command	• Possible Decoder Expansion	• Probable Decoder Expansion
Telemetry		• Data Modes for Capsule Telemetry
Scan Control	• Removal of Mars Gates	
Science	• Passive Cooling of IRS • Possible TV Field of View Changes	No Estimate
Cabling		• Three Inflight Disconnects
Mechanical Devices	• High Gain and Maneuver Antenna Deployment • High Gain Antenna Articulation • Modified Separation Mechanics	• Spacecraft Separation Mechanics • Modified Orbiter Separation Mechanics • New High Gain Antenna Deployment
Propulsion	• New	• New Tanks and Supports for (Orbital Entry Capsule)
Structure	• Strengthened Adapter	• Capsule Adapter • Spacecraft Adapter • Strengthened Octagon for (Orbital Entry Capsule)

TABLE 4.6-2. ORBITER PROPULSION SUMMARY, POINT DESIGN 2A

ΔV (Total)		1495
Weights (lb)		
	Capsule	1882
	Orbiter	930
	Adapter	200
(1)	Propulsion (dry)	153
(2)	Residuals	29
(3)	Total propellant and pressurant	825
(1) + (2)	Burnout	182
(1) + (3)	Propulsion system	978
Volumes (in.)		
	Propellant tank diameter	22
	Pressurant tank diameter	11
Burn time (insertion) (sec)		730
Spacecraft launch weight (lb)		3990

TABLE 4.6-3. ORBITER PROPULSION SUMMARY, POINT DESIGN 2B

ΔV (Total)		1495
Weights (lb)		
	Capsule	1463
	Orbiter	930
	Adapter	165
(1)	Propulsion (dry)	153
(2)	Residuals	29
(3)	Total propellant and pressurant	825
(1) + (2)	Burnout	182
(1) + (3)	Propulsion system	978
Volume (in.)		
	Propellant tank diameter	22
	Pressurant tank diameter	11
Burn time (insertion) (sec)		730
Spacecraft launch weight (lb)		3536

4.7 PROBABILITY OF SUCCESS - POINT DESIGN 2

4.7.1 INTRODUCTION

A key factor in evaluating a design concept is the determination of the probability of success of the configuration. This determination is primarily beneficial at the early concept design state in performing trade-off evaluations of several potential design configurations. As the design evolves from conceptual towards final, the merit of the quantitative value shifts from comparative to predictive.

A probability of success determination was performed for the conceptual mission as defined by Point Design 2. Due to the early stage of the design, it was necessary to perform this determination based on many assumptions. These are listed below. In general, it can be stated that failure rate data was based on information known concerning components of similar generic or complexity definition. It was also assumed that the new development items required for this mission will be developed, tested, and qualified before being flown.

Due to these assumptions, and the uncertainty of sterilization influence on some of the components, the predictive value of the determination may not be accurate. However, since the same assumptions and methodologies were used on all determinations during the study, the comparative value of the determinations are significant.

4.7.2 RESULTS

Probability of success values were determined for both the Capsule systems and for the booster and Orbiter systems of the mission. The procedures used in performing these determinations are presented in Sections 4.7.3 and 4.7.4 below. A summary of the determinations, by major mission phase, is shown in table 4.7.2-1.

This tabulation indicates that the value obtained, under the study ground rules stated in the preceding paragraph for the probability of success of the total mission is 0.699. This is the probability of obtaining proper functioning of all mission equipment, as required, for the duration of the mission from launch to completion of one full diurnal cycle on the Martian surface.

TABLE 4.7.2-1. MISSION SUCCESS PROBABILITY, POINT DESIGN 2

Mission Phase	Booster and Orbiter		Capsule		Combined	
	Phase	Cumulative	Phase	Cum.	Phase	Cum.
Launch/Cruise	.807	.807	.958	.958	.773	.773
Separation and Entry	.998	.805	.951	.911	.949	.773
Orbit Achievement	.989	.796		.911	.989	.725
Landed Operation	.997	.794	.967	.881	.964	.699

4.7.3 CAPSULE ANALYSIS

This section presents the procedure followed in analyzing the Mars Hard Lander System Point Design for the probability of successfully accomplishing its intended functions.

4.7.3.1 Assumptions

The assumptions and ground rules used in the analysis were as follows:

1. A component would not fail under non-operating conditions.

2. The probabilities of success of all components were considered to be statistically independent. This permitted the use of the product rule of assessing the system and subsystem success probabilities. In the case of redundant application, the above ground rule applied to the component function.

3. The success probability of the structure, aeroshell and impact attenuation was assumed equal to unity (1.0).

4. The probability of success of the system or its components was defined as being equal to the probability of zero (0) functional failures.

5. The mission phases and time of each phase upon which the analysis was based are as follows:

Phase	
Launch/Cruise	3,936 hr
Pre-entry	24.1 hr
Entry	0.34 hr
Landed Operation	24.6 hr

6. The assessment for the success probability of a component during any given phase reflects only the time during the phase in which it operates.

7. If any portion of a component operated during a particular phase, the entire component was assessed for its success probability.

8. The success probability of the various system components was based on failure data of components which were similar or identical in function or of equivalent complexity.

4.7.3.2 Procedure

4.7.3.2.1 Component Success Probability

The probability of success of time (or cycle) sensitive components was obtained using the following expression:

$$R_c = e - \lambda t \quad (1)$$

where:

R_c = probability of success

λ = failure rate in failures/hr (or cycle)

t = operating time (hr) or cycles

For redundant application of a component, the following expression was used to obtain the probability of success of the function:

$$R = [1 - (1 - R_c)^n] \quad (2)$$

where:

R = probability of success of the function

R_c = probability of success of the component

n = number of components in the redundant group.

For components which are not time (or cycle) sensitive, such as squib valves, the success probability reflects the results of successes versus trials using appropriate statistical techniques.

4.7.3.2.2 Subsystem Success Probability

The probability of success of a subsystem for any given phase was obtained using the following expression:

$$R(S'S)_p = \pi_i \; R_i \quad (3)$$

where:

$R(S'S)_p$ = probability of success of the subsystem in the phase

R_i = probability of success of the i^{th} component or function (for redundant application) for the phase being considered

π = symbol for product

The probability of success of a subsystem over its entire mission was obtained using the following expression.

$$R\ (S/S)_M = \pi_j\ R\ (S'S)_j \tag{4}$$

where: $R\ (S/S)_M$ = probability of success of the subsystem over the missions.

$R\ (S/S)_j$ = probability of success of the subsystem for the j^{th} mission phase.

4.7.3.2.3 System Success Probability

The probability of success of the system for any given phase was obtained using the following expression.

$$R\ (System)_p = \pi_k\ R\ (S'S)_k \tag{5}$$

where:

$R\ (System)_p$ = probability of success of the system in the phase

$R\ (S/S)_k$ = probability of success of the k^{th} subsystem for the phase being considered.

The probability of success of the system over the entire mission was obtained using the following expression.

$$R\ (System)_M = \pi_k\ R\ (S/S)_{M_k} \tag{6}$$

where:

$R\ (System)\ M$ = probability of success of the system for the mission

$R\ (S'S)_{M_k}$ = probability of success of the k^{th} subsystem for the mission

4.7.3.2.4 Orbiter Support Analysis

The probability of success of the Mars Hard Lander for the i^{th} mission phase, reflecting the success probability of the booster and spacecraft (in support of Capsule operations) and the Capsule system is given by:

$$R\ (MHL)_i = R\ (Booster)_i \cdot R\ (Spacecraft)_i \cdot R\ (Capsule)_i \tag{7}$$

The cumulative probability of success of the Mars Hard Lander for the i^{th} mission phase is given by:

$$R\ (MHL;\ cumulative) = \prod_{i-1}^{i} R\ (MHL) \qquad (8)$$

where:

$R\ (MHL)_{i-1}$ = independent probability of success of the MHL for the $(i-1)^{th}$ phase as obtained form (7)

$R\ (MHL)_i$ = independent probability of success of the MHL for the i^{th} phase as obtained from (7)

The cumulative success probability for each of the systems are similarly obtained from (8).

4.7.3.3 Results

4.7.3.3.1 Component Success Probabilities

The success probability for the components (or functions in the case of redundant applications) comprising Point Design 2 for the Mars Lander System is summarized in table 4.7.3-1 for each of the mission phases described in para 4.7.3.1.

The values appearing in the table were computed using expressions (1) or (2) described in para 4.7.3.2 as applicable, for time (or cycle) sensitive components. These values reflect failure rate data from the sources indicated in the table. Non-time (or cycle) sensitive component success probabilities were obtained directly from the indicated source.

4.7.3.3.2 System and Subsystem Success Probabilities

The success probabilities for the subsystems and systems which define Point Design 2 are summarized in table 4.7.3-2 for each of the phases described in para 4.7.3.1 and the total mission. The values appearing in the table were obtained using expressions (3), (4), (5) and (6) described in para 4.7.3.2.

4.7.3.4 Redundancy Considerations

A Failure Mode Effects Analysis (FMEA) was performed as part of the Capsule analyses. Due to the conceptual state of the mission design, this was performed on a quantitative rather than a quantitative basis. The primary purpose of this analysis was to point out potential problem areas for redundancy considerations.

TABLE 4.7.3-1. RELIABILITY ESTIMATES, POINT DESIGN 2 COMPONENTS

Description	Reliability				Data Source
	Launch and Cruise	De-orbit	Entry	Landed Operation	
EP&D Subsystem					
Battery, Operational (1)	-	.9999	.9981	.9993	ERSR-TT Program
Battery, Entry (Dual)	-	.9999	-	-	
Battery, T/C (Dual)	-	.9999	-	-	
Programmer, Lander (1)	-	.9999	.9944	.9942	REA-MBRV Program
Voltage Regulator, A (1)	-	.9999	.9999	.9999	RFMA-MK12 Program
Voltage Regulator, B (1)	-	.9999	.9996	.9999	
Voltage Regulator, C (1)	.9999	.9999	-	-	
Regulator, Charge (1)	.9999	-	-	-	REA-Voyager Study
Module, Diode Block (2)	-	.9998	-	-	RFMA-TT Program
Module, Diode Block (1)	-	-	.9999	-	
Battery, H.R. (Dual)	-	-	.9999	.9999	ERSR-TT Program
Module, Power Distribution	-	.9999	-	-	REA-MK12 Program
Filter, EMC, A (1)	-	.9999	-	-	RFMA-TT Program
Filter, EMC, B (1)	-	.9999	-	-	
Filter, EMC, C (1)	-	-	.9999	.9999	
Module, Thermal Relay (2)	-	.9998	-	-	
Module, Thermal Relay (1)	-	-	.9999	.9999	
Battery, Dual	.9999	.9999	-	-	ERSR-TT Program
Control, Power-C	.9999	.9999	-	-	REA-MK12 Program
Control, Power-L	-	.9999	.9988	.9999	
Programmer, Dual-C	-	.9999	-	-	RFMA-TT Program
Switch, Hg (Dual)	-	-	-	.9999	FARADA
Switch, Breaker and Limit	-	.9999	-	-	FARADA
Switch, Power Transformer	.9999	-	-	-	REA-MBRV Program
Pressurization and Venting Subsystem					
Valve, Vent	.9999	-	-	-	FARADA
Separation Subsystem					
Release, Hot-Wire (4)	-	.9996	-	-	RFMA-MK12 Program
Nut, Explosive (4)	-	.9894	-	-	FARADA
Nut, Explosive (4)	-	.9894	-	-	FARADA
Scientific Payload Subsystem					
Transducer, Temperature -A (4)	-	-	.9997	-	FARADA
Transducer, Temperature -L (4)	-	-	-	.9981	
Transducer, Pressure -A (6)	-	-	.9996	-	
Transducer, Pressure -L (2)	-	-	-	.9940	
Accelerometer, Tri-Axial (1)	-	-	.9983	-	
Release, Hatch Cover (1)	-	-	-	.9999	
Solenoid, Camera Release (4)	-	-	-	.9987	
Camera, Facsimile (4)	-	-	-	.9996	
Sensor, Wind Velocity (10)	-	-	-	.9972	
Sensor, Moisture (1)	-	-	.9999	.9997	
Spectrometer, Mass (1)	-	-	.9997	-	
Inclinometer (1)	-	-	-	.9996	
Comp, Surface (1)	-	-	-	.9960	FARADA
Attitude Control and Propulsion					
Tank, N_2	.9992	.9999	-	-	FARADA
Valve, Squib	-	.9999	-	-	
Valve, Fill	.9994	.9999	-	-	
Tank, Hydrazine	.9992	.9997	-	-	
Disc, Burst	.9999	.9999	-	-	FARADA

Legend
- RFMA - Reliability Figure of Merit Analysis
- REA - Reliability Estimate Analysis
- ERSR - Equipment Reliability Status Report

TABLE 4.7.3-1. RELIABILITY ESTIMATES, POINT DESIGN 2 COMPONENTS (Cont'd)

Description	Reliability				Data Source
	Launch and Cruise	De-orbit	Entry	Landed Operation	
Attitude Control and Propulsion (Cont'd)					
Valve, Solenoid (12)	-	.9999	-	-	FARADA
Gyro, Rate	-	.9993	-	-	
Amplifier	-	.9997	-	-	
Detector, Threshold	-	.9994	-	-	
Driver, Pneumatic	-	.9993	-	-	
Generator, R.R.	-	.9996	-	-	
Switch	-	.9995	-	-	
Rocket, Retro	-	.9999	-	-	
Ejector, Nozzle	-	.9975	-	-	FARADA
Retardation Subsystem					
G-Switch	-	-	.9991	-	MBRV Program
Mortar, Drogue	-	-	.9999	-	
Fitting, Main Release (3)	-	-	.9997	-	
Fitting, Drogue Release	-	-	.9999	-	
Switch, Impact	-	-	.9999	-	
Parachute Assembly	-	-	.9999	-	MBRV Program
Telecommunication Subsystem					
Transmitter, VHF	-	.9998	.9999	.9999	RFMA-MK12 Program
Conditioner, Signal Data	-	.9999	.9999	.9997	
Antenna, VHF (2)	-	.9999	.9999	.9999	FARADA
Core, Memory	-	.9999	.9999	.9996	
Processor, Data	-	.9999	.9999	.9999	RFMA-MK12 Program
Diplexer (2)	-	-	.9999	.9999	FARADA
Communicator, Cruise	.9999	-	-	-	
Switch, Microwave (2)	-	-	-	.9989	
Receiver, Beacon VHF	-	-	-	.9940	RFMA-MK12 Program
Sensor, Temperature (18)	.9961	.9982	-	-	FARADA
Sensor, Pressure (8)	.9982	.9992	-	-	
Sensor, Linear Velocity (12)	.9988	.9988	-	-	
Conditioner, Firing Checkout (1)	.9999	.9999	-	-	RFMA-MK12 Program
Sensor, Power Supply	.9999	.9999	-	-	MIL HDBK-217A
Conditioner, Signal-C	.9999	.9999	-	-	RFMA- MK12 Program
Sensor, Voltage Regulator	.9999	-	-	-	MIL HDBK-217A
Detector, Separation Load (2)	-	.9999	-	-	Accelerometer est.
Indicator, A/S Rel (2)	-	.9999	-	-	Sep. Switch est.
Conditioner, Linear Velocity Data	.9999	-	-	-	RFMA-MK12 est.
Multicoder	-	.9999	.9999	.9999	PCM est.- MBRV
Sensor, Link Tensile (4)	.9996	-	-	-	Strain Gage est.
Accelerometer, Impact	-	-	.9999	-	FARADA
Processor, Impact Data	-	-	.9999	-	Computer est.
Electrical Interface					
IFD, Capsule-Spacecraft	.9992	-	-	-	MIL-HDBK-217A MK12 RFMA
IFD, A/S-Lander	.9992	.9999	.9999	-	
IFD, T/C-Lander	.9992	.9999	-	-	
Safe-Arm, Lander	.9992	.9999	.9999	.9999	
Safe-Arm, Aeroshell	.9992	.9999	-	-	
Safe-Arm, Canister	.9992	-	-	-	
Fitting, Coaxial Data	.9999	-	-	-	
Fitting, Coaxial Interface	.9999	-	-	-	
Fitting, Coaxial VHF	.9999	-	-	-	MIL-HDBK-217A MK12 RFMA
Thermal Control Subsystem					
Heater	.9896	.9999	-	-	FARADA
Thermostat	.9843	.9999	-	-	FARADA

Legend
- RFMA - Reliability Figure of Merit Analysis
- REA - Reliability Estimate Analysis
- ERSR - Equipment Reliability Status Report

TABLE 4.7.3-2. RELIABILITY SUMMARY, POINT DESIGN 2 CAPSULE SYSTEM AND SUBSYSTEMS

Subsystem	Mission Phase				$R_M = \pi R_p$
	Launch and Cruise	De-orbit	Entry	Landed Operation	
EP&D	.9995	.9981	.9904	.9928	.9808
Attitude Control and Propulsion	.9977	.9934	-	-	.9911
Pressure and Venting	.9999	-	-	-	.9999
Separation	-	.9784	-	-	.9784
Telecommunications	.9921	.9950	.9991	.9917	.9780
Thermal Control	.9740	.9998	-	-	.9738
Scientific Payload	-	-	.9972	.9828	.9800
Retardation	-	-	.9984	-	.9984
Electrical I/F	.9949	.9996	.9998	.9999	.9942
$R_p = \pi$ R(S/S)	.9586	.9646	.9849	.9675	.8810

During the FMEA, it was learned that the items that had the greatest criticality and risk of failure were the canister heater and thermostat and the operational battery. The former were of high risk due to the long duty cycle during the interplanetary cruise. The latter was critical due to its requirement to perform all Capsule operations. Redundancy inclusions were provided for these items; a standby parallel thermal control system and internal cell redundancy in the battery.

In addition to these items, many other redundancy inclusions are provided in the Capsule design. A typical listing of some of these inclusions together with the type of redundancy used is shown below. Other redundancy provisions such as backup gate or switching signals and backup time signals are also provided but not included in the listing.

Item	Type Redundancy
Operational Battery	Internal
Canister Heater and Thermostat	Parallel
Dual Battery	Internal
Thermal Batteries	Parallel
Programmer - Lander	Internal
Charge Regulator	Internal
Blocking Module	Internal
Power Distribution Module	Internal
Thermal Relay Module	Internal
Dual Programmer	Internal
Hg Switch	Parallel
Breaker and Limiter Unit	Internal
Spin Initiator	Parallel Squibs
De-spin Initiator	Parallel Squibs
Rocket Initiator	Parallel Squibs
Temperature Transducers	Parallel
Pressure Transducers	Parallel
UHF Antenna	Parallel

4.7.4 ORBITER SUPPORT ANALYSIS

4.7.4.1 Introduction

Probability of success determinations for the Booster and Orbiter systems were performed for those functions which support and/or contribute to the success of the

Capsule and its mission. Flight operations were based on a direct entry reference mission with a flight time of 164 days.

4.7.4.2 Assumptions

The assumptions made and the ground rules followed in the analysis were as follows:

1. Only those functions required for the success of the Capsule missions were included.

2. The Orbiter is assumed to use 1971 equipment hardware with only minor modifications.

3. The spacecraft support is required for a one day landed mission.

4. The reliability or criticality of the ground support functions have not been included in the study.

4.7.4.3 Procedure and Data Sources

In arriving at the reliability estimates, the tools and failure rate data bases developed during the Voyager Task C redundancy and Task D Design studies conducted for JPL, as modified by more recent studies, were used. These procedures are described in detail in the reference documents shown in Section 4.8. In summary, these can be stated as follows:

1. Minuteman level parts and Minuteman and Apollo failure rates were used to the greatest extent possible.

2. Curves developed during the studies showing the projected reliability growth for inertial components and integrated circuits were used.

3. Factors to reflect (1) parts reliability growth and (2) upgrading to a high reliability status were used to obtain failure rates for sources other than Minuteman and Apollo.

4. Where failure rate data was lacking, or inadequate, failure rates were derived by comparing the part in question with another part of similar construction or performance for which reliability information was available.

4.8 REFERENCES

4-1. RF Transparent, Energy Absorbing, Structural Elements, Phase II Final Report Prepared for JPL under Contract No. 950964, August 1964, GE-MSD Document No. 64SD4329.

4-2. Development of Energy Dissipating Plastic Honeycomb, Quarterly Progress Report Nos. 7 and 8, Contract No. 951172, JPL, GE-MSD Document No. 66SD4390.

4-3. Failure Rate Data Base for Spacecraft Redundancy Study, VOY-C3-TR8.

4-4. Reliability Characteristics of Voyager Components - Voyager Spacecraft Redundancy Study, VOY-C3-TR7.

4-5. Voyager Final Report, Phase IA, Task C, Volume 4, Application of Redundancy Study, July 28, 1967, VOY-CO-FR, prepared for JPL under contract 951112.

4-6. Voyager Spacecraft Final Report, Phase B, Task D. Volume II (Book 1 of 5), Systems Description, October 2, 1967, under contract NAS 8-22603.